

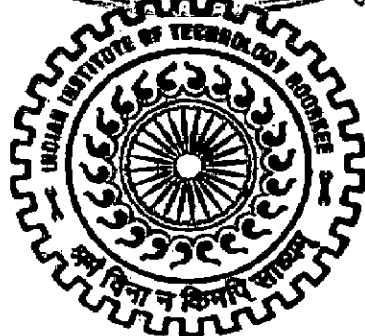
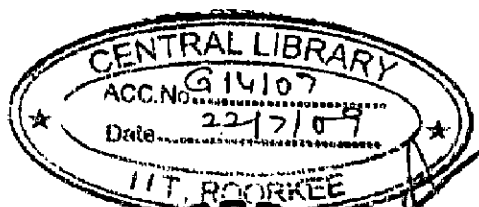
# HOT CORROSION BEHAVIOUR OF CONVENTIONAL AND NANOSTRUCTURED COATINGS ON SUPERALLOYS

## A THESIS

*Submitted in partial fulfilment of the requirements for the award of the degree*  
*of*  
**DOCTOR OF PHILOSOPHY**  
*in*  
**METALLURGICAL AND MATERIALS ENGINEERING**

*by*

**MAHESH R ANWAR**

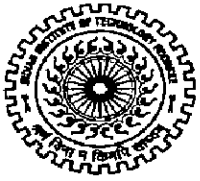


**DEPARTMENT OF METALLURGICAL AND MATERIALS ENGINEERING  
INDIAN INSTITUTE OF TECHNOLOGY ROORKEE  
ROORKEE - 247 667 (INDIA)**

**AUGUST, 2008**

©INDIAN INSTITUTE OF TECHNOLOGY ROORKEE, ROORKEE, 2008  
ALL RIGHTS RESERVED

# INDIAN INSTITUTE OF TECHNOLOGY ROORKEE ROORKEE



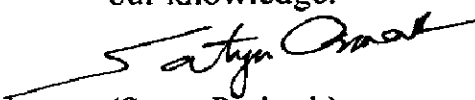
## CANDIDATE'S DECLARATION

I hereby certify that the work which is being presented in the thesis entitled **HOT CORROSION BEHAVIOUR OF CONVENTIONAL AND NANOSTRUCTURED COATINGS ON SUPERALLOYS**, in partial fulfilment of the requirements for the award of the Degree of Doctor of Philosophy and submitted in the Department of Metallurgical & Materials Engineering of the Indian Institute of Technology Roorkee, Roorkee, is an authentic record of my own work carried out during a period from Jan. 2005 to Aug. 2008 under the supervision of Dr. R. Jayaganthan, Assistant Professor and Dr. Satya Prakash, Professor, Metallurgical and Materials Engineering Department, Indian Institute of Technology Roorkee, Roorkee.

The matter presented in this thesis has not been submitted by me for the award of any other degree of this or any other institute.

  
(MAHESH R ANWAR)

This is to certify that the above statement made by the candidate is correct to the best of our knowledge.

  
(Satya Prakash)  
Supervisor

  
(R. Jayaganthan)  
Supervisor

Date: 13.08.08

The Ph.D. Viva-Voce Examination of **Mr. Mahesh R Anwar**, Research Scholar, has been held on .....

Signature of Supervisors

Signature of External Examiner

Material degradation at high temperatures is a serious problem in several high technology based industries. Gas turbines in aircraft, fossil fueled power plants, refineries and petrochemical industries, and heating elements for high temperature furnaces are some examples, where corrosion either limits their use or reduces their life, considerably affecting the efficiency. Understanding the behaviour of metals and alloys at elevated temperatures, especially their corrosion behaviour and providing protective surface layers has become an object of scientific investigation since long time. Hot corrosion is an accelerated oxidation of material at elevated temperatures, induced by a thin film of fused salt deposits. In hot corrosion, metals and alloys are subjected to degradation at much higher rates than in gaseous oxidation, with porous non-protective oxide scale formed at the surface and sulphides permeating into the substrate. Hot corrosion was first recognized as a serious problem in the year 1940 in connection with the degradation of fireside boiler tubes in coal-fired steam generating plants. Later on, it became a topic of importance and popular interest in the late 60s as gas turbine engines of military aircraft suffered severe corrosion during the Vietnam conflict during operation over seawater.

The hot corrosion of an alloy usually occurs in the environments where molten salts such as sulphates ( $\text{Na}_2\text{SO}_4$ ), chlorides ( $\text{NaCl}$ ) or oxides ( $\text{V}_2\text{O}_5$ ) are deposited onto the surfaces. Sodium vanadyl vanadate ( $\text{Na}_2\text{O} \cdot \text{V}_2\text{O}_4 \cdot 5\text{V}_2\text{O}_5$ ), which melts at a relatively low temperature  $550^\circ\text{C}$  is found to be the most common salt deposit on boiler superheaters. Superalloys are well known candidates for such high temperature applications. Although the superalloys have adequate mechanical strength at elevated temperatures, they often lack resistance to oxidizing/corroding environments. Use of inhibitors like  $\text{MgO}$ ,  $\text{CeO}_2$ ,  $\text{CaO}$ ,  $\text{MnO}_2$ , etc. have already been investigated in the laboratory at Metallurgical and Materials Engg, IIT Roorkee, and decrease in the extent of corrosion in the most aggressive environment of  $\text{Na}_2\text{SO}_4$ -60% $\text{V}_2\text{O}_5$  at  $900^\circ\text{C}$  has been achieved. However, the major problem being envisaged is the application of these inhibitors to the hot metal surface. Another countermeasure against the hot corrosion and oxidation constitutes the use of protective coatings. Furthermore, use of plasma sprayed coatings on boiler steels and HVOF sprayed coatings on superalloys to investigate the hot corrosion resistance have been carried out in this department and the better resistance to hot corrosion in a very aggressive environment of  $\text{Na}_2\text{SO}_4$ -60% $\text{V}_2\text{O}_5$  at  $900^\circ\text{C}$  has been achieved. The literature on hot corrosion behaviour of

Ni-5Al, NiCrAl and ceria added NiCrAlY coatings deposited on superalloys by HVOF and sputtering techniques is very limited.

Owing to the aforementioned facts, the present work has been focused to evaluate the hot corrosion behaviour of Ni-5Al, NiCrAl and NiCrAlY-0.4wt%CeO<sub>2</sub> coatings deposited by HVOF spray process and Ni-Al and NiCrAl films deposited by RF magnetron sputtering process on Ni and Fe based superalloys in air, molten salt (Na<sub>2</sub>SO<sub>4</sub>-60%V<sub>2</sub>O<sub>5</sub>) at 900°C in the laboratory under cyclic conditions, and in actual industrial environment in a coal fired boiler of a thermal power plant. The behaviour of these coatings in different degrading environments will be helpful in choosing the suitable coating for the hot section components of the gas turbine and boiler applications. The results have been critically analysed and discussed in the light of existing literature to propose an insight into the corrosion mechanisms manifested in both coated and bare superalloys. The whole work has been presented in 9 chapters.

**Chapter-1** contains a brief introduction as to hot corrosion phenomenon and its deleterious impact on the various engineering equipments and components. The remedial measures to obviate this problem are also briefly discussed.

**Chapter-2** presents the literature review on various aspects and mechanism of high temperature oxidation and hot corrosion. The high temperature oxidation/corrosion studies reported by various researchers relevant to the current work have been critically reviewed; particularly those conducted on similar Ni- and Fe-based alloys in air and molten salt environments. The various preventive measures have been summarised along with the description of HVOF spray process and RF magnetron sputtering process. The studies related to hot corrosion behaviour of coatings have also been reviewed. The problem has been formulated based on the available literature on hot corrosion behavior of coated and bare superalloys for the high temperature applications.

**Chapter 3** presents the experimental techniques and procedures employed for applying the coatings and their characterisation, oxidation studies in air, molten salt environment, and in the actual coal fired boiler environment. The specifications of the equipments and other instruments used for the present investigation and the techniques used to analyse the corrosion products are described bellow.

The HVOF spray coatings were deposited at M/s Metallizing Equipments Company Pvt Ltd, Jodhpur, India, on Ni- and Fe- based superalloys. These superalloys were procured from Mishra Dhatu Nigham Ltd., Hyderabad (India). Three types of coatings formulated were Ni-5Al, NiCrAl and NiCrAlY-0.4wt%CeO<sub>2</sub>. As-sprayed coatings were characterised by

metallography, FESEM, EDAX and X-ray mapping analysis. Mechanical properties such as bond strength and microhardness of the coatings have been evaluated. Surface roughness of the as sprayed coatings was also measured. The RF magnetron sputtering process was used to deposit nanostructured coatings (Ni-Al and NiCrAl) on the superalloys. The thin films were formulated in the Centre of Nanoscience Laboratory, Indian Institute of Technology Roorkee. The as deposited films were characterised by XRD, AFM, FESEM/EDAX analyses.

The corrosion behaviour of uncoated and coated superalloys has been studied in the air as well as in the aggressive environment of molten salt ( $\text{Na}_2\text{SO}_4\text{-60\%V}_2\text{O}_5$ ) in the laboratory furnace for 100 cycles. Each cycle consisted of 1 hour heating at  $900^\circ\text{C}$  followed by 20 minutes cooling to ambient temperature. At the end of each cycle, the specimens were critically examined regarding the colour, luster, tendency to spall and adherence of scale and then subjected to weight change measurements. The molten salt studies were performed by applying a uniform layer ( $3\text{-}5\text{ mg/cm}^2$ ) of the mixture of  $\text{Na}_2\text{SO}_4\text{-60\%V}_2\text{O}_5$  on the preheated samples ( $250^\circ\text{C}$ ) with the help of camel hair brush. XRD and FESEM/EDAX analytical techniques were used to identify the phases obtained and the elemental analysis of the surface scale, respectively. The corroded samples were then cut across the cross-sections for analyzing its composition by X-ray mapping analysis.

**Chapter-4** describes the detailed investigation of HVOF sprayed Ni-5Al coatings and RF magnetron sputtered Ni-Al film on Ni- and Fe-based superalloys, which includes, the characterisation of HVOF sprayed Ni-5Al coatings and RF magnetron sputtered film, oxidation studies in air at  $900^\circ\text{C}$  under cyclic conditions and hot corrosion studies in a very aggressive environment of ( $\text{Na}_2\text{SO}_4\text{-60\%V}_2\text{O}_5$ ) at  $900^\circ\text{C}$  in laboratory under cyclic conditions. Techniques such as XRD, FESEM, EDAX and X-ray mapping were used to analyse the as sprayed coatings and the corroded specimens after oxidation studies in air and molten salt environment.

The porosity of the coating was found to be around 2.0%. The bond strength of the coating was measured as per ASTM standard C633-01 and found to be 43 MPa. The splats formed are rich in nickel and aluminum moved to the periphery of the nickel rich splats. The as sprayed Ni-5Al coating indicates minor diffusion of alloying elements from the substrate into the coating. Oxidation studies were carried out on both bare and coated superalloy substrates in air at  $900^\circ\text{C}$  for 100 cycles. Among the three-coated superalloys, Superfer 800 substrate has shown the better resistance to oxidation. The protective nature of the Ni-5Al coated superalloys was due to the formation of protective oxide scales such as NiO,  $\text{Al}_2\text{O}_3$  and  $\text{Cr}_2\text{O}_3$ . Hot corrosion studies were conducted on bare as well as HVOF-coated superalloy

specimens in a molten salt ( $\text{Na}_2\text{SO}_4\text{-60\%V}_2\text{O}_5$ ) environment at  $900^\circ\text{C}$  under cyclic conditions. The coatings and the oxide scale formed on the exposed surface were found to be intact with the superalloys. Superfer 800 with Ni-5Al coating has provided a good protection to the superalloys in the given molten salt environment. In case of RF magnetron sputtered Ni-Al coating, the weight gain was comparatively lower than the HVOF sprayed coatings in oxidation studies. The lower weight gain may be attributed to the formation of oxide layer on the surface at a rapid rate due to the nanograins formed on the as deposited film. In molten salt tests, the RF sputtered Ni-Al film has shown comparatively higher weight gain. The possible reason could be sputtering of the thin scale during the initial period of exposure.

**Chapter-5** contains the investigation of HVOF sprayed NiCrAl coatings and RF magnetron sputtered NiCrAl film on Ni- and Fe-based superalloys. The characterisation of HVOF sprayed NiCrAl coating and RF sputtered film has been discussed in detail. Oxidation studies in air at  $900^\circ\text{C}$  under cyclic conditions and hot corrosion studies in a very aggressive environment of ( $\text{Na}_2\text{SO}_4\text{-60\%V}_2\text{O}_5$ ) at  $900^\circ\text{C}$  under cyclic conditions are reported in detail. XRD, FESEM, EDAX and X-ray mapping techniques were used to analyse the as sprayed and corroded products after oxidation studies in different environments.

The porosity of the coating was found to be around 1.7%. The microhardness of the coating was in the range of 278 - 351 Hv. The bond strength of the coating was found to be 59 MPa. Nickel and chromium were coexisting in the splats and aluminum along the splat boundaries. In the as sprayed coating, minor diffusion of alloying elements was noticed from the substrate into the coating. Oxidation kinetics was established at  $900^\circ\text{C}$  for 100 cycles by thermogravimetric analysis. The NiCrAl coated Superni 750 alloy (SN 750) provided a better protection among the coated superalloys investigated. The NiCrAl deposited coatings on Ni- and Fe-based superalloys indicate dense and adherent with the substrates. The scale formed on the coated superalloys provided a better oxidation resistance at  $900^\circ\text{C}$  under cyclic conditions. The NiCrAl coated Superni 750 has provided better hot corrosion resistance amongst the coated superalloys in the molten salt environment due to the formation of spinels on the surface and a thick band of  $\text{Cr}_2\text{O}_3$  observed along the coating-substrate interface contributed to the added protection to the substrate alloy, resulting in the least weight gain among the three coated superalloys. In case of RF magnetron sputtered NiCrAl coating, the weight gain was comparatively lower than the HVOF sprayed coatings after exposure to air at  $900^\circ\text{C}$  for 100 cycles. However, in molten salt environment, the scale spalled during the period of exposure indicating a higher weight gain.

**Chapter-6** describes the detailed investigation of HVOF sprayed NiCrAlY-0.4wt%CeO<sub>2</sub> coatings on Ni- and Fe-based superalloys. The characterisation of HVOF sprayed NiCrAl coatings has been discussed in detail. Oxidation studies in air at 900°C under cyclic conditions and hot corrosion studies in a very aggressive environment of (Na<sub>2</sub>SO<sub>4</sub>-60%V<sub>2</sub>O<sub>5</sub>) at 900°C under cyclic conditions are discussed. Techniques such as XRD, FESEM, EDAX and X-ray mapping are used to analyse the as sprayed coatings and the corroded specimens after oxidation studies in air and molten salt environment.

The porosity of the coating was found to be around 1.4%. The microhardness of the coating was in the range of 649 - 753 Hv. The bond strength of the coating was found to be 45 MPa. Nickel and chromium were coexisting in the splats and aluminum along the splat boundaries. In the as sprayed coating, minor diffusion of alloying elements was noticed from the substrate into the coating. Presence of Ce and Y was observed in the coating. Oxidation kinetics was established at 900°C for 100 cycles by thermogravimetric analysis. All the coated superalloys followed the parabolic rate law in the given environment. The better protection of the NiCrAlY-0.4wt%CeO<sub>2</sub> coated superalloys may be attributed to the formation of oxides of aluminum, chromium, nickel and spinel of nickel and chromium.

The coated superalloys after exposure to molten salt environment at 900°C for 100 cycles showed comparatively very little weight gain and the scale formed on the surface were dense and adherent to superalloy substrates. The NiCrAlY-0.4wt%CeO<sub>2</sub> coating has led to the reduction in weight per unit area of about 1/20 in Superni 76, whereas 1/50 and 1/100 for Superni 750 and Superfer 800, respectively. The formations of oxides of nickel, chromium, aluminum, and spinel of nickel and chromium as indicated by XRD analysis provide a better protection to the superalloys in the given environment. Furthermore, the formation of ceria in the scale and the possible formation of cerium vanadates (CeVO<sub>4</sub>) might have contributed for better corrosion resistance of the superalloys in the given environment.

**Chapter 7** includes the detailed study of uncoated Superfer 800, HVOF sprayed Ni-5Al, NiCrAl and NiCrAlY-0.4wt%CeO<sub>2</sub> coatings and RF magnetron sputtered films (Ni-Al and NiCrAl) on Fe- based superalloy in the actual environment of the coal fired boiler. A 2 mm hole was drilled in the specimens and the uncoated and coated specimens were hanged in the low temperature superheater zone of the coal fired boiler of Guru Gobind Singh Super Thermal Power Plant, Ropar, Punjab, India, by using stainless steel wires. The temperature of the zone was around 700°C ±10°C. Hot corrosion studies were performed for 100 cycles, each cycle consists of 100 hours exposure followed by 1 hour cooling at ambient temperature. The



specimens were visually examined at the end of each cycle for any change in colour, luster, spalling tendency and other physical changes of the scale, if any. Weight change measurements were made at the end of each cycle but it could not be of much use for predicting hot corrosion behaviour of suspected spalling and ash deposition on the samples. The extent of corrosion has been evaluated by measuring thickness of the unreacted portion of the samples after the total exposure of 1000 hours. The different phases and their distribution in the hot corroded specimens were analysed by using XRD, FESEM/EDAX and X-ray mapping.

**Chapter-8** describes the comparative performance of the uncoated, HVOF coated and RF magnetron sputtered films on superalloys in air, molten salt ( $\text{Na}_2\text{SO}_4\text{-60\%V}_2\text{O}_5$ ) environment as well as in the actual working environment of the coal fired boiler at  $700^\circ\text{C}$  under cyclic conditions.

**Chapter-9** includes conclusions of the present investigation and a scope for the future work.

# ACKNOWLEDGEMENTS

---

---

I would like to express my immense sense of gratitude to **Dr. R. Jayaganthan**, Asst. Professor and **Dr. Satya Prakash**, Professor and Ex-Head, Department of Metallurgical and Materials Engineering (MMED), Indian Institute of Technology, Roorkee for their valuable and intellectual guidance throughout the tenure of this work. They have been a motivating and driving force where targets appeared to be arduous during the course of work. Without their timely help, constructive criticism, positive attitude and painstaking efforts, it would have been impossible to complete this thesis in the present form.

I am highly indebted to Dr. S. K. Nath, Professor and Head, MMED for his co-operation in extending the necessary facilities and supports during the concluding phase of this work. I am very grateful to Prof. V. K. Tewari, Prof. P. S. Mishra for their valuable suggestions during the course of this work. I wish to record a deep sense of gratitude to Head, Institute Instrumentation Centre (IIC), Indian Institute of Technology Roorkee for extending necessary facilities during the experimental and analysis work.

I am highly obliged to Council of Scientific and Industrial Research (CSIR) Govt of India, New Delhi for providing financial assistance through Senior Research Fellowship. I wish to express my sincere thanks to Dr. Ramesh Chandra, Associate Professor, Institute Instrumentation Centre, Indian Institute of Technology, Roorkee for providing the sputtering facility during the course of the study. Deep sense of gratitude is acknowledged to my research committee members, Prof. P.S. Mishra, Prof. B.K.Mishra and Prof S.K.Nath for reviewing this thesis.

I express my sincere thanks to Mr. K. Ramesh (GM) Marketing, Mr. Sridhar and Mr I.S.N.Murty, Mishra Dhatu Nigam Ltd, Hyderabad, India, for providing the superalloys for the present research work. Special thanks are also due to Mr. S.C. Modi, Director and Mr. Ankur Modi, Executive Director, Mr.(Late) S. S. Gehlot, DGM-Marketing, Er. Karunanidhi, and Mr Naresh, Metallizing Equipments Company Pvt., Ltd, Jodhpur, India for providing the HVOF coating facility.

My sincere thanks to the technical and administrative staff of the MMED, especially to Mr. R. S. Sharma, Mr. Shamsheer Singh, Mr. N. K. Seth, Mr. Vidya Prakash, Mr. T. K. Sharma, Mr. R. K. Sharma, Mr. H. K. Ahuja, Mr. Shakti Gupta, Mr. S. N. Kaushik, Mr.

Sanjay, Mr. Yogesh Goel, Mr. Vedprakash and Mr. M. Aslam, who helped me in all possible ways during my experimental work.

I convey my sincere thanks to Mr. J. S. Bhatia, Senior Executive Engineer, Guru Gobind Singh Super Thermal Power Plant, Ropar, Punjab, India, for allowing the hot corrosion experiments in the actual coal fired boiler environment.

I am highly obliged to Prof. Sanjay Sampath and Dr. J. L. Smialek, and Prof. S. K. Roy for sending the softcopy of their valuable papers. My sincere thanks to Prof. Vikram Jayaram, Department of Metallurgical Engineering, Indian Institute of Science, Bangalore, for providing facilities to carry out the SEM/EDAX analyses.

I would like to thank Mr. Shivakumar, Mr. S. D. Sharma, Mrs. Rekha Sharma, and Mr. T. K. Ghosh of IIC, IIT, Roorkee for carrying out XRD, SEM and X-ray mapping analysis work respectively. Thanks are also due to Mr. Puran Sharma for preparing high quality micrographs. Sincere thanks are acknowledged to Mr. Narendra Kumar for typesetting of thesis manuscript.

I wish to thank my friends and colleagues especially Mr. Subhash Kamal, Mr. Prashanth. K.S and Mr. C. Ramprasad for their inspiration and moral support during the course of the work. Thanks are also due to Dr Arivazhgan, Dr. Harpreet Singh, Dr. T.S.Sidhu, Dr. Hazoor Singh, Mr. Susantha Panigrahi, Mr. Vipin. Chawla, Mr. Rahul Sharma, Mr. Pawan, Mr. Ananth, Mr. Bansi P. Agarwal, Mr. Devakumar, Mr. J. Sharanabasawaraj, Mr. Ramesh, Mr. Jayaprakash and Mr. Santosh Vishwakarma for their everlasting support.

I would like to humbly dedicate this thesis to my parents who are the source of inspiration behind this research work. I am highly grateful to my brothers Dr. Lingaraj and Mr. Sangamesh for their moral support and co-operation during the course of this work. I would like to express my admiration for parents-in-law, brother-in-law and sister-in-law, who have always been the inspiration and encouraging force for me. I would like to thank my wife, Lakshmi, for her persistent moral support and help during the preparation of the thesis manuscript.

Above all, I am highly indebted to almighty God who blessed me with spiritual support and fortitude at each and every stage of this work.

**(MAHESH R ANWAR)**

# CONTENTS

	Page No.	
<i>Candidate's Declaration</i>	i	
<i>Abstract</i>	ii	
<i>Acknowledgements</i>	viii	
<i>List of figures</i>	xvii	
<i>List of Tables</i>	xxxv	
<i>Research Papers Presented/Published</i>	xxxvi	
<i>Abbreviations</i>	xxxviii	
<b>CHAPTER 1</b>	<b>INTRODUCTION</b>	<b>1</b>
<b>CHAPTER 2</b>	<b>LITERATURE REVIEW</b>	<b>5</b>
<b>2.1</b>	<b>HIGH TEMPERATURE OXIDATION</b>	<b>5</b>
<b>2.1.1</b>	<b>Oxidation of Superalloys</b>	<b>12</b>
<b>2.2</b>	<b>HOT CORROSION</b>	<b>14</b>
<b>2.2.1</b>	<b>High Temperature (Type I) Hot Corrosion (HTHC)</b>	<b>14</b>
<b>2.2.2</b>	<b>Low Temperature (Type II) Hot Corrosion (LTHC)</b>	<b>15</b>
<b>2.2.3</b>	<b>Hot Corrosion of Superalloys</b>	<b>15</b>
<b>2.2.4</b>	<b>Mechanisms of Hot Corrosion</b>	<b>17</b>
<b>2.2.5</b>	<b>Salt fluxing reactions</b>	<b>18</b>
<b>2.2.5.1</b>	<i>Basic Fluxing Mode</i>	<b>19</b>
<b>2.2.5.2</b>	<i>Acidic Fluxing Mode</i>	<b>19</b>
<b>2.2.6</b>	<b>Chemistry of Salts</b>	<b>20</b>
<b>2.2.6.1</b>	<i>Chemistry and Phase Stability of Na<sub>2</sub>SO<sub>4</sub> Salt</i>	<b>20</b>
<b>2.2.6.2</b>	<i>Vanadate Solution Chemistry</i>	<b>20</b>
<b>2.2.6.3</b>	<i>Chemistry of salts in combustion of Coal/Fuel Oils</i>	<b>21</b>
<b>2.3</b>	<b>STUDIES ON Na<sub>2</sub>SO<sub>4</sub>-V<sub>2</sub>O<sub>5</sub> INDUCED HOT CORROSION</b>	<b>23</b>

<b>2.4</b>	<b>HOT CORROSION STUDIES IN ENERGY GENERATION SYSTEMS</b>	<b>25</b>
<b>2.5</b>	<b>PREVENTIVE MEASURES AGAINST HOT CORROSION</b>	<b>27</b>
<b>2.6</b>	<b>PROTECTIVE COATINGS</b>	<b>28</b>
<b>2.7</b>	<b>HVOF THERMAL SPRAYING</b>	<b>32</b>
<b>2.8</b>	<b>SPUTTERING PROCESS</b>	<b>34</b>
<b>2.9</b>	<b>ROLE OF METALLIC COATINGS</b>	<b>37</b>
<b>2.10</b>	<b>PROBLEM FORMULATION</b>	<b>38</b>
<b>CHAPTER 3</b>	<b>EXPERIMENTAL TECHNIQUES AND PROCEDURES</b>	<b>43</b>
<b>3.1</b>	<b>SELECTION OF SUBSTRATE MATERIALS</b>	<b>43</b>
<b>3.2</b>	<b>DEVELOPMENT OF COATINGS BY HVOF PROCESS</b>	<b>43</b>
	<b>3.2.1 Preparation of Substrate Materials</b>	<b>43</b>
	<b>3.2.2 Alloy Powders for Coatings</b>	<b>43</b>
	<b>3.2.3 Formulation of Coatings</b>	<b>45</b>
	<b>3.2.3.1 By HVOF spray process</b>	<b>45</b>
	<b>3.2.3.2 By RF magnetron sputtering process</b>	<b>46</b>
<b>3.3</b>	<b>CHARACTERISATION OF COATINGS</b>	<b>48</b>
	<b>3.3.1 Specimen Preparation</b>	<b>48</b>
	<b>3.3.2 Measurement of Coating Thickness</b>	<b>48</b>
	<b>3.3.3 Measurement of Porosity</b>	<b>48</b>
	<b>3.3.4 Measurement of Microhardness</b>	<b>49</b>
	<b>3.3.5 Measurement of Surface Roughness</b>	<b>49</b>
	<b>3.3.6 Measurement of Bond Strength</b>	<b>49</b>
	<b>3.3.7 X-ray diffraction (XRD) Analysis</b>	<b>49</b>
	<b>3.3.8 Scanning Electron Microscopy (SEM) and Energy Dispersive X-Ray (EDAX) Analysis</b>	<b>50</b>
	<b>3.3.9 X-ray mapping</b>	<b>51</b>

<b>3.4</b>	<b>HIGH TEMPERATURE OXIDATION AND HOT CORROSION STUDIES</b>	<b>51</b>
3.4.1	Experimental Setup	51
3.4.2	Oxidation Studies in Air	52
3.4.3	Hot Corrosion Studies in Molten Salt ( $\text{Na}_2\text{SO}_4$ -60% $\text{V}_2\text{O}_5$ )	52
	3.4.3.1 <i>Molten Salt Coating</i>	52
	3.4.3.2 <i>Hot Corrosion Studies</i>	52
3.4.4	Studies in Industrial environment	52
<b>3.5</b>	<b>ANALYSIS OF CORROSION PRODUCTS OF OXIDATION IN AIR AND MOLTEN SALT</b>	<b>53</b>
3.5.1	Visual Observation	53
3.5.2	Thermogravimetric Studies	54
3.5.3	X-ray diffraction (XRD) Analysis	55
3.5.4	FESEM/EDAX Analysis	55
	3.5.4.1 <i>Surface Morphology</i>	55
	3.5.4.2 <i>Cross-Sectional Morphology</i>	55
3.5.6	X-ray mapping	56
<b>Chapter 4</b>	<b>Ni-5Al COATING</b>	<b>57</b>
4.1	Microstructure of the substrate superalloys	57
<b>Part I : HVOF SPRAYED COATINGS</b>		<b>59</b>
<b>4.2</b>	<b>Characterisation of the coatings</b>	<b>59</b>
4.2.1	Intrioduction	59
4.2.2	Experimental Procedure	61
4.2.3	Results	61
4.2.4	Discussion	70
4.2.5	Conclusions	72
<b>4.3</b>	<b>Oxidation Studies in air</b>	<b>73</b>
4.3.1	Introduction	73
4.3.2	Experimental procedure	74

4.3.3	Results	74
4.3.4	Discussion	86
4.3.5	Conclusions	88
<b>4.4</b>	<b>Hot Corrosion studies in molten salt environment</b>	<b>89</b>
4.4.1	Introduction	89
4.4.2	Experimental Design	90
4.4.3	Results	90
4.4.4	Discussion	104
4.4.5	Conclusions	108
 <b>Part II : RF MAGNETRON SPUTTERED COATINGS</b>		<b>109</b>
<b>4.5</b>	<b>Characterisation and Oxidation Studies</b>	<b>109</b>
4.5.1	Introduction	109
4.5.2	Experimental details	110
4.5.3	Results	110
4.5.4	Discussion	124
4.5.5	Conclusions	125
<b>4.6</b>	<b>Hot corrosion studies in molten salt environment</b>	<b>126</b>
4.6.1	Introduction	126
4.6.2	Experimentation	127
4.6.3	Results	127
4.6.4	Discussion	136
4.6.5	Conclusions	137
 <b>Chapter 5 NiCrAl COATINGS</b>		<b>138</b>
<b>Part I : HVOF SPRAYED COATINGS</b>		<b>138</b>
<b>5.1</b>	<b>Characterisation of the coatings</b>	<b>138</b>
5.1.1	Intrioduction	138
5.1.2	Experimental Details	139
5.1.3	Results	140

5.1.4	Discussion	153
5.1.5	Conclusions	155
<b>5.2</b>	<b>Oxidation Studies in air</b>	<b>157</b>
5.2.1	Introduction	157
5.2.2	Experimental details	158
5.2.3	Results	158
5.2.4	Discussion	172
5.2.5	Conclusions	174
<b>5.3</b>	<b>Hot Corrosion studies in molten salt environment</b>	<b>175</b>
5.3.1	Introduction	175
5.3.2	Experimental Details	177
5.3.3	Results	177
5.3.4	Discussion	188
5.3.5	Conclusions	191
<b>Part II : RF MAGNETRON SPRAYED COATINGS</b>		<b>192</b>
<b>5.4</b>	<b>High temperature Oxidation studies in air</b>	<b>192</b>
5.4.1	Introduction	192
5.4.2	Experimental Details	193
5.4.3	Results	193
5.4.4	Discussion	206
5.4.5	Conclusions	207
<b>5.5</b>	<b>Hot corrosion studies in molten salt environment</b>	<b>208</b>
5.5.1	Introduction	208
5.5.2	Experimental Details	208
5.5.3	Results	208
5.5.4	Discussion	218
5.5.5	Conclusions	219



<b>Chapter 6 NiCrAlY-0.4wt%CeO<sub>2</sub> COATINGS</b>	220
<b>6.1 Characterisation of the coatings</b>	220
6.1.1 Introduction	220
6.1.2 Experimental Procedure	221
6.1.3 Results	221
6.1.4 Discussion	232
6.1.5 Conclusions	234
<b>6.2 Oxidation Studies in air</b>	236
6.2.1 Introduction	236
6.2.2 Experimental procedure	237
6.2.3 Results	237
6.2.4 Discussion	249
6.2.5 Conclusions	252
<b>6.3 Hot Corrosion studies in molten salt environment</b>	253
6.3.1 Introduction	253
6.3.2 Experimental Details	254
6.3.3 Results	254
6.3.4 Discussion	265
6.3.5 Conclusions	268
<b>Chapter 7 HOT CORROSION STUDIES IN INDUSTRIAL ENVIRONMENT</b>	269
<b>7.1 Experimental details</b>	269
<b>7.2 Results and Discussion</b>	270
<b>7.3 Summary of results</b>	295
<b>7.4 Comprehensive discussion</b>	297
7.4.1 Uncoated superalloy	297
7.4.2 HVOF coated Superfer 800	298
7.4.2.1 Ni-5Al coating	298
7.4.2.2 NiCrAl coating	299

7.4.2.3	NiCrAlY-0.4wt%CeO <sub>2</sub> coating	299
7.4.3	RF magnetron sputtered Superfer 800	300
7.4.3.1	Ni-Al coating	300
7.4.3.2	NiCrAl coating	301
<b>Chapter 8</b>	<b>COMPARATIVE DISCUSSION</b>	<b>302</b>
8.1	Oxidation in air	302
8.2	Molten salt environment	303
8.3	Industrial environment	304
<b>Chapter 9</b>	<b>CONCLUSIONS</b>	<b>307</b>
	<b>SUGGESTIONS FOR FUTURE WORK</b>	<b>311</b>
	<b>REFERENCES</b>	<b>312</b>

## LIST OF FIGURES

Figure No.	Particulars	Page No.
Fig. 2.1	Schematic representation showing transient oxidation and subsequent development of a healing $\text{Cr}_2\text{O}_3$ -rich layer on Ni-20%Cr at high temperature (Stott, 1998).	7
Fig. 2.2	Alloy oxidation mechanisms, with the corresponding morphologies of the oxide layers.	9
Fig. 2.3	Schematic cross sections of an A-B alloy where both components form stable oxides but BO is more stable than AO. (a) Alloy dilute in B showing internal oxidation of B under an external layer of AO. (b) Alloy concentrated in B showing continuous external BO.	10
Fig. 2.4	Schematic representation of the process of nucleation of microcracks within the scale (a) or at the scale/metal interface (b) by dislocation sliding and the formation of dislocation pile-ups at obstacles (grain boundaries, scale/metal interface). The microcrack is indicated by the black area. The situation is shown for compressive stresses but is equivalent for tensile stresses.	11
Fig. 2.5	Schematic diagram to illustrate the conditions that develop during the initiation and the propagation of hot corrosion attack, and to identify the factors that determine the time at which the transition from the initiation to the propagation stage occurs (Pettit and Meier, 1985).	16
Fig. 2.6	Schematic representation of the reaction sequence during low-temperature hot corrosion of a Co-30%Cr alloy exposed to $\text{O}_2$ - $\text{SO}_2$ - $\text{SO}_3$ environment where $\text{Na}_2\text{SO}_4$ - $\text{CoSO}_4$ liquid and $\text{Co}_3\text{O}_4$ are stable. At higher concentration of $\text{SO}_3$ where $\text{Co}_3\text{O}_4$ is unstable at the gas-salt interface, the outward migrating cobalt will form $\text{CoSO}_4$ (s) or $\text{Co}_3\text{O}_4$ and $\text{CoSO}_4$ (s).	18

<b>Fig. 2.7</b>	Na-Cr-S-O phase stability diagram for 1200 K (Rapp, 1986).	22
<b>Fig. 2.8</b>	Phase stability diagram for Na-V-S-O system at 900°C (Hwang and Rapp, 1989).	23
<b>Fig. 2.9</b>	Phase Diagram for Na <sub>2</sub> SO <sub>4</sub> -V <sub>2</sub> O <sub>5</sub> System (Otero et al, 1987).	25
<b>Fig. 2.10</b>	Coating deposition technologies (Bhushan and Gupta, 1991).	31
<b>Fig. 2.11</b>	Schematic cross-section of diamond jet spray gun (Stokes & Looney, 2001).	33
<b>Fig. 2.12</b>	Schematic of simplified sputtering systems (a) DC, (b) RF (Ohring, 2002).	36
<b>Fig. 2.13</b>	Types of high-temperature attack for metallic coatings (aluminide, chromide, MCrAlY, etc.) on nickel-base superalloys with approximate temperature regimes and severity of attack.	38
<b>Fig. 3.1</b>	HVOF system (Hipojet 2100) used in the current research work	47
<b>Fig. 3.2</b>	RF Magnetron sputtering system used in the current research work	47
<b>Fig. 3.3</b>	Analysis of fly ash (a) FESEM morphology and (b) EDAX compositional analysis.	54
<b>Fig. 4.1</b>	Optical micrographs of the substrate superalloys (a) Superni 76, (b) Superni 750 and (c) Superfer 800	58
<b>Fig. 4.2</b>	SEM image of Ni-5Al powder used for coating	61
<b>Fig. 4.3</b>	SEI showing the cross-section morphology of Ni-5Al coatings on (a) Superni 76, (b) Superni 750 and (c) Superfer 800.	62
<b>Fig. 4.4</b>	Microhardness profiles for HVOF sprayed Ni-5Al coatings on the different superalloys.	64
<b>Fig. 4.5</b>	Optical micrograph of the surface of as-sprayed Ni-5Al coatings on (a) Superni 76; (b) Superni 750; and (c) Superfer 800.	64
<b>Fig. 4.6</b>	X-ray diffraction pattern of as sprayed Ni-5Al coating on	65

different superalloy substrates.

<b>Fig. 4.7</b>	SEM image of as-sprayed Ni-5Al coating on Superfer-800 showing (a) surface morphology and (b) EDAX analysis of as-sprayed Ni-5Al coating showing elemental composition (wt.%) at selected points on Superfer 800.	66
<b>Fig. 4.8(a)</b>	Composition image (SEI) and X-ray mapping of the cross-section of the as sprayed Ni-5Al coating on Superni 76.	67
<b>Fig. 4.8(b)</b>	Composition image (SEI) and X-ray mapping of the cross-section of the as sprayed Ni-5Al coating on Superni 750.	68
<b>Fig. 4.8(c)</b>	Composition image (SEI) and X-ray mapping of the cross-section of the as sprayed Ni-5Al coating on Superfer 800.	69
<b>Fig. 4.9</b>	Surface macrographs of Ni-5Al-coated (a) Superni 76; (b) Superni 750; and (c) Superfer 800 after 100 hr exposure to air at 900°C.	75
<b>Fig. 4.10</b>	Mass gain/area vs Time (no of cycles) plot for Ni-5Al coated samples oxidized in air at 900°C for 100 cycles.	76
<b>Fig. 4.11</b>	(Mass gain/area) <sup>2</sup> vs time plot for Ni-5Al coated superalloy substrates oxidized in air at 900°C for 100 cycles.	77
<b>Fig. 4.12</b>	Bar chart showing cumulative weight gain per unit area for bare and Ni-5Al coated superalloys subjected to cyclic oxidation for 100 cycles at 900°C.	78
<b>Fig. 4.13</b>	X-ray diffraction pattern of Ni-5Al coated on superalloys subjected to cyclic oxidation in air at 900°C.	79
<b>Fig. 4.14</b>	Surface-scale morphology and EDAX patterns from different spots on uncoated superalloys oxidized at 900°C for 100 cycles of (a) Superni 76, (b) Superni 750 and (c) Superfer 800.	80
<b>Fig. 4.15</b>	Surface-scale morphology and EDAX patterns from different spots on Ni-5Al coated superalloys oxidized at 900°C for 100 cycles of (a) Superni 76, (b) Superni 750 and (c) Superfer 800.	81

<b>Fig. 4.16(a)</b>	Composition image (BSEI) and X-ray mapping of the cross-section of the Ni-5Al coated superalloy Superni 76 subjected to cyclic oxidation at 900°C after 100 cycles.	83
<b>Fig. 4.16(b)</b>	Composition image (BSEI) and X-ray mapping of the cross-section of the Ni-5Al coated superalloy Superni 750 subjected to cyclic oxidation at 900 °C after 100 cycles.	84
<b>Fig. 4.16(c)</b>	Composition image (BSEI) and X-ray mapping of the cross-section of the Ni-5Al coated superalloy Superfer 800 subjected to cyclic oxidation at 900 °C after 100 cycles.	85
<b>Fig. 4.17</b>	Schematic diagram showing possible oxidation mode for the Ni-5Al coated Superni 76 at 900°C for 100 cycles.	87
<b>Fig. 4.18</b>	Surface macrographs of bare Superni 76 (a), Superni 750 (b), Superfer 800 (c) and Ni-5Al coated Superni 76 (d), Superni 750 (e) and Superni 800 (f) after 100 hr exposure to molten salt ( $\text{Na}_2\text{SO}_4\text{-60}\%\text{V}_2\text{O}_5$ ) environment at 900°C.	91
<b>Fig. 4.19</b>	Mass gain/area vs number of cycles plot for bare and Ni-5Al coated superalloys subjected to $\text{Na}_2\text{SO}_4\text{-60}\%\text{V}_2\text{O}_5$ environment at 900°C for 100 cycles.	92
<b>Fig. 4.20</b>	$(\text{Mass gain/area})^2$ vs. number of cycles for bare and Ni-5Al coated superalloys subjected to $\text{Na}_2\text{SO}_4\text{-60}\%\text{V}_2\text{O}_5$ environment at 900°C for 100 cycles.	93
<b>Fig. 4.21</b>	Bar chart showing cumulative weight gain per unit area for bare and Ni-5Al coated superalloys subjected to cyclic oxidation for 100 cycles at 900°C.	93
<b>Fig. 4.22</b>	X-ray diffraction pattern of Ni-5Al coated superalloys after 100h exposure to molten salt ( $\text{Na}_2\text{SO}_4\text{-60}\%\text{V}_2\text{O}_5$ ) environment at 900°C.	95
<b>Fig. 4.23</b>	SEM/EDAX analysis of the bare superalloys, (a) Superni 76; (b) Superni 750; and (c) Superfer 800 exposed to molten salt ( $\text{Na}_2\text{SO}_4\text{-60}\%\text{V}_2\text{O}_5$ ) environment at 900°C after 100 cycles.	96

<b>Fig. 4.24</b>	Surface-scale morphology and EDAX patterns from different spots on Ni-5Al coated (a) Superni 76; (b) Superni 750 and (c) Superfer 800 in molten salt ( $\text{Na}_2\text{SO}_4\text{-60\%V}_2\text{O}_5$ ) environment at 900°C after 100 cycles.	97
<b>Fig. 4.25</b>	Oxide scale morphology and variation of elemental composition across the cross-section of the Ni-5Al coated (a) Superni 76, (b) Superni 750 and (c) Superfer 800 subjected to the cyclic oxidation at 900°C in molten salt environment after 100 cycles.	99
<b>Fig. 4.26(a)</b>	Composition image (BSEI) and X-ray mapping of the cross-section of SN-76 coated with Ni-5Al subjected to cyclic oxidation in $\text{Na}_2\text{SO}_4\text{-60\%V}_2\text{O}_5$ environment at 900°C.	101
<b>Fig. 4.26(b)</b>	Composition image (BSEI) and X-ray mapping of the cross-section of SN-750 coated with Ni-5Al subjected to cyclic oxidation in $\text{Na}_2\text{SO}_4\text{-60\%V}_2\text{O}_5$ environment at 900°C.	102
<b>Fig. 4.26(c)</b>	Composition image (BSEI) and X-ray mapping of the cross-section of SF-800 coated with Ni-5Al subjected to cyclic oxidation in $\text{Na}_2\text{SO}_4\text{-60\%V}_2\text{O}_5$ environment at 900°C.	103
<b>Fig. 4.27</b>	Schematic diagram showing the possible hot corrosion mode for the Ni-5Al coated Superni 750 exposed to the $\text{Na}_2\text{SO}_4\text{-60\%V}_2\text{O}_5$ environment at 900°C for 100 cycles.	107
<b>Fig. 4.28</b>	The image of Ni-Al target after sputtering process.	111
<b>Fig. 4.29</b>	XRD patterns indicating the Ni-Al film deposited on different superalloy substrates by RF magnetron sputtering.	111
<b>Fig. 4.30</b>	AFM images of Ni-Al film on (a) Superni 76, (b) Superni 750 and (c) Superfer 800 by RF magnetron sputtering.	112
<b>Fig. 4.31</b>	Surface morphology and EDAX analysis of Ni-Al film deposited on (a) Superni 76, (b) Superni 750 and (C) Superfer 800 alloy.	113
<b>Fig. 4.32</b>	Thickness of Ni-5Al film deposited on superalloy by RF magnetron sputtering.	114
<b>Fig. 4.33</b>	Cross sectional EDAX analysis of RF magnetron sputtered Ni-5Al film on Superni 750.	114

<b>Fig. 4.34</b>	Surface macrographs of RF sputtered Ni-Al films on (a) Superni 76, (b) Superni 750, and (c) Superfer 800 after 100 h exposure to air at 900°C.	116
<b>Fig. 4.35</b>	Mass gain/area versus number of cycles plot for Ni-Al coated specimens oxidized in air at 900 °C for 100 cycles.	117
<b>Fig. 4.36</b>	(Mass gain/area) <sup>2</sup> versus number of cycles plot for Ni-Al coated superalloy specimens oxidized in air at 900°C for 100 cycles.	117
<b>Fig. 4.37</b>	Bar chart showing cumulative weight gain per unit area for uncoated and RF sputtered Ni-Al film on superalloys subjected to cyclic oxidation for 100 cycles at 900°C.	118
<b>Fig. 4.38</b>	X-ray diffractograms of Ni-Al coated thin films on (a) SN 76, (b) SN 750 and (c) SF 800 after oxidation at 900°C for 100 cycles.	118
<b>Fig. 4.39</b>	Surface scale morphology and EDAX composition of Ni-Al coated thin film after oxidation studies on (a) SN 76, (b) SN 750 and (c) SF 800.	120
<b>Fig. 4.40(a)</b>	Compositional image (SEI) and X-ray mapping of the cross-section of Ni-Al coated Superni-76 subjected to cyclic oxidation in air at 900°C.	121
<b>Fig. 4.40(b)</b>	Compositional image (SEI) and X-ray mapping of the cross-section of Ni-Al coated Superni 750 subjected to cyclic oxidation in air at 900°C	122
<b>Fig. 4.40(c)</b>	Compositional image (SEI) and X-ray mapping of the cross-section of Ni-Al coated Superfer 800 subjected to cyclic oxidation in air at 900°C.	123
<b>Fig. 4.41</b>	Surface macrographs of RF sputtered Ni-Al films on (a) Superni 76, (b) Superni 750, and (c) Superfer 800 after 100 h exposure to molten salt environment at 900°C.	129
<b>Fig. 4.42</b>	Mass gain/area versus number of cycles plot for Ni-Al coated specimens oxidized in molten salt environment at 900°C for 100 cycles.	129
<b>Fig. 4.43</b>	(Mass gain/area) <sup>2</sup> versus number of cycles plot for Ni-Al coated superalloy specimens after exposure to molten salt environment at 900°C for 100 cycles.	130



<b>Fig. 4.44</b>	Bar chart showing cumulative weight gain per unit area for uncoated and RF sputtered Ni-Al film on superalloys subjected to molten salt environment at 900°C for 100 cycles	130
<b>Fig. 4.45</b>	X-ray diffractograms of Ni-Al coated thin films on (a) Superni 76, (b) Superni 750 and (c) Superfer 800 after cyclic oxidation in molten salt environment at 900°C.	131
<b>Fig. 4.46</b>	Surface scale morphology and EDAX composition of Ni-Al coated thin film for (a) Superni 76, (b) Superni 750 and (c) Superfer 800 after exposure to molten salt environment at 900°C.	132
<b>Fig. 4.47(a)</b>	Compositional image (SEI) and X-ray mapping of the cross-section of Ni-Al coated Superni-76 subjected to molten salt environment at 900°C.	133
<b>Fig. 4.47(b)</b>	Compositional image (SEI) and X-ray mapping of the cross-section of Ni-Al coated Superni 750 subjected to molten salt environment at 900°C.	134
<b>Fig. 4.47(c)</b>	Compositional image (SEI) and X-ray mapping of the cross-section of Ni-Al coated Superfer 800 subjected to molten salt environment at 900°C.	135
<b>Fig. 5.1</b>	Surface FESEM photographs of as sprayed NiCrAl coating showing the top surface after polishing on (a) Superni 76; (c) Superni 750; (e) Superfer 800 and cross sectional details of (b) Superni 76; (d) Superni 750 and (f) Superfer 800.	140
<b>Fig. 5.2</b>	Microhardness profiles for HVOF sprayed NiCrAl coatings on the different superalloys.	142
<b>Fig. 5.3</b>	Photograph of the surfaces of a NiCrAl coated specimen after it was pulled apart in the tensile test machine.	142
<b>Fig. 5.4</b>	X-ray diffraction pattern of NiCrAl powder used for coating.	143
<b>Fig. 5.5</b>	X-ray diffraction patterns of NiCrAl coating on Ni- and Fe-based superalloys in as sprayed condition.	143
<b>Fig. 5.6</b>	FESEM micrographs of as sprayed NiCrAl coating showing the surface microstructure on superalloys (a) Superni 76; (b) Superni 750 and (c) Superfer 800.	144

<b>Fig. 5.7</b>	Cross-section morphology of NiCrAl coated superalloys in as sprayed condition of (a) Superni 76, (b) Superni 750 and (c) Superfer 800.	145
<b>Fig. 5.8a-i</b>	Compositional image and X-ray mapping of the cross-section of the as sprayed NiCrAl coating on Superni 76 superalloy.	147
<b>Fig. 5.8a-ii</b>	Compositional image and X-ray mapping of the enlarged splat of the as sprayed NiCrAl coating on Superni 76.	148
<b>Fig. 5.8b-i</b>	Compositional image and X-ray mapping of the cross-section of the as sprayed NiCrAl coating on Superni 750.	149
<b>Fig. 5.8b-ii</b>	Compositional image and X-ray mapping of the enlarged splat of the as sprayed NiCrAl coating on Superni 750.	150
<b>Fig. 5.8c-i</b>	Compositional image and X-ray mapping of the cross-section of the as sprayed NiCrAl coating on Superfer 800 superalloy.	151
<b>Fig. 5.8c-ii</b>	Compositional image and X-ray mapping of the enlarged splat of the as sprayed NiCrAl coating on Superfer 800.	152
<b>Fig. 5.9</b>	Surface macrographs of NiCrAl coated (a) Superni 76; (b) Superni 750; and (c) Superfer 800 after 100 hr exposure to air at 900°C.	160
<b>Fig. 5.10</b>	(Weight gain/area) <sup>2</sup> vs. number of cycles plots for the uncoated and coated NiCrAl superalloys subjected to cyclic oxidation for 100 cycles at 900°C.	161
<b>Fig. 5.11</b>	(Weight gain/area) <sup>2</sup> vs. number of cycles plots for the uncoated and coated NiCrAl superalloys subjected to cyclic oxidation for 100 cycles at 900°C.	161
<b>Fig. 5.12</b>	Bar chart showing cumulative weight gain per unit area for bare and NiCrAl coated superalloys subjected to cyclic oxidation for 100 cycles at 900°C.	162
<b>Fig. 5.13</b>	X-Ray Diffractograms of bare superalloys subjected to cyclic oxidation after 100 hour exposure to air at 900°C.	163
<b>Fig. 5.14</b>	X-Ray Diffractograms of NiCrAl coated superalloys subjected to cyclic oxidation after 100 hour exposure to air at 900°C.	163

<b>Fig. 5.15</b>	Surface scale morphology and EDAX analysis from different points on NiCrAl coated superalloys oxidized at 900 °C for 100 cycles of (a) Superni 76, (b) Superni 750 and (c) Superfer 800.	166
<b>Fig. 5.16</b>	Oxide scale morphology and the variation in the elemental composition across the cross section of HVOF coated NiCrAl on (a) Superni 76; (b) Superni 750 and (c) Superfer 800 oxidised in air at 900°C after 100 cycles.	167
<b>Fig. 5.17(a)</b>	Composition image and X-ray mapping of the cross-section of the NiCrAl coated superalloy Superni 76 subjected to cyclic oxidation in air at 900°C after 100 cycles.	169
<b>Fig. 5.17(b)</b>	Composition image and X-ray mapping of the cross-section of the NiCrAl coated superalloy Superni 750 subjected to cyclic oxidation in air at 900°C after 100 cycles.	170
<b>Fig. 5.17(c)</b>	Composition image and X-ray mapping of the cross-section of the NiCrAl coated superalloy Superfer 800 subjected to cyclic oxidation in air at 900°C after 100 cycles.	171
<b>Fig. 5.18</b>	Schematic diagram showing possible oxidation mode for the NiCrAl coated Superni 76 at 900 °C for 100 cycles.	174
<b>Fig. 5.19</b>	Mass gain per area versus number of cycles of bare and NiCrAl coated superalloys after exposure to molten salt environment ( $\text{Na}_2\text{SO}_4\text{-60\%V}_2\text{O}_5$ ) at 900°C for 100 cycles.	178
<b>Fig. 5.20</b>	(Mass gain/area) <sup>2</sup> vs. number of cycles for bare and NiCrAl coated superalloys subjected to molten salt environment ( $\text{Na}_2\text{SO}_4\text{-60\%V}_2\text{O}_5$ ) at 900°C for 100 cycles.	179
<b>Fig. 5.21</b>	Bar chart showing cumulative weight gain per unit area for bare and NiCrAl coated superalloys subjected to molten salt environment at 900°C for 100 cycles.	179
<b>Fig. 5.22</b>	X-Ray Diffraction pattern of NiCrAl coated superalloys after 100h exposure to molten salt ( $\text{Na}_2\text{SO}_4\text{-60\%V}_2\text{O}_5$ ) environment at 900°C.	180

<b>Fig. 5.23</b>	Surface-scale morphology and EDAX patterns from different spots on NiCrAl coated (a) Superni 76, (b) Superni 750 and (c) Superfer 800 in molten salt ( $\text{Na}_2\text{SO}_4\text{-60\%V}_2\text{O}_5$ ) environment at $900^\circ\text{C}$ after 100 cycles.	181
<b>Fig. 5.24</b>	Oxide scale morphology and variations of elemental composition across the cross-section of HVOF coated and hot corroded in $\text{Na}_2\text{SO}_4\text{-60\%V}_2\text{O}_5$ environment at $900^\circ\text{C}$ for 100 cycles. (a) Superni 76; (b) Superni 750 and (c) Superfer 800.	183
<b>Fig. 5.25(a)</b>	Composition image (SEI) and X-ray mapping of the cross-section of Superni 76 coated with NiCrAl subjected to cyclic oxidation in $\text{Na}_2\text{SO}_4\text{-60\%V}_2\text{O}_5$ environment at $900^\circ\text{C}$ .	185
<b>Fig. 5.25(b)</b>	Composition image (SEI) and X-ray mapping of the cross-section of Superni-750 coated with NiCrAl subjected to cyclic oxidation in $\text{Na}_2\text{SO}_4\text{-60\%V}_2\text{O}_5$ environment at $900^\circ\text{C}$ .	186
<b>Fig. 5.25(c)</b>	Composition image (SEI) and X-ray mapping of the cross-section of Superfer-800 coated with NiCrAl subjected to cyclic oxidation in $\text{Na}_2\text{SO}_4\text{-60\%V}_2\text{O}_5$ environment at $900^\circ\text{C}$	187
<b>Fig. 5.26</b>	Schematic diagram showing possible hot corrosion mode for the NiCrAl coated Superfer 800 exposed to $\text{Na}_2\text{SO}_4\text{-60\%V}_2\text{O}_5$ environment at $900^\circ\text{C}$ for 100 cycles.	190
<b>Fig. 5.27</b>	The image of the targets after RF magnetron sputtering process.	194
<b>Fig. 5.28</b>	XRD patterns indicating the NiCrAl film deposited on different superalloy substrates by RF magnetron sputtering.	194
<b>Fig. 5.29</b>	AFM images of NiCrAl deposited film on (a) Superni 76, (b) Superni 750 and (c) Superfer 800 by RF magnetron sputtering.	195
<b>Fig. 5.30</b>	Surface morphology and EDAX analysis of NiCrAl film deposited on (a) Superni 76, (b) Superni 750 and (c) Superfer 800 alloy.	196

<b>Fig. 5.31</b>	Surface macrographs of NiCrAl deposited film on (i) Superni 76, (ii) Superni 750, (iii) Superfer 800 after 100 h exposure to air at 900°C indicating spalled scale powder.	198
<b>Fig. 5.32</b>	(Mass gain/area) versus number of cycles plot for uncoated and NiCrAl coated film on superalloy specimens oxidized in air at 900°C for 100 cycles.	198
<b>Fig. 5.33</b>	(Mass gain/area) <sup>2</sup> versus number of cycles plot for uncoated and NiCrAl coated films on superalloy specimens oxidized in air at 900°C for 100 cycles.	199
<b>Fig. 5.34</b>	Bar chart showing cumulative weight gain per unit area for uncoated and NiCrAl deposited film on superalloys subjected to cyclic oxidation for 100 cycles at 900 °C.	199
<b>Fig. 5.35</b>	X-ray diffractograms of oxidised scale of the NiCrAl coated films on Superni 76, Superni 750 and Superfer 800 after 100 cycles at 900°C.	200
<b>Fig. 5.36</b>	Surface scale morphology and EDAX composition of Ni-Al coated thin film after oxidation studies on (a) Superni 76, (b) Superni 750 and (c) Superfer 800.	201
<b>Fig. 5.37(a)</b>	Compositional image and X-ray mapping of the cross-section of NiCrAl coated Superni-76 subjected to cyclic oxidation in air at 900°C.	203
<b>Fig. 5.37(b)</b>	Compositional image and X-ray mapping of the cross-section of NiCrAl coated Superni 750 subjected to cyclic oxidation in air at 900 °C.	204
<b>Fig. 5.37(c)</b>	Compositional image and X-ray mapping of the cross-section of NiCrAl coated Superfer 800 subjected to cyclic oxidation in air at 900°C.	205
<b>Fig. 5.38</b>	Surface macrographs of RF sputtered NiCrAl films on (a) Superni 76, (b) Superni 750, and (c) Superfer 800 after 100 hr exposure to molten salt environment at 900°C.	210
<b>Fig. 5.39</b>	Mass gain/area versus number of cycles plot for NiCrAl coated specimens oxidized in molten salt environment at 900°C for 100 cycles.	211

<b>Fig. 5.40</b>	(Mass gain/area) <sup>2</sup> versus number of cycles plot for NiCrAl after exposure to molten salt environment at 900°C for 100 cycles.	211
<b>Fig. 5.41</b>	Bar chart showing cumulative weight gain per unit area for uncoated and RF sputtered NiCrAl film on superalloys subjected to molten salt environment at 900°C for 100 cycles.	212
<b>Fig. 5.42</b>	X-ray diffractograms of NiCrAl coated thin films on (a) Superni 76, (b) Superni 750 and (c) Superfer 800 after 100 hrs exposure to molten salt environment at 900°C.	212
<b>Fig. 5.43</b>	Surface scale morphology and EDAX composition of Ni-Al coated thin film for (a) Superni 76, (b) Superni 750 and (c) Superfer 800 after exposure to molten salt environment at 900°C.	213
<b>Fig. 5.44(a)</b>	Compositional image (SEI) and X-ray mapping of the cross-section of NiCrAl coated Superni 76 subjected to molten salt environment at 900°C.	215
<b>Fig. 5.44(b)</b>	Compositional image (SEI) and X-ray mapping of the cross-section of NiCrAl coated Superni 750 subjected to molten salt environment at 900°C.	216
<b>Fig. 5.44(c)</b>	Compositional image (SEI) and X-ray mapping of the cross-section of NiCrAl coated Superfer 800 subjected to molten salt environment at 900°C.	217
<b>Fig. 6.1</b>	FESEM image showing the (a) morphology of NiCrAlY-0.4wt%CeO <sub>2</sub> powder, (b) ceria distribution along the splat boundaries in the polished as sprayed sample.	222
<b>Fig. 6.2</b>	EDAX analysis of dark areas in HVOF sprayed coating show O, Al, Ni, Cr peaks.	222
<b>Fig. 6.3</b>	Back scattered electron image (BSEI) of coated superalloys showing the cross sectional details for (a) Superni 76, (b) Superni 750 and (c) Superfer 800.	223
<b>Fig. 6.4</b>	Microhardness profiles for HVOF sprayed NiCrAlY-0.4wt% CeO <sub>2</sub> coatings on the superalloys.	224
<b>Fig. 6.5</b>	Fracture surfaces of a HVOF sprayed NiCrAlY-0.4wt% CeO <sub>2</sub> coated specimen after ASTM C633 tensile test.	225

<b>Fig. 6.6</b>	XRD diffractograms of HVOF sprayed NiCrAlY-0.4 wt%CeO <sub>2</sub> coating on different superalloy substrates.	225
<b>Fig. 6.7</b>	FESEM/EDAX analysis of as sprayed NiCrAlY-0.4wt%CeO <sub>2</sub> coating showing surface morphology and elemental composition at different spots on (a) Superni 76, (b) Superni 750 and (c) Superfer 800.	226
<b>Fig. 6.8</b>	Elemental composition across the cross-section of the HVOF sprayed NiCrAlY-0.4wt% CeO <sub>2</sub> coating on (a) Superni 76, (b) Superni 750 and (c) Superfer 800.	227
<b>Fig. 6.9(a)</b>	Compositional image (SEI) and X-ray mapping of the cross-section of the as sprayed NiCrAlY-0.4wt%CeO <sub>2</sub> coating on Superni 76.	229
<b>Fig. 6.9(b)</b>	Compositional image (SEI) and X-ray mapping of the cross-section of the as sprayed NiCrAlY-0.4wt%CeO <sub>2</sub> coating on Superni 750.	230
<b>Fig. 6.9(c)</b>	Compositional image (SEI) and X-ray mapping of the cross-section of the as sprayed NiCrAlY-0.4wt%CeO <sub>2</sub> coating on Superfer 800.	231
<b>Fig. 6.10</b>	Surface photograph of the NiCrAlY-0.4wt% CeO <sub>2</sub> coating oxidised in air at 900°C for 100 cycles for (a) Superni 76, (b) Superni 750 and (c) Superfer 800.	239
<b>Fig. 6.11</b>	Mass gain/area versus. Number of cycles for bare and NiCrAlY-0.4wt%CeO <sub>2</sub> coated superalloys oxidised in air at 900°C for 100 cycles.	239
<b>Fig. 6.12</b>	(Mass gain/area) <sup>2</sup> vs. number of cycles for bare and NiCrAlY-0.4wt%CeO <sub>2</sub> coated superalloys oxidised in air at 900°C for 100 cycles.	240
<b>Fig. 6.13</b>	Cumulative weight gain per unit area for bare and NiCrAlY-0.4wt%CeO <sub>2</sub> coated superalloys subjected to cyclic oxidation in air at 900°C for 100 cycles.	241
<b>Fig. 6.14</b>	X-ray diffraction pattern of NiCrAlY-0.4wt%CeO <sub>2</sub> coated superalloys after oxidation in air for 100 h at 900°C.	241

<b>Fig. 6.15</b>	Surface-scale morphology and EDAX analysis of NiCrAlYCeO <sub>2</sub> coated (a) Superni 76, (b) Superni 750 and (c) Superfer 800 alloys after oxidation for 100 cycles at 900°C.	244
<b>Fig. 6.16</b>	Cross sectional morphology and variation of elemental composition across the cross-section of the NiCrAlY-0.4wt% CeO <sub>2</sub> coated (a) Superni 76, (b) Superni 750 and (c) Superfer 800 subjected to the cyclic oxidation at 900°C after 100 cycles.	245
<b>Fig. 6.17(a)</b>	Composition image (SEI) and X-ray mapping of the NiCrAlY-0.4wt%CeO <sub>2</sub> coated Superni 76 subjected to cyclic oxidation in air at 900°C.	246
<b>Fig. 6.17(b)</b>	Composition image (SEI) and X-ray mapping of the NiCrAlY-0.4wt%CeO <sub>2</sub> coated Superni 750 subjected to cyclic oxidation in air at 900°C.	247
<b>Fig. 6.17(c)</b>	Composition image (SEI) and X-ray mapping of the NiCrAlY-0.4wt%CeO <sub>2</sub> coated Superfer 800 subjected to cyclic oxidation in air at 900°C.	248
<b>Fig. 6.18</b>	Schematic diagram showing probable oxidation mechanism for the NiCrAlY-0.4wt%CeO <sub>2</sub> coated Superni 750 exposed to air at 900°C for 100 cycles.	251
<b>Fig. 6.19</b>	Surface macrographs of bare Superni 76 (a), Superni 750 (b), Superfer 800 (c) and NiCrAlY-0.4wt%CeO <sub>2</sub> coated Superni 76 (d), Superni 750 (e) and Superni 800 (f) after 100 cycles in 40%Na <sub>2</sub> SO <sub>4</sub> -60%V <sub>2</sub> O <sub>5</sub> environment at 900°C.	255
<b>Fig. 6.20</b>	Mass gain/area versus. number of cycles for bare and NiCrAlY-0.4wt%CeO <sub>2</sub> coated superalloys subjected to 40% Na <sub>2</sub> SO <sub>4</sub> - 60% V <sub>2</sub> O <sub>5</sub> environment at 900°C for 100 cycles.	257
<b>Fig. 6.21</b>	(Mass gain/area) <sup>2</sup> vs. number of cycles for bare and NiCrAlY-0.4wt%CeO <sub>2</sub> coated superalloys subjected to 40% Na <sub>2</sub> SO <sub>4</sub> -60% V <sub>2</sub> O <sub>5</sub> environment at 900°C for 100 cycles.	257



<b>Fig. 6.22</b>	Cumulative weight gain per unit area for bare and NiCrAlY-0.4wt%CeO <sub>2</sub> coated superalloys subjected to cyclic oxidation in air at 900°C for 100 cycles.	258
<b>Fig. 6.23</b>	X-Ray Diffraction pattern of NiCrAlY-0.4wt%CeO <sub>2</sub> coated superalloys after 100h exposure to 40% Na <sub>2</sub> SO <sub>4</sub> - 60%V <sub>2</sub> O <sub>5</sub> environment at 900°C.	259
<b>Fig. 6.24</b>	Surface-scale morphology and EDAX patterns from different spots on NiCrAlY-0.4wt%CeO <sub>2</sub> coated (a) Superni 76, (b) Superni 750 and (c) Superfer 800 in 40% Na <sub>2</sub> SO <sub>4</sub> – 60% V <sub>2</sub> O <sub>5</sub> environment at 900°C after 100 cycles.	261
<b>Fig. 6.25(a)</b>	Composition image (SEI) and X-ray mapping of the cross-section of Superni-76 coated with NiCrAlY-0.4wt%CeO <sub>2</sub> subjected to cyclic oxidation in 40% Na <sub>2</sub> SO <sub>4</sub> -60%V <sub>2</sub> O <sub>5</sub> environment at 900°C.	262
<b>Fig. 6.25(b)</b>	Composition image (SEI) and X-ray mapping of the cross-section of Superni 750 coated with NiCrAlY- 0.4wt%CeO <sub>2</sub> subjected to cyclic oxidation in 40% Na <sub>2</sub> SO <sub>4</sub> -60%V <sub>2</sub> O <sub>5</sub> environment at 900°C.	263
<b>Fig. 6.25(c)</b>	Composition image (SEI) and X-ray mapping of the cross-section of Superfer 800 coated with NiCrAlY-0.4wt%CeO <sub>2</sub> subjected to cyclic oxidation in 40% Na <sub>2</sub> SO <sub>4</sub> -60%V <sub>2</sub> O <sub>5</sub> environment at 900°C.	264
<b>Fig. 6.26</b>	Schematic diagram showing the possible hot corrosion mode for the NiCrAlY-0.4wt%CeO <sub>2</sub> coated Superfer 800 exposed to the 40%Na <sub>2</sub> SO <sub>4</sub> -60%V <sub>2</sub> O <sub>5</sub> environment at 900°C for 100 cycles.	267
<b>Fig. 7.1</b>	Macrographs of the (a) uncoated, and HVOF sprayed (b) Ni-5Al, (c) NiCrAl and (d) NiCrAlY-0.4wt%CeO <sub>2</sub> coated on Superfer 800 after 1000 hrs exposure to low temperature superheater zone of the boiler at 700 °C.	271
<b>Fig. 7.2</b>	Macrographs of RF magnetron sputtered (a) Ni-Al and (b) NiCrAl coated films on Superfer 800 after 1000 hrs exposure to low temperature superheater zone of the boiler at 700 °C.	271

<b>Fig. 7.3</b>	Weight change vs. time plots for the uncoated and HVOF coated Superfer 800 subjected to 1000 hrs cyclic exposure to low temperature superheater zone of the coal fired boiler at 700 °C.	273
<b>Fig. 7.4</b>	Weight change vs. time plots for the RF sputtered Ni-Al and NiCrAl coated films on Superfer 800 subjected to 1000 hrs cyclic exposure to low temperature superheater zone of the coal fired boiler at 700 °C.	273
<b>Fig. 7.5</b>	(Weight gain/area) <sup>2</sup> vs. number of hours plots for the uncoated and HVOF coated Superfer 800 subjected to 1000 hrs cyclic exposure to low temperature superheater zone of the coal fired boiler at 700°C.	275
<b>Fig. 7.6</b>	(Weight gain/area) <sup>2</sup> vs. number of hours plots for the RF magnetron sputtered Ni-Al and NiCrAl coated Superfer 800 subjected to 1000 hrs cyclic exposure to low temperature superheater zone of the coal fired boiler at 700°C.	275
<b>Fig. 7.7</b>	BSE images for the uncoated and HVOF coated Superfer 800 after 1000 hrs exposure to low temperature superheater zone of the coal fired boiler at 700 °C: (a) Uncoated superalloy (b) Ni-5Al coated, (c) NiCrAl coated (d) NiCrAlY-0.4wt%CeO <sub>2</sub> coated	276
<b>Fig. 7.8</b>	Bar charts indicating the scale/coating thickness for the bare and HVOF coated Superfer 800 after 1000 hrs exposure to the coal fired boiler at 700 °C	276
<b>Fig. 7.9</b>	BSE images for the RF sputtered (a) Ni-Al and (b) NiCrAl films on Superfer 800 after 1000 hrs exposure to low temperature superheater zone of the coal fired boiler at 700 °C.	277
<b>Fig. 7.10</b>	Bar charts indicating the scale/coating thickness for the RF sputtered Ni-Al and NiCrAl film on Superfer 800 after 1000 hrs exposure to the coal fired boiler at 700 °C.	277
<b>Fig. 7.11</b>	X-ray diffraction patterns for the (i) uncoated and HVOF sprayed (ii) Ni-5Al, (iii) NiCrAl, (iv) NiCrAlY-0.4wt%CeO <sub>2</sub> coatings on Superfer 800 after 1000 hrs exposure to low temperature superheater zone of the coal fired boiler at 700 °C.	280

<b>Fig. 7.12</b>	X-ray diffraction patterns of RF sputtered (i) Ni-Al and (ii) NiCrAl coatings on Superfer 800 after 1000 hrs exposure to low temperature superheater zone of the coal fired boiler at 700 °C.	280
<b>Fig. 7.13</b>	FESEM/EDAX analysis showing elemental composition (wt.%) for the bare and HVOF coated Superfer 800 after 1000 hrs exposure to low temperature superheater zone of the coal fired boiler at 700 °C: (a) Bare Superfer 800 (b) Ni-5Al coated (c) NiCrAl coated (d) NiCrAlY-0.4wt%CeO <sub>2</sub> coated.	281
<b>Fig. 7.14</b>	FESEM/EDAX analysis showing elemental composition (wt.%) for the RF sputtered (a) Ni-Al and (ii) NiCrAl films on Superfer 800 after 1000 hrs exposure to low temperature superheater zone of the coal fired boiler at 700 °C.	282
<b>Fig. 7.15</b>	Oxide scale morphologies and variations of elemental composition (wt%) across the cross section of (a) bare and (b) HVOF sprayed Ni-5Al coating on Superfer 800 after 1000 hrs exposure to low temperature superheater zone of the coal fired boiler at 700 °C.	285
<b>Fig. 7.16</b>	Oxide scale morphologies and variations of elemental composition (wt%) across the cross section of HVOF sprayed (a) NiCrAl and (b) NiCrAlY-0.4wt%CeO <sub>2</sub> coating on Superfer 800 after 1000 hrs exposure to low temperature superheater zone of the coal fired boiler at 700 °C.	286
<b>Fig. 7.17</b>	Oxide scale morphologies and variations of elemental composition (wt%) across the cross section of RF sputtered (a) Ni-Al and (b) NiCrAl films on on Superfer 800 after 1000 hrs exposure to low temperature superheater zone of the coal fired boiler at 700 °C.	287
<b>Fig. 7.18</b>	Composition image (BSEI) and X-ray mappings across the cross-section of uncoated Superfer 800 after 1000 hrs exposure to low temperature superheater zone of the coal fired boiler at 700 °C.	289
<b>Fig. 7.19</b>	Composition image (BSEI) and X-ray mappings across the cross-section of HVOF sprayed Ni-5Al coated Superfer 800 after 1000 hrs exposure to low temperature superheater zone of the coal fired boiler at 700 °C.	290

<b>Fig. 7.20</b>	Composition image (BSEI) and X-ray mappings across the cross-section of HVOF sprayed NiCrAl coated Superfer 800 after 1000 hrs exposure to low temperature superheater zone of the coal fired boiler at 700 °C.	291
<b>Fig. 7.21</b>	Composition image (BSEI) and X-ray mappings across the cross-section of HVOF sprayed NiCrAlY-0.4wt%CeO <sub>2</sub> coated Superfer 800 after 1000 hrs exposure to low temperature superheater zone of the coal fired boiler at 700 °C.	292
<b>Fig. 7.22</b>	Composition image (BSEI) and X-ray mappings across the cross-section of RF sputtered Ni-Al film on Superfer 800 after 1000 hrs exposure to low temperature superheater zone of the coal fired boiler at 700 °C.	293
<b>Fig. 7.23</b>	Composition image (BSEI) and X-ray mappings across the cross-section of RF sputtered NiCrAl film on Superfer 800 after 1000 hrs exposure to low temperature superheater zone of the coal fired boiler at 700 °C.	294
<b>Fig. 8.1</b>	Bar charts showing cumulative weight gain (mg/cm <sup>2</sup> ) for the uncoated and coated superalloys subjected to cyclic oxidation in air at 900°C for 100 cycles.	304
<b>Fig. 8.2</b>	Bar charts showing cumulative weight gain (mg/cm <sup>2</sup> ) for the uncoated and coated superalloys subjected to cyclic oxidation in Na <sub>2</sub> SO <sub>4</sub> -60%V <sub>2</sub> O <sub>5</sub> environment at 900°C for 100 cycles.	305
<b>Fig. 8.3</b>	Bar charts indicating the scale/coating thickness for the (a) uncoated Superfer 800; (b) HVOF coated Ni-5Al; (c) HVOF coated NiCrAl; (d) HVOF coated NiCrAlY-0.4wt%CeO <sub>2</sub> ; (e) RF sputtered Ni-Al and (f) RF sputtered NiCrAl coated Superfer 800 after 1000 hrs exposure to the coal fired boiler at 700 °C.	306
<b>Fig. 8.4</b>	Bar charts showing weight gain for the (a) uncoated Superfer 800; (b) HVOF coated Ni-5Al; (c) HVOF coated NiCrAl; (d) HVOF coated NiCrAlY-0.4wt%CeO <sub>2</sub> ; (e) RF sputtered Ni-Al and (f) RF sputtered NiCrAl coated Superfer 800 after 1000 hrs exposure to the coal fired boiler at 700°C.	306

# LIST OF TABLES

Table No.	Particulars	Page No.
Table 2.1	Comparison of characteristics for various thermal spray processes.	34
Table 3.1	Nominal composition and industrial applications of the superalloys used	44
Table 3.2	Composition of the alloy powders, shape and size of the particles.	45
Table 3.3	Process parameters employed during HVOF coating.	45
Table 3.4	Process parameters employed during RF magnetron sputtering process	46
Table 4.1	Coating thickness and porosity values of as sprayed Ni- 5Al coating on different superalloys.	62
Table 4.2	Parabolic rate constant, $k_p$ values of uncoated and coated superalloys subjected to air oxidation at 900°C.	77
Table 4.3	Parabolic rate constant, $k_p$ values of bare and Ni-5Al coated by HVOF process after hot corrosion studies at 900°C	94
Table 5.1	Parabolic rate constant, $k_p$ values of uncoated and NiCrAl coated superalloys subjected to air oxidation at 900°C	162
Table 5.2	Parabolic rate constant, $k_p$ values of bare and NiCrAl coated by HVOF process after hot corrosion studies at 900°C.	180
Table 6.1	Parabolic rate constants of bare and coated superalloys under the similar conditions.	240
Table 6.2	Parabolic rate constants of bare and coated superalloys under the similar conditions.	258
Table 7.1	Summary of the results for uncoated and coated Superfer 800 exposed to low temperature superheater zone of the coal fired boiler at around 700°C 1000 hours.	295

# RESEARCH PAPERS PRESENTED/PUBLISHED

---

---

Research papers published out of the present investigation, in the peer-reviewed journals as well as presented/published in the conferences, are as follows

## (A) REFERRED JOURNALS

1. **Mahesh**, R. A., Jayaganthan, R., and Prakash, S., (2008), "Oxidation behavior of HVOF sprayed Ni-5Al coatings deposited on Ni- and Fe-based superalloys under cyclic condition", *Materials Science and Engineering A*, 475 (2008) 327-335.
2. **Mahesh**, R. A., Jayaganthan, R., and Prakash, S., (2008), "Oxidation behaviour of selected Ni- and Fe- based superalloys in air at 900°C under cyclic conditions", *Transactions of the Indian Institute of Metals Journal*, Vol. 61, No. 1, (2008), 45-49.
3. **Mahesh**, R. A., Jayaganthan, R., and Prakash, S., (2008), "A study on hot corrosion behaviour of Ni-5Al coatings on Ni- and Fe-based superalloys in an aggressive environment at 900°C", *Journal of Alloys and Compounds*, 460 (2008), 220-231.
4. **Mahesh**, R. A., Jayaganthan, R., and Prakash, S., (2008), "Microstructural Characteristics and Mechanical properties of HVOF Sprayed NiCrAl Coating on Superalloys", *Journal of Alloys and Compounds*, (in press) (doi: 10.1016/j.jallcom.2008.01.025).
5. **Mahesh**, R. A., Rao, G., Jayaganthan, R., and Prakash, S., (2008), "Hot corrosion behaviour of HVOF sprayed NiCrAlY-0.4wt%CeO<sub>2</sub> coatings on superalloys in an aggressive environment at 900°C", *Corrosion Engineering Science and Technology*, (in press) (doi: 10.1179/174327808X303473).
6. **Mahesh**, R. A., Jayaganthan, R., and Prakash, S., (2008), "Evaluation of Hot Corrosion Behaviour of HVOF Sprayed NiCrAl coating on Superalloys at 900 Degree C", *Materials Chemistry and Physics*, Vol. 111, (2008), 524-533.
7. **Mahesh**, R. A., Jayaganthan, R., and Prakash, S., (2008), "Characterisation of HVOF sprayed NiCrAlY-0.4wt%CeO<sub>2</sub> Coatings on Superalloys", *Surface Engineering*, (in press) (doi: 10.1179/174329408X326362).
8. **Mahesh**, R. A., Jayaganthan, R., and Prakash, S., (2008), "Microstructural Characterization and hardness evaluation of HVOF Sprayed Ni-5Al coatings on Ni and Fe - based superalloys", *Journal of Materials Processing Technology* (Provisional acceptance).

9. **Mahesh, R. A., Jayaganthan, R., and Prakash, S., (2008),** “High Temperature Cyclic Oxidation behavior of Magnetron Sputtered Ni-Al thin films on Ni- and Fe-based superalloys”, *Materials Chemistry and Physics* (Provisional Acceptance).
10. **Mahesh, R. A., Jayaganthan, R., and Prakash, S., (2008),** “High temperature cyclic oxidation behaviour of HVOF sprayed NiCrAlY-0.4 wt% CeO<sub>2</sub> coatings on Ni and Fe-based superalloys”, *Surface and coating Technology* (under revision).
11. **Mahesh, R. A., Jayaganthan, R., and Prakash, S., (2008)** “High Temperature Oxidation studies on HVOF sprayed NiCrAl coatings on superalloys”, *Journal of Thermal Spray Technology* (under review).

**(B) NATIONAL/INTERNATIONAL CONFERENCES PROCEEDINGS**

12. **Mahesh, R. A., Subhash, K., Ankur, M., Jayaganthan, R., and Prakash, S., (2008),** “Degradation Behavior of HVOF sprayed Ni-based coatings on superalloy in 40%Na<sub>2</sub>SO<sub>4</sub>-60%V<sub>2</sub>O<sub>5</sub> environment at 900°C”, *International Thermal Spray Conference-08*, during 02-04 June, 2008, Maastricht, Netherlands. Abstract No:1556 (CDROM).
13. **Mahesh, R. A., Jayaganthan, R., and Prakash, S., (2007),** “Some studies on the hot corrosion behavior of Superalloys in aggressive environment at 900°C”, 16<sup>th</sup> *International Conference on Processing and Fabrication of Advanced Materials (PFAM16)*, 17-19 December, 2007, Singapore. pp 313-323.
14. **Mahesh, R. A., Jayaganthan, R., and Prakash, S., (2007),** “On the Role of HVOF Sprayed Coatings to Combat Hot Corrosion” *Corcon 2007*, International conference of corrosion, 26-28 September, 2007, Mumbai, India. (Poster presentation, CDROM)
15. **Mahesh, R. A., Jayaganthan, R., and Prakash, S., (2007),** “Hot Corrosion Behaviour of HVOF sprayed Ni-5Al coatings on Ni based superalloy” *Global Conference on Production and Industrial Engineering (An International Conference)*, 22-24 March, NIT- Jalandhar, India, (CDROM).

## ABBREVIATIONS

---

---

HVOF	High Velocity Oxy-Fuel
RF	Radio Frequency
FESEM	Field Emission Scanning Electron Microscope
BSEI	Back Scattered Electron Image
XRD	X-ray Diffraction
EDAX	Energy Dispersive X-ray Analysis
EPMA	Electron Probe Micro Analyser
$k_p$	Parabolic Rate Constant
hr	Hour
min	Minute
m.p.	Melting Point
Wt%	Weight Percentage
LPG	Liquid Petroleum Gas
fcc	Face Centered Cubic
Hv	Vickers Hardness



## **INTRODUCTION**

---

---

Material degradation at high temperatures is a serious problem in several high tech industries. Gas turbines in aircraft, fossil fueled power plants, refineries and petrochemical industries, and heating elements for high temperature furnaces are some examples, where corrosion either limits their use or reduces their life, considerably affecting the efficiency. The major challenge facing the power generation and aerospace industries is to use superior materials with increased efficiencies and adhere to the stringent environmental regulations, while ensuring reliability, availability, maintainability and cost are not compromised. Understanding the behaviour of metals and alloys at elevated temperatures, especially their corrosion behaviour and providing protective surface layers has become an object of scientific investigation since long time.

Materials for high-temperature applications are generally selected for specific properties such as strength, creep, mechanical and/or thermal fatigue. Although protective surface treatments are widely used at low temperatures yet the use of these at elevated temperatures is more recent. During their use at high temperature, these mechanical properties may degrade as a result of interactions with corrosive environments.

Corrosion is a natural electrochemical/chemical phenomena commonly defined as the deterioration of a substance (usually metal) or its properties as a consequence of its reaction with the environment. It is important to understand the nature of all types of environmental degradation of metals and alloys as vividly as possible so that preventive measures against metal loss and failures can be economically devised to ensure safety and reliability in the use of metallic components (Buta and Prakash, 2006).

Hot corrosion was first recognised as a serious problem in the year 1940 in connection with the degradation of fireside boiler tubes in coal-fired steam generating plants. Since then, the problem has been observed in boilers, internal combustion engines, gas turbines, fluidized bed combustion and industrial waste incinerators (Khanna and Jha, 1998). Hot corrosion became a topic of importance and popular interest in the late 1960s as gas turbine engines of military aircraft suffered severe corrosion during the operation over sea water in the Vietnam war. Metallographic inspection of failed parts often showed the presence of sulphides of nickel and chromium, so the mechanism was initially called as “sulphidation” (Rapp, 1986 and 2002).

According to a recent study, corrosion of metals costs the United States over \$300 billion per year (4.2% GNP). This is more than the cost of annual floods and fires. An estimated 40% of total US steel production goes to replacement of corroded parts and products (Priyantha et al, 2003). As far as India is concerned, the corrosion costs may touch Rs. 24000 crore (Rs. 240000 million), which include materials used in building structures, bridges, chemical plants, offshore platforms, power plants, ships, pipe lines for transportation of hydrocarbon, electrical and electronics components (Gupta, 2003).

A case study of boiler tube failure in coal fired boilers has been conducted by Prakash et al, (2001) covering 1 year and it was observed that more than 50% of the failures were attributed to the hot corrosion and erosion due to ash. Cheruvu et al, (2006) reported that the replacement cost of the hot section components alone can exceed 35% of the cost of a new unit. Although corrosion problems cannot be completely remedied, it is estimated that corrosion-related costs can be reduced more than 30% by development and use of better corrosion control technologies. From human safety point of view, corrosion is considered more disastrous, as premature failure of operating equipments or structures results in human injury or even loss of life.

The gas turbine engine provides one of the harshest environments challenging materials today. Engine components are subjected to rigorous mechanical loading conditions, high temperatures, and corrosive and/or erosive media. Historically, engine manufacturers have applied protective coatings to increase the durability and field performance of alloys or composite materials. Advanced engine designs as well as the development of processing technologies have led to the development of many new and improved coating systems in a variety of engine component applications (DeMasi-Marcin and Gupta, 1994).

High temperature oxidation and hot corrosion i.e., molten salt corrosion present the most deleterious forms of surface degradation which can lead to the loss of mechanical strength and catastrophic failure of structural and engineering components. High temperature oxidation and hot corrosion are routinely encountered in superalloys which operate in high temperature and corrosive environments. An understanding of long term high temperature oxidation and hot corrosion behaviors of materials are extremely important.

Ni- and Fe-based superalloys are used as structural components in various applications such as gas turbines, steam boilers, heat exchangers, aeroengines and industrial springs as they possess superior mechanical properties, and corrosion and oxidation resistance to some extent. These superalloys cannot provide high-temperature corrosion resistance without affecting its mechanical properties as tailoring of microstructural and

compositional parameters to achieve the former would have adverse influence on the latter. Therefore, protective coatings are essential to provide the high temperature oxidation and corrosion resistance to the superalloys in order to realize the long service life of the components even in harsh environments, especially in industrial gas turbines and boilers. It is well known in the literature that degradation by high temperature oxidation is one of the main failure modes of hot section components in gas turbines (Liu et al, 2001).

The knowledge of oxidation behavior of high-temperature coatings is important to extend the limits of use of superalloys at upper end of their performance capabilities without altering the mechanical properties of the substrate materials while protecting them against wear or corrosion (Sidky and Hocking, 1999). The performance of materials used in high temperature environment is often controlled by its ability to form the protective oxide scale on the surface (Graham and Hussey, 1995). The alloys or coatings designed to resist oxidizing environments at high temperatures should be capable of forming thermodynamically stable, slow growing, and adherent surface oxide scales (Toma et al, 2000). Hence, the oxidation resistance of superalloys under cyclic high temperature environments has become a vital issue.

According to Gurrappa (2001), the role of the coating is to provide a metal surface composition which will react with the environment to produce the most protective scale possible combining corrosion resistance with long term stability and resistance to cracking or spallation under mechanical and thermal stresses induced during the operation of the component. Goward (1998) opined that a complete understanding of oxide adherence is still elusive and is one of the most important areas of research, for both coatings and superalloys, to provide further advances in engine efficiency and service life. Research and development on coatings for diffusion, overlay and thermal barrier systems deserves equally strong support. He further predicted that the future for coating science and technology is brighter than ever in the current millennium. In future, as the quest for fuel efficiency forces us to ever higher temperatures and larger plants (with huge capital investments), molten salt corrosion will become potentially even more critical, and we may anticipate a new level of need to understand, and to develop materials and means to combat, corrosion by fused salts and slags.

Sidky and Hocking (1999) have observed that the coatings produced by plasma spray process are porous; this reduces their strength and decreases their corrosion resistance. The HVOF process is one of the most popular thermal spraying technologies and has been widely adopted by many industries due to its flexibility, cost effectiveness and the superior quality of the coatings produced. The main advantages of HVOF process is the shorter residence time in

the flame and the higher kinetic energy of the impacting particles. This produces a dense coating with less degradation of the powder during spraying (Nicholls, 2000).

Metal tube corrosion is a major operating problem because it results in downtime and periodic shutdowns in waste-to-energy (WTE) power plants and accounts for a significant fraction of the total operating cost of WTE plants. Metallic coatings and corrosion resistant alloys such as stainless steels and nickel-base alloys are often used to protect boilers from corrosion and represent a large use of valuable resources. The need to protect materials in gas turbines has resulted in a wide variety of corrosion-resistant coatings which are applied by a number of different processes, and are specific for different applications and corrosive environments (Streief, 1993).

The present study has been focused to comparatively evaluate the hot corrosion behaviour of Ni-5Al, NiCrAl and NiCrAlY-0.4wt% CeO<sub>2</sub> coatings by HVOF spray process and Ni-Al and NiCrAl films deposited by RF magnetron sputtering process on Ni and Fe based superalloys in air, molten salt (Na<sub>2</sub>SO<sub>4</sub>-60%V<sub>2</sub>O<sub>5</sub>) at 900°C and in actual industrial environment in a coal fired boiler of a thermal power plant. The behaviour of these coatings in different degrading environments will be helpful in choosing the suitable coating for the hot section components of the gas turbine and boiler applications.

# LITERATURE REVIEW

---

---

*This chapter contains a comprehensive review of the literature with a special reference to oxidation and hot corrosion of metals and alloys, and protective coatings. HVOF thermal spray process and RF magnetron sputtering process are described in brief. The problem has been formulated after critical analysis of the literature at the end of this chapter.*

### 2.1 HIGH TEMPERATURE OXIDATION

The oxidation behaviour of materials at elevated temperatures is of paramount importance, especially in many domains of material science and engineering e.g. high temperature processes in chemical industry or metal production and fabrication. It is essential to control high temperature oxidation by thorough understanding of oxidation kinetics. An oxidation reaction between a metal (M) and the oxygen gas (O<sub>2</sub>) to form the oxide M<sub>a</sub>O<sub>b</sub> is given below



This reaction can be considered as a special case of heterogeneous reaction. Knoll et al, (1999) have reported that the reaction path and the oxidation behaviour may depend on a variety of factors, and the reaction mechanisms often proven to be complex. For example, the initial step in the metal-oxygen reaction is the adsorption of the gas on the metal surface. As the reaction proceeds, individual separated oxide nucleus formed on the surface continues to grow laterally to form a continuous oxide film on the metal surface. Thus, the oxide film separates the metal from the gas and the reaction mechanism changes completely. The reaction can only proceed by a solid-state diffusion of one or both of the reactants through the oxide film. At high temperature, the oxidation of many metals is found to follow parabolic time dependence;

$$x^2 = k_p t + C \quad (2.2)$$

where 'x' is the scale thickness in dimensions of length, k<sub>p</sub> represents the parabolic rate constant and t is the time. High temperature parabolic oxidation signifies that a thermal diffusion process is the rate determining step. Khanna (2005) has also reported that most metals and engineering alloys follow parabolic kinetics at elevated temperatures. The oxide growth process is usually governed by the diffusion of ions or electrons through the initially formed oxide scale. Mondal et al, (2007) have reported that the oxidation behavior is governed by the inward oxygen diffusion and oxide growth follows a parabolic rate law.

Oxidation is the most important high temperature corrosion reaction. Metals and alloys are oxidised when heated to elevated temperatures in air or in highly oxidising atmospheres with excess air or oxygen. Many metallic components, such as retorts in heat treatment furnaces, furnace heater tubes and coils in chemical and petrochemical plants, water walls and combustors and transition ducts in gas turbines, are subjected to oxidation (Lai, 2007). Oxidation, in real sense, is the formation of the oxide scale. If the formed oxide scale is thin, slow growing, and adherent, it protects the substrate from further oxidation. However, if the scale spalls frequently, the metal is consumed continuously and the material ultimately fails (Khanna, 2005).

Metals and alloys constitute the most important group among engineering materials, and the demand for metallic materials with higher strength and special properties is on the increase with the advancement of technology. However a serious drawback of metallic materials is the deterioration in properties originating from their interaction with the environments in which they are expected to perform. Often this leads to a premature failure of metallic components with the allied hazards of plant shutdown and loss of economy, environmental pollution, and risk to human lives. The annual direct loss of natural resources, i.e., metals, due to environmental degradation is also substantial. The nature of degradation of materials varies from environment to environment, although some factors (e.g., loss of ductility, cracking) may be common to several of them. (Chatterjee et al, 2001). He et al., (2001) reported that both mechanical properties and oxidation resistance of materials must be considered for its use in high temperature applications. Creep, mechanical fatigue, thermal fatigue, oxidation and sulfidation are the main possible causes of failure of a turbine blade in a hot station.

According to Stott (1998), the establishment of an oxide scale on an alloy occurs by a nucleation and growth process. When the clean component is exposed to an oxygen-rich gas, small, impinging nuclei of all the thermodynamically stable oxides develop on the surface. These initial nuclei of oxide coalesce rapidly to give a complete layer. During this initial or transient stage, the rate of oxidation is rapid, all the elements in the alloy oxidize and the amounts of the various oxides in the layer are approximately proportional to the concentration of the elements in the alloy. Once the transient oxide layer has been established, it continues to grow following diffusion of metal ions to the scale/gas interface or oxygen to the scale/alloy interface. The rate of thickening of the layer is determined by the temperature, the oxygen pressure and the spatial distribution, the amount, the composition, and the structure of the initial oxide phases (Chattopadhyay and Wood, 1970).

Stott (1998) reported that for oxidation of Ni-20%Cr alloy, approximately 80% of the surface is covered by the NiO phase and 20% by the Cr<sub>2</sub>O<sub>3</sub> phase in the initial stages, (neglecting any NiCr<sub>2</sub>O<sub>4</sub> that may develop), the faster-growing NiO phase overgrows the Cr<sub>2</sub>O<sub>3</sub> phase and a transient oxide scale layer of NiO develops, incorporating the other transient oxide phases. At the same time, the thermodynamically favored oxide (Cr<sub>2</sub>O<sub>3</sub> on Ni-20%Cr) attempts to establish as a complete layer at the base of the transient oxide scale layer. This is achieved after a short period for this alloy at high temperatures (> 600°C). Sufficient Cr<sub>2</sub>O<sub>3</sub> nuclei develop in the alloy, at or close to the alloy/scale interface, to coalesce and form a complete layer, the oxygen activity at the transient oxide scale layer/alloy interface being sufficiently high to oxidize selectively chromium in the alloy. This has been shown schematically in Fig 2.1. The rate of oxidation is then controlled by transport of reactants across this Cr<sub>2</sub>O<sub>3</sub>-rich layer, a much slower process than across the initially formed NiO-rich layer. He concluded that the oxide scale which forms at the steady state depends, in general, on various factors such as alloy composition, temperature, oxygen partial pressure, diffusivity in the alloy, interdiffusion coefficients, growth rates of various oxides, microstructure and surface condition of the alloy, and mechanical properties.

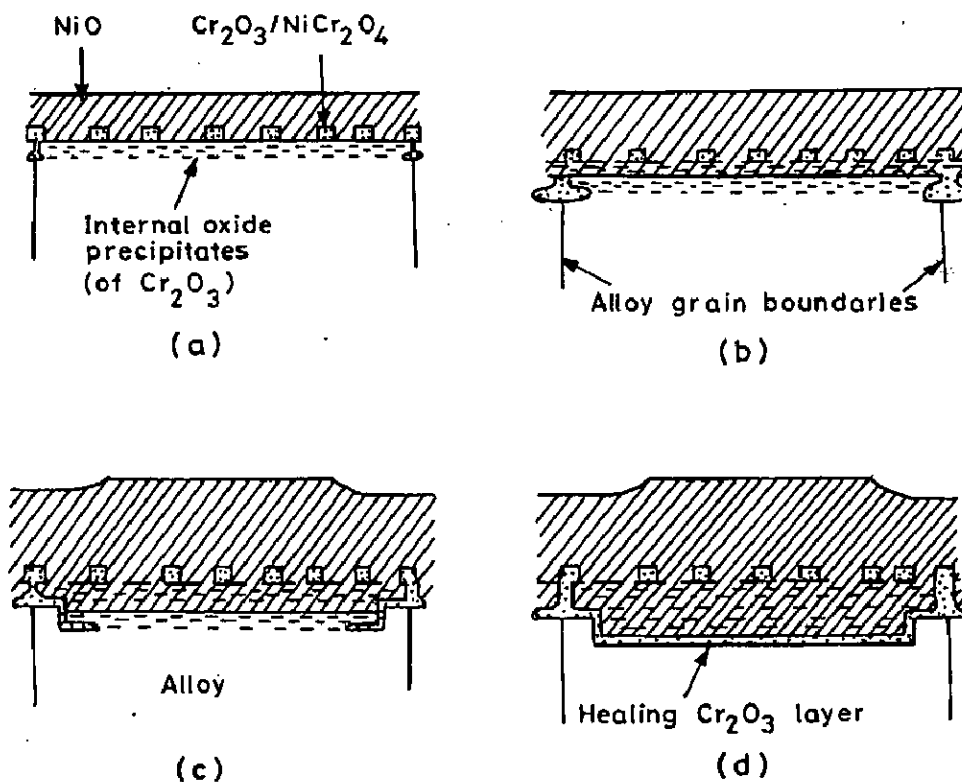


**Fig. 2.1:** Schematic representation showing transient oxidation and subsequent development of a healing Cr<sub>2</sub>O<sub>3</sub>-rich layer on Ni-20%Cr at high temperature (Stott, 1998).

According to Dieter (2007), the study of the oxidation behaviour of binary alloys AB highlights the most important oxidation mechanisms of multi-component alloys. The two components of a binary alloys in general do not have the same affinity for oxygen and therefore do not oxidise at the same rate. Two distinct types of behaviour are observed: (i) if the affinity for oxygen of A is much greater than that of B, A will undergo selective oxidation; (ii) if A and B have comparable affinities for oxygen, they undergo simultaneous oxidation. The alloy oxidation mechanism has been depicted in Fig 2.2.

Smialek (2001) opined that the successful application of many materials at high temperature requires excellent high-temperature properties such as long-term mechanical and chemical stability. He has observed that the surface stability of the candidate material is necessary to prevent rapid material consumption at high temperatures. In general, this dictates that the exposed material is able to form a slow-growing, stable, adherent surface scale that serves to protect the underlying substrate material. He has explained that most of the scales have a very fine grain size, often submicron during the first few hours of oxidation. Since bulk diffusion in many stoichiometric oxides is relatively slow, short-circuit processes such as grain boundary diffusion dominates the overall process. Consequently, the factors affecting grain boundary diffusion, e.g. grain growth and aleovalent impurity segregation, have a considerable effect on the net growth rate and may cause deviations from true parabolic kinetics. In addition to scale growth kinetics, scale adhesion in cyclic exposures also must be considered for continuous protection to prevent rapid metal consumption upon reoxidation. According to Murthy et al. (1994), one of the prerequisites of any structural material is its stability towards environmental degradation caused by means of localised, general corrosion.

Liu et al, (2001) has described the high temperature oxidation behavior of aluminide coatings on cobalt base superalloy in air, in which during the initial oxidation stage, the oxidation rate of the coating was controlled by the air/coating interface reaction, presenting the rapid increase in the weight gain. Al selectively oxidised to form a perfect protective  $\text{Al}_2\text{O}_3$  scale leading to the oxidation process to change from original directive reaction between alloy and air into the diffusion reaction of outward metal cations and inward oxygen anions through the oxide scale. They observed that  $\theta\text{-Al}_2\text{O}_3$  has faster growth rate as compared to that of  $\alpha\text{-Al}_2\text{O}_3$ . Rybicki et al, (1989) proved by TGA that  $\theta\text{-Al}_2\text{O}_3$  has the fastest growth rate among all alumina phases. The higher the oxidation temperature,  $\alpha\text{-Al}_2\text{O}_3$ , forms easily as compared to  $\theta\text{-Al}_2\text{O}_3$ .



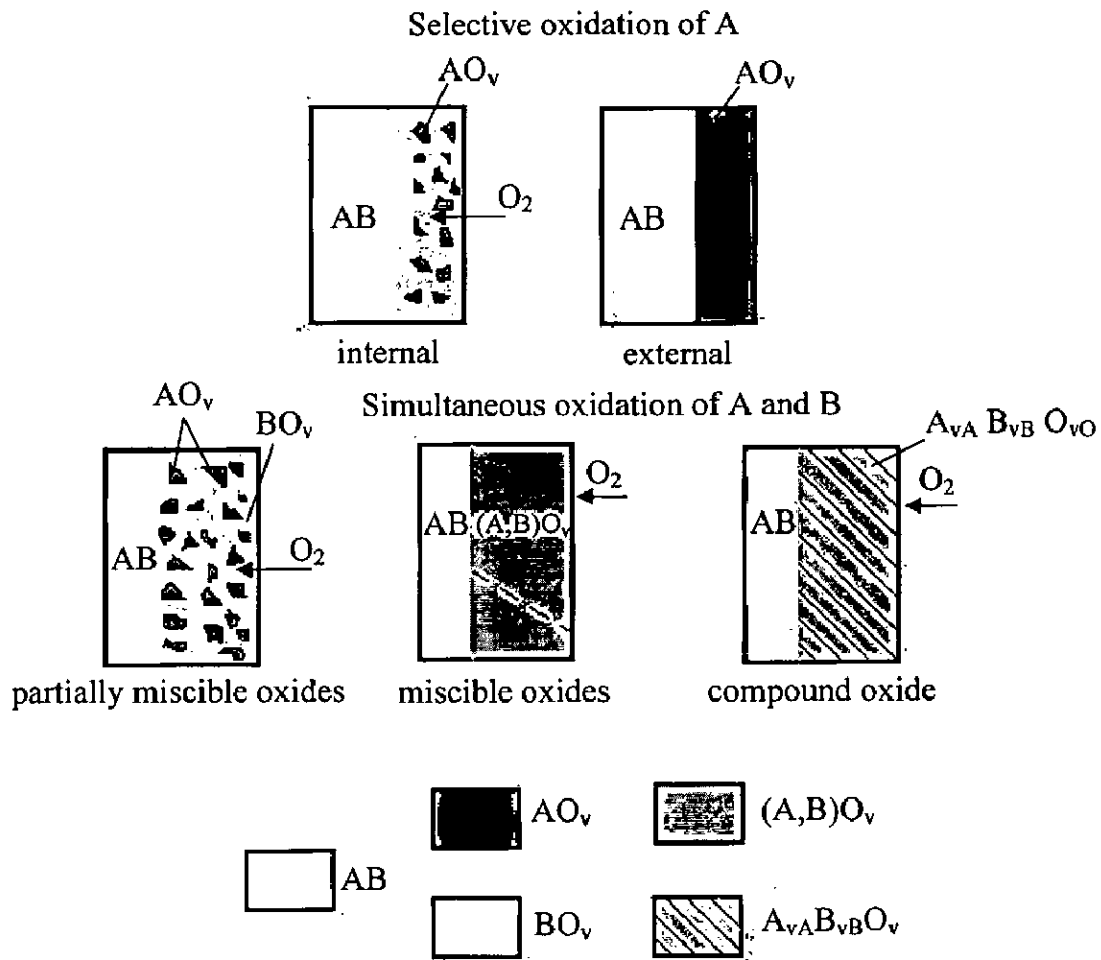


**Fig. 2.2:** Alloy oxidation mechanisms, with the corresponding morphologies of the oxide layers (Dieter, 2007).

Whittle (1983) explained the typical oxidation process of binary alloy where the oxides of both A and B are stable in the gas but BO is more stable than AO (in superalloys, A generally represents Ni or Co and B represents Cr, Al etc) as shown in Fig. 2.3. Thus the alloying element B, which forms a very stable and slow growing oxide, is added in the superalloy in sufficient quantity to form a protective surface layer by selective oxidation. The selective oxidation process is very important because it allows the most thermodynamically stable oxide to cover the entire alloy surface. It is the primary method used to develop oxidation resistance on the structural alloys presently in use.

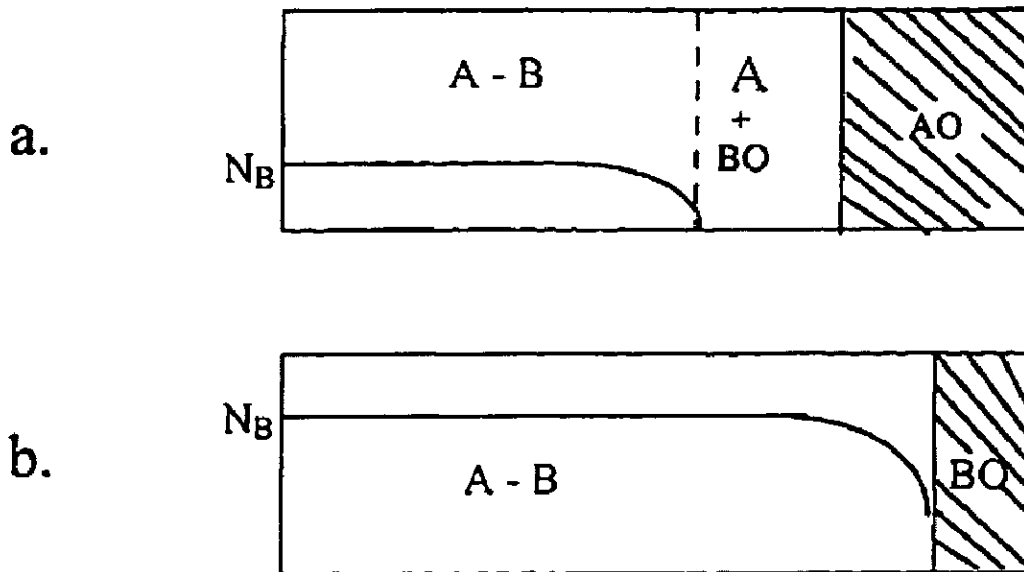


**Fig. 2.3:** Schematic cross sections of an A-B alloy where both components form stable oxides but BO is more stable than AO. (a) Alloy dilute in B showing internal oxidation of B under an external layer of AO. (b) Alloy concentrated in B showing continuous external BO (Whittle, 1983)

Hussain et al, (1994) have opined that oxidation at high temperature involves the oxidation of selective elements, formation of oxide scales and internal oxidation. The phenomenon is too complex to be understood in simple terms of diffusion processes. Knowledge of reaction kinetics and the nature of the surface scales formed during oxidation are important for assessing the degradation characteristics of materials in high-temperature applications.

Schutze (1993) has explained that the resistance of protective oxide scales against cracking by mechanical stresses is very much dependent on the size and distribution of physical defects in the oxide. Fig 2.4 illustrates that even in more or less perfect oxide scales, the movement of dislocations may lead to the nucleation of microcracks. This nucleation will take place at sites where dislocation motion is impeded, e.g. at grain boundaries where dislocation pile-ups lead to the formation and growth of microcracks. This effect may occur within the oxide scale but also at the oxide/metal interface as illustrated in Fig. 2.4 (b). Under the effect of mechanical stresses, these microcracks will grow in a stable manner until they reach a critical state for spontaneous scale failure. He concluded that the size of the physical defects and their number should be as small as possible, the scale thickness should be as low as possible and the oxide intrusions improve scale adhesion by the reduction of interfacial stresses for the optimum behavior of protective oxide scale.

Li et al. (2003) have reported that although considerable insight has been accumulated on mechanisms of high temperature oxidation, from both engineering and more fundamental studies, reaction mechanisms are often not fully understood. They further stated that the degradation by oxidation is one of the main failure modes of hot-section components in the gas turbines, so an understanding of the oxidation phenomenon is very necessary, particularly for the superalloys (Li et al, 2003). Plenty of literature is available on the high temperature oxidation of metals and alloys, which is difficult to review in a comprehensive manner in such a short space. As an alternative, it is proposed to overview the high temperature corrosion, especially, some recent studies conducted by various researchers in the field, which may form a basis for the formulation the problem.

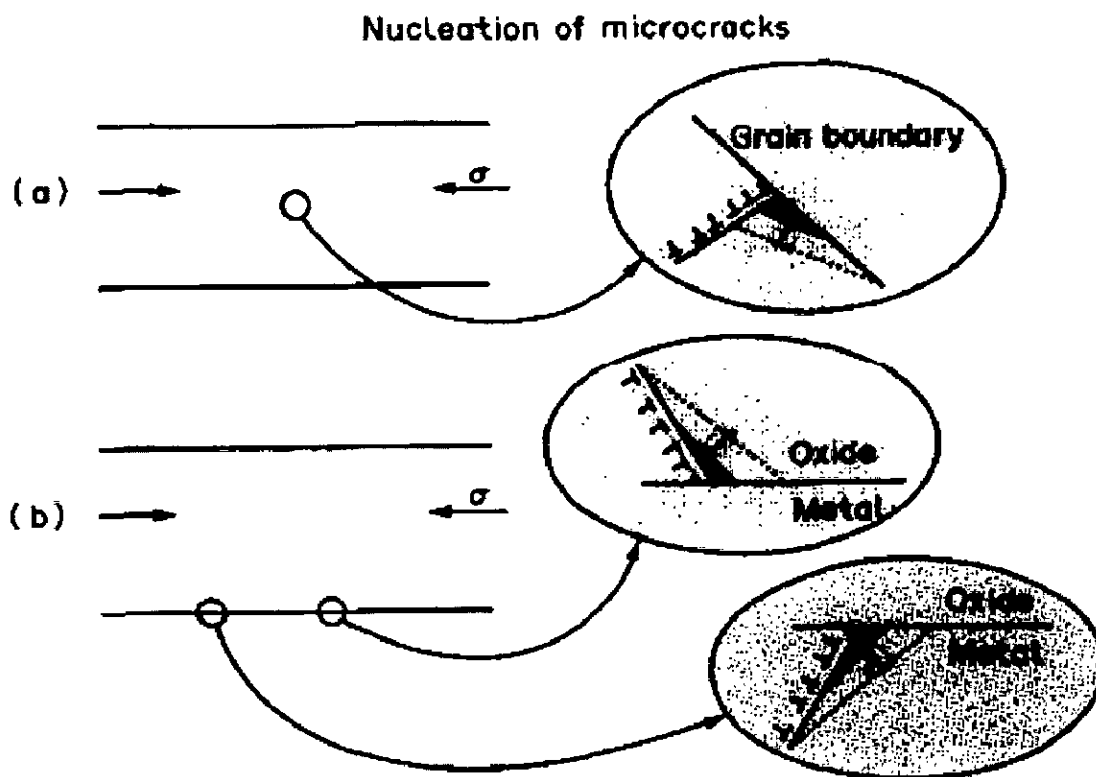


**Fig. 2.4:** Schematic representation of the process of nucleation of microcracks within the scale (a) or at the scale/metal interface (b) by dislocation sliding and the formation of dislocation pile-ups at obstacles (grain boundaries, scale/metal interface). The microcrack is indicated by the black area. The situation is shown for compressive stresses but is equivalent for tensile stresses (Schutze, 1993).

### 2.1.1 Oxidation of Superalloys

The superalloys have been developed to achieve oxidation resistance by utilising the concept of selective oxidation. The selective oxidation approach to obtain oxidation resistance in superalloys consists of oxidising essentially only one element in the superalloy and relying upon this element's oxide for protection. For effective protection, it is anticipated that the oxide should cover the whole surface of the alloy and it must be an oxide through which the diffusion of the reactants takes place at comparatively slow rates. Nickel-, cobalt- and iron-base superalloys make use of the selective oxidation of the aluminium or chromium to develop oxidation resistance (Pettit and Meier, 1985). Further, Pettit and Meier (1985) have reported that the selective oxidation processes are affected by a number of factors such as alloy composition, alloy surface conditions, gas environment and cracking of the oxide scale. Cyclic oxidation conditions wherein the oxide scales crack and spall, as well as certain phases present in the superalloys, both affect the capability to selectively oxidise aluminium or chromium in the superalloys.

Haugsrud (2003) revisited the high temperature oxidation mechanism of Ni with an extensive review and experimental studies conducted to study the oxidation behaviour of Ni in the range 500-1300°C and oxygen pressure from  $1 \times 10^{-4}$  to 1 atm. The oxidation behaviour according to a parabolic rate law at 1100°C and its reaction rate was found to be governed by outward lattice diffusion of Ni via either singly or doubly charged Ni vacancies. At lower temperature, the oxidation mechanism has been reported to be more complex and contradictions are found in the literature. Short circuit mechanisms of both Ni and oxygen are of importance, where the influence of oxygen transport increases with decreasing temperature. Further, he concluded that the mechanism of oxygen ingress is not fully clear, but since the oxygen diffusivity in NiO is too slow to account for the inward growth, oxygen is assumed to penetrate the scale as gaseous species.

Li et al (2003) have studied the oxidation of single crystal Ni-base superalloy in air at 800 and 900°C for exposures up to 1925 hrs. They reported that oxidation rate of single crystal Ni-base superalloy at 900°C was slower than that at 800°C. The scale formed at 900°C was more uniform and consists of several layers, an NiO outer layer, a spinel-rich sublayer and an  $\alpha$ -Al<sub>2</sub>O<sub>3</sub> inner layer provides a good oxidation resistance.

Huang et al. (2005) have examined the behaviour of directionally solidified Ni-based superalloy during isothermal oxidation at 1000, 1050 and 1100°C and the cyclic oxidation behaviour at 1000°C. They reported that the alloy exhibited a two stage parabolic oxidation

kinetics at 1000-1100°C and in cyclic oxidation, the alloy showed no weight loss even after 1100 cycles. Large population of faceted and needle-like AlN precipitates were observed on the alloy subsurface regions.

Pettit and Meier (1985) opined that during isothermal oxidation of Ni-base superalloys, Cr<sub>2</sub>O<sub>3</sub> and Al<sub>2</sub>O<sub>3</sub> scales are formed. Whereas, under cyclic conditions, depletion of chromium and aluminium results eventually in formation of NiO scale. Some alloys facilitate the formation of the NiO scale much more rapidly than the others. They further concluded that the application of aluminide coatings to two nickel based superalloys B-1900 and Mar M200 makes them remain in alumina scale formation range for even longer times than obtained for the uncoated alloys. The time, over which nickel base superalloys can be protective, external scales of alumina or chromia are affected by temperature, the gas environment and alloy composition. Generally, the superalloys remain alumina or chromia formers for longer times as the aluminium or chromium concentrations are increased. Other elements such as yttrium or cerium can extend this time as these elements improve the oxide scale adherence. Further, the alloys which are in alumina formers generally have better oxidation resistance than the chromia formers since diffusion through the alumina scales is generally slower than through chromia.

As far as the Co- and Fe-based superalloys are concerned, they usually cannot be made to contain enough aluminium to permit them to be alumina formers as it will have detrimental effect on their mechanical properties. Therefore, the oxidation resistance of Co- and Fe-based superalloys depends solely on the formation of chromia scales. However, the oxidation resistance of Co- and Fe-base superalloys is inferior to that of Ni-base superalloys. Furthermore, even when considering the Ni-base superalloys that are chromia formers, as degradation begins i.e. the chromia scales are damaged, the less protective oxides formed on the Ni-base alloys contain significant amount of nickel oxide as compared to cobalt and iron oxides on the cobalt and iron-base superalloys, respectively. Since nickel oxides are more protective than cobalt and iron oxides, the oxidation resistance drop-off is more abrupt in the case of the Co- and Fe-base superalloys (Pettit and Meier, 1985).

Khalid et al, (1999) have examined the high temperature oxidation behaviour of Incoloy 800H and Incoloy 825 at 1000 and 1200°C. Incoloy 800H exhibited compact, dense and adherent oxide layer, whereas the Incoloy 825 decomposed completely into the oxide. They reported the presence of coarse Ti-rich inclusions which indicates less dissolution of Ti in the alloy. Harpreet et al. (2005A) have carried out high temperature oxidation studies of plasma sprayed coatings (NiCrAlY, Ni-20Cr, Ni3Al and Stellite-6) on iron based superalloy

at 900°C under cyclic conditions for 50hrs. They have reported that the coatings exhibited fairly good adherence to the substrate superalloy and developed oxide scales that would protect the substrate from oxidation.

Hussain et al, (1994) have studied the comparison of the oxidation kinetics of four commercial heat-resisting alloys namely Hastelloy C-4, SS 304L, Incoloy 800H and Incoloy 825, in air from 600 to 1200°C. Hastelloy C-4 was found to be the most resistant to oxidation for temperatures upto 1000°C following a cubic-rate law. SS 304L was reported to be oxidised in the form of stratified nodules of two distinct layers, which grow in opposite directions at the metal-oxide interface irrespective of time and temperature of oxidation. Incoloy 800H and Incoloy 825 showed similar kinetics, following parabolic-rate law at 1000°C and 1200°C. They also observed the deleterious effect of Mo on the oxidation resistance of Incoloy 825.

## **2.2 HOT CORROSION**

Metals and alloys sometimes experience accelerated oxidation when their surfaces are covered with a thin film of fused salt in an oxidizing gas atmosphere at elevated temperatures. This is known as hot corrosion where a porous non-protective oxide scale is formed at the surfaces and sulphides in the substrate (Rapp and Zhang, 1994).

If concentration of the sulphate exceeds the saturation vapour pressure at the operating metal temperature for turbine blades, vanes and energy generation components (700-1100°C), then  $\text{Na}_2\text{SO}_4$  will deposit on the surface of these components. At higher temperatures, these deposits of  $\text{Na}_2\text{SO}_4$  are molten (m.p.884°C) and can cause accelerated attack of Ni- and Co-base superalloys. Further, the accelerated corrosion can also be caused by other salts, such as vanadates or sulphates-vanadate mixtures and in the presence of solid or gaseous salts such as chlorides.

### **2.2.1 High Temperature (Type I) Hot Corrosion (HTHC)**

High temperature (Type I) hot corrosion (HTHC) is observed mainly within the temperature range 850-950°C with the condensation of fused alkali metal salts on the surface of the component. The dominant salt in HTHC is  $\text{Na}_2\text{SO}_4$  due to its high thermodynamic stability. The macroscopic appearance of HTHC is manifested in many cases as severe peeling of the metal and by significant colour changes (greenish tone, resulting from the formation of NiO) in the area of the accelerated attack (Eliaz et al, 2002).

## 2.2.2 Low Temperature (Type II) Hot Corrosion (LTHC)

This form of corrosion is observed mainly within the temperature range 650-800°C (Nicholls, 2000; Wright, 1987). LTHC occurs well below the melting point of pure Na<sub>2</sub>SO<sub>4</sub>. The reaction product morphology for this type of corrosion can be characterised by a non-uniform attack in the form of pits, with only little sulphide formation close to the alloy/scale interface and little depletion of Cr or Al in the alloy substrate (Rapp and Zhang, 1994). The formation of low melting point eutectics causes typical LTHC pitting for instance the formation of Na<sub>2</sub>SO<sub>4</sub>-NiSO<sub>4</sub> eutectics for nickel-based superalloys. Wright (1987) suggested that a high partial pressure of SO<sub>3</sub> in the gaseous phase is required for the LTHC reactions to occur, in contrary to HTHC. The localized nature of attack is related to localized failure of the scale as a result of thermal cycling, erosion, or chemical reactions. As opposed to Type I hot corrosion, in Type II, neither microscopic sulphidation nor chromium depletion are generally observed (Driver et al, 1981; Santorelli et al, 1989).

## 2.2.3 Hot Corrosion of Superalloys

Hot corrosion degradation process of the superalloys usually consists of two stages, namely, an initiation stage and a propagation stage (Pettit and Meier, 1985 and Pettit and Giggins, 1987). Pettit and Meier (1985) reported that all corrosion resistant alloys degrade via these two stages and it is the result of using selective oxidation to develop oxidation or corrosion resistance. They elaborated that the conditions causing hot corrosion therefore only shorten the time for which the superalloys can form protective alumina or chromia scales via selective oxidation. Such conditions are depicted schematically in Fig. 2.5.

During the initiation stage of hot corrosion, superalloys are degraded at rates similar to those that would have prevailed in the absence of the deposits. Elements in the alloy are oxidised and electrons are transferred from metallic atoms to the reducible substances in the deposit. Consequently, the reaction product barrier that forms beneath the deposit on the alloy surface usually exhibits primarily those features resulting from the gas-alloy reaction (Pettit and Giggins, 1987).

In some cases of hot corrosion, an increasing amount of sulphide particles become evident in the alloy beneath the protective reaction product barrier. In other, small holes become evident in the protective reaction product barrier where the molten deposit begins to penetrate it. Eventually, the protective barrier formed via selective oxidation is rendered ineffective, and the hot corrosion process enters into the propagation stage. Obviously in attempting to develop resistance to hot corrosion, it is important to ensure the superalloys remain in the initiation stage as long as possible (Pettit and Meier, 1985).

Numerous factors affect the time at which the hot corrosion process moves from the initiation stage into the propagation stage as shown in Fig. 2.5. These factors also play the dominant role in determining the type of reaction product that is formed in the propagation stage. These factors are also responsible for variety of hot corrosion processes that have been observed when superalloys are exposed to different environments (Pettit and Meier, 1985). The propagation stage of the hot corrosion sequence is the stage for which the superalloy must be removed from service, since this stage always has much larger corrosion rates than for the same superalloy in the initiation stage (Pettit and Meier, 1985 and Pettit and Giggins, 1987).

## HOT CORROSION CHRONOLOGY

### Initiation Stage

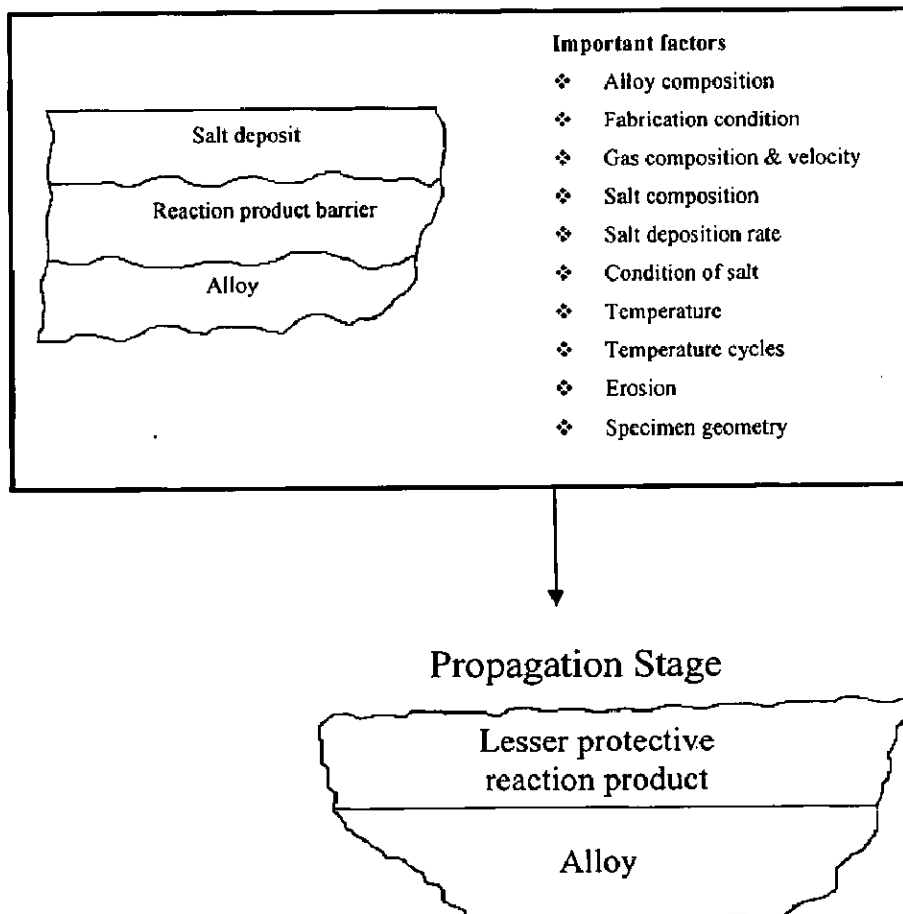


**Fig. 2.5:** Schematic diagram to illustrate the conditions that develop during the initiation and the propagation of hot corrosion attack, and to identify the factors that determine the time at which the transition from the initiation to the propagation stage occurs (Pettit and Meier, 1985).



## 2.2.4 Mechanisms of Hot Corrosion

Several mechanisms have been proposed to describe the phenomenon of hot corrosion (Goebel and Pettit, 1970A, Goebel and Pettit, 1970B, Beltran and Shores, 1972, Rapp and Goto, 1981, Rapp, 1986, Pettit and Giggins, 1987, Stringer, 1987, Otsuka and Rapp, 1990 and Zhang et al, 1993). Eliaz et al, (2002) have reported that the failures of turbine materials are often attributed to the initiation of high temperature hot corrosion (HTHC) to failure of the protective oxide layer, which allows the molten salt to access directly the substrate metal. This failure may result from erosion, thermal stresses, erosion-corrosion, chemical reactions, etc. The mechanisms proposed for the HTHC propagation stage are the sulphidation-oxidation mechanism and the salt fluxing mechanisms (Stringer, 1987).

According to Rapp and Goto (1981), the oxide soluble in molten  $\text{Na}_2\text{SO}_4$  as a function of the acidity of the salt. They reported that a negative gradient of the solubility of the protective oxide in the salt film at the oxide/salt interface should lead to oxide dissolution at this interface and to precipitation of a non-protective oxide away from the interface, where the solubility is lower. Fluxing arises in this case only because of the local variation of sodium oxide activity and/or oxygen partial pressure across the salt film, without any necessity of sulphide-forming reaction. This mechanism can explain a self-sustaining process of dissolution of the protective oxide to maintain an accelerated corrosion attack (Stringer, 1987).

The effect of vanadium on HTHC has also been studied by different researchers. Bornstein et al, (1973) and Goebel et al, (1973) opined that a self-sustained acidic dissolution of the protective  $\text{Cr}_2\text{O}_3$  or  $\text{Al}_2\text{O}_3$  scales could take place when the salt film contains vanadium, because  $\text{V}_2\text{O}_5$  is a strong acidic oxide.

Luthra (1983) explained the phenomenon of LTHC with the help of a common model, according to which LTHC follows two stages. In the first stage, liquid sodium-cobalt sulphate is formed on the surface, whereas in the second stage, propagation of the attack takes place, as shown in Fig. 2.6. The propagation is suggested to occur via migration of  $\text{SO}_3$  and cobalt inward and outward, respectively, through the liquid salt.

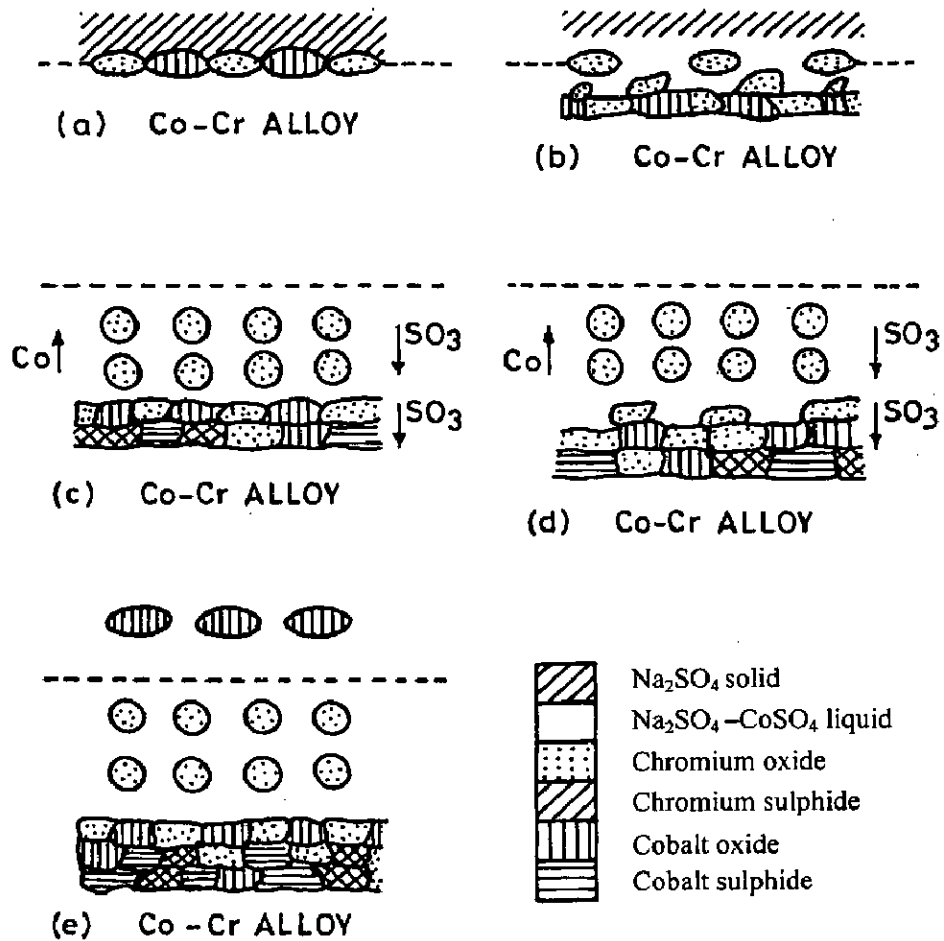


**Fig. 2.6:** Schematic representation of the reaction sequence during low-temperature hot corrosion of a Co-30%Cr alloy exposed to O<sub>2</sub>-SO<sub>2</sub>-SO<sub>3</sub> environment where Na<sub>2</sub>SO<sub>4</sub>-CoSO<sub>4</sub> liquid and Co<sub>3</sub>O<sub>4</sub> are stable. At higher concentration of SO<sub>3</sub> where Co<sub>3</sub>O<sub>4</sub> is unstable at the gas-salt interface, the outward migrating cobalt will form CoSO<sub>4</sub> (s) or Co<sub>3</sub>O<sub>4</sub> and CoSO<sub>4</sub>(s) (Luthra, 1983).

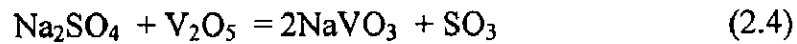
### 2.2.5 Salt-fluxing Reactions

The salt fluxing reactions for superalloys may be either acidic or basic in nature. The process by which the reaction product barrier becomes non-protective due to the formation of species which are soluble in the liquid deposit are called "fluxing" reactions.

Dissolution of protective oxides on the acidic side is termed as 'acidic fluxing' and on the basic side as 'basic fluxing'. In molten sulphate deposit, the following equilibrium can be used to define the acidity or basicity:



With the equilibrium constant,  $K = \frac{P_{SO_3}}{a_{O^{2-}}}$  where  $P_{SO_3}$  is the pressure of  $SO_3$  and  $a_{O^{2-}}$  is the activity of the oxide ions in the melt. The acidity increases as the  $P_{SO_3}$  is increased. The acidity is not controlled by the  $P_{SO_3}$  in the gas alone when there are other gradients in the system. For example  $V_2O_5$  can react with  $Na_2SO_4$  to increase the acidity of the melt via reaction:



Molybdenum and Tungsten in the alloy can create similar effects when their oxides are formed as corrosion products (Pettit and Giggins, 1987). The initial concept of basic fluxing was first proposed by Bornstein and Decrescent (1970) and then described in thermodynamic terms for the hot corrosion of nickel by Goebel and Petit (1970A, 1970B).

### 2.2.5.1 Basic Fluxing Mode

Basic fluxing reactions occur because sulphur is removed from the  $Na_2SO_4$  and consequently oxide scale ions are produced which react with the protective oxide scale. It is important to notice that the concentration of oxide ions available for basic fluxing is limited by the amount of the deposit present upon the surface of the superalloy. Hence, basic fluxing reactions are not self-sustaining, but require a continuous source of  $Na_2SO_4$  in order for this type of degradation to proceed indefinitely (Pettit and Meier, 1985).

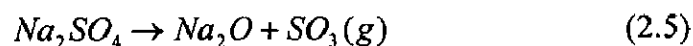
### 2.2.5.2 Acidic Fluxing Mode

The acidic fluxing reactions involve the development of non protective reaction products on superalloys as a result of a liquid deposit on the surface of the superalloy which has a deficiency of oxide ions. The deficiency of oxide ions in the  $Na_2SO_4$  can arise due to an acidic component present in the gas or an acidic phase formed as an oxidation product upon the superalloy. When the acidic component is present in the gas, the nonprotective oxide scale ensues due to rapid transport of certain ionic species in the acidic melt. If the melt becomes acidic due to formation of an oxide from an element in the superalloy, the attack becomes self-sustaining even with a small amount of  $Na_2SO_4$ . The refractory elements Mo, W and V form oxides that cause  $Na_2SO_4$  to become acidic and hence, these elements when oxidised in the presence of  $Na_2SO_4$  deposit on superalloys usually cause catastrophic self-sustaining hot corrosion via acidic fluxing (Pettit and Meier, 1985).

## 2.2.6 Chemistry of Salts

### 2.2.6.1 Chemistry and Phase Stability of Na<sub>2</sub>SO<sub>4</sub> Salt

Oxyanion melts of alkali nitrates, carbonates, hydroxides and sulphates exhibit an acid base character whereby the acid components may be considered as NO<sub>2</sub>(g), CO<sub>2</sub>(g), H<sub>2</sub>O(g) or SO<sub>3</sub>(g) respectively. Although the use of the Lux-Flood selection of NO<sub>3</sub><sup>-</sup>, CO<sub>3</sub><sup>2-</sup>, OH<sup>-</sup> and SO<sub>4</sub><sup>2-</sup> as the basic components is common for such fused salts, the oxide ion can be alternatively chosen as the Lewis base in common for all of these salts (Rapp, 1986 and 2002). For a melt of pure Na<sub>2</sub>SO<sub>4</sub> (m.p. 884<sup>0</sup>C), there exists the equilibrium as given below:

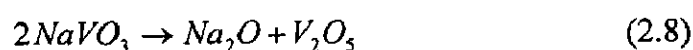
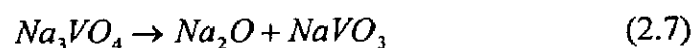


According to Rapp (1986), in examining the expected stability of the protective oxide Cr<sub>2</sub>O<sub>3</sub>, with respect to dissolution either as acidic solutes such as Cr<sub>2</sub>(SO<sub>4</sub>)<sub>3</sub> or as basic solutes such as Na<sub>2</sub>CrO<sub>4</sub> or NaCrO<sub>2</sub>, the phase stability diagram for the Cr-S-O system can be superimposed on that for Na-S-O, as shown in Fig. 2.7. The two abscissa scales at the bottom and top of figure provide alternate parameters for melt basicity (or acidity). Under no conditions is the metal chromium stable in contact with Na<sub>2</sub>SO<sub>4</sub> at 1200 K (927<sup>0</sup>C) (Rapp, 1986).

### 2.2.6.2 Vanadate Solution Chemistry

Vanadium is a transition element that may exist in various oxidation states, with + 5 and + 4 valences, usually the most stable (Hwang and Rapp, 1989). Rapp and Goto (1981) have suggested that the presence of such multivalent transition metal ions in a fused salt deposit could greatly accelerate the hot corrosion rate either by counterdiffusion of the multivalent cations or else by electron hopping, which would provide the fast transport of charge through the salt film.

The phase stability diagram for the Na-V-S-O system at 900<sup>0</sup>C reported by Hwang and Rapp (1989) has been shown in Fig. 2.8. The dashed lines present the isoactivity lines for the vanadate species in the salt solution. They determined the dependence of the equilibrium concentrations of various vanadate solutes in the sodium sulphate-vanadate solutions on the melt basicity by considering following equilibrium reactions:

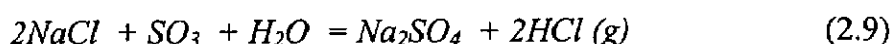


The equilibrium concentration of each vanadium compound varies continuously with melt basicity. Na<sub>3</sub>VO<sub>4</sub> is the dominant component in the melt at basicity less than 8.2 and

$V_2O_5$  is dominant at basicity greater than 16.3. For basicities between 8.2 and 16.3,  $NaVO_3$  is the most important vanadium solute (Hwang and Rapp, 1989).

### 2.2.6.3 Chemistry of salts in combustion of Coal/Fuel Oils

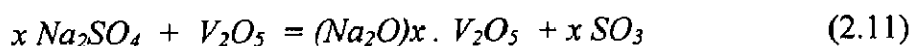
According to Khanna and Jha (1998), the sulphur present in coal and fuel oils yields  $SO_2$  on combustion which is partially oxidised to  $SO_3$ . The  $NaCl$  (either as impurities in the fuel or in the air) reacts with  $SO_3$  and water vapour at combustion temperatures to yield  $Na_2SO_4$  as below:



Pure  $Na_2SO_4$  has a melting point of  $884^\circ C$ , but with the dissolved salts, e.g.  $NaCl$  or other metal sulphates, its melting point is lowered.  $Na_2SO_4$  is deposited on metal/alloy surfaces, and at lower temperatures  $Na_2SO_4$  can further react with  $SO_3$  to form sodium pyrosulphate,  $Na_2S_2O_7$ , with a melting point of  $401^\circ C$ .



Small amount of vanadium (V) may also present in fuel oils which on combustion forms  $V_2O_5$ . This may further react with  $Na_2SO_4$  to form low melting sodium vanadates which are highly corrosive:



Thus, metals and alloys in combustion gases are exposed to various corrosives such as  $O_2$ ,  $SO_2/SO_3$ , molten salts, e.g.  $Na_2SO_4$  or sulphate mixtures, sodium vanadates,  $NaCl$  etc. (Khanna and Jha, 1998).

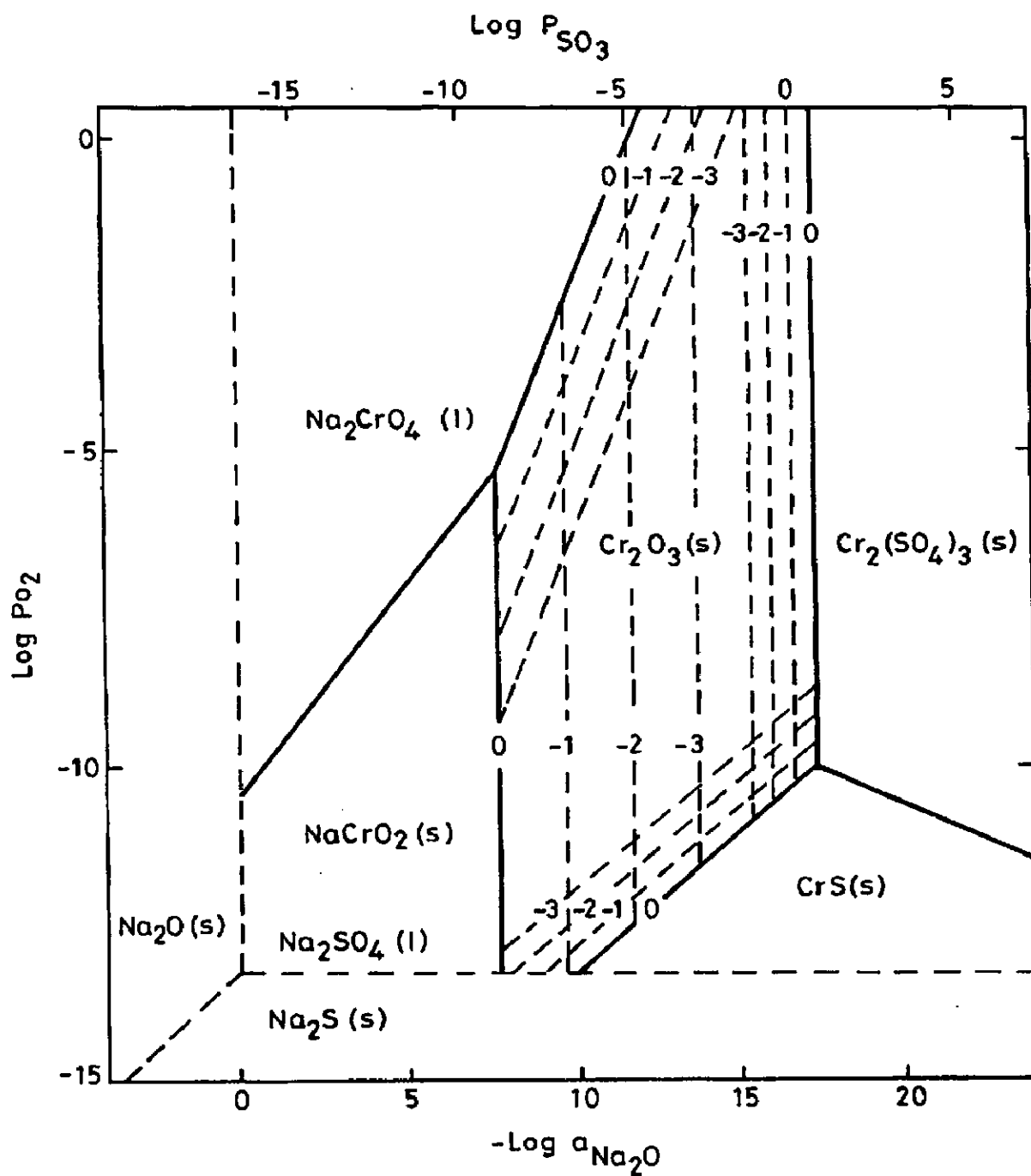
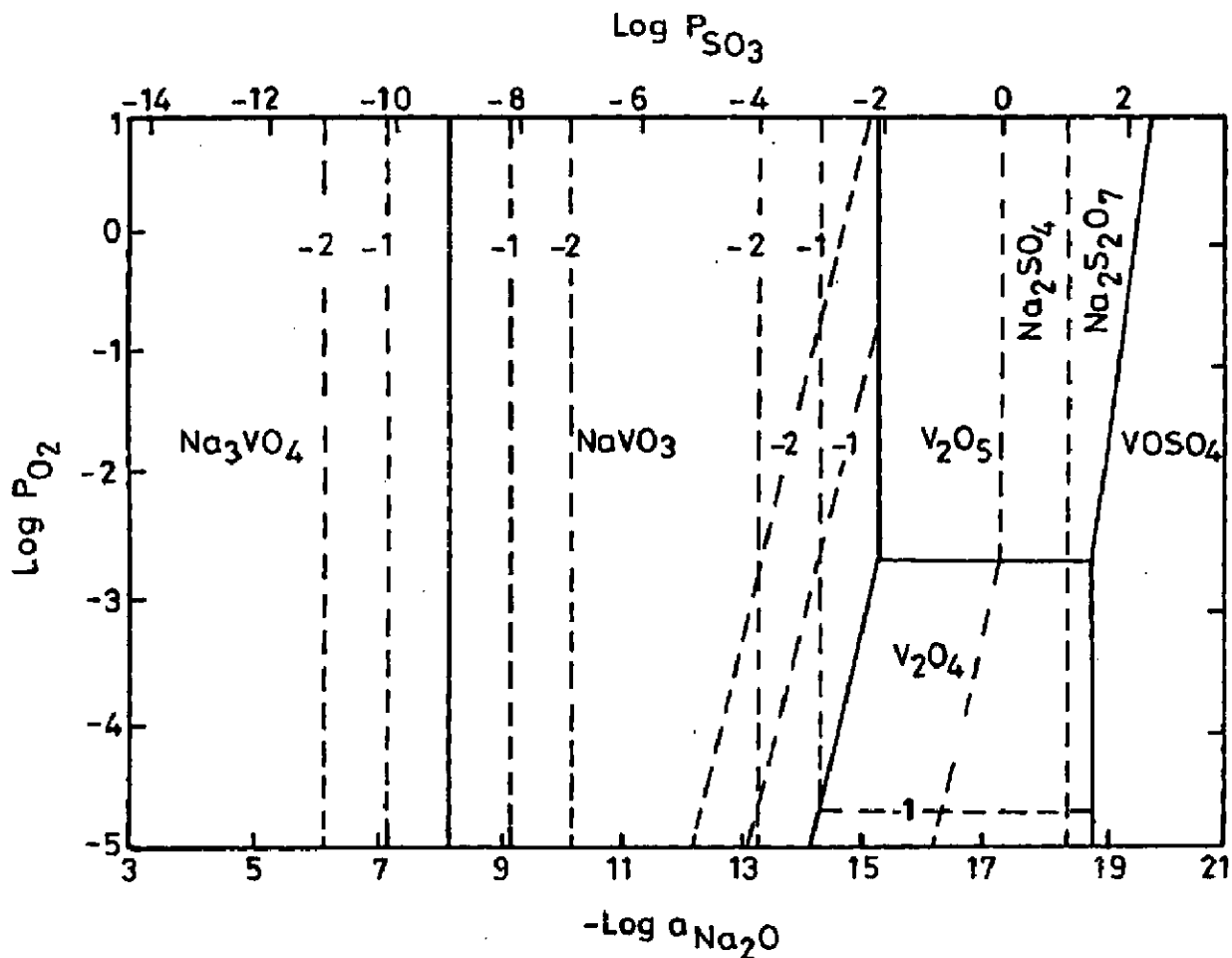


Fig. 2.7: Na-Cr-S-O phase stability diagram for 1200 K (Rapp, 1986).



**Fig. 2.8:** Phase stability diagram for Na-V-S-O system at 900 °C (Hwang and Rapp, 1989).

### 2.3 STUDIES ON $\text{Na}_2\text{SO}_4$ - $\text{V}_2\text{O}_5$ INDUCED HOT CORROSION

Kolta et al, (1972) have studied the kinetics of the reactions between  $\text{Na}_2\text{SO}_4$  (X) and  $\text{V}_2\text{O}_5$  (Y) and reported that the rate of reaction depended both on the temperature (600-1300°C) and the molar ratios of X: Y. They found that with increase in the reaction period (>30 min.), there was decrease in reaction rate which finally reached to zero order. This decrease in the reaction rate has been attributed to the formation of vanadosulphate complexes such as  $(\text{NaV}_3\text{O}_8)_2 \cdot \text{Na}_2\text{SO}_4$  and  $(\text{NaVO}_3)_2 \cdot \text{Na}_2\text{SO}_4$  which get decomposed at higher temperatures giving the meta- and pyro-vanadates respectively.

According to Otero et al, (1987),  $\text{Na}_2\text{SO}_4$ -60% $\text{V}_2\text{O}_5$  deposit was detected on a number of components in actual service which were operated at high temperature and were in contact

with high-temperature gases from combustion of fuels, containing certain amounts of impurities, i.e. Na, V, S etc. The presence of sulphur and its oxidised compounds were reported to favour the formation of isolated lobes with radial morphology having great permeability to facilitate the access of oxygen, which further led to reduction in the protective character of scale. The presence of vanadium and its oxidised products was observed to generate compounds with aciculate morphology, identified to look like alkaline vanadate complexes. These aciculated shapes further contribute to reduce the protective character of the scale. The equilibrium diagram for  $\text{Na}_2\text{SO}_4\text{-V}_2\text{O}_5$  is shown in Fig. 2.9 and the mixture of  $\text{Na}_2\text{SO}_4\text{-60\%V}_2\text{O}_5$  is seen to be the lowest eutectic temperature.

According to Kofstad (1988), during combustion, the vanadium contaminants are oxidized to the higher valence vanadium oxides ( $\text{V}_2\text{O}_4$  and  $\text{V}_2\text{O}_5$ ) and sodium vanadates are formed by the reaction of vanadium oxides and sodium salts, e.g.  $\text{Na}_2\text{SO}_4$ . The composition of the vanadates may be presented in a simplified form as  $(\text{Na}_2\text{O})_x\text{V}_2\text{O}_5$ , but the detailed compositions of the individual vanadates may be more complex as part of the vanadium may be in the +IV state. The solid compounds comprise  $(\text{Na}_2\text{O})_x\text{V}_2\text{O}_4(\text{V}_2\text{O}_5)_{12-x}$  (often termed  $\beta$  bronze),  $(\text{Na}_2\text{O})_5(\text{V}_2\text{O}_4)_x(\text{V}_2\text{O}_5)_{12-x}$  ( $K$  bronze),  $\text{NaVO}_3$  (sodium metavanadate),  $\text{Na}_4\text{V}_2\text{O}_7$  (sodium pyrovanadate) and  $\text{Na}_3\text{VO}_4$  (sodium orthovanadate). A notable feature of the vanadates is that they have relatively low melting points, which extend from  $535^\circ\text{C}$  upwards. Furthermore, metal oxides dissolved in the vanadates may suppress the melting points and eutectic temperatures even further. He further reported that the slags developed on valves in diesel engines consist predominantly of sodium sulphate and sodium vanadates and have a melting points as low as  $400^\circ\text{C}$ .

Molten vanadates flux is oxide ceramics and its solubilities of metal oxides may be high and are dependent on the Na:V ratio. The solubilities of  $\text{Cr}_2\text{O}_3$  and  $\text{Fe}_2\text{O}_3$  are highest at Na:V ratios close to 5:12 and it is about 50 mol.%. For  $\text{NiO}$ , the solubility is about 60 mol. % for Na : V = 3 : 2 and decreases to about 55 mol.% for Na : V = 5 : 12. As  $\text{V}_2\text{O}_5$  is acidic, it will in general react with more basic oxides to form the corresponding vanadates. Gonzalez-Rodriguez et al (2006) have evaluated the corrosion resistance of three heat resistant alloys (Fe-Cr-Ni) in molten vanadium pentaoxide ( $\text{V}_2\text{O}_5$ ), sodium sulphate ( $\text{Na}_2\text{SO}_4$ ), and 80(mol%)  $\text{V}_2\text{O}_5\text{-20Na}_2\text{SO}_4$  at 600, 700 and  $800^\circ\text{C}$ , respectively, and 800, 900 and  $1000^\circ\text{C}$  for  $\text{Na}_2\text{SO}_4$ . They reported that vanadium compounds such as  $\text{Na}_2\text{O.V}_2\text{O}_4.\text{V}_2\text{O}_5$  and  $5\text{Na}_2\text{O.V}_2\text{O}_4.11\text{V}_2\text{O}_5$  as one of the most aggressive corrosion products and presence of these compounds will increase the corrosiveness of the salt.



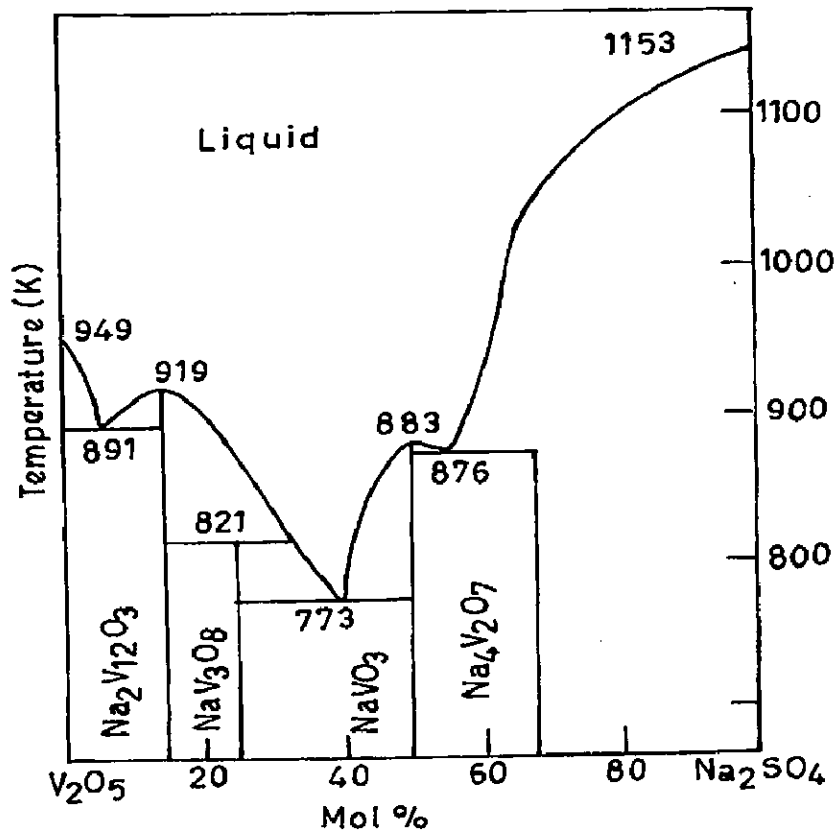


Fig. 2.9: Phase Diagram for Na<sub>2</sub>SO<sub>4</sub>-V<sub>2</sub>O<sub>5</sub> System (Otero et al, 1987)

## 2.4 HOT CORROSION STUDIES IN ENERGY GENERATION SYSTEMS

The use of residual fuel oil refinery furnaces, boilers and gas turbines is limited by the severe degradation of materials. Residual fuel oil contains sodium and sulphur as impurities, which form compounds such as Na<sub>2</sub>SO<sub>4</sub>, V<sub>2</sub>O<sub>5</sub> and complex vanadates by reaction in the combustion systems. These compounds deposit on the surface of the materials and induce accelerated attack generally known as hot corrosion (Deb et al, 1996).

An extensive review on fuel ash corrosion was made by Srivastava et al, (1997). They reported that the fuel ash corrosion of boilers and super-heater tubes is a matter of great concern since it affects the performance of thermal power stations by lowering their efficiency to significantly below the anticipated level. The dangers of corrosion, in a conventional steam power plant, limit the temperature of the super-heat and recovery of low grade energy from the flue gases; this usually prevents any further gain in thermodynamic efficiency of the system. Further, they reported that sulphidation kinetics are several orders of magnitude higher than oxidation rates because of the higher diffusivity of sulphides in iron based alloys.

The failure of wall tubes and superheater has been frequently blamed on alkali-pyrosulphates ( $\text{Na}_2\text{S}_2\text{O}_7$  and  $\text{K}_2\text{S}_2\text{O}_7$ ) which have a high chemical activity towards metal. While sulphates are implicated in providing a molten film on moderate to high temperature metallic surfaces, causing eventually metal wastage and corrosion; the pyrosulphate ( $\text{K}_2\text{S}_2\text{O}_7$ ) exists in boiler furnaces only at temperatures upto about 783 K and  $\text{Na}_2\text{S}_2\text{O}_7$  upto about 673 K. Neither of these compounds is likely to exist as deposits on superheaters, where there is insufficient  $\text{SO}_3$  (Krisch, 1963).

Otsuka (2002) has reported that for boiler tubes suffering severe fireside corrosion, sulphate and chloride salts concentrate at the deposit/scale interface, and become partially fused since these salts contain alkali metals of sodium and potassium. For boilers burning dirty oil, vanadium in the fuel condenses as  $\text{V}_2\text{O}_5$  on tube surface to form low melting point, oxygen fast-diffusing, fused salt film. Condensation/accumulation of low melting-point salts from flue-gas on tube surface is considered a root cause for the severe wastage of tube materials, since salts containing chlorides and sulphates of sodium and potassium, and of vanadium oxides in some cases, easily liquefy at the operating metal temperatures. In most cases, hot corrosion caused predominantly by low melting-point fused salts in the slag deposits.

Boilers and other steam power plant equipments are subjected to a wide variety of failures involving one or more of several mechanisms. Overheating is reported to be the main cause of failure in steam generators. A survey compiled (Metals Handbook, 1975) over a period of 12 years, encompassing 413 investigations, listed overheating as the cause in 201 failures or 48.7% of those investigated. Fatigue and corrosion fatigue were listed as the next most common causes of failure accounting for 89 failures or 21.5%. Corrosion, stress corrosion and hydrogen embrittlement caused a total of 68 failures or 16.5%. Defective or improper material has been cited as the cause of most of the remaining failures (13.3%). Although "defective material" is often blamed for a failure but this survey indicates that statistically, it is one of the least likely causes of failure in power plant equipments

Sidhu et al, (2006A) have studied the hot corrosion behaviour of high velocity-oxy fuel (HVOF) sprayed NiCrBSi and Stellite-6 coatings on a nickel-based superalloy in an actual industrial environment of a coal fired boiler. The cyclic studies were performed in the platen superheater zone of a coal fired boiler where the temperature was around 900 °C for 1000 hours duration. They reported that Stellite-6 coating found to be effective in imparting better hot corrosion resistance on nickel based superalloy in the coal fired boiler environment due to the formation of oxides of chromium and cobalt, and spinels of cobalt–chromium ( $\text{CoCr}_2\text{O}_4$ ) and nickel–chromium ( $\text{NiCr}_2\text{O}_4$ ). Furthermore, they have also reported that the

better hot corrosion resistance of the Ni- 20Cr wire coated alloy in the coal fired boiler environment is mainly attributed to the formation of a thick band of chromium oxide just above the scale–substrate interface and chromium oxide stringers along the splat boundaries, as well as to the nickel oxide and the dense and uniform fine grain structure of the as sprayed coating (Sidhu et al, 2006B).

Buta and Prakash (2006) have investigated the erosion-corrosion behaviour of plasma as sprayed and laser remelted Stellite-6 coatings on boiler tube steels (GrA1, T11 and T22) in the actual coal fired boiler environment at 755°C for 1000 hours. They observed that the coated steels were found to possess higher resistance to erosion-corrosion than the uncoated steels. The highest degradation resistance of coated T11 steel coated and subsequently laser remelted coatings are due to the presence of thick and continuous layer of chromium at the bond coat-substrate interface.

Zhao S, et al (2005A) studied the corrosion of a nickel-based superalloy, INCONEL alloy 740, at 550 and 700°C using a simulated pulverized coal-fired environment as coal ash plus flue gas. They reported the formation of thin oxide scale on the samples corroded at 550 °C. The hot corrosion, which was characterized by a pitting attack with no internal sulphidation and alloy depletion resulted from sulphidation mechanism. They further reported that the hot corrosion of the alloy at 700 °C consisted of two stages. The oxidation and sulphidation of alloy took place in the initial stage, during which the fluxing of oxide scale did not occur. Due to the oxidation of cobalt on the surface of oxide scale, the hot corrosion proceeded to the propagation stage during which stable  $\text{CoSO}_4$  melt formed by inward migration of  $\text{SO}_3$  and the outward migration of cobalt, and the internal sulphidation reaction proceeded as well.

Prakash et al, (2001) reported a case study on boiler tube failure in the coal fired power plants in north-western region of India, covering a period of one year. . They described that total 89 failures occurred in the study period, out of which 50 failures were attributed to the hot corrosion and erosion by ash. They further investigated five samples of failed boiler tubes selected randomly from the same installation. They found overheating as another main cause of tube failures.

## **2.5 PREVENTIVE MEASURES AGAINST HOT CORROSION**

Preventive measures against metal losses and failures due to corrosion should be economically devised to ensure safety and reliability in the use of metallic components.

Resistance to high temperature corrosion of metals/alloys can be achieved by the establishment and maintenance of an impervious, stable, inert, adherent, protective layer on the substrate during the service period. (Chatterjee et al, 2001).

The corrosion control in highly aggressive applications requires careful selection of materials. Nickel-based superalloys exhibit good mechanical properties and superior corrosion resistance at higher temperatures and are used as base materials for many hot components. However, the hot corrosion is inevitable when these alloys are used at higher temperatures for longer periods of time in an extreme environment (Goebel et al, 1973; Sims, 1987).

Although corrosion problems cannot be completely remedied, it is estimated that corrosion-related costs can be reduced by more than 30% with development and use of better corrosion control technologies. Corrosion control measures include corrosion inhibitors, cathodic protection, and coatings (Priyantha et al, 2003). Heath et al, (1997) have suggested the number of countermeasures to control the excessive material damage in variety of corrosive environments including proper alloy selection, optimum design of components, injecting chemical additives, shielding of substrates and protective coatings. Eliaz et al, (2002) have also suggested that hot corrosion of gas turbine components could be controlled by employing proper selection of structural alloys, application of coatings, washing of hot parts, air filtering and control of both fuel cleanliness and composition. Rajan and Zhou (2004) suggested that the application of a surface engineering technique is the most appropriate method to further enhance the corrosion resistance.

## **2.6 PROTECTIVE COATINGS**

A coating can be defined as a layer of material, formed naturally or synthetically or deposited artificially on the surface of an object made of another material, with the aim of obtaining required technical or decorative properties (Burakowski and Wierzchon, 1999). Surface coatings are one of the cost-effective approaches against surface failure. In the last few decades, development of protective coatings has become an active area in the field of materials engineering (Wang and Chen, 2003). In a wide variety of applications, materials have to operate under severe conditions such as erosion, corrosion and oxidation at higher temperature in hostile chemical environments. Therefore, surface modification of these components is necessary to protect them against various types of degradation (Pawlowski, 1995). Coatings can be thought of as engineering solutions to enhance surfaces against wear,

corrosion, thermal degradation and other surface phenomenon. Acceptable coatings are generally characterised by good adhesion, substrate compatibility and low porosity (Handbook, Thermal Spray Tech, 2004).

Coatings provide a way of extending the limits of use of materials at the upper end of their performance capabilities by allowing the mechanical properties of the substrate materials to be maintained while protecting them against wear or corrosion by applying a protective coating (Sidky and Hocking, 1999). Coatings can add value to products upto 10 times the cost of the coating (Matthews et al, 1998). The use of hard material coatings reduces the problem of corrosion, erosion and wear of the surface in petrochemical industries (Scrivani et al, 2001). According to Sivakumar and Mordike (1989), high temperature coatings are designed to increase the life of the underlying alloy during service. Coatings also help in eliminating or reducing the critical and scarce raw materials used in the preparation of the alloys. The coating composition is selected to form the protective scale depending upon the environment it has to combat.

The hot components of gas turbines and energy systems operating in aggressive environments are subjected to different types of high temperature corrosion, including oxidation, sulphidation, carburization, chlorination, erosion and hot corrosion induced by molten salts (Streief, 1993). He suggested that high temperature coatings are mandatory to protect structural alloys and/or to extend service life of hot section components in gas turbines for both aircraft and industrial applications. According to Rhys-Jones and Swindells (1985), the most common methods used to combat hot corrosion problems in gas turbine involves the utilization of surface coatings. Gurumoorthy et al, (2007) have reported that cobalt-based Stellite-6 and Stellite-12 alloys, which have excellent resistance to wear at elevated temperature and corrosion, are extensively used for hard facing of nuclear power plant components, especially in surfacing of valves.

The desire for higher operating temperature, improved performance, extended component lives, and cleaner and more fuel-efficient power plant/processes places severe demands on the structural materials used to construct such a high-temperature plant. As a result, many components operating at high temperature within such plants are coated or surface treated (Nicholls, 2000). The demand for protective coatings has increased recently for almost all types of superalloys with improved strength, since high-temperature corrosion problem has become much more significant for these alloys with increasing operating temperatures of modern heat engines (Yoshida, 1993).

### **2.6.1 Coating Processes**

The commonly employed methods of applying metallic coatings have been enlisted in Fig. 2.10 (Bhushan and Gupta, 1991). From a production point of view, three methods are in current use, these being chemical vapour deposition (CVD), physical vapour deposition (PVD) and thermal spraying (metal spraying). A serious drawback of the pack process (CVD) is the inclusion of pack particles in the coating, which can lead to coating failure (Nicoll, 1984).

Ilavsky et al. (2000) reported that the thermally sprayed coatings have often superior properties, lower application cost and less environmental issues as compared to other industrially used coatings such as CVD, PVD, hard chromium plating. Moreover, Nicholls and Stephenson (1995) revealed that overlay coatings performed better than diffusion coatings at higher temperatures.

The current common coating deposition processes used in gas turbine engine applications are chemical vapor deposition (CVD), physical vapor deposition (PVD), thermal spraying, diffusion and electroplating. Since the CVD process is a non-line-of-sight technique, proper masking and tooling are the major design considerations and it is expensive (DeMasi-Marcin and Gupta, 1994). Pratt and Whitney initiated a program in the late 1960 to develop coatings with compositions nominally independent of substrates, and with capabilities for tailoring to the wide range of requirements of gas turbine applications (Goward, 1998).

### **2.6.2 Thermal Spray Coating Processes**

Thermal spraying is considered to have been started with the works of M.U. Schoop, who in 1910 developed a system of spraying of metallic powder using the energy of combustion. The brilliant idea of using fine atomised metallic particles for production of coatings came to Schoop when he played with his son throwing small balls of lead to the wall. Two years later, in 1912 the first system of spraying of wire was invented and this process was used for deposition of zinc coatings to increase the corrosion resistance of the substrates (Sobolev et al, 2004). The thermal spraying technologies expanded in the 1970 due to development of thermal plasmas, and the increasing demand of high temperature and wear resistant materials and coating systems (Knotek, 2001). In the 1990s, thermal spraying was highly available and had become a standard tool for improving surfaces in most industries. Thermal spraying is the application of a material (the consumable) to a substrate by melting the material into droplets and impinging the softened or molten droplets on a substrate to form a continuous coating (Budinski, 1998).

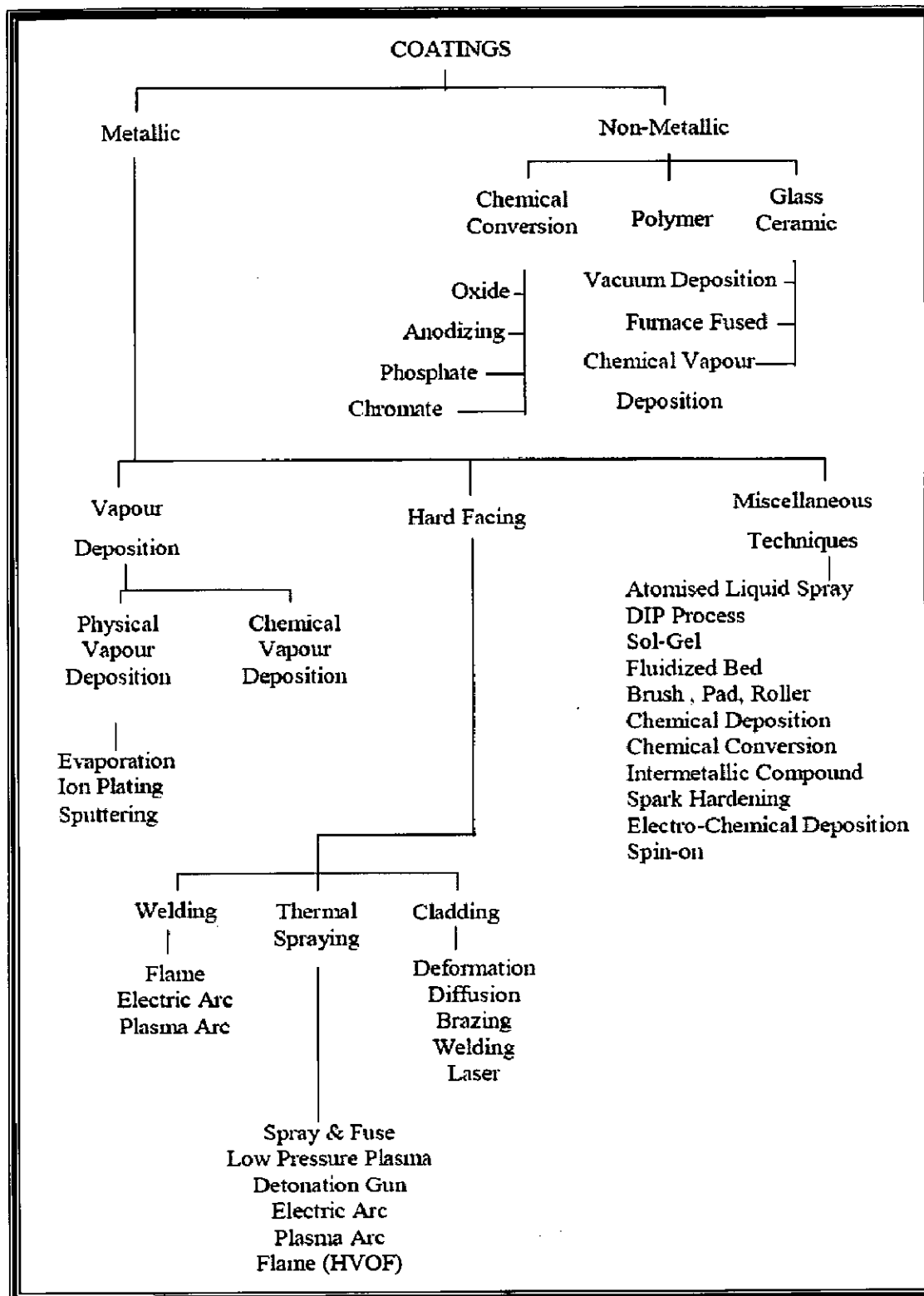


**Fig. 2.10:** Coating deposition technologies (Bhushan and Gupta, 1991).

Generally, any material which does not decompose, vaporize, sublime, or dissociate on heating, can be thermally sprayed. Consequently a large class of metallic and nonmetallic materials (metals, alloys, ceramics, cermets, and polymers) can be deposited by thermal spraying. In thermal spraying, the initial coating material (materials in the form of rod, wire, or powder) is heated, generally to a molten state and projected onto a receiving surface, known as a substrate. The use of thermal spraying ranges across many manufacturing processes, from the automotive (Nakagawa et al., 1994; Nicoll, 1994), through to the space exploration industry (Nguyentat et al, 1992). Metals, carbides and cermets are the most widely used coating materials, however the spraying of polymers has also been researched (Varacalle et al, 1996; Kawase and Nakano, 1996).

## **2.7 HIGH VELOCITY OXY-FUEL (HVOF) THERMAL SPRAYING**

High velocity oxy-fuel (HVOF) processes belong to the family of thermal spraying technologies and are capable of producing coatings with lower porosity, higher hardness, superior bond strength and less decarburization than many of the other thermal spraying methods (Pawlowski, 1995; Smith and Knight, 1995; Herman et al, 2000; Modi and Calla, 2001; Wang and Shui, 2002). The schematic cross-section of diamond jet spray gun is shown in Fig. 2.11. In HVOF spray process, powder material is melted by the use of combustion of oxygen and a fuel gas and is propelled at a high velocity by the use of compressed air, towards a surface. Propylene, propane, hydrogen, acetylene, methane, ethylene, crylene, SPRAL 29 kerosene, MAPP (methyleacetylene-propadiene-stabilised gas), LPG etc. are used as combustion fuels. In the combustion zone, the powder material enters the flame, where it becomes molten or semi-molten, depending on the melting temperature and the feed rate of the material. During HVOF spraying, hypersonic gas velocities of about  $1800 \text{ ms}^{-1}$  and the flame temperature of above  $2800^\circ\text{C}$  are achieved. The high kinetic energy of the powder particles in HVOF spray process results in the deposition of high quality coatings (Sobolev et al, 2004). The main advantage of HVOF process is the shorter residence time in the flame and the higher kinetic energy of the particles impacting. This produces a dense coating with less degradation of the powder during spraying (Nicholls, 2000).



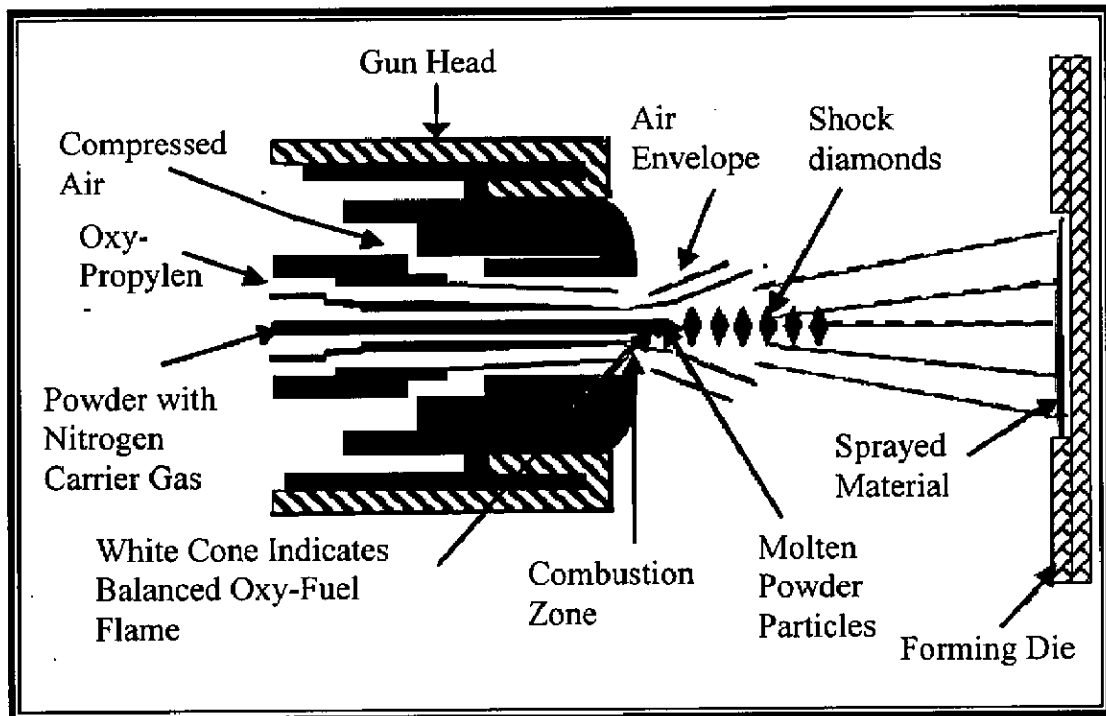


**Fig. 2.11:** Schematic cross-section of diamond jet spray gun (Stokes & Looney, 2001).

The main characteristics of HVOF spraying compared to plasma spraying are associated with higher particle velocities and lower temperatures of the powder particles (Sobolev et al, 2004). The HVOF coatings are widely used in various engineering components for combating wear and corrosion including propellers, pump impellers and casings, super-heaters and pre-heaters of boilers, valve bodies/trim and pipe systems (Tan et al, 2005). The important characteristics associated with these thermal spray techniques are reported in Table 2.1 (Bhushan and Gupta, 1991; Sobolev et al, 2004). Particle speed, flame temperature and spray atmosphere are the main parameters, which differentiate the various spraying techniques. Coating porosity, bond strength and oxide content are typical properties influenced by the coating procedure.

**Table 2.1:** Comparison of characteristics for various thermal spray processes (Bhushan and Gupta, 1991; Sobolev et al, 2004).

Deposition Technique	Heat source	Propellant	Material feed type	Typical temp. (°C)	Particle velocity m/s	Coating materials	Relative bond strength	Porosity level %volume
Electric Arc	Arc between electrodes	Air	Wire	6000	240	Ductile materials	Good	8-15
Plasma Arc Spraying	Plasma Arc	Inert Gas	Powder	16000	120-600	Metallic, ceramic, plastic and compounds	Very Good to Excellent	2-5
Low Pressure Plasma Spraying	Plasma Arc	Inert Gas	Powder	16000	900	Metallic, ceramic, plastic and compounds	Excellent	<5
Spray & Fuse	-	-	Powder	-	-	Fusible metals	Excellent	<0.5
Flame Spraying	Oxyacetylene/ Oxyhydrogen	Air	Powder	3000	30-120	Metallic and ceramics	Fair	10-20
Detonation Gun Spraying	Oxygen/ Acetylene/ Nitrogen Gas Detonation	Detonation Shock Waves	Powder	4500	800	Metallic, ceramic, plastic and compounds	Excellent	0.1 to 1
High Velocity Oxy-fuel (HVOF)	Oxy-propylene/ hydrogen/ propane/ LPG	Combustion Jet	Powder/wire	3000	800	Metallic and ceramic	Excellent	0.1-2

## 2.8 SPUTTERING PROCESS

Sputtering is a momentum transfer process in which a fast ion (e.g.  $Ar^+$ ) collides with an atom from a cathode surface and sputters it out towards a substrate (Sidky and Hocking, 1999). The process deposits thin, adherent films, usually of metal, in a plasma environment on virtually any substrate. Sputtering is the only deposition method that does not depend on melting points and vapour pressures of refractory compounds such as carbides, nitrides, silicides, and borides. As a result, films of these materials can be sputtered directly onto

surfaces without altering substrate properties. Sputtering process can be divided into four major categories namely, DC, AC (mostly RF), reactive and magnetron. The sputtering processes are basically configured as planar diodes with facing anode and cathode electrodes as shown in Fig. 2.12 (Ohring, 2002).

### **2.8.1 Magnetron Sputtering Process**

Magnetron sputtering is a powerful and flexible technique which can be used to coat virtually any workpiece with a wide range of materials - any solid metal or alloy and a variety of compounds (Ohring, 2002). Magnetron sputtering creates fields which cause the electrons (emitted from the cathode) to follow long helical paths which results in many more collisions with the argon gas atoms and so generate many more  $\text{Ar}^+$  ions for sputtering (Sidky and Hocking, 1999). Magnetron sputtering is practiced in DC, AC, and RF as well as reactive variants and has significantly enhanced the efficiency of these processes. Important implications of the process are higher deposition rates, low voltage operation than for DC sputtering, reduced operating pressures (Ohring, 2002).

Prior to the sputtering procedure, a vacuum of less than one ten millionth of an atmosphere ( $3 \times 10^{-6}$  torr) must be achieved. From this point, a closely controlled flow of an inert gas such as argon is introduced. This raises the pressure to the minimum needed to operate the magnetrons, although it is still only a few ten thousandth of atmospheric pressure. When power is supplied to a magnetron, a negative voltage of typically -300V or more is applied to the target. This negative voltage attracts positive ions to the target surface at speed. Generally, when a positive ion collides with atoms at the surface of a solid, an energy transfer occurs. If the energy transferred to a lattice site is greater than the binding energy, primary recoil atoms can be created which can collide with other atoms and distribute their energy via collision cascades. A surface atom becomes sputtered if the energy transferred to it normal to the surface is larger than about 3 times the surface binding energy (approximately equal to the heat of sublimation). The sputter process has almost no restrictions in the target materials, ranging from pure metals where a d.c.-power supply can be used to semiconductors and isolators which require a r.f.-power supply or pulsed dc. Deposition can be carried out in either non reactive (inert gas only) or reactive (inert & reactive gas) discharges with single or multi-elemental targets. Radio frequency sputtering can be used for insulators (which are unable to be sputtered by other techniques because they get charged). Electrons in the plasma

prevent charging and ion plating then occurs in the appropriate half cycles (Sidky and Hocking, 1999).

According to Smith (1995), electrons operating in the glow region acquire enough energy to cause ionizing collisions. At radio frequencies, voltage can be coupled through any kind of impedance so that the electrodes need not be conductors.

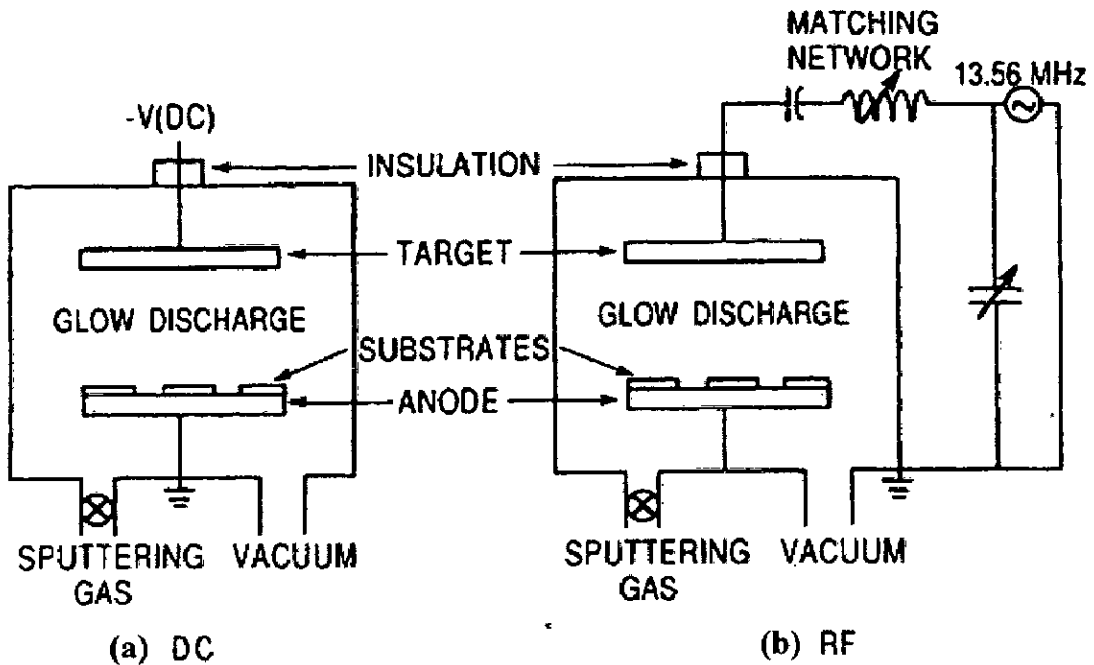


**Fig. 2.12:** Schematic of simplified sputtering systems (a) DC, (b) RF (Ohring, 2002).

### 2.8.2 Target Self-Bias

RF sputtering essentially works because the target self-biases to a negative potential. Once this happens, it behaves like a DC target where positive ion bombardment sputters away atoms for subsequent deposition. Negative target bias is a consequence of the fact that electrons are considerably more mobile than ions and have little difficulty in following the periodic change in the electric field. The disparity in electron and ion mobilities means that isolated positively charged electrodes draw more electron current than comparably isolated negatively charged electrodes draw positive ion current.

As the pulsating AC signal is applied to the target, a large initial current is drawn during the positive half of the cycle. However, only a small ion current flows during the second half of the cycle. This enables a net current averaged over a complete cycle to be different from zero, but this cannot happen because no charge can be transferred through the capacitor. Therefore the operating point on the characteristic shifts to a negative voltage, the target bias, where no net current flows (Ohring, 2002). In the present investigation, RF magnetron sputtering is used for depositing the thin films on the superalloy substrates.

## **2.9 ROLE OF METALLIC COATINGS**

At high temperatures, coatings that protect against oxidation form a compact, adherent oxide scale that provides a barrier between the high-temperature gases and the underlying metal (National Materials Advisory Board, 1996). Gurrappa (2003) suggested that the coating used at high-temperature should have a composition that will react with the environment to produce the most protective scale possible, provide corrosion resistance with long term stability and have resistance to cracking or spallation under mechanical and thermal stresses induced during operation of the components. Further, the protective oxide scale should not react with the corrosive environment and at the same time, it should not allow the corrosive species to diffuse through the coating.

High temperature coatings are used to protect many engineering components from environmental degradation. The operating temperature and the nature of the corrodant dictate the choice of the coating (Sivakumar and Mordike, 1989). Guilemany et al, (2002) have reported that in case of the metallic coatings, thicker layer provides better resistance against corrosion. Fig.2.13 shows the types of high-temperature attack for metallic coatings (aluminide, chromide, MCrAlY, etc.) on nickel-base superalloys with approximate temperature regimes and severity of attack (National Materials Advisory Board, 1996).

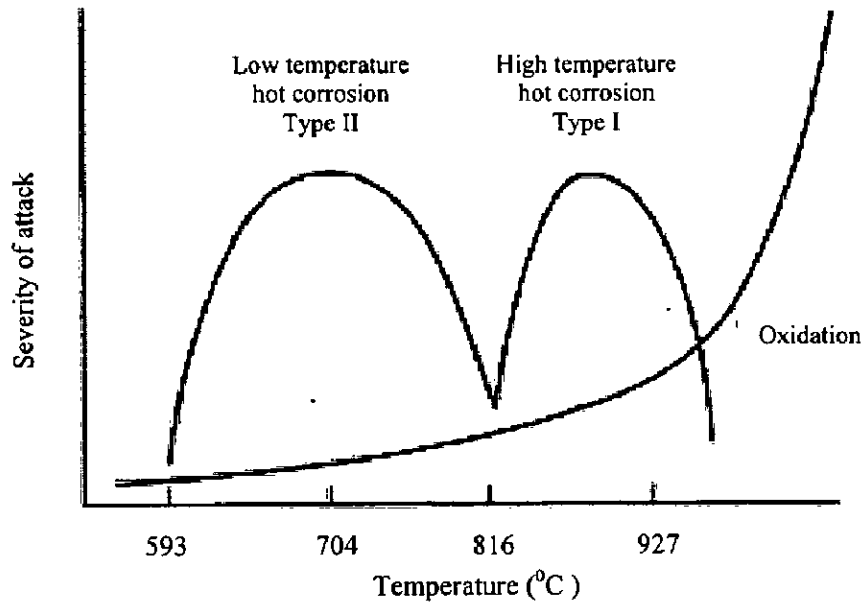


**Fig. 2.13:** Types of high-temperature attack for metallic coatings (aluminide, chromide, MCrAlY, etc.) on nickel-base superalloys with approximate temperature regimes and severity of attack (National Materials Advisory Board, 1996).

## 2. 10 PROBLEM FORMULATION

### 2.10.1 Scope

Power plants are one of the major industries which encounter severe corrosion problems resulting in the substantial losses. The problem is becoming more prominent as the plants are getting older. The super-heater and re-heaters tubes of the steam generating system are subjected to fireside corrosion, resulting in tube wall thinning and premature failure. Protective coatings are used to decrease maintenance costs of these components. Hot corrosion degradation of materials has also been identified as a serious problem in other high-temperature applications such as in waste incinerations, diesel engines, gas turbines, coal gasification plants, and chemical plants etc.

The combustion of coal generates very corrosive media particularly near the super-heater tubes (Weulersse-mouturat et al, 2004). For boiler tubes suffering from severe fire-side corrosion, sulphate salts concentrate at the deposit/scale interface and become partially fused because these salts contain alkali metals of sodium and potassium. Condensation/accumulation of low melting-point salts from flue gas on tube surface is considered a root cause for the severe wastage of tube materials (Otsuka, 2002).

Ni- and Fe- based superalloys are used in the high temperature applications such as gas turbine parts, aviation and industrial springs, steam boilers, furnace equipments etc. Although the superalloys have adequate mechanical strength for such high temperature applications, yet they are prone to degradation by high temperature oxidation/corrosion during long term exposures. Chatterjee et al, (2001) have reported that, in general, the behaviour of the protective coatings in environments of their use and its interactions with the substrate during high-temperature performance is not well understood. Uusitalo et al, (2003) have also suggested that there is a need to investigate the high-temperature corrosion behaviour of the thermal spray coated materials in different aggressive environments.

Therefore, the superalloys need to be protected, but the protection system must be practical, reliable and economically viable. It is reported in the literature that hot corrosion problem could be arrested through some preventive measures; prominent among them being controlling process parameters, use of inhibitors, application of protective coatings etc. Further, the use of inhibitors is not easily viable due to practical implications in injecting these inhibitors along with the fuel in the combustion chamber in an actual industrial environment (Tiwari and Prakash, 1998 and Gitanjaly et al, 2002). In this regard, use of the protective coatings has been identified as a potential area for the present research.

In an earlier work conducted by Buta Singh (2003) in our department, laser remelting of the plasma sprayed coatings was attempted to eliminate the porosity of the coatings. However, he observed that these laser remelted coatings showed slightly inferior hot corrosion resistance in molten salt environment as compared to the as coated samples. This behaviour was attributed to the presence of vertical cracks in the laser remelted samples after exposure to hot corrosion, through which the oxidising environment could reach the substrate steels. Harpreet Singh (2005A) has studied oxidation behaviour of plasma sprayed NiCrAlY, Ni-20Cr, Stellite-6 and Ni<sub>3</sub>Al coatings on Ni- and Fe-based superalloys and in all the cases, NiCrAlY was used as a bond coat. He reported that NiCrAlY coating on Fe-based superalloy has provided the best protection in both air and molten salt environment. Sidhu T S., (2006) has studied the hot corrosion behaviour of HVOF sprayed coatings in the laboratory as well as in actual industrial boiler environment and concluded that Ni-20Cr coating provided highest protection; whereas, Stellite-6 coating provided the least resistance to the molten salt environment in the laboratory. In case of industrial environment, he reported that Ni-20Cr showed a better resistance and the least resistance was observed in case of Cr<sub>3</sub>C<sub>2</sub>-NiCr coatings. He further explained that the high chromium content in Cr<sub>3</sub>C<sub>2</sub>-NiCr coating resulted in the formation of thick network of chromium oxide around the nickel rich splats and

responsible for spallation and disintegration of the coating due to the difference in coefficient of thermal expansion of oxide scale, the coating and the substrate.

### **2.10.2 Aim**

In the present investigation, an attempt has been made to comparatively evaluate the high temperature oxidation and hot corrosion behaviour of HVOF sprayed Ni-5Al, NiCrAl and NiCrAlY-0.4wt%CeO<sub>2</sub> coatings and RF magnetron sputtered Ni-Al and NiCrAl films on Ni- and Fe-based superalloys. Numerous research workers have reported the inter-diffusion of the elements between the coating and the substrate during the high temperature exposures (Smeggil and Bornstein, 1983; Buta Singh, 2003; Sundararajan et al, 2004A; Prakash et al, 2005; Harpreet Singh et al, 2005C and 2005D; Xiao et al, 2006).

It is well known in the literature that the Ni-based coatings are used in applications where wear resistance combined with oxidation or hot corrosion resistance are required (Edris et al, 1997; Knight and Smith, 1992). Ni-5Al, NiCrAl coatings are widely used as bond coat between the substrate and top coating as it exhibit good oxidation and abrasion resistance at high temperatures. NiCrAlY coating is widely used as bond coat for thermal barrier coatings and also as overlay coatings for high temperature applications. Literature is scarce on oxidation in air and hot corrosion in molten salt environment of the aforementioned coatings. Therefore, a thorough investigation of the hot corrosion behaviour of the coatings in different environments as well as in actual boiler environment is envisaged in the present work.

According to Shifler (2004), the high-temperature coatings on various superalloy substrates behaved differently during 1000 hours of exposure in a Type I hot corrosion environment at 899°C. He further reported that differences in chemical compositions between a coating and a substrate alloy can lead to inter-diffusion between these materials that can modify the oxidation and corrosion resistance of the coating and the mechanical properties of the coating-substrate system. He suggested that the stress state may also significantly influence and increase the magnitude of the inter-diffusion that may lead to deleterious precipitation reactions. Sundararajan et al, (2005) reported that diffusion of elements adjacent to the coating-substrate interface induces microstructural changes. Therefore, several superalloys have been chosen for the study to understand the effect of the composition of the substrate alloy on the hot corrosion behaviour of a particular coating.

An investigation of high temperature oxidation behaviour of these coatings in air and in molten salt environment at 900°C has been made in the laboratory tube furnace. It



was also decided to investigate the behaviour of bare superalloys under similar conditions of accelerated oxidation tests to predict the usefulness of the coatings by different processes. Oxidation time was selected to be 100 cycles (each cycle of 1 hour heating followed by 20 minutes cooling in air). Experiments were proposed to be conducted in a silicon tube furnace because both furnaces as well as burner rig tests are capable of reproducing the corrosion observed in service (Saunders and Nicholls, 1984). The temperature of study was kept high (900°C) as this will also take into consideration the overheating effects in case of boilers, which has been identified as the major cause of failure (Metals Handbook, 1975). Moreover, at 900°C, the rate of high temperature hot corrosion (HTHC) has been reported to be the severest shown in Fig. 2.13 (National Materials Advisory Board, 1996). In addition, the hot corrosion behaviour of coated specimens was studied in the actual industrial environment of a power plant where these coatings are intended to be used.

The hot corrosion environment selected for the present study is  $\text{Na}_2\text{SO}_4$ -60% $\text{V}_2\text{O}_5$ , which constitutes an eutectics with a low melting point of 550°C and provides a very aggressive environment for accelerated testing under simulated laboratory conditions (Tiwari, 1997). Barbooti et al, (1988) reported that sodium vanadyl vanadate ( $\text{Na}_2\text{O} \cdot \text{V}_2\text{O}_4 \cdot 5\text{V}_2\text{O}_5$ ) is the common salt deposit on boiler superheaters, which melts at a relatively low temperature 550°C. This environment will also be pertinent to the gas turbines as the predominant species in the salt deposits forming on gas turbine surfaces are  $\text{Na}_2\text{SO}_4$ ,  $\text{V}_2\text{O}_5$  and  $\text{Na}_2\text{V}_2\text{O}_6$  (Luthra & Spacil, 1982). According to Goward (1998), the corrosion in boilers and turbines is of similar kind. The testing of the coatings in air environment has been conducted, which provides useful information regarding the adhesion of the coatings and the spalling tendency of their oxide scales (Burman and Ericsson, 1983), apart from air oxidation behaviour of the coatings.

It is aimed to conduct the experiment under cyclic conditions as these conditions constitute more realistic approach towards solving the problem of metal corrosion in actual applications, where conditions are more or less cyclic, rather than isothermal (Sadique et al, 2000). Hancock and Hurst (1974) also emphasised that all potential commercial alloys should be subjected to thermal cyclic mode of testing to consider the effect of surface stresses developed due to disparity in coefficients of expansion of the base alloy, coating and oxide. Further, it could be seen from the literature survey that relatively fewer studies are reported on hot corrosion of HVOF sprayed coatings under cyclic conditions and literature is very scarce on oxidation and hot corrosion behaviour of sputtered films on superalloys.

In order to establish the performance of these coatings and bare superalloys in the actual working conditions in which they may be used, it has been planned to study the

coatings in the operational environment of the coal fired boiler at Guru Gobind Singh Super Thermal Plant, Ropar, Punjab, India. The tests have been designed to expose the coated as well as the uncoated samples for 1000 hours to the combustion environment of the coal fired boiler in the regions of low temperature superheater zone, where temperature is around 700 °C with variation of  $\pm 10$  °C. It has been aimed to conduct the study under cyclic conditions for 10 cycles, each cycle consisting of 100 hours duration heating followed by 1 hour cooling at the ambient conditions.

Thermogravimetric (weight change with time) studies were to be done under cyclic conditions in air and 40%Na<sub>2</sub>SO<sub>4</sub>-60%V<sub>2</sub>O<sub>5</sub> environments to establish the kinetics of corrosion. Standard techniques such as X-ray Diffractometer (XRD), Scanning Electron Microscope (SEM), Energy Dispersive X-ray Analysis (EDAX) and Electron Micro Probe Analyser (EPMA)/X-ray mapping analysis were used to characterise the as sprayed coating and the oxidation/corrosion products, with an attempt to understand and propose mechanisms for the high temperature corrosion.

# EXPERIMENTAL TECHNIQUES AND PROCEDURES

---

---

*This chapter presents the experimental techniques and procedures employed for deposition and characterisation of coatings, oxidation in air and hot corrosion studies and analysis of the corrosion products. Specifications of the equipments used are also incorporated.*

### 3.1 SELECTION OF SUBSTRATE MATERIALS

The substrate materials for the study have been selected after consultation with Mishra Dhatu Nigam Ltd, Hyderabad (India). The Ni-based superalloys namely Midhani Grades Superni 76 and Superni 750, and Fe-based superalloy namely Superfer 800 have been used in the present study. The alloys were procured in the rolled sheet form. The nominal composition and industrial applications of these alloys are given in Table 3.1.

### 3.2 DEVELOPMENT OF COATINGS BY HVOF PROCESS

#### 3.2.1 Preparation of Substrate Materials

The specimens with dimensions measuring approximately 20mm X 15mm X 5mm were cut from the alloy sheets. The specimens were polished with SiC papers down to 180 grit and subsequently grit blasted by alumina (Grit 45) before deposition of the coatings by HVOF spray process for developing better adhesion between the substrate and the coatings.

#### 3.2.2 Alloy Powders for Coatings

Three types of commercially available alloy powders namely Ni-5Al (MEC-1037A), NiCrAl (MEC-1047A) and NiCrAlY (H. C. Starck) were chosen for HVOF spray deposition on the three superalloy substrates. The chemical composition and particle size of all the alloy powders are reported in Table 3.2. The first two powders namely Ni-5Al and NiCrAl were supplied by HVOF gun manufacturer, Metallizing Equipments Company Private Limited, Jodhpur, India. In case of NiCrAlY alloy powder, a rare earth namely CeO<sub>2</sub> (0.4 wt %) with 99.99% purity was added and mixed in the laboratory ball mill for 6 hours to form a uniform and homogeneous mixture. Srinivas et al, (2004) have also reported the method of mechanical alloying by a ball mill to formulate Al-Cu-Fe powder. It is important to mention here that these commercial alloy powders have been selected for depositing the coatings on the superalloy substrates as the characterisation and oxidation studies of these coatings on the superalloy substrates are scarce in the literature.

**Table 3.1:** Nominal composition and industrial applications of the superalloys used

Sl. No.	Alloy Midhani Grade (Similar grade)	Chemical Composition (wt.%)													Recommended Application (Manufacturer's Catalogue)
		Fe	Ni	Cr	Ti	W	P	Al	Mo	Mn	Si	Co	C	S	
1.	Superni 76 (Hastelloy X)	19.69	Bal	21.49	-	0.6	0.005	-	9.05	0.29	0.39	1.6	0.086	0.002	Gas Turbine parts
2.	Superni 750 (Inconel X-750)	7.32	Bal	15.28	2.37	-	0.85	0.59	-	0.06	0.07	0.0	0.07	0.004	Gas turbine parts. Aviation and Industrial springs, bolts, bellows
5.	Superfer 800 (Incoloy 800)	Bal	30.8	19.5	0.44	-	-	0.34	-	1.0	0.6	-	0.10	0.006	Steam boilers, furnace equipment, heat exchangers and piping in chemical industry, reformer, baffle plates/tubes in fertilizer plants

**Table 3.2:** Composition of the alloy powders, shape and size of the particles.

Alloy powders	Chemical Composition (Wt. %)	Shape	Particle Size
Ni-5Al Powder (MEC- 1037)	95Ni-5Al	Irregular	45 $\mu$ to 90 $\mu$
NiCrAl Powder (MEC-1047)	Ni-17.92Cr-6.66Al-0.29Fe-0.66Mn-0.054C-0.90Si	Irregular	44 $\mu$ to 120 $\mu$
NiCrAlY+CeO <sub>2</sub> Powder	Ni-22.1Cr-10.4Al-1.01Y-0.4CeO <sub>2</sub>	Spherical	-45 +5 $\mu$

### 3.2.3 Formulation of The Coatings

#### 3.2.3.1 HVOF spray process

The coatings were developed in collaboration with M/S Metallizing Equipment Co. Pvt. Ltd., Jodhpur (India) with Hipojet-2100 HVOF system as shown in Fig. 3.1 using liquefied petroleum gas (LPG) as a fuel. Optimized spray parameters were used to deposit the coatings. During the deposition, the process parameters were kept constant throughout the coating process. The specimens were cooled with the compressed air jets during and after spraying. The process parameters employed during HVOF coating are presented in Table 3.3.

**Table 3.3:** Process parameters employed during HVOF coating.

Parameters	Hipojet-2100
Oxygen flow rate (m <sup>3</sup> /s)	0.0042
Fuel (LPG) flow rate (m <sup>3</sup> /s)	0.0010
Air flow rate (m <sup>3</sup> /s)	0.0010
Spray distance (mm)	200
Feed rate (gm/min)	
• Ni-5Al powder	38
• NiCrAl powder	51
• NiCrAlY- CeO <sub>2</sub>	44
Fuel pressure (N/mm <sup>2</sup> )	0.59
Oxygen Pressure (N/mm <sup>2</sup> )	0.78
Air Pressure (N/mm <sup>2</sup> )	0.59

### 3.2.3.2 RF Magnetron Sputtering Process

The thin films (Ni-Al, NiCrAl) were deposited on Ni- and Fe-based superalloys by RF magnetron sputtering process. The system used for the deposition of the films is shown in Fig. 3.2. The substrate was mirror polished and cleaned by acetone prior to the deposition of the film. The sputtering target was prepared by thermal spraying of the required powder on 50.8 mm diameter and 5 mm thick stainless steel disc. Table 3.4 show the conditions employed in this study for the deposition of the films on Ni- and Fe-based superalloys. XRD (Bruker AXS) measurements were made using  $\text{CuK}\alpha$  radiation to characterize the NiAl, NiCrAl thin films. The scan rate used was  $1^\circ/\text{min}$  and the scan range was from  $10$  to  $110^\circ$ . The grain size of the thin films was estimated from the Scherrer formula (Cullity, 1970), as given in Eq. (1).

$$D = \frac{0.9\lambda}{B\cos\theta} \quad (3.1)$$

where  $\lambda$ ,  $\theta$  and  $B$  are the X-ray wavelength ( $1.54056\text{\AA}$ ), Bragg diffraction angle and line width at half maximum, respectively. An instrumental broadening of  $0.1^\circ$  has been taken into account for the size calculations. The surface topography and microstructure were studied using scanning probe microscope (NT-MDT: NTEGRA Model) and field emission scanning electron microscopy (FESEM), respectively.

**Table 3.4:** Process parameters employed during RF magnetron sputtering process

Parameter	Condition
Substrate	Ni and Fe based superalloys
Base pressure	$3 \times 10^{-6}$ Torr
Deposition pressure	10 mTorr
RF power	190 W
Substrate temperature	$250^\circ\text{C}$
Deposition Time	2 hr 30 min.
Target to substrate distance	50 mm
Deposition atmosphere	Ar

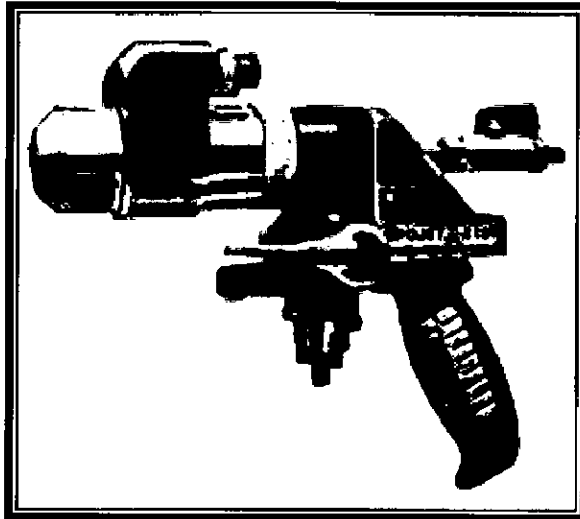


**Fig. 3.1:** HVOF system (Hipojet 2100) used in the current research work.

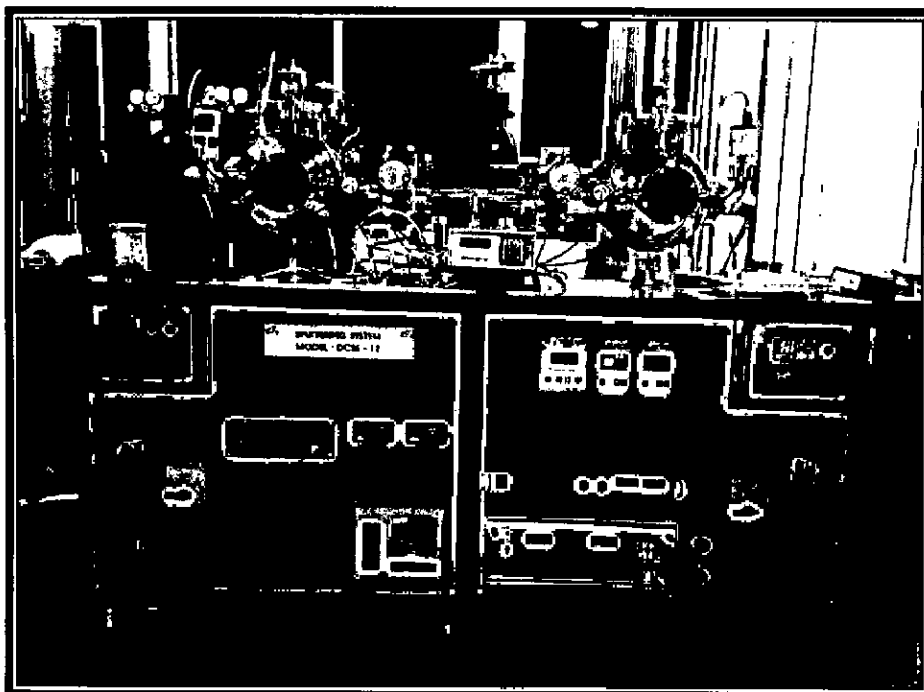


**Fig. 3.2:** RF Magnetron sputtering system used in the current research work.

### **3.3 CHARACTERISATION OF THE COATINGS**

#### **3.3.1 Specimen Preparation**

The as coated specimens were cut with a diamond cutter (Buehler's Precision Diamond Saw, Model ISOMET 1000, made in USA) across its cross-section and subsequently hot mounted in Buehler's transoptic powder (20-3400-080). Then, the mounted specimens were polished manually down to 1000 grit SiC emery papers. Finally, the specimens were mirror polished on a cloth polishing wheel machine with 0.05  $\mu\text{m}$  alumina powder suspension. The specimens were washed properly with flowing water, and dried in hot air to remove any moisture.

#### **3.3.2 Measurement of Coating Thickness**

The thickness was monitored during the process of HVOF spraying process with a Minitest-2000 thin film thickness gauge (made in Germany, precision  $\pm 1 \mu\text{m}$ ). Efforts were made to obtain the coatings with uniform thickness. The thickness of some of the as-sprayed specimens were further verified by cutting along the cross-section and mounted, as explained in Section 3.3.1. A Scanning Electron Microscope (LEO 435VP, Leo Electron Microscopy Ltd., Cambridge, UK) with an attached Robinson Back Scattered Detector (RBSD) was used for some of the specimens and also field emission scanning electron microscope (FEI Quanta 200F, Made in Czech Republic) was used to obtain the back scattered electron (BSE) images. The average coating thickness was measured from the BSE images at different locations.

#### **3.3.3 Measurement of Porosity**

The HVOF coated specimens were polished to reveal microstructure of the coatings. A Zeiss Axiovert 200MAT inverted optical microscope, fitted with imaging software Zeiss Axiovert 200 MAT Inverted Optical Microscope with AxioVision release 4.1 (Germany) was used for microstructural characterization. The porosity values of the coating were measured by processing its optical micrographs with an image analyzer in Axiovision multiphase release 4.1 software based on ASTM (American Society for Testing and Materials) B276. The computer analysis system determines the pore area size in the view field by converting the pore areas (grey-level areas) into a background colour such as red while the rest of the microstructure remains in its original colour. The area of one feature is numerically related to the total area of the picture, as the program counts the number of one colour type pixels (red) and sets that as a ratio of the total number of pixels in the picture (total area). A total of 10 images were taken on each coating at different location and the average values are reported.



### 3.3.4 Measurement of Microhardness

For obtaining microhardness of the HVOF sprayed coatings, the specimens were cut, mounted and polished as explained in section 3.3.1. The microhardness of the as sprayed coatings was measured by using Miniload 2 Microhardness Tester (Leitz, Germany) fitted with a Vickers pyramidal diamond indenter. A 15 g (147.1mN) load was applied to the indenter for penetration of as sprayed coatings. Hardness value was calculated from the relation  $Hv = 1854.4 \times \frac{F}{d^2}$  where 'F' is the load in grams and 'd' is the diameter of the indenter in micrometer. Each reported value of the microhardness is the average value of five measurements. These microhardness values are plotted as a function of distance from the coating/substrate interface in the subsequent chapters.

### 3.3.5 Measurement of Surface Roughness

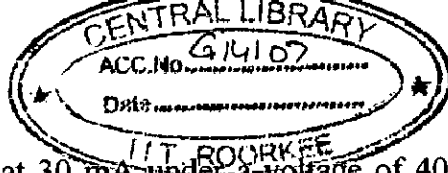
The surface roughness ( $R_a$ ) values of the HVOF sprayed as coated specimens were measured using Surface Roughness Tester (Mitutoyo SJ-201, Japan). Each reported value of surface roughness ( $R_a$ ) is the mean of five observations taken at different locations. The centre line average (CLA) method was used to obtain the  $R_a$  values. The surface roughness values are presented in following chapters

### 3.3.6 Measurement of Bond Strength

The bond strength of the HVOF sprayed coatings was tested using the ASTM standard C633-01. This test method covers the determination of the degree of adhesion (bonding strength) of a coating to a substrate or the cohesion strength of the coating in a tension normal to the surface. The test consists of coating one face of a substrate fixture, bonding this coating to the face of a loading fixture, and subjecting this assembly of coating and fixtures to a tensile load normal to the plane of the coating. A data acquisition system has continuously recorded the tensile load exerted by the machine. It is adapted particularly for testing coatings applied by thermal spray, which is defined to include the combustion flame, plasma arc, two-wire arc, high-velocity oxygen fuel, and detonation processes for spraying feedstock, which may be in the form of, wire, rod, or powder. A total of three specimens were tested and average value of the bond strength is reported.

### 3.3.7 X-Ray Diffraction (XRD) Analysis

XRD analysis was carried out for both the alloy powders as well as HVOF coated specimens to identify the various phases present on their surfaces. The X-ray diffraction patterns were obtained by a Bruker AXS D-8 Advance Diffractometer (Germany) with  $CuK_{\alpha}$



radiation and nickel filter at 30 mA under a voltage of 40 kV. The specimens were scanned with a scanning speed of 2°/min in 2 $\theta$  range of 10° to 110° and the intensities were recorded. Assuming height of the most prominent peak as 100%, the relative intensities were calculated for all the peaks. The diffractometer interfaced with Bruker DIFFRAC<sup>plus</sup> X-Ray diffraction software provides 'd' values directly on the diffraction pattern. These 'd' values were then used for identification of various phases with the help of JCPDS data cards.

### **3.3.8 Scanning Electron Microscopy (SEM) and Energy Dispersive X-ray Analysis (EDAX) Analysis**

#### **3.3.8.1 Surface Morphology/EDAX Analysis**

The surface morphologies of the alloy powders and HVOF coated specimens were studied with the help of a Scanning Electron Microscope (LEO 435VP, Leo Electron Microscopy Ltd., Cambridge, UK) and field emission scanning electron microscope (FEI Quanta 200F, Made in Czech Republic) with an aim to understand the morphology of the alloy powders and to identify inclusions, unmelted, partially melted particles and pores in the as sprayed coatings. Surface EDAX analysis of some of the samples was carried out for the coated specimens on Joel Scanning Electron Microscope (JSM-840A) fitted with EDAX attachment of Oxford ISIS300 (made in England) at Indian Institute of Science, Bangalore (India). The equipment could directly indicate the elements or phases (oxides) present at a point alongwith their compositions (weight %) based on built-in EDAX software. Most of the samples characterized using field emission scanning electron microscope (FEI Quanta 200F, Made in Czech Republic) fitted with EDAX Genesis software attachment. The EDAX genesis software directly indicates the elements or phases (oxides) present at a point alongwith their compositions (weight %). Although the compositions correspond to selected points on the as-sprayed surfaces, still the data could be useful to understand the formation of desired compositions in the coatings. The EDAX analysis was carried out at some selected points of interest on the coating structure in order to understand the formation of desired compositions in the coatings. SEM morphologies of the alloy powders and SEM/EDAX analysis for the HVOF coated specimens are reported in subsequent chapters of this thesis.

#### **3.3.8.2 Cross Sectional Analysis**

BSEI/EDAX analysis along the cross-sections of some coated specimens was carried out. The sample was prepared as explained in the section 3.3.1. The analysis was carried out using a Scanning Electron Microscope of JEOL with EDAX attachment of

Oxford (England) and also using FESEM. The back scattered electron images were taken and the EDAX analysis was performed across the cross section to ascertain elemental composition (weight %) at different points as well as to identify the presence of various elements along the cross-section of the coatings.

### **3.3.9 X-ray Mapping Analysis**

To obtain cross-sectional analysis of the different elements present in the coatings, the specimens were cut along the cross-section, mounted and polished in accordance with the procedure already discussed in section 3.3.1. The polished specimens were coated with carbon/gold before performing the X-ray mapping analysis. In this analysis, first secondary image of representative area of the specimen was recorded followed by elemental X-ray mapping of that particular area. The selected area has three regions i.e. substrate, coating and some epoxy region. X-ray mappings were obtained for all the elements of the substrate and the coatings, but only those mappings are reported which indicates the presence of some element. X-ray mapping analysis of the samples was done on field emission scanning electron microscope (FEI Company, Quanta 200F) with EDAX attachment.

## **3.4 HIGH TEMPERATURE OXIDATION AND HOT CORROSION STUDIES**

### **3.4.1 Experimental Setup**

Oxidation and hot corrosion studies were conducted at 900<sup>0</sup>C in a laboratory silicon carbide tube furnace (Digitech, India make). The furnace was calibrated to an accuracy of  $\pm 5^{\circ}\text{C}$  using Platinum/Platinum-13% Rhodium thermocouple fitted with a temperature indicator of Electromek (Model-1551 P), India. The uncoated as well as the coated specimens were polished down to 1 $\mu\text{m}$  alumina wheel cloth polishing to obtain similar condition of reaction before being subjected to corrosion run. The physical dimensions of the specimens were then recorded carefully with vernier caliper to evaluate their surface areas. Subsequently, the specimens were washed properly with acetone and dried in hot air to remove the moisture. During experimentation, the prepared specimen was kept in an alumina boat and the weight of boat and specimen was measured. The alumina boats used for the studies were pre heated at a constant temperature of 1200<sup>0</sup>C for 12 hours and it was assumed that their weight would remain constant during the course of high temperature cyclic oxidation/corrosion study. Then, the boat containing the specimen was inserted into hot zone of the furnace maintained at a temperature of 900<sup>0</sup>C. The weight of the boat loaded with the

specimen was measured after each cycle during the corrosion run, the spalled scale if any was also considered during the weight change measurements. Holding time in the furnace was one hour in still air followed by cooling at the ambient temperature for 20 minutes. Following this, weight of the boat along with specimen was measured and this constituted one cycle of the oxidation study. Electronic Balance Model CB-120 (Contech, Mumbai, India) having a sensitivity of  $10^{-3}$  g was used to conduct the thermogravimetric studies. The specimens were subjected to visual observations carefully after the end of each cycle with respect to colour or any other physical aspect of the oxide scales being formed. All oxidation and hot corrosion studies were carried out for 100 cycles. The reproducibility in the experiments was established by repeating hot corrosion experiments for five cases.

### **3.4.2 Oxidation Studies in Air**

The oxidation tests at 900°C were performed on all three base superalloys (mirror polished) as well as HVOF spray coated superalloys in laboratory furnace up to 100 cycles as discussed in section 3.4.1.

### **3.4.3 Hot Corrosion Studies in Molten Salt ( $\text{Na}_2\text{SO}_4$ -60% $\text{V}_2\text{O}_5$ )**

#### **3.4.3.1 Molten Salt Coating**

The HVOF spray coated as well as uncoated specimens (mirror polished) were prepared for studies as discussed in section 3.4.1. The specimens were then heated in an oven upto 250°C and a salt mixture of  $\text{Na}_2\text{SO}_4$ -60% $\text{V}_2\text{O}_5$  dissolved in distilled water was coated on all the surface of the warm polished specimens with the help of a camel hair brush. Amount of the salt coating was kept in the range of 3.0-5.0 mg/cm<sup>2</sup>. The salt coated specimens as well as the alumina boats were then dried in the oven for 3 hours at 100°C and weighed before being exposed to hot corrosion tests.

#### **3.4.3.2 Hot Corrosion Studies**

The uncoated as well as HVOF spray coated specimens after application of salt coating were subjected to hot corrosion in the laboratory furnace at 900°C for 100 cycles as discussed in section 3.4.1.

### **3.4.4 Studies in Industrial Environment**

The uncoated as well as HVOF coated superalloy specimens were exposed to the low temperature superheater zone of the coal fired boiler of Stage-I at Guru Gobind Singh Super Thermal Power Plant, Ropar, Punjab (India). This zone was selected for the present study as

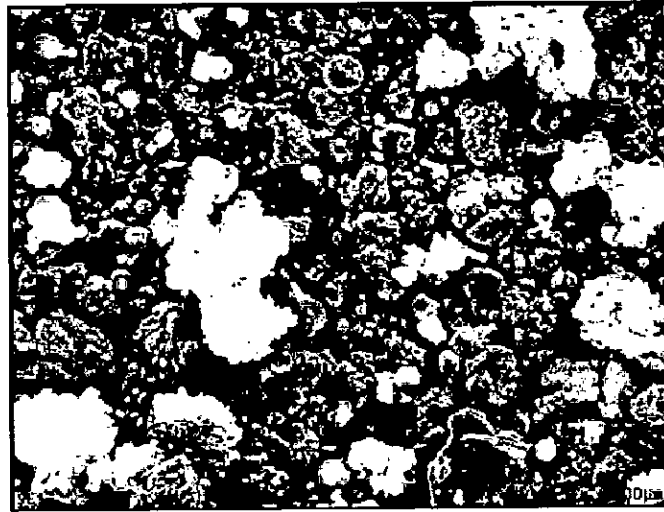
many breakdowns occurred in this power plant due to hot corrosion degradation of the superheater tubes of the coal fired boilers. A hole of 1.2 mm diameter was drilled in all the specimens to hang them in the boiler for experimentation. The coated specimens were cleaned with acetone and the uncoated specimens were polished down to 1 $\mu$ m alumina on a cloth polishing wheel machine to obtain similar conditions of reaction on the surface of all the specimens. The physical dimensions of the specimens were measured with a digital vernier caliper, to evaluate their surface areas. To measure the thickness loss during experimentations, the average thickness of each specimen (average of 10 measurements) was measured using micrometer screw gauge, before exposing them to the boiler environment. The coated as well as uncoated specimens were then hanged with the help of a stainless steel wire through the soot blower dummy points at 42 m height from the base of the boiler. The specimens were exposed to the combustion environment for 10 cycles. Each cycle consisted of 100 hours heating followed by 1 hour cooling at ambient conditions. The flue gas temperature was about 700 °C with variation of  $\pm 10$  °C and the volumetric flow of the flue gas was around 527 m<sup>3</sup>/s. The FESEM/EDAX analysis of the fly ash is shown in Fig. 3.3. After the end of each cycle, the specimens were subjected to careful visual observation for any change in the surface texture and weight of the specimens were measured subsequently using an Electronic Balance Libror AEU-210 (Japan having a sensitivity of 10<sup>-4</sup> g).

### **3.5 ANALYSIS OF CORROSION PRODUCTS OF OXIDATION IN AIR AND MOLTEN SALT**

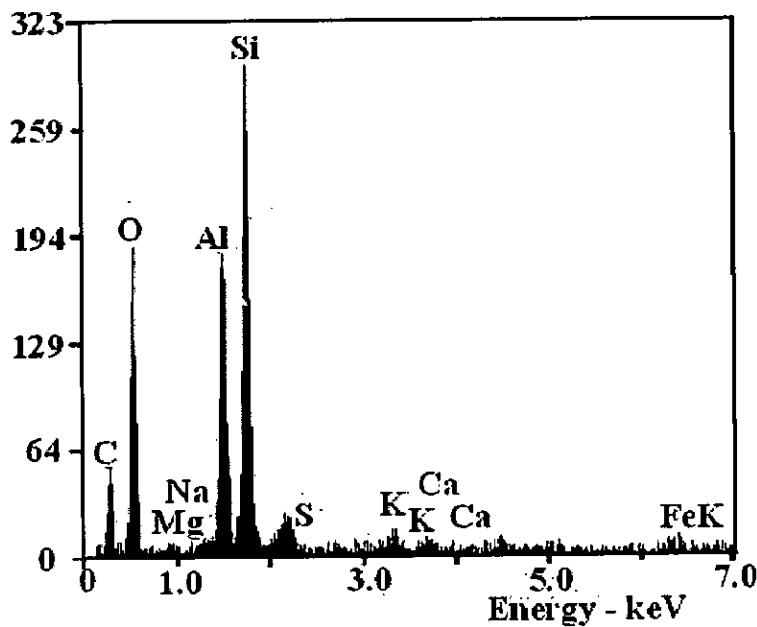
All the specimens subjected to oxidation, hot corrosion as well as in the boiler environments were analysed for the characterisation of corrosion products. The surface and the cross-section of the corroded specimens were analysed by using various analytical techniques such as XRD, FESEM/EDAX, and X-ray mapping analyses.

#### **3.5.1 Visual Observation**

Visual examination was made carefully after each cycle and changes in colour, luster, adherence-spalling tendency, and growth of cracks in the coatings/oxide scales were recorded. After the completion of 100 cycles (each cycle of 1 hr heating and 20 minutes cooling) in laboratory and 10 cycles (each cycle of 100 hr heating and 1hr cooling) in case industrial environment, the specimens were finally examined and their macrographs were taken. The physical conditions of the exposed specimens such as changes in the color, spallation, disintegration of the coating, cracks in the surface etc, if any, can be observed from the macrographs. The macrographs were obtained on a Stemi 2000C Stereo Microscope (Carl Zeiss Jena GmbH, Germany), fitted with a Sony Cyber-Shot DSC-S85 Digital Still Camera.



(a)



(b)

<i>Element</i>	<i>Wt%</i>	<i>At%</i>
<i>CK</i>	26.96	38.82
<i>OK</i>	37.21	40.22
<i>MgK</i>	00.26	00.18
<i>AlK</i>	10.43	06.69
<i>SiK</i>	19.68	12.12
<i>SK</i>	00.17	00.09
<i>KK</i>	01.05	00.46
<i>CaK</i>	00.87	00.37
<i>FeK</i>	02.61	00.81
<i>Matrix</i>	Correction	ZAF

**Fig. 3.3:** Analysis of fly ash (a) FESEM morphology and (b) EDAX compositional analysis.

### 3.5.2 Thermogravimetric Studies

The weight change values were measured at the end of each cycle to establish the kinetics of corrosion. The weight change data was plotted with respect to number of cycles for each specimen and the plots are given in the subsequent chapters. However, in case of the specimens exposed to the industrial environment, the actual working conditions of the coal fired boiler in a thermal power plant, the spalled scale could not be collected and incorporated in the mass change. In this case, the weight change consists of a weight gain owing to the

formation of the oxide scales and a weight loss due to the suspected spalling and fluxing of the oxide scales. Therefore, the net weight change in the industrial environment represents the combined effects of these two processes. The weight change data was plotted with respect to number of hours for each specimen and the plots are presented in subsequent chapters.

### **3.5.3 X-ray Diffraction (XRD) Analysis**

For identification of different phases formed in the oxides scales of oxidized/hot corroded specimens after 100 cycles in the laboratory and in actual industrial environment, X-ray diffractometer has been used as described in section 3.3.8.

### **3.5.4 SEM/EDAX Analysis**

#### **3.5.5.1 Surface Morphology**

SEM/EDAX analysis of some of the oxidized/hot corroded specimen surfaces after 100 cycles was conducted at Indian Institute of Science, Bangalore (India), and the details regarding the equipment are provided in section 3.3.9.1. The specimens were scanned under the microscope and the critical areas of interests were photographed with an aim to identify the micro cracks, voids, inclusions and surface morphology of the scale. Point analysis by EDAX was carried out on various locations on these identified areas of interest to understand composition (weight %) of various phases in the oxide scales. Although these compositions correspond to selected points on the surfaces, the data could still be useful to support the formation of various phases in the oxide scales.

#### **3.5.4.2 Cross-Sectional Morphology**

SEM/EDAX analysis for some of the selected specimens was carried out along their cross-sections using FESEM attached with genesis EDAX software. Cross-sectional BSE images were taken at some points of interest including scale/coating and substrate. The elemental composition (weight %) was carried out by EDAX analysis at various points along the cross-section. An approximate distribution of various elements across the thickness of the scales is estimated using these data. In some cases, the oxide scale thickness was also measured from these BSE images.

### **3.5.5 X-ray Mapping Analysis**

For detailed cross-sectional analysis, the specimens were cut along the cross-section, mounted and polished in accordance with the procedure already discussed in section 3.3.1 and subjected to EPMA/X-ray mapping analysis. The details regarding the EPMA/X-ray mapping equipment and preparation of the specimens have already been discussed in section 3.3.10 of this chapter.

During EPMA analysis, the specimen was moved along the cross-section and the elemental X-ray mappings were obtained for some critical area of interest on each specimen with the secondary electron image. X-ray mappings were obtained for all the elements present in the substrate, the coatings and the environment of study, but only those maps in which an element was identified in substantial concentrations have been reported in respective chapters.



# *Chapter 4*

## **Ni-5Al COATING**

---

---

*This chapter has been divided into two parts, first part presents the detailed analysis of HVOF sprayed Ni-5Al coating on Ni-and Fe-based superalloys and characterizations of coatings for the properties relevant to high temperature applications. The second part contains the detailed analysis of RF magnetron sputtered coatings on superalloys. The results of oxidation in air and hot corrosion studies for both the coatings are discussed in this chapter.*

### **4.1 MICROSTRUCTURES OF THE SUBSTRATE SUPERALLOYS**

The optical micrographs of the substrate superalloys are shown in Fig. 4.1. The microstructures of the superalloys have been explained with reference to international Standard superalloys given in Metals Handbook (1972) and ASM Handbook (1995). The microstructures of Superni 76 and Superni 750, Figs. 4.1 (a) and (b) respectively, exhibit a nickel-rich  $\gamma$ -solid solution matrix. Carbide particles are dispersed in the gamma matrix of Superni 76 and Superni 750. Twin boundaries are also visible in the structure of Superni 750 and Superfer 800 alloys. The microstructure of the Superfer 800H, Fig. 4.1(c), consists of a solid solution matrix in which some of the grains are delineated by particles of precipitated carbides at the grain boundaries and by twinning lines (Metals Handbook, 1972).

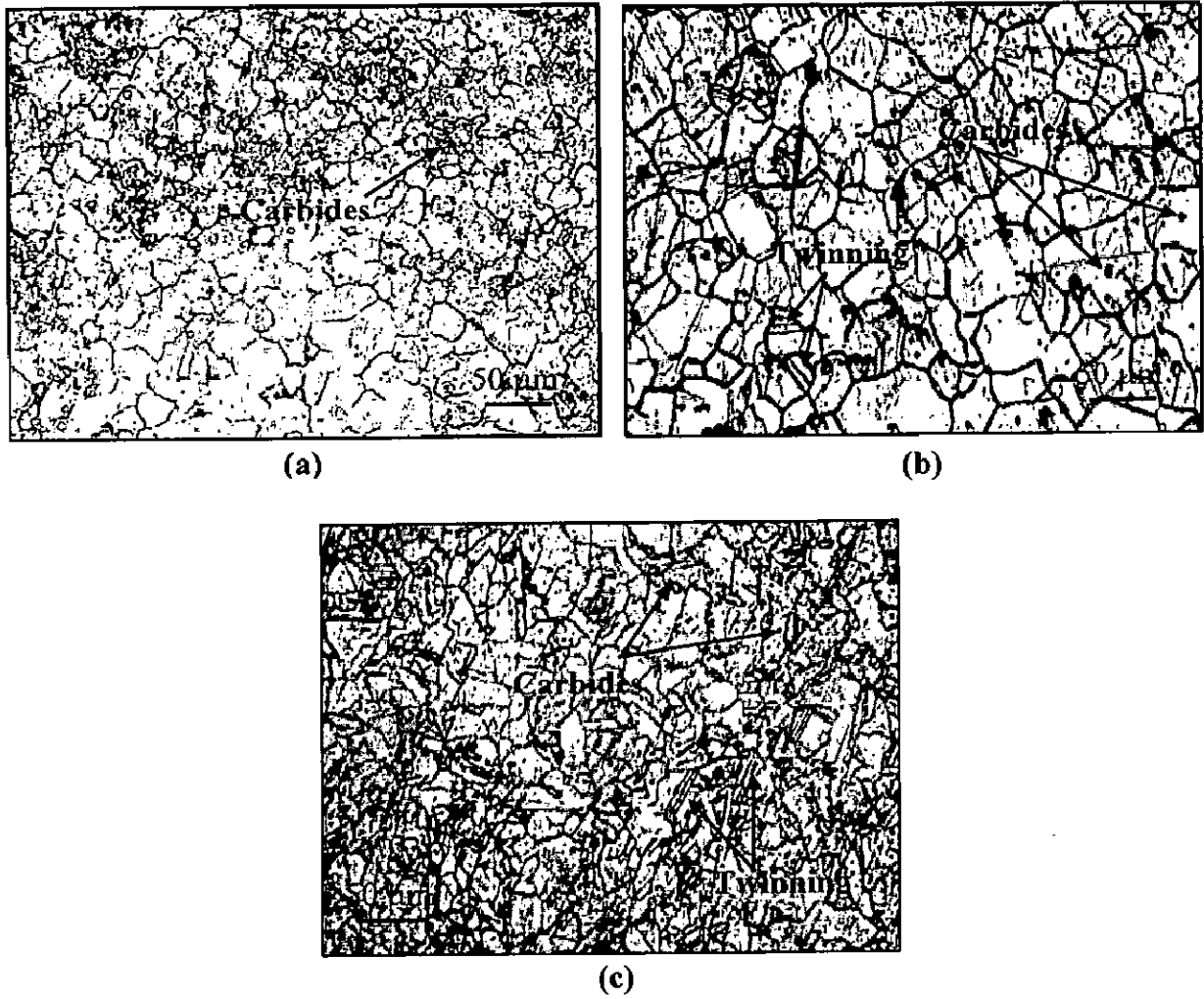


**Fig. 4.1:** Optical micrographs of the substrate superalloys  
 (a) Superni 76      (b) Superni 750      (c) Superfer 800

## **Part I – HVOF sprayed coatings**

### **4.2 CHARACTERISATION OF THE COATING**

#### **4.2.1 Introduction**

Thermal sprayed NiAl coating is widely used as bond coat between the superalloy substrate and top coating as it exhibits good oxidation and abrasion resistance at high temperatures. NiAl intermetallic compounds show excellent resistance in high temperature corrosive environments due to the formation of a continuous, compact and adherent alumina scale (Hearley et al, 2000). Ni-Al based compounds is a very promising high-temperature material owing to its high melting point (1911 K), low density (5890 kgm<sup>-3</sup>), high thermal conductivity (76Wm<sup>-1</sup>K<sup>-1</sup>) and excellent corrosion resistance at high temperatures. These features permit to use Ni–Al as a coating for high-temperature applications (Sierra and Vazquez, 2005). It is reported in the literature that that HVOF sprayed Ni-Al based coatings on steel substrates consisted of high quality contact to the surface, highly dense structure, low oxide and porosity contents (Culha et al, 2008).

It is well known in the literature that the Ni-based coatings are used in applications where wear resistance combined with oxidation or hot corrosion resistance is required (Edris et al, 1997; Knight and Smith, 1992) and also as bond coats for thermal barrier coatings (TBCs) on turbine components, as restorative layers for machine parts, as bond coats in internal combustion engine cylinders, for corrosion protection of boiler tubes and in numerous other applications requiring wear, high temperature and corrosion-resistant surfaces (Sampath et al, 2004).

Sampath et al, (2004) reported in their study on Ni-5wt%Al bond coats that thermal and kinetic energy together controlled the flattening behavior of the particles forming the splats. Further, they also observed that the elastic modulus, thermal conductivity and hardness were relatively higher in case of HVOF deposit. The properties of coatings produced from different composition of Ni-Al wire and powders and the effects of different spaying techniques have been studied extensively by various researchers (Sampath et al, 1987, Sampath et al, 2004, Khor and Loh, 1994, Geibel et al, 1996). In the recent years, several alternative thermal spray processes have evolved as a means of depositing thermal spray coatings in general and Ni-5wt%Al bond coats in particular.

High velocity oxy-fuel (HVOF) thermal spray is a well-established thermal spray technique used for depositing the coatings on materials used in the high temperature applications. The process typically involves melting the material either in the form of powder or wire, which is propelled at a higher velocity to deposit them on substrate. Due to the high impact velocity of particles, the coatings show a high adhesive strength and cohesive

strength of individual splats, uniform microstructure, high density and low porosity (Scrivani et al, 2001; Stewart et al, 1999; Picas et al, 2003; Wirojanupatump et al, 2001). In recent times, thermally sprayed nickel based superalloy coatings are used in various applications requiring wear and high-temperature corrosion-resistant surfaces (Pawlawski, 1995; Ilavsky et al, 2000). This HVOF process is reported to be versatile technology and has been adopted by many industries due to flexibility, cost effectiveness and the superior quality of coating produced (Stokes and Looney, 2004). HVOF thermally sprayed coatings are used in a wide range of other applications such as the gas turbine, petroleum (Moskowitz, 1992), chemical, paper/pulp (Matsubara and Tomiguchi, 1992), automotive (Byrnes and Kramer, 1994; Fukutome et al, 1995) and manufacturing industries (Perkin Elsmar, 1989).

The high velocity oxy-fuel (HVOF) process is widely used to deposit various types of coatings, which have low porosity and high hardness and are relatively well bonded to the substrate being protected (Sidhu et al, 2006C). The effect of thermal spraying process on microstructure and mechanical properties of Ni-5wt% Al coating deposited on steel substrate has been studied by Sampath et al, (2004). It is shown in their study that the superior elastic and plastic properties of HVOF sprayed Ni-5Al coating as compared to air plasma sprayed (APS) and twin wire-arc sprayed (TWA) are due to formation of denser coating with less porosity and less oxide content in the former process. Deshpande et al, (2006) have studied the mechanisms of oxidation and its influence on microstructural evolution of Ni-5wt% Al coatings deposited using HVOF, APS, and Wire Arc spraying. They observed that in flight oxidation is common in APS, Wire Arc and Wire fed HVOF spraying but oxidation of splat surface occurs for the powder fed HVOF. It is reported in their study that the high quality of the HVOF sprayed Ni-5wt% Al coatings is due to its less porosity and oxide contents when compared to that of APS and Wire Arc sprayed coatings. It is reasoned that the slightly lower temperature, higher viscosity, and higher particle velocities during HVOF spraying of Ni-5wt% Al coatings are responsible for obtaining denser coatings with less undesirable features of inclusions and oxides. Although the HVOF sprayed Ni-5wt% Al coatings on steel substrates have been reported in the literature, the microstructural features of Ni-5Al coatings on different superalloy substrates were not studied so far. The three superalloys viz. Superni 76 (similar to Hastelloy X), Superni 750 (similar to Inconel X-750) and Superfer 800 (similar to Incoloy 800) are used in gas turbine parts, aviation and industrial springs, bolts, bellows, furnace equipment, steam boiler, heat exchanger and piping in chemical industry. Therefore, the present work has been focused to investigate the microstructural features of HVOF sprayed Ni-5Al deposited on three different super alloy substrates namely Superni 76 (SN 76), Superni 750 (SN 750) and Superfer 800 (SF 800) by using optical and SEM/EDAX. The formation of different phases and the chemical composition of Ni-5Al coatings are

analyzed by XRD and distribution of different elements by X-ray mapping analysis, respectively. The porosity and thickness of the Ni-5Al coatings are measured from their respective optical and SEM micrographs. Microhardness, surface roughness and bond strength of the coatings were also measured.

## 4.2.2 Experimental Procedure

The details of the substrate material, coating formulation and characterisation of the coating are explained in Chapter 3.

## 4.2.3 Results

### 4.2.3.1 Measurement of coating thickness

The SEM image of the Ni-5Al powder particles used for coating is shown in Fig. 4.2. The thickness of Ni-5Al coating is measured from its back-scattered electron images obtained at the cross section of the mounted samples. Fig. 4.3 shows the Secondary electron image (SEI) of the coating and its thickness values are reported in Table 4.1.

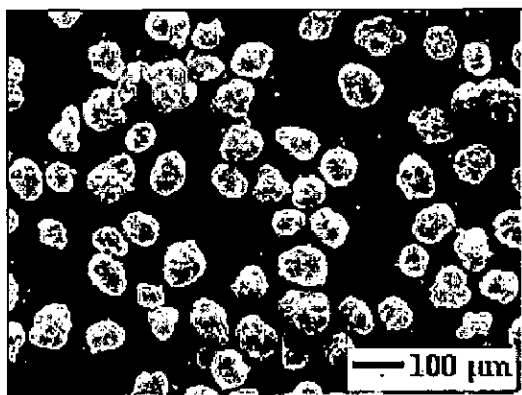


**Fig. 4.2:** SEM image of Ni-5Al powder used for coating

### 4.2.3.2 Measurement of Porosity of the Coating

Porosity is one of the essential parameters of the coatings need to be quantified as it affects the corrosion resistance of the thermal spray coatings by providing preferential paths for corrosive species to penetrate through the coatings and reach the substrate. It is well established that the dense coatings usually provide better corrosion resistance than porous coatings (Sidhu et al, 2006D). Zeiss Axiovert 200MAT inverted optical microscope with stereographic image analysis software based on ASTM B276 is used to measure the surface porosity of the coating. The polished specimen is unetched and free of grinding and polishing marks before scanning the specimen surface under the optical microscope at the appropriate

magnification. The optical micrographs obtained at different areas on the specimen surface are processed by imaging analysis software to calculate the porosity contents. Porosity of HVOF sprayed Ni-5Al coatings is found to be around 2% and reported in Table 4.1.

**Table 4.1:** Coating thickness and porosity values of as sprayed Ni-5Al coating on different superalloys.

Substrate material	Average coating thickness	Porosity value (in %)
Superfer 800	200 $\mu\text{m}$	2.0
Superni 76	174 $\mu\text{m}$	2.0
Superni 750	194 $\mu\text{m}$	1.8

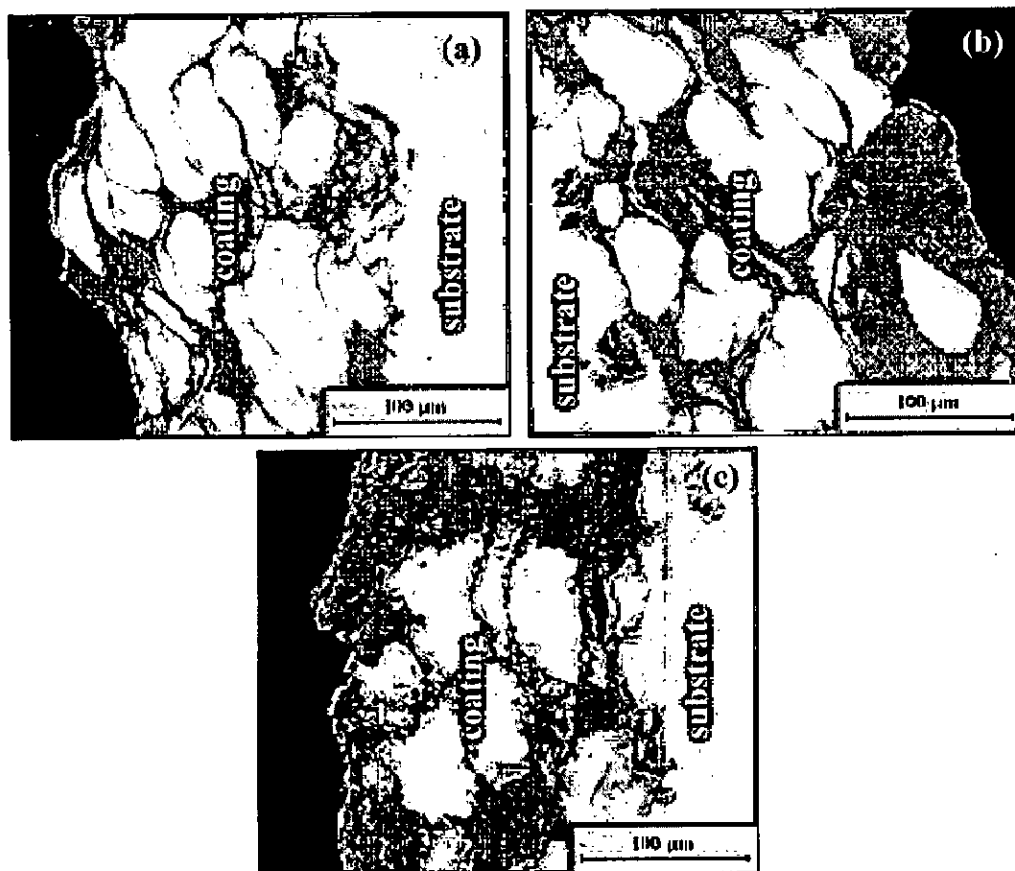


**Fig. 4.3:** SEI showing the cross-section morphology of Ni-5Al coatings on (a) Superni 76, (b) Superni 750 and (c) Superfer 800.

#### **4.2.3.3 Surface roughness (Ra) values of the as sprayed coatings**

The surface roughness (Ra) values of the as sprayed coatings were found to be in the range of 9.22 – 9.45  $\mu\text{m}$ . The centre line average (CLA) method was used to obtain the Ra values.

#### **4.2.3.4 Bond strength of the coatings**

The bond strength of the Ni-5Al coatings was measured on three specimens as per ASTM standard C633-01. The coating failed at the substrate-coating interface while remaining attached to the adhesive. Average bond strength of 43 MPa was observed for the coatings.

#### **4.2.3.5 Microhardness of the coatings**

The microhardness profile along the cross-section of the substrate and the coatings as a function of distance from the coating substrate interface is shown in Fig. 4.4. The microhardness of the coating is found to vary with the distance from the coating-substrate interface. A maximum value of 250Hv and a minimum value of 210 Hv are obtained in case of Ni-5Al coating on Superfer 800. A maximum hardness value of 262 Hv and a minimum value of 245 Hv are obtained for Superni 76. Superni 750 showed hardness values with maximum of 272 Hv and a minimum of 232 Hv

#### **4.2.3.6 Cross sectional morphology of the coatings**

Ni-5Al coatings are deposited by moving the HVOF gun on a stationary substrate and the required thickness of the coating is achieved by varying the number of passes. Lamellar structure of splats is observed in the coatings as shown in Fig. 4.3. Few unmelted, partially melted particles and inclusions are observed in the microstructure. It is evident that the coating is dense with porosity determined around 2%. Tiny sized inclusions are indicated in the coating or at the coating-substrate interface in the form of dark spots. A minor amount of oxides may have been formed in the coating as a result of oxidation of in-flight particles between successive runs and appeared in the intersplat region oriented parallel to the substrate surface.

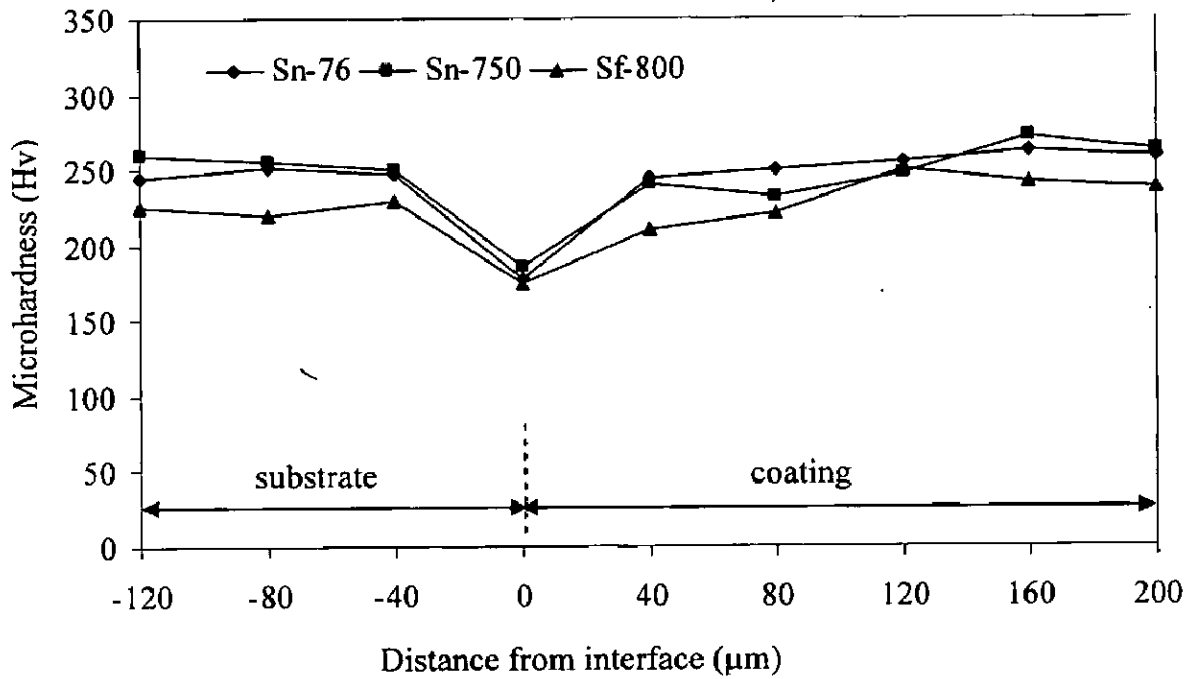


**Fig. 4.4:** Microhardness profiles for HVOF sprayed Ni-5Al coatings on the different superalloys.

#### 4.2.3.7 Surface morphology of the coatings

The optical micrographs of surface of the as sprayed Ni-5Al coating after polishing are shown in Fig. 4.5. Globular morphology is evident from the microstructure. It shows lower porosity and inclusions. Porosity and inclusions are identified based on their contrast as black spots with some depth and dark spots of in-plane orientation, respectively.

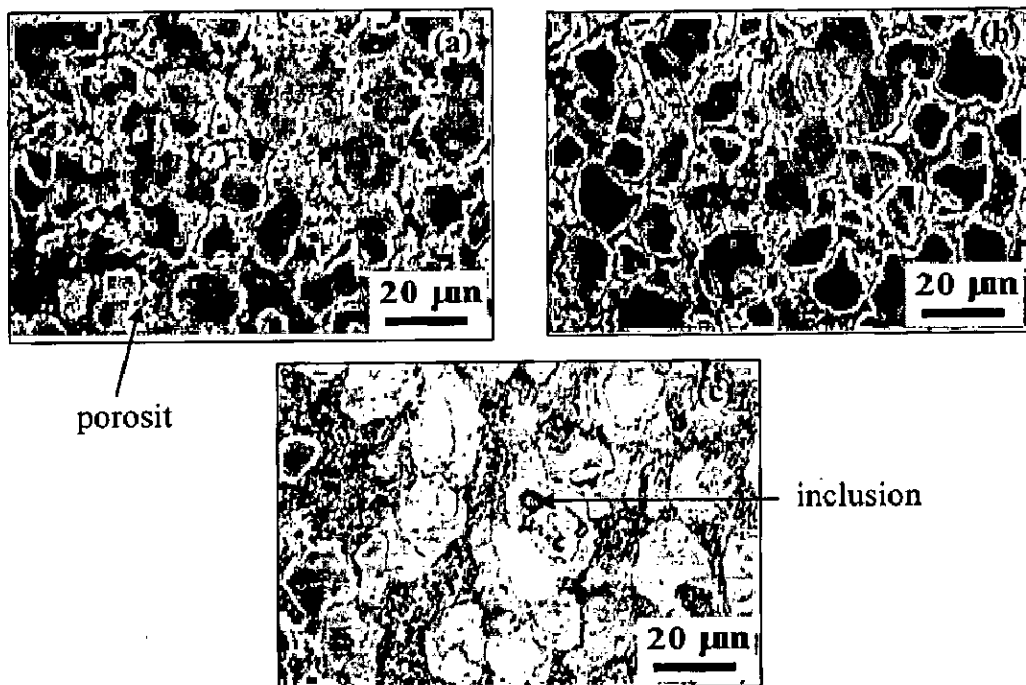


**Fig. 4.5:** Optical micrograph of the surface of as-sprayed Ni-5Al coatings on (a) Superni 76; (b) Superni 750; and (c) Superfer 800



#### 4.2.3.8 X-Ray Diffraction analysis

The XRD patterns of HVOF sprayed Ni-5Al coatings on three different superalloy substrates are shown in Fig. 4.6. As sprayed coatings revealed the presence of phases such as Al, Ni, and AlNi.

#### 4.2.3.9 SEM/EDAX analysis

The SEM micrographs and the elemental compositions of Ni-5Al coating on Superfer 800 are shown in Fig 4.7 (a) and (b), respectively. Dense structure with lower porosity is observed in the coating microstructure and also it is free from cracks. Black spot in the microstructure is identified as porosity. The formation of coating with dense microstructure is attributed to the high velocity of impinging molten particles. The globular particles in coating microstructure are rich in nickel as observed by the EDAX analysis. The splat boundaries are consisting of mainly aluminum.

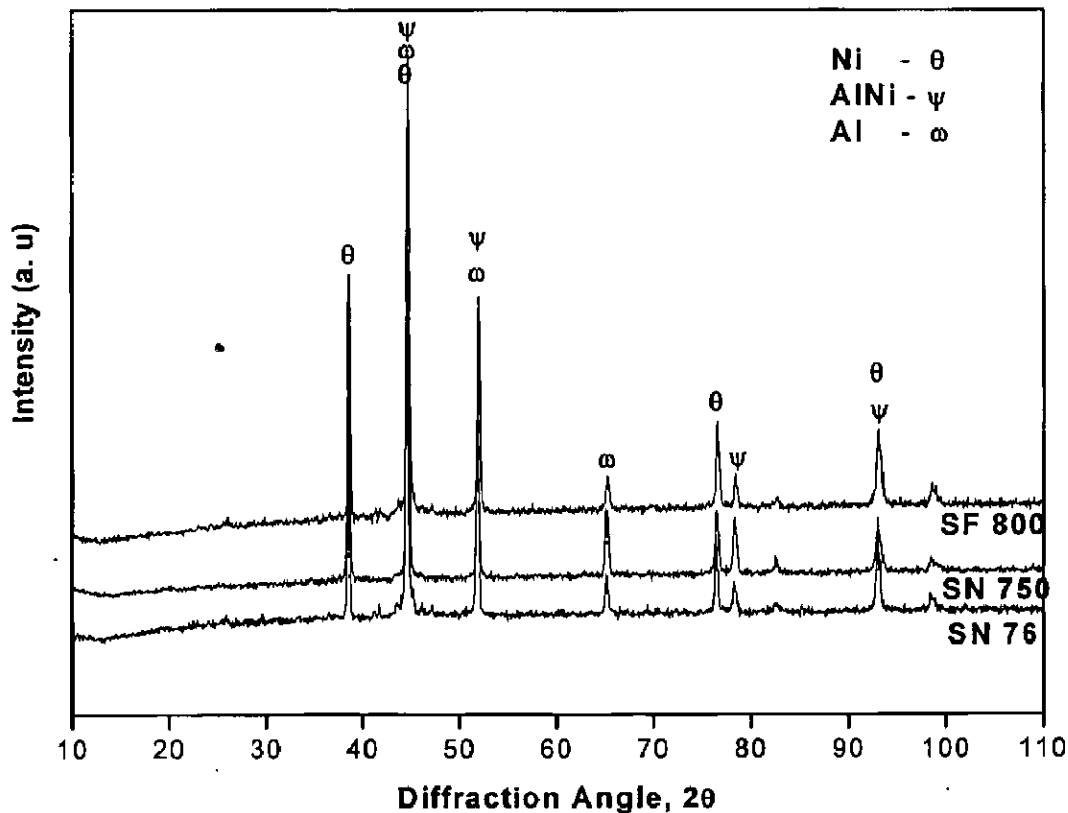


**Fig. 4.6:** X-ray diffraction pattern of as sprayed Ni-5Al coating on different superalloy substrates.

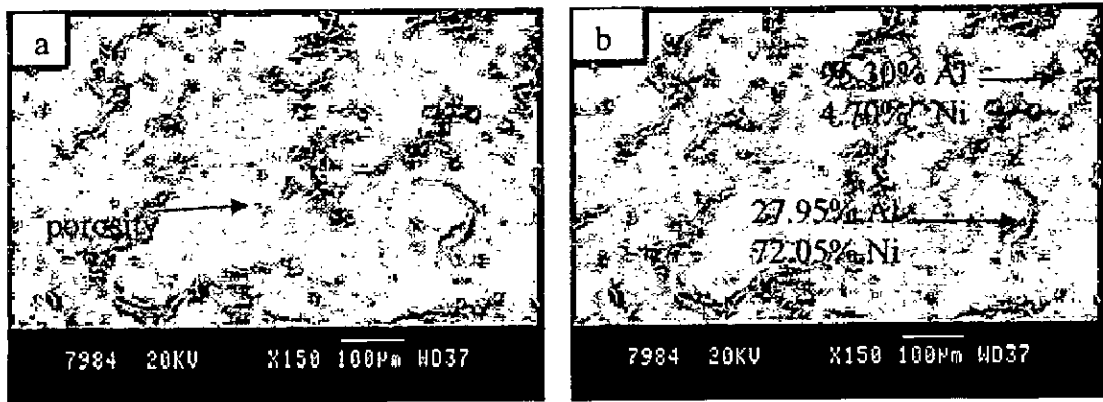


**Fig. 4.7:** SEM image of as-sprayed Ni –5Al coating on Superfer-800 showing (a) surface morphology and (b) EDAX analysis of as-sprayed Ni –5Al coating showing elemental composition (wt. %) at selected points on Superfer 800.

#### 4.2.3.10 X-ray mapping of the different elements

As sprayed Ni-5Al coated specimens on different superalloy substrates are cut by using Buehler ISOMET 1000 precision saw across its cross-sections and mounted in transoptic mounting resin and subsequently mirror polished to obtain the X-ray mapping of different elements. The elemental mapping of the coatings showed that the nickel splats are unoxidised and aluminum has moved to the splat boundaries and coexists with oxygen. Few elements such as Cr, Fe, S, and W have diffused in traces from the Superni 76 substrate into the coating as observed in Fig. 4.8(a). In case of Superni 750, apart from the coating elements, a slight amount of 'P' has diffused along with Cr, Fe, and S from the substrate into the coating as observed in Fig. 4.8(b). Trace amounts of Cr, Fe, S, and P have diffused from the substrate into the coating in case of Superfer 800, which is evident from the Fig. 4.8(c). It is noticed that wherever nickel is present, aluminum is absent.

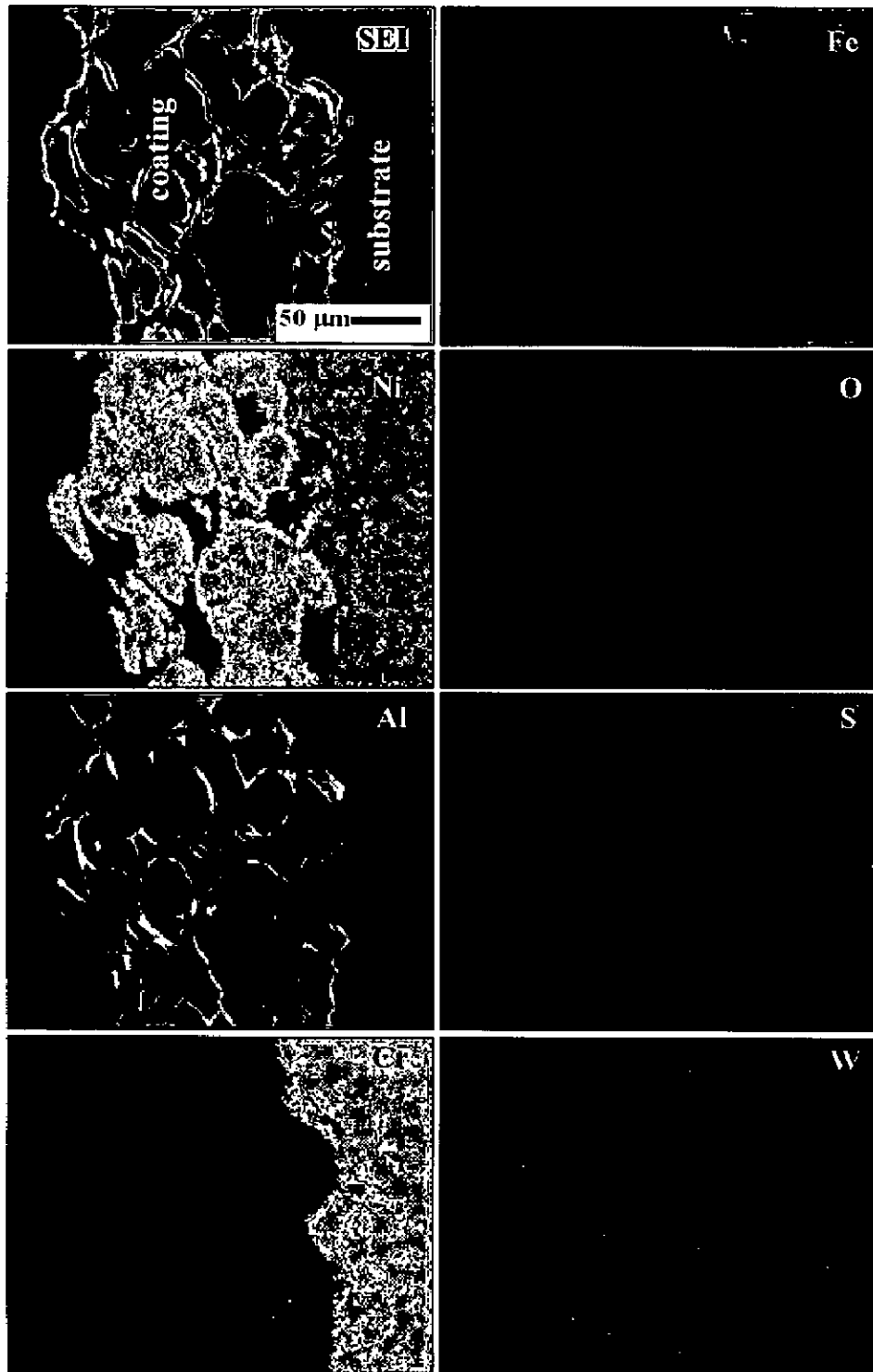


**Fig. 4.8(a):** Composition image (SEI) and X-ray mapping of the cross-section of the as sprayed Ni-5Al coating on Superni 76.

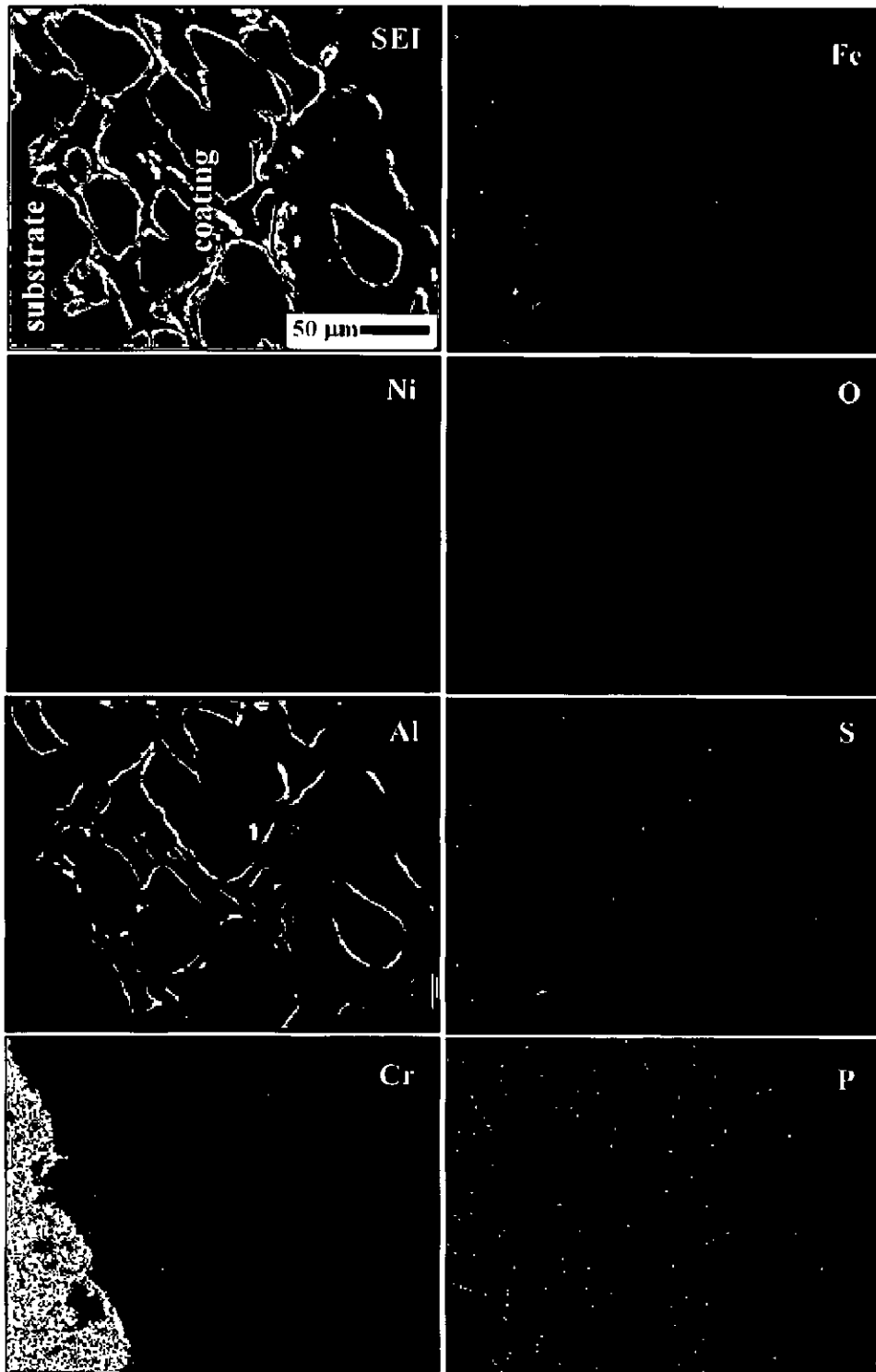


**Fig. 4.8(b):** Composition image (SEI) and X-ray mapping of the cross-section of the as-sprayed Ni-5Al coating on Superni 750.

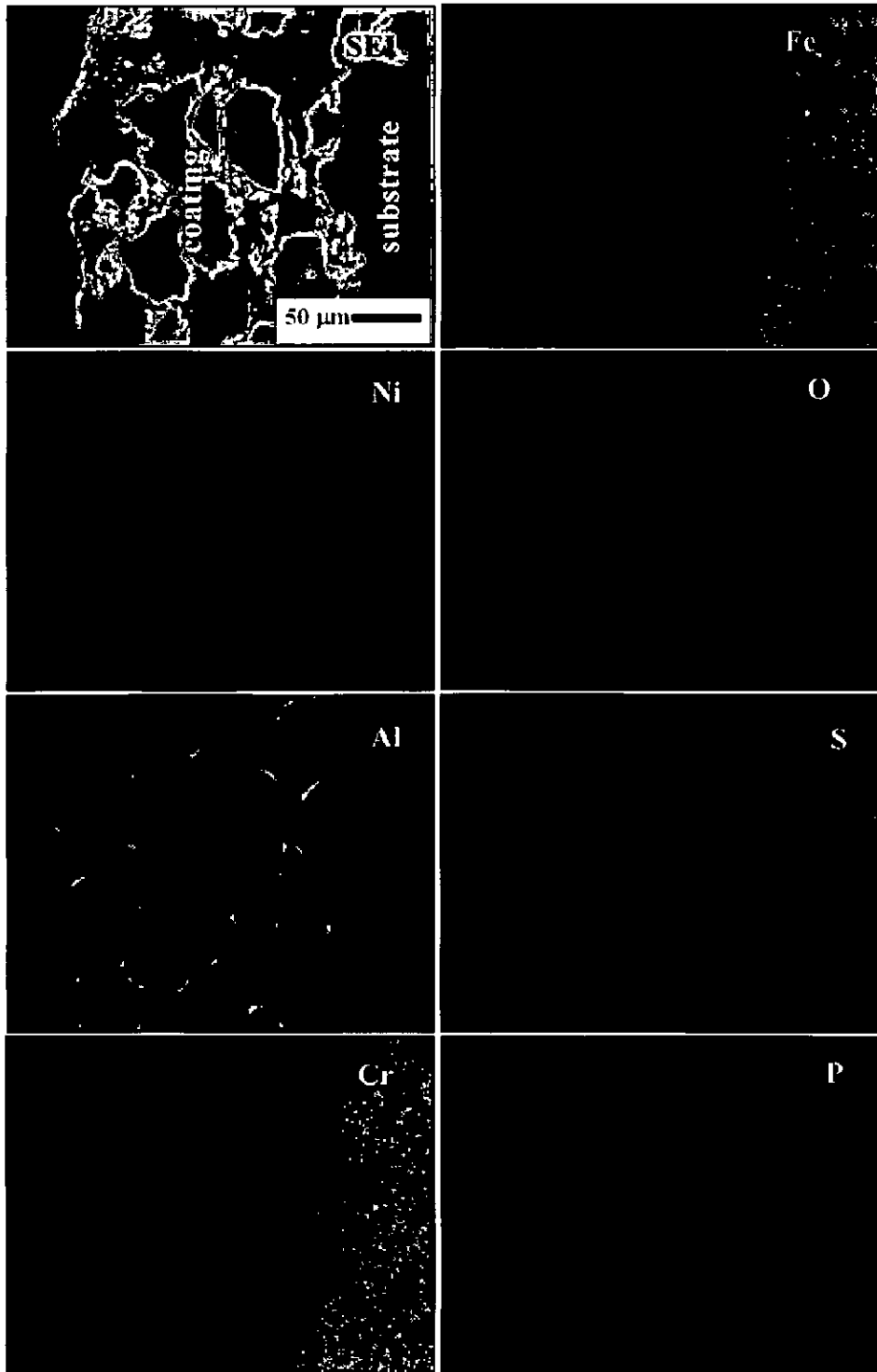


**Fig. 4.8(c):** Composition image (SEI) and X-ray mapping of the cross-section of the as sprayed Ni-5Al coating on Superfer 800.

#### 4.2.4 Discussion

HVOF process with LPG fuel is used to deposit successfully Ni-5Al coating on Ni- and Fe-based superalloy substrates in the present work. LPG fuel is chosen as it is very cost effective when compared to hydrogen fuel. The coatings obtained are having dense microstructure and lower porosity which may be attributed to the higher velocity, relatively lower temperatures, and higher impact force of the powder particles on the substrate material.

Fig. 4.3 shows the cross-section morphology of the coatings on different superalloy substrates. The coating exhibit characteristic splat like, layered morphologies due to the deposition and re-solidification of molten or semi molten droplets. Since the HVOF splats are less fragmented during deposition, it flattens well and improves the contact between splats and substrate. Flattening of the HVOF splats is governed by its high Re number as reported in (Sampath et al, 2004) work. The physical features of splats dictate the structure of dense coating and thereby its mechanical and corrosion resistant properties. During HVOF spraying of powders, long axis of the impacted splats is oriented parallel to the substrate surface resulting in nearly lamellar microstructures. It is seen that the coating obtained are homogeneous and dense on all the superalloy substrates.

The measured surface porosity of the Ni-5Al coatings in the present work is around 2% and it is in accordance with the porosity values of HVOF sprayed NiAl coatings reported in the literature (Sampath et al, 2004; Deshpande et al, 2006; Culha et al, 2007). The coating microstructure is comprised of unmelted particles and inclusions but its content is very less as compared to that of the coatings deposited by other process techniques such as APS and Wire Arc (Deshpande et al, 2006). The high degree of flattening and very less splat fragmentation during HVOF spraying of Ni-5Al powders contribute for the less porosity value in the as deposited coating. An increase in kinetic energy of the powder particles would also reduce the porosity in the deposit. The thickness of the Ni-5Al coating is measured along the cross sectional images of the randomly selected samples obtained using RBSD in SEM and it is found to be in the range of 174-200  $\mu\text{m}$ . Uniform thickness of the coating ensures good adherence over the substrates but very high thickness variation across the coatings might have lead to its disintegration.

Hardness is the most frequently quoted mechanical property of the coatings (Tucker Jr R.C, 1994). Fig. 4.4 shows the profiles of microhardness of the coatings along the cross-section on all the three different superalloy substrates used in the present investigation. It is evident from this figure that the microhardness of the coating varies with the distance from

coating-substrate interface. The non-uniformity of the hardness values of the coatings, along the distance on all the substrates, probably is attributed to the microstructural changes along the cross-section of the coatings. These microstructural changes might be due to the presence of porosity; oxidised, melted, unmelted and semi-melted particles in the coating structure as observed in SEM and optical micrographs. The hardness of coatings on three different superalloy substrates was measured and they lie in the range of 210-272 Hv. Buta Singh et al, (2005A); Hazoor et al, (2006), and Mahesh et al, (2008A), have also reported the variation in the hardness values along the cross section of the as sprayed coatings. An increase in hardness value of coating with depth is attributed to the presence of oxide and the lower hardness value in some location of the coating may be due to the slight amount of porosity. However, the bond strength of the coating also depends on process variables such as high kinetic energy and thermal energy of the particles, which increases the splat-splat interaction for the improved adhesion between interlayer and intersplats. The very fine globular grain morphology of the splats contributes for the higher hardness values of HVOF sprayed coatings. In addition to that, the compressive residual stress in the HVOF sprayed coatings would also contribute for the improved bond strength and hardness as it facilitates the better adhesion of coatings on the substrate. The slight variation in hardness values may be attributed to the microstructural changes along the cross-section of the coating as observed in the SEM and optical micrographs.

The surface roughness values of the coatings were found to be in the range of 9.22-9.45  $\mu\text{m}$  which is identical to the findings of Culha et al, (2007). The average bond strength of the coatings was 43 MPa. It has been reported that high velocity of sprayed particles and its improved melting improves adhesion of the coatings to the substrate (Wang Y.Y et al, 2006). The enhancement of coating strength is due to the deep penetration of droplets into surface cavities of the substrate prior to freezing process. It is heavily dependent on fluid flow and heat transfer characteristics of droplets. The surface roughness and temperature as identified by Pershin et al, (2003) also contribute for the tailoring the properties of the coatings.

It is evident from the XRD pattern of Ni-5Al coating on three different superalloy substrates, shown in Fig. 4.6, that the major phase is Ni-based fcc structure with AlNi and Al as the other phases. The results of XRD are further supplemented by EDAX analysis, which confirmed the presence of Ni and Al.

It is observed from the secondary electron images and elemental X-ray mapping along the cross-section of Ni-5Al coated substrates (Fig.4.8) that the core and outer surface of the splats is composed of predominantly Ni and Al, respectively. The difference in surface tension values of Ni (1.778 N/m) and Al (1.007 N/m) might have contributed for the partial dissociation of Ni and Al in the splat. However, Al has the stronger tendency to dissolve in Ni to form solid solutions, as indicated in XRD analysis, to form the atomized Ni-5wt%Al alloy. It may be mentioned that in the HVOF spraying process, slight in-flight oxidation of aluminum might have also occurred.

#### **4.2.5 Conclusions**

The HVOF technique has been used to deposit Ni-5Al coatings on three different superalloy substrates and the coatings were characterized for their microstructural features, hardness, and bond strength in the present work. The following observations were made based on the present study.

1. The coatings on three different superalloy substrates (Superni 76, Superni 750 and Superfer 800) exhibited a dense and uniform lamellar structure with the porosity value around 2.0%.
2. The presence of Ni, Al, and NiAl phases has been confirmed by XRD analysis.
3. Optical microstructure of the coating reveals the globular splats structure after polishing. The as sprayed coating indicated lower porosity with minor inclusions.
4. The splats are rich in nickel and wherever nickel is present, aluminum is absent. Aluminum is existing along the intersplat boundaries.
5. The diffusion of alloying elements (Cr, Fe, W, P, S) from superalloy substrates into the coatings has been confirmed by X-ray mapping analysis.



## 4.3 OXIDATION STUDIES IN AIR

### 4.3.1 Introduction

Ni and Fe- based superalloys are used as structural components in various applications such as gas turbines, steam boilers, heat exchangers, aeroengines and industrial springs as they possess superior mechanical properties, and corrosion and oxidation resistance to some extent. These superalloys cannot provide high-temperature corrosion resistance without affecting its mechanical properties as tailoring of microstructural and compositional parameters to achieve the former would have adverse influence on the latter. Therefore, protective coatings are essential to provide the high temperature oxidation and corrosion resistance to the superalloys in order to realize the long service life of the components even in harsh environments, especially in industrial gas turbines. It is well known in the literature that degradation by high temperature oxidation is one of the main failure modes of hot section components in gas turbines (Liu et al, 2001). The knowledge of oxidation behaviour of high temperature coatings is important to extend the limits of use of superalloys at upper end of their performance capabilities without altering the mechanical properties of the substrate materials while protecting them against wear or corrosion (Sidky and Hocking, 1999).

To realize the superior performance of the superalloys, aluminides based coatings are applied, traditionally, using various process routes such as pre-aluminisation and pre-oxidation, pack cementation (Lih et al, 1992, Lih et al, 1993), alternative element doping (Beele et al, 1997; Czech et al, 1995) and surface remelting (He, J. L., et al, 2001). The oxidation behavior of NiAl has been reviewed by Grabke (1999) and it is reported that the formation of fast growing metastable phases such as  $\gamma$ ,  $\delta$ , and  $\theta$   $\text{Al}_2\text{O}_3$  at  $1000^\circ\text{C}$  takes place before it transforms into a stable phase,  $\alpha$   $\text{Al}_2\text{O}_3$  with longer duration exposure. The metastable phases are undergrown by  $\alpha$   $\text{Al}_2\text{O}_3$  and alloying elements such as Cr, Y, and Ce, which promotes its nucleation rate, accelerates the formation of  $\alpha$   $\text{Al}_2\text{O}_3$ . The formation of voids and cavities beneath the oxide scale, due to the consumption of Al and inward diffusion of Ni, lead to decreased oxide adherence and spallation of the scale upon temperature changes. The hot corrosion mechanism of intermetallic compound  $\text{Ni}_3\text{Al}$  has been investigated by Lee and Lin (2003) and they found that the formation of spinel phase  $\text{NiAl}_2\text{O}_4$  provides a better hot corrosion resistance than NiO due its thermodynamically lower solubility in the molten salt. They proposed that the oxide solubility and sulphur penetration rate control the corrosion process of NiAl in the molten salt environment at 800 and  $1000^\circ\text{C}$ .

The cyclic oxidation behavior of HVOF sprayed Ni-5Al coating on Ni and Fe based super alloys is scarce in the literature. Furthermore, the cyclic conditions constitute a more realistic approach towards solving the problem of metal corrosion (oxidation) in actual applications, where conditions are more or less cyclic, rather than isothermal (Sadique et al, 2000). Ni-5Al coating is expected to provide better ductile properties and coefficient of thermal expansion compatibility with the substrate and thereby it could reduce the spallation problem resulting from cyclic oxidation at high temperature when compared to  $\gamma'$ -Ni<sub>3</sub>Al and  $\beta$  NiAl coating. Therefore, the present work has been focused to investigate the cyclic oxidation behavior of HVOF sprayed Ni-5Al coatings on Ni and Fe-based superalloys, in air environment, at 900°C. The Ni-5Al coatings were characterized by XRD, SEM/EDAX and X-ray mapping analyses.

### **4.3.2 Experimental Procedure**

The details of the substrate material, coating formulation and oxidation studies of the coating are explained in section 3.4 and 3.5 of Chapter 3.

### **4.3.3 Results**

#### **4.3.3.1 Visual Observation**

The surface macrograph of Ni-5Al coated superalloys after 100 cycles exposure to air at 900°C is shown in Fig. 4.9. A visual observation of Ni-5Al coated Superni 76 alloy (Fig. 4.9a) at 900°C, after fifth cycle, showed the formation of light grey color on its surface and subsequently turned into a dark grey after tenth cycles. Few grey patches were also observed on the surface of the coating. Some amount of micro sputtering was manifested at the end of 48<sup>th</sup> cycle. In case of Ni-5Al coated Superni 750 alloy (Fig. 4.9b), a light green color was observed on the surface of the coating, after sixth cycle, and then it transformed into a dark grey during the course of the experiment. The Ni-5Al coated Superfer 800 alloy (Fig. 4.9c) showed a dark grey color on the surface of the coating at the end of second cycle. Some amount of superficial spalling was noticed at the end of fourth cycle. This may be due to the loosely bond particles on the surface of the coating.

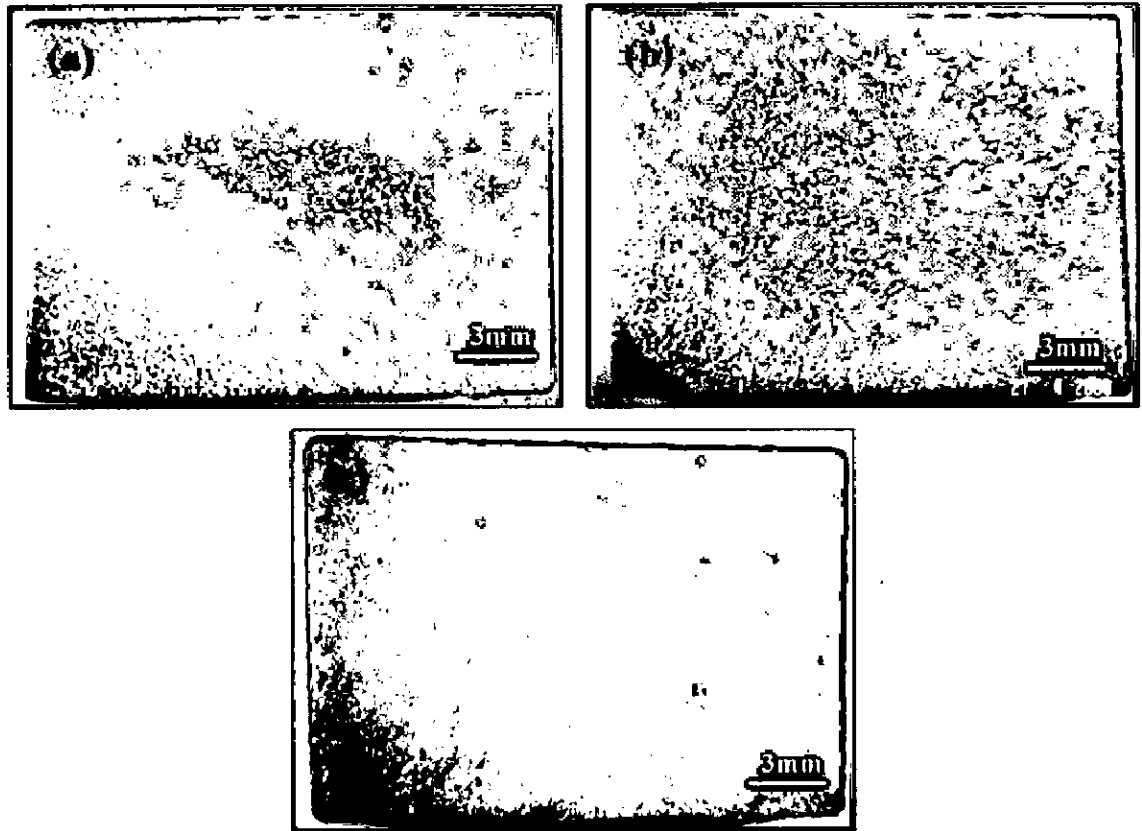


**Fig. 4.9:** Surface macrographs of Ni-5Al-coated (a) Superni 76; (b) Superni 750; and (c) Superfer 800 after 100 hr exposure to air at 900 °C.

#### 4.3.3.2 Oxidation studies in air

The weight gain per unit area versus number of cycles plots for the bare and coated alloys is depicted in Fig.4.10. In all cases, during the initial stages, the rates of oxidation are higher which gradually levels off. The weight gain per unit area square plotted against number of cycles indicates that there are slight deviations from the parabolic law. The maximum weight gain ( $\text{mg}/\text{cm}^2$ ) was obtained in case of Superni 750 bare alloy whereas least weight gain was observed with Superfer 800 bare alloy. In case of Ni-5Al coated Superfer 800 alloy, the weight gain was least but Ni-5Al coated Superni 750 has shown the highest weight gain.

The parabolic rate constant  $k_p$  values for uncoated and Ni-5Al coated superalloy substrates subjected to air oxidation at 900°C after 100 cycles are shown in Table 4.2. The  $k_p$

values decreases for all coated superalloys thereby indicating lower oxidation rates for the coated superalloys.

The uncoated Superni 750 showed a higher mass gain as compared to coated one. Ni-5Al coated Superfer 800 has shown a lower mass gain whereas coated Superni 76 revealed a higher mass gain which is 45% more than that of the former. The mass gain data reveals that the bare superalloys, in general, are prone to oxidation attack, whereas Ni-5Al coatings are found to be successful in lowering appreciably the extent of oxidation. Fig. 4.11 presents the square of mass gain per unit area as a function of time expressed in the number of cycles to confirm the parabolic oxidation behavior. The coating protects the superalloy substrates by acting as diffusion barriers to the corroding species. Fig. 4.12 shows the cumulative weight gain/unit area in all three cases of uncoated/coated superalloys.

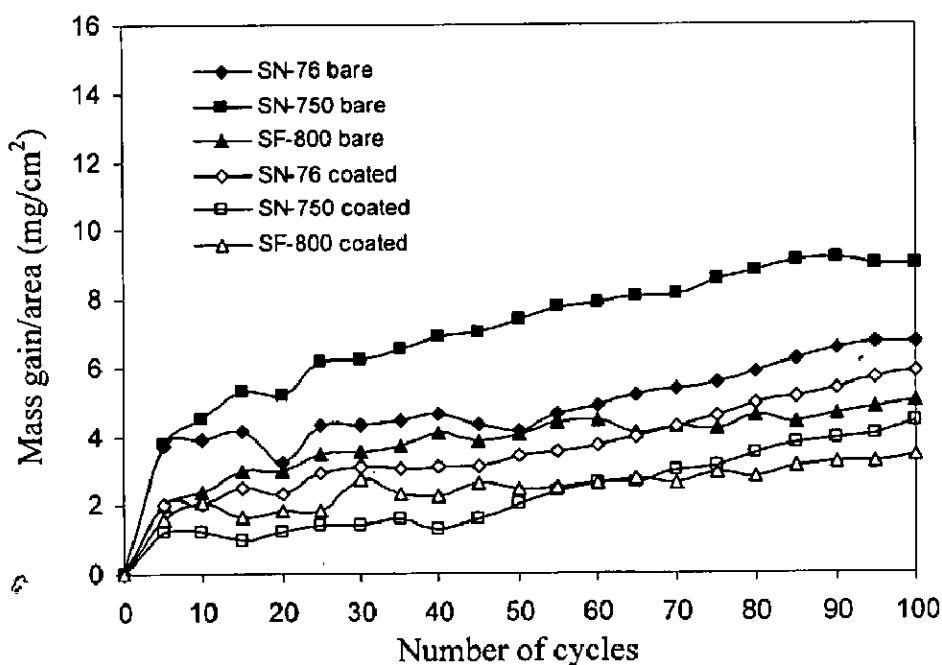


**Fig. 4.10:** Mass gain/area vs Time (no of cycles) plot for Ni-5Al coated samples oxidized in air at 900°C for 100 cycles.

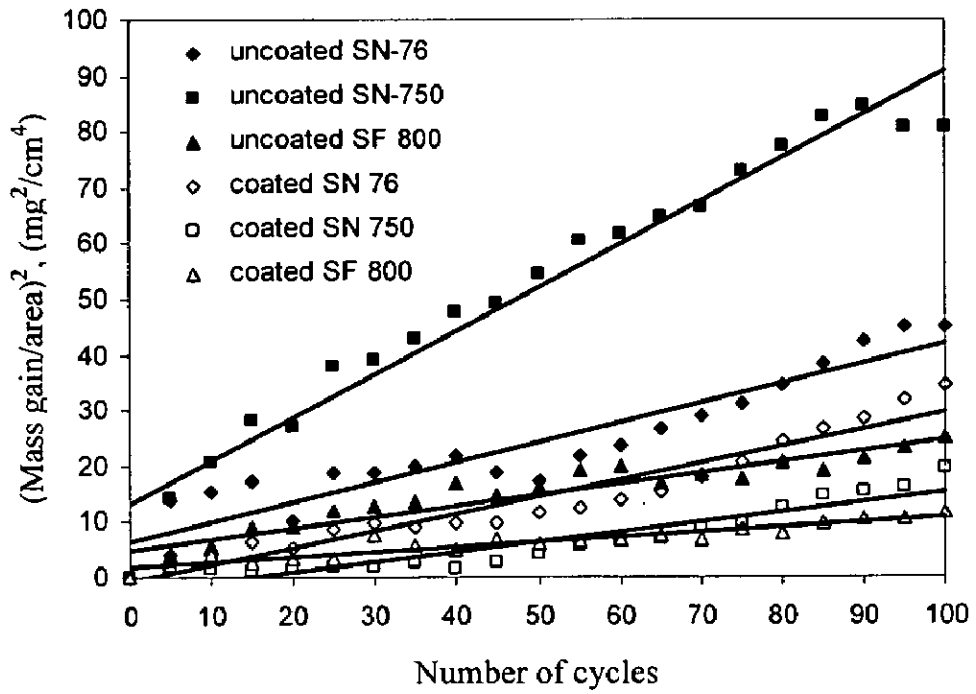


**Fig. 4.11:**  $(\text{Mass gain/area})^2$  vs time plot for Ni-5Al coated superalloy substrates oxidized in air at  $900^\circ\text{C}$  for 100 cycles.

**Table 4.2:** Parabolic rate constant,  $k_p$  values of uncoated and coated superalloys subjected to air oxidation at  $900^\circ\text{C}$

Superalloy substrate	$k_p \times 10^{-10} \text{ gm}^2 \text{ cm}^{-4} \text{ s}^{-1}$
Uncoated Superni 76	1.0
Uncoated Superni 750	2.15
Uncoated Superfer 800	0.55
Coated Superni 76	0.84
Coated Superni 750	0.50
Coated Superfer 800	0.249

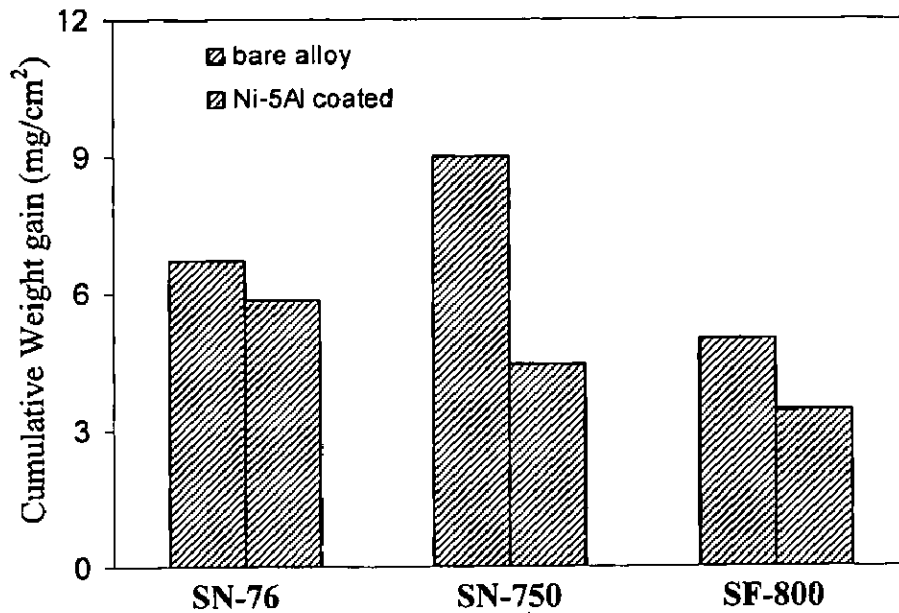


**Fig. 4.12:** Bar chart showing cumulative weight gain per unit area for bare and Ni-5Al coated superalloys subjected to cyclic oxidation for 100 cycles at 900°C.

### 4.3.3.3 Surface scale analysis.

#### 4.3.3.3.1 X-ray diffraction.

X-ray diffractograms of the Ni-5Al coated superalloy substrates after cyclic oxidation in air for 100 cycles at 900°C are shown in Fig. 4.13. All the coated and oxidized superalloys have indicated the formation of similar phases and the main phases analyzed by XRD analysis are NiO, Ni<sub>2</sub>O<sub>3</sub>, α-Al<sub>2</sub>O<sub>3</sub>, AlNi, and Ni<sub>2</sub>Al<sub>3</sub>. In Superni 76 alloy, Cr<sub>2</sub>O<sub>3</sub> has been observed as shown in Fig. 4.13.

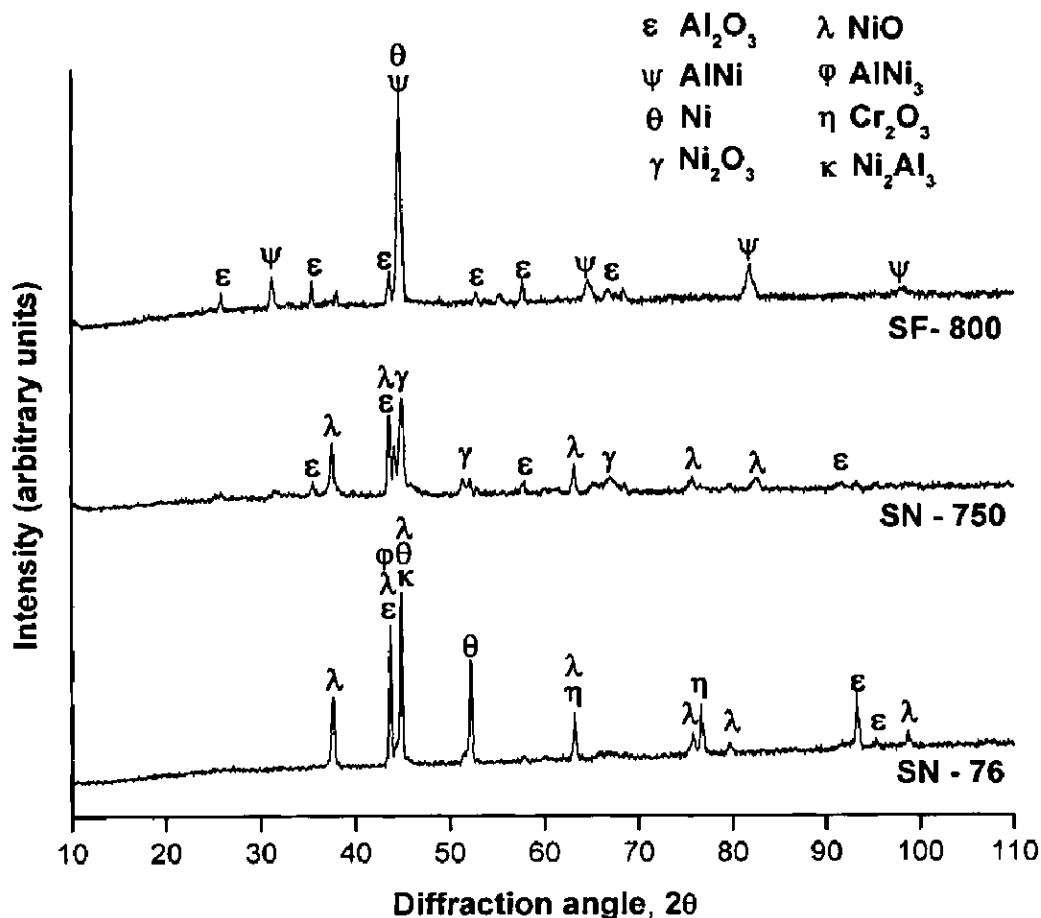


**Fig. 4.13:** X-Ray Diffraction pattern of Ni-5Al coated on superalloys subjected to cyclic oxidation in air at 900°C.

#### 4.3.3.3.2. Surface scale morphology

SEM micrographs along with EDAX analysis of uncoated superalloys oxidized at 900°C for 100 cycles at some selected sites of interest are shown in Fig. 4.14. The uncoated Superni 76 alloy shows the presence of nodules and the spalled regions in the subscale. The elongated nodules, with directionality, are seen in uncoated Superni750 and they are rich in  $\text{Cr}_2\text{O}_3$ . The uncoated Superfer 800 alloy shows the presence of oxide scale such as  $\text{Cr}_2\text{O}_3$  and NiO. The top scale is rich in  $\text{Cr}_2\text{O}_3$  and other oxides such as  $\text{TiO}_2$ , NiO,  $\text{Fe}_2\text{O}_3$  and MnO have formed. The scale formed was fragile and it showed some cracks in it. The SEM micrographs and compositions of Ni-5Al coated superalloys oxidized at 900°C for 100 cycles are shown in Fig. 4.15. In case of Ni-5Al coated Superni 76 alloy, the scanning electron micrograph (Fig 4.15a) shows the splats consisting of mainly nickel and the surrounding region contains  $\text{Al}_2\text{O}_3$  and NiO. X-ray diffraction results also confirmed the formation of

aluminum oxide and nickel oxide. The SEM micrograph of Ni-5Al coated Superni 750 alloy (Fig 4.15b) shows scale morphology where a scale rich in  $\text{Al}_2\text{O}_3$  has formed. It is observed that oxidation has taken place along the splat boundaries as well as at the splats where the scale is enriched in NiO. The Ni-5Al coated Superfer 800 alloy (Fig 4.15c) shows a massive scale consisting of mainly  $\text{Al}_2\text{O}_3$  with spalled regions indicating a subscale containing some amount of NiO and  $\text{Cr}_2\text{O}_3$ .

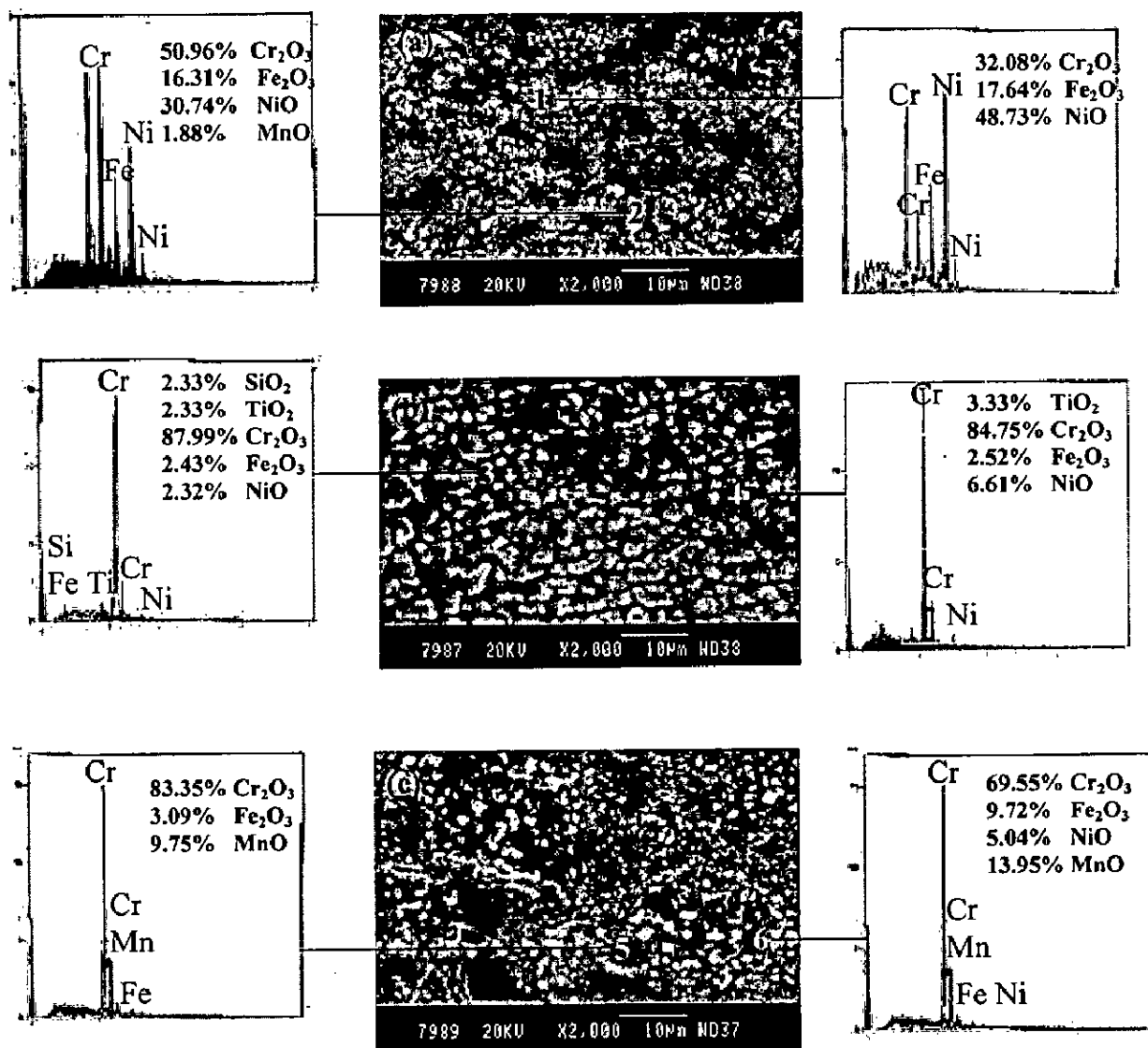


**Fig. 4.14:** Surface-scale morphology and EDAX patterns from different spots on uncoated superalloys oxidized at  $900^\circ\text{C}$  for 100 cycles of (a) Superni 76, (b) Superni 750 and (c) Superfer 800.



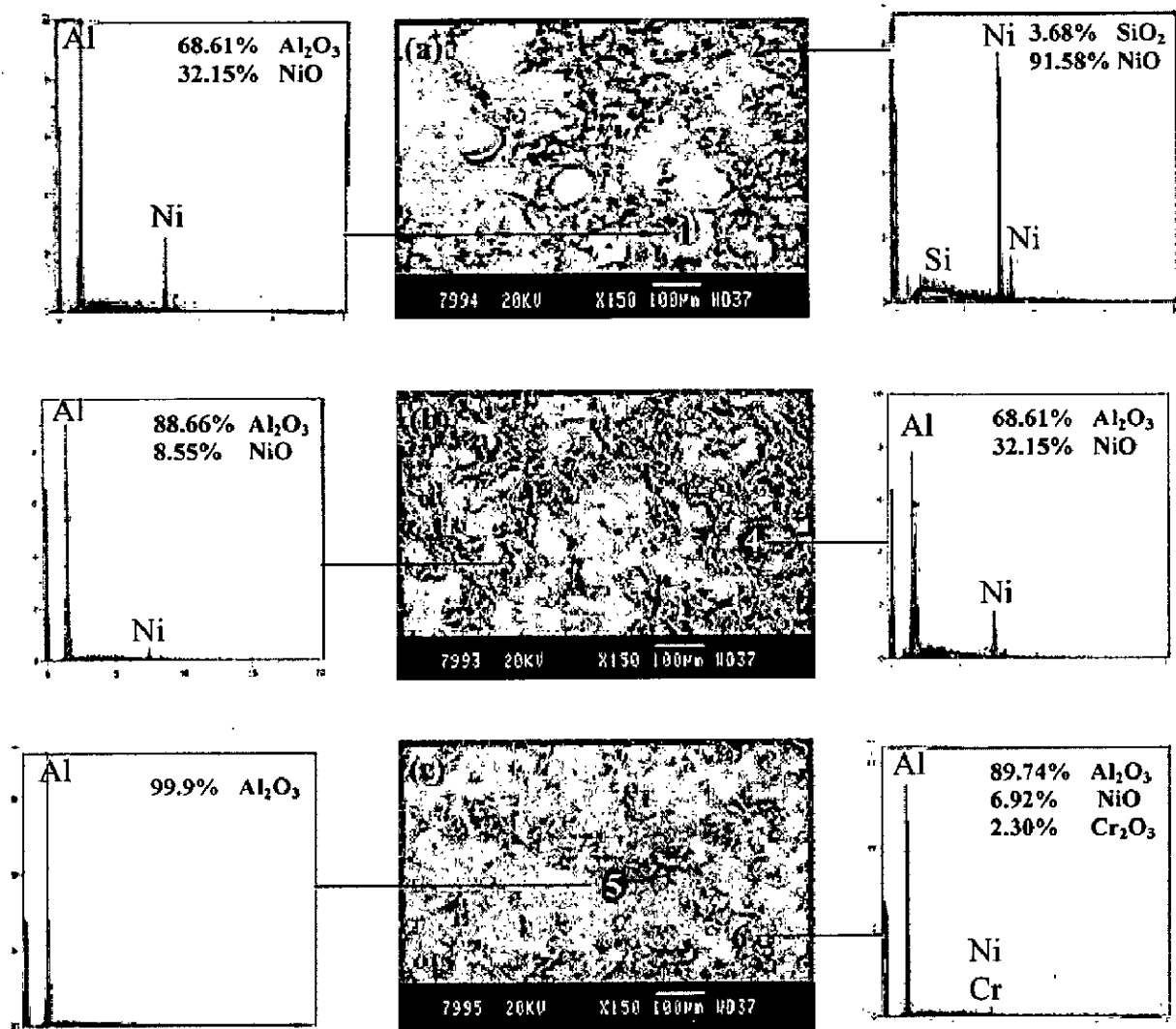


**Fig. 4.15:** Surface-scale morphology and EDAX patterns from different spots on Ni-5Al coated superalloys oxidized at 900°C for 100 cycles of (a) Superni 76, (b) Superni 750 and (c) Superfer 800.

#### 4.3.3.4 Cross sectional analysis of the scale

The oxidized samples were cut across the cross section using Buehler Isomet 1000 precision saw and mounted in transoptic mounting resin and subsequently mirror polished to obtain X-ray mapping of different elements as shown in Fig. 4.16.

X-ray mappings for oxidised Ni-5Al coated Superni 76, Fig. 4.16(a) indicate the formation of scale containing mainly nickel rich splats and aluminum at the splat boundaries. Oxygen and aluminum are coexisting in the oxidised coating. Small amount of chromium, iron, manganese and tungsten have diffused from the substrate into the coating. In case of oxidised Ni-5Al coated Superni 750, Fig. 4.16(b), nickel rich splats are clearly seen and wherever nickel is present aluminum is absent. Al is found around the splat boundaries. A band of chromium is present near the coating substrate interface. There is a presence of iron, manganese and titanium in traces in the oxidized coating. X-ray mappings for oxidised Ni-5Al coated Superfer 800 are shown in Fig. 4.16(c). A thick band rich in chromium is present near the coating substrate interface. Perceptible amount of iron has diffused from the substrate into the coating. Aluminum and oxygen are coexisting in the coating. Small amount of manganese and silicon have diffused from the substrate into the coating.

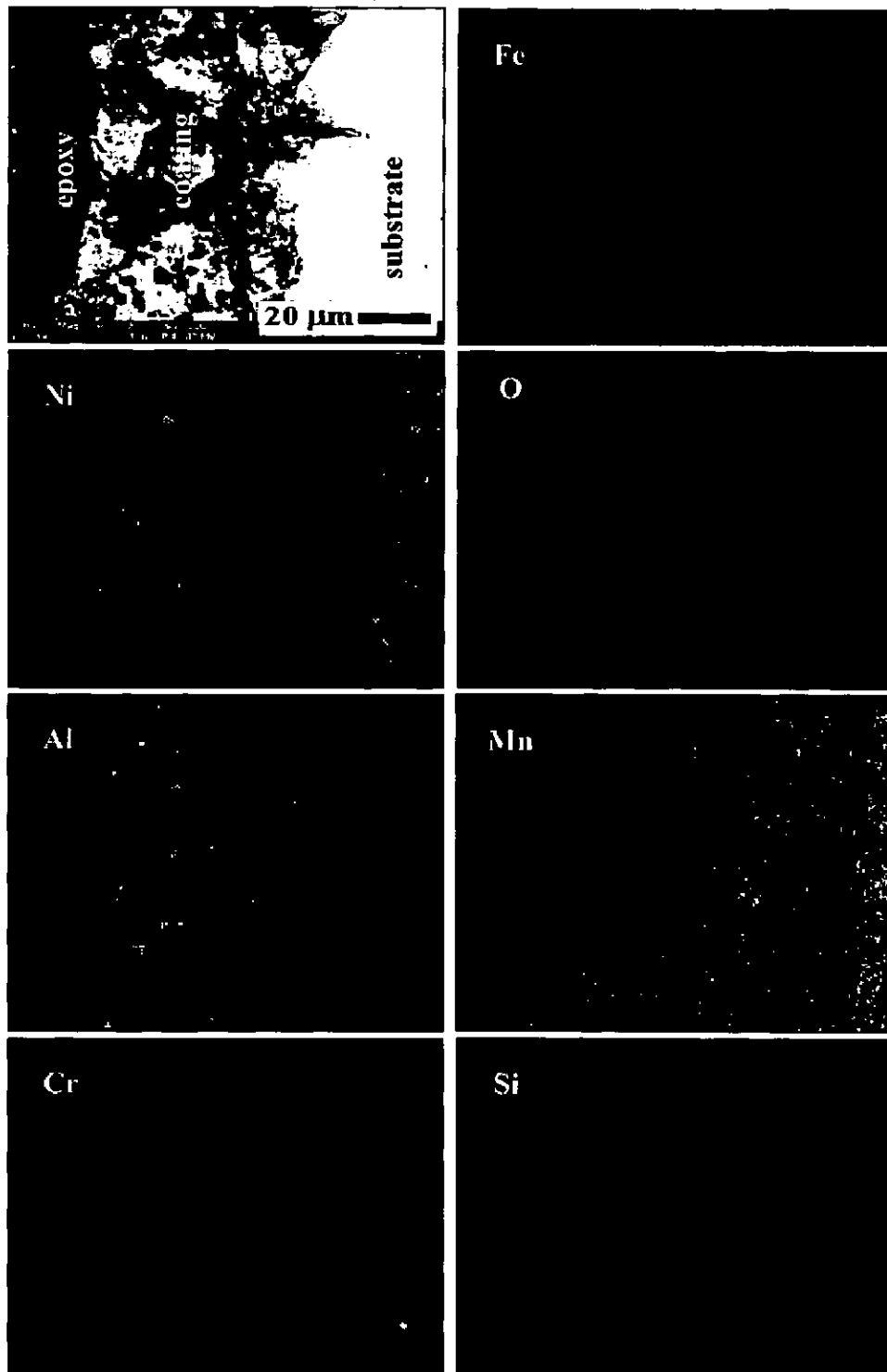


**Fig. 4.16(c):** Composition image (BSEI) and X-ray mapping of the cross-section of the Ni-5Al coated superalloy Superfer 800 subjected to cyclic oxidation at 900 °C after 100 cycles.

#### 4.3.3.5 Discussion

HVOF process has successfully been used to obtain Ni-5Al coatings on Superni 76, Superni 750 and Superfer 800 in the present investigation. Fig. 4.3 shows the cross-section morphology of the Ni-5Al coating on different superalloys and it exhibits characteristic splat like, layered morphologies due to the deposition and re-solidification of molten or semi molten droplets. The microhardness profiles of the Ni-5Al coating on superalloy substrates vary with the distance from coating-substrate interface and they lie within the range from 210 to 272 Hv. The variation in the hardness may be attributed to the presence of oxides in the coating and also to the slight amount of porosity.

It is well known that the performance of HVOF sprayed coatings in high temperature corrosive environment depends on the several factors such as porosity, inclusions, oxides, and size and shape of the splat microstructures as reported in the literature (Dent et al, 1999). The high temperature cyclic oxidation behavior of Ni-5Al coated superalloys follows a parabolic trend as evident from the results of thermogravimetric data reported in Fig.4.11. The parabolic kinetic behavior is due to the diffused controlled mechanism operating at 900°C under cyclic conditions. The weight gains per unit area in case of Ni-5Al coated Superni 750 has reduced to 51% as compared to that of uncoated Superni 750. Further, there is a reduction of 12.65% and 31.94% weight gain per unit area in the case of coated Superni 76 and Superfer 800 alloys, respectively.

The slight deviations from the parabolic rate of cyclic oxidation of the coating may be attributed to the formation and rapid growth of inhomogeneous oxides during oxidation process as reported by Choi et al, (2002). The rapid weight gain of the coated alloys was observed only during initial cycles of oxidation study and it may be because of the rapid formation of oxides at the coating-splat boundaries as well as due to the penetration of the oxidizing species along the splat boundaries/open pores. However, the coating subsequently becomes dense and movement of oxidizing species to the inner portion of the coating gets slowed down once the oxides are formed at places of porosity and splat boundaries. This would relatively minimize the weight gain and result in the steady state oxidation behavior with the prolonged exposure time. It is evident from the XRD results of the oxidized coated alloys that  $\text{Al}_2\text{O}_3$  and NiO are the major phases and  $\text{Cr}_2\text{O}_3$  and Ni are also present. The presence of these phases is further

supported by EDAX and X-ray mapping analysis. In case of Superfer 800 alloy, the X-ray mapping shows that there is a continuous band of chromium at the substrate-coating interface. This chromium oxide band may be the one which provides protection against further oxidation. On the basis of the results of XRD, SEM/EDAX (surface and cross-section), and X-ray mapping analyses, schematic representation of the possible oxidation mode for the Ni-5Al coated Superni 76 at 900°C after 100 cycles is shown in Fig. 4.17.

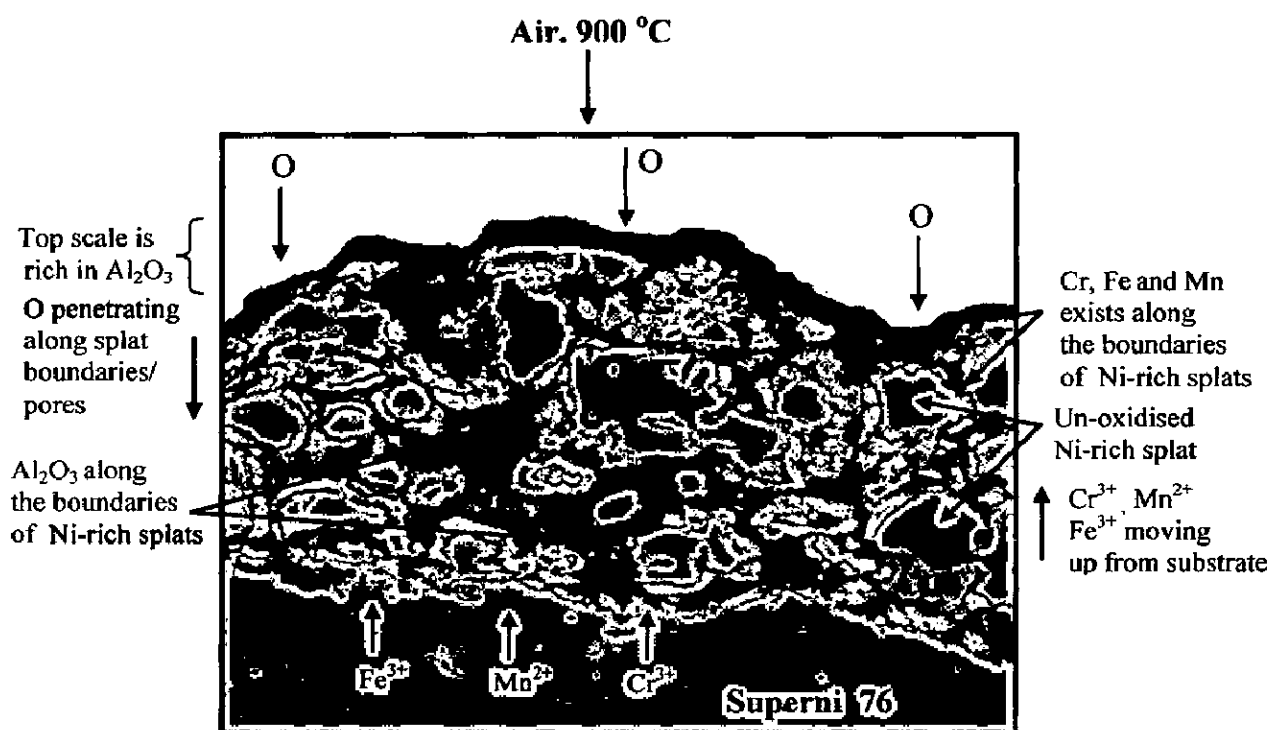


**Fig. 4.17:** Schematic diagram showing possible oxidation mode for the Ni-5Al coated Superni 76 at 900 °C for 100 cycles.

#### 4.3.3.6 Conclusions

The high temperature oxidation behaviour of HVOF sprayed Ni-5Al coatings on Superni 76, Superni 750 and Superfer 800 alloys in air at 900°C have been investigated and the following conclusions are made.

1. HVOF process using LPG as fuel gas could be used successfully to deposit Ni-5Al coating on the given Ni- and Fe- based superalloys. The coatings are dense and free of cracks and having a porosity of around 2%.
2. The HVOF Ni-5Al coated superalloys when subjected to cyclic oxidation at 900°C developed a protective oxide scale mainly consisting of NiO, Al<sub>2</sub>O<sub>3</sub> and some amount of Cr<sub>2</sub>O<sub>3</sub> as confirmed by EDAX.
3. In case of uncoated superalloys, the weight gain is high in Superni 750 alloy followed by Superni 76 and Superfer 800 respectively.
4. Ni-5Al coating has led to the reduction in weights of about 13% in Superni 76, whereas 51% and 32% for Superni 750 and Superfer 800 alloys respectively. The Ni-5Al coating has provided the necessary protection to the superalloy substrates which followed the sequence:

Superni 750 > Superfer 800 > Superni 76

5. The oxidation behaviour of Ni-5Al coated Superni 750 and Superfer 800 is found to be nearly parabolic but a slight deviation is observed for coated Superni 76 substrate.
6. In case of Superfer 800, a thick band of chromium is formed at the substrate-coating interface, which might have enhanced the protection to the substrate resulting in a minimum weight gain.
7. The oxide scale formed is adherent to the coating and its spallation is negligible.

## **4.4 HOT CORROSION STUDIES IN MOLTEN SALT ENVIRONMENT**

### **4.4.1 Introduction**

Advances in the development of high temperature materials and cooling schemes are expected to increase the life time of gas turbines, boilers, and industrial waste incinerators with their improved strength, creep and fatigue properties. The combination of high temperature with contaminants of environment and low-grade fuels, such as sodium, sulphur, vanadium, and chlorine, manifested in the gas turbine environments require special attention as they lead to the phenomenon of hot corrosion. This form of corrosion consumes the material at an unpredictably rapid rate (Eliaz et al, 2002). The corrosive nature of the gaseous environment may cause rapid material degradation and result in premature failure of components (Danyluk and Park, 1979; Wang, D, 1988). The usage of residual fuel oil refinery furnaces, boilers and gas turbines is limited by the severe degradation of materials (Deb et al, 1996). Unlike the conventional concept of frequent renewal of the superheaters made of low cost materials, the new concept exploits the high performance corrosion-resistant materials to realise the reduction of overall plant costs (Kawahara, 2002).

A case study of boiler tube failure in coal fired boilers has been conducted by Prakash et.al, (2001) covering one year and it was observed that more than 50% of the failures were attributed to the hot corrosion and erosion due to ash. Although corrosion problems cannot be completely remedied, it is estimated that corrosion related costs could be reduced by more than 30% with the development and use of better corrosion control technologies such as corrosion inhibitors, cathodic protection and coatings (Priyantha et al, 2003). Coatings can add value to products up to 10 times the cost of the coating (Matthews et al, 1998). Nickel aluminide coatings are of relatively recent origin (Malik et al, 1992) and they are reported to possess high-temperature mechanical strength as well as oxidation resistance (He et al, 2001; Schneibel, 1999). It has been reported in the literature that nickel aluminide coatings on steel have improved the oxidation and corrosion resistance as well as the elevated temperature tribological properties of the substrate (He et al, 2001; La et al, 1999). One of the most common methods used to combat hot corrosion problems in gas turbines involves the utilization of surface coatings. Coatings for superalloys are usually designed in such a way that on exposure to reactive environments, the selective oxidation of an element occurs to form a protective oxide film such as  $\text{Cr}_2\text{O}_3$ ,  $\text{Al}_2\text{O}_3$  or  $\text{SiO}_2$  (Rhys-Jones, 1985).

There is no available literature on the behaviour of Ni-5Al coatings on superalloys subjected to molten salt environment under cyclic conditions. Therefore, an attempt has been made in the present investigation to develop Ni-5Al coating by HVOF process on the

superalloys and investigate its high temperature corrosion behaviour under cyclic conditions at 900°C in an aggressive environment of Na<sub>2</sub>SO<sub>4</sub>-60%V<sub>2</sub>O<sub>5</sub>. The hot corrosion environment, Na<sub>2</sub>SO<sub>4</sub>-60%V<sub>2</sub>O<sub>5</sub> has been selected in the present investigation because it simulates similar conditions of the molten sulfate-vanadate deposits resulting from the condensation of combustion products of low-grade fuels (Sidhu et al, 2007). These low melting compounds react and dissolve the protective oxides formed on the components of boilers and turbines. Further, a mixture of Na<sub>2</sub>SO<sub>4</sub> and V<sub>2</sub>O<sub>5</sub> in the ratio of 40:60 constitutes eutectic with a low melting point of 550°C and provides a very aggressive environment for hot corrosion to occur (Tiwari, 1997). The cyclic conditions were chosen to create a very aggressive environment for corrosion attack. The cyclic conditions constitute a more realistic approach towards solving metal corrosion problems. Thermogravimetric (weight change with time) technique is used to approximate the kinetics of corrosion of coated and bare superalloy substrates. XRD, and SEM/EDAX and X-ray mapping analyses techniques have been used to characterize the corrosion products formed during hot corrosion studies under cyclic conditions.

#### **4.4.2 Experimental Design**

The substrate materials, coating formulation and the hot corrosion studies are explained in detail in section 3.4.3 and 3.5 of Chapter 3.

#### **4.4.3 Results**

##### **4.4.3.1 Visual observation**

In case of bare Superni 76 alloy, Fig. 4.18(a), spalling was observed after the completion of 2<sup>nd</sup> cycle. A brownish grey scale appeared on the surface and the scale turned dark in color with the course of the study. A small amount of sputtering was observed after 21 cycles and a crack was seen on the oxide scale. The spalled scale was included in the boat during the mass change measurements, whereas in case of bare Superni 750 alloy, Fig. 4.18(b), brown color was observed after 2<sup>nd</sup> cycle, which turned into dark brown after subsequent cycles. After the completion of 7 cycles, spalling of the scale was observed in. In case of bare Superfer 800 alloy, Fig. 4.18(c), brown color was observed after the 2<sup>nd</sup> cycle, which turned dark during the study. The spallation of the scale has started after 10<sup>th</sup> cycle and it was included during the mass change measurements. The spalling after few cycles might have resulted from the different co-efficient of thermal expansion (or mismatch) of coating and scale.

The Ni-5Al coated Superni 76 showed a brown color after the 2<sup>nd</sup> cycle, which turned light brown after 6<sup>th</sup> cycle. After completion of 16 cycles, light brown colour with green patches was observed on the surface of the sample which lasted upto 100 cycles. The oxide scale was



intact with the coating and marginal spalling was observed from the surface as shown in Fig 4.18(d). In case of coated Superni 750, green color was seen on the surface after 3<sup>rd</sup> cycle, which turned dark brown after 5<sup>th</sup> cycle. A little amount of spalling and sputtering of the scale were observed during the course of the study as observed from Fig 4.18(e). Few patches of light green color appeared on the surface of the substrate and lasted up to the end of the study, while in case of Superfer 800, the scale formed on the surface were brown in color. The scale started spalling from the surface after 11 cycles and it was marginal. Some spalling was observed after 18<sup>th</sup> cycle in the form of fine powder. Final scale was adherent with a light green patch on it as shown in Fig 4.18(f) with further exposure upto 100 cycles.

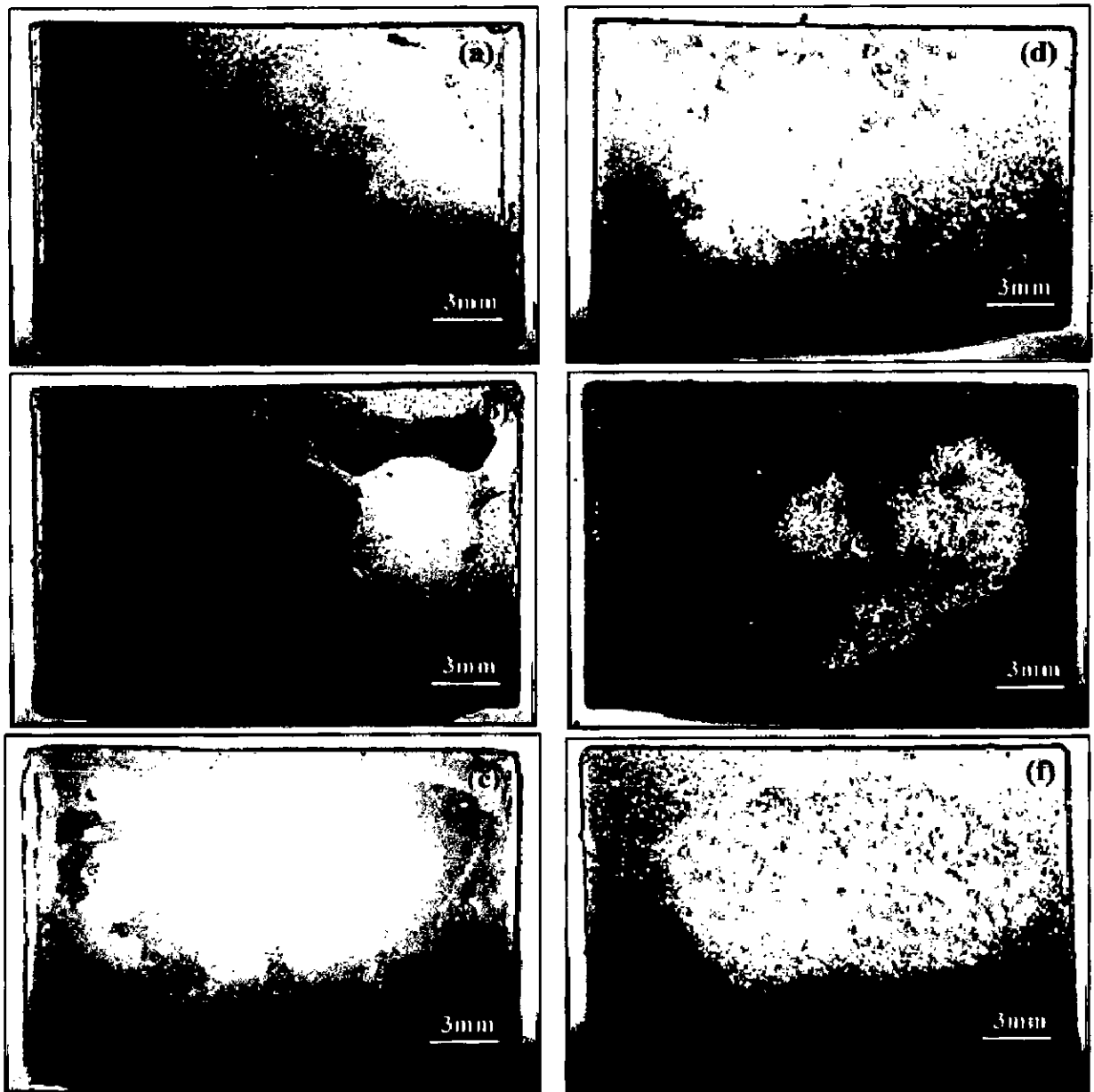


**Fig. 4.18:** Surface macrographs of bare Superni 76 (a), Superni 750 (b), Superfer 800 (c) and Ni-5Al coated Superni 76 (d), Superni 750 (e) and Superni 800 (f) after 100 hr exposure to molten salt ( $\text{Na}_2\text{SO}_4$ -60% $\text{V}_2\text{O}_5$ ) environment at 900°C.

#### 4.4.3.2 Corrosion Kinetics in molten salt environment

The mass gain per area versus number of cycles plots for the bare as well as coated superalloys in the presence of molten salt ( $\text{Na}_2\text{SO}_4\text{-60\%V}_2\text{O}_5$ ) environment under cyclic conditions is shown in Fig. 4.19. It is observed that the mass gain of the coated superalloys is lower as compared to that of bare superalloys in the molten salt environment. Superfer 800 coated with Ni-5Al has shown a minimum mass gain. Superni 750 coated with Ni-5Al has shown a slightly higher mass gain. The weight gain data indicates that the bare superalloys are prone to hot corrosion attack whereas the HVOF sprayed Ni-5Al coating provided a better protection to the superalloys from hot corrosion to a considerable extent.

The parabolic rate constant  $k_p$  is calculated from the slope of the linear regression fitted line. The nature of fit, a parabolic rate law, for hot corrosion experiments is also shown in Fig. 4.20. There is a visible deviation from the parabolic rate law in case of bare superalloy substrates whereas the Ni-5Al coated specimens follow the parabolic behaviour upto 100 cycles. The parabolic rate constant for bare and Ni-5Al coated superalloys is shown in Table 4.3. The cumulative weight gain/unit area in all three cases of bare/coated superalloys is plotted as shown in Fig. 4.21.

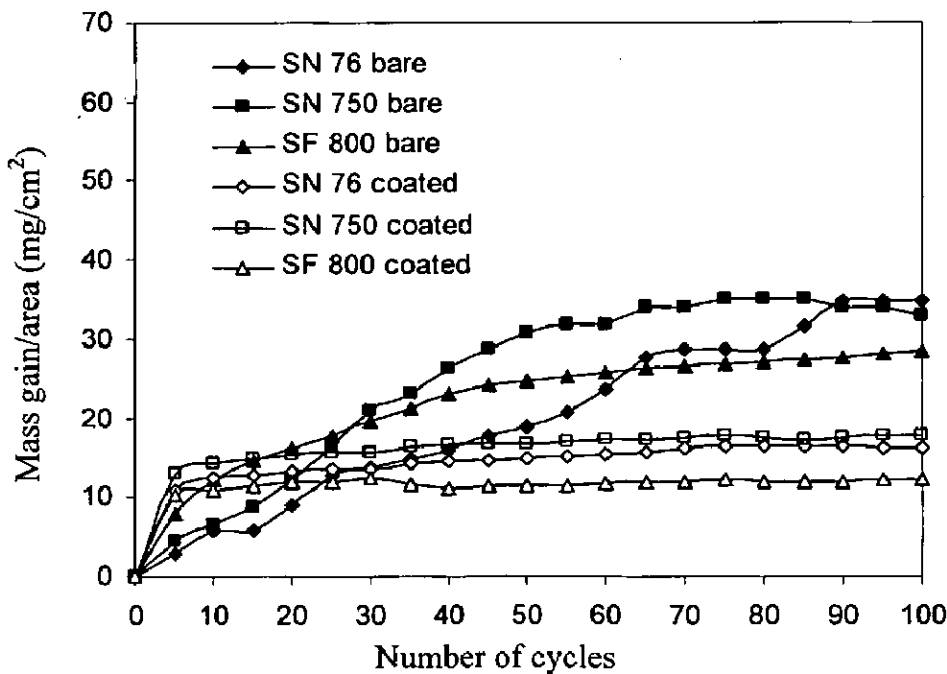


**Fig. 4.19:** Mass gain/area vs number of cycles plot for bare and Ni-5Al coated superalloys subjected to  $\text{Na}_2\text{SO}_4\text{-60\%V}_2\text{O}_5$  environment at  $900^\circ\text{C}$  for 100 cycles.

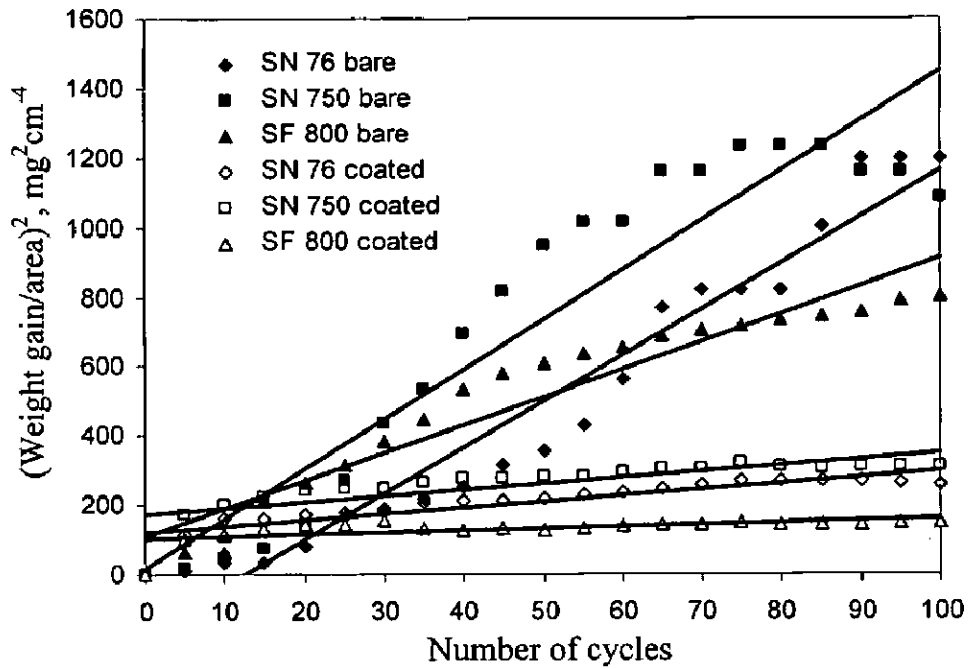


**Fig. 4.20:**  $(\text{Mass gain/area})^2$  vs. number of cycles for bare and Ni-5Al coated superalloys subjected to  $\text{Na}_2\text{SO}_4$ -60% $\text{V}_2\text{O}_5$  environment at  $900^\circ\text{C}$  for 100 cycles.

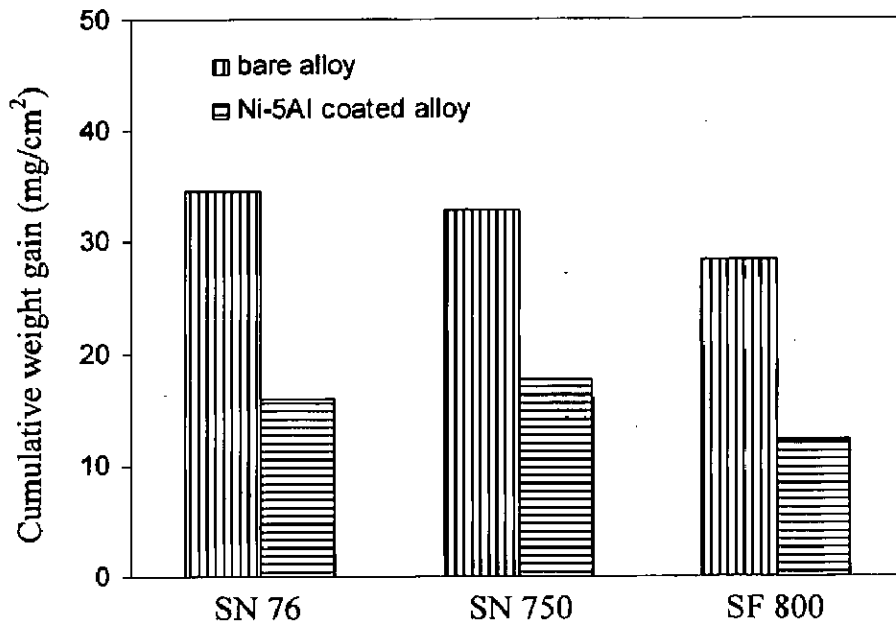


**Fig. 4.21:** Bar chart showing cumulative weight gain per unit area for bare and Ni-5Al coated superalloys subjected to cyclic oxidation for 100 cycles at  $900^\circ\text{C}$ .

**Table 4.3:** Parabolic rate constant,  $k_p$  values of bare and Ni-5Al coated by HVOF process after hot corrosion studies at 900°C

Substrate	$k_p$ values( $10^{-10} \text{ gm}^2 \text{ cm}^{-4} \text{ s}^{-1}$ )
bare Superni 76	37.08
bare Superni 750	39.71
bare Superfer 800	22.36
coated Superni 76	5.08
coated Superni 750	5.01
coated Superni 800	1.63

#### 4.4.3.3 X-Ray Diffraction Analysis

The XRD analysis was carried out with Bruker AXS D-8 Advance Diffractometer (Germany) with  $\text{CuK}\alpha$  radiation. The XRD patterns of the hot corroded samples after 100 cycles are shown in Fig. 4.22. XRD patterns of the Ni-5Al coatings revealed that the presence of  $\text{NiO}$ ,  $\text{NiAl}_2\text{O}_4$ ,  $\text{NiCr}_2\text{O}_4$  and  $\text{Al}_2\text{O}_3$  as the main phases. Furthermore, very weak phases indexed as belonging to  $\text{Cr}_2\text{O}_3$ ,  $\text{FeVO}_4$  and  $\text{MnO}$  are identified.

#### 4.4.3.4 SEM/EDAX analysis of the scale

##### 4.4.3.4.1 Surface analysis

SEM micrographs with EDAX analysis (Jeol Scanning Microscope (JSM-840A) with EDAX attachment, Link ISIS) at some selected points of interest of hot corroded bare samples are shown in Fig 4.23. The scale formed on the bare Superni 76 shows (Fig. 4.23 a) spalling tendency and EDAX analysis shows the presence of  $\text{Cr}_2\text{O}_3$ ,  $\text{Fe}_2\text{O}_3$  and  $\text{NiO}$  phases in the scale. In case of bare Superni 750 alloy, (Fig. 4.23b), large numbers of small pores are seen on the surface of the specimen. The major oxide formed on the surface of Superni 750 is nickel oxide along with small percentage of  $\text{Cr}_2\text{O}_3$ ,  $\text{Fe}_2\text{O}_3$  and  $\text{V}_2\text{O}_5$ . The SEM micrograph of bare Superfer 800 (Fig. 4.23c), indicates few cracks on the surface and the surface scale consists of  $\text{Cr}_2\text{O}_3$ ,  $\text{Fe}_2\text{O}_3$ ,  $\text{NiO}$  and  $\text{MnO}$  as revealed by EDAX analysis.

The SEM images showing the surface morphology of Ni-5Al coated superalloys after cyclic hot corrosion studies at 900°C are given in Fig. 4.24. For Superni 76 (Fig 4.24a), the point analysis shows the higher percentages of NiO, Cr<sub>2</sub>O<sub>3</sub> and Al<sub>2</sub>O<sub>3</sub> along with presence of Fe<sub>2</sub>O<sub>3</sub> and Na<sub>2</sub>O. The EDAX of Superni 750 scale indicated the dominance of Al<sub>2</sub>O<sub>3</sub> in the shining area (point 2) along with NiO and Cr<sub>2</sub>O<sub>3</sub>. NiO occurs as the main phases along with Fe<sub>2</sub>O<sub>3</sub> in the black area (point 1) as shown in Fig. 4.24b. The scale of Superfer 800 specimen, Fig 4.24c, indicated Al<sub>2</sub>O<sub>3</sub> as the main phase with NiO and Na<sub>2</sub>O as the other phases.

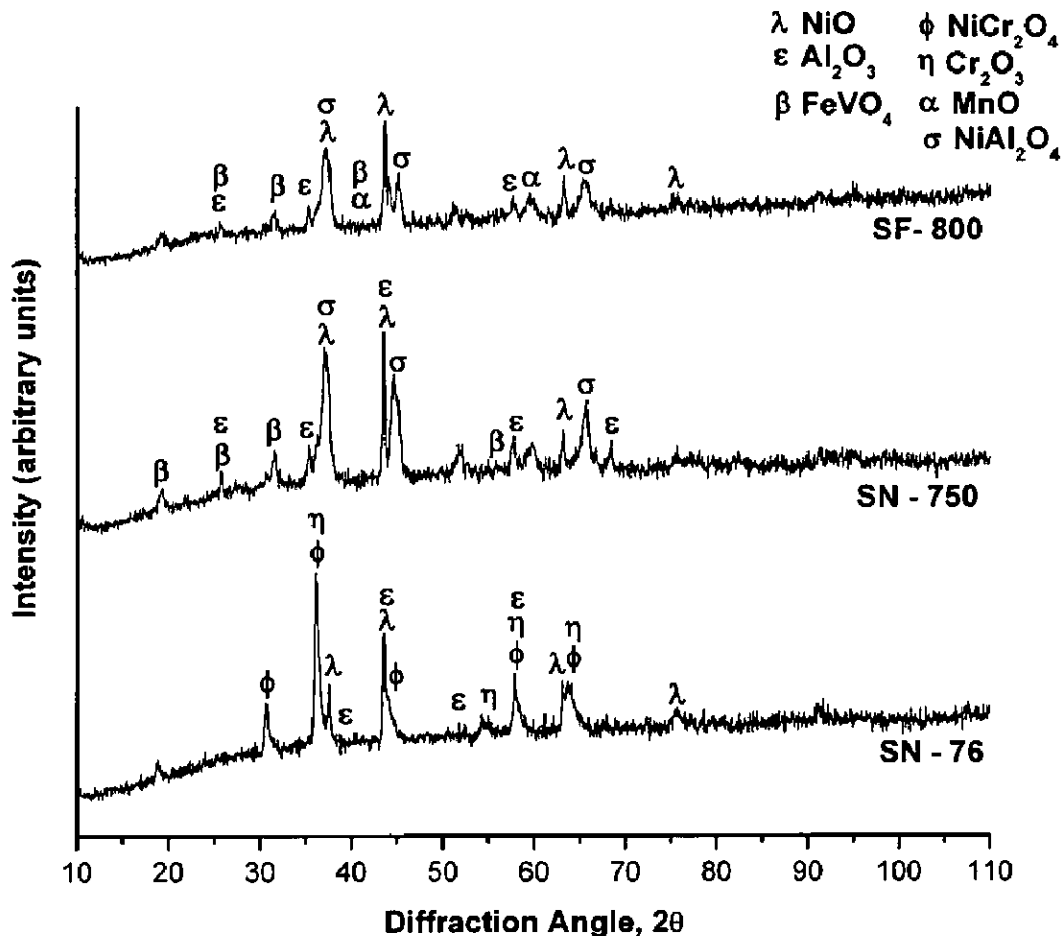


**Fig. 4.22:** X-ray diffraction pattern of Ni-5Al coated superalloys after 100h exposure to molten salt (Na<sub>2</sub>SO<sub>4</sub>-60%V<sub>2</sub>O<sub>5</sub>) environment at 900°C.

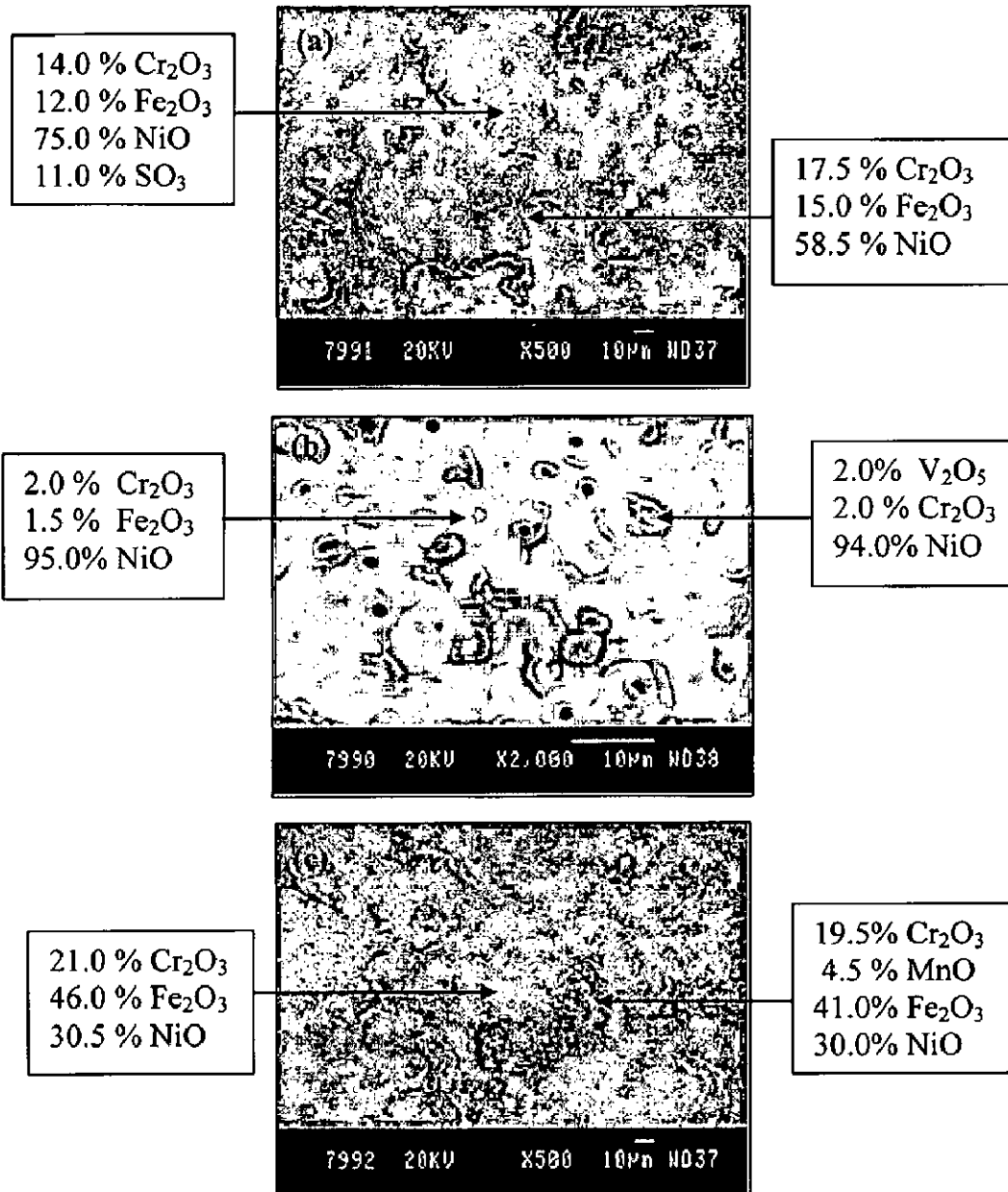


**Fig. 4.23:** SEM/EDAX analysis of the bare superalloys, (a) Superni 76; (b) Superni 750; and (c) Superfer 800 exposed to molten salt ( $\text{Na}_2\text{SO}_4$ -60% $\text{V}_2\text{O}_5$ ) environment at 900°C after 100 cycles.

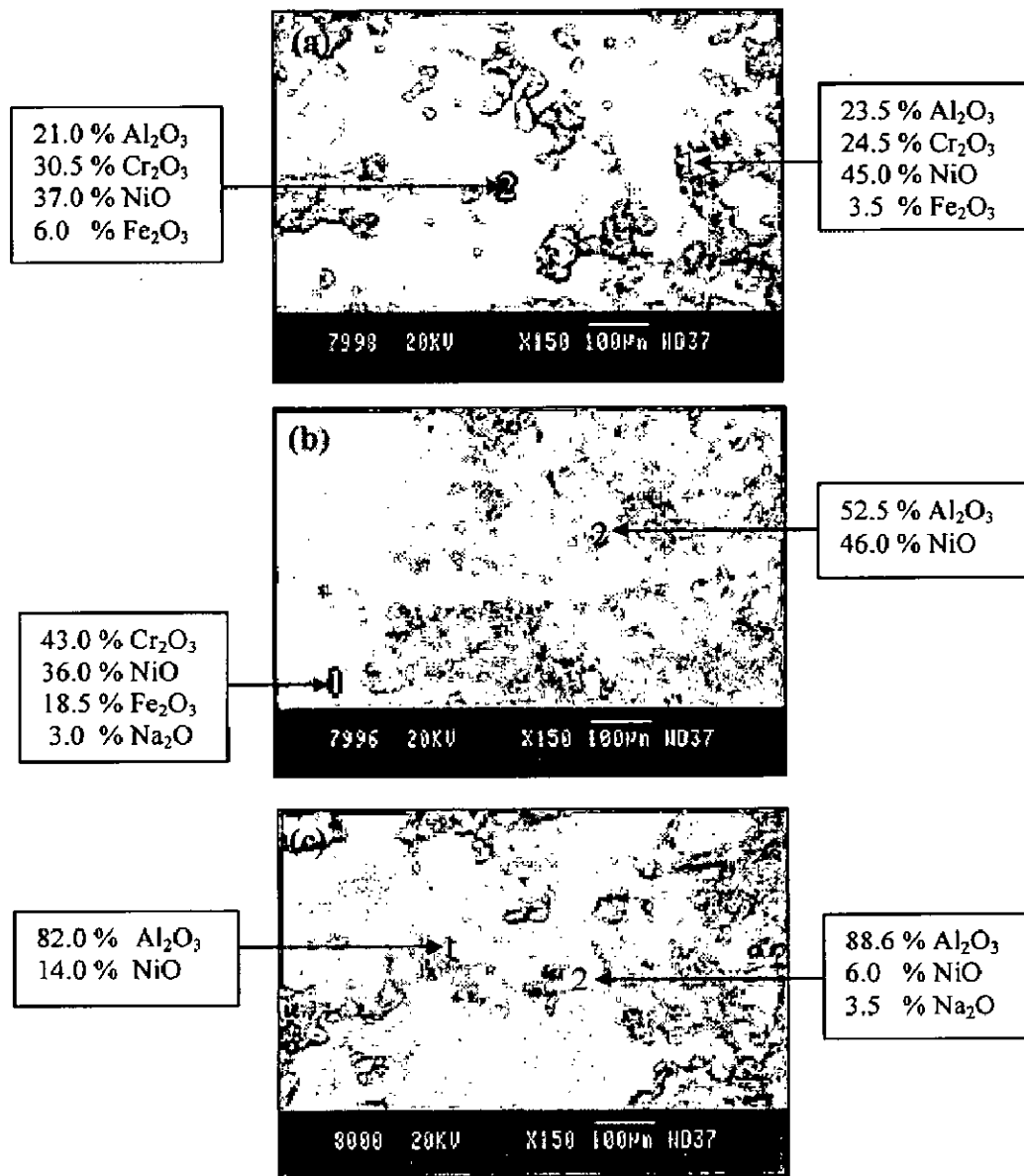


**Fig. 4.24:** Surface-scale morphology and EDAX patterns from different spots on Ni-5Al coated (a) Superni 76; (b) Superni 750 and (c) Superfer 800 in molten salt ( $\text{Na}_2\text{SO}_4$ -60% $\text{V}_2\text{O}_5$ ) environment at 900°C after 100 cycles.

#### 4.4.3.4.2. Cross sectional analysis

EDAX analysis was carried out at different points of interest along the cross section of HVOF sprayed Ni-5Al coated corroded samples viz. Superni 76, Superni 750 and Superfer 800 as shown in Fig. 4.25 using Field Emission Scanning Electron Microscope (FESEM,

FEI, Quanta 200F) company, with EDAX Genesis software attachment. EDAX analysis of the oxide scale across the cross section of Ni-5Al coated Superni 76 alloy after 100 cycles at 900°C in molten salt environment indicates a light grey layer in the top part of the scale (point 1) shown in Fig 4.25a, which is rich with oxides of nickel. The presence of about 28 wt% oxygen at point 1 shows that oxygen has penetrated through the scale formed on the Ni-5Al coated Superni 76. Point 2 in Fig.4.25a, indicates the presence of oxides Ni, Al and Cr. Al and Cr are present at the Ni splat boundaries. The points 3, 4 and 5 show the presence of higher amount of Ni and oxygen in lower amount, which indicate that Ni has partially oxidized. EDAX analysis for Fe, Cr and Mn elements revealed outward diffusion from the substrate.

For SN 750 alloy with Ni-5Al coating indicates that the oxide scale is intact and the upper layer is rich in NiO and Al<sub>2</sub>O<sub>3</sub>. Presence of oxygen indicates the penetration through the oxide scale formed on the coating. EDAX analysis indicated that the inner layer (point 3, 4) in Fig. 4.25b composed of aluminum, nickel, chromium, oxygen and iron. Little amount of oxygen is present near the coating-substrate interface, which might have penetrated during the initial period of exposure.

In case of Ni-5Al coated SF 800 alloy, the formation of oxides of Ni, Cr, and Al are observed. The light grey color at the upper layer indicates the presence of nickel oxide (point 1 and 2) in Fig. 4.25c. The black contrast area indicates the presence of chromium (point 3). Some cracks are observed on the upper part of the coating. EDAX analysis at point 4 shows a lower amount of oxygen indicating the partial oxidation of nickel. Point 5 indicates the presence of nickel, chromium, aluminum and oxygen. Very little amount of oxygen is present near the coating substrate interface, suggesting that some oxygen might have penetrated during initial cycles of hot corrosion runs. The splat boundaries and pores present in the coating are clogged due to formation of oxides, which might have blocked the penetration of reacting species towards the base alloy.



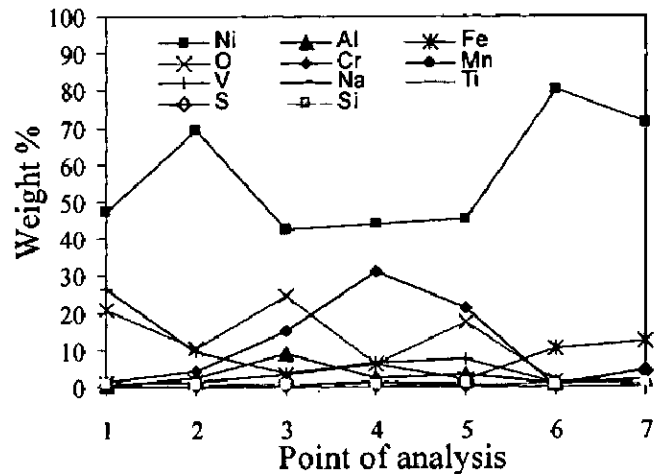
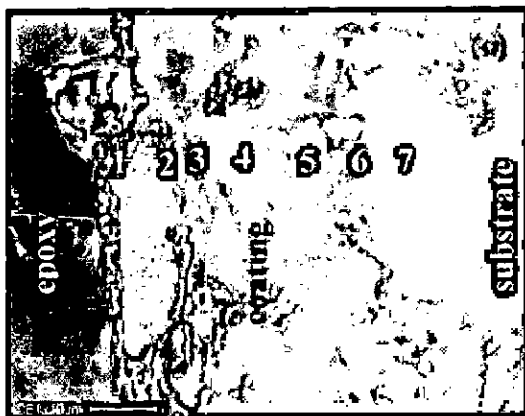
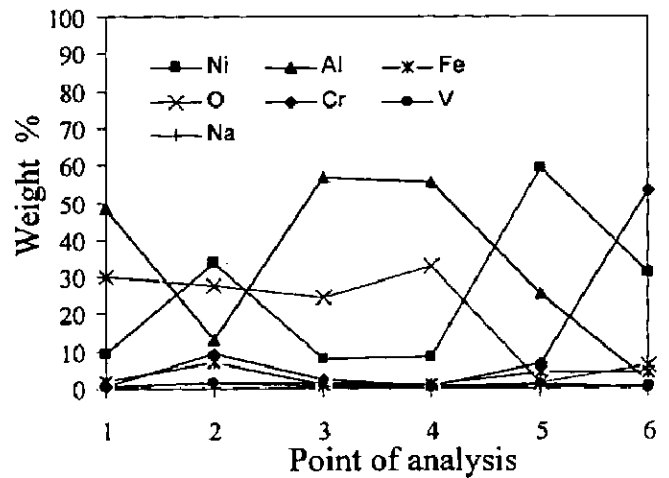
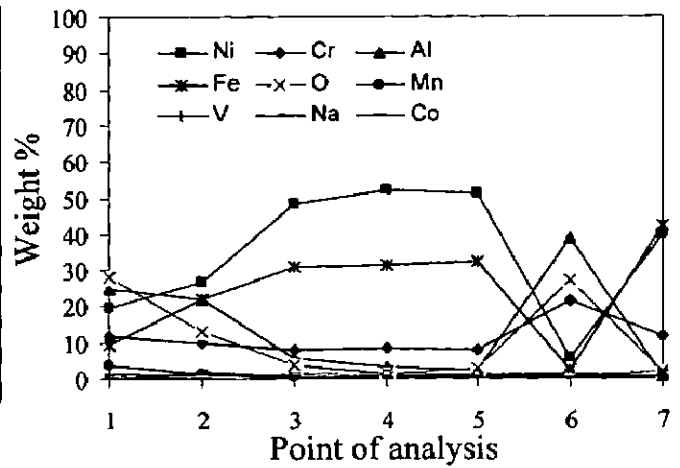
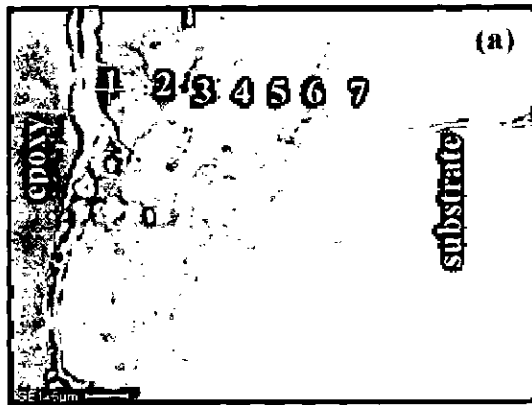


**Fig. 4.25:** Oxide scale morphology and variation of elemental composition across the cross-section of the Ni-5Al coated (a) Superni 76, (b) Superni 750 and (c) Superfer 800 subjected to the cyclic oxidation at 900°C in molten salt environment after 100 cycles.

#### 4.4.3.5 X-ray mapping of different elements

The corroded samples were cut using Buehler ISOMET 1000 precision saw and then it is mounted in transoptic powder for mirror polishing prior to studying its cross sectional features. The polished samples were then carbon coated to facilitate the X-ray mapping of different elements present across the corroded samples by using FESEM (FEI, Quanta 200F) as shown in Fig. 4.26. X-ray mapping for the Ni-5Al coated on Superni 76 at 900°C after 100 cycles in molten salt ( $\text{Na}_2\text{SO}_4\text{-60\%V}_2\text{O}_5$ ) environment is shown in Fig.4.26a. The elemental maps for Ni, Cr, Fe and O indicates that the scale is mainly rich in oxides of nickel, chromium and iron. Aluminum oxide is present in the subscale regions. Small amount of sodium has diffused from the environment into the scale through the splat boundaries as seen in the Fig 4.25a. Traceable amount of Mo has diffused into the coating from the substrates. The scale of Ni-5Al coated Superni 750 indicates the top scale mainly consists of aluminum oxide and nickel oxide as shown in Fig. 4.26b. The elemental maps reveal that the Ni rich splats, which are present beneath the top scale are mostly unoxidised. Chromium and Iron shows a relatively higher percentage near the coating-substrate interface indicating their diffusion from the substrate to coating. Sodium and silicon are also found in the scale in very small amount, which may have diffused along the splat boundaries. The X-ray mapping for Ni-5Al coated on Superfer 800 alloy is shown in Fig. 4.26c. A dense and thick scale consisting mainly of aluminum and nickel oxide is observed. Fe and Cr are present near the coating-substrate interface indicating the diffusion behaviour of the substrate into the coating. Higher percentage of iron has diffused into the substrate compared to the chromium. Titanium has migrated from the substrate to the coating and is present along splat boundaries. Streaks of manganese oxide are present in the oxidized coating near the substrate coating interface.

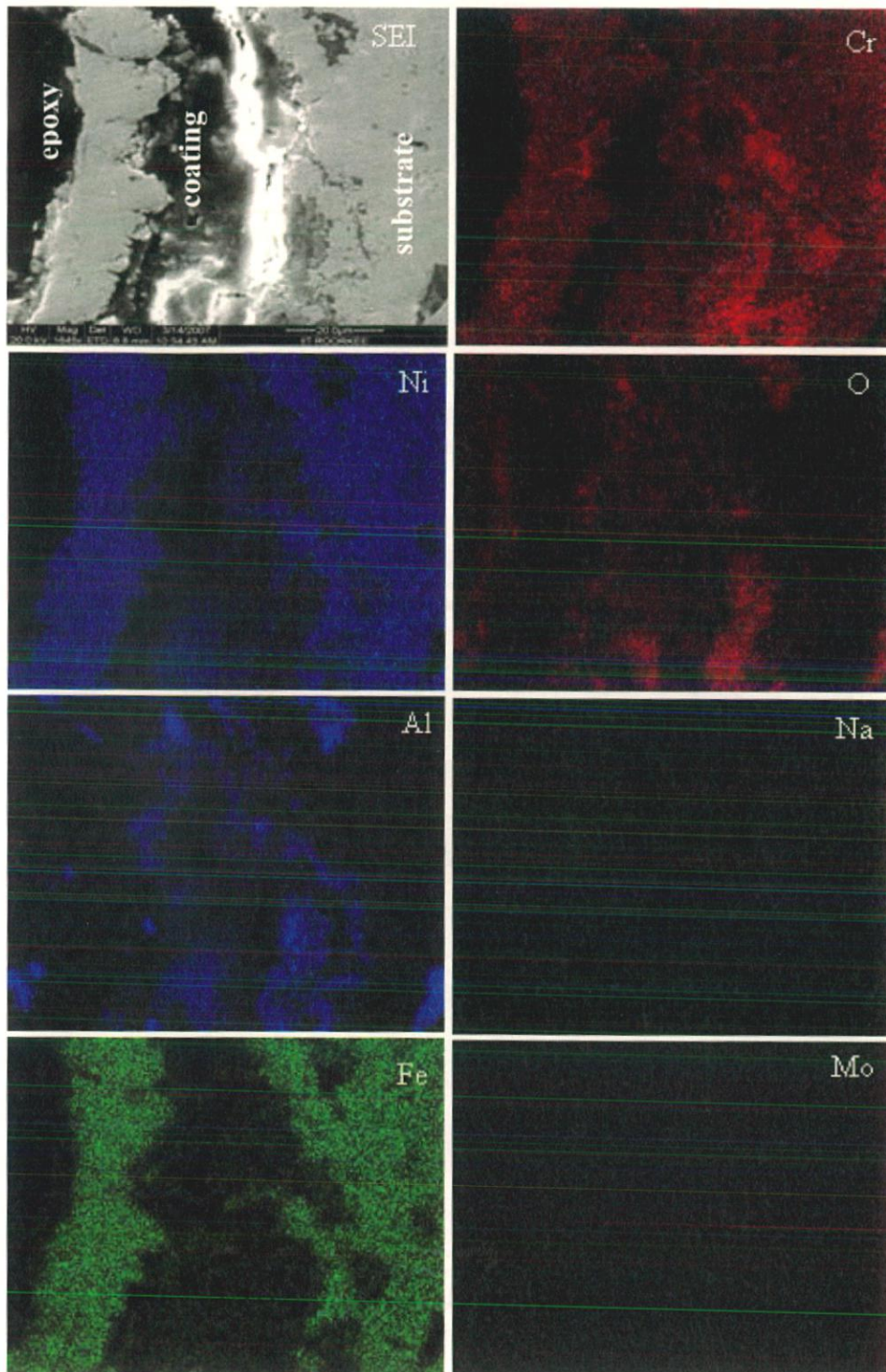


**Fig. 4.26(a):** Composition image (BSEI) and X-ray mapping of the cross-section of SN-76 coated with Ni-5Al subjected to cyclic oxidation in  $\text{Na}_2\text{SO}_4$ -60% $\text{V}_2\text{O}_5$  environment at 900°C.

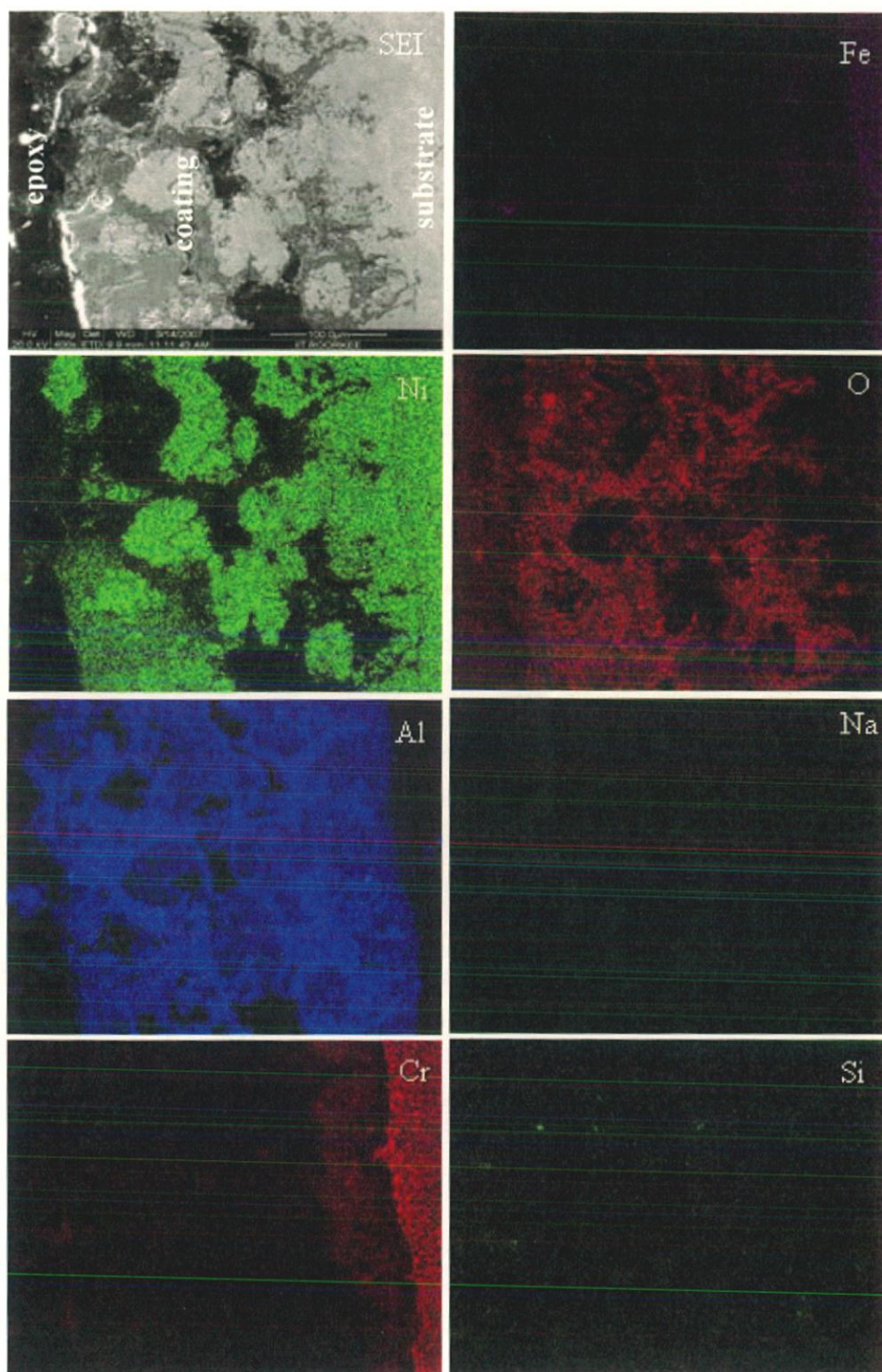


**Fig. 4.26(b):** Composition image (BSEI) and X-ray mapping of the cross-section of SN-750 coated with Ni-5Al subjected to cyclic oxidation in  $\text{Na}_2\text{SO}_4\text{-60\%V}_2\text{O}_5$  environment at  $900^\circ\text{C}$ .

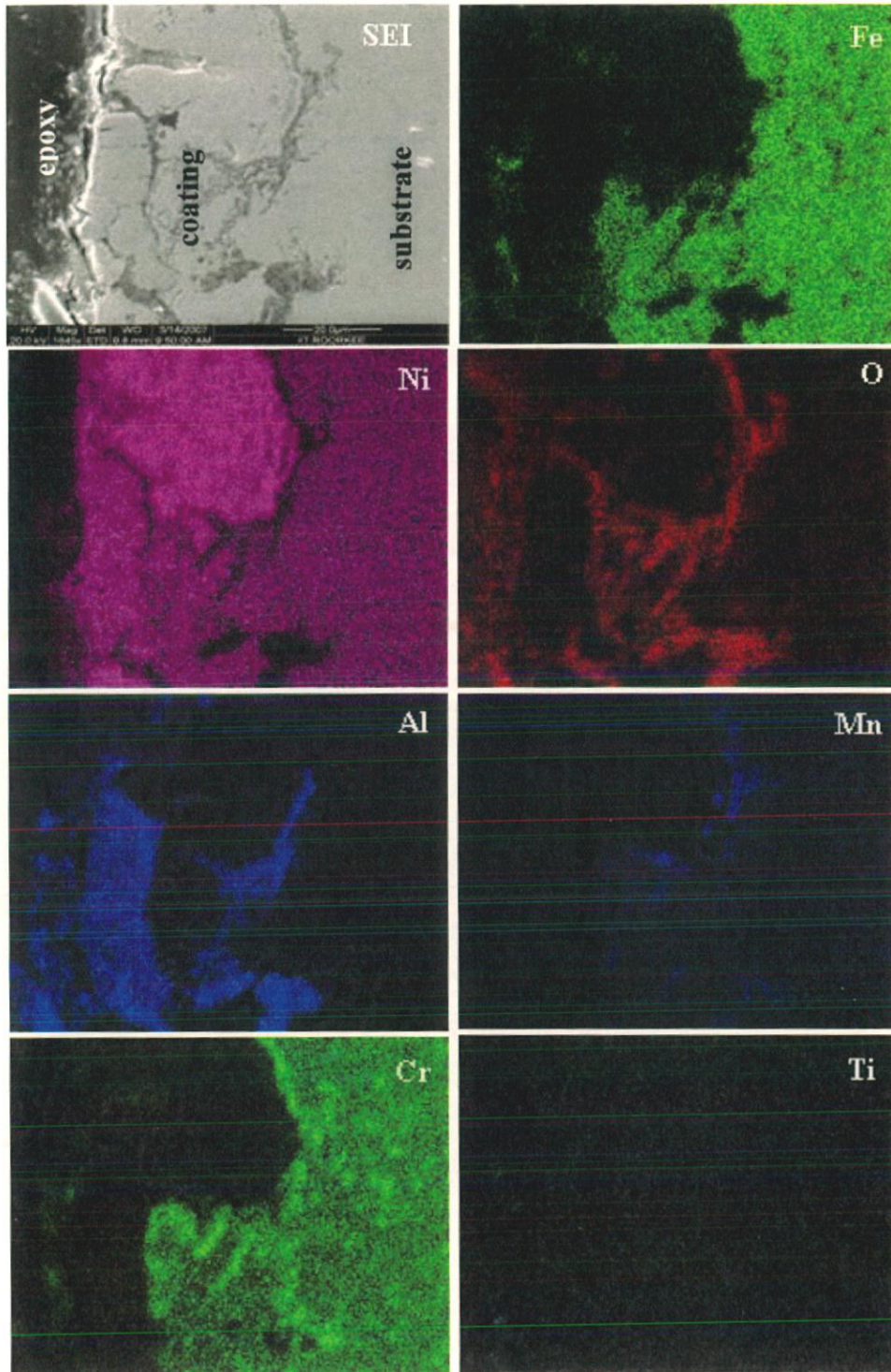
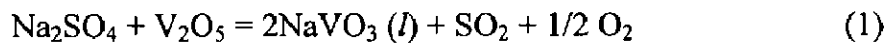


**Fig. 4.26(c):** Composition image (BSEI) and X-ray mapping of the cross-section of SF-800 coated with Ni-5Al subjected to cyclic oxidation in  $\text{Na}_2\text{SO}_4$ -60% $\text{V}_2\text{O}_5$  environment at  $900^\circ\text{C}$ .

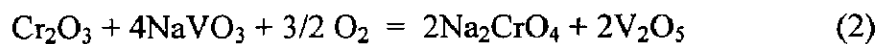
#### 4.4.4 Discussions

The surface macrographs of bare and Ni-5Al coated superalloys after hot corrosion studies are shown in Fig. 4.18. It is observed from the macrographs that the oxide scale was intact with the coating and marginal spalling was observed from the surface. Few light green patches were seen on the surface of the corroded samples. The greenish color of the scale in the case of coated superalloys may be attributed to the presence of NiO in the scale, which is identical to the findings of Bornstein et al, (1975) and Buta Singh, (2003).

The mass gain of the bare alloys is gradual whereas the mass gain of the Ni-5Al coated superalloys was high during the initial stages and then it becomes nearly constant as observed in Fig. 4.19. The rapid increase in the mass gain during the initial period of exposure to molten salt environment at 900°C may be due to the rapid diffusion of oxygen through the molten salt layer. Kolta et al, (1972) proposed that in the temperature range of 900°C, the Na<sub>2</sub>SO<sub>4</sub> and V<sub>2</sub>O<sub>5</sub> will combine to form NaVO<sub>3</sub>, as represented by eq. (1) having a melting point of 610°C.



This NaVO<sub>3</sub> acts as a catalyst and also serves as an oxygen carrier to the base alloy through the open pores present on the surface, which will lead to the rapid oxidation of the base elements of the substrates to form a protective oxide scale. Hence, an increase in the mass gain of the bare superalloys occurs in the early stages of hot corrosion. There may also be simultaneous dissolution of Cr<sub>2</sub>O<sub>3</sub> in the molten salt due to the reaction (Seiersten and Kofstad, 1987; Swaminathan et al, 1993)



During the subsequent cycles, the formations of oxides have blocked the diffusion of corrosive species by covering the pores and the splat boundaries. The formation of oxides at the splat boundaries is confirmed by the X-ray mapping analysis (Fig. 5.24). The rapid increase in the mass gain during the initial period was also reported by Sidhu et al (2006E), Harpreet Singh et.al, (2005C), Tiwari and Prakash, (1997) and Ul-Hamid, (2003) during their studies on the hot corrosion of superalloy materials.

In case of coated alloys, aluminum from the coating and chromium, iron and titanium diffused from the alloy and gets oxidized and nickel splats have remained unoxidised. Once these oxides of aluminum, chromium has formed at the intersplat regions, they block the diffusion of corrosive species across the coating. Therefore, in the initial stages, oxidation

rate is fast, afterwards the curve levels off indicating the protection provided by the partially oxidized coating. This coating was compact and adherent upto 100 cycles.

The parabolic rate constant for the bare superalloy is found to be greater than that of Ni-5Al coated superalloys. It can be inferred that the HVOF sprayed Ni-5Al coating has provided the necessary protection to the superalloys. Particularly, Ni-5Al coated on Superfer 800 has shown a high resistance to hot corrosion and provided the best protection.

The XRD analysis (Fig. 4.22) of the Ni-5Al coated superalloys after hot corrosion study at 900°C in molten salt environment indicates that the Ni-5Al coating has provided the better protection to the superalloys, which may be due to the formation of  $\alpha$ -Al<sub>2</sub>O<sub>3</sub>, NiO, Cr<sub>2</sub>O<sub>3</sub>, as confirmed by EDAX analysis. These oxides are very protective as reported by Ul-Hamid, (2003) and Sundararajan et.al, (2004A). The presence of NiAl<sub>2</sub>O<sub>4</sub> and NiO also reported by Lee and Lin (2003) during their hot corrosion studies on Ni<sub>3</sub>Al intermetallic compound at 800 and 1000°C. They opined that the NiAl<sub>2</sub>O<sub>4</sub> spinel might have better hot corrosion resistance than NiO since the solubility of NiAl<sub>2</sub>O<sub>4</sub> spinel is thermodynamically smaller than that of NiO in the molten salt. The role of coating is sacrificial as it act as reservoir for the formation of oxides or spinels. In case of coated Superfer 800 alloy, protective oxides such as Al<sub>2</sub>O<sub>3</sub>, NiO and NiAl<sub>2</sub>O<sub>4</sub> spinel have provided the best protection to the substrate alloy. Other oxides formed after the exposure to molten salt environment are, NiCr<sub>2</sub>O<sub>4</sub>, FeVO<sub>4</sub> and MnO.

EDAX analysis (Fig.4.23) revealed that in the case of bare Superni 750 after exposing to molten salt environment, small pores are seen thereby indicating possible escape of vapourised phases. These pores can help corroding species to easily penetrate into the substrate and cause the damage. Whereas, in the case of Superni 76 and Superfer 800 the mass gain was comparatively lower. The EDAX analysis of the scale for the Ni-5Al coated (Fig.4.24) specimens has shown Al<sub>2</sub>O<sub>3</sub>, Cr<sub>2</sub>O<sub>3</sub>, Fe<sub>2</sub>O<sub>3</sub> and NiO phases. The presence of these oxides at the surface decrease oxygen availability in the underlying alloy and favor the most thermodynamically stable oxide i.e. Cr<sub>2</sub>O<sub>3</sub> (Ul-Hamid, 2003). The results of EDAX are further supplemented by XRD analysis, which confirmed the presence of Al<sub>2</sub>O<sub>3</sub>, NiO, and Cr<sub>2</sub>O<sub>3</sub>. The Ni-5Al coating on all the superalloys was effective in reducing the hot corrosion in the given molten salt environment, thus indicating the protective nature of the coating used.

Cross sectional EDAX analysis for coated Superni 76 alloy Fig. 4.25a indicates that the top scale is rich in NiO. The presence of oxides of Al and Cr in the subscale region might have acted as diffusion barrier to the inward diffusion of corrosive species. Formation of

small amount of  $\text{Fe}_2\text{O}_3$  as indicated by EDAX and supported by X-ray mapping may be due to their diffusion of Fe from substrate to coating at high temperature. For Ni-5Al coated SN 750 alloy, it is indicated that the oxide scale is intact and the upper layer is rich in nickel oxide and aluminum oxide. Nickel rich splats are present in the subscale regions which are unoxidised as observed from Fig. 4.25b. In case of Ni-5Al coated SF 800 alloy Fig. 4.25c, protective oxides of nickel, chromium and aluminum have formed on the surface. Thereafter, the splat boundaries and pores present in the coating are clogged due to formation of oxides, which might have blocked the penetration of reacting species towards the base alloy. Small amount of chromium, iron and titanium have diffused from the substrate into the coating at high temperature.

The elemental mapping shows that the in case of Ni-5Al coated Superni 76 alloy Fig. 4.26a, nickel, chromium, aluminum, iron and oxygen coexists with each other suggesting the formation of oxides of nickel, chromium, aluminum and iron which is well supported by surface XRD and EDAX analysis. Iron and chromium have diffused into the coating from the substrate. The scale of Ni-5Al coated Superni 750 indicates the top scale is rich in aluminum oxide and splats of unoxidised nickel, beneath the top surface are found as shown in Fig. 4.26b. Aluminum is found at the periphery of nickel rich splats. At some places, nickel and oxygen coexists indicating the formation of nickel oxide on the top surface. The elemental maps reveal that the Ni rich splats mostly unoxidised beneath the top scale. This is confirmed by cross sectional XRD and EDAX analysis. A band of chromium is present near the coating substrate interface. The X-ray mapping for Ni-5Al coated on Superfer 800 alloy is shown in Fig. 4.26c which indicates that nickel is partially oxidized and aluminum is found at the nickel rich splat boundaries. A dense and thick scale consisting of aluminum, nickel and oxygen coexist suggesting the formation of oxides of aluminum and nickel. A thick band of chromium is present near the coating substrate interface. The results are confirmed with surface EDAX and XRD analysis. On the basis of the results of X-ray mapping, SEM, EDAX (surface/cross-section) and XRD analyses, schematic representation of the possible hot corrosion mode for the Ni-5Al coated Superni 750 subjected to the molten salt environment for 100 cycles at  $900^\circ\text{C}$  is shown in Fig. 4.27.



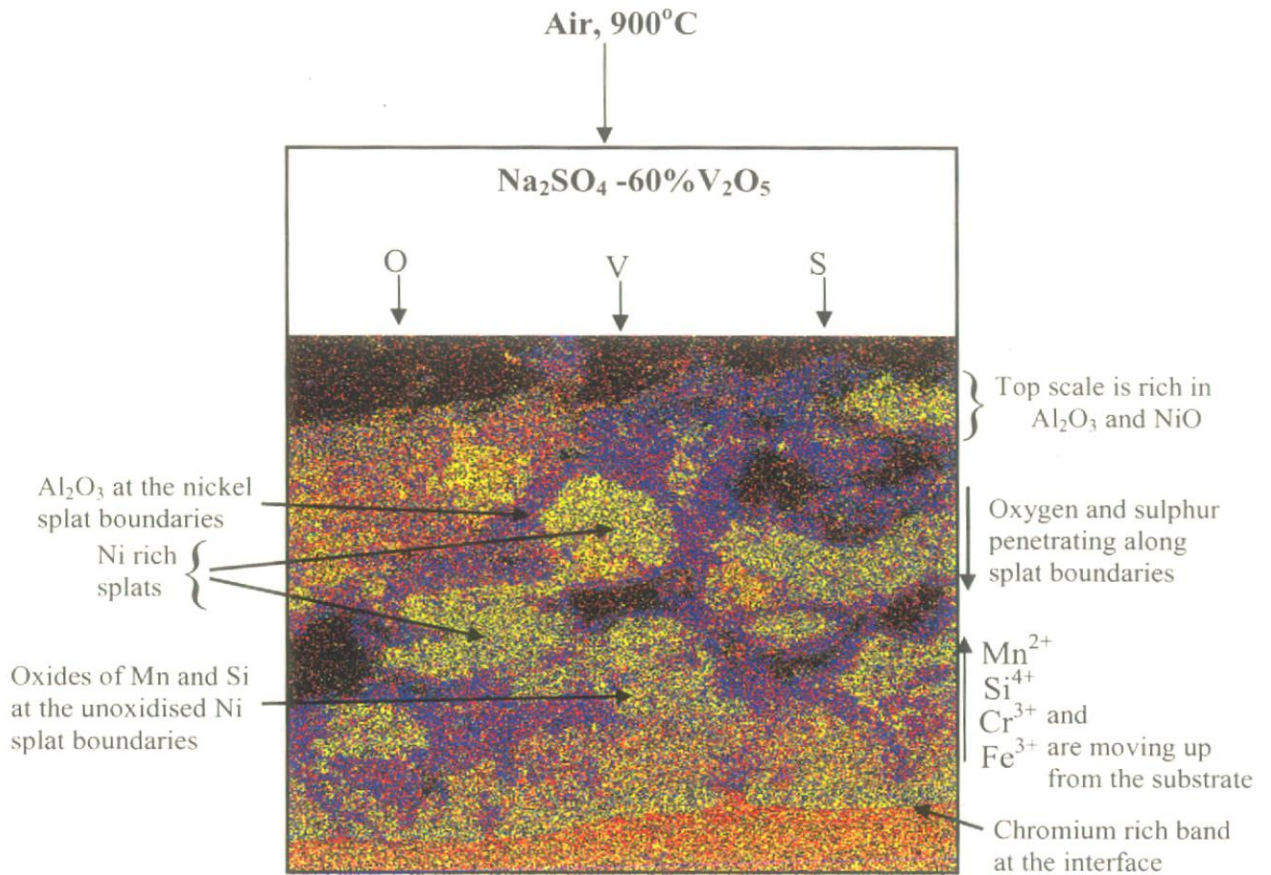


**Fig. 4.27:** Schematic diagram showing the possible hot corrosion mode for the Ni-5Al coated Superni 750 exposed to the Na<sub>2</sub>SO<sub>4</sub>-60 %V<sub>2</sub>O<sub>5</sub> environment at 900°C for 100 cycles.

#### 4.4.5 Conclusions

The hot corrosion behaviour of HVOF sprayed Ni-5Al coatings on Superni 76, Superni 750 and Superfer 800 alloys in aggressive environment of  $\text{Na}_2\text{SO}_4$ -60% $\text{V}_2\text{O}_5$  at 900°C has been investigated and the following conclusions are made.

1. The HVOF sprayed Ni-5Al coating indicated improved resistance to hot corrosion behaviour as compared to bare superalloys in the aggressive environment of  $\text{Na}_2\text{SO}_4$ -60% $\text{V}_2\text{O}_5$  at 900°C.
2. The bare superalloys have shown extensive spalling and peeling of the scale and the mass gain was relatively more than the Ni-5Al coated superalloys.
3. The colour of the oxide scale formed on the surface of the coated specimens is brown colour with green patches after exposing to the molten salt environment at 900°C.
4. The parabolic rate constants of Ni-5Al coated superalloys are much lower than the bare superalloys subjected to cyclic oxidation in molten salt environment indicating the protective behaviour of the HVOF sprayed Ni-5Al coating.
5. Ni-5Al coating has led to the reduction in weights of about 53%, 46% and 57% for Superni 76, Superni 750 and Superfer 800 alloys respectively. The necessary protection of the Ni-5Al coating to the substrates in molten salt environment which followed the sequence:

Superfer 800 > Superni 76 > Superni 750

6. The hot corrosion resistance of Ni-5Al coated Superfer 800 is better compared to other two Ni-5Al coated superalloys in the given molten salt environment. This may be due to the presence of thick band of chromium near the coating substrate interface. The better hot corrosion resistance may also be attributed to the formation of  $\text{NiAl}_2\text{O}_4$  spinels revealed by XRD analysis. The scale formed on the surface is compact and adherent to the coating.
7. There is a perceptible diffusion of some elements from the substrate to the coating as observed in the elemental mapping analysis.

## **Part II – RF Magnetron Sputtered coatings**

### **4.5 CHARACTERISATION AND OXIDATION STUDIES**

#### **4.5.1 Introduction**

Ni–Al alloys exhibit a wide range of favorable physical and mechanical characteristics, such as low density, high melting temperature, high thermal conductivity, attractive stiffness, good oxidation resistance, and metal-like electrical conductivity. This makes Ni–Al of interest for various applications including high pressure turbine blades, interconnections in electronic components, high temperature corrosion protective coatings, surface catalysts, high-current vacuum circuit breakers, and electronic metallizations in semiconductor heterostructures, microelectronics (Chang et al, 2006; Zhong et al, 2000), high temperature environmental coatings (Goward, 1970). The importance of these intermetallic materials stems from: (i) excellent resistance to oxidation; (ii) maintaining strength at high temperature; and (iii) low density (Rastogi, et al, 1994). Aluminide coatings deposited either by pack cementation or by chemical vapor deposition techniques (CVD), have been applied to gas turbine vane and blade airfoils since approximately 1970 (Goward, 1998). Lee et al. (1995) fabricated very thin ( $t = 100$  nm) Ni-Al underlayer films using magnetron sputtering and a target which was a Ni-Al material with the same composition as desired in the film. Thin-film nickel aluminides are generally produced by solid-state reactions between Ni and Al during heating of the Ni Al multilayer thin films. The other possibilities of forming NiAl thin films are to use dual magnetron co-sputter deposition of Ni Al alloy targets or Ni and Al separate targets, and to deposit films from a NiAl compound target. However, there is no reported literature on the latter technique (Zhong et al, 2000). For high temperature aerospace applications, two types of diffusion techniques at 1000-1100°C are generally employed in order to form the NiAl-type protective coatings (Pichoir, 1978).

As per the knowledge of the authors, literature is very scarce on the high temperature oxidation behavior of Ni-Al thin films on Ni and Fe-based superalloys deposited by RF magnetron sputtering process. In the present work, an attempt has been made to characterise and study the high temperature oxidation behaviour of Ni-Al thin films on Ni and Fe- based superalloys in air at 900°C under cyclic conditions. The oxidised specimens were characterised using the combined techniques of XRD and FESEM attached with EDS.

## 4.5.2 Experimental Details

The experimental details of the RF magnetron sputtering process are explained in section 3.2.3.2 of Chapter 3. Fig.4.28 shows the image of the Ni-Al targets after RF magnetron sputtering process.

## 4.5.3 Results

### 4.5.3.1 Characterisation of the Ni-Al film

#### 4.5.3.1.1 XRD analysis of the as deposited Ni-Al film

The XRD patterns of Ni-Al films deposited on different superalloy substrates for a period of 2 hour and 30 minutes is shown in Fig.4.29. The main phase obtained in case of SN 76 and SN 750 was  $\gamma$ -Ni and in case of SF 800 the main phase obtained was AlNi<sub>3</sub>. The XRD results indicated that the deposited film has a crystallite size of 8 nm, 9 nm and 16 nm for SN 76, SN 750 and SF 800 respectively.

#### 4.5.3.1.2 AFM analysis of the as deposited Ni-Al film

The surface morphology of the films was studied using atomic force microscope (NT-MDT: NTEGRA Model) in semi-contact mode. Fig. 4.30 shows the AFM images of the films deposited on different superalloy substrates. The surface roughness of the deposited film in case of SN 76 was around 58 nm and for SN 750 and SF 800 is 32 nm, 60 nm, respectively.

#### 4.5.3.1.3 FESEM/EDAX analysis of the Ni-Al film

The Ni-Al films deposited by RF magnetron sputtering on all three superalloys are shown in Fig.4.31. It is noticed from the FESEM/EDAX analysis that in case of SN 76 and SN 750 alloy, the deposited film is rich in nickel with small amount of aluminum. The film was deposited uniformly over the entire surface of the specimens. Fig. 4.32 shows the cross sectional image of the Ni-Al film deposited on SN 750 alloy. The coating thickness was measured at different locations along the cross section for all the three superalloys. The thickness of the film was found to be around 3- 4  $\mu$ m for the given process parameters. EDAX analysis was carried out at different points of interest along the cross section of Ni-Al deposited film on SN 750 as shown in Fig. 4.33 using Field Emission Scanning Electron Microscope with EDAX Genesis software attachment. It is noticed that the film is rich in nickel with aluminum in small amounts.

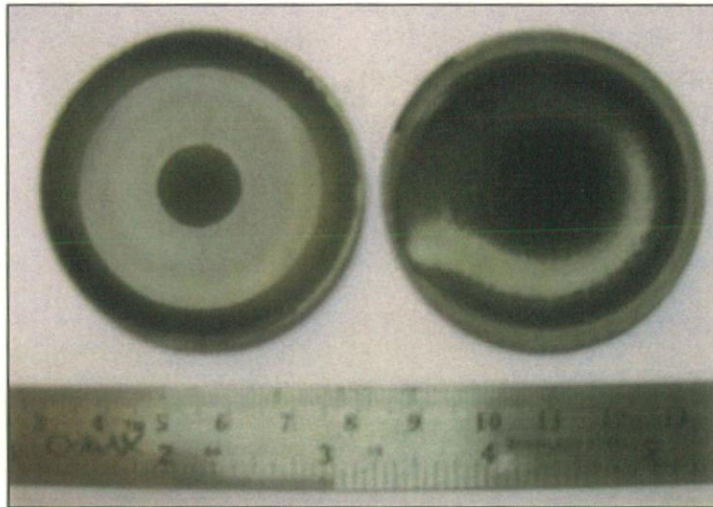


**Fig. 4.28:** The image of Ni-Al target after sputtering process.

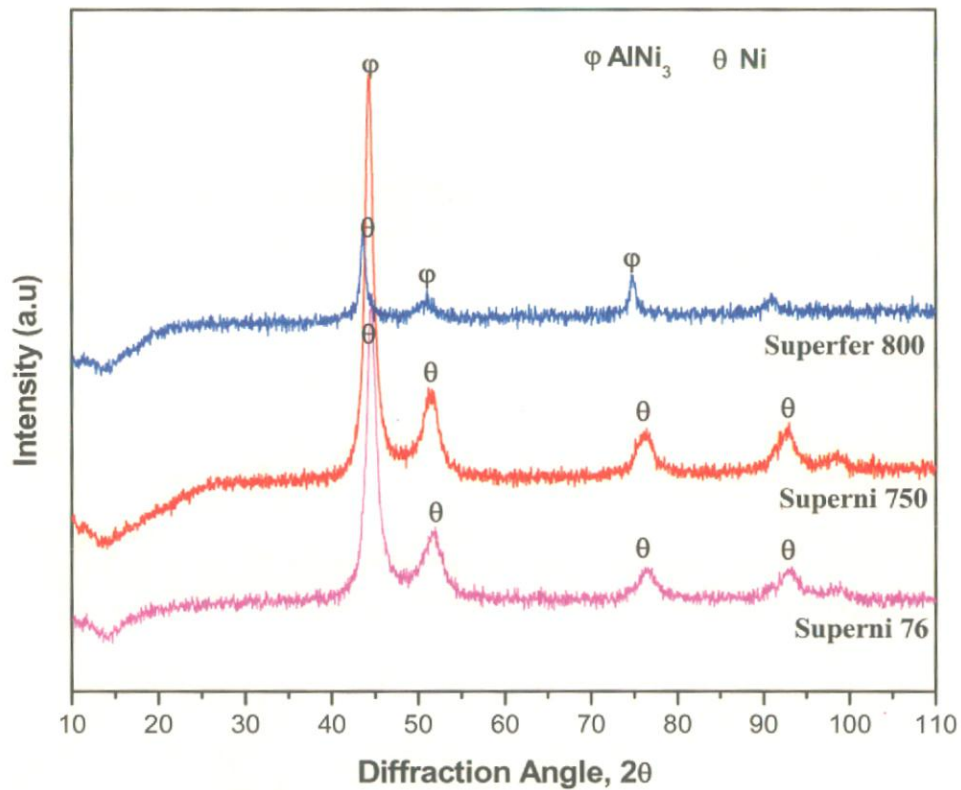


**Fig. 4.29:** XRD patterns indicating the Ni-Al film deposited on different superalloy substrates by RF magnetron sputtering.

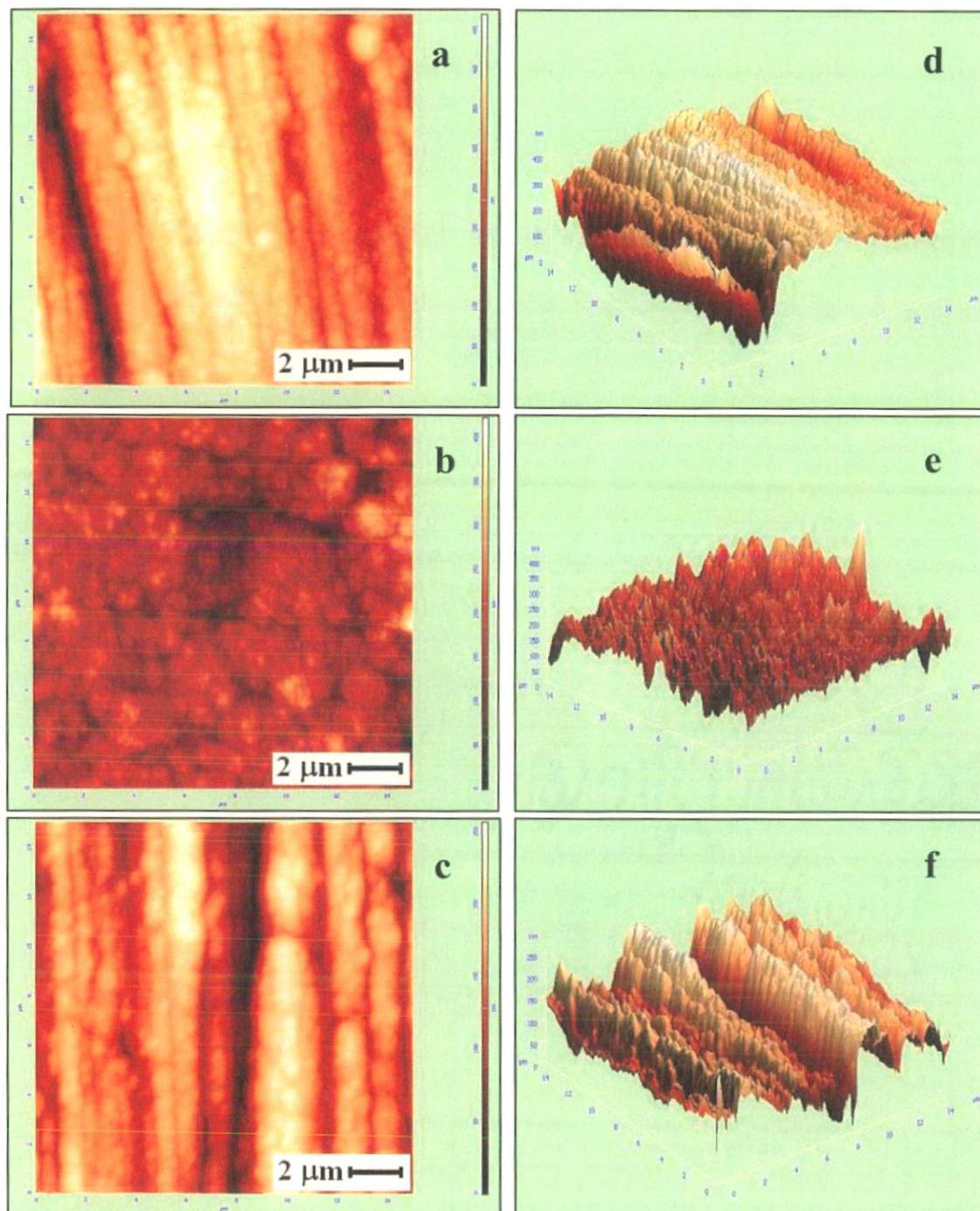


**Fig. 4.30:** AFM images of Ni-Al film on (a) Superni 76, (b) Superni 750 and (c) Superfer 800 by RF magnetron sputtering.

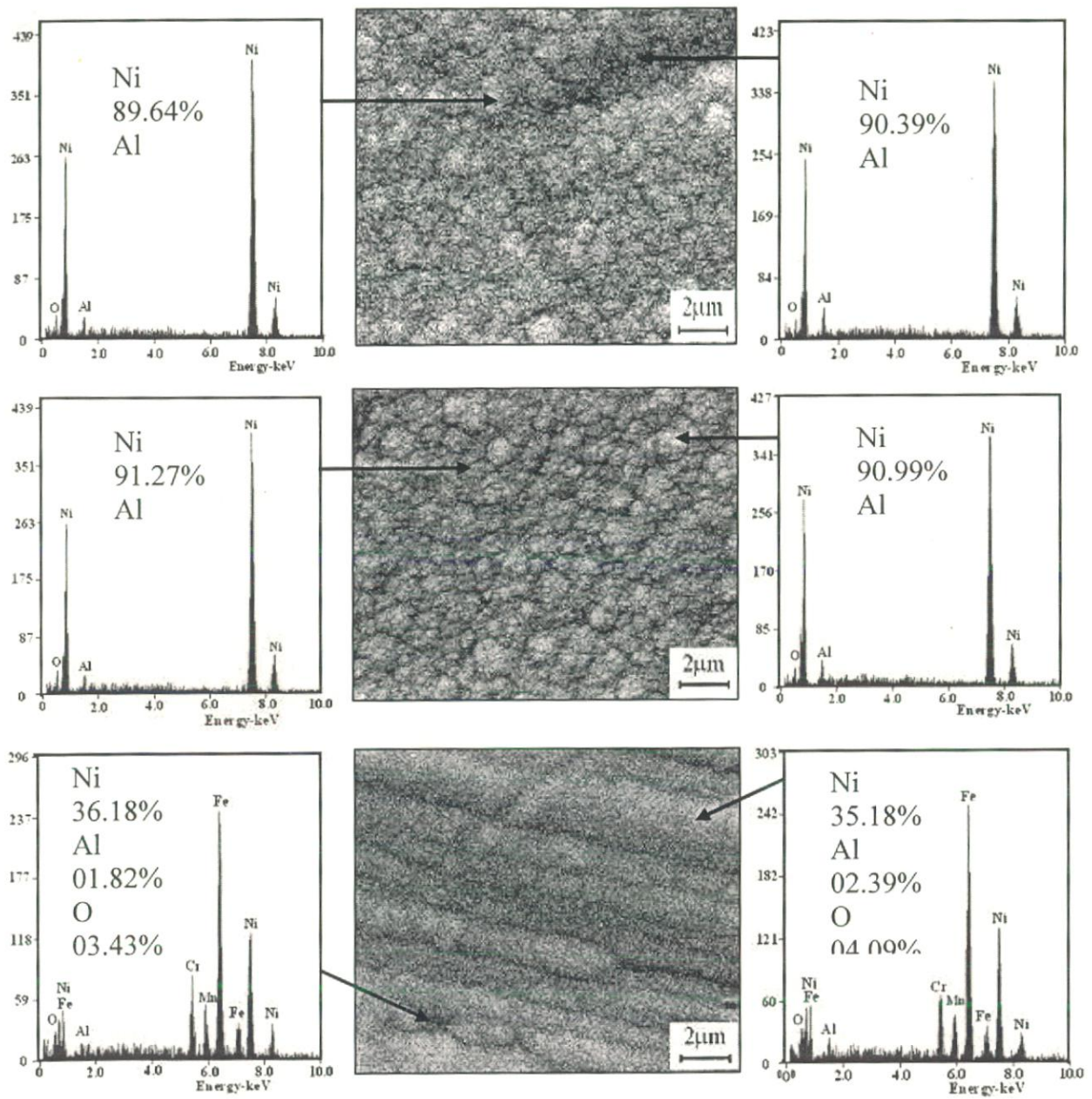


**Fig.4.31:** Surface morphology and EDAX analysis of Ni-Al film deposited on (a) Superni 76, (b) Superni 750 and (c) Superfer 800 alloy.

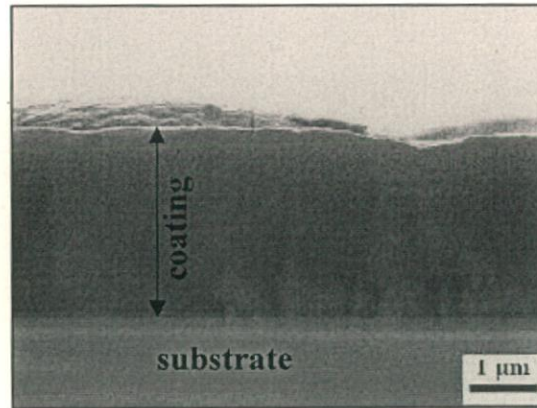


**Fig. 4.32:** Thickness of Ni-Al film deposited on superalloy by RF magnetron sputtering.

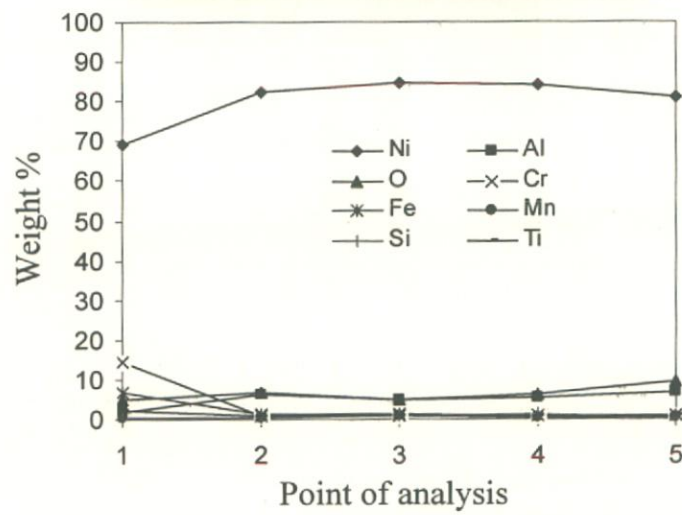
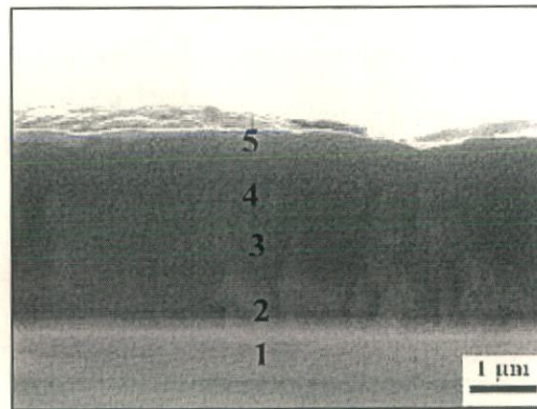


**Fig. 4.33:** Cross sectional EDAX analysis of RF magnetron sputtered Ni-Al film on Superni 750.



### 4.5.3.2 Oxidation Studies In air

#### 4.5.3.2.1 Visual Observations after cyclic oxidation studies

The macrographs of the coated oxidised specimens after 100 cycles exposure in air is shown in Fig. 4.34. In case of coated Superni 76, the surface of the specimen turned into light grey in color after the completion of second cycle. Microspattering of the coating was observed after the completion of third cycle. The microspalling of the coating continued upto seventh cycle. The spalling of the scale has reduced with further exposure. After the completion of 100 cycles, the surface of the specimen turned into a mixture of greenish and brown color as shown in Fig. 4.34(a).

In case of coated Superni 750, the surface of the specimen turned into greenish color after the completion of second cycle. The coating cracked at the edges after second cycle. The coating started spalling after second cycle and continued upto ninth cycle. The spalling of the coating stopped after ninth cycle and the color of the specimen turned greenish in color after 100 cycles as shown in Fig. 4.34(b).

In case of coated Superfer 800, the surface of the specimen turned grey in color after the completion of second cycle. Microspalling of the coating was observed after third cycle. The microspalling of the coating was observed upto six cycles and then stopped. The surface indicated a grey color after the completion of 100 cycles as indicated in Fig. 4.34(c).

#### 4.5.3.2.2 Cyclic oxidation studies at 900°C in air

The weight gain per unit area versus number of cycles plots for the bare and coated alloys is depicted in Fig.4.35. The weight gain is high in case of bare (uncoated) superalloys compared to Ni-Al deposited superalloys under the same conditions. In case of coated Superni 76 and Superfer 800 superalloys, the weight loss was observed after 3<sup>rd</sup> cycle and 10th cycle of the experiment. In case of coated Superni 750, microspalling of the coating was observed after second cycle and continued upto ninth cycle. Furthermore, adherent oxide scale was formed on the surface of the coated specimens during subsequent cycles and further spallation has stopped. The square of weight gain per unit area versus number of cycles indicates that the Ni-Al coated Superni 76 and Superfer 800 followed the parabolic rate law whereas, coated Superni 750 alloy slightly deviated from the parabolic rate law as observed from Fig.4.36. The bare alloys slightly deviate from the parabolic rate law. The maximum weight gain ( $\text{mg}/\text{cm}^2$ ) was observed in case of bare SN 750 whereas bare SF 800 shows a minimum weight gain in the given environment. In case of coated superalloys, SF 800 alloy indicated the least weight gain and coated SN 750 has shown the higher weight gain. The parabolic rate constant  $k_p$  were obtained from the slope of the linear regression fitted line

(cumulative weight gain / area)<sup>2</sup> versus number of cycles. The nature of fit, parabolic rate law, for oxidation experiments are also shown in Fig. 4.36. The  $k_p$  values for the bare SN 76, Sn 750 and SF 800 are  $1.0 \times 10^{-10} \text{ g}^2 \text{ cm}^{-4} \text{ s}^{-1}$ ,  $2.15 \times 10^{-10} \text{ g}^2 \text{ cm}^{-4} \text{ s}^{-1}$  and  $0.55 \times 10^{-10} \text{ g}^2 \text{ cm}^{-4} \text{ s}^{-1}$  respectively. Whereas, the parabolic rate constants in case of Ni-Al coated SN 76, SN 750 and SF 800 are  $0.06 \times 10^{-10} \text{ g}^2 \text{ cm}^{-4} \text{ s}^{-1}$ ,  $0.29 \times 10^{-10} \text{ g}^2 \text{ cm}^{-4} \text{ s}^{-1}$  and  $0.032 \times 10^{-10} \text{ g}^2 \text{ cm}^{-4} \text{ s}^{-1}$ , respectively. The cumulative weight gain/unit area for bare and Ni-Al coated superalloys is shown in Fig. 4.37.

#### 4.5.3.2.3 Surface scale analysis

##### 4.5.3.2.3.1 X ray diffraction analysis

X-ray diffractograms of the Ni-Al coated films on superalloy substrates after cyclic oxidation in air for 100 cycles at 900°C are shown in Fig. 4.38. The oxides formed on the scale of the Ni-Al coated SN 76 superalloy consists of NiO, Fe<sub>2</sub>O<sub>3</sub>, Ni and AlNi. In case of coated SN 750, the scale consists only NiO. The oxide formed on the scale of the coated SF 800 indicates the formation of Al<sub>2</sub>O<sub>3</sub>, MnFe<sub>2</sub>O<sub>4</sub> and AlNi<sub>3</sub>.

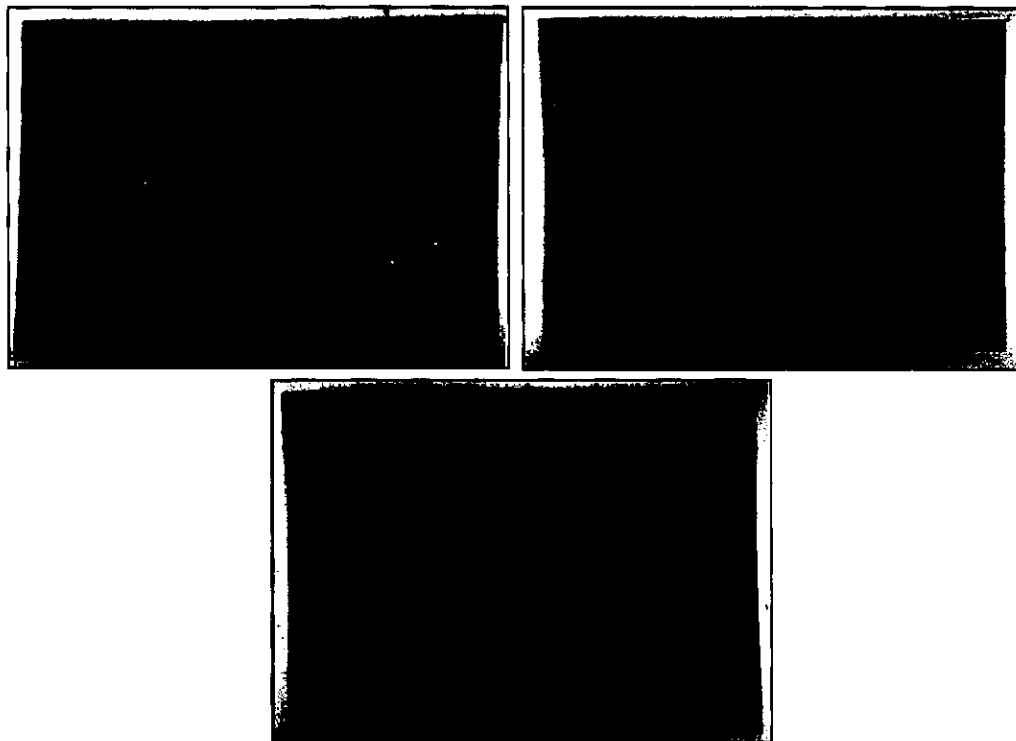


**Fig. 4.34:** Surface macrographs of RF sputtered Ni-Al films on (a) Superni 76, (b) Superni 750, and (c) Superfer 800 after 100 h exposure to air at 900°C.

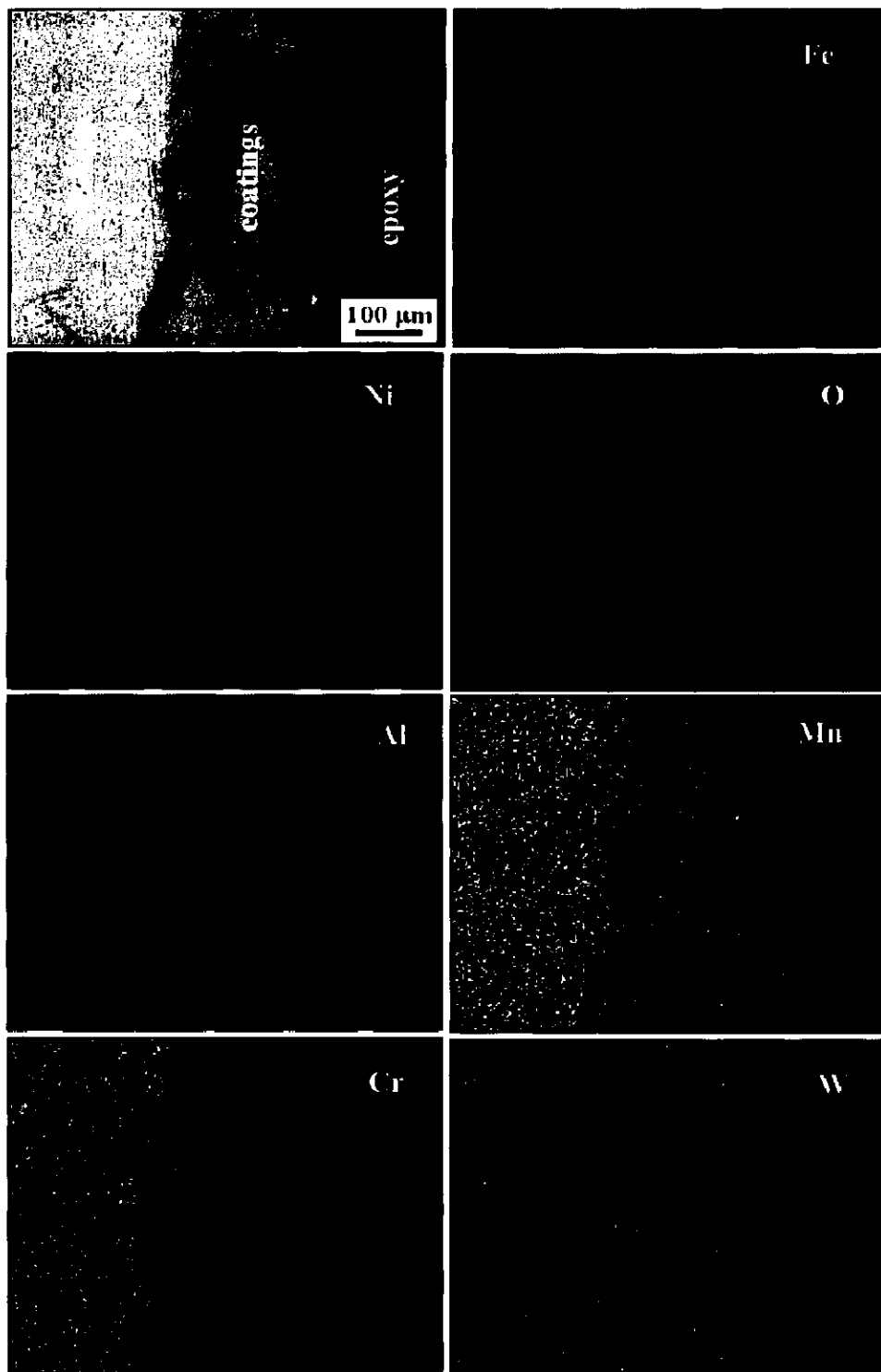


**Fig. 4.16(a):** Composition image (BSEI) and X-ray mapping of the cross-section of the Ni-5Al coated superalloy Superni 76 subjected to cyclic oxidation at 900 °C after 100 cycles.

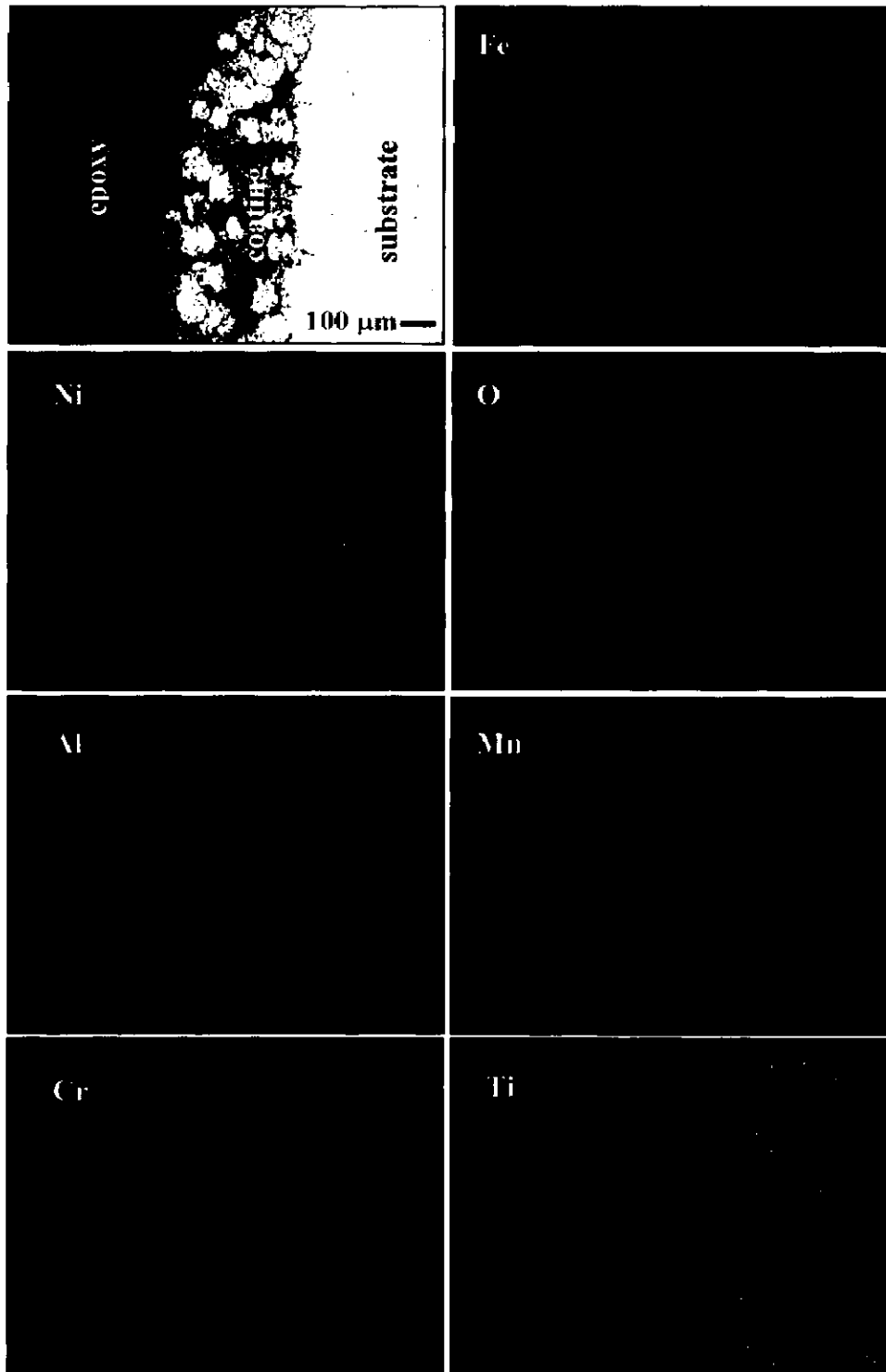


**Fig. 4.16(b):** Composition image (BSEI) and X-ray mapping of the cross-section of the Ni-5Al coated superalloy Superni 750 subjected to cyclic oxidation at 900 °C after 100 cycles.

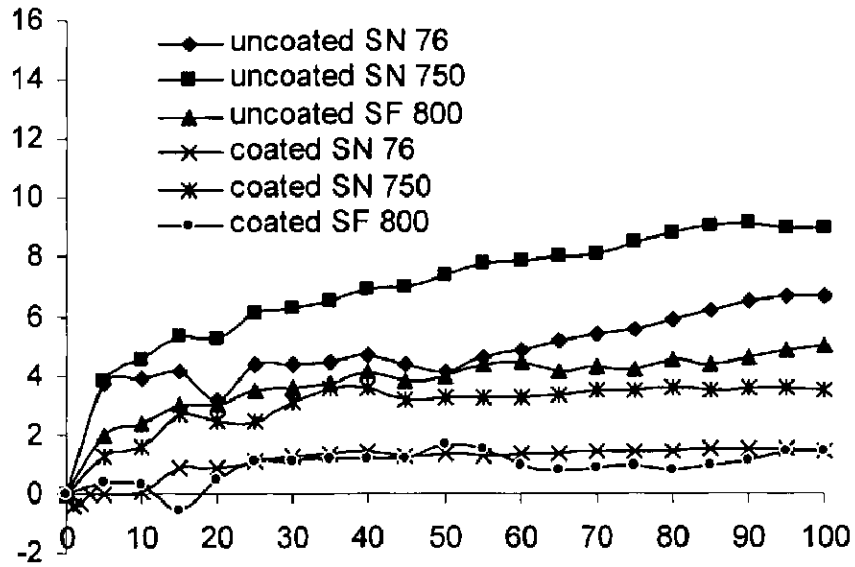


**Fig. 4.35:** Mass gain/area versus number of cycles plot for Ni-Al coated specimens oxidized in air at 900 °C for 100 cycles.

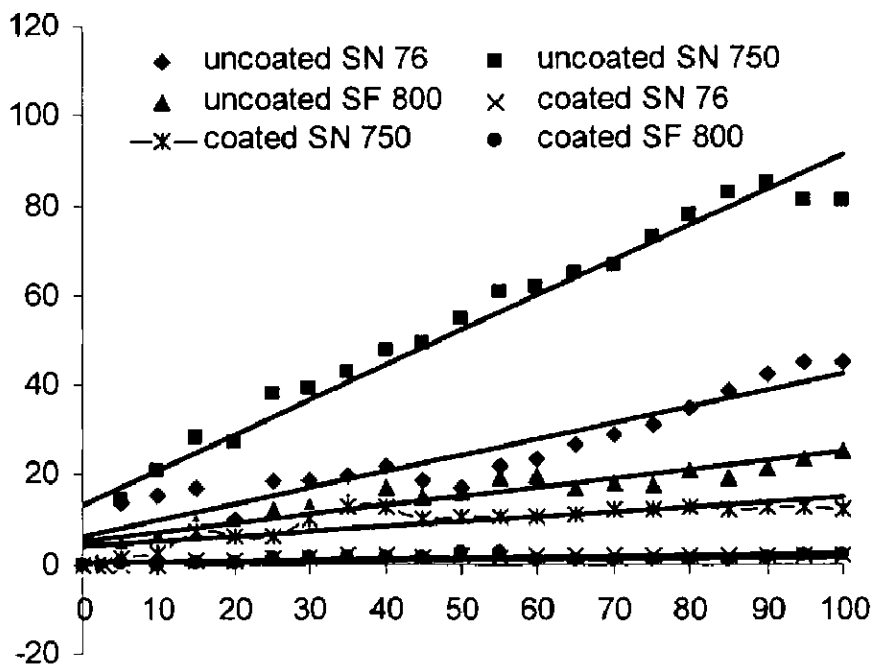


**Fig. 4.36:**  $(\text{Mass gain/area})^2$  versus number of cycles plot for Ni-Al coated superalloy specimens oxidized in air at 900°C for 100 cycles.

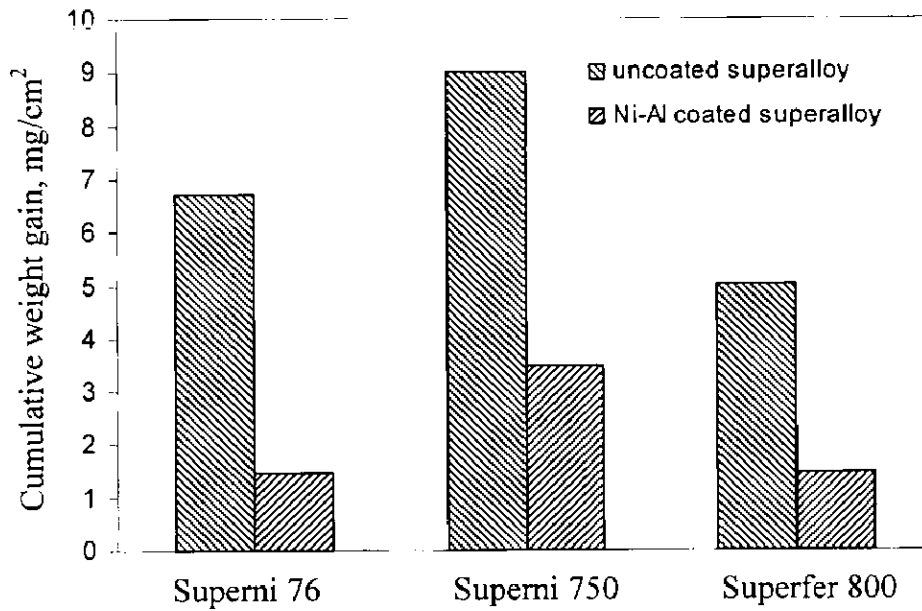


**Fig. 4.37:** Bar chart showing cumulative weight gain per unit area for uncoated and RF sputtered Ni-Al film on superalloys subjected to cyclic oxidation for 100 cycles at 900°C.

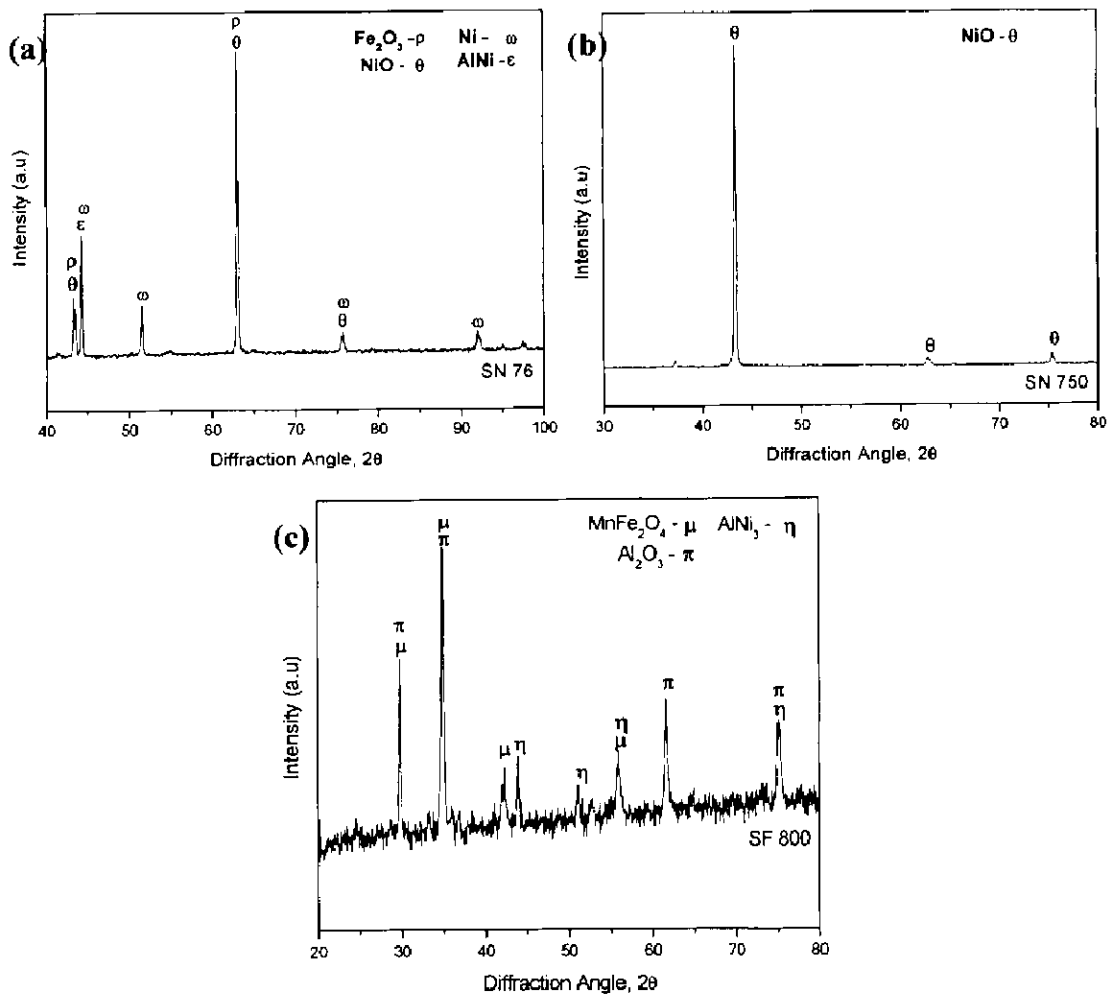


**Fig. 4.38:** X-ray diffractograms of Ni-Al coated thin films on (a) SN 76, (b) SN 750 and (c) SF 800 after oxidation at 900°C for 100 cycles.

#### **4.5.3.2.3.2 SEM/EDAX analysis of the surface scale**

The surface scale morphology of the coated superalloys oxidised at 900°C for 100 cycles is shown in Fig. 4.39. It is observed that the scale formed on the surface of the Ni-Al coated SN 76 and SN 750 superalloys indicate that the formation of irregular shaped granules. NiO is the prominent phase formed on the surface in both the cases. XRD results also confirmed the formation of NiO phases. Furthermore, oxides of aluminum, chromium oxide, iron and manganese have formed on the surface scale. In case of SF 800 alloy, the surface scale consists of small spherical particles in agglomerated form and mainly consists of iron oxide. The as coated Ni-Al film also indicated the presence of iron in higher amount. Other oxides formed on the surface of the oxidised SF 800 alloy are NiO, Al<sub>2</sub>O<sub>3</sub>, Cr<sub>2</sub>O<sub>3</sub> and MnO.

#### **4.5.3.2.4 X-ray mapping analysis**

Compositional image (SEI) and the elemental mapping analysis of RF sputtered Ni-Al films on different superalloys are shown in Fig. 4.40. In case of Ni-Al coated Superni 76 Fig 4.40(a), the scale formed on the surface contains mainly nickel and aluminum is present along the interface. Oxygen is present on the top surface and also along the interface and coexists with aluminum. Presence of chromium, iron, manganese and tungsten were observed in the scale. In case of coated Superni 750, Fig 4.40(b), chromium has moved from the substrate into the coating. Aluminum has moved from the coating into the substrate and existing with oxygen along the interface. Ti and Al are found existing together. In case of coated Superfer 800 Fig 4.40(c), chromium has depleted in the region near to the coating-substrate interface. Aluminum is rich in the area where chromium is depleted. Chromium has moved from the substrate into the coating, but Al has moved from the coating into the substrate.

The X-ray mapping analysis of different elements indicates that the scale formed on the surface consists of mainly nickel. Presence of higher amount of chromium, iron and manganese in the scale may be due to the deposition of these elements from the steel target. Aluminum is present only along the interface and coexists with oxygen.

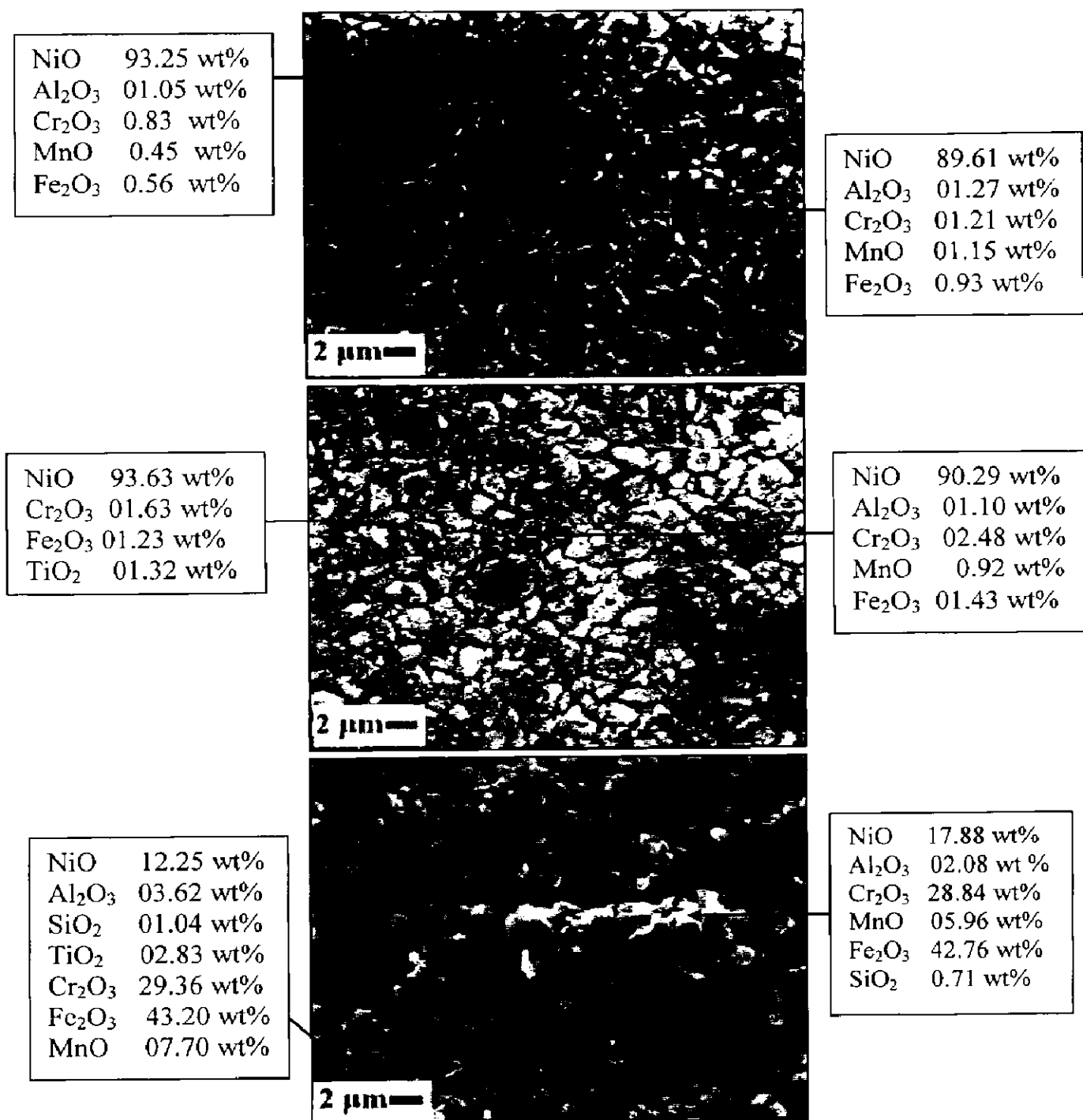


**Fig. 4.39:** Surface scale morphology and EDAX composition of Ni-Al coated thin film after oxidation studies on (a) SN 76, (b) SN 750 and (c) SF 800.



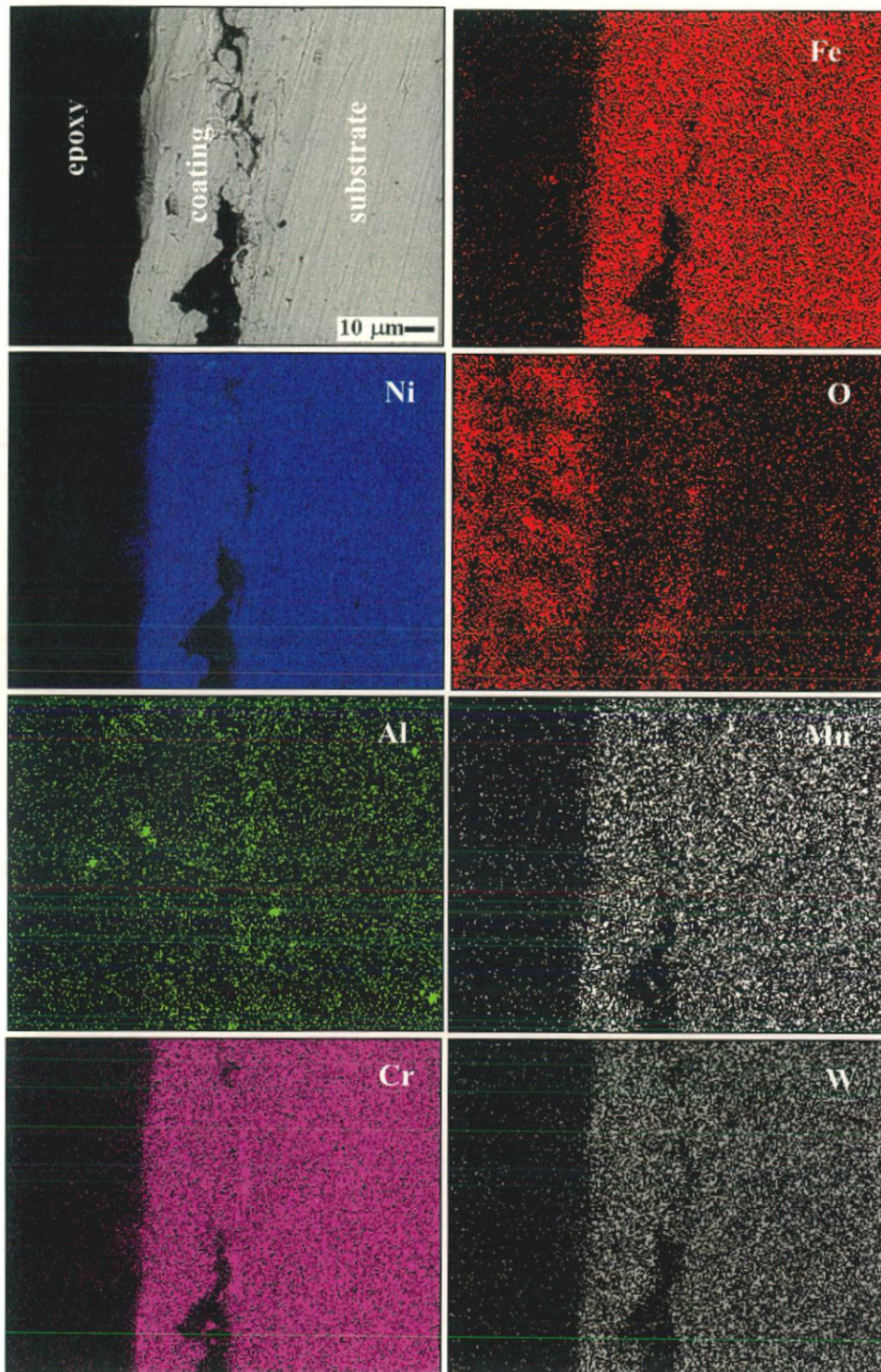


**Fig. 4.40(a):** Compositional image (SEI) and X-ray mapping of the cross-section of Ni-Al coated Superni-76 subjected to cyclic oxidation in air at 900°C.

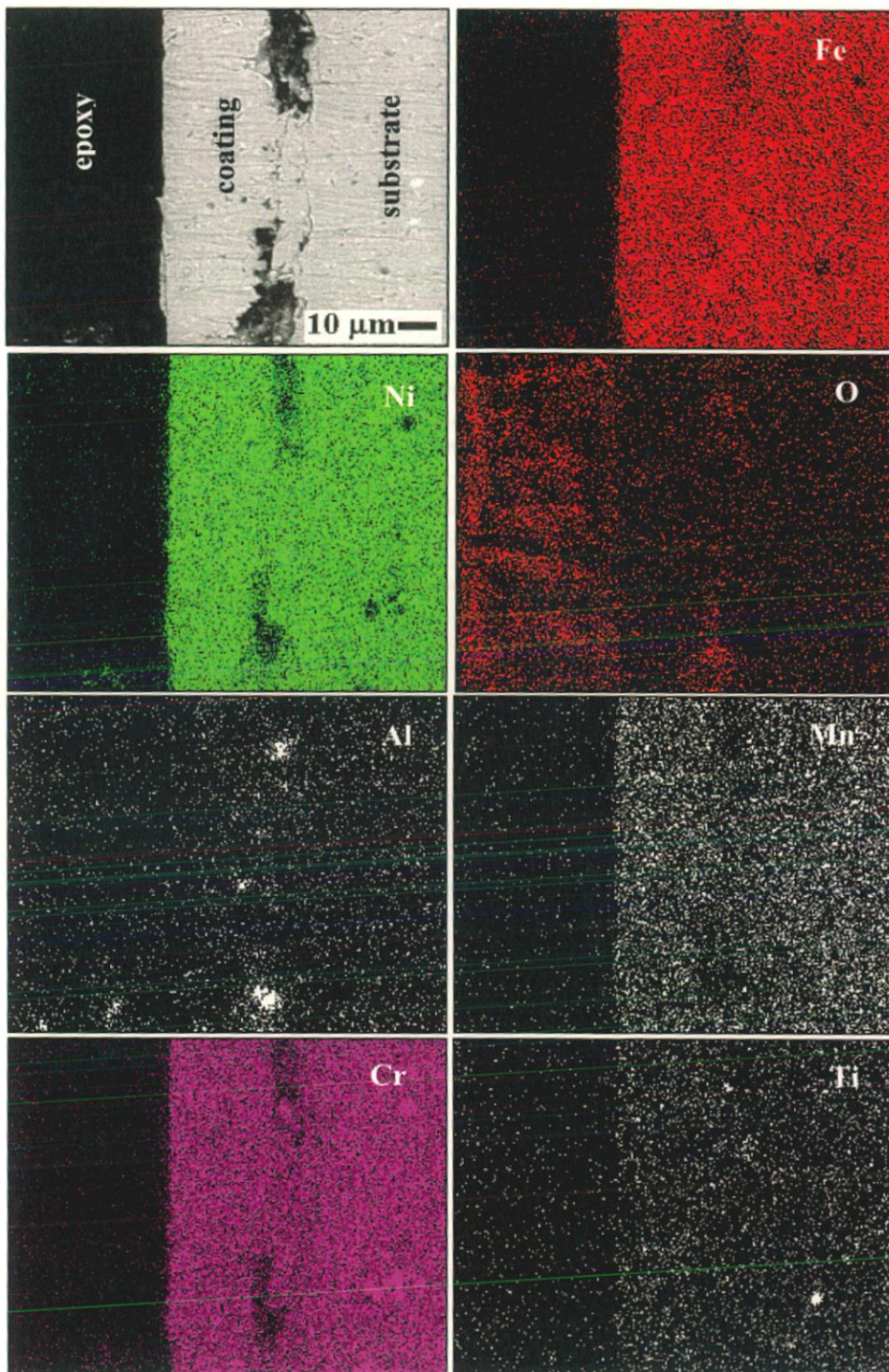


**Fig. 4.40(b):** Compositional image (SEI) and X-ray mapping of the cross-section of Ni-Al coated Superni 750 subjected to cyclic oxidation in air at 900°C.

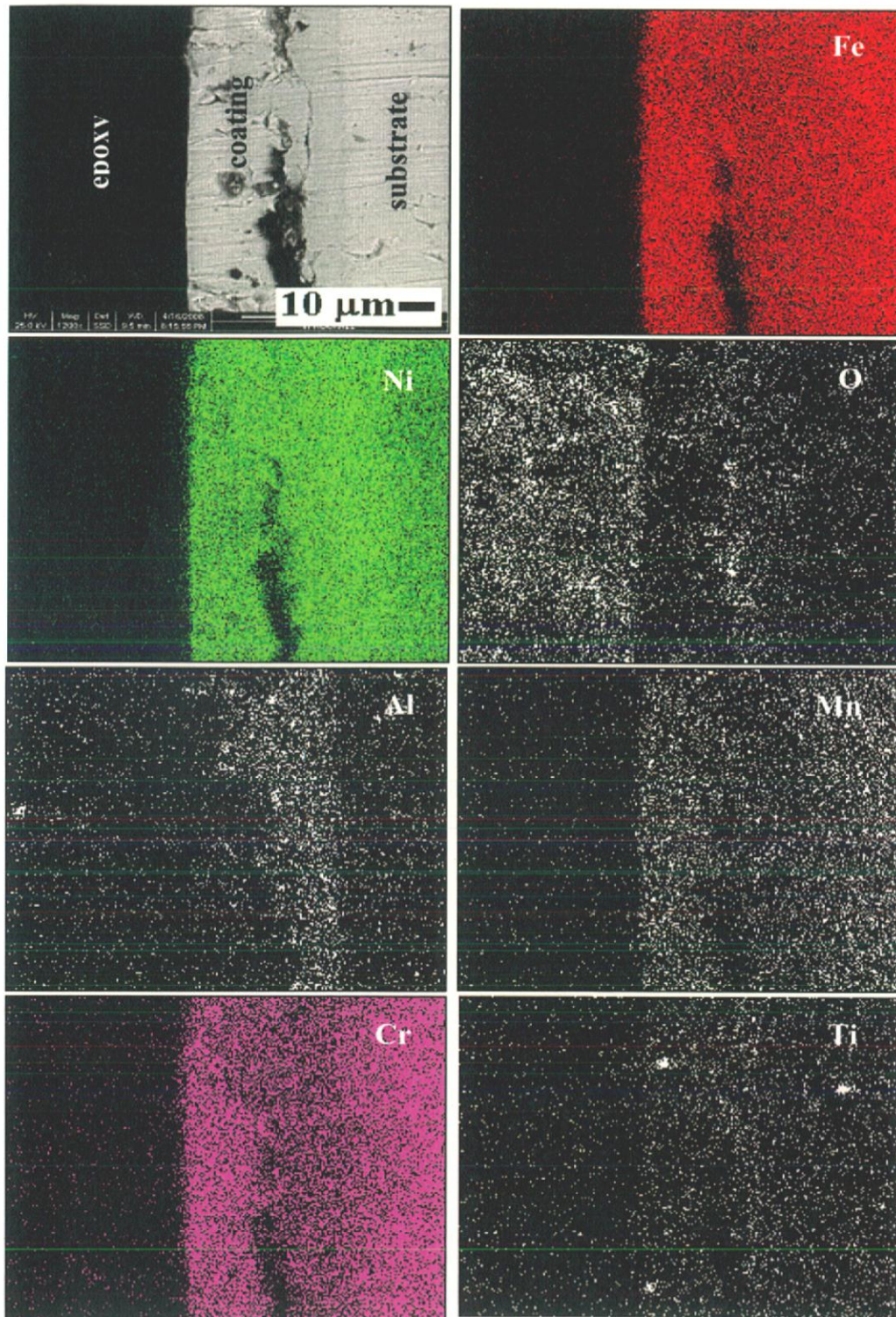


**Fig. 4.40(c):** Compositional image (SEI) and X-ray mapping of the cross-section of Ni-Al coated Superfer 800 subjected to cyclic oxidation in air at 900°C.

#### 4.5.4 Discussion

The Ni-Al film was deposited uniformly on all the superalloy substrates by RF magnetron sputtering process. The deposited film consists of spherical shaped particles in case of SN 76 and SN 750 alloy; whereas, in case of Superfer 800 alloy, the particle shape was not clearly visible in SEM micrograph. The deposited film has a crystallite size of 8.1 nm, 9.22 nm and 16.04 nm for SN 76, SN 750 and SF 800 respectively as observed from the XRD analysis. FESEM analysis of the as deposited film indicated the presence of oxygen in the film due to the oxidation of Ni-5Al coating during thermal spraying process on the steel target. In case of SF 800 alloy, presence of higher amount of iron in the deposited film may be due to the diffusion of iron from the steel target into the Ni-5Al coating during thermal spraying process. Small amount of oxygen and manganese has also diffused into the coating during thermal spraying process.

The weight loss was observed in SN 76 and SF 800 alloy and this may be attributed to the spalling of the scale formed on the surface of the coated specimens during initial stages of the oxidation study. The high temperature oxidation behaviour of the Ni-Al coated film on superalloys mostly followed the parabolic rate law. There is a slight deviation in parabolic rate law in case of coated SN 750. This may be due to the formation of rapid inhomogeneous scale on the surface of the superalloy as identified by our earlier work on thermal sprayed coating (Mahesh et al, 2008B). The formation of oxide layer would minimize the weight gain and the steady state oxidation behaviour can be obtained for longer duration of exposure. The  $k_p$  values are lower for all Ni-Al coated superalloys thereby indicating better resistance to oxidation in the given environment at 900°C.

The XRD analysis of SN 76 indicates that the formation of NiO, Fe<sub>2</sub>O<sub>3</sub>, Ni and AlNi occurs on the top surface of oxidised sample. In case of SN 750 superalloy, NiO is the only phase detected by XRD after oxidation. Whereas, in case of SF 800, Al<sub>2</sub>O<sub>3</sub>, AlNi<sub>3</sub> and spinel of manganese and iron are formed on the top scale which is supplemented by EDAX analysis of the top surface. FESEM analysis of the coated SN 76 and coated SN 750 shows the formation of NiO as the main phase with small amount of Al<sub>2</sub>O<sub>3</sub>. In case of coated SF 800, the top scale contain higher amount of Fe<sub>2</sub>O<sub>3</sub>, along with NiO and Cr<sub>2</sub>O<sub>3</sub>. Some alloying elements from the steel target might have diffused into the Ni-5Al wire coating during thermal spraying on steel target and got oxidised.

#### 4.5.5 Conclusions

1. The Ni-Al film was successfully deposited using RF magnetron sputtering process under the employed conditions with a thickness of around 3  $\mu\text{m}$ . The AFM analysis indicates the film was uniformly deposited on the surface of all the specimens and the surface roughness of film was in the range 31 – 60 nm.
2. The XRD analysis of the as deposited film indicates the grains is in the nanoscale range of 8 - 21 nm.
3. The XRD analysis of the as coated film revealed the presence of face center cubic Ni rich phase in case of Superni 76 and Superni 750 alloys, whereas  $\text{Al}_2\text{O}_3$ ,  $\text{AlNi}_3$  and spinel of Mn and Fe phases were detected in case of Superfer 800 alloy.
4. The surface and cross sectional EDAX analysis of the as deposited film indicates the presence of Ni in higher amounts, which is further supported by XRD analysis.
5. The weight gain of the Ni-Al coated superalloys was lower as compared to that of bare superalloys. The oxidation behaviour of the Ni-Al coated SN 76 and SF 800 superalloys was nearly parabolic and in case of coated SN 750, a slight deviation was observed.
6. The smaller grains help in fast diffusion of elements through the grain boundaries and helps in selective oxidation of the elements such as nickel and aluminum to form a protective layer on the coated specimen surface and thus prevents the permeation of oxidising species.
5. Among the three coated superalloys, SF 800 indicated a better resistance to oxidation at 900°C under cyclic conditions.

## 4.5 HOT CORROSION STUDIES IN MOLTEN SALT ENVIRONMENT

### 4.5.1 Introduction

Aluminide coatings deposited either by pack cementation or by chemical vapor deposition techniques (CVD), have been applied to gas turbine vane and blade airfoils since approximately 1970. Over 80% of all coated first stage blade airfoils are estimated to be coated by these techniques, indicating the enormous market share captured by these coatings. More recently, aluminide coatings were recognized as suitable bond coats for thermal barrier coatings (TBCs) (Leyens et al, 2000). NiAl intermetallic compound is a material of great interest in high temperature applications, due to its combination of low density, high melting point, and high thermal conductivity, and in particular to its excellent oxidation resistance.

Yang et al, (2001) have reported that for a cast NiAl alloy many voids of different sizes formed along the alloy/scale interface, after 100 cycles at 1000°C. Furthermore, they observed that the voids are deleterious to the adhesion of the scale and cracks also were observed in the scale. However, for a cast NiAlY alloy and a NiAl microcrystalline coating, the scales were continuous and appear in good contact with their substrates. Spallation was observed for cast NiAl during cyclic oxidation test, while no such behavior was detected for cast NiAlY and the NiAl coating.

In the Ni-Al system, thin film research is motivated by an increasing industrial interest to develop special coatings for advanced engineering applications, including low density wear-resistant materials, high-temperature structural materials and state-of-the-art microelectronics, where interconnects and transition-metal aluminides on compound semiconductors are of paramount importance (Almeida et al, 2000).

Geng et al, (2003) have studied the high temperature oxidation behavior of a sputtered pure Ni nanocrystalline coating at 700–900°C. The study showed that the nanocrystallization provides significant contribution for the rapid oxidation during the early stage mainly owing to the increase of grain boundary. As time increases, the oxidation quickly slows down probably due to rapid grain growth of the NiO oxide at high temperature, which reduce the Ni outward diffusivity through NiO layer.

Lou et al, (1996) have examined the oxidation behavior of sputtered microcrystalline coating of superalloy K17F at 900 and 1000°C. They observed that during isothermal oxidation of cast K17F alloy, at the initial stage of oxidation, the oxide scale which formed

on the surface consists of complex oxides of Ni, Cr, Ti, after 20 hour of oxidation,  $\text{Al}_2\text{O}_3$  predominates with some oxides of Ni, Cr, Ti. After 500 hours oxidation, the scale has transformed into complex oxides of  $\text{TiO}_2$ , spinel and a little  $\text{Al}_2\text{O}_3$ . During cyclic oxidation, complex and nonuniform oxide scales of  $\text{TiO}_2$ ,  $\text{NiCr}_2\text{O}_4$ , and  $\alpha\text{-Al}_2\text{O}_3$  formed on the as-cast K17F. Acoustic Emission (AE) analysis indicated that spallation of the oxide scale occurred in the cooling stage for the as-cast alloy, but no AE signal was detected for the as-sputtered microcrystalline coating.

Literature is very scarce on hot corrosion behaviour of Ni-Al sputter deposited films on Ni- and Fe- based superalloys. In the present investigation, an attempt has been made to study the hot corrosion behaviour of Ni-Al sputter deposited films on Ni- and Fe-based superalloys in molten salt (40% $\text{Na}_2\text{SO}_4$ -60% $\text{V}_2\text{O}_5$ ) environment at 900°C under cyclic conditions. The corrosion products formed on the superalloy substrates were characterised by XRD, SEM/EDAX and X-ray mapping techniques. Thermogravimetric technique was used to approximate the kinetics of corrosion.

## **4.5.2 Experimentation**

The details of the substrate material, coating formulation and oxidation studies of the coating are explained in section 3.4 and 3.5 of Chapter 3.

## **4.5.3 Results**

### **4.5.3.1 Visual Observation**

The photograph of Ni-Al coated specimens after hot corrosion studies in molten salt environment at 900°C for 100 cycles are shown in Fig. 4.41. In case of Ni-Al coated Superni 76 alloy (Fig.4.41a), after completion of 3<sup>rd</sup> cycle, grey color was observed on the surface of the specimen. During the course of the experiment, green patches with grey background was observed after seven cycles. The microspalling of the scale in the form of fine powder was observed at the end of fourth cycle. The microspalling subsequently reduced as the time of the experiment is increased. In case of Ni-Al coated Superni 750 alloy (Fig 4.41b), grey color was observed on the specimen after three cycles, which subsequently turned into green patches with grey background after the completion of six cycles. The microspalling was noticed after eight cycles, whereas in case of Ni-Al coated Superfer 800 alloy (Fig.4.41c), the

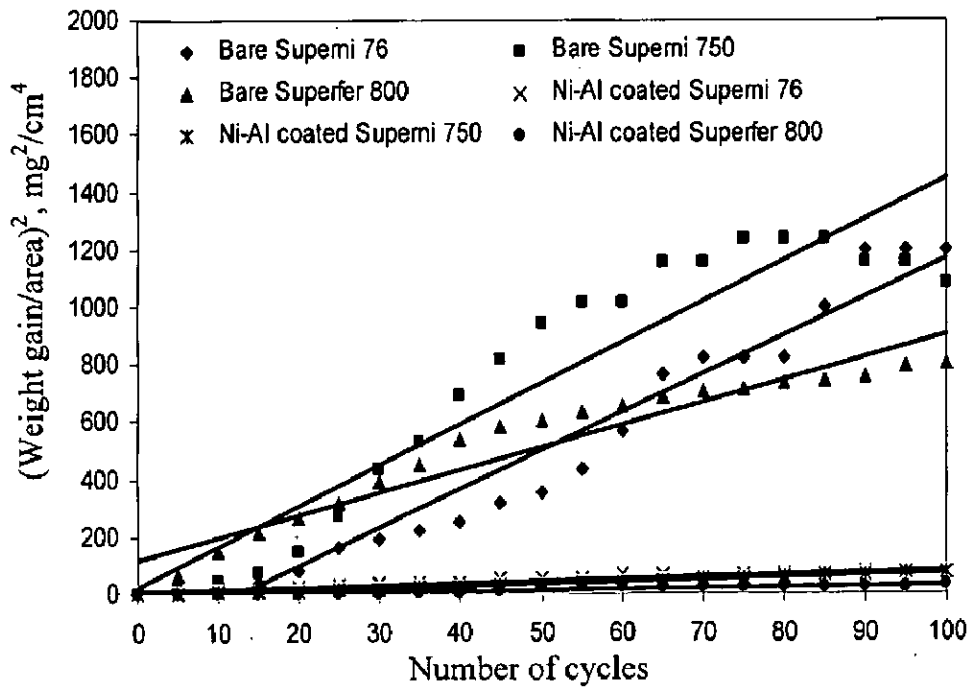


**Fig. 4.43:** (Mass gain/area)<sup>2</sup> versus number of cycles plot for Ni–Al coated superalloy specimens after exposure to molten salt environment at 900°C for 100 cycles.

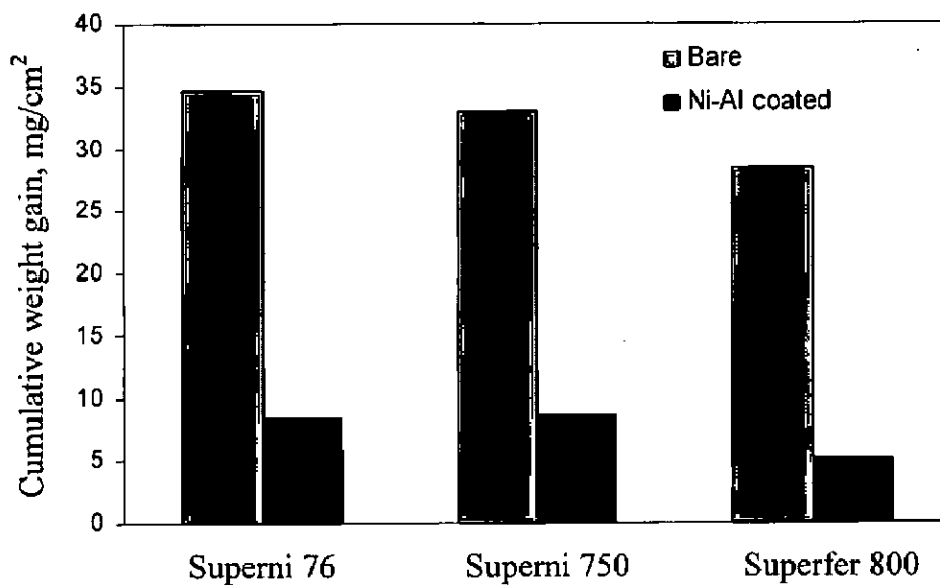


**Fig. 4.44:** Bar chart showing cumulative weight gain per unit area for uncoated and RF sputtered Ni–Al film on superalloys subjected to molten salt environment at 900°C for 100 cycles



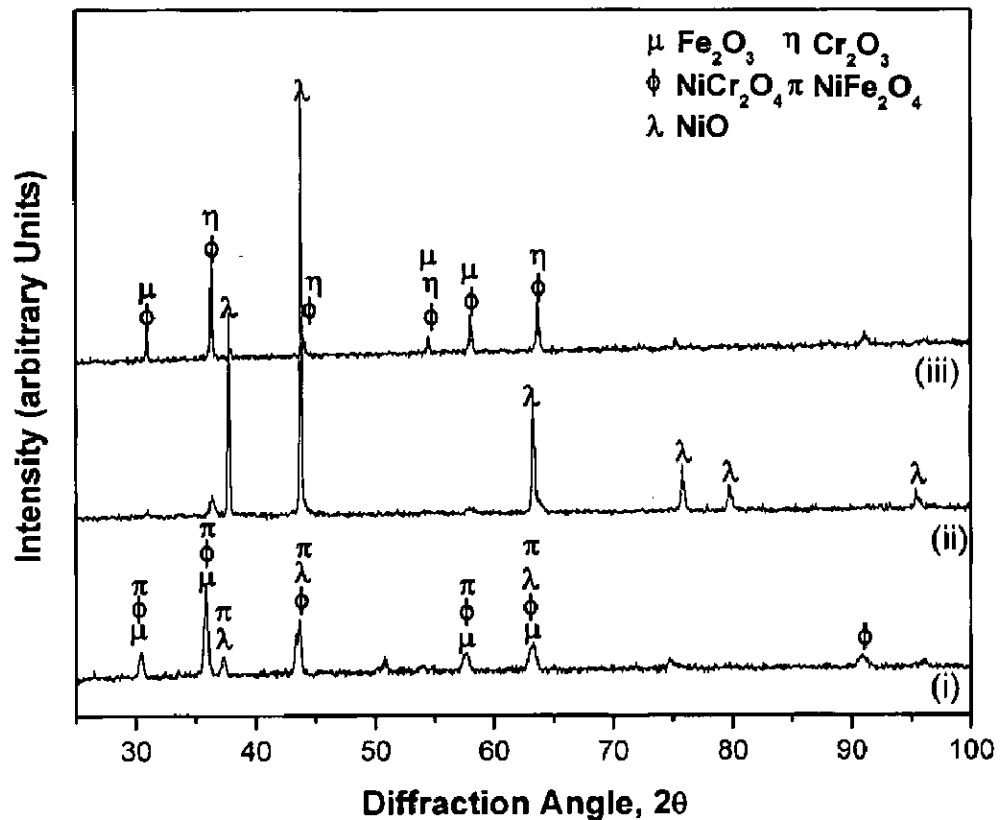


**Fig. 4.45:** X-ray diffractograms of Ni-Al coated thin films on (a) Superni 76, (b) Superni 750 and (c) Superfer 800 after cyclic oxidation in molten salt environment at 900°C.

#### 4.5.3.4 FESEM/EDAX analysis

##### 4.5.3.4.1 Surface analysis

SEM micrographs showing the surface morphology and EDAX analysis (FEI Company, Quanta 200F attached with V5.21 genesis EDAX software) at some selected points of interest of hot corroded Ni-Al coated specimens are shown in Fig. 4.46. The scale formed on Ni-Al coated Superni 76 alloy shows (Fig. 4.46a) the nodules of NiO on the top scale and presence of Cr<sub>2</sub>O<sub>3</sub> and Fe<sub>2</sub>O<sub>3</sub> in the subscale regions. The microspalling of the scale was observed in the form of fine powder. The SEM analysis for Ni-Al coated Superni 750 alloy (Fig. 4.46b) indicates at some locations the scale was spalled. The EDAX analysis indicates NiO as a dominant oxide. In case of Ni-Al coated Superfer 800 (Fig. 4.46c) alloy, the scale formed on the surface consists of small spherical nodules having NiO, Cr<sub>2</sub>O<sub>3</sub> and Fe<sub>2</sub>O<sub>3</sub> as main phases.

##### 4.5.3.5 X-ray mapping analysis

The corroded samples were cut using Buehler ISOMET 1000 precision saw and then they were mounted in transoptic powder. The samples were mirror polished before studying its

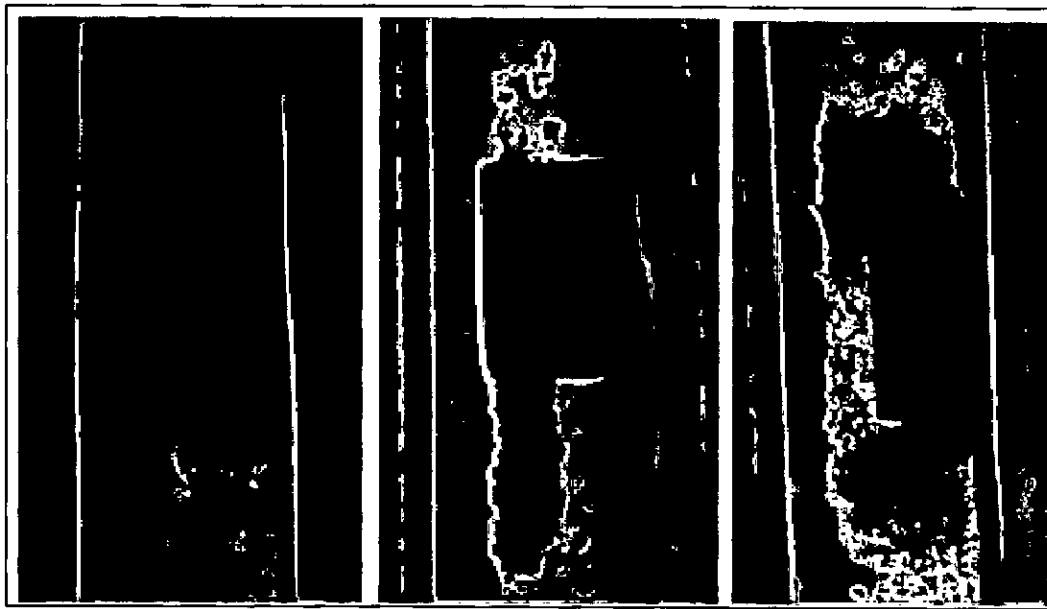
scale started spalling after fourth cycles and the color of the specimen after completion of three cycles was found grey. The microspalling was continued upto ten cycles and then slowly reduced. The color of the specimen subsequently turned into dark grey.

#### 4.5.3.2 Corrosion Kinetics in molten salt environment

The mass gain per unit area versus number of cycles plots for the bare as well as coated superalloys in the presence of molten salt ( $\text{Na}_2\text{SO}_4$ -60% $\text{V}_2\text{O}_5$ ) environment under cyclic conditions is shown in Fig. 4.42. It is noticed that the mass gain of the coated superalloys is much lower compared to that of bare superalloys in the molten salt environment. The Ni-Al coated Superfer 800 alloy indicated a minimum mass gain, whereas, Ni-Al coated Superni 76 alloy has indicated higher mass gain. The higher mass gain in case of bare superalloys indicates that they are more prone to hot corrosion attack. The parabolic rate constant  $k_p$  is calculated from the slope of the linear regression fitted line from  $(\text{mass gain/area})^2$  versus number of cycles and is found to be  $1.98 \times 10^{-10} \text{ g}^2\text{cm}^{-4}\text{s}^{-1}$ ,  $2.13 \times 10^{-10} \text{ g}^2\text{cm}^{-4}\text{s}^{-1}$  and  $0.94 \times 10^{-10} \text{ g}^2\text{cm}^{-4}\text{s}^{-1}$  for Ni-Al coated Superni 76, Superni 750 and Superfer 800 respectively. The nature of fit, a parabolic rate law, for hot corrosion experiments is also shown in Fig. 4.43. The bare superalloys slightly deviated from the parabolic rate law, whereas the Ni-Al sputtered specimens followed the parabolic behaviour up to 100 cycles. Fig. 4.44 shows the cumulative weight gain/unit area in all three cases of bare/coated superalloys.

#### 4.5.3.3 X-ray diffraction analysis

The XRD analysis of the hot corroded samples after 100 cycles is shown in Fig.4.45. The XRD analysis was carried out with Bruker AXS D-8 Advance Diffractometer (Germany) with  $\text{Cu K}_\alpha$  radiation. XRD patterns of the Ni-Al coated Superni 76 after exposure to molten salt environment at  $900^\circ\text{C}$  revealed the presence of NiO,  $\text{Fe}_2\text{O}_3$ ,  $\text{NiCr}_2\text{O}_4$  and  $\text{NiFe}_2\text{O}_4$  phases. In case of Ni-Al coated Superni 750 alloy, only NiO phase was observed after 100 cycles, whereas in case of Ni-Al coated Superfer 800 alloy, XRD revealed the presence of  $\text{Fe}_2\text{O}_3$ ,  $\text{Cr}_2\text{O}_3$ , and  $\text{NiCr}_2\text{O}_4$  phases.



(a) Superni 76

(b) Superni 750

(c) Superfer 800

**Fig. 4.41:** Surface macrographs of RF sputtered Ni-Al films on (a) Superni 76, (b) Superni 750, and (c) Superfer 800 after 100 h exposure to molten salt environment at 900°C.

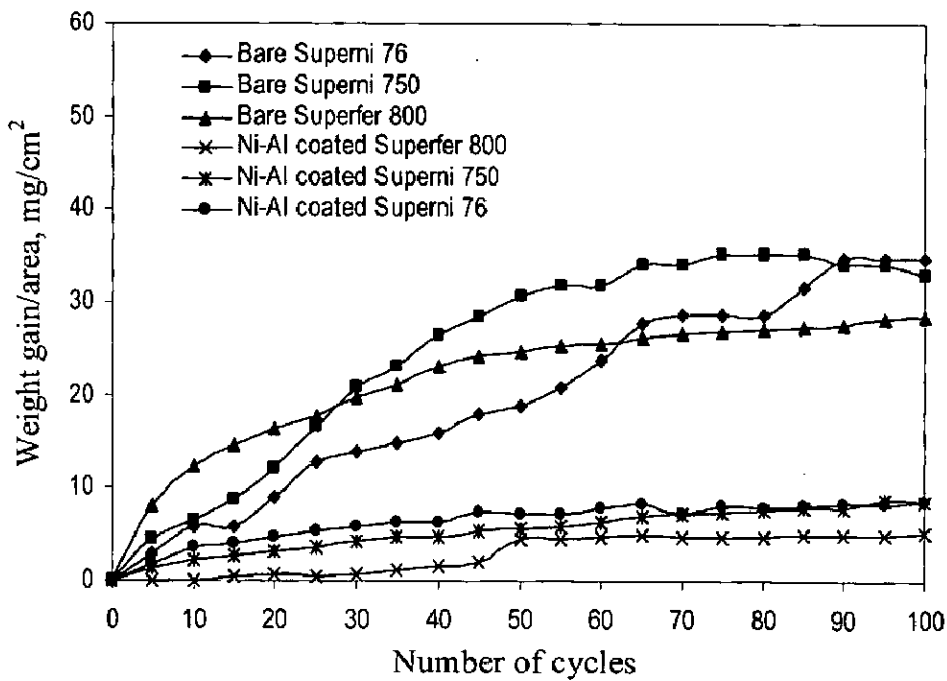


**Fig. 4.42:** Mass gain/area versus number of cycles plot for Ni-Al coated specimens oxidized in molten salt environment at 900 °C for 100 cycles.

cross sectional features. The polished samples were then gold coated to facilitate the X-ray mapping of different elements present across the corroded samples by using FESEM (FEI, Quanta 200F). X-ray mapping for the coated Ni-Al film on Ni- and Fe-based superalloy after hot corrosion studies is shown in Fig. 4.47. The scale consists of mainly nickel, aluminum is present wherever nickel is absent. Oxygen is coexisting with aluminum and presence of chromium and iron in the scale may be attributed to the diffusion from the substrate and /or during the deposition, iron might have deposited from the steel target on to the substrate. Small amount of silicon has migrated from the substrate into the scale.

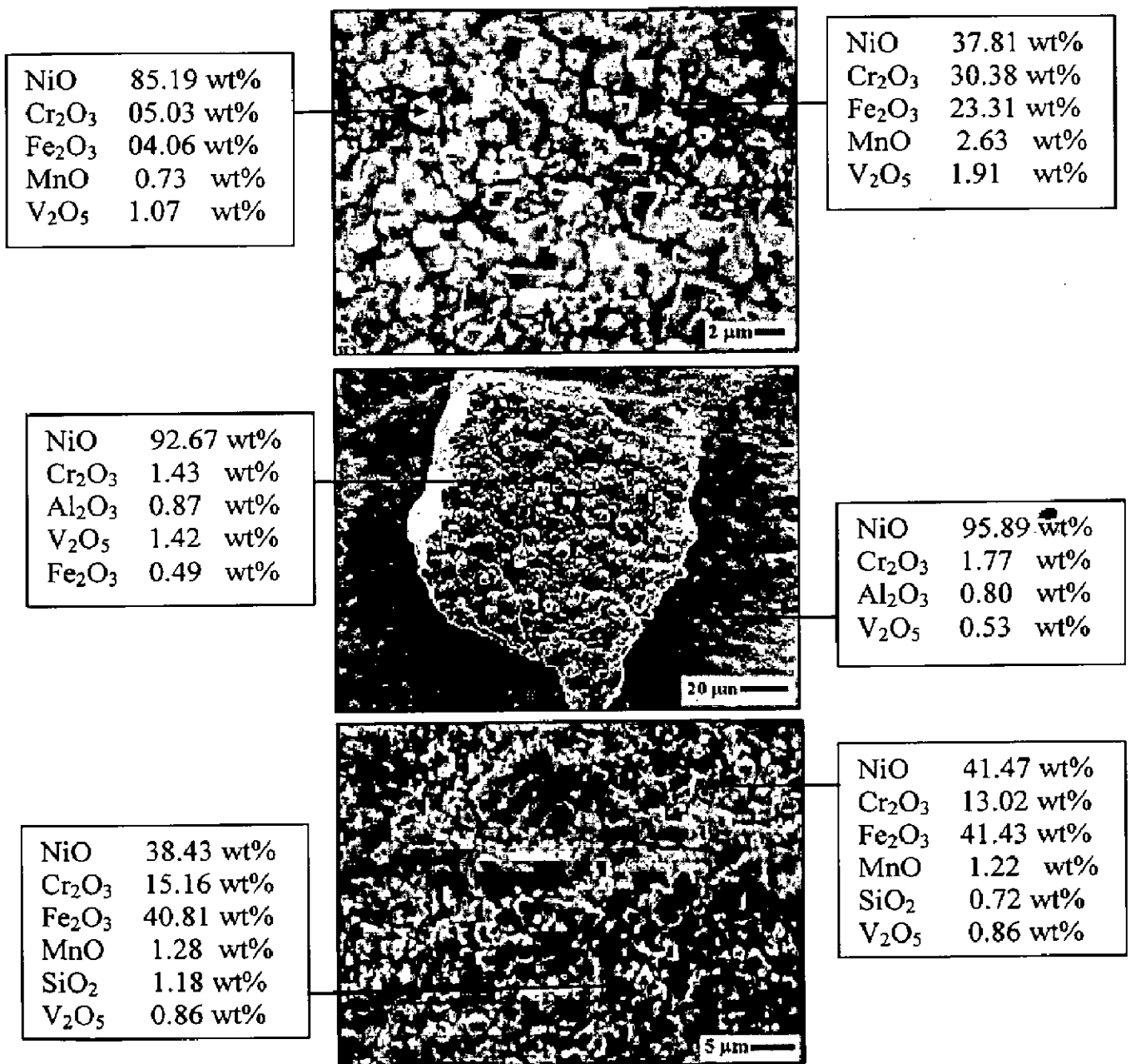


**Fig. 4.46:** Surface scale morphology and EDAX composition of Ni-Al coated thin film for (a) Superni 76, (b) Superni 750 and (c) Superfer 800 after exposure to molten salt environment at 900°C.

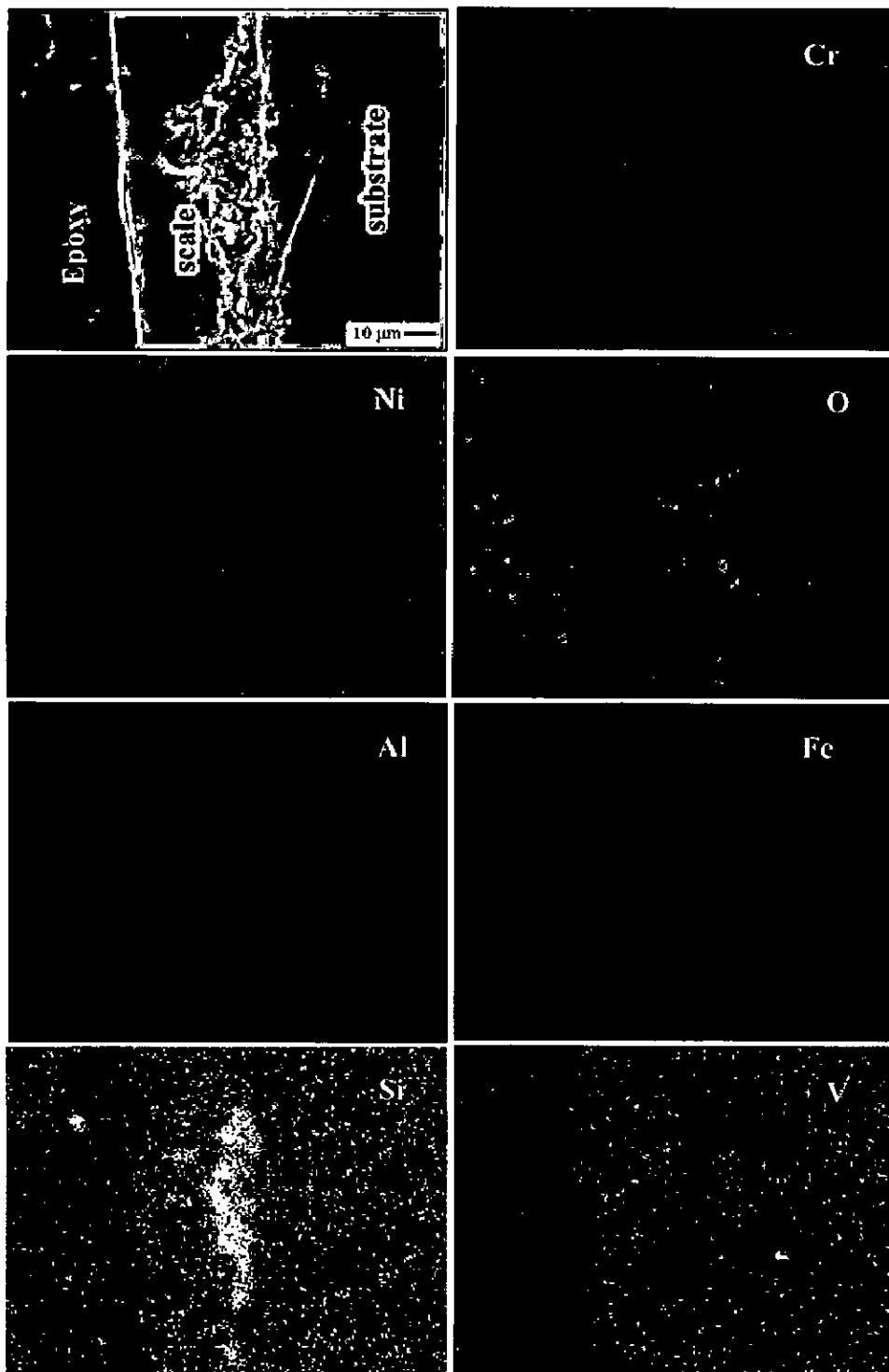


**Fig. 4.47(a):** Compositional image (SEI) and X-ray mapping of the cross-section of Ni-Al coated Superni-76 subjected to molten salt environment at 900°C.

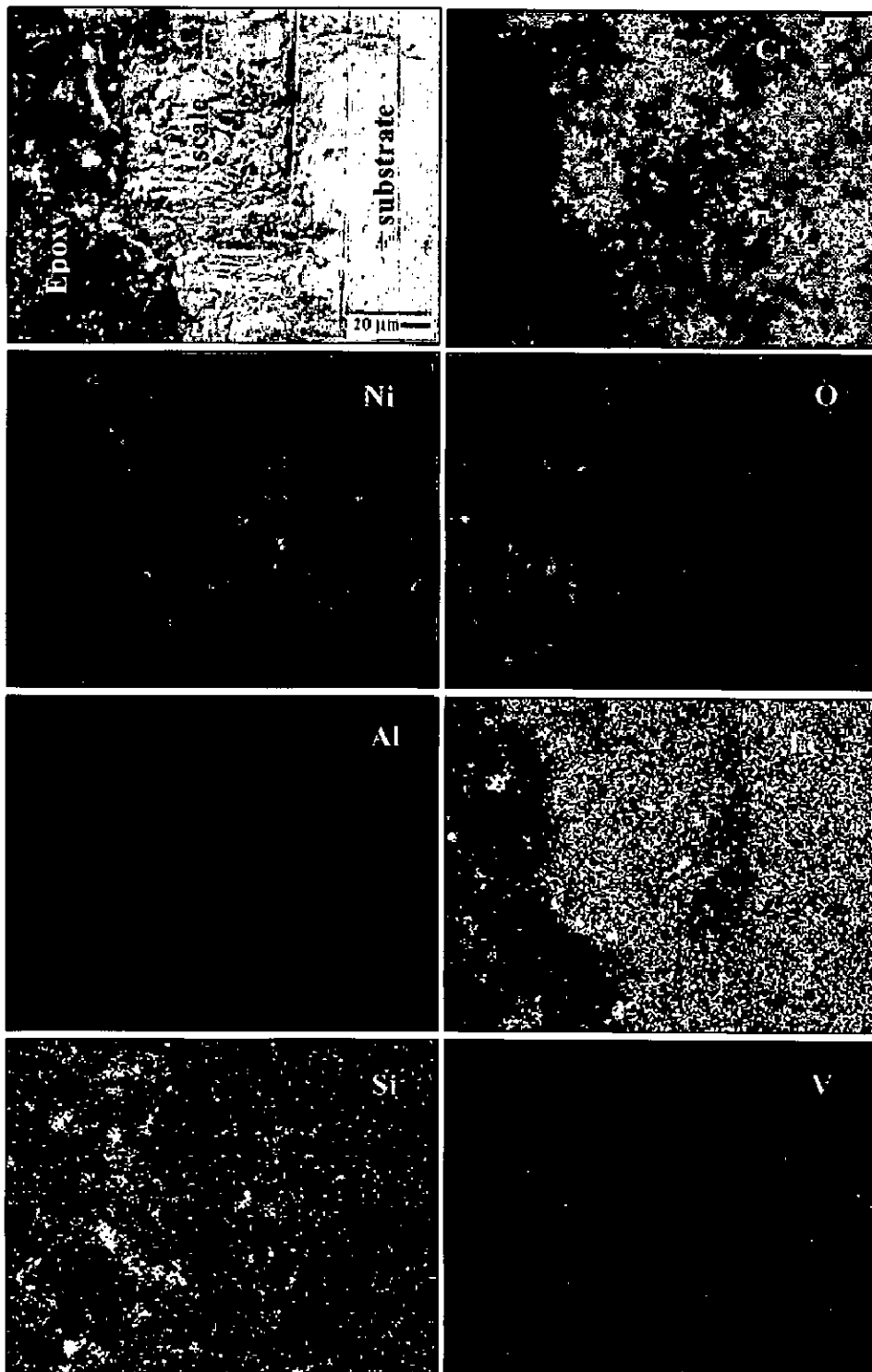


**Fig. 4.47(b):** Compositional image (SEI) and X-ray mapping of the cross-section of Ni-Al coated Superni 750 subjected to molten salt environment at 900°C.

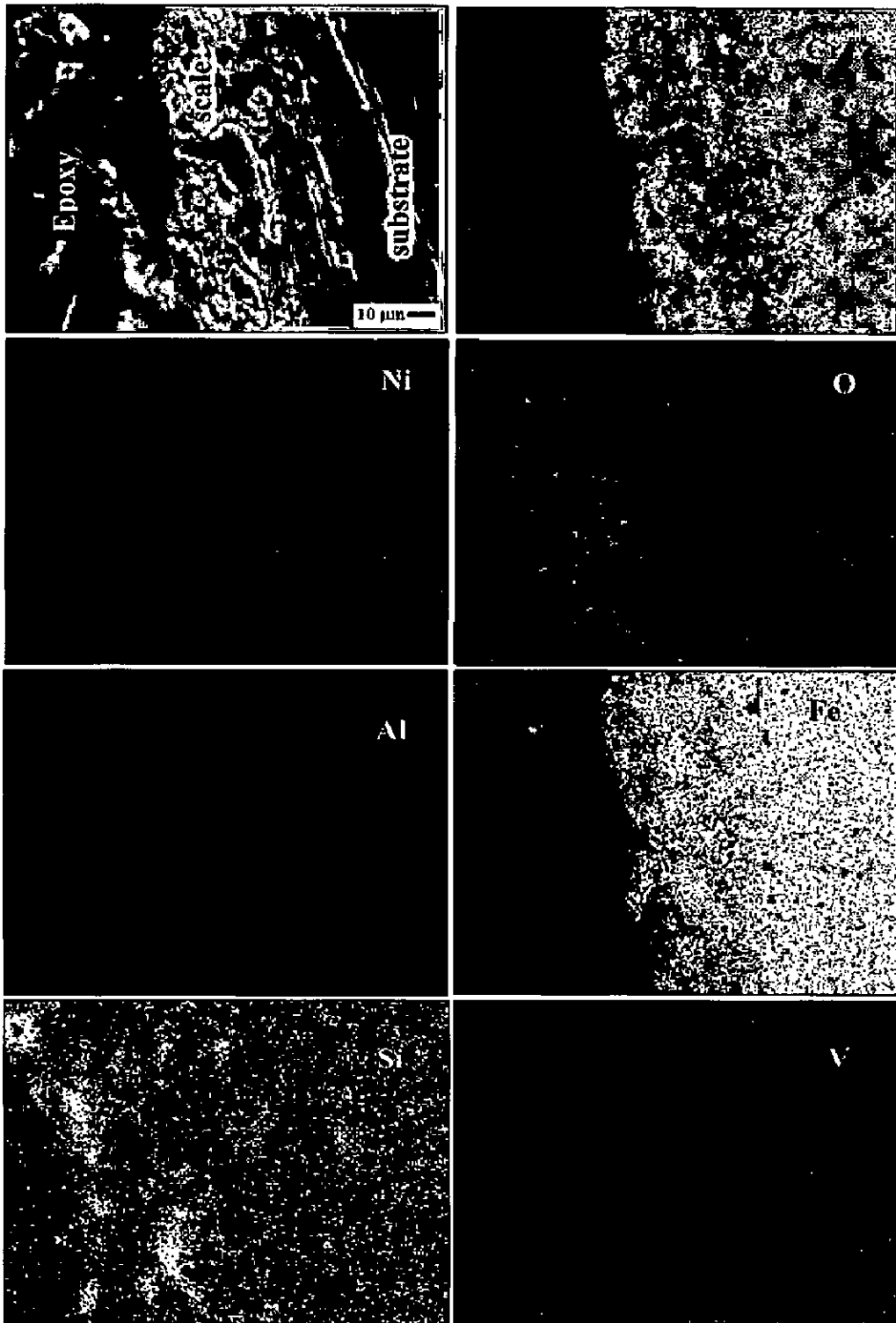


**Fig. 4.47(c):** Compositional image (SEI) and X-ray mapping of the cross-section of Ni-Al coated Superfer 800 subjected to molten salt environment at 900°C.

#### 4.5.4 Discussion

The surface macrographs of Ni-Al coated superalloys after hot corrosion studies are shown in Fig. 4.41. It is observed from the macrographs that microspalling of the scale was occurred during the initial period of exposure to molten salt environment. During the course of the experiments, the spalling tendency of the scale from the surface stopped. The scale formed on the corroded surface was having some green patches with grey background which may be attributed to the presence of NiO in the scale, which is identical with the findings of (Mahesh et al, 2007; Bornstein et al, 1975; Buta Singh, 2003). The presence of NiO is further supported by XRD and SEM/EDAX analysis. The uncoated specimen showed a significant spalling during cyclic oxidation in the given environment with a substantial weight gain (Fig 4.42). The mass gain of the bare alloys during the initial period was high and then becomes gradual during the course of the exposure at 900°C. The weight gain is relatively high during the initial period of exposure, which may be attributed to the formation of NaVO<sub>3</sub> which acts as a catalyst and also serves as oxygen carrier to the base alloy, leading to rapid oxidation of the basic elements of the superalloy thereby forming the protective oxide scales. After the initial period of high corrosion rate, it has been observed that the rate of corrosion tends to be nearly uniform with the increase in the period of exposure. In the case of coated superalloys subjected to cyclic oxidation in the given environment, significant weight gains were noticed in the early cycles of the exposure, but it became almost uniform with the exposure time obeying the parabolic rate law. The parabolic rate constant for the bare superalloy is found to be greater than that of NiAl coated superalloys. It can be inferred that the RF sputtered Ni-Al coating has provided the better protection to the superalloys.

The XRD analysis (Fig. 4.45) of the coated superalloys after hot corrosion study at 900°C in molten salt environment indicates that the coating has provided the better protection to the superalloys. The protection to the superalloys from hot corrosion might be due to the formation of oxides of nickel, chromium and spinel of nickel and chromium. The formation of spinels on the top scale may further enhance the oxidation resistance due to their much smaller diffusion coefficients of the cations and anions than those in their parent oxides (Chatterjee et al, 2001). EDAX analysis on the surface indicated the presence of oxides of nickel, chromium and iron. Nickel oxide is present on the surface of the scale, whereas, chromium and iron oxides are present in the subscale regions. The



presence of chromium and iron in the scale indicates that during the deposition of the Ni-Al film from the steel target, chromium and iron might have also got deposited on the superalloy substrate and eventually oxidised at 900°C. X-ray mapping analysis (Fig. 4.47) shows that the scale is rich in nickel and oxygen is coexisting with aluminum. The presence of chromium and iron in the scale was noticed and small amount of alloying element such as silicon has migrated from the substrate into the scale.

#### **4.5.5 Conclusions**

1. The RF magnetron sputtering process has been successfully used to deposit Ni-Al films on Ni- and Fe-based superalloys in the present work.
2. The coated superalloys after exposure to molten salt environment at 900°C for 100 cycles showed comparatively a very little weight gain compared to the bare superalloys in the given environment. Minor spalling of the oxide scale was observed during the initial period of exposure.
3. The parabolic rate constant for the coated superalloys was found to be very less as compared to the bare superalloys.
4. The formation of oxides of nickel, chromium and spinel of nickel and chromium has lead to better resistance of the coated superalloys in the molten salt environment.

*A detailed analysis of HVOF sprayed NiCrAl coatings on Ni-and Fe-based superalloy is presented in the first part of this chapter. In the second part, the detailed analyses of RF magnetron sputtered NiCrAl coatings on superalloys are made. The studies on characterisation, air oxidation and hot corrosion of NiCrAl coatings are discussed in this chapter.*

### **Part I – HVOF sprayed coatings**

## **5.1 CHARACTERISATION OF THE COATING**

### **5.1.1 Introduction**

The properties of thermal sprayed coating materials used for high temperature oxidation and hot corrosion protection are generally a sensitive function of their chemical compositions and microstructural features. The microstructural uniformity has long been considered necessary to improve the thermal, chemical and mechanical properties of coatings deposited on the substrate alloys used for fabricating turbine components in high temperature applications. In a wide variety of applications, for example, in aero and thermal power plants mechanical components, especially turbine engines have to operate under severe conditions, such as high load, speed, temperature and hostile chemical environments. The turbine engine hot section components are designed to provide only the structural integrity and mechanical reliability in the actual service conditions but not the high temperature protection, as it is not possible to provide both of them simultaneously. Therefore, the surface modification of these components is necessary in order to protect them against various types of degradation (Buta Singh et al, 2005A). There is an increased attention towards the plant efficiency of fossil power plants to meet the stringent environmental regulations along with ensuring plant reliability, availability and maintainability without compromising the cost (Stott, 1989; Fitzer and Schlichting, 1981). Materials used in the thermal power plant should withstand against creep and oxidation at high temperature (Sundararajan et al, 2003). It is known from the literature (Tobe, 1998) that properties worth of 3 to 5% of gross domestic products (GDP) are lost by corrosion in every year in the developed countries. It is recognized worldwide that corrosion including oxidation is still one of the biggest technical challenges posed to the mankind. It is a proven fact that an application of thermal spray coatings on the materials used for high temperature application is one of the strongest protective weapons against high

temperature oxidation and hot corrosion. The MCrAlY (where M = Ni, Co or Fe) based coatings deposited on the superalloys extend the latter service life by providing the required corrosion protection, through the formation of protective and well adherent oxide scales in the high temperature environment. It is very essential that the coating constitutes the desirable chemical compositions and microstructural morphologies, which should react with the environment and produce a slow growing and continuous protective oxide scale so as to preclude the corrosive species to diffuse into the coating-substrate interface (Gurrappa, 2001). HVOF spray process is used to coat the powder as it could operate at atmospheric pressure and more importantly, the investment and operation costs are much lower than that of the other thermal spray processes operated in vacuum (Lugscheider et al, 1998).

Although thermal spray technology is well advanced, the microstructural characteristics of the coatings are not well quantified via experimental and theoretical studies. Especially, there is no reported literature on the microstructural features and bond strength of the HVOF sprayed NiCrAl coating on the three superalloys such as Superni 76 (SN 76), Superni 750 (SN 750), and Superfer 800 (SF 800) chosen in the present investigation. It is very important to realise that characterizations of morphologies such as splats structure, shape, porosity, and compositional features of the coatings are critical for understanding the way thermal spray coatings behave and formulate guidelines for improving coating performance in the future. The NiCrAl coatings on superalloys can be used at elevated temperatures above 900°C, where pure NiCr coatings could not be used due to the formation and evaporation of chromium oxide at high temperature. High temperature oxidation and corrosion studies of NiCrAl bulk alloys is reported in the literature (Khanna et al, 1993; Santoro et al, 1978; Santoro, 1979) but there is no such studies on HVOF sprayed NiCrAl coating on the superalloy substrates chosen in the present work. Therefore, the present research work has been focused to characterise the microstructural and compositional features of HVOF sprayed NiCrAl coatings on Ni- and Fe-based superalloys. The NiCrAl coatings on superalloy substrates were characterised with respect to their microstructures, porosity, microhardness, bond strength and phase formation using the combined techniques of optical microscopy, X-ray diffraction (XRD), field emission scanning electron microscopy/energy-dispersive X-ray analysis (FESEM/EDAX) and X-ray mapping.

### **5.1.2 Experimental Details**

The details of the substrate material, coating formulation and characterisation of the coating are explained in Chapter 3 (Experimental chapter).

## 5.1.3 Results

### 5.1.3.1 Porosity and thickness of the coatings

The FESEM image of the as sprayed NiCrAl coating after polishing is shown in Fig. 5.1. Porosity measurements were done for NiCrAl coated superalloys, which were found to be around 1.7%. The standard deviation of 0.336 for NiCrAl coated Superni 76 and 0.244, 0.235 for coated Superni 750 and Superfer 800, respectively, were observed. The thickness of the NiCrAl coated samples were measured by back scattered electron image (BSEI) across the cross section of the mounted samples shown in Fig. 5.1 (b), (d), (f). The coating thickness was measured at different locations along the cross section for all the three superalloys. The average coating thickness of 175  $\mu\text{m}$ , 139  $\mu\text{m}$  and 97  $\mu\text{m}$  was found in the case of Superni 76, Superni 750 and Superfer 800 respectively.

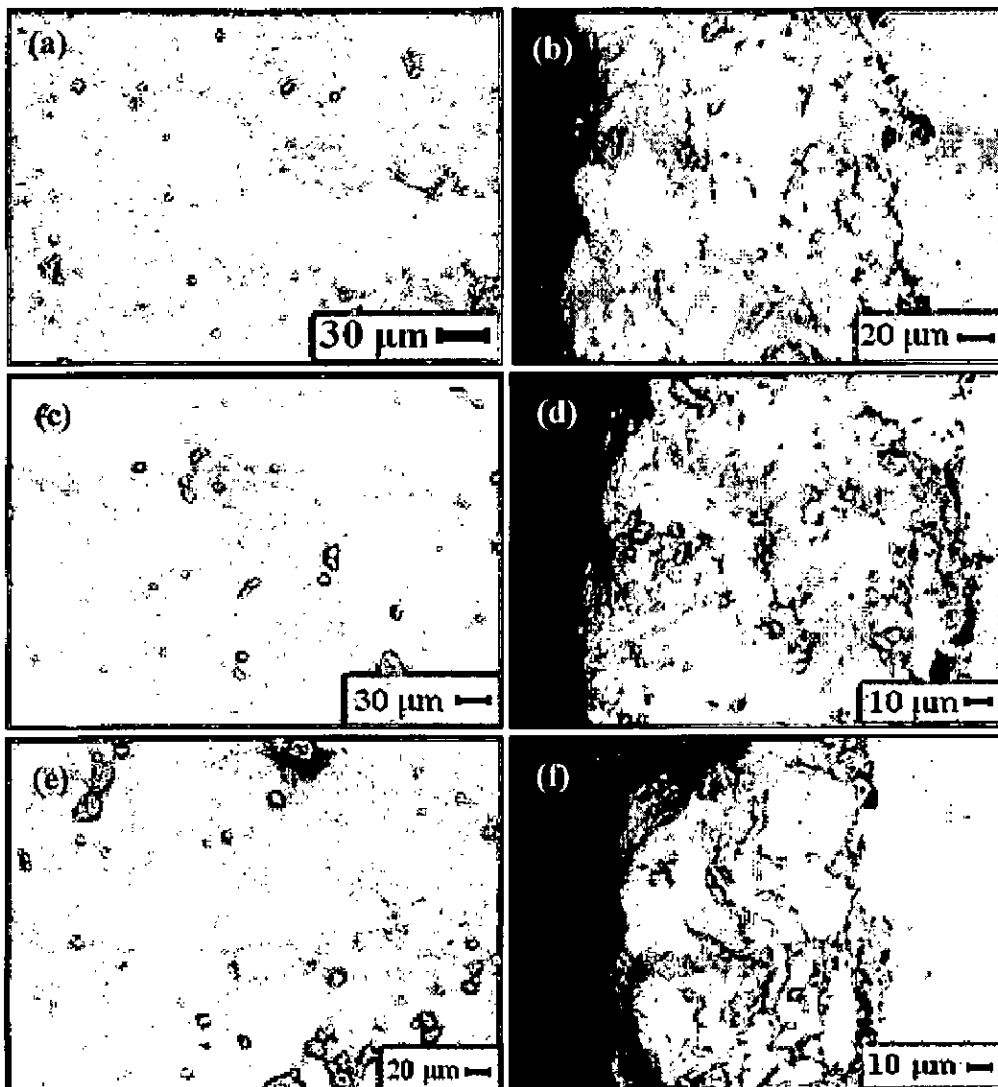


**Fig. 5.1:** Surface FESEM photographs of as sprayed NiCrAl coating showing the top surface after polishing on (a) Superni 76; (c) Superni 750; (e) Superfer 800 and cross sectional details of (b) Superni 76; (d) Superni 750 and (f) Superfer 800.

### **5.1.3.2 Microhardness of the coatings**

The microhardness data of the coatings is plotted in the Fig. 5.2, which shows the hardness profiles along the cross section of the coatings as a function of distance from the coating–substrate interface. The hardness of the substrates was found to be in the range of 216–290 Hv, whereas the hardness of the coatings varied with the distance from the coating–substrate interface. A maximum of 351 Hv and a minimum of 278 Hv were observed in case of coated Superni 76. In case of coated Superni 750, a maximum of 342 Hv and a minimum of 278 Hv were found, whereas coated Superfer 800 alloy indicated a maximum value of 324 Hv and a minimum value of 285 Hv.

### **5.1.3.3 Surface roughness (Ra) values of the as sprayed coatings**

The surface roughness (Ra) values of the as sprayed coatings were found to be in the range of 10.36 – 11.01  $\mu\text{m}$ . The centre line average (CLA) method was used to obtain the Ra values.

### **5.1.3.4 Bond strength of NiCrAl coatings**

The photograph of the surfaces of a coated specimen after pulling apart in the tensile test machine is shown in Fig. 5.3. The coating failed at the substrate-coating interface while remaining attached to the adhesive. An average bond strength of 59 MPa was observed.

### **5.1.3.5 X-ray diffraction (XRD) analysis**

The XRD patterns of the NiCrAl powder and NiCrAl coated superalloys are shown in Fig. 5.4 and Fig. 5.5, respectively. The feedstock powder and the NiCrAl coated superalloys mainly comprised of nickel based fcc phase. Further, they revealed the presence of chromium and aluminum as the minor phases.

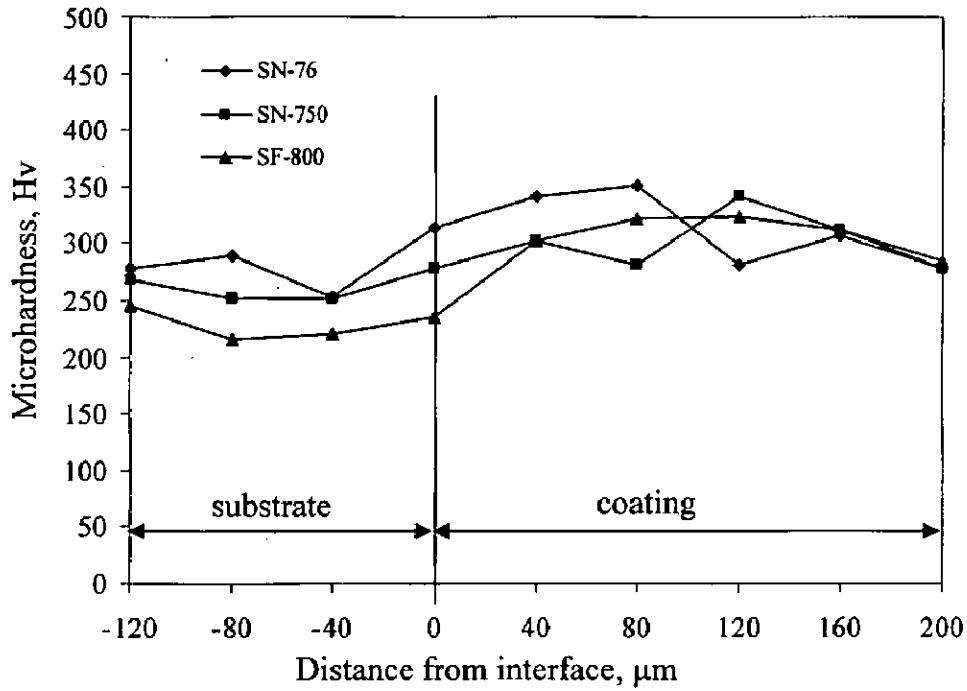


**Fig. 5.2:** Microhardness profiles for HVOF sprayed NiCrAl coatings on the different superalloys.

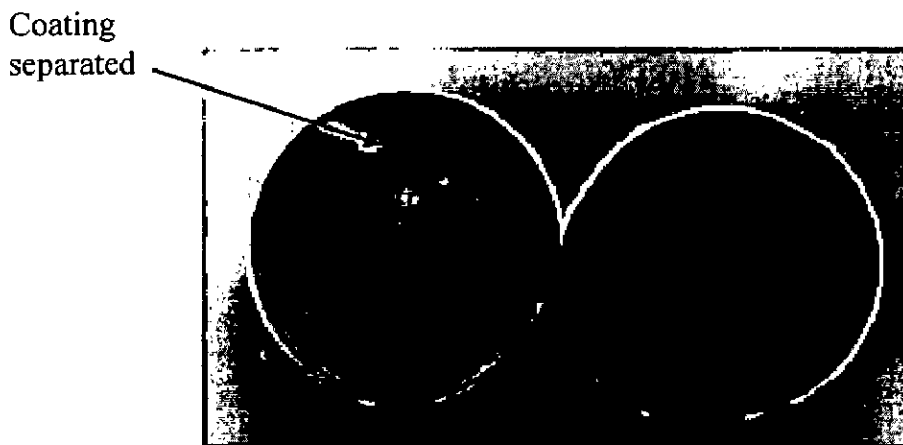


**Fig. 5.3:** Photograph of the surfaces of a NiCrAl coated specimen after it was pulled apart in the tensile test machine.

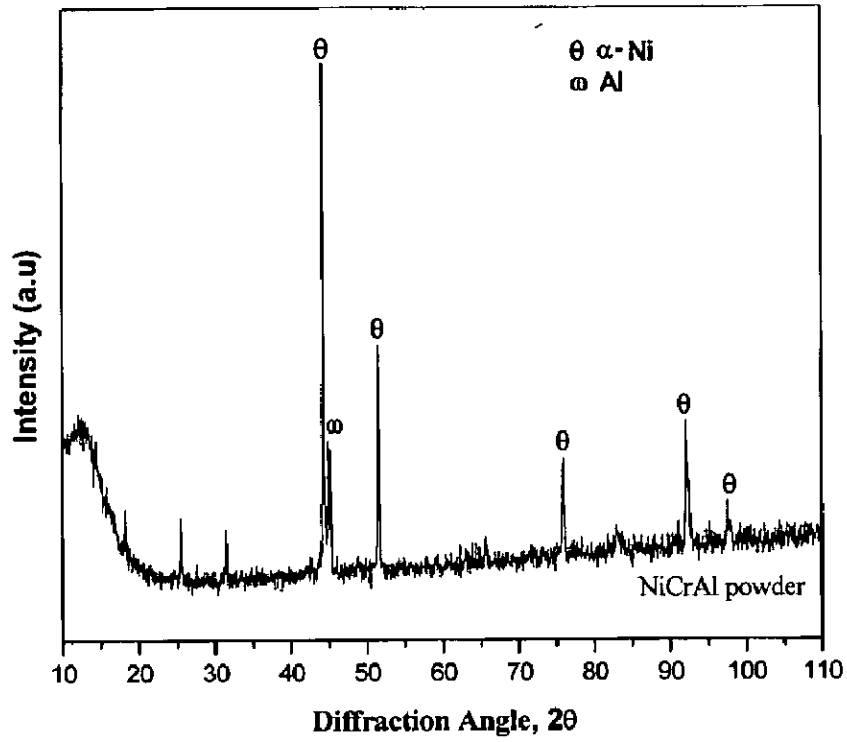


**Fig. 5.4:** X-ray diffraction pattern of NiCrAl powder used for coating.

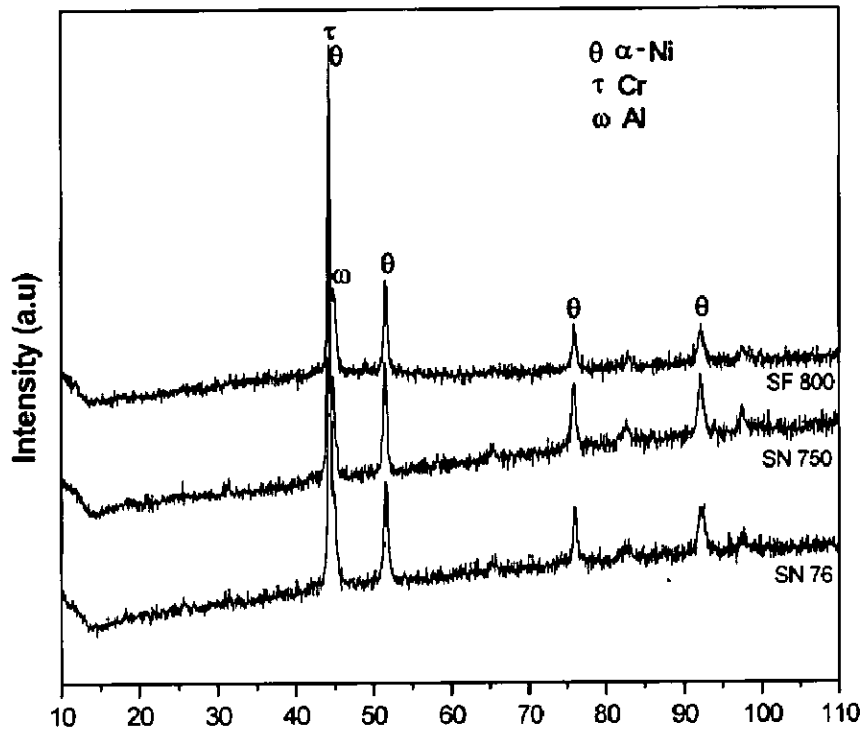


**Fig. 5.5:** X-ray diffraction patterns of NiCrAl coating on Ni- and Fe-based superalloys in as sprayed condition.

### 5.1.3.6 FESEM/EDAX analysis

#### 5.1.3.6.1 Surface morphology of the as sprayed coating

The FESEM images of surface microstructure of the as sprayed NiCrAl coating on the superalloy are depicted in Fig.5.6. It is observed that the splats have formed without any sign of cracking or disintegration. Few partially melted powder particles were noticed in the as sprayed coating. The coating in general consists of irregular shaped splats distributed uniformly throughout with distinct splat boundaries, which represents the typical HVOF spraying process. The coating contains some oxide stringers which may be due to the in-flight oxidation during spraying process and/or preexisting in the feed material along with small voids in the as sprayed microstructure. In general, the NiCrAl coating formed is uniform and adherent with the superalloy substrates.

#### 5.1.3.6.2 EDAX cross sectional analysis

The cross-sectional images and the corresponding EDAX analysis was carried out at different points of interest for NiCrAl coated superalloys viz. Superni 76, Superni 750 and Superfer 800 as shown in Fig. 5.7. It is seen that nickel is predominately present in the coating with chromium in small amounts and aluminum is located at the Ni splat boundaries. Al is absent wherever Ni is identified. The black areas at the coating–substrate interface are identified as the oxides of aluminum.

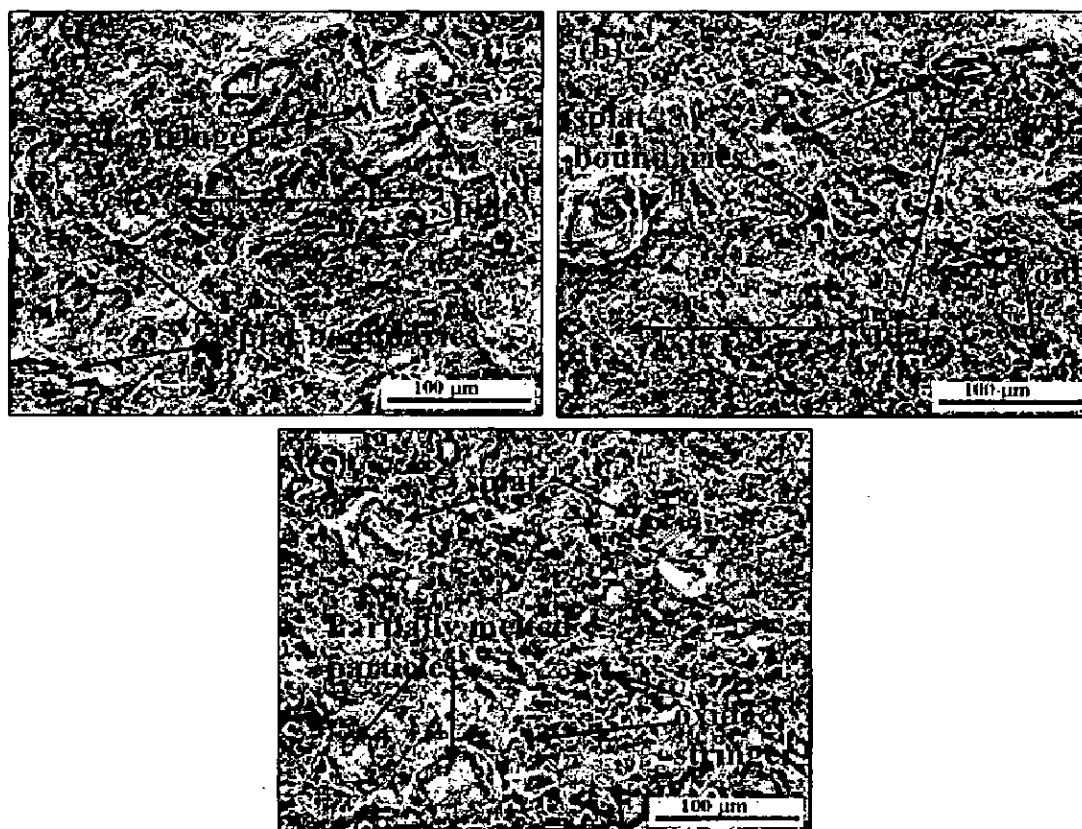


**Fig.5.6:** FESEM micrographs of as sprayed NiCrAl coating showing the surface microstructure on superalloys (a) Superni 76; (b) Superni 750 and (c) Superfer 800.



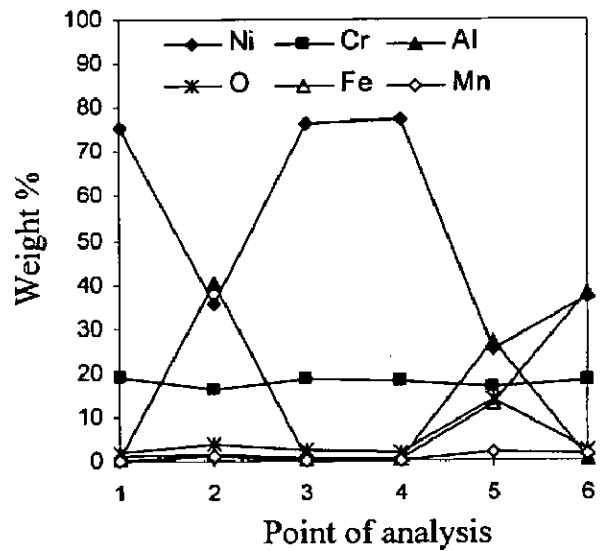
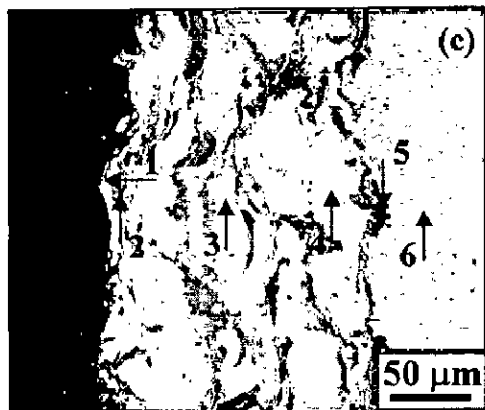
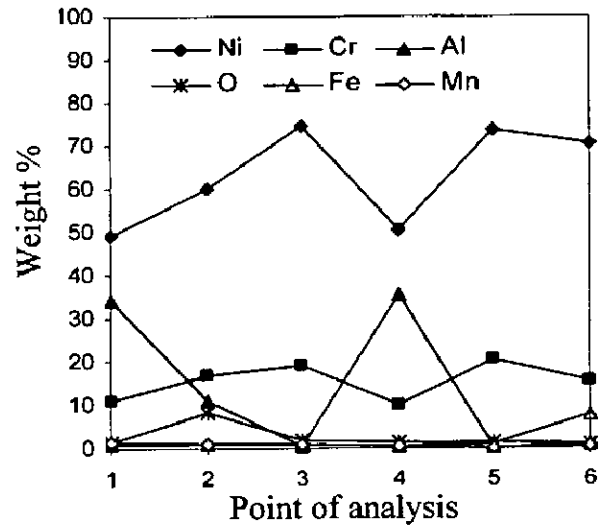
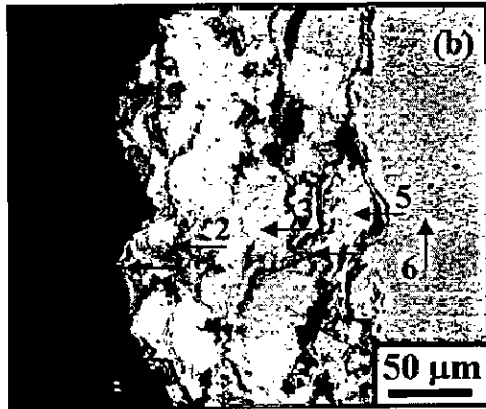
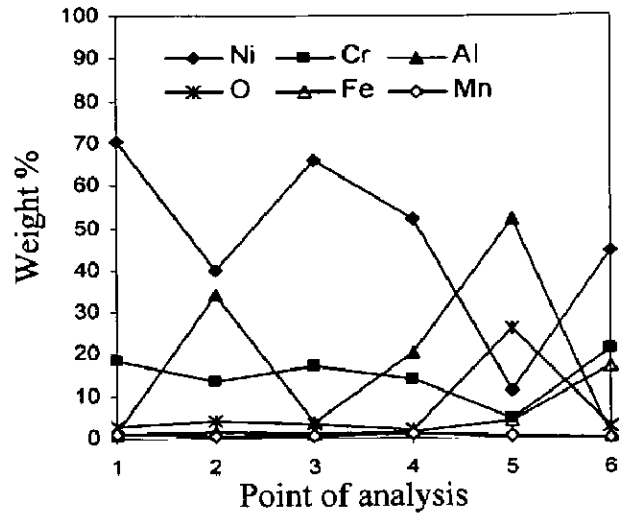
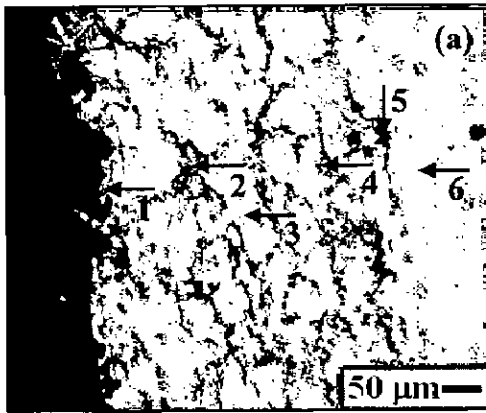


**Fig. 5.7:** Cross-section morphology of NiCrAl coated superalloys in as sprayed condition of (a) Superni 76, (b) Superni 750 and (c) Superfer 800.

### 5.1.3.7 X-ray mapping

X-ray mapping of different elements in the NiCrAl coated superalloy samples are shown in Fig. 5.8. Coated Superni76 shown in Fig. 5.8 (a) illustrate that Ni and Cr are distributed uniformly throughout the coating; whereas, aluminum is found along the splat boundaries. A small amount of oxygen might have penetrated into the coating during spraying process. Nickel and chromium are found at the location where aluminum is absent. In case of Superni 750, aluminum and oxygen coexists as observed in the X-ray mapping shown in Fig. 5.8 (b). A small amount of silicon has diffused from the substrate into the coating and is present along the intersplat boundaries. A traceable amount of Fe and Mn have migrated from the substrate into the coating. The Fig. 5.8 (c) shows X-ray mapping of coated Superfer 800, in which nickel and chromium uniformly exist together in the coating, whereas, aluminum exists along the nickel splat boundaries. Small amount of Fe has diffused from the substrate into the coating along the intersplat region and forms a thin band at the surface as seen from the X-ray mapping. Trace amounts of Mn and Si have diffused from the substrate into the coating through the intersplat regions.

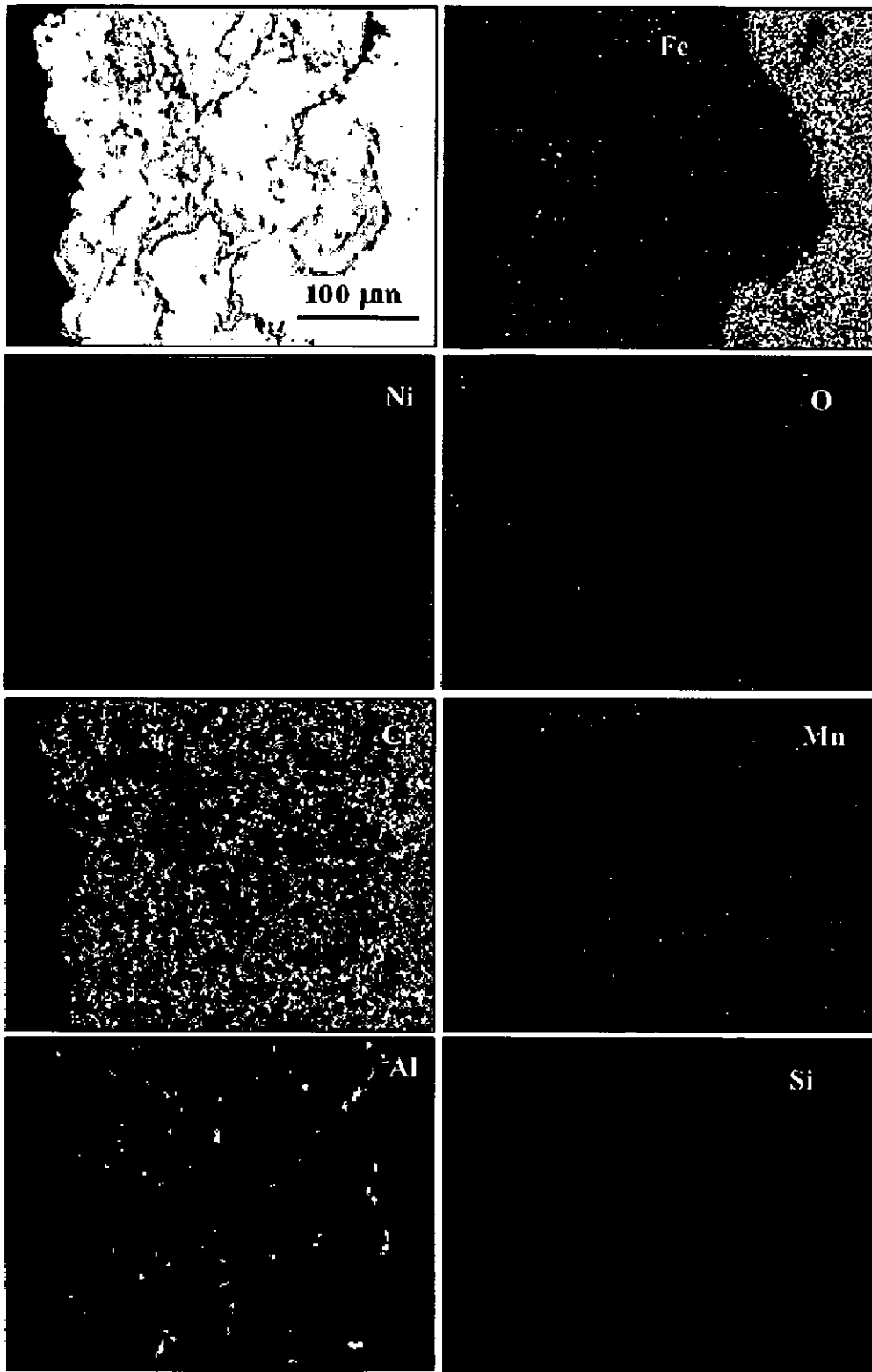


**Fig. 5.8 (a)- i:** Compositional image and X-ray mapping of the cross-section of the as sprayed NiCrAl coating on Superni 76 superalloy.

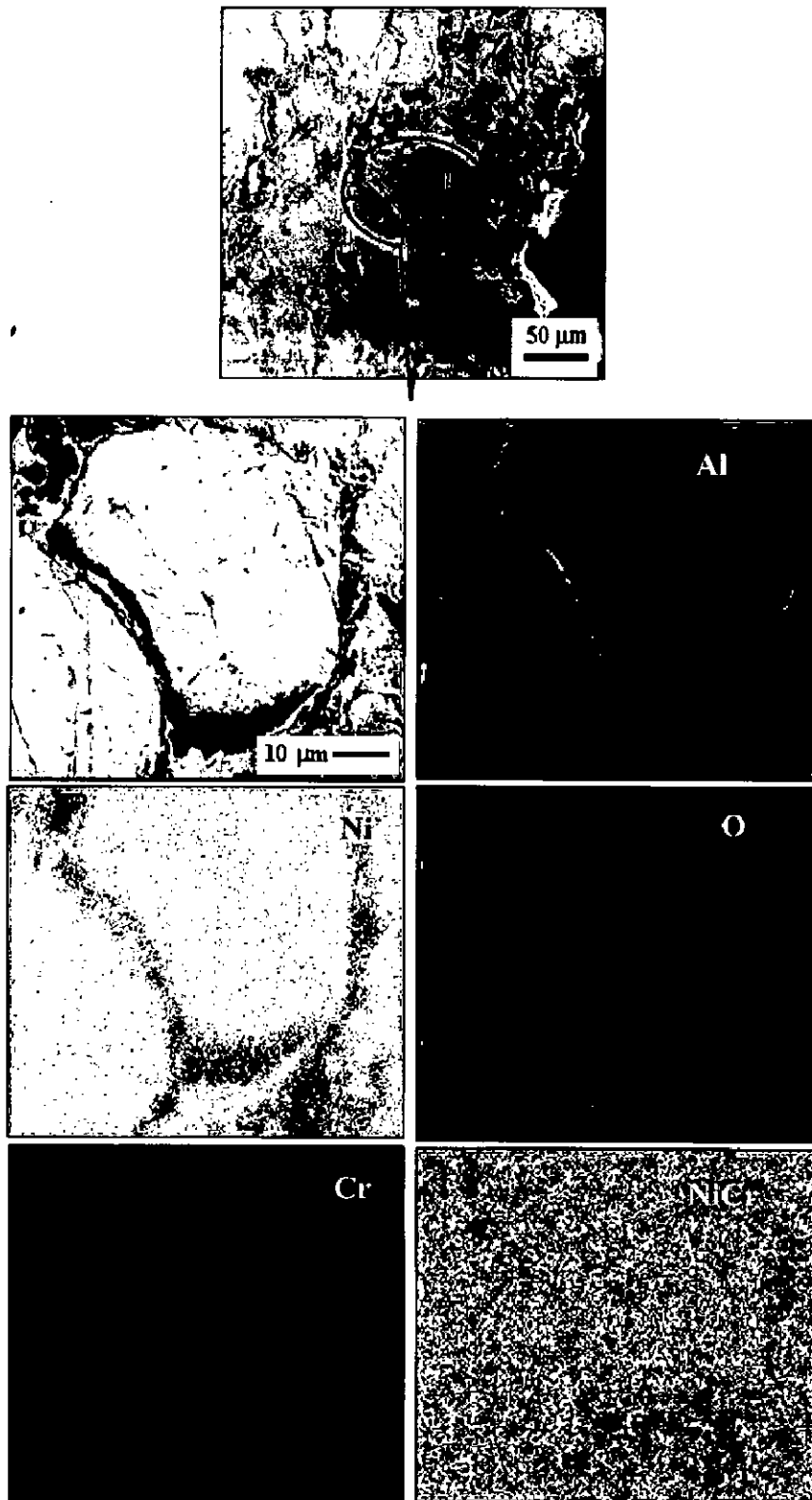


**Fig. 5.8 (a)-ii:** Compositional image and X-ray mapping of the enlarged splat of the as sprayed NiCrAl coating on Superni 76.

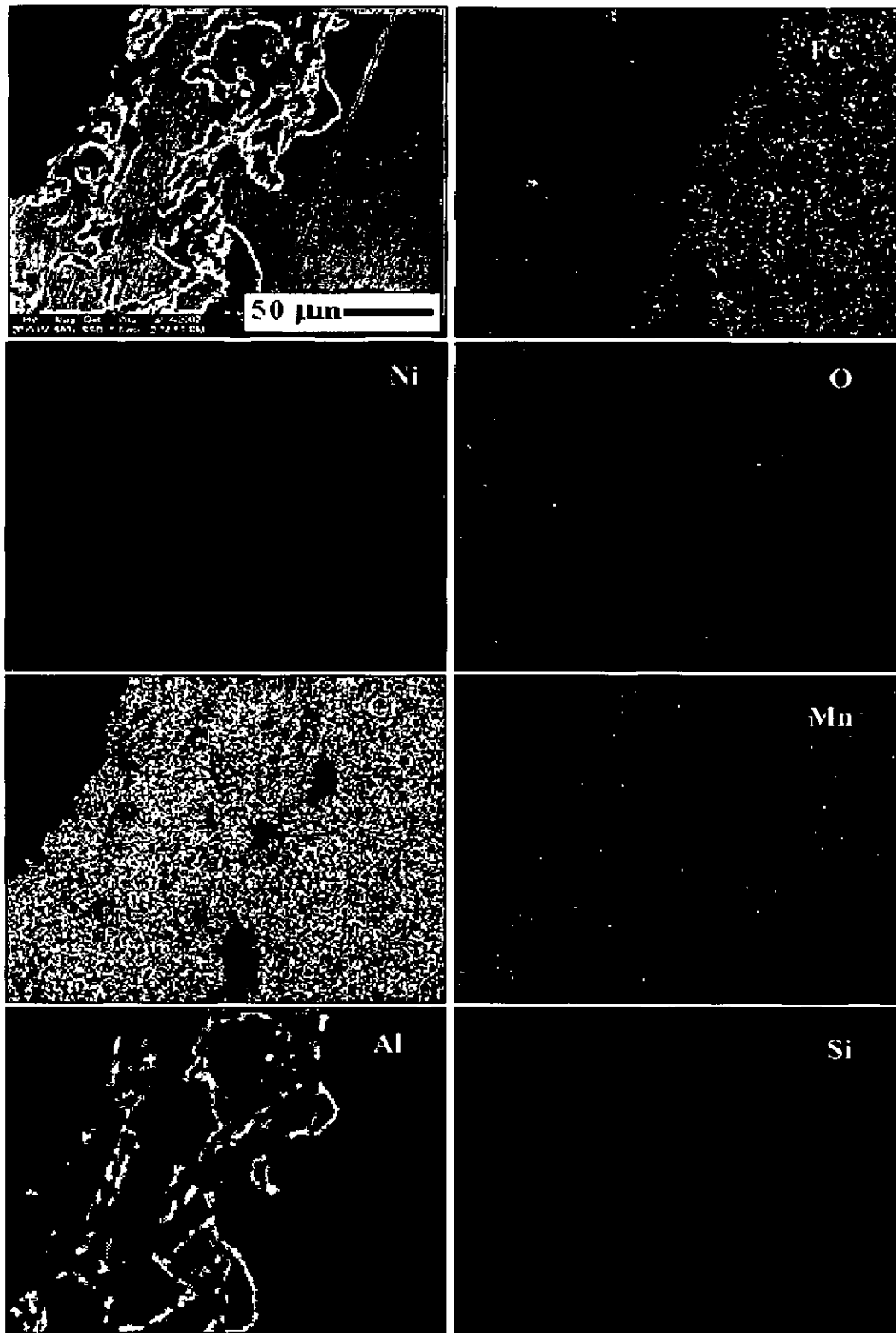


**Fig. 5.8 (b)-i:** Compositional image and X-ray mapping of the cross-section of the as sprayed NiCrAl coating on Superni 750.

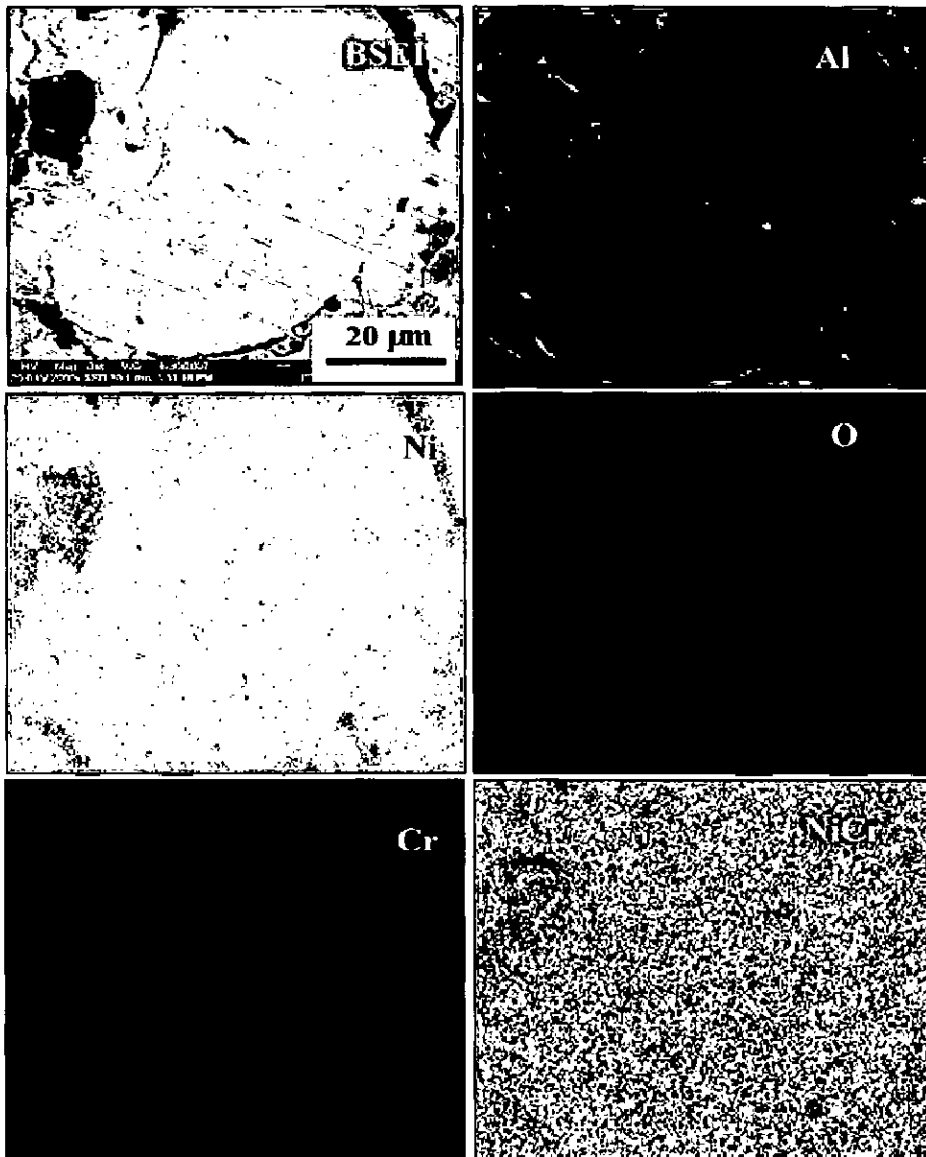
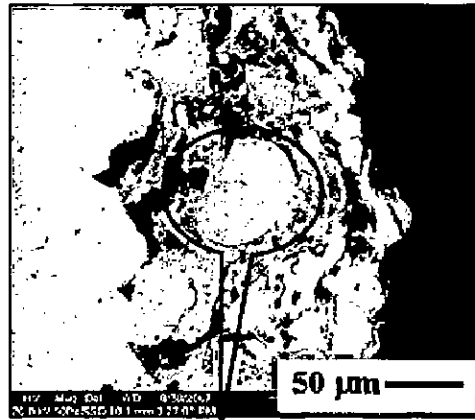


**Fig. 5.8(b)-ii:** Compositional image and X-ray mapping of the enlarged splat of the as sprayed NiCrAl-coating on Superni 750.

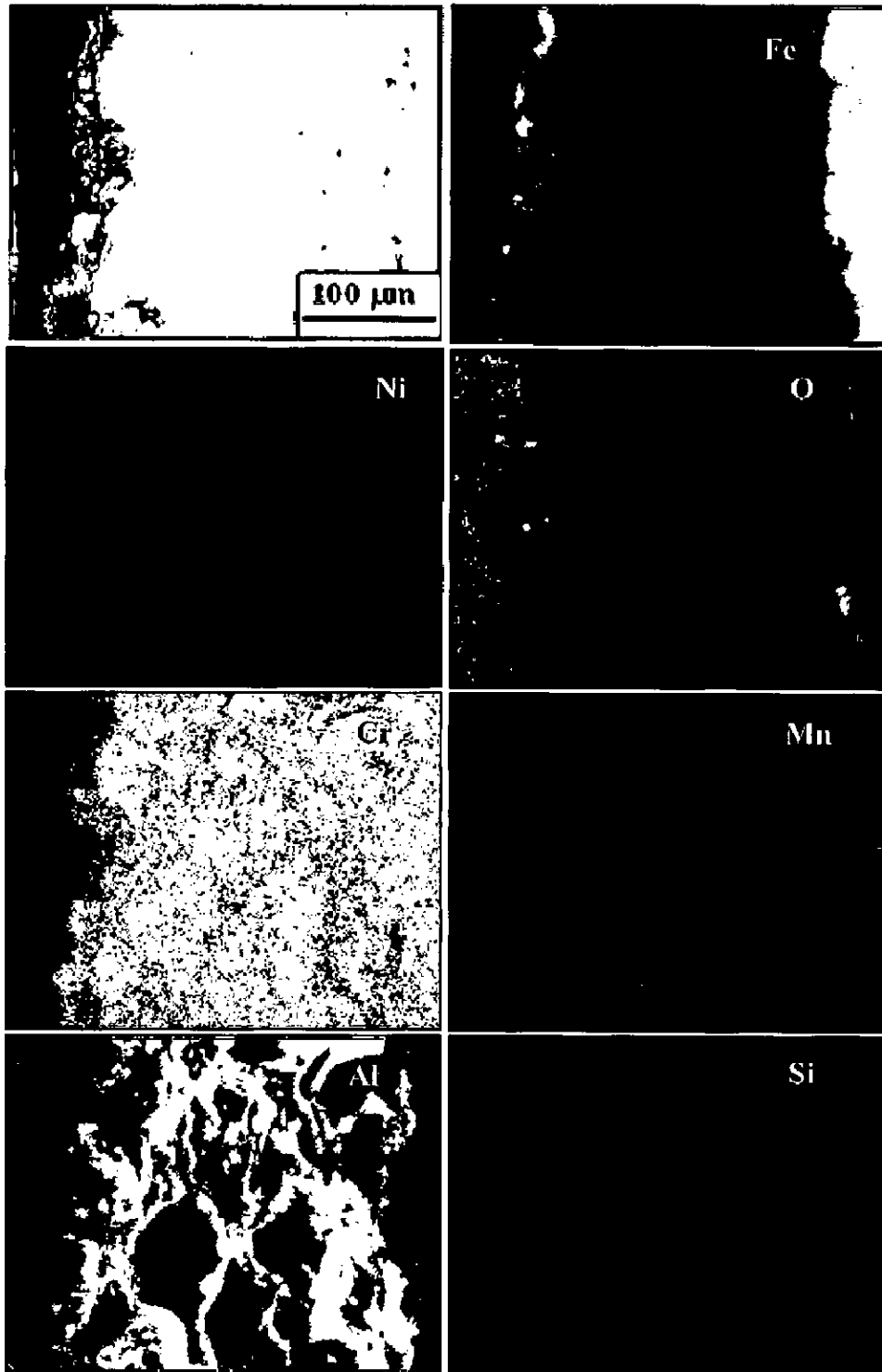


**Fig. 5.8(c)-i:** Compositional image and X-ray mapping of the cross-section of the as sprayed NiCrAl coating on Superfer 800 superalloy.

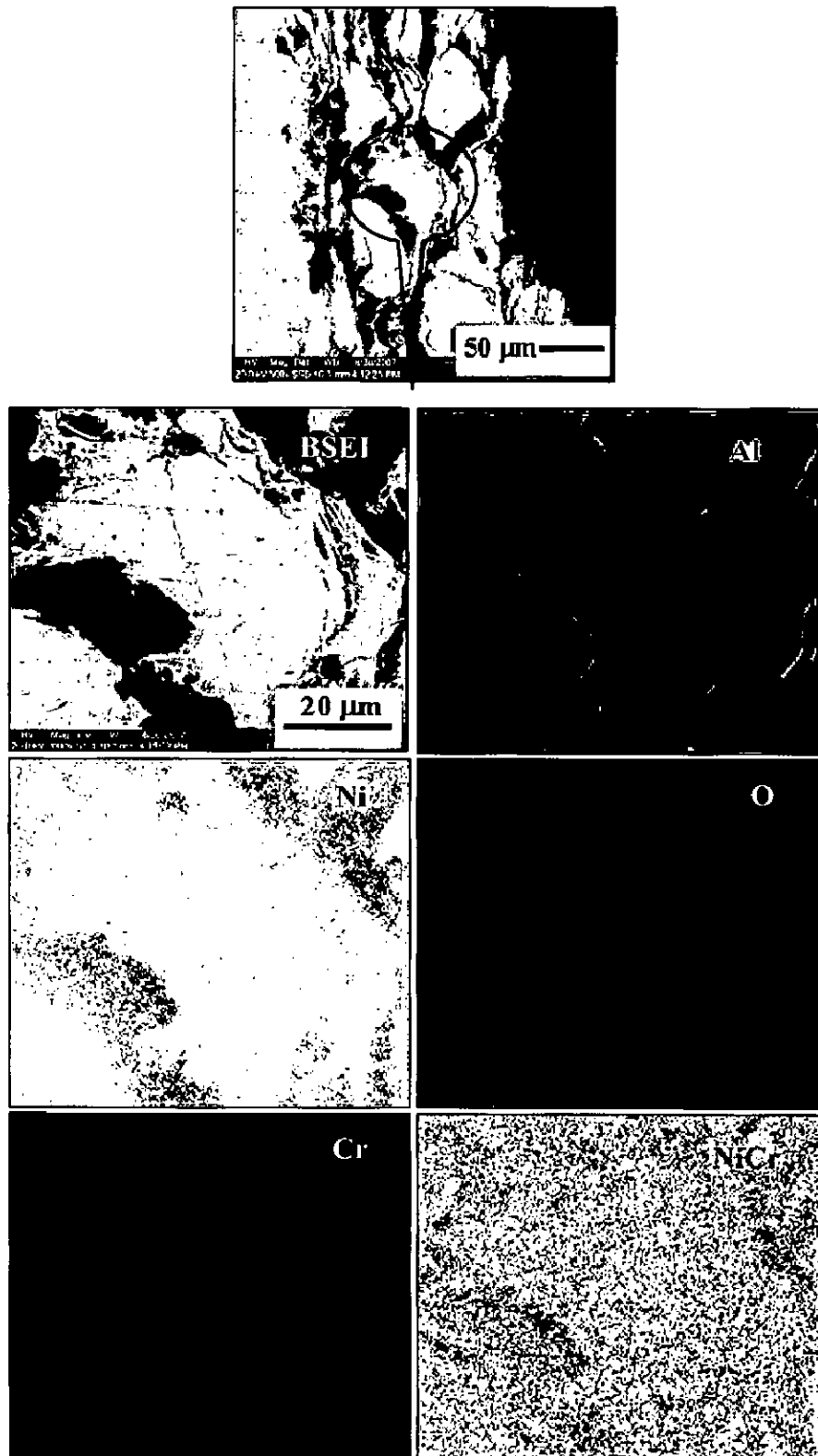


**Fig. 5.8 (c)-ii:** Compositional image and X-ray mapping of the enlarged splat of the as sprayed NiCrAl coating on Superfer 800.



#### 5.1.4 Discussion

HVOF process has been found successful in depositing the NiCrAl coating on superalloys in the present work. Higher velocity of particles results in higher bond strengths and lower porosity as the particle has less time to cool down at high velocities. It is well known that porosity of the coatings affects the corrosion resistance of thermal spray coatings. Dense coatings usually provide a better corrosion resistance than the porous coatings as porosities can do harm to the persistent corrosion resistance of the coating (Zhao, W.M., et al, 2004; Zhao, W.M., et al, 2005). The porosity of the NiCrAl coatings has been found to be less than 1.70%. Fig. 5.1 shows the surface morphology of the as sprayed coating on different superalloys chosen in the present work. The coating obtained was dense and have a layered structure due to deposition and resolidification of the molten and semi molten particles which is similar to the findings of Dent et al, (2001). It could be noted that the long axis of the deposited splats are parallel to the substrate surface. The deposited coatings possess porosity, melted, unmelted particles, oxidized particles and inclusions. Some particles might have oxidized due to the inflight oxidation during the deposition of successive passes. Dent et al, (2001) and Sidhu et al. (2006F) also observed the inflight oxidation of the powders during HVOF spraying.

Hardness is one of the important mechanical property of the coatings need to be measured to ensure its reliability in the actual applications (Tucker, 1994). It is found that the microhardness value of the coating varies along the cross section and it may be due to the presence of porosity, oxide inclusions, melted, unmelted particles in the coating as seen in the FESEM micrograph (Fig. 5.6). These variations in microhardness values are in tandem with that of the hardness values measured for the thermal sprayed coatings reported in the earlier literature (Buta Singh, 2005A; Dent et al, 2001; Hazoor et al, 2006; Sidhu et al, 2006G). The higher value of hardness near the coating-substrate interface might be partly contributed by the work-hardening effect of sandblasting of the substrate prior to the coating process as suggested by Sundararajan et al,(2004B) and also perhaps due to the high-speed impact of the coating particles as suggested by Hidalgo et al, (1997, 1998, 1999). The surface roughness values were found to be slightly higher due to the coarse particles used for coating. Surface roughness is one of the important parameters of the HVOF sprayed coatings need to be measured for its better performance in the high temperature applications. For example, in thermal power plants, the coatings employed on the boiler components are subjected to solid particle erosion and therefore it is essential to ensure the erosion resistance of the coatings

with respect to its surface features such as surface roughness, morphology of the grain, etc. It may be mentioned that higher surface roughness of the coated component would result in the higher erosion rate.

The bond strength is an important property of the thermally sprayed coating. It is generally believed that high velocity of spray particle and an improved melting benefit the adhesion of a coating to substrate (Wang, Y.Y., et al, 2006). Coating strength is enhanced if droplets penetrate deep into surface cavities of the substrate before they freeze. The coating properties are therefore highly dependent on fluid flow and heat transfer during droplet impact and are affected by both surface roughness and temperature (Pershin et al, 2003). A study on the adhesive strength of HVOF coatings using nickel-based alloy powders revealed that the adhesive strength is slightly decreased with the improvement of the melting state of the particles when the coating strength reaches to over 40 MPa (Li C.J., et al, 2001). It is reported in the literature that the HVOF metallic coating deposited with well-melted particles yielded a limited adhesive strength from 40 MPa to 50 MPa (Li and Li, 1998), while the coating deposited by partially melted particles yielded a higher adhesive strength. A good melting does not necessarily correspond to good adhesion under the HVOF spraying condition; on the contrary, a limited melting, corresponds to spray particles in a solid-liquid state, results in good adhesion with HVOF coating as reported in the literature (Li C.J., et al, 2001). The HVOF sprayed NiCrAl coatings on the superalloys failed at the coating-substrate interface and the average bond strength was found to be 59 MPa in the present work. Normally, the HVOF-sprayed coatings tend to exhibit higher bond strength levels than those of atmospheric plasma sprayed (APS) coatings (Pawlawski, 1995) and it is because of higher particle velocities attained by the HVOF-sprayed particles when compared to APS process.

The XRD analysis of the feedstock powder and as-sprayed coatings indicates nickel as a prominent phase with weak peaks of chromium and aluminum. The results of XRD are further supplemented by EDAX analysis, which confirms the presence of Ni in higher amount at certain intervals. The X-ray mapping analysis of NiCrAl coated superalloys indicates that the core of the splat is rich in nickel and chromium; where as aluminum is present along the splat boundaries and it is also seen at locations where nickel and chromium are absent.

X-ray mapping of NiCrAl coated Superni 76 Fig.5.8(a)-i indicate that nickel and chromium coexists together. Oxygen has also diffused into the coating and is present at the splat boundaries. Iron has diffused from the substrate into the coating and present along the intersplat regions. Fig 5.8(a)-ii shows the enlarged area of the splat and it consists of both

nickel and chromium as evident from the EDAX analysis, which is further supplemented by XRD analysis. Chromium is coexisting with aluminum at the splat boundaries. A thick irregular band of aluminum is found at the coating substrate interface. An in-flight oxidation of aluminum might have occurred during the coating process. A small amount of manganese and silicon have migrated from the substrate into the coating.

In case of Superni 750, Fig. 5.8(b)-i, the X-ray mapping shows that the splats are rich in nickel and chromium. The dark area near the coating-substrate interface indicates the presence of aluminum oxide, which may be attributed to the in-flight oxidation of aluminum during coating process. Traceable amount of iron, manganese and silicon have diffused from the substrate into the coating. The enlarged area of the splat is shown in Fig.5.8(b)-ii. Nickel and chromium are coexisting in the splats and aluminum is present at the boundary with chromium. The X-Ray mapping of NiCrAl coated Superfer 800, Fig. 5.8(c)-i depicts that the splats are rich in nickel and chromium. Presence of thin band of iron on the surface indicates the diffusion of the substrate elements during coating process. A thick band of aluminum is present along the coating-substrate interface. Fig. 5.8(c)-ii indicates the enlarged area of the splat, which consists of nickel and chromium, which is further confirmed by XRD analysis. Aluminum is present along the splat boundaries and coexists with chromium. Small amount of manganese and silicon have also diffused from the substrate into the coating and are present along the splat boundaries.

### **5.1.5 Conclusions**

1. The HVOF spray process has been successfully used to deposit dense, adherent and homogeneous coatings on the three different superalloy substrates in the present work.
2. The coatings on all the three superalloys exhibited uniform lamellar structure with a porosity value around 1.7%. The as sprayed coatings showed roughness values in the range of 10.36-11.01  $\mu\text{m}$ .
3. The hardness of the three superalloy substrates were in the range of 216–290 Hv, whereas the hardness value of NiCrAl coating on these substrates varied between 278-351 Hv. It may be mentioned that the hardness values of the coatings varied across the coating-substrate interface and found to be nearly equal on the coating surface.

4. The bond strength value of the HVOF sprayed NiCrAl coating was found to be 59MPa. The higher values of bond strength can be attributed to the higher particle velocities attained by the HVOF process.
5. The XRD analysis of the as sprayed NiCrAl coatings on three different superalloys revealed the presence of nickel (fcc) as a dominant phase with minor intensity peaks of chromium, aluminum, which was further supplemented by cross sectional EDAX analysis and X-ray mapping of the coated alloys.
6. The X-ray mapping analysis of the three-coated alloys indicated that nickel and chromium co-exists in the splats and aluminum along the splat boundaries. The dark area near the coating substrate interface indicates the presence of aluminum oxide, which may be attributed to the in-flight oxidation of aluminum during coating process.
7. Traceable amount of iron, manganese and silicon have migrated from the substrate into the coating indicating the diffusion of the substrate elements into the coating during HVOF spraying process.

## 5.2 OXIDATION STUDIES IN AIR

### 5.2.1 Introduction

The performance of materials used in high temperature environment is often controlled by its ability to form the protective oxide scale on the surface (Graham and Hussey, 1995). The specific alloys or coatings designed to resist oxidizing environments at high temperatures should be capable of forming thermodynamically stable, slow growing, and adherent surface oxide scales (Toma et al, 2000). Gas turbine technology for power generation and aero engine applications places an increasing demand on the superior performance of Ni- and Fe-based superalloys. The hot section components, made up of superalloys, in gas turbine engines are subjected to repeated thermal cycles and fail due to high temperature oxidation during operation. The operating temperature of modern gas turbine engines is increasing gradually to realize the improved efficiency at the lower cost (Goward, 1998). Hence, the oxidation resistance of superalloys under cyclic high temperature environments has become a vital issue. Although numerous studies in the literature reported the oxidation behaviour of bulk alloys (Khanna et al, 1993), the development of HVOF sprayed NiCrAl alloy coatings on superalloys as protective coatings is scarce in the literature.

Nesbitt and Heckel (1984) have modeled the degradation of Ni-Cr-Al overlay coatings on Ni-22 at.%Cr substrate occurred due to oxidation accompanied by thermal cycling. The coating-substrate interdiffusion caused the reduction of aluminum content of the coating and leaving the formation of considerable porosity at the coating-substrate interface during cyclic oxidation at 1150°C as reported in their work. Lowell et al, (1982) investigated the high velocity oxidation and hot corrosion behavior of NiCrAl and FeCrAl base oxide dispersion strengthened (ODS) alloys. It was reported in their work that the austenitic Ni-base ODS alloys showed a poor oxidation resistance as compared to ferritic base ODS alloys. The better performance of ferritic Fe-base alloys is due to its lower thermal expansion, which results in less stress in the oxide due to thermal cycling and it does not lead to spallation. They reported that the high thermal expansion of Ni-base ODS alloys directly leads to spalling during cycling from 1100°C to room temperature. Barrett et al, (1981) carried out the cyclic oxidation tests on Ni-Cr-Al-1.10 w/o Zr alloys in static air at 1100 and 1200°C and showed that a small addition of Zr improves the oxidation resistance of NiCrAl alloys due to the strong oxide-metal bond, which does not cause spallation at the oxide-metal interface.

In recent years, HVOF thermal spray technique is extensively used for depositing protective coatings of various materials on a wide variety of substrates (Edris and McCartney,

1997) due to the high quality of coatings with minimal porosity and low oxide content achievable in this technique (Sobolev et al, 2004). The heat source for particle melting comes from a combustion reaction in this technique and it does not cause degradation of the mechanical properties of the alloy substrates. Goward (1998) reported that a complete understanding of oxide adherence is still elusive and is one of the most important areas of research, for both coatings and superalloys, to improve upon the engine efficiency and service life.

Owing to the importance of combating the high temperature oxidation of superalloys, the present work has been focused to assess the oxidation kinetics of bare and NiCrAl coated superalloys at 900°C in air under cyclic conditions. In the actual industrial applications, these superalloys experience cyclic conditions of mechanical loading, temperature and atmosphere (Raffaitin et al, 2006). An attempt has been made to produce a dense, adherent and protective NiCrAl coating on Ni- and Fe-based superalloys in the present investigation. The corrosion rate of bare and coated superalloys has been evaluated by monitoring the weight gain data as a function of time. XRD, FESEM/EDAX, and X-ray mapping techniques have been employed to understand the nature, composition and protective properties of the oxide scales formed on both bare and coated superalloys during exposure to elevated temperature.

## **5.2.2 Experimental details**

The substrate materials, coating formulation and the hot corrosion studies are explained in detail in section 3.4.3 and 3.5 of Chapter 3.

## **5.2.3 Results**

### **5.2.3.1 Visual observation**

The surface macrograph of oxidised specimens of NiCrAl coated superalloys after 100 cycles exposure to air at 900°C is shown in Fig. 5.9. In case of NiCrAl coated Superni 76 alloy (Fig. 5.9a), light greenish colour was observed after second cycle during the experiment which turned into light grey after seven cycles. The spalling of the scale in the form of powder was seen after 22 cycle and continued for 28 cycle. The surface of the oxidised specimen indicated grey colour after 100 cycles. In case of NiCrAl coated Superni 750 alloy (Fig. 5.9b), a light green color was observed on the surface of the coating, after third cycle, and then it transformed into a grey during the course of the experiment. Spalling in the form of powder was noted after fourth cycle during the experiment and it continued upto eight

cycles. The scale on the surface turned into grey colour after 100 cycles. The surface in case of NiCrAl coated Superfer 800 alloy (Fig. 5.9c) showed a grey color on the surface of the coating at the end of third cycle. Microsputtering of the scale was noticed after sixth cycle during the experiment and continued for few cycles. The surface of the specimen became grey colour after 100 cycles.

### 5.2.3.2 Oxidation Kinetics

The weight gain per unit area of the sample is calculated as a function of time, expressed as the number of cycles as shown in Fig. 5.10. The total weight gain at the end of 100 cycles for bare Superni 76, 750 and Superfer 800 has been found to be 6.72, 9.0 and 5.01 mg/cm<sup>2</sup> respectively. The weight gain was very rapid during the initial period of exposure in all the three bare superalloys. The total weight gain in case of NiCrAl coated Superni 76, Superni 750 and Superfer 800 was found to be 5.57, 5.42 and 4.96 mg/cm<sup>2</sup> respectively. The (weight gain/area)<sup>2</sup> versus the number of cycles for both bare superalloys and NiCrAl coated superalloys are shown in Fig. 5.11. It is inferred from the weight gain plots that the total weight gain in case of NiCrAl coated superalloys was marginally lower than that of the bare superalloys.

The rapid increase in weight gain in case of NiCrAl coated superalloys during the initial period of exposure is due to the formation of oxides at the surface as well as the penetration of the oxidizing species along the intersplat boundaries/open pores. The coating subsequently becomes dense and diffusion of oxidizing species to the inner portion of the coating gets slowed down once the oxides are formed at places of porosity and splat boundaries. The high temperature oxidation behavior of the NiCrAl coated superalloys follows nearly the parabolic trend. This would relatively minimize the rate of weight gain and result in the steady state oxidation behavior with the prolonged exposure time. The diffusion controlled mechanism operates at 900°C under cyclic conditions. Table 5.1 shows the parabolic rate constant for bare and NiCrAl coated superalloys after oxidation studies. The cumulative weight gain per unit area for bare and NiCrAl coated superalloys subjected to cyclic oxidation at 900°C for 100 cycles is depicted in Fig. 5.12.

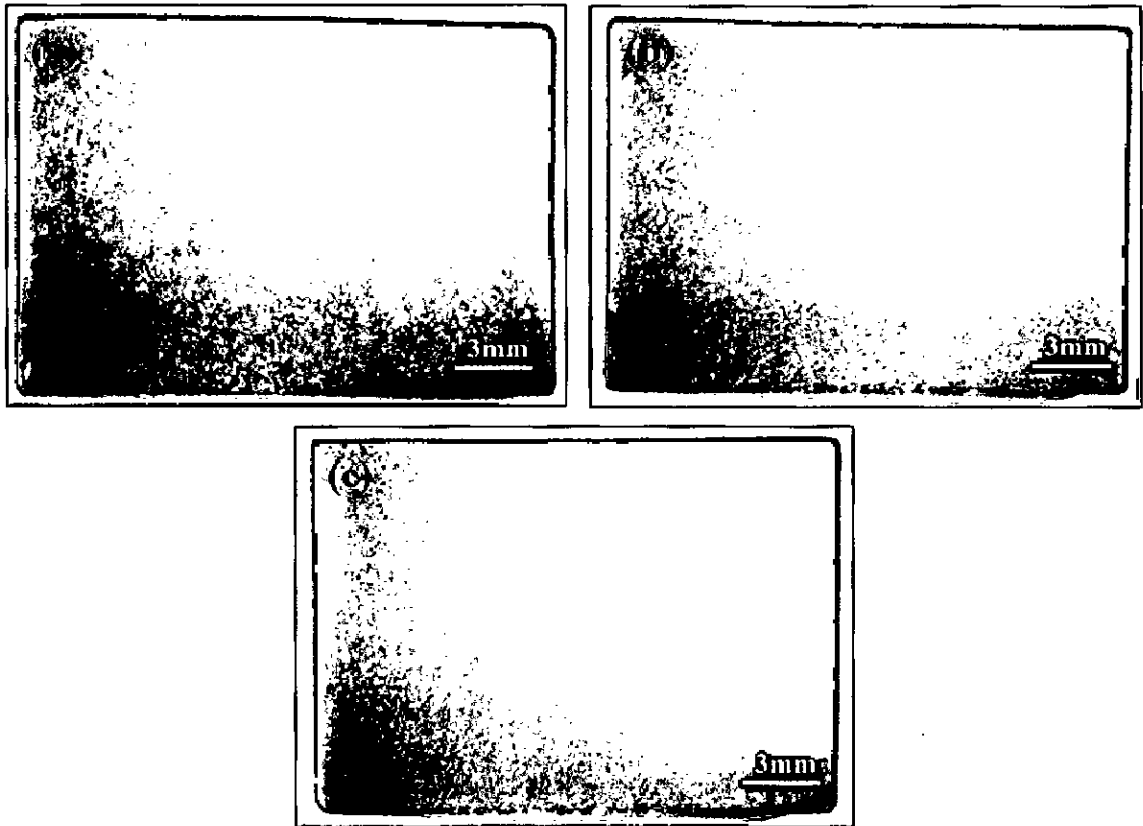


**Fig. 5.9:** Surface macrographs of NiCrAl coated (a) Superni 76; (b) Superni 750; and (c) Superfer 800 after 100 hr exposure to air at 900°C.



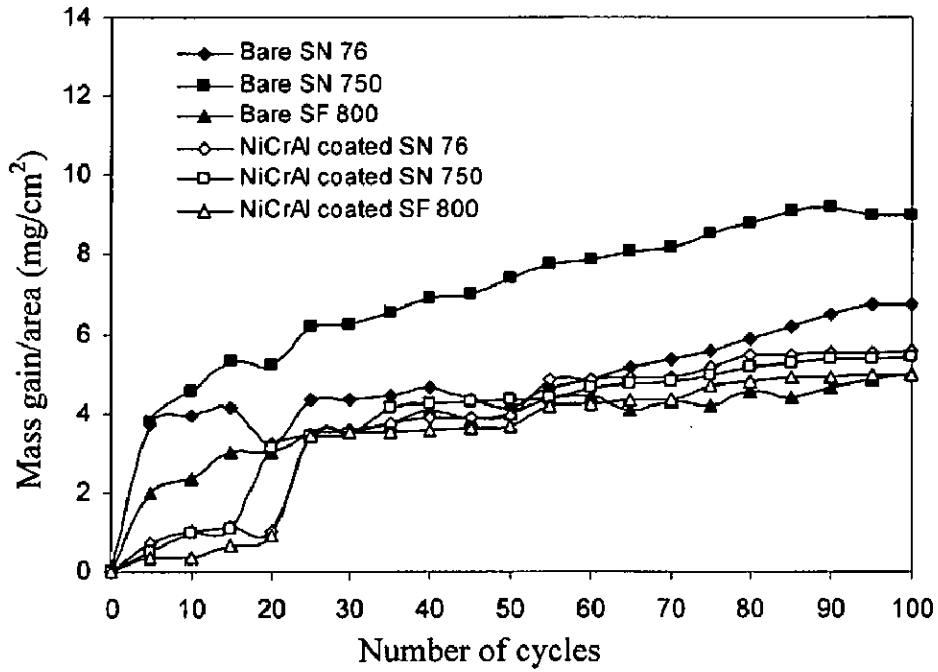


**Fig.5.10:**  $(\text{Weight gain/area})^2$  vs. number of cycles plots for the uncoated and coated NiCrAl superalloys subjected to cyclic oxidation for 100 cycles at  $900^\circ\text{C}$ .

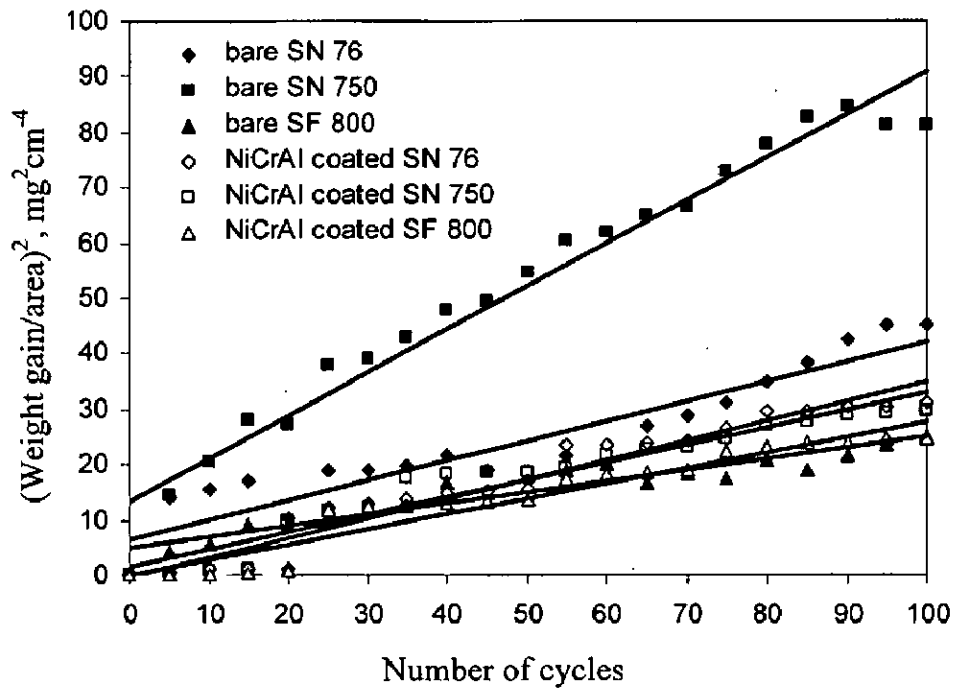


**Fig.5.11:**  $(\text{Weight gain/area})^2$  vs. number of cycles plots for the uncoated and coated NiCrAl superalloys subjected to cyclic oxidation for 100 cycles at  $900^\circ\text{C}$ .

**Table 5.1:** Parabolic rate constant,  $k_p$  values of uncoated and NiCrAl coated superalloys subjected to air oxidation at 900°C.

Superalloy substrate	$k_p \times 10^{-10} \text{ gm}^2 \text{ cm}^{-4} \text{ s}^{-1}$
Uncoated Superni 76	1.0
Uncoated Superni 750	2.15
Uncoated Superfer 800	0.55
NiCrAl coated SN 76	1.0
NiCrAl coated SN 750	0.8
NiCrAl coated SF 800	0.7

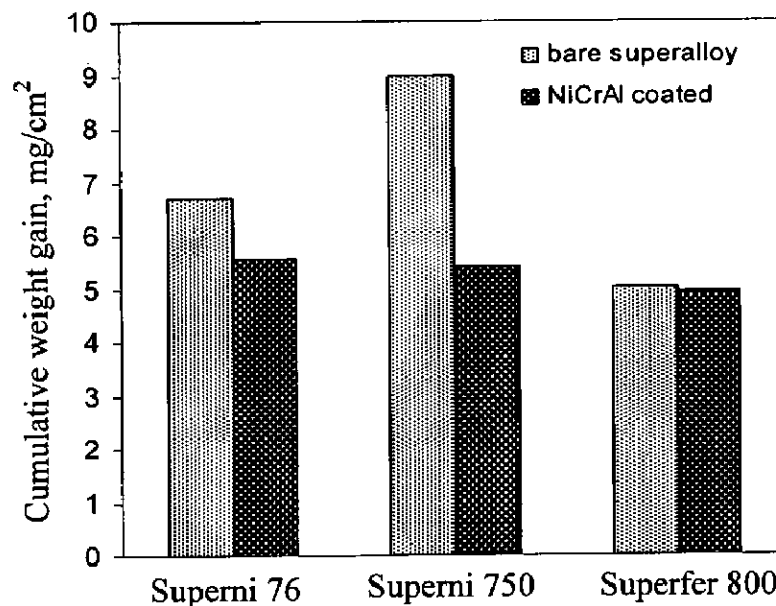


**Fig. 5.12:** Bar chart showing cumulative weight gain per unit area for bare and NiCrAl coated superalloys subjected to cyclic oxidation for 100 cycles at 900°C.

### 5.2.3.3 X-ray diffraction analysis

X-ray Diffractograms of bare superalloys subjected to cyclic oxidation after 100 hour exposure to air at 900°C is shown in Fig. 5.13. The oxide phases found were  $\text{Al}_2\text{O}_3$ ,  $\text{Cr}_2\text{O}_3$ , NiO,  $\text{Fe}_2\text{O}_3$  and  $\text{NiCr}_2\text{O}_4$ . X-ray diffractograms of NiCrAl coated superalloys oxidised in air at 900°C under cyclic conditions are shown in Fig. 5.14. No oxide phases detected in XRD results after oxidation studies at 900°C in all the three superalloy substrates. The major phases formed are AlNi, Ni, and Cr along with weak phases of  $\text{Al}_2\text{O}_3$ .

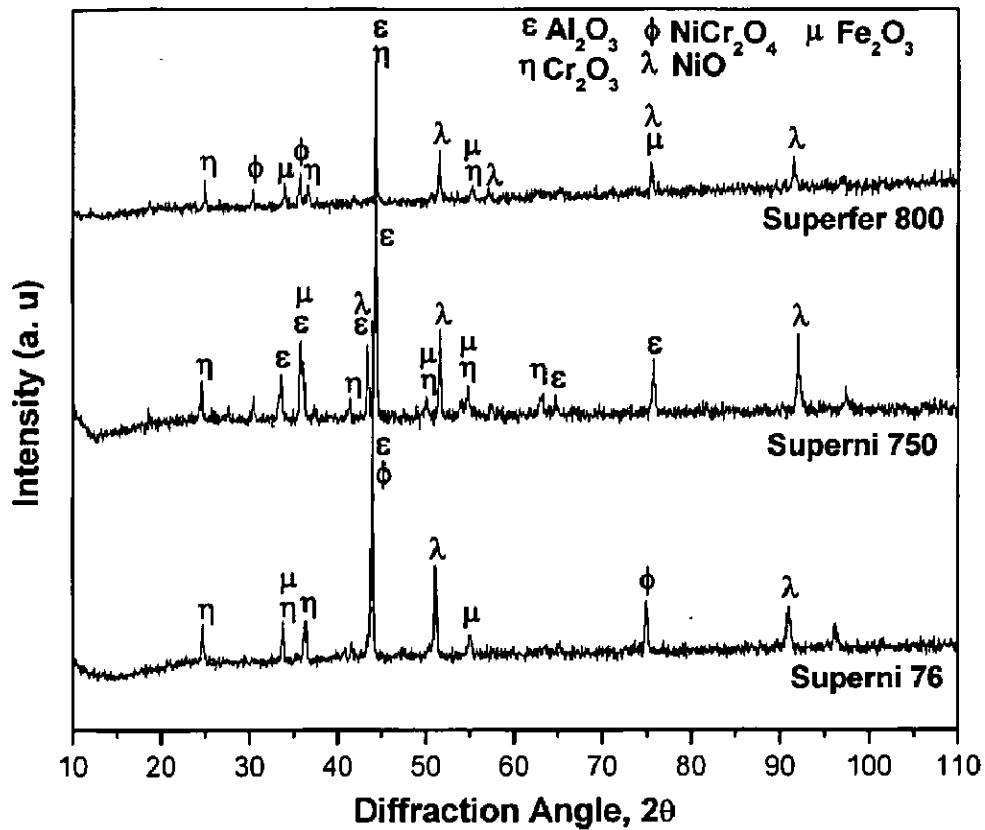


**Fig.5.13:** X-Ray Diffractograms of bare superalloys subjected to cyclic oxidation after 100 hour exposure to air at 900°C.

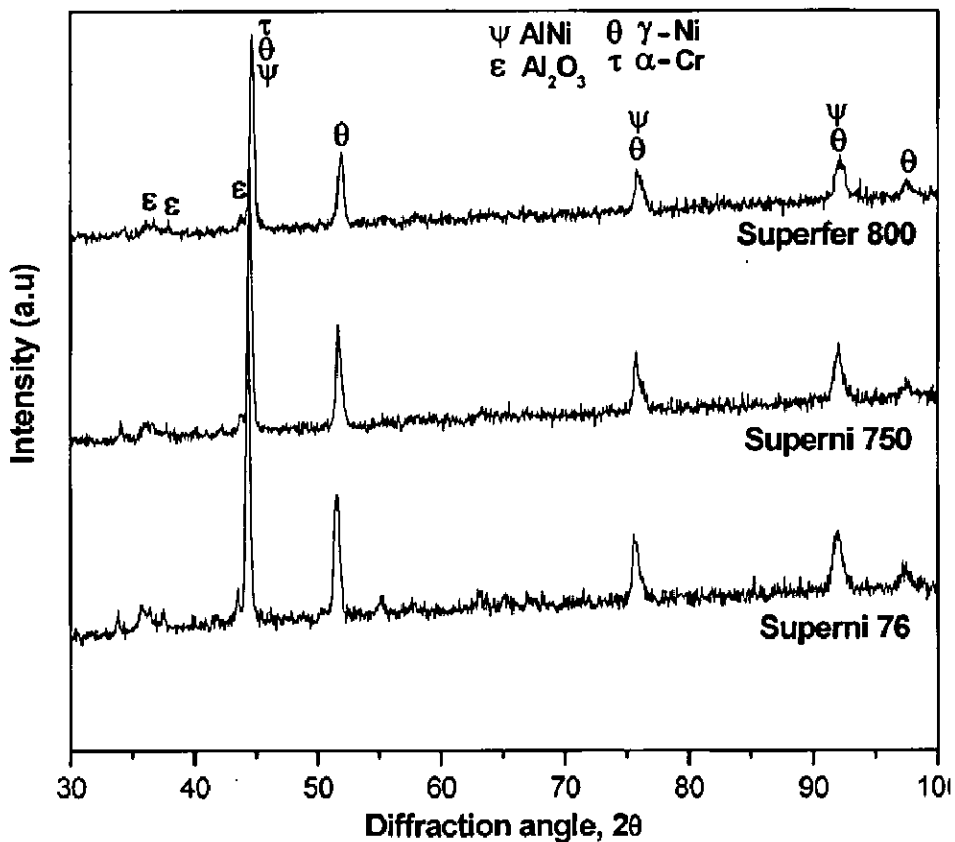


**Fig.5.14:** X-Ray Diffractograms of NiCrAl coated superalloys subjected to cyclic oxidation after 100 hour exposure to air at 900°C.

### **5.2.3.4 Diffusion of species and reaction products**

#### **5.2.3.4.1 Surface scale analysis**

The SEM/EDAX micrographs of the surface morphology of the NiCrAl coatings oxidised at 900°C under cyclic conditions are shown in Fig.5.15. The oxide scale for the coated Superni 76 after oxidation studies indicated a dominance of NiO with Cr<sub>2</sub>O<sub>3</sub>. A small amount of oxides of Si, Mn, Fe and W are found in the oxide scale but Al<sub>2</sub>O<sub>3</sub> is found at the splat boundaries. In case of coated Superni 750, the scale is rich in Cr<sub>2</sub>O<sub>3</sub> along with the presence of NiO. Other oxides such as SiO<sub>2</sub>, MnO, and Fe<sub>2</sub>O<sub>3</sub> are found on the surface of samples. Al<sub>2</sub>O<sub>3</sub> is present in the splat boundary area as noticed for Superni 76. The oxide scale in case of coated Superfer 800 alloy showed the presence of NiO, Cr<sub>2</sub>O<sub>3</sub> and Al<sub>2</sub>O<sub>3</sub> in the region of splat boundaries. Other oxides formed on the surface are SiO<sub>2</sub>, MnO, and Fe<sub>2</sub>O<sub>3</sub>.

#### **5.2.3.4.2 Cross sectional scale analysis**

The EDAX analysis at the selected points of interest across the cross section of the NiCrAl coated Superni 76, Superni 750, and Superfer 800 oxidised in air at 900°C after 100 cycles is shown in Fig. 5.16. The scale is found to be adherent and continuous with the substrate. The EDS analysis of oxidised NiCrAl coated Superni 76 (Fig.5.16a) shows that oxygen is not present at point 1 which indicates that the substrate superalloy remained unaffected during the oxidation studies. The dark phase at the coating-substrate interface (point 2) is found to be rich with Al and O<sub>2</sub> is an inclusion of aluminum oxide. It is believed that the some alumina particles might be retained in the asperities during the grit blasting of the substrate prior to the deposition of the coatings and appeared in the interface as an oxide. The white phase (point 3) region is consisted of Ni-rich splats which are presumed to be unoxidised as oxygen is found to be absent at this point. The presence of oxide stringers (point 4) indicates the possible in-flight oxidation of the coating powder during deposition over the substrate superalloys. The presence of aluminum, chromium and nickel with oxygen at the splat boundaries (point 5) in the upper part of the scale indicates the formation of oxides during the initial period of exposure wherein the oxidizing species enter into the coating through open pores and along the splat boundaries. The weight percent of chromium

and oxygen increases appreciably at the top scale (point 6) where Ni and Al decreases substantially which indicates that the top scale might be rich in oxides of chromium.

The EDAX analysis of oxidised NiCrAl coated Superni 750 (Fig.5.16b) indicates the presence of higher weight percent of Ni with small amount of chromium and aluminum and absence of oxygen at point 1 in the substrate. The white phase at point 2 indicates the unoxidised Ni-rich splat. There is a substantial decrease in the weight percent of Ni with appreciable increase in the weight percent of chromium and aluminum (point 3) indicating the formation of oxides at the splat boundary. The increase in aluminum and nickel with the presence of oxygen at point 4 indicates the formation of oxides of aluminum and nickel and as one moves further chromium content starts decreasing. The presence of Ni-rich splats at point 5 which are presumed to be unoxidised indicates the as sprayed nature of the scale. The top scale (point 6) consists of higher amount of nickel and small amount of chromium with oxygen which indicates that the top scale mainly consists of oxides of nickel and chromium.

In case of oxidised NiCrAl coated Superfer 800 (Fig. 5.16c), the EDAX analysis shows that the presence of Fe and Ni with small amount of chromium and aluminum and absence of oxygen at point 1. The dark phase (point 2) at the coating-substrate indicates the presence of aluminum oxide. The white phase at point 3 shows the Ni-rich splat with small amount of chromium and the absence of oxygen which indicates that the Ni rich splats are unoxidised. At point 5, there is a substantial decrease in the weight percent of Ni and Cr with appreciable increase in the weight percent of aluminum and oxygen, which indicates the presence of aluminum oxide at the inter splat boundaries. The top scale of the point 6 consists of higher amount of nickel and small amount of chromium and oxygen.

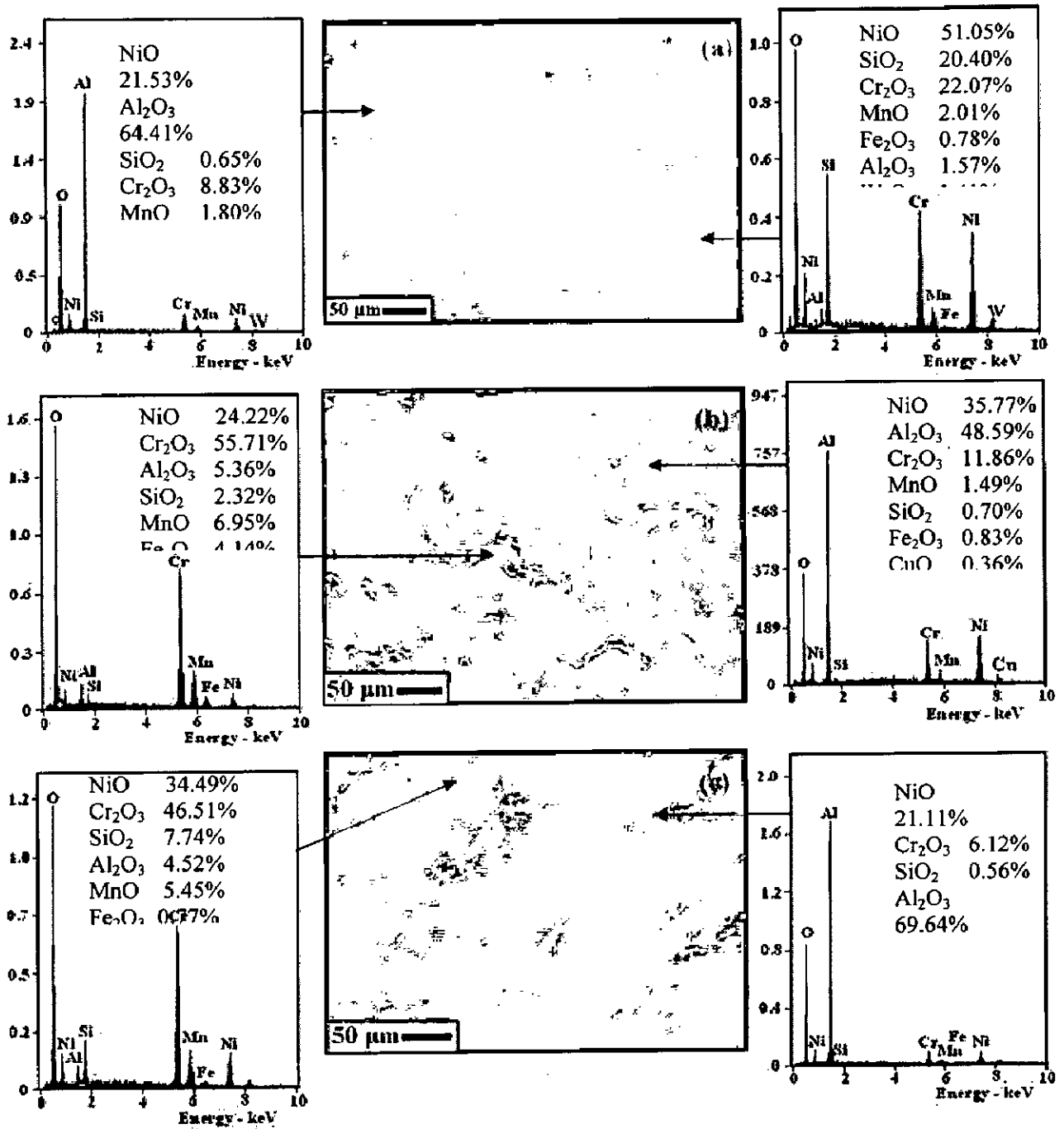


**Fig.5.15:** Surface scale morphology and EDAX analysis from different points on NiCrAl coated superalloys oxidized at 900 °C for 100 cycles of (a) Superni 76, (b) Superni 750 and (c) Superfer 800.

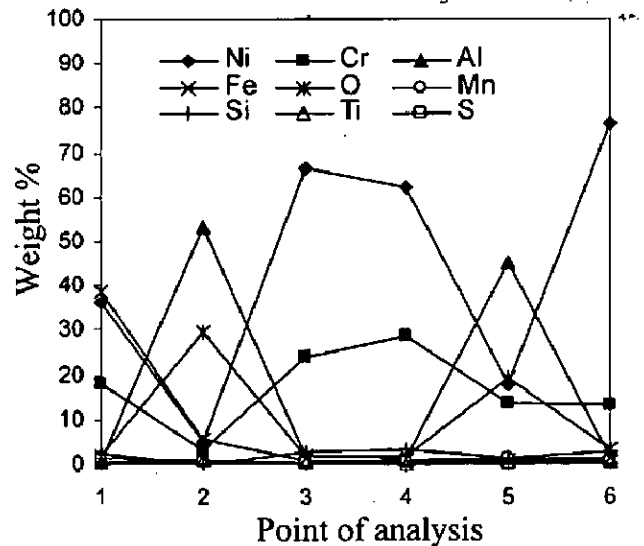
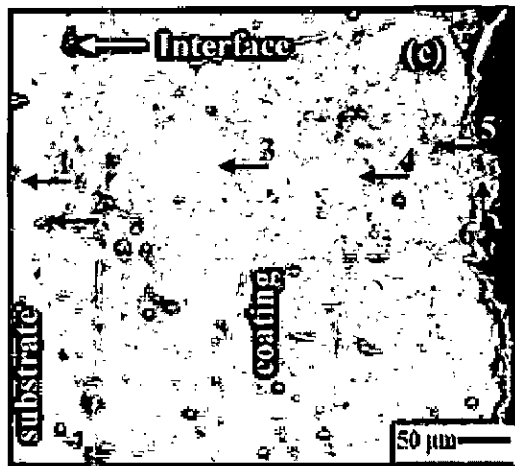
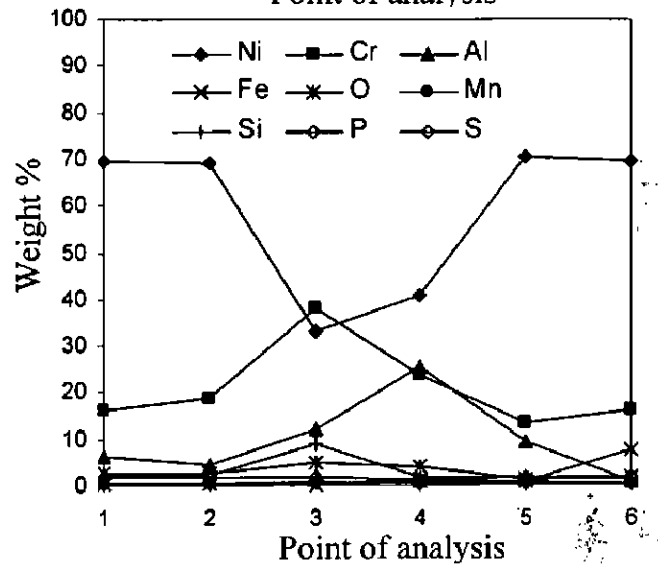
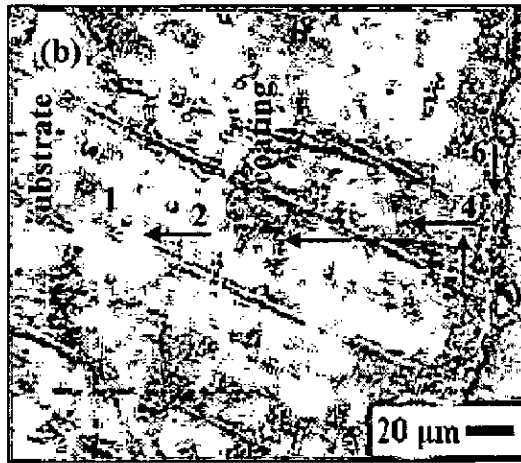
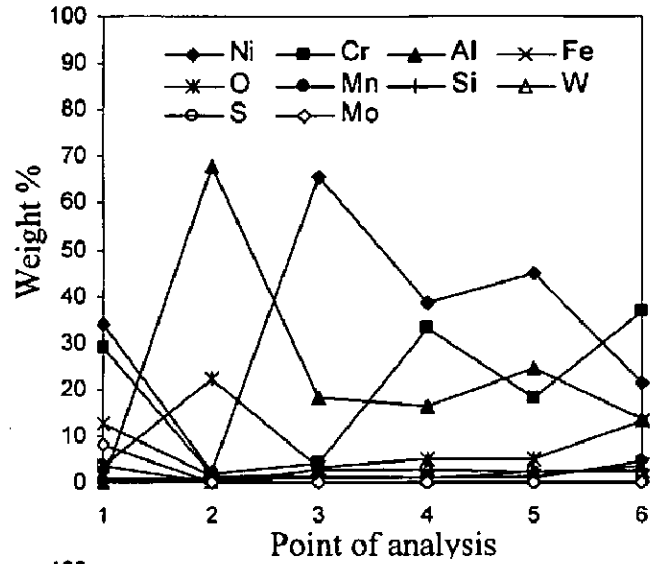
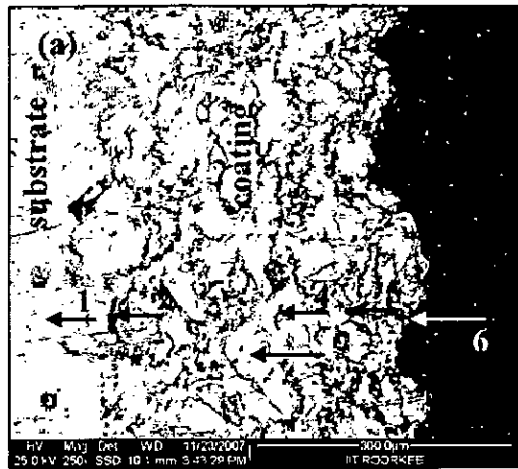


**Fig.5.16:** Oxide scale morphology and the variation in the elemental composition across the cross section of HVOF coated NiCrAl on (a) Superni 76; (b) Superni 750 and (c) Superfer 800 oxidised in air at 900°C after 100 cycles.

### 5.2.3.5 X-ray mapping analysis

The X-ray mapping analysis for Superni 76 (Fig.5.17 a) shows that the splats are rich in Ni and Cr, aluminum is present at the splat boundaries only. Wherever Ni is present, Al is absent. The dark phase at the coating substrate interface indicates the coexistence of aluminum and oxygen which is supplemented by cross sectional EDS analysis. Most of the Ni rich splats are unoxidised, whereas in the top scale region, Ni and Cr are partially oxidised. In the intersplat regions, oxygen, chromium and aluminum are coexisting indicating the formation of chromium oxide and aluminum oxide. Alloying elements like Fe, Mn and Si have diffused from the substrate into the coating along the splat boundaries and got oxidised. In case of coated Superni 750 (Fig.5.17 b), the splats are mainly consisting of Ni and Cr. Al is present at the intersplat regions. It is clearly noticed that wherever Ni and Cr are present, Al is absent. Oxygen is found to be dispersed in the coating. The dark phase at the coating substrate interface indicates the presence of Al and oxygen indicating the formation of aluminum oxide which is supported by cross sectional EDS analysis. Nickel and chromium are partially oxidised on the top surface. Small amount of Fe, Mn and Si have migrated from the substrate into the coating and oxidised at the intersplat boundaries.

X-ray mapping analysis in case of Superfer 800 (Fig.5.17 c) shows that the splats are rich in nickel and chromium. Most of the splats formed are unoxidised. Al is present along the intersplat boundaries and coexisting with oxygen. Ni, Cr and Al present in the top surface of the scale are oxidised. A small amount of iron has penetrated from the substrate into the coating surface indicating the diffusion behavior of the substrate. Elements like Mn and Si have migrated along the intersplat boundaries from the substrate into the coating and oxidised.



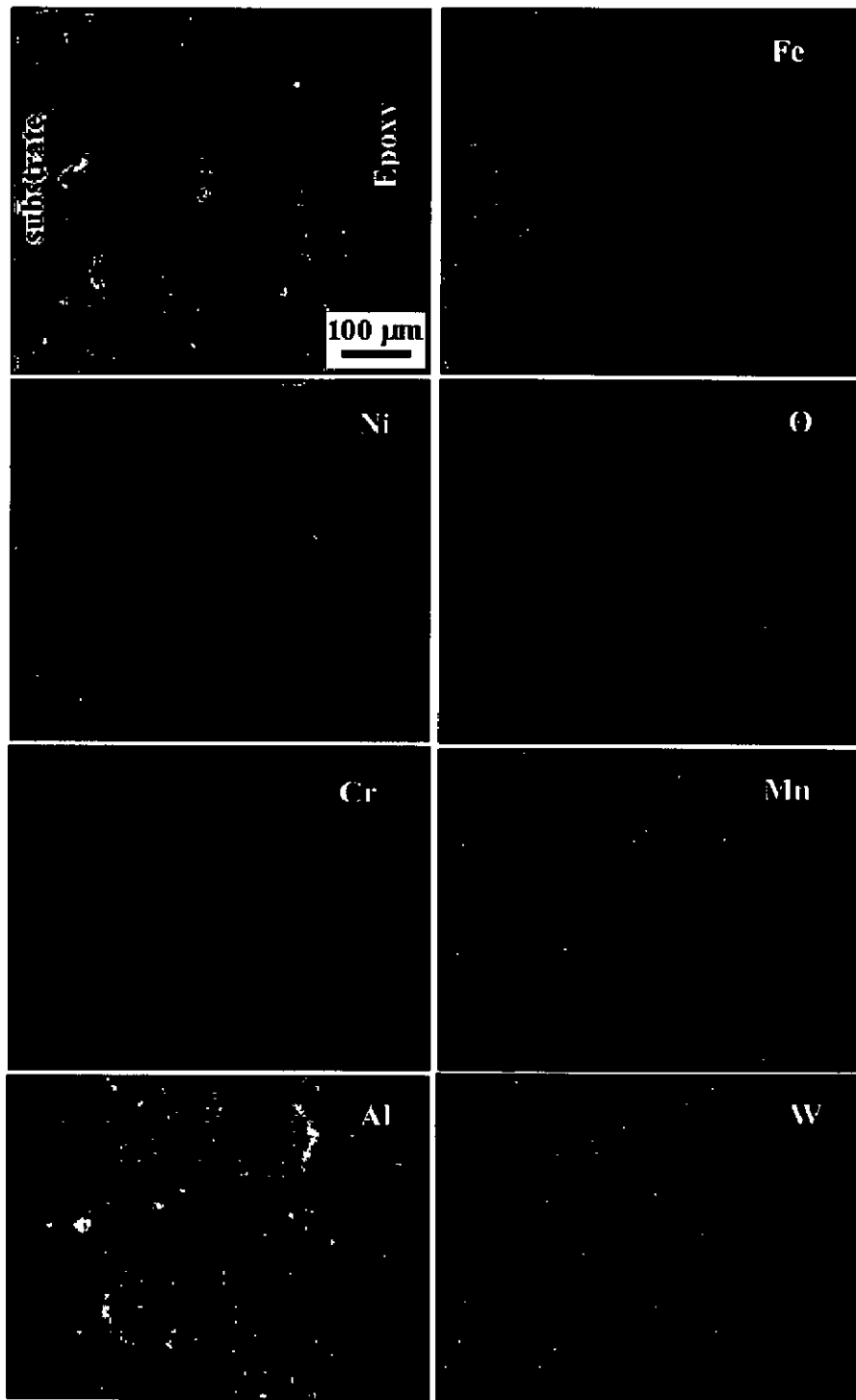


**Fig.5.17(a):** Composition image and X-ray mapping of the cross-section of the NiCrAl coated superalloy Superni 76 subjected to cyclic oxidation in air at 900°C after 100 cycles.

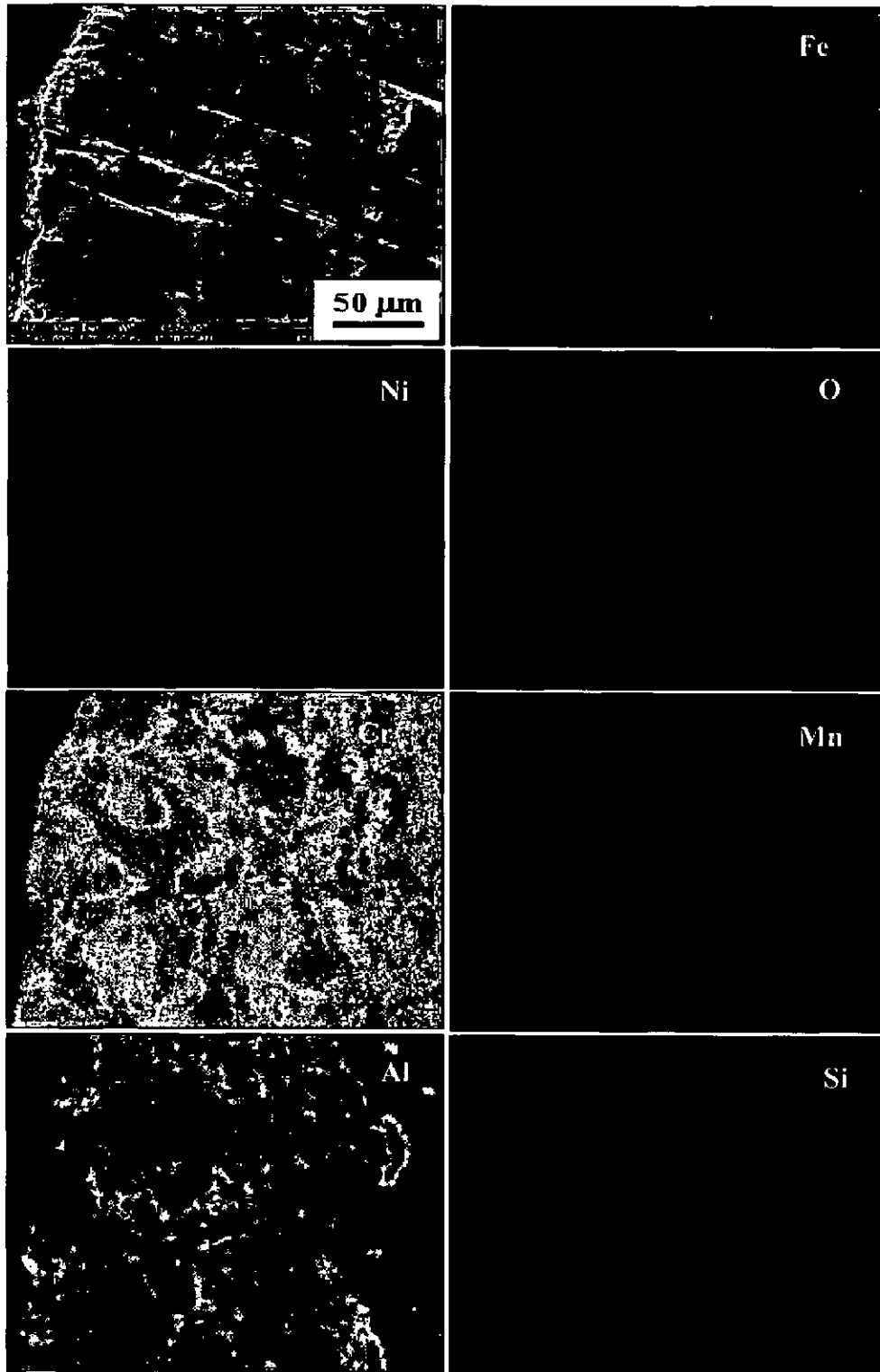


**Fig.5.17(b):** Composition image and X-ray mapping of the cross-section of the NiCrAl coated superalloy Superni 750 subjected to cyclic oxidation in air at 900°C after 100 cycles.

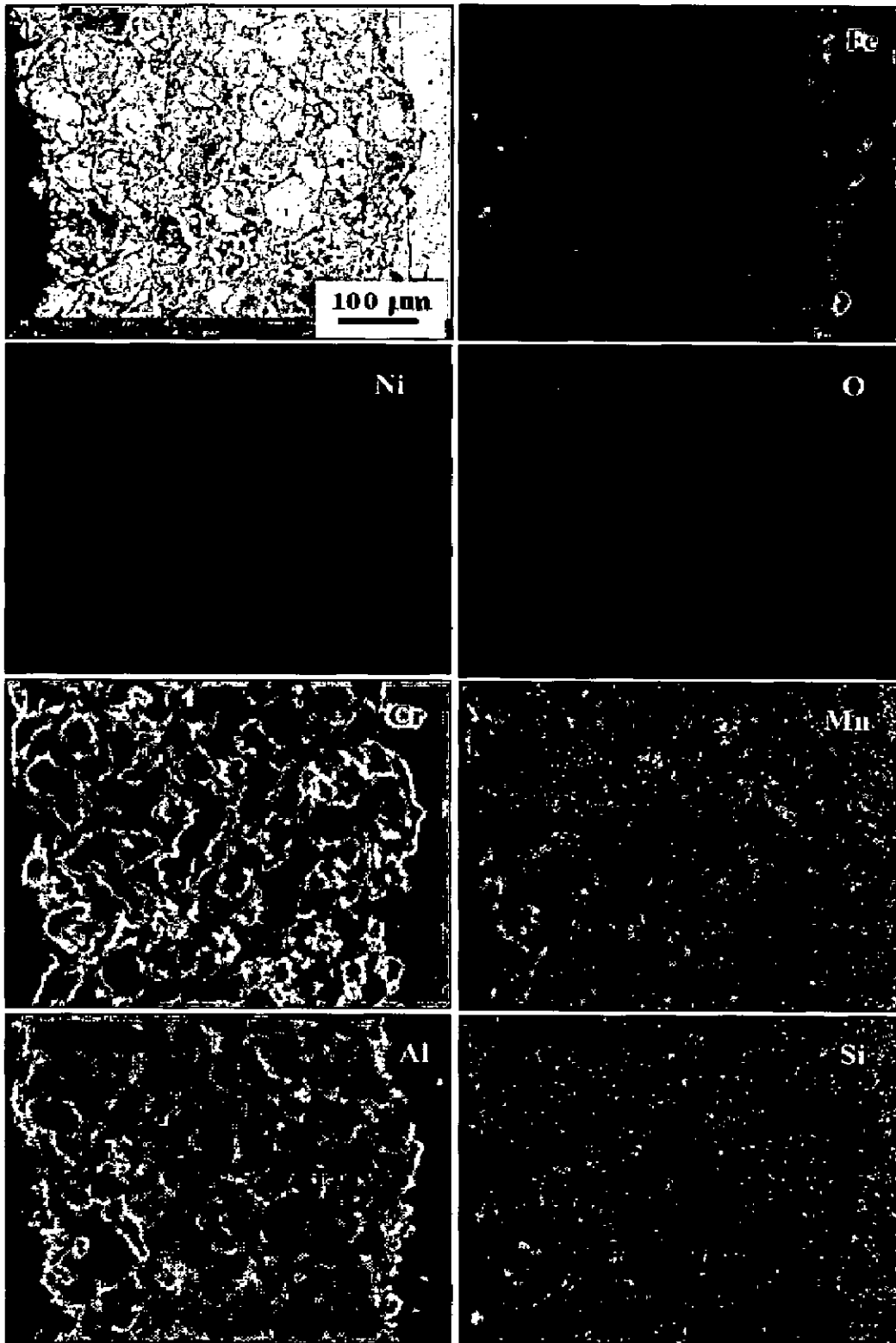


**Fig.5.17(c):** Composition image and X-ray mapping of the cross-section of the NiCrAl coated superalloy Superfer 800 subjected to cyclic oxidation in air at 900°C after 100 cycles.

## 5.2.4 Discussion

The surface of the oxidised specimens are observed carefully after each cycle during the experiment and it is noticed that in all the cases grey colour is seen (Fig. 5.9) on the surface after 100 cycles. The high temperature oxidation of HVOF sprayed NiCrAl coating on superalloys has followed a diffusion controlled mechanism at 900°C, which is noticed by the parabolic behavior of the weight gain per unit area versus number of cycles plots as shown in Fig.5.10. The results are similar to the findings of Harpreet Singh et.al, (2005B), Buta Singh et.al, (2005B) and Mahesh. et al, (2008B). The slight deviation from the parabolic rate behavior of cyclic oxidation of the coating may be attributed to the formation and rapid growth of inhomogeneous oxides during oxidation process as reported by Choi et al, (2002). The weight gain per unit area in case of NiCrAl coated Superni 76 has got reduced to 17% of the uncoated Superni 76. Further, in case of coated Superni 750 and Superfer 800 alloys, there is a reduction of 40% and 1% weight gain per unit area respectively.

The HVOF sprayed NiCrAl coatings on superalloys (Fig.5.6) indicated the typical splat surface morphology without cracks or sign of disintegration. Few partially melted powder particles have been noticed in the as sprayed coating. The coating in general consists of irregular shaped splats distributed uniformly throughout the coating with distinct splat boundaries which represents the typical HVOF spraying process. Pawlowski (1995) also reported that the thermal sprayed coating composed of lamellae formed from molten, partially molten and unmelted particles. Wigren and Tang (2001) have observed the microstructure of thermally sprayed coating consisting of multiphase matrix (often a mixture of hard, soft and amorphous), pores, oxides, delaminations, crack, grit residue and unmelted particles. According to their observation, the diffusion of oxidising species into the coating through the open pores found in the as sprayed coating is completely blocked by the formation of continuous oxide layer on the surface of the coating. The similar mechanism holds good for the protective nature of the oxide film which forms on the coated superalloys subjected to cyclic oxidation at 900°C in the present work.

XRD analysis (Fig.5.14) of NiCrAl coated superalloys oxidised in air at 900°C under cyclic conditions indicates the presence of AlNi, Ni, Cr as major phases along with weak phases of Al<sub>2</sub>O<sub>3</sub>. However, no oxide phases detected in XRD results after oxidation studies at

900°C in all the three coated superalloy substrates. Choi et al, (2002) have reported the similar phases in plasma sprayed NiCrAlY coatings oxidised at 1000°C. The EDAX analysis (Fig.5.15) of the surface of NiCrAl coated superalloys after oxidation at 900°C shows the formation of a thin oxide layer consisting of NiO, Cr<sub>2</sub>O<sub>3</sub>, Al<sub>2</sub>O<sub>3</sub> and other oxides formed on the surface are SiO<sub>2</sub>, MnO, and Fe<sub>2</sub>O<sub>3</sub> due to the diffusion of elements from the substrate into the coating. The presence of these oxides at the surface decrease the oxygen availability in the underlying alloy and favor the most thermodynamically stable oxide i.e. Cr<sub>2</sub>O<sub>3</sub> (Ul-Hamid, 2003).

The cross sectional EDAX analysis for coated Superni 76 (Fig.5.16a) shows the top scale consisting of oxides of Ni, Cr and Al. Formation of these oxides on the surface acts as diffusion barrier to the inward diffusion of oxidising species. For the coated Superni 750 (Fig.5.16b), it is observed that the scale formed is intact and the top surface consists of nickel oxide and chromium oxide. Nickel-rich splats are present in the subscale regions which are mostly unoxidised. In case of coated Superfer 800, (Fig. 5.16c), the protective oxides of nickel, chromium and aluminum have formed on the surface. All the NiCrAl coated superalloys show the absence of oxygen in the substrates after oxidation run. The oxide scales formed are adherent and intact with the surface during the course of the cyclic oxidation for 100 hours.

The X-ray mapping analysis of the oxidised NiCrAl coated superalloy samples indicates the presence of thin oxide layer on the top surface of the coating. Most of the coating is unoxidised in the subscale region which indicates the as sprayed nature of the coating. The oxides formed on the surface as well as at the intersplat boundaries clog the pores and prevent the penetration of the reacting species towards the substrate alloy, thereby suppresses the further oxidation of the alloys. On the basis of the results of XRD, FESEM/EDAX (surface and cross-section), and X-ray mapping analyses, schematic representation of the possible oxidation mode for the NiCrAl coated Superni 76 at 900°C after 100 cycles is shown in Fig. 5.18.

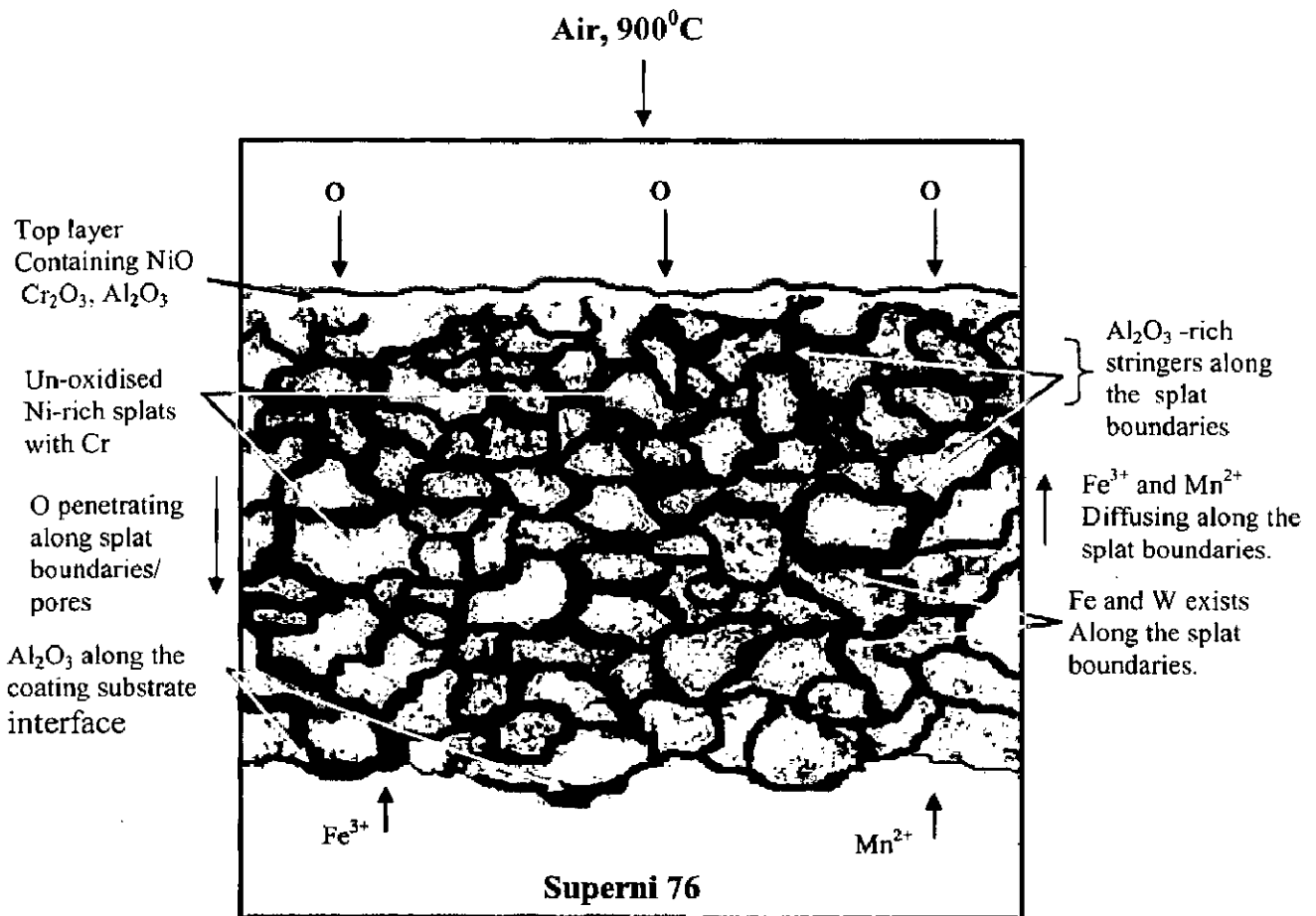


**Fig. 5.18:** Schematic diagram showing possible oxidation mode for the NiCrAl coated Superni 76 at 900 °C for 100 cycles.

### 5.2.5 Conclusions

The high temperature oxidation behavior of HVOF sprayed NiCrAl coatings on Superni 76, Superni 750 and Superfer 800 alloys in air at 900°C have been investigated and the following conclusions are made.

- (1) The NiCrAl deposited coatings on Ni- and Fe-based superalloys indicate dense and adherent with the substrates. The scale formed on the coated superalloys provided a better oxidation resistance at 900°C under cyclic conditions.
- (2) The NiCrAl coated superalloys when subjected to cyclic oxidation at 900°C developed a protective oxide scale mainly consisting of NiO, Cr<sub>2</sub>O<sub>3</sub> and Al<sub>2</sub>O<sub>3</sub> as confirmed by EDAX and X-ray mapping analysis.
- (3) The oxidation behavior of NiCrAl coated superalloys followed the parabolic rate law and the oxide scale formed is adherent to the coating and only microspalling is observed during the experiment.
- (4) NiCrAl coating on the superalloys has led to the reduction in weights of about 17% in Superni 76, whereas 40% and 1% for Superni 750 and Superfer 800 alloys, respectively.
- (5) It is evident from the X-ray mapping analysis that the oxide formed at the splat boundaries of oxidised HVOF sprayed NiCrAl coatings consisted of mainly oxides of aluminum and chromium.

## **5.3 HOT CORROSION STUDIES IN MOLTEN SALT ENVIRONMENT**

### **5.3.1 Introduction**

Hot corrosion was first recognized as a serious problem in the 1940's in connection with the degradation of fireside boiler tubes in coal-fired steam generating plants, internal combustion engines, gas turbines, fluidized bed combustion and industrial waste incinerators (Khanna and Jha, 1998). High temperature oxidation and hot corrosion are routinely encountered in superalloys, which operate in high temperature and corrosive environments in land-based turbine and aero gas turbine engines. An understanding of the long-term high temperature corrosion behaviors is extremely important. Gurrappa (2003) reported that number of components of gas turbine have undergone severe corrosion, causing failures to occur. Investigations confirmed that the failures were due to corrosion, in which there was extensive penetration of the materials by sulphur, oxygen, carbon etc, leading to the formation of metal sulphides, oxides, carbides etc, which in turn, reduced the mechanical properties of the components resulting in catastrophic failures. The use of high-strength nickel-base alloys for long periods of time at temperatures above about 871°C requires the application of protective coatings to prevent excessive surface degradation by oxidation and related processes (Goward and Boone, 1971). It is now generally accepted that hot corrosion of alloys used for gas-turbine blades is caused by a deposit of sulfate resulting from the ingestion of salts in the engine and sulfur from the combustion of fuel. In order to enhance the corrosion resistance of alloys, protective coatings, have been developed (Geng et al, 2002). High-temperature protective coatings used in gas turbine components must withstand extremely severe environmental conditions (Bettridge et al, 1986; Mevrel, 1989). The primary aim of the coating/surface treatment is the ability to produce a stable, slow-growing surface oxide providing a barrier between the coated alloy and the environment (Nicholls, 2000). In fact, coatings are playing a significant role in today's military and gas turbine engines to extend the life or enhance the performance of components. About 75% of all the components in jet engines are coated (Wolfe and Singh, 1998). Although protective surface treatments are widely used at low temperature, the use of these at elevated temperature is more recent. Current high temperature applications are limited largely to the aerospace industries. Enormous challenge exists to develop and to apply the coating technologies to other high temperature applications such as process industries and diesel engines (Stroosnijder et al, 1994).

Santoro and Barrett (1978) reported that the hot corrosion resistance of nickel-chromium-aluminum alloys was examined by cyclically oxidizing sodium sulfate-coated specimens in still air at 900°, 1000° and 1100°C. They found that the alloys melted in zirconia crucibles and without annealing had significantly greater hot corrosion resistance at 1100°C than alloys melted in alumina crucibles and annealed. Nesbitt and Heckel (1984) studied the degradation of a NiCrAlZr overlay coating on the Ni-Cr substrate by low-pressure plasma spray process. They reported that the coating failure occurred as a result of insufficient aluminum transport in the coating towards the oxide scale, which resulted in considerable porosity at the coating-substrate interface following cyclic oxidation at 1150°C. Khanna et al, (1993) during their study on the mechanism of the oxidation of NiCrAl-base alloys in air and air containing sulphur dioxide have reported that the material with a smaller grain size helps in faster diffusion of protective oxide-forming element through grain boundaries, thus causing faster development of the protective scale in the very initial stages of oxidation, while a larger grain size would take a longer time. They observed that the forged alloy formed protective scale very rapidly due to its smaller grain size and prevented direct reaction of SO<sub>2</sub> with the alloy constituents, whereas in the cast alloy due to a delay in the formation of the protective layer in the initial stages of oxidation due to larger grain size, the direct reaction with SO<sub>2</sub> resulted in severe attack. Barrett et al, (1981) studied the effect of zirconium on the cyclic oxidation of NiCrAl alloys at 1100° and 1200°C in static air. They noted that the depth of attack and the degree of oxide penetration strongly depended upon the zirconium content of the alloy. The zirconium free alloy had a massive penetration of aluminum oxide, small amount of zirconium led to minimum penetration and with increased zirconium content, the oxide penetration was less pronounced.

Due to the flexibility and cost effectiveness, HVOF has been widely adopted in many industries (Stokes and Looney, 2001) such as aerospace, automotive and other industries (Sidhu et al, 2006H). Therefore, in this study, HVOF has been selected to deposit the coatings on the Ni and Fe based superalloys.

The present research work has been focused to investigate the hot corrosion behaviour of HVOF-sprayed NiCrAl coatings on Ni- and Fe based superalloys in an aggressive environment of Na<sub>2</sub>SO<sub>4</sub>-60%V<sub>2</sub>O<sub>5</sub> molten salt at 900°C under cyclic conditions. The high temperature corrosion behavior of these thermal sprayed coatings on the chosen superalloy substrates is not reported in the literature so far. Long-term exposure of the coatings in the aggressive high temperature environment with characterization of the failure mechanisms is essential for estimating the protection capability of the coatings (Uusitalo et al, 2003). The



molten salt environment (40% Na<sub>2</sub>SO<sub>4</sub>-60%V<sub>2</sub>O<sub>5</sub>) is selected in the present investigation. The cyclic conditions are chosen to create a very aggressive environment for corrosion attack. Thermogravimetric (weight change with time) technique is used to approximate the kinetics of corrosion of coated and bare superalloy substrates. Techniques such as XRD, and SEM/EDAX and X-ray mapping analyses are used to characterise the corrosion products formed during hot corrosion studies under cyclic conditions.

### 5.3.2. Experimental Details

The substrate materials, coating formulation and the hot corrosion studies are explained in detail in section 3.4.3 and 3.5 of Chapter 3.

### 5.3.3 Results

#### 5.3.3.1 Corrosion Kinetics in molten salts

The weight gain/unit area results for bare and NiCrAl coated superalloys exposed to the Na<sub>2</sub>SO<sub>4</sub>-60% V<sub>2</sub>O<sub>5</sub> salt mixture at 900°C for 100 cycles are shown in Fig.5.19. The Ni-based uncoated superalloy Superni 750 (SN 750) shows the maximum weight gain, whereas bare Superfer 800 (SF 800) shows the minimum among all the superalloys. The weight decreases in case of SN 750 over the last 20 cycles. The spalling and sputtering of the scale was observed in case of bare superalloys during the study. There is a visible deviation from parabolic behavior in case of uncoated superalloys during the course of the experiment.

Among the NiCrAl coated superalloys, Superni 750 has shown minimum weight gain, whereas Superni 76 has shown maximum weight gain, which is around 3 times than that for Superni 750. In Fig. 5.20, (mass gain/area)<sup>2</sup> versus number of cycles data are plotted to show conformance with the parabolic rate law. Table 5.2 shows the calculated values of the parabolic rate constant  $k_p$  for the specimens studied. Fig. 5.21 shows the cumulative weight gain/unit area in all the three cases in the form of histogram.

#### 5.3.3.2 X-ray Diffraction Analysis (XRD)

The XRD phases revealed for the NiCrAl coated samples after hot corrosion studies for 100 cycles are shown in Fig. 5.22. The analysis showed that the coated Superni 76 specimen has NiCr<sub>2</sub>O<sub>4</sub>, NiO and Cr<sub>2</sub>O<sub>3</sub> phases in its scale along with relatively weak peaks of NiFe<sub>2</sub>O<sub>4</sub> phase. In the scale of coated Superni 750, NiCr<sub>2</sub>O<sub>4</sub>, Cr<sub>2</sub>O<sub>3</sub>, Al<sub>2</sub>O<sub>3</sub> and NiO were indicated as predominant phases alongwith NiFe<sub>2</sub>O<sub>4</sub> as a minor phase. Whereas, in the scale

of coated Superfer 800 (SF 800), the phases like NiO, NiCr<sub>2</sub>O<sub>4</sub>, Cr<sub>2</sub>O<sub>3</sub>, Fe<sub>2</sub>O<sub>3</sub> and Al<sub>2</sub>O<sub>3</sub> were observed from X-ray diffraction analysis.

### 5.3.3.3 Surface morphology of the Scales

SEM micrographs showing surface morphology of the NiCrAl coated superalloy specimens after cyclic hot corrosion for 100 cycles at 900°C are reported in Fig. 5.23. Compositions of various oxides are calculated by default with the help of EDAX software loaded on the machine (FESEM, FEI- Quanta 200F). The EDAX analysis of the scale for the coated Superni 76 specimen (Fig. 5.23a) has shown NiO, Cr<sub>2</sub>O<sub>3</sub> and Al<sub>2</sub>O<sub>3</sub> along with V<sub>2</sub>O<sub>5</sub>, SiO<sub>2</sub>, MnO phases. Some cracks are also observed in the surface scale and minor microspalling is seen during the course of the study. For coated Superni 750 (Fig. 5.23b), the point analysis shows higher percentages of NiO alongwith the presence of Cr<sub>2</sub>O<sub>3</sub>, Al<sub>2</sub>O<sub>3</sub>, and V<sub>2</sub>O<sub>5</sub>. The surface scale indicates that the scale formed is adherent with negligible cracks on the surface. The EDAX analysis of coated Superfer 800 (Fig. 5.23c) scale indicated presence of NiO, Cr<sub>2</sub>O<sub>3</sub>, Al<sub>2</sub>O<sub>3</sub> and V<sub>2</sub>O<sub>5</sub>. Minor cracks have developed on the surface with some amount of microspalling of the scale. Although these compositions correspond to point analysis, the data is useful to support the formation of various phases in the oxide scales.

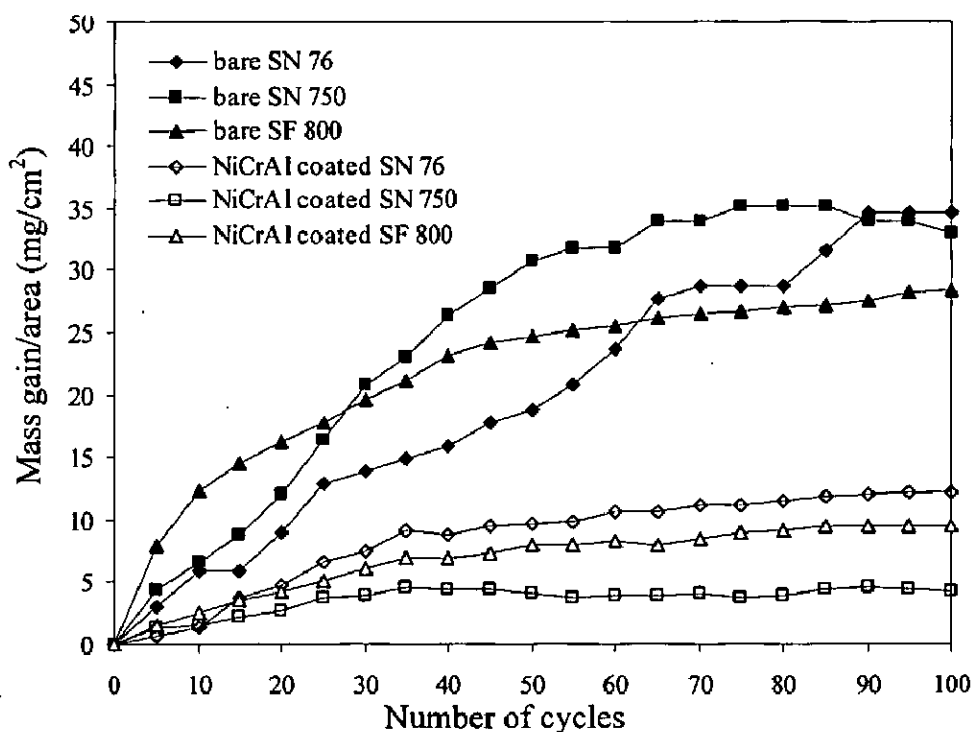


**Fig. 5.19:** Mass gain per area versus number of cycles of bare and NiCrAl coated superalloys after exposure to molten salt environment (Na<sub>2</sub>SO<sub>4</sub>-60%V<sub>2</sub>O<sub>5</sub>) at 900°C for 100 cycles.

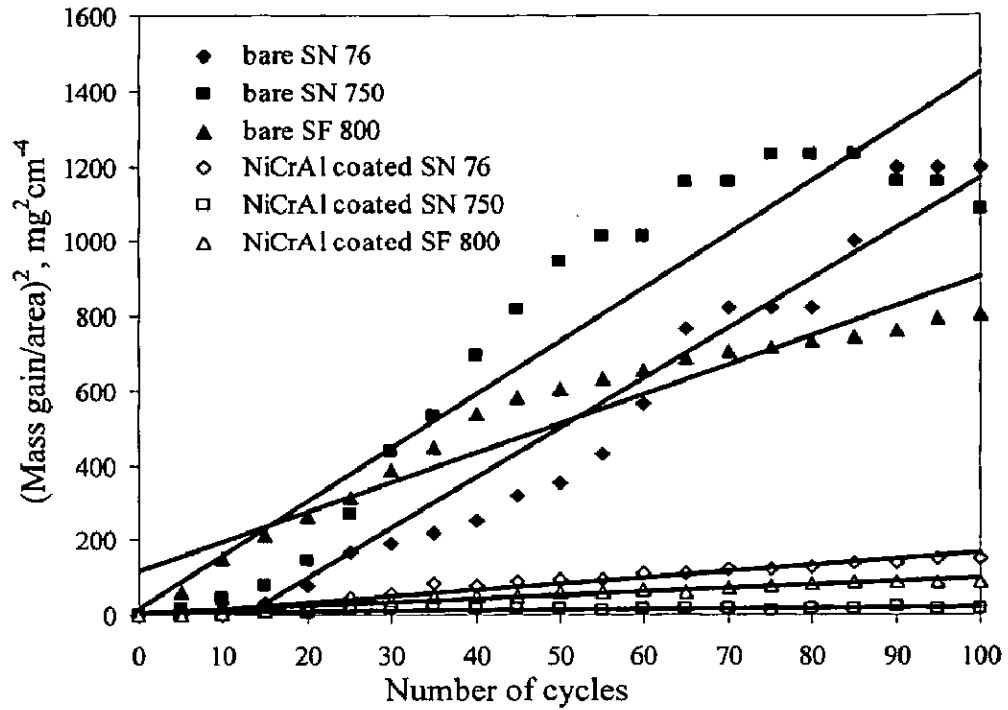


**Fig. 5.20:**  $(\text{Mass gain/area})^2$  vs. number of cycles for bare and NiCrAl coated superalloys subjected to molten salt environment ( $\text{Na}_2\text{SO}_4\text{-60\%V}_2\text{O}_5$ ) at  $900^\circ\text{C}$  for 100 cycles.

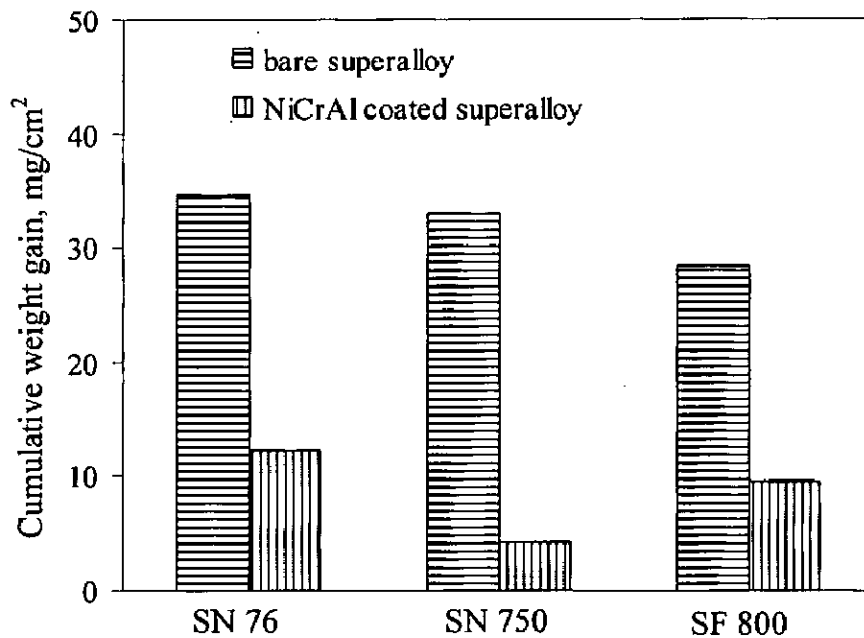


**Fig. 5.21:** Bar chart showing cumulative weight gain per unit area for bare and NiCrAl coated superalloys subjected to molten salt environment at  $900^\circ\text{C}$  for 100 cycles.

**Table 5.2:** Parabolic rate constant,  $k_p$  values of bare and NiCrAl coated by HVOF process after hot corrosion studies at 900°C.

Substrate	$k_p$ values( $10^{-10} \text{ gm}^2\text{cm}^{-4}\text{s}^{-1}$ )
bare Superni 76	37.08
bare Superni 750	39.71
bare Superfer 800	22.36
NiCrAl coated Superni 76	4.56
NiCrAl coated Superni 750	0.42
NiCrAl coated Superfer 800	2.73

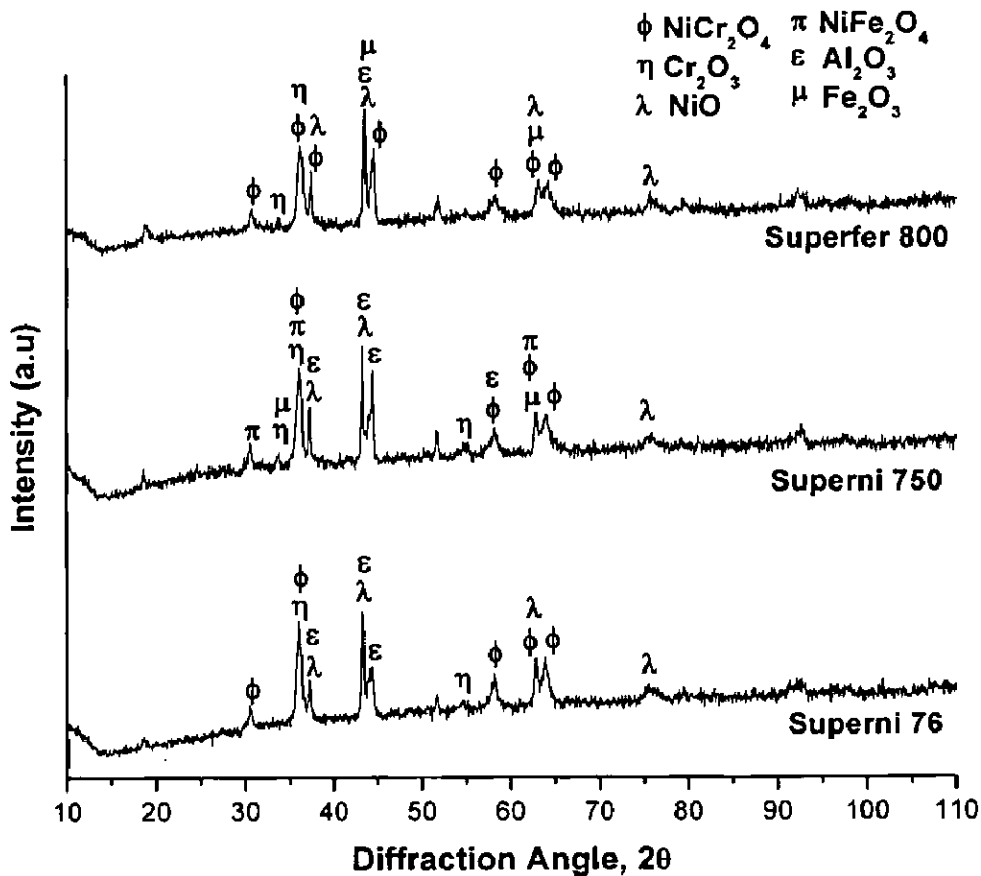


**Fig. 5.22:** X-Ray Diffraction pattern of NiCrAl coated superalloys after 100h exposure to molten salt ( $\text{Na}_2\text{SO}_4$ -60% $\text{V}_2\text{O}_5$ ) environment at 900°C.

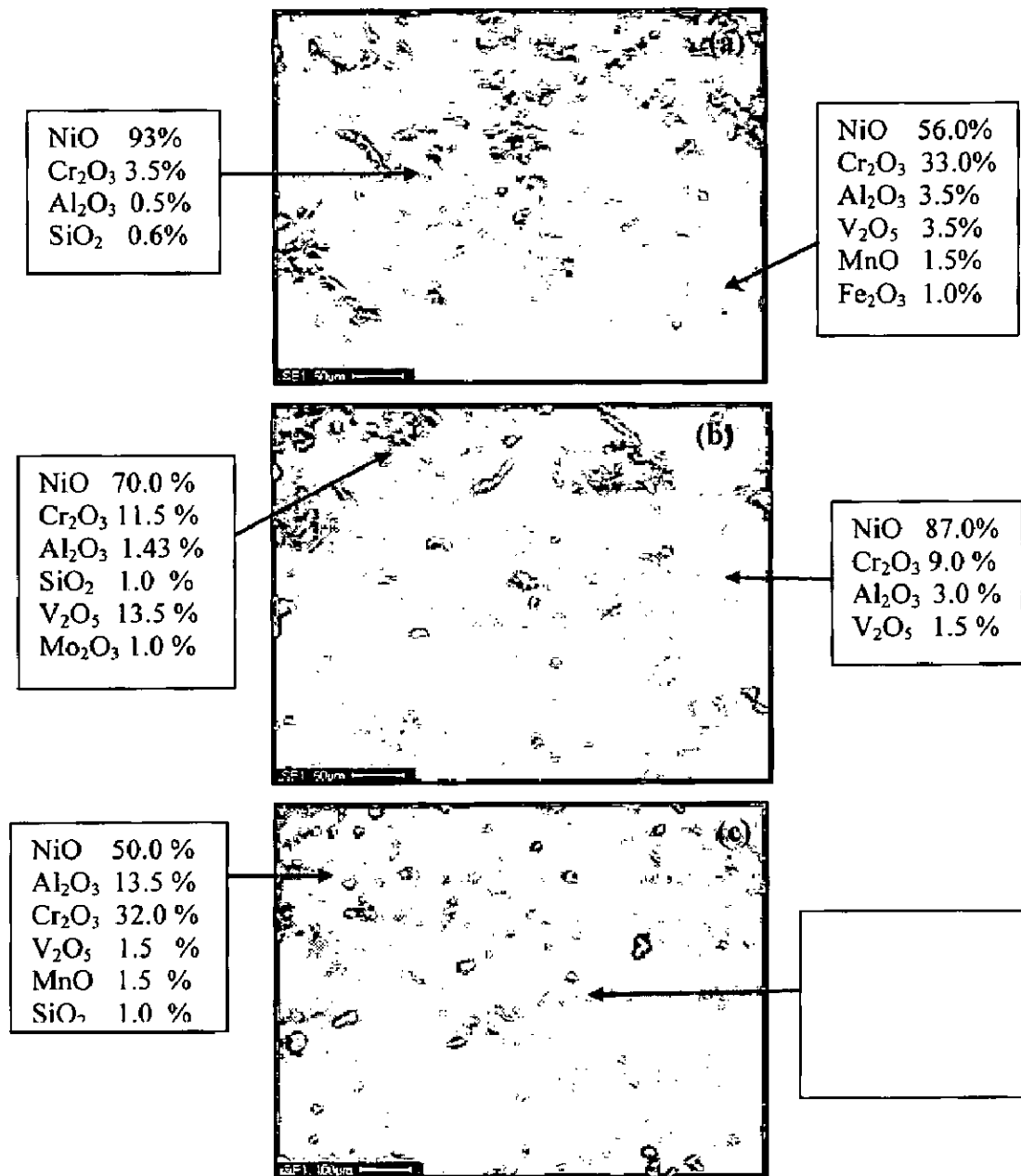


**Fig. 5.23:** Surface-scale morphology and EDAX patterns from different spots on NiCrAl coated (a) Superni 76, (b) Superni 750 and (c) Superfer 800 in molten salt ( $\text{Na}_2\text{SO}_4\text{-60}\%\text{V}_2\text{O}_5$ ) environment at 900°C after 100 cycles.

#### 5.3.3.4 Cross sectional EDAX analysis of the scale

The cross sectional oxide scale morphology of the corroded samples is shown in Fig. 5.24. The cross sectional EDAX analysis shows that the top scale (Point 6) of the coated Superni 76 (Fig. 5.24a) sample consists of mainly chromium oxide along with oxides of nickel and aluminum. The point 3 and 5 shows the presence of oxides of aluminum and chromium along the nickel rich splat boundaries. Oxygen has penetrated into the coating through the splat boundaries and open pores. Points 2 and 4 show the nickel rich splats are in unoxidised state. Point 1 in the substrate shows the absence of oxygen, thereby indicating the better protection in the given environment. Small amount of S and V are present in the top scale indicating the interaction with the molten salt.

In case of coated Superni 750 (Fig.5.24b), the top scale (Point 6) consists of oxides of nickel, chromium and aluminum. Cross sectional EDAX analysis shows that the contrast grey phase (Point 2, 3 and 5) mainly consists of chromium and aluminum. The existence of significant quantity of oxygen points out that this phase may be rich in aluminum and chromium oxide. The white phase (Point 4) indicates the unoxidised nickel rich splat in the coating. Point 1 in the substrate alloy shows absence of oxygen. It is noticed from the EDAX analysis that the top scale consists of small amount of vanadium.

In case of coated Superfer 800 (Fig.5.24c), the upper most scale (Point 6) consists of mainly chromium oxide along with oxides of nickel and aluminum. EDAX analysis at point 5 shows the presence of chromium and aluminum along the splat boundaries. The white phases (Points 3 and 4) are identified as unoxidised nickel rich splats spread uniformly over the coating. EDAX analysis at point 2 shows the presence of aluminum oxide along the interface. The substrate alloy (Point 1) nickel, iron and chromium with negligible amount of oxygen.

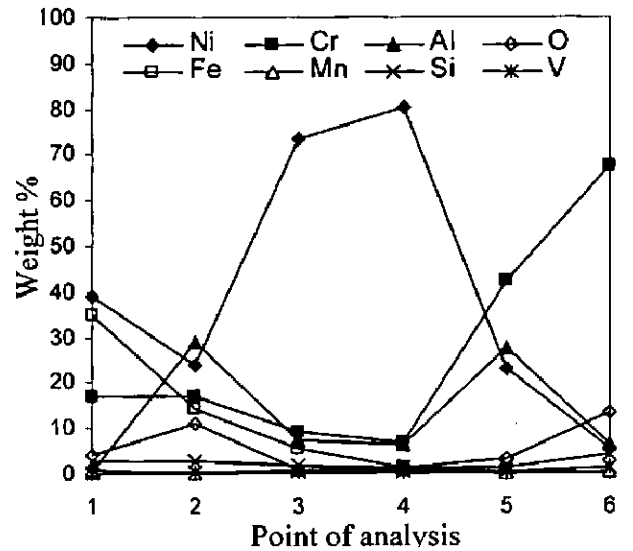
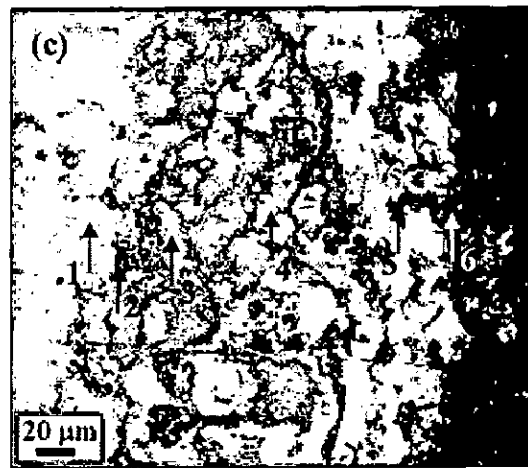
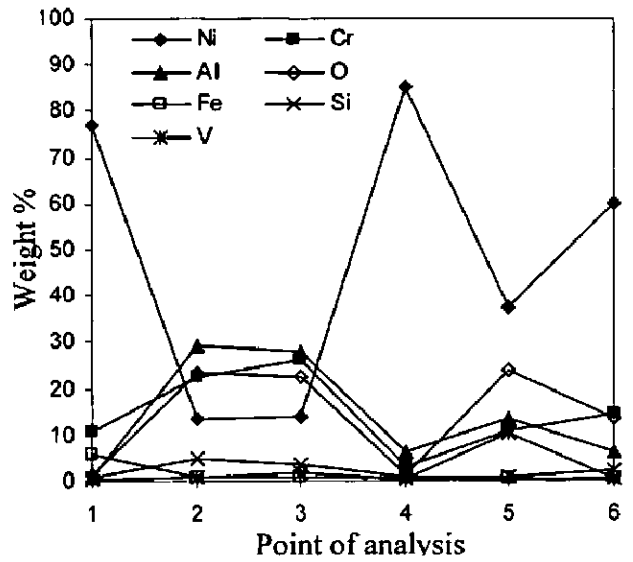
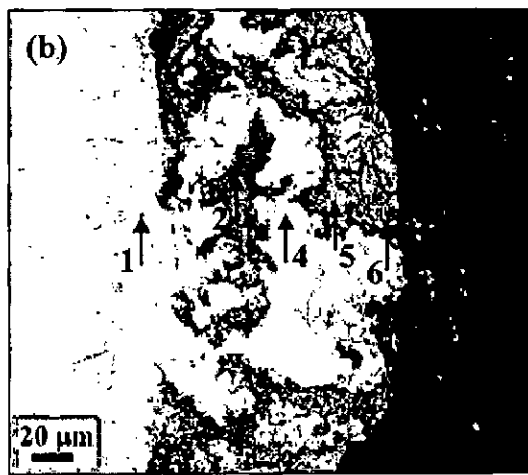
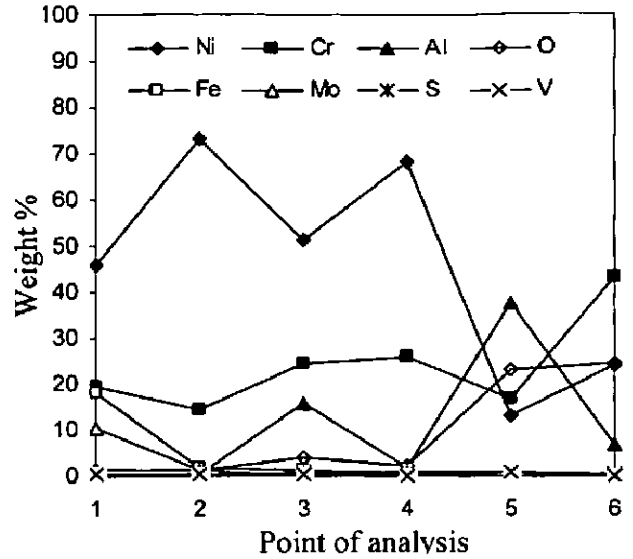
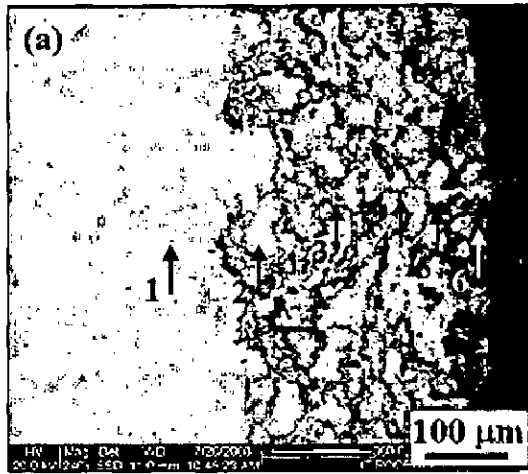


**Fig. 5.24:** Oxide scale morphology and variations of elemental composition across the cross-section of HVOF coated and hot corroded in  $\text{Na}_2\text{SO}_4$ -60% $\text{V}_2\text{O}_5$  environment at 900 °C for 100 cycles. (a) Superni 76; (b) Superni 750 and (c) Superfer 800.

### 5.3.3.5 X-ray mapping of different elements

SEI and elemental mapping for HVOF sprayed NiCrAl coatings on Superni 76, Superni 750 and Superfer 800 after cyclic oxidation in  $\text{Na}_2\text{SO}_4$ -60% $\text{V}_2\text{O}_5$  environment at 900°C are shown in Fig.5.25. The scale formed on the NiCrAl coated superalloys was dense and continuous. In case of NiCrAl coated Superni 76 (Fig.5.25a), the upper scale consists of nickel oxide and chromium oxide is present in the subscale region. Aluminum and chromium are present along the nickel splat boundaries with oxygen forming aluminum oxide and chromium oxide. A thick band of chromium oxide is present near the coating-substrate interface. Alloying elements such as Fe, S and Mn have diffused from the substrate into the coating along the intersplat regions as observed from the X-ray mapping.

The X-ray mapping for NiCrAl coated Superni 750 indicates that the top scale mainly consists of chromium oxide. Nickel oxide is present in the subscale region as shown in Fig. 5.25b. Aluminum and chromium coexists along the splat boundaries. The coating is dense and adherent and it has retained the as-sprayed structure. Oxygen might have diffused into the coating through the splat boundaries and through the pores during the initial period of exposure. A thick band of chromium and aluminum oxide is present near the coating-substrate interface. Some amount of Mn has diffused from the substrate into the coating and S from the environment.

The X-ray mapping for NiCrAl coated on Superfer 800 alloy is shown in Fig.5.25c. The top scale consists of oxides of nickel, chromium and aluminum. Nickel and chromium are existing in the splats. Aluminum and chromium are present at the splat boundaries along with oxygen forming oxides of aluminum and chromium oxide. A band of aluminum oxide is present at the coating substrate-interface, where nickel and chromium are absent. A small amount of Ti and Mn have migrated from the substrate into the coating as observed from the elemental mapping. Streaks of manganese oxide are present in the oxidized coating at the splat boundaries.



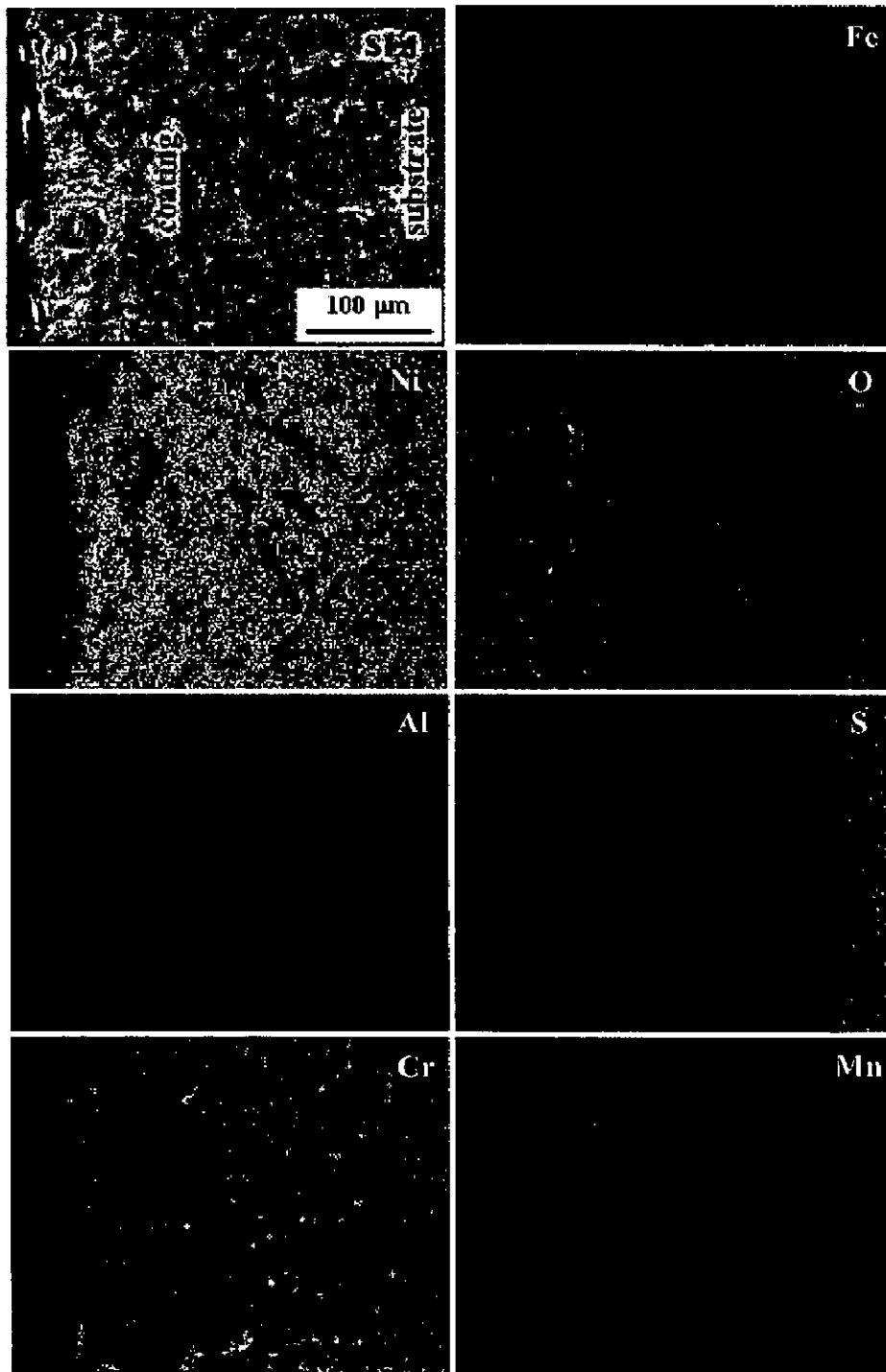


**Fig. 5.25(a):** Composition image (SEI) and X-ray mapping of the cross-section of Superni - 76 coated with NiCrAl subjected to cyclic oxidation in  $\text{Na}_2\text{SO}_4\text{-60\%V}_2\text{O}_5$  environment at  $900^\circ\text{C}$ .

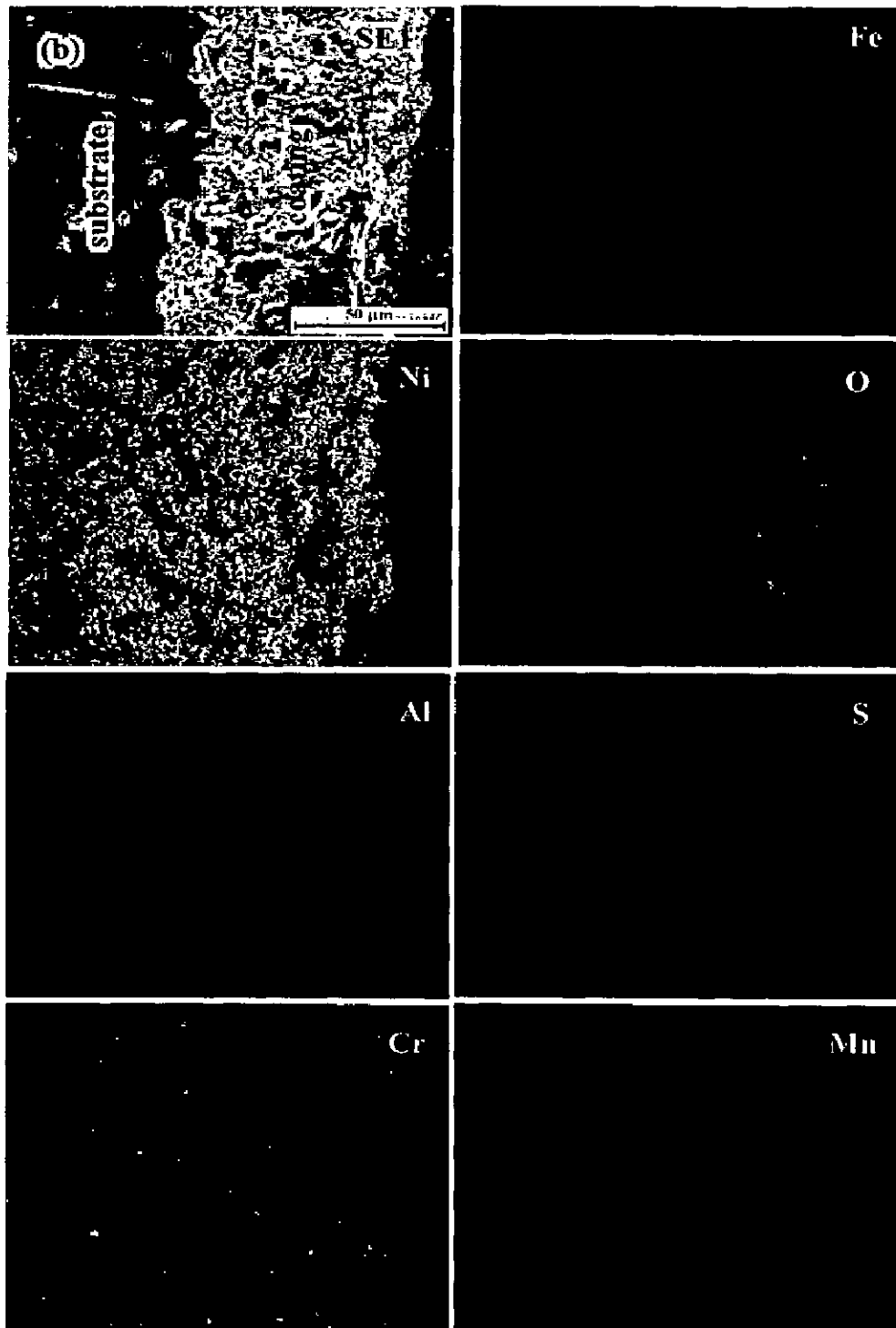


**Fig. 5.25(b):** Composition image (SEI) and X-ray mapping of the cross-section of Superni-750 coated with NiCrAl subjected to cyclic oxidation in  $\text{Na}_2\text{SO}_4$ -60% $\text{V}_2\text{O}_5$  environment at  $900^\circ\text{C}$ .

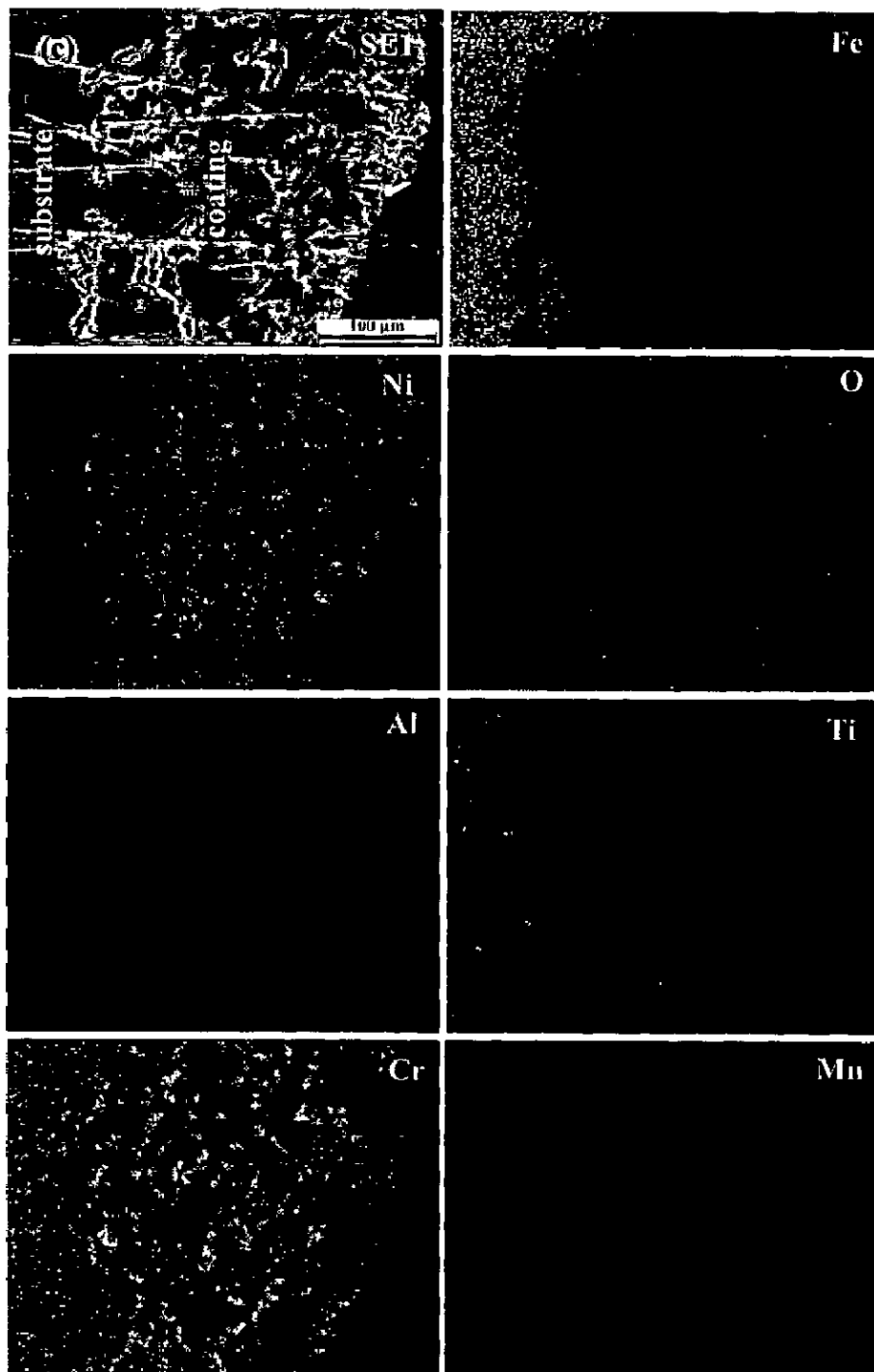


**Fig. 5.25(c):** Composition image (SEI) and X-ray mapping of the cross-section of Superfer-800 coated with NiCrAl subjected to cyclic oxidation in  $\text{Na}_2\text{SO}_4$ -60% $\text{V}_2\text{O}_5$  environment at 900°C

### 5.3.4 Discussion

The surface condition of the samples was observed carefully after each cycle. Finally a greenish color scale on the surface of the samples was observed after exposure to molten salt environment for 100 cycles. Microspalling of the scale in the form of fine powder was observed after 21 cycles. The superficial microspalling was reduced during the subsequent cycles of the study in coated Superni 76 alloy. In case of coated Superni 750, superficial microspalling of the scale was observed after 36, 53 and 59 cycle, whereas in case of Superfer 800, microspalling in the form of fine powder was seen after 10 cycles. Some cracks were also seen near the edges of the samples after exposure to molten salt environment at 900°C.

The weight gain for bare superalloys increases continuously, whereas for coated superalloys, it is relatively high during the initial stages of the hot corrosion study but subsequently the increase in weight gain is gradual (Fig. 5.19). A similar weight change trend had been observed by Tiwari (1997) for the bare superalloy substrates.

According to Hwang and Rapp (1989), sodium sulfate and vanadium oxide reacts as represented by equation (1)



These sodium vanadates are highly corrosive and can markedly increase the rate of oxidation of nickel base superalloys and they are more volatile and rapidly vaporize from the surface. Hence, an increase in the mass gain of bare superalloys occurs during the early stages of hot corrosion. The initial high oxidation rate of the coated specimens might be attributed to the rapid formation of oxides at the splat boundaries and within open pores due to the penetration of the oxidizing species.

The EDAX analysis at the cross section (Fig. 5.24) shows the formation of aluminum oxide, chromium oxide at the splat boundaries. The formation of oxides is further supported by the X-ray mapping analysis (Fig. 5.25). These oxides might have blocked the pores and splat boundaries and acts as a diffusion barrier to the inward diffusion of corroding species. This might be the reason for steady state oxidization with the progress of the exposure time. The rapid increase in the mass gain during the initial period was also reported by Sidhu et al, (2006E), Harpreet Singh et.al, (2005C), Tiwari and Prakash (1997) and Ul-Hamid (2003) during their studies on the hot corrosion of superalloy materials. The parabolic rate constant for the bare superalloys is higher than that of NiCrAl coated superalloys. It can be inferred

from the parabolic rate constant value that the NiCrAl coating has provided the necessary protection to the alloys in molten salt environment at 900°C.

The scale formed on the surface of the NiCrAl coated superalloys is compact and showed very little spalling. In case of Superni 76, the top surface scale mainly consists of NiO and Cr<sub>2</sub>O<sub>3</sub> as revealed by XRD and EDAX analysis (Fig. 5.22 and Fig. 5.23a) and confirmed by X-ray mapping (Fig. 5.25a) of different elements. In case of Superni 750, the surface scale is rich in NiO on the scale and beneath this scale, a thick band of Al<sub>2</sub>O<sub>3</sub> and Cr<sub>2</sub>O<sub>3</sub> is present along unoxidised nickel rich splats, which prevents/reduces the further diffusion of corrosive species into the coating. This is well supported by EDAX and XRD analysis and further confirmed by X-ray mapping analysis. The presence of spinel phases on the surface scale as indicated by XRD analysis may further enhance the corrosion resistance due to much lower diffusion coefficients of the cations and anions in the spinel phases than those in the parent oxide phases (Chatterjee et al, 2001). Formation of small amounts of oxides of iron and manganese as indicated by XRD/EDS/X-ray mapping analysis may be due to the diffusion from the substrate into the coating.

Cross sectional EDAX analysis of coated superalloys indicate that the oxide scale is intact with the coating and the top layer of the scale consists oxides of chromium, nickel and aluminum. The presence of oxides of Al and Cr along the splat boundaries might have acted as diffusion barrier by clogging the splat boundaries and open pores present in the coating to the inward diffusion of corrosive species towards the base alloy. Presence of small amount of oxides of vanadium in the top oxide layer (Fig. 5.24) is supported by EDAX analysis of the oxide scale formed on the surface (Fig. 5.23). Formation of oxides of aluminum and chromium along the nickel rich splat boundaries is further confirmed by X-ray mapping analysis. EDAX analysis indicated the presence of small amount of Fe<sub>2</sub>O<sub>3</sub> on the oxide scale which may be attributed to the diffusion of Fe from substrate to coating at high temperature, is further supported by XRD and X-ray mapping analyses. Small amount of manganese and titanium have diffused from the substrate into the coating at high temperature. On the basis of the results of XRD, FESEM/EDAX (surface and cross-section), and X-ray mapping analyses, schematic representation of the possible oxidation mode for the NiCrAl coated Superni 76 at 900°C after 100 cycles is shown in Fig. 5.26.

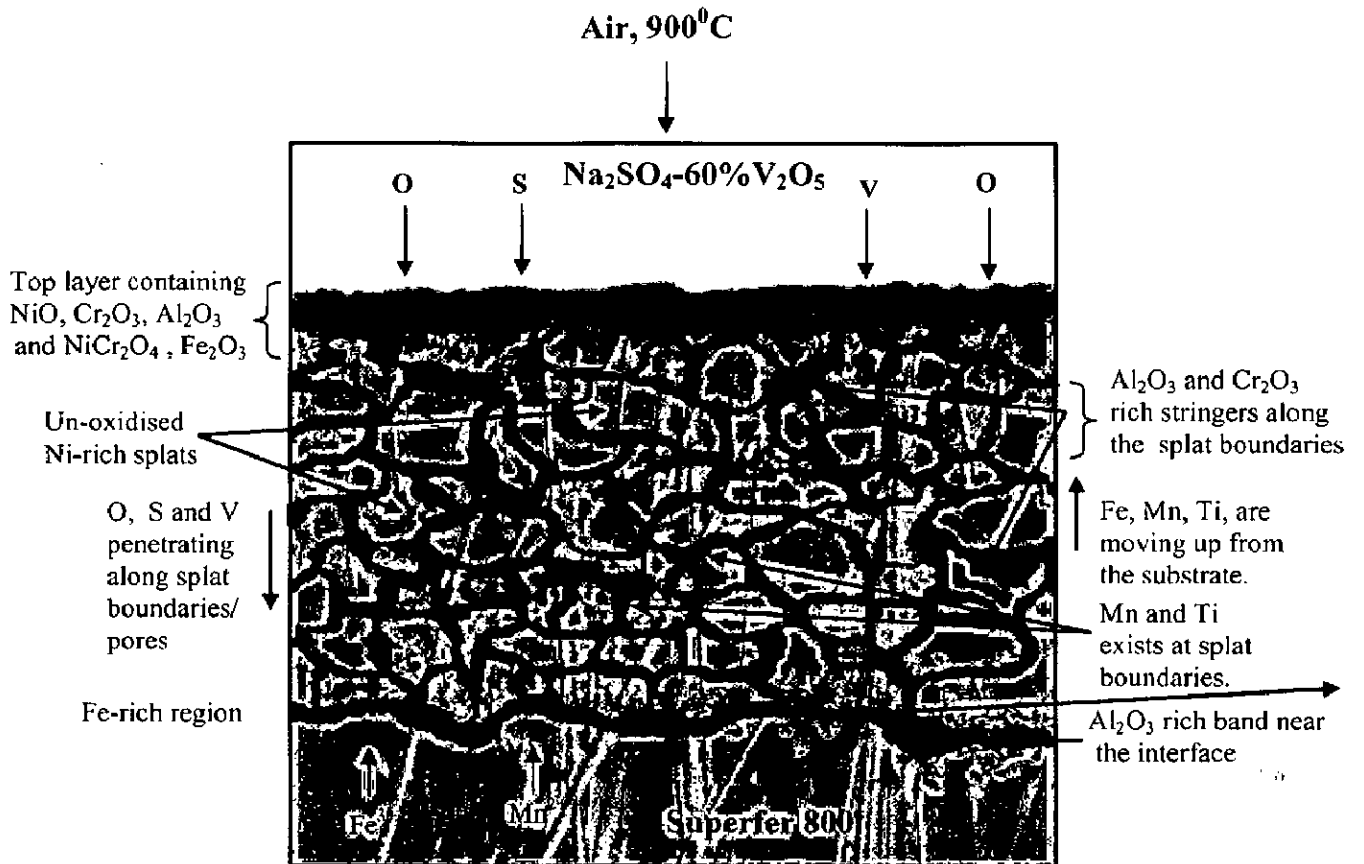


**Fig. 5.26:** Schematic diagram showing possible hot corrosion mode for the NiCrAl coated Superfer 800 exposed to Na<sub>2</sub>SO<sub>4</sub>-60%V<sub>2</sub>O<sub>5</sub> environment at 900 °C for 100 cycles.

### 5.3.5 Conclusions

1. HVOF sprayed NiCrAl coatings are effective in providing necessary resistance to molten salt ( $\text{Na}_2\text{SO}_4\text{-60\%V}_2\text{O}_5$ ) corrosion to the Ni- and Fe-based superalloys in the present investigation at  $900^\circ\text{C}$  under cyclic conditions for 100 hours.
2. In case of all three coated superalloys after cyclic exposure to given environment indicates a uniform and adherent scale with greenish color. There is a superficial microspalling from the surface and along the edges. However, in case of bare superalloys, intense spalling and sputtering of the scale is observed during the course of hot corrosion experiment and therefore, ultimate weight gain was high.
3. The NiCrAl coated superalloys under hot corrosion conditions followed the parabolic law and its parabolic rate constants are lower as compared with that of bare alloys under the same conditions there by indicating the protective nature of NiCrAl coating.
4. The weight gains in case of NiCrAl coated superalloys in the molten salt environment of 100 cycles followed the sequence

Superni 76 > Superfer 800 > Superni 750

Whereas, the weight gain of the bare alloys in the given environment at  $900^\circ\text{C}$  followed the sequence

Superni 76 > Superni 750 > Superfer 800

5. Maximum reduction in weight gain as compared to the exposed bare alloy is noticed for Superni 750 i.e. 88%, whereas, for Superni 76 and Superfer 800, it is nearly same i.e. around 66%.
6. In case of coated superalloys, the oxidation took place along the splat boundaries forming  $\text{Cr}_2\text{O}_3$  and  $\text{Al}_2\text{O}_3$  thereby stopping ingress of corrosive species towards the base alloy. Nickel in splats remains unoxidised even after exposure for 100 cycles at  $900^\circ\text{C}$ . Further, some spinels of  $\text{NiCr}_2\text{O}_4$  and  $\text{NiFe}_2\text{O}_4$  have also formed on the surface. A thick band of  $\text{Cr}_2\text{O}_3$  is observed in the case of coated Superni 750 along the coating-substrate interface, which might have contributed to the added protection of the substrate alloy resulting in the least weight gain among the three coated superalloys.
7. Some alloying elements have diffused from the substrate to the coating as observed in the elemental X-ray mapping analysis.

## Part II – RF Magnetron Sputtered coatings

### 5.4 HIGH TEMPERATURE OXIDATION STUDIES IN AIR

#### 5.4.1 Introduction

Magnetron sputter deposition is one of the most important techniques to produce thin films. Sputter deposition processes have been applied to produce overlay coatings for turbine components to improve oxidation resistance (Liu and Gao, 1998). Ni-Cr-Al ternary alloys are widely used for turbine blades, engine parts and many high temperature resistant components in energy production, aerospace and chemical industries. Since the 1970s, over-lay coatings of these alloys have been effectively used to provide oxidation and corrosion protection for the components exposed to hot gases. The effectiveness of these coatings very much depends on the presence of Al and/or Cr in the coatings to form a protective, self-healing scale of alumina or chromia (Liu et al, 1998). Microstructures have also been found to affect the high temperature corrosion resistance of many alloys. Merz (1979) and Basu and Yurek (1991) showed that a small grain size promoted the formation of  $\text{Cr}_2\text{O}_3$  protective scales on stainless steels.

Ni-Cr-Al alloys are the main components of certain coatings used on Ni-base superalloys, therefore, the study of the oxidation of Ni-Cr-Al alloys is beneficial to the understanding of oxide formation of the complex coated superalloys (Chen and Lou, 1999). Recently, nanocrystalline coatings prepared by the magnetron sputtering technique have attracted much attention. The nanocrystalline coatings (Ni-3Cr-20Al) on the substrates of the same materials such as Ni-based superalloys K38G, K17F and LDZ125 showed excellent oxidation resistance by developing a unitary layer of  $\text{Al}_2\text{O}_3$  (Chen and Lou, 2000). There is no reported literature on the high temperature oxidation studies of RF-Magnetron sputtered NiCrAl films on superalloys. Therefore, in the present work, the oxidation behaviour of NiCrAl thin film deposited by RF magnetron sputtering was studied at  $900^\circ\text{C}$ , which represents the average service temperature for turbine components as reported by Liu and Gao (1998). The oxide scale formed on the surface of the film was analysed by various techniques like XRD, AFM, FESEM/EDAX and X-ray mapping analysis.



## 5.4.2 Experimental Details

The details of the experimental procedure used for deposition of NiCrAl films by RF magnetron sputtering process are explained in detail in section 3.2.3.2 of Chapter 3. The image of the targets after RF magnetron sputtering process is shown in Fig. 5.27.

## 5.4.3 Results

### 5.4.3.1 Characterisation of the NiCrAl film

#### 5.4.3.1.1 XRD analysis

The X-ray diffraction pattern of NiCrAl films deposited on different superalloy substrates is shown in Fig.5.28. The main phases obtained in case of Superni 76 and Superni 750 was NiAl and Cr. In case of SF 800, Ni<sub>3</sub>Al phase was identified as the main phase in the as deposited condition. The crystallite size of the deposited film was measured from XRD analysis. The results indicated that the deposited film has a crystallite size of 17 nm for Superni 76, 21 nm for Superni 750 and 8 nm for Superfer 800.

#### 5.4.3.1.2 AFM analysis of the as deposited NiCrAl film

The surface topography of the films was studied using atomic force microscope (NT-MDT: NTEGRA Model) in semi-contact mode. Fig. 5.29 shows the AFM images of the films deposited on different superalloy substrates. The surface roughness of the deposited film was around 32 nm, 57 nm and 63 nm for Superni 76, Superni 750 and Superfer 800, respectively.

#### 5.4.3.1.3 FESEM/EDAX analysis of the as deposited film

The EDAX analysis of the as deposited NiCrAl film on Ni- and Fe-based superalloys is shown in Fig. 5.30. In case of Superni 76, the EDAX analysis indicates the presence of higher amount of Ni (30 wt %) along with chromium (15 wt%) and aluminum (5 wt %). Presence of iron (47 wt%) in the as deposited film indicates its deposition from the steel targets. In case of Superni 750 and Superfer 800 alloys, the EDAX analysis of the as deposited film shows that the amount of nickel reduced drastically in the deposited film and also the aluminum amount has reduced. The chromium amount remains almost same. It is very interesting to see that the amount of iron has increased to a considerable extent in the deposited film. The higher wt % of iron in the deposited film indicates the possibility of iron deposition from the steel target. It is noticed from the Fig. 5.27 that a small impression is formed on the targets indicating the deposition of iron from the target.

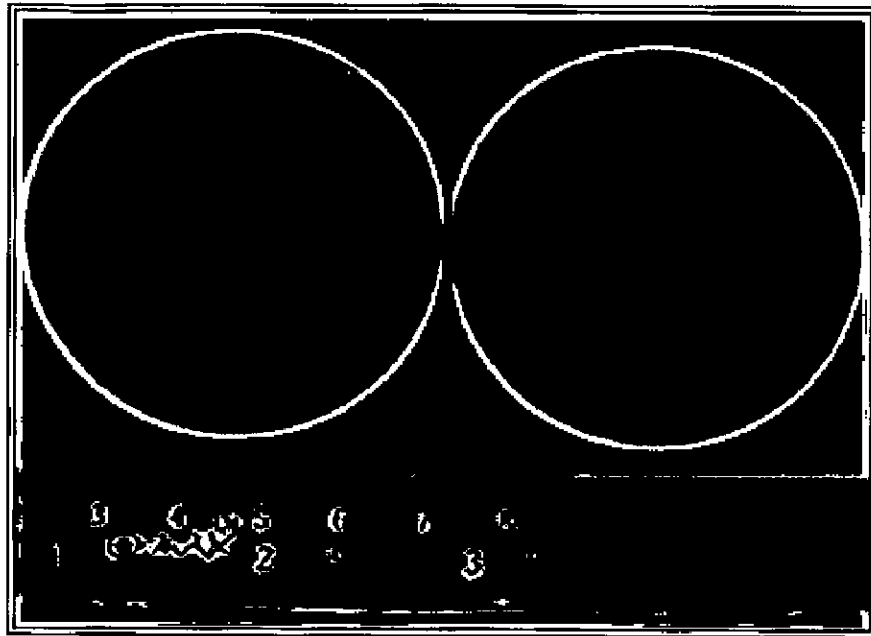


**Fig. 5.27:** The image of the targets after RF magnetron sputtering process.

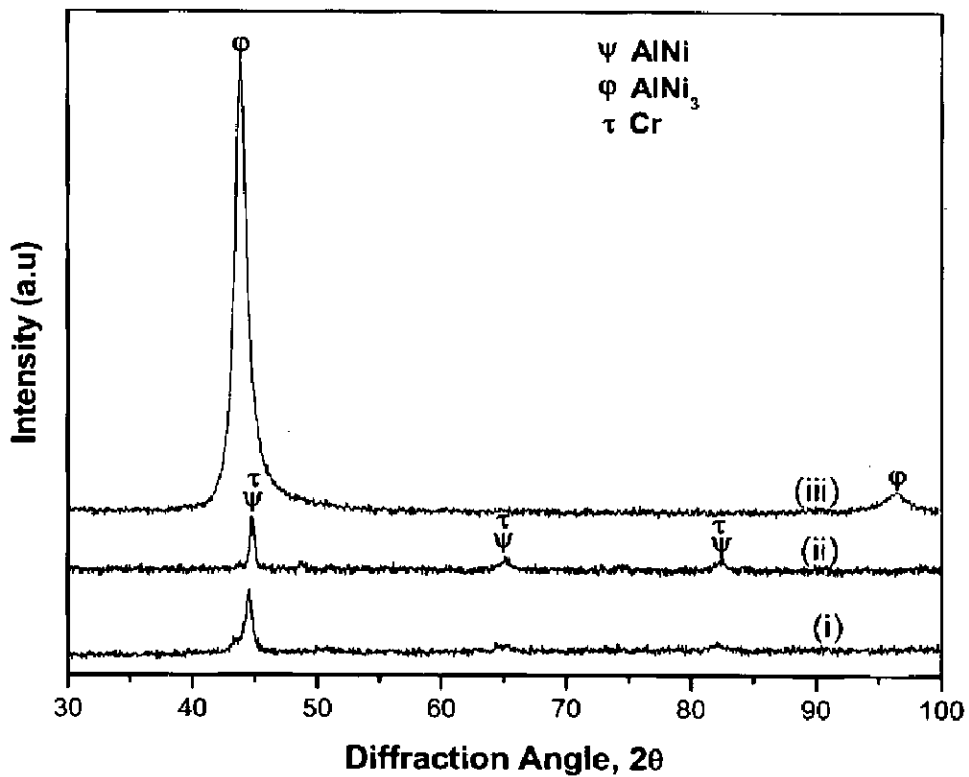


**Fig. 5.28:** XRD patterns indicating the NiCrAl film deposited on different superalloy substrates by RF magnetron sputtering.

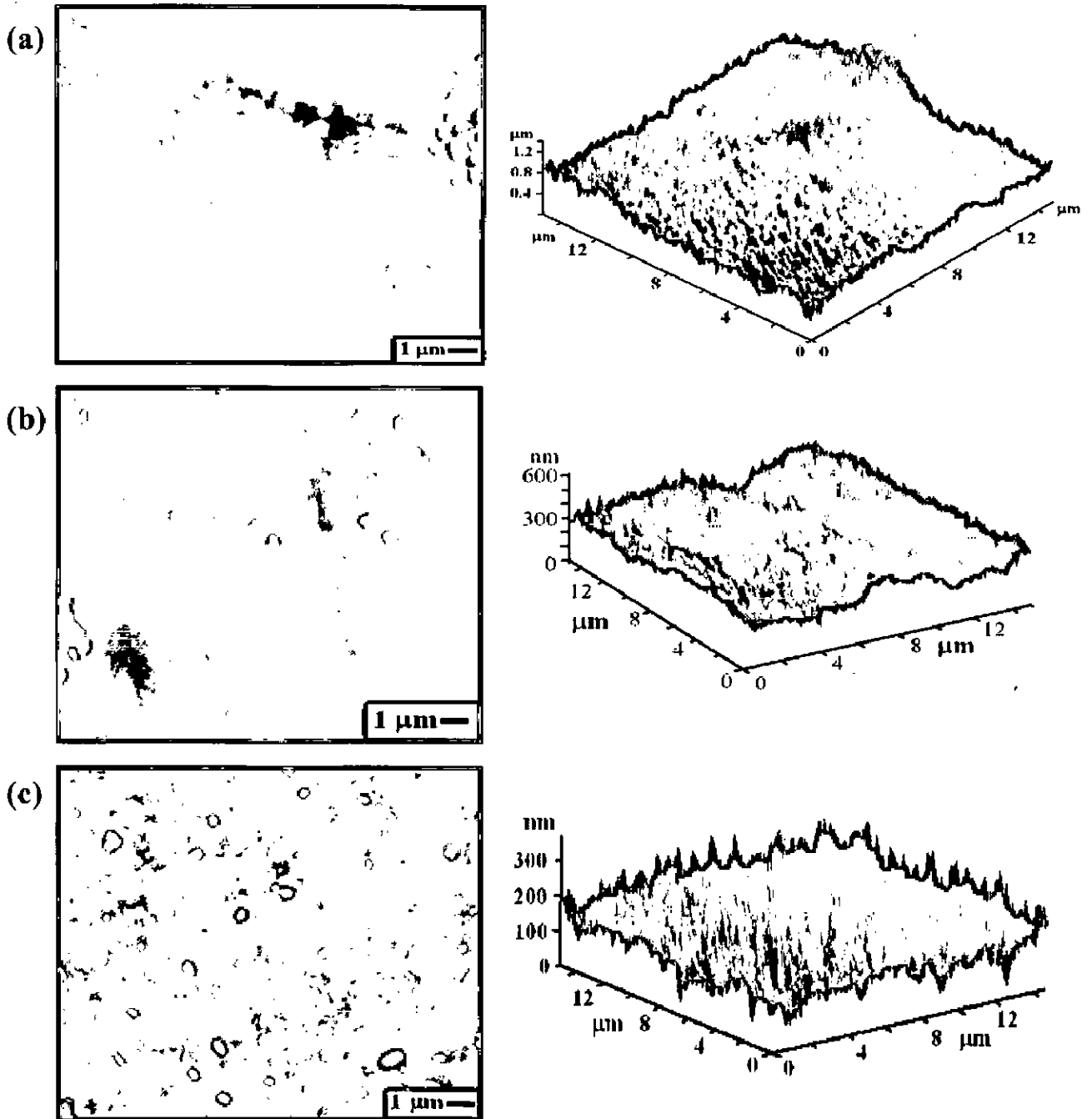


**Fig. 5.29:** AFM images of NiCrAl deposited film on (a) Superni 76, (b) Superni 750 and (c) Superfer 800 by RF magnetron sputtering.

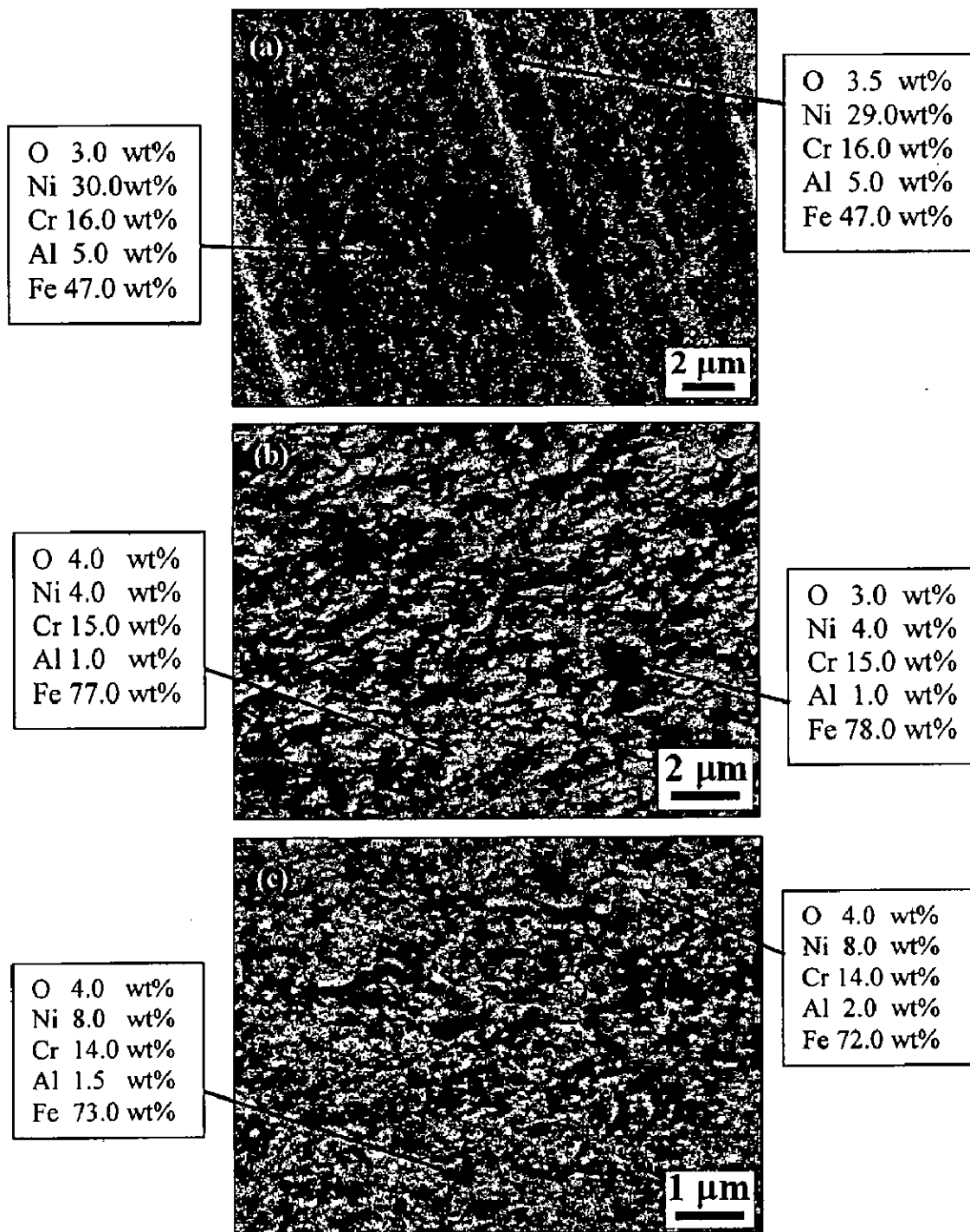


**Fig.5.30:** Surface morphology and EDAX analysis of NiCrAl film deposited on (a) Superni 76, (b) Superni 750 and (c) Superfer 800 alloy.

### 5.4.3.2 Oxidation Studies

#### 5.4.3.2.1 Visual Observations after oxidation studies

The oxidised NiCrAl deposited films on superalloy specimens after 100 cycles at 900°C are shown in Fig. 5.31. In case of NiCrAl coated Superni 76 alloy, Fig.5.31(i), the film spalled in the form of powder after the completion of 2<sup>nd</sup> cycle. The color of the surface became grey and the spalling stopped after completion of 4<sup>th</sup> cycle. The specimen turned dark grey in color with further exposure. In case of NiCrAl coated Superni 750 alloy Fig. 5.31(ii), the microspalling of the film started after the completion of 2<sup>nd</sup> cycle in the form of fine powder. The surface of the specimen showed grey colored patches with black background. The microspalling of the film stopped completely after the completion of 4<sup>th</sup> cycle. The surface of the specimen turned dark grey after the completion of 8<sup>th</sup> cycle. The NiCrAl coated Superfer 800 alloy, Fig. 5.31(iii), also showed a similar behaviour when exposed to high temperature in air.

#### 5.4.3.2.2 Cyclic oxidation studies at 900°C in air

The weight gain per unit area versus number of cycles plots for the bare and coated alloys is depicted in Fig.5.32. The weight gain in case of bare (uncoated) superalloys was high compared to NiCrAl deposited superalloys under the same conditions. The coated Superni 750 indicated minimum weight gain compared to coated Superni 76 and Superfer 800 alloys. During the initial period of exposure, little microspalling was observed and as the exposure time increased the spalling completely got arrested and an adherent scale formed on the surface of the coated specimens.

The square of weight gain per unit area versus number of cycles indicates that the NiCrAl coated specimens followed the parabolic rate law, whereas, uncoated specimens slightly deviated from the parabolic rate law as shown in Fig. 5.33. The parabolic rate constant  $k_p$  values for the NiCrAl coated Superni 76, Superni 750 and Superfer 800 are  $0.072 \times 10^{-10} \text{ g}^2 \text{ cm}^{-4} \text{ s}^{-1}$ ,  $0.022 \times 10^{-10} \text{ g}^2 \text{ cm}^{-4} \text{ s}^{-1}$  and  $0.13 \times 10^{-10} \text{ g}^2 \text{ cm}^{-4} \text{ s}^{-1}$ , respectively. The bar chart indicating the cumulative weight gain of uncoated and NiCrAl coated superalloys is shown in Fig. 5.34.

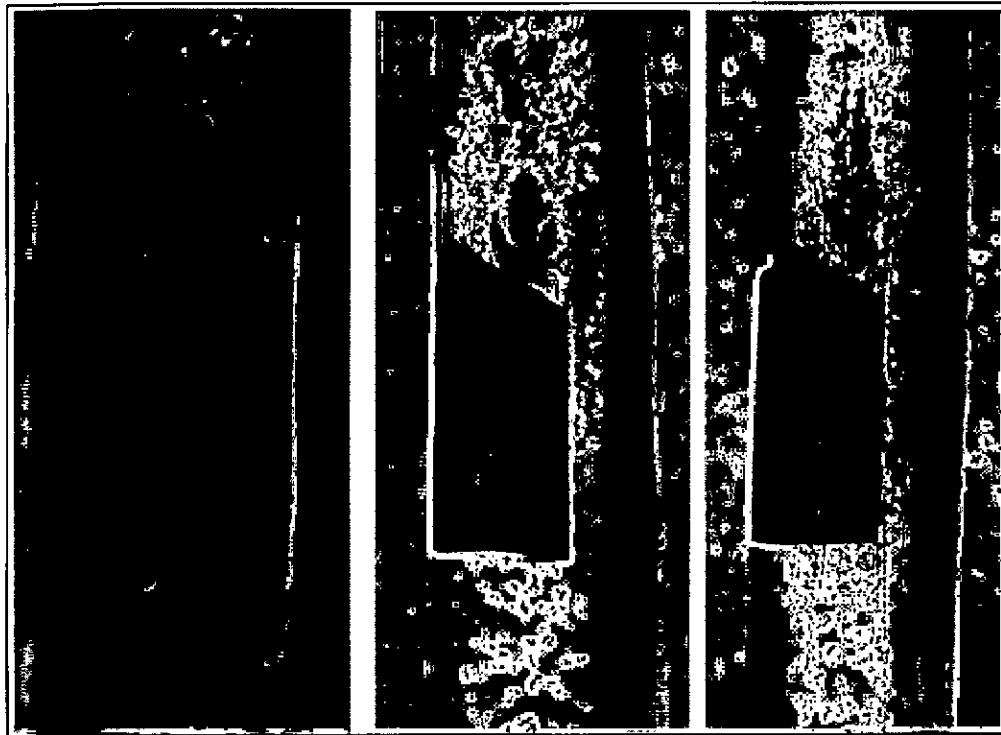


**Fig. 5.31:** Surface macrographs of NiCrAl deposited film on (i) Superni 76, (ii) Superni 750, (iii) Superfer 800 after 100 h exposure to air at 900°C indicating spalled scale powder.

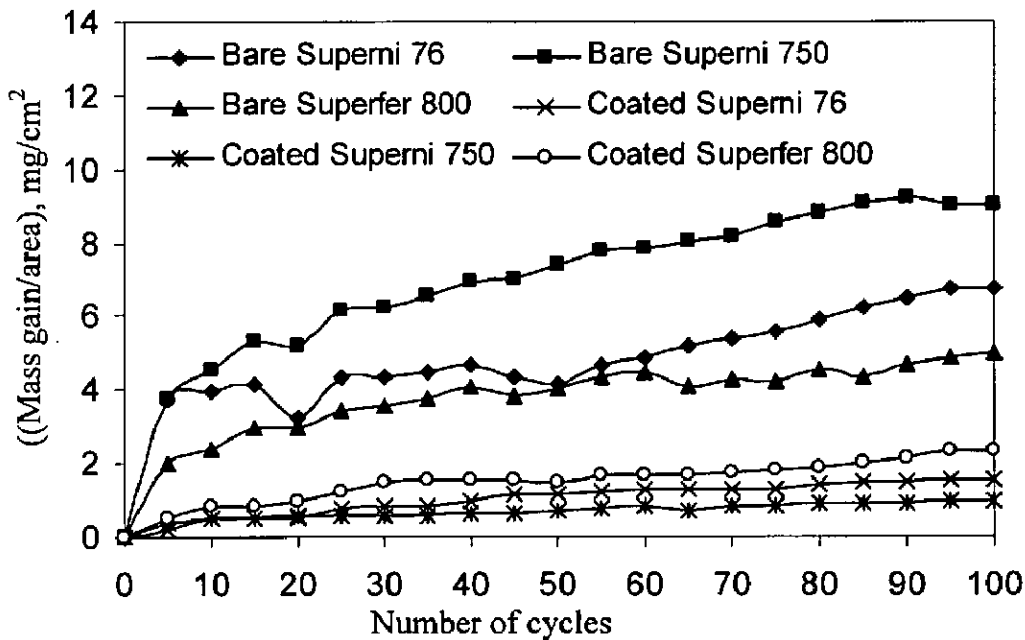


**Fig. 5.32:** (Mass gain/area) versus number of cycles plot for uncoated and NiCrAl coated film on superalloy specimens oxidized in air at 900°C for 100 cycles.

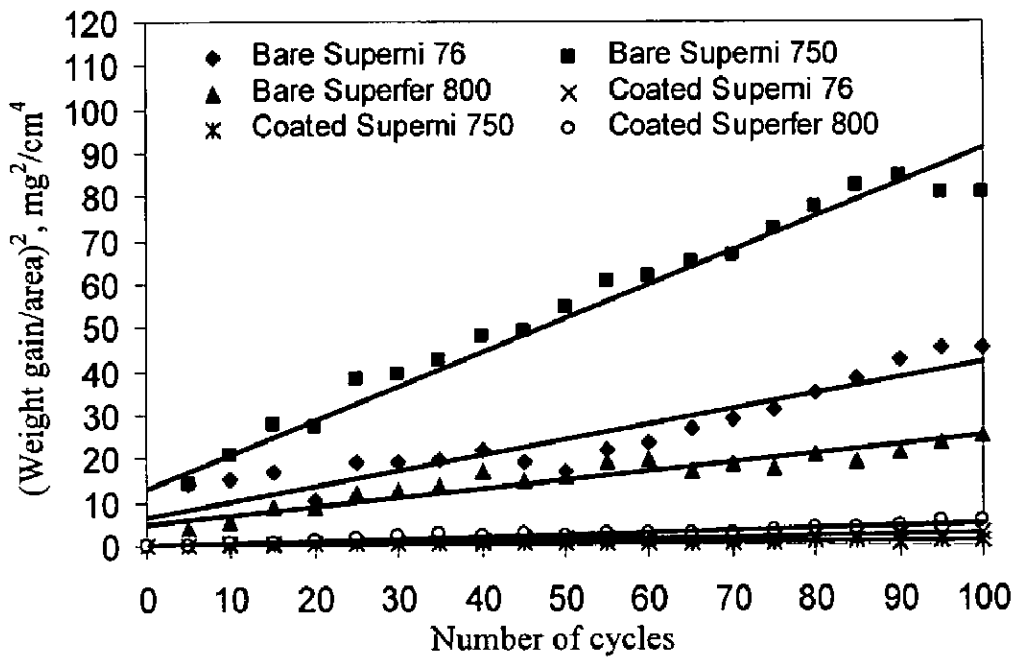


**Fig. 5.33:**  $(\text{Mass gain/area})^2$  versus number of cycles plot for uncoated and NiCrAl coated films on superalloy specimens oxidized in air at  $900^\circ\text{C}$  for 100 cycles.

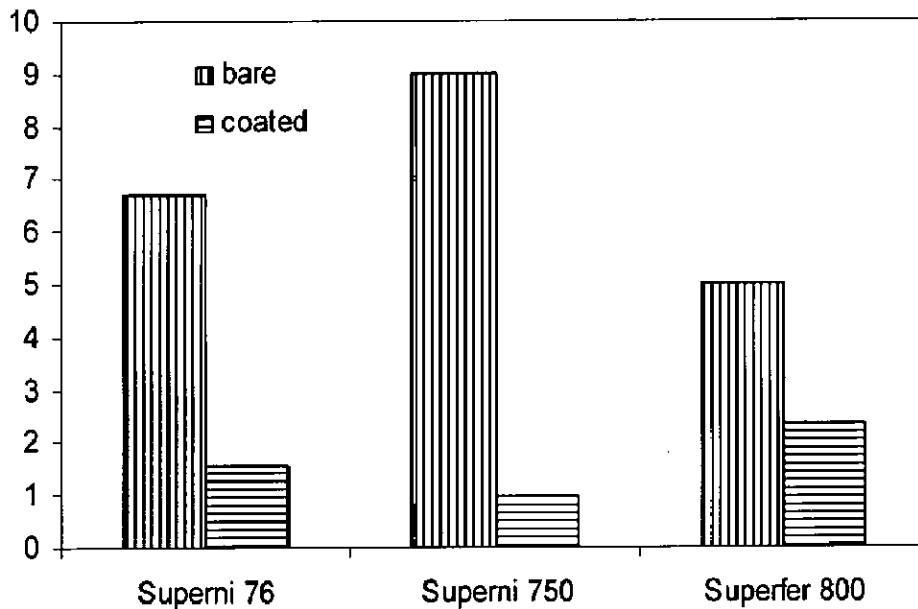


**Fig. 5.34:** Bar chart showing cumulative weight gain per unit area for uncoated and NiCrAl deposited film on superalloys subjected to cyclic oxidation for 100 cycles at  $900^\circ\text{C}$ .

### 5.4.3.2.3 Surface scale analysis

#### 5.4.3.2.3.1 X ray diffraction analysis

X-ray diffractograms of the NiCrAl coated films on superalloy substrates after cyclic oxidation in air for 100 cycles at 900°C are shown in Fig. 5.35. The oxides formed on the scale of the NiCrAl coated Superni 76 superalloy consists of Fe<sub>2</sub>O<sub>3</sub>, NiCr<sub>2</sub>O<sub>4</sub> and MnO<sub>2</sub>. In case of coated Superni 750 and Superfer 800 alloy, the scale consists of Fe<sub>2</sub>O<sub>3</sub>, MnO<sub>2</sub> and MnFe<sub>2</sub>O<sub>4</sub>.

#### 5.4.3.2.3.2 FESEM/EDAX analysis of the top surface of the scale

The FESEM micrographs indicating the surface scale morphology of the NiCrAl films on superalloys oxidised at 900°C for 100 cycles is shown in Fig. 5.36. It is observed that the scale formed on the NiCrAl coated Superni 76 indicates the presence of oxygen, Mn, Fe and Cr. In case of coated Superni 750, the surface scale consists of oxygen, chromium, manganese and iron. The scale formed is adherent with the coating and minor spalling is indicated. In case of coated Superfer 800 alloy, the surface scale consists of small irregular shaped granules. The surface scale mainly consists of oxygen, manganese, chromium and iron. Nickel and aluminum are present in minor amounts.

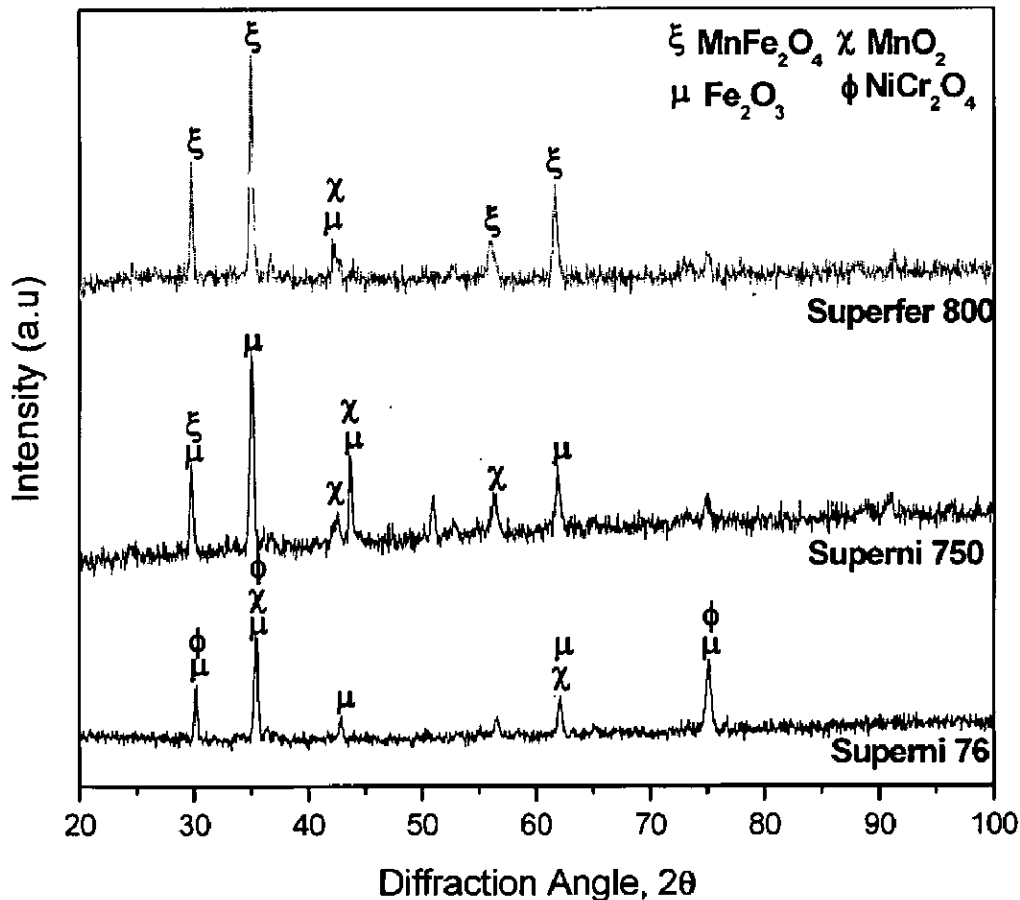


**Fig. 5.35:** X-ray diffractograms of oxidised scale of the NiCrAl coated films on Superni 76, Superni 750 and Superfer 800 after 100 cycles at 900°C.



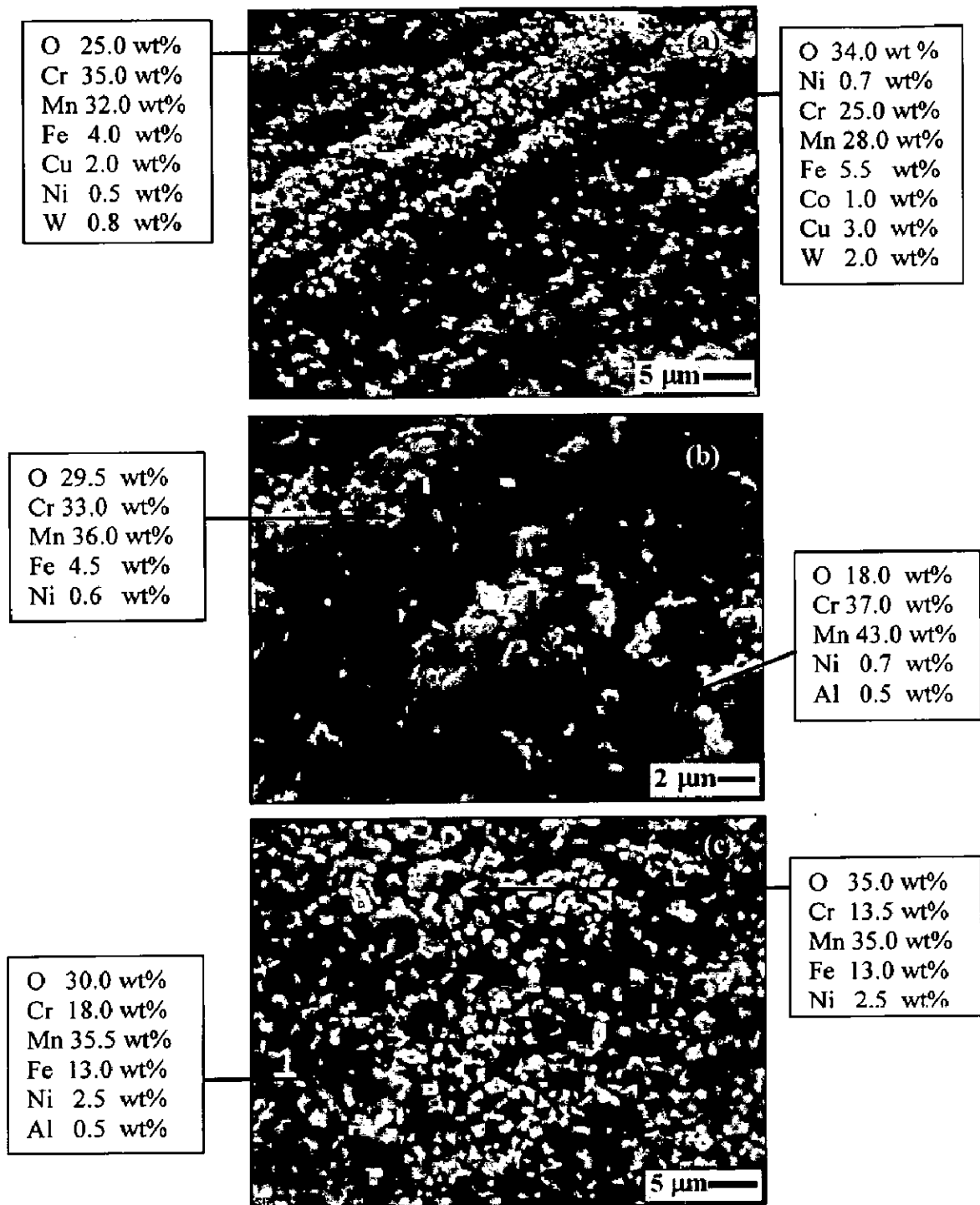


**Fig. 5.36:** Surface scale morphology and EDAX composition of Ni-Al coated thin film after oxidation studies on (a) Superni 76, (b) Superni 750 and (c) Superfer 800.

#### ***5.4.3.2.4 X ray mapping analysis of the cross-section***

The elemental mapping of NiCrAl deposited film on Superni 76, Superni 750 and Superfer 800 after cyclic oxidation at 900°C is shown in Fig. 5.37. The film formed on the NiCrAl coated superalloys is uniform and continuous. In case of NiCrAl coated film on Superni 76, Fig. 5.37(a), the film is unoxidised and consists of mainly nickel, chromium and iron. Oxygen is present on the top surface of the film and coexisting with aluminum along the coating-substrate interface. Alloying elements such as Mn and W have diffused from the substrate into the coating as observed from the X-ray mapping.

In case of coated Superni 750 alloy Fig 5.37(b), the topmost surface of the film consists of chromium, iron and oxygen. Nickel has depleted from the substrate. Chromium has migrated and formed a band in the substrate which is also coexisting below the nickel rich band. The presence of iron in the film may be attributed either to the migration from the substrate or probable deposition from the steel target. Streak of titanium is observed just above the chromium rich band.

In case of NiCrAl coated Superfer 800, Fig. 5.37(c), the top surface of the film consists of nickel, chromium and iron with oxygen. Presence of manganese in the film is noticed from the X-ray mapping analysis. Aluminum is existing wherever nickel is absent in the film. Aluminum and chromium are coexisting in the in the film. Few specs (points) of oxygen are present only at the film-substrate interface.

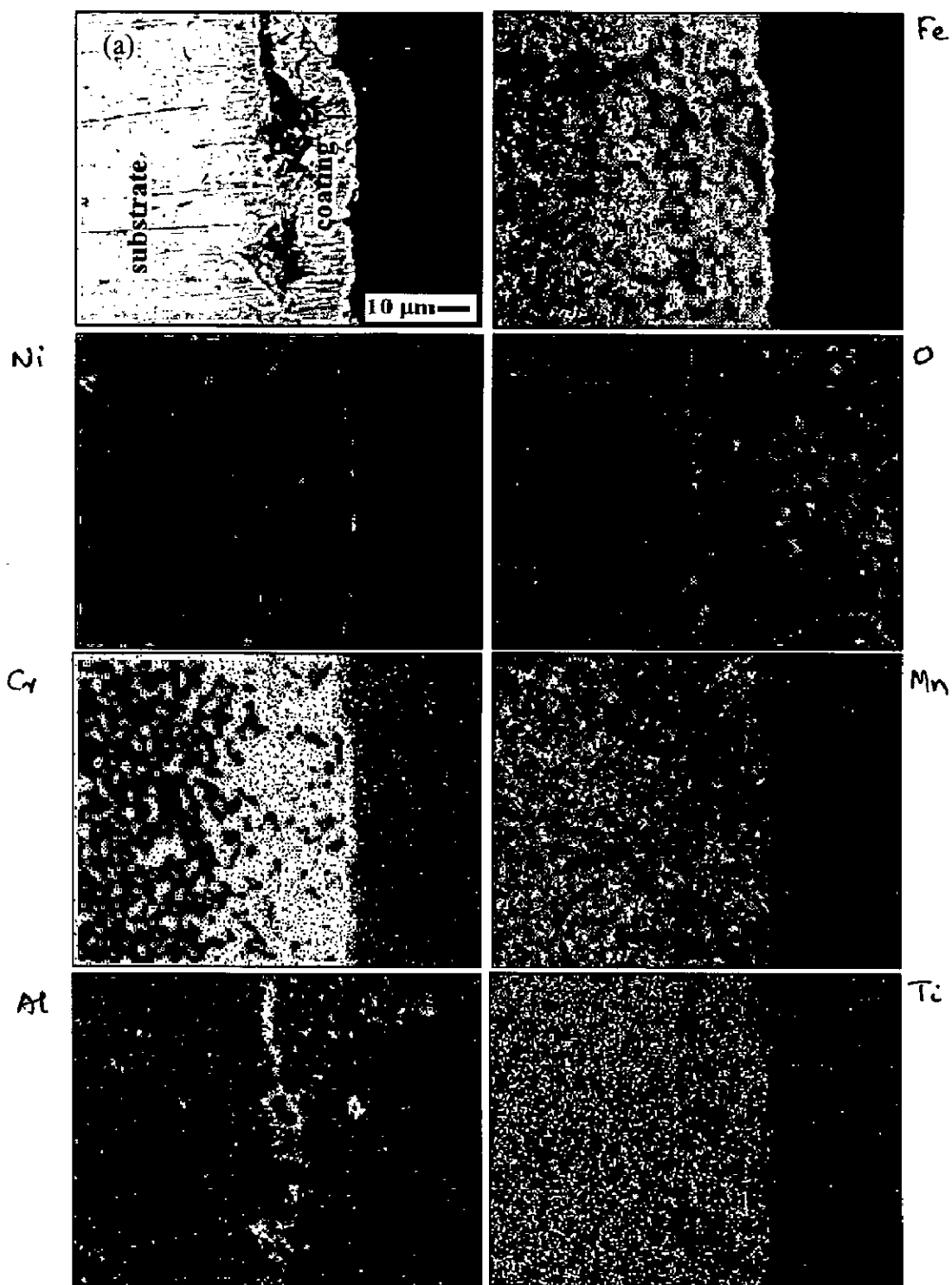


**Fig. 5.37(a):** Compositional image and X-ray mapping of the cross-section of NiCrAl coated Superni-76 subjected to cyclic oxidation in air at 900 °C.

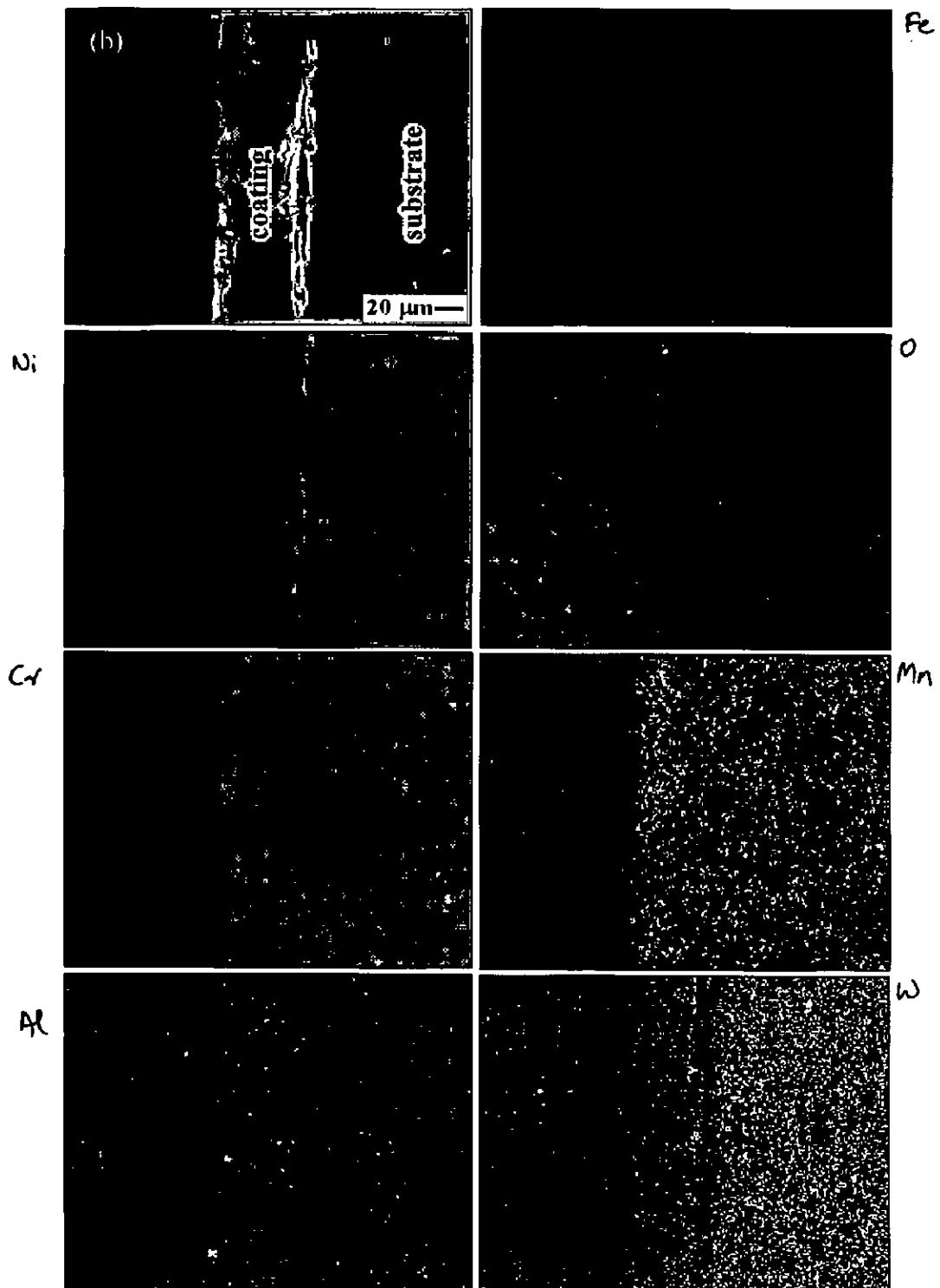


**Fig. 5.37(b):** Compositional image and X-ray mapping of the cross-section of NiCrAl coated Superni 750 subjected to cyclic oxidation in air at 900 °C.

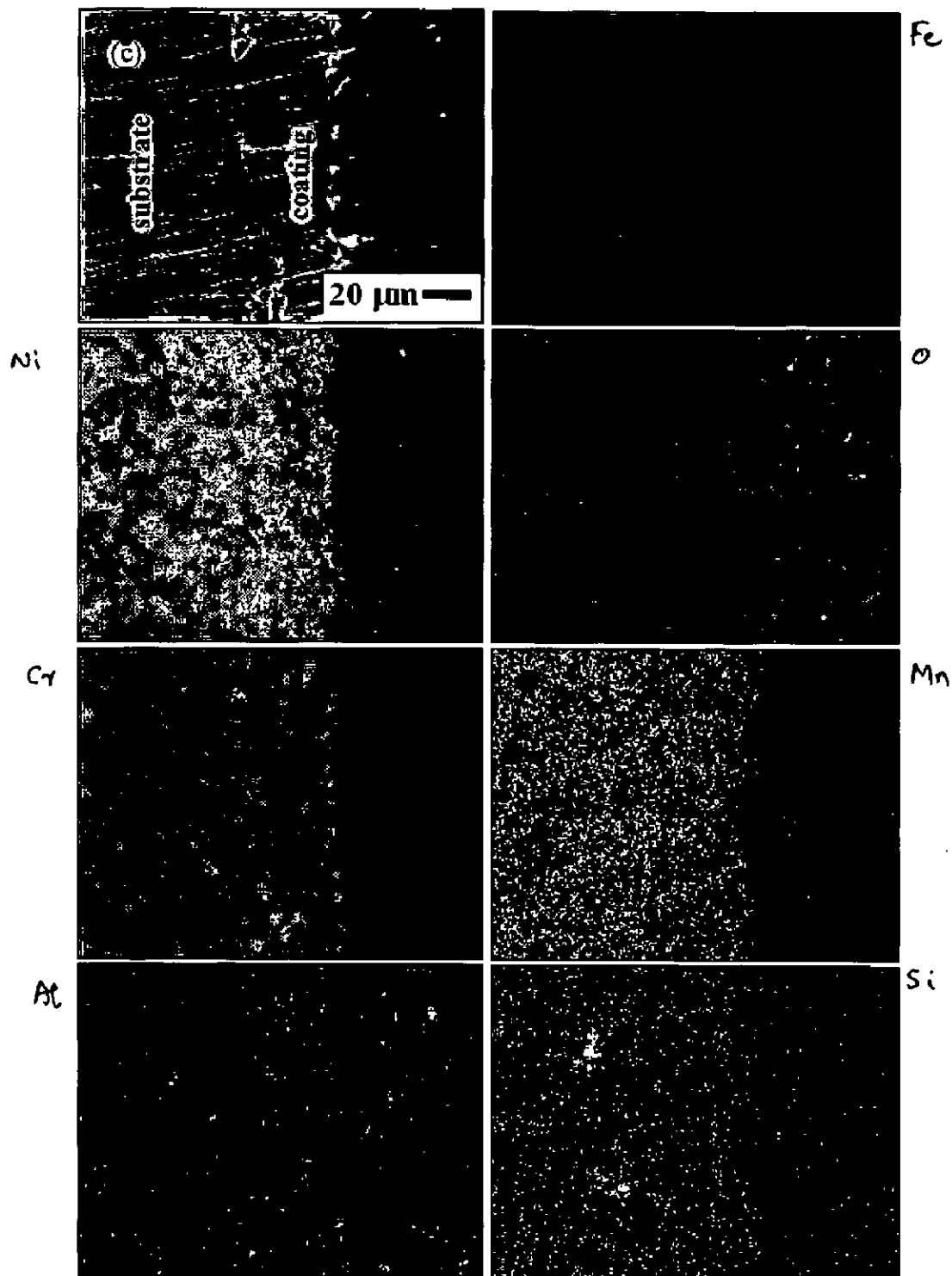


**Fig. 5.37(c):** Compositional image and X-ray mapping of the cross-section of NiCrAl coated Superfer 800 subjected to cyclic oxidation in air at 900 °C.

#### 5.4.4 Discussion

The NiCrAl film was deposited successfully on all the superalloy substrates by RF magnetron sputtering process. The deposited film has a crystallite size of 17 nm, 21 nm and 8 nm for Superni 76, Superni 750 and Superfer 800, respectively, as observed from the XRD (Fig. 5.28) analysis. The surface topography of the films indicated the deposited film was uniform throughout the surface as shown in Fig. 5.29. The surface roughness of the deposited films was found around 32 nm, 57 nm and 63 nm for Superni 76, Superni 750 and Superfer 800, respectively. The surface macrograph of the NiCrAl deposited film after 100 cycles of exposure at 900°C are shown in Fig. 5.31. It is observed from the macrographs that the microspalling in the form of fine powder was observed during the initial period of exposure. The oxide scale became dense and adherent with further exposure.

The weight gain of the bare alloys was high during the initial period of exposure and then becomes gradual with the course of the experiment. The uncoated specimens indicated the spalling of the oxide scale after some cycles of exposure and again fresh surface is exposed to the environment and thus increasing the weight. The uncoated superalloys deviated from the parabolic rate law. The NiCrAl coated film on superalloys showed lower weight gain. A thin oxide scale formed on the surface was uniform over the surface and adherent with the NiCrAl film. Minor microspalling in the form of fine powder was observed during the course of the study. The high temperature oxidation behaviour of NiCrAl coated specimens followed the parabolic rate law and the parabolic rate constant ( $k_p$ ) values for the coated specimens were much lower than the uncoated superalloys exposed in the same environment thereby indicating better resistance to oxidation.

The XRD analysis of coated Superni 76 indicates that the formation of  $Fe_2O_3$ ,  $NiCr_2O_4$  and  $MnO_2$  on the top surface of oxidised sample. In case of coated Superni 750 and Superfer 800 alloy, presence of  $Fe_2O_3$ ,  $MnO_2$  and  $MnFe_2O_4$  were also observed in the oxide scale. EDAX analysis of the oxidised scale indicates the presence of oxygen, chromium, manganese and iron. Presence of some alloying elements of the base alloy was also noted in the oxide scale. The cross-sectional X-ray mapping analysis indicates that a very thin oxide scale formed on the surface is continuous and dense. The oxide scale consists of chromium, iron, manganese and nickel. Oxygen is coexisting with aluminum and also present on the top surface of the scale. The grain size of the deposited film is in the range of 8 – 21 nm. The smaller grains help in faster diffusion of elements through the grain boundaries and help in selective oxidation of the elements such as aluminum, chromium and nickel and form a

protective layer on the surface of the coated specimen and prevent the diffusion of oxidising species into the base alloy. The presence of aluminum in the film is low and aluminum oxide which formed on the surface during the oxidation study might have spalled during cyclic conditions. Presence of chromium oxide on the oxidised specimen might have provided better protection in the given environment. Presence of manganese and iron in the film may be attributed to the probable deposition from the steel target. Some alloying elements such as Co, Cu, W and Ti might have diffused from the substrate into the film during high temperature exposure.

### 5.4.5 Conclusions

1. The NiCrAl film was successfully deposited using RF magnetron sputtering process under the employed conditions. It was observed from the AFM analysis that the film was uniformly deposited on the surface of all the specimens and the surface roughness of film was in the range 32 – 63 nm.
2. The XRD analysis of the as deposited film indicates the grains is in the nanoscale range of 8-21nm.
3. The XRD analysis of the oxidised film revealed the presence of  $MnO_2$ ,  $Fe_2O_3$ ,  $NiCr_2O_4$  and  $MnFe_2O_4$ .
4. The weight gain of the NiCrAl coated superalloys was lower as compared to that of bare superalloys. The oxidation behaviour of NiCrAl coated specimens followed the parabolic rate law.
5. NiCrAl coating has led to the reduction in weights of about 78% in Superni 76, whereas 89% and 54% for Superni 750 and Superfer 800 alloys, respectively. The NiCrAl coating has provided the necessary protection to the superalloy substrates in the given environment. Among the three coated superalloys, Superni 750 indicated a better resistance to oxidation at 900°C under cyclic conditions.
6. The smaller grains help in faster diffusion of elements through the grain boundaries and help in selective oxidation of the elements such as aluminum, chromium and nickel and form a protective layer on the surface of the coated specimen and prevent the diffusion of oxidising species into the base alloy.
7. Some alloying elements such as Mn, Ti and W might have diffused from the substrate into the oxide scale at high temperature.

## **5.5 HOT CORROSION STUDIES IN MOLTEN SALT ENVIRONMENT**

### **5.5.1 Introduction**

The increase of surface temperature of component in modern gas turbines leads to an enhanced oxidation attack of the blade coating (Guo et al, 2006). High-temperature oxidation and hot corrosion of the superalloys pose serious problem to the gas turbines. The resistance of metals and alloys relies on the protectiveness of oxide scales formed on their surfaces during service. The formation and growth of oxide scales are determined by an extensive range of parameters, including the alloy composition and the oxidizing environment. Therefore, it may be very difficult to establish a continuous, protective scale under some conditions (Zhu et al, 1995). It is well known in the literature that the nanostructured coatings provide a better corrosion resistance at high temperature due to the formation of continuous protective layer assisted by the enhanced diffusivity of atoms in the coating (Geng et al, 2003; Ren and Wang, 2006; Chen and Lou, 2003). Wang X.Y., and Li (2002) have reported that the effect of the nanostructure on the material corrosion resistance has not been well understood although the improved corrosion resistance has been observed for the nanostructured materials.

The objective of the present work is to investigate the hot corrosion behaviour of nanostructured coatings of NiCrAl obtained by RF magnetron sputtering process on Ni- and Fe-based superalloys. The hot corrosion study was carried out in aggressive environment of molten salt (40%Na<sub>2</sub>SO<sub>4</sub>-60%V<sub>2</sub>O<sub>5</sub>) at 900°C under cyclic conditions. Techniques such as XRD, SEM/EDAX and X-ray mapping were used to analyse the corroded specimens after exposure. Thermogravimetric (weight change with time) technique was used to approximate the kinetics of corrosion.

### **5.5.2 Experimental Details**

The details of the substrate material, coating formulation and hot corrosion studies of the RF sputtered NiCrAl films are explained in section 3.2.3.2 of the Chapter 3.

### **5.5.3 Results**

#### **5.5.3.1 Visual Observation**

The photograph of NiCrAl coated specimens after hot corrosion studies in molten salt environment at 900°C for 100 cycles are shown in Fig. 5.38. In case of NiCrAl coated Superni 76 alloy (Fig. 5.38a), after completion of 2<sup>nd</sup> cycle, grey color was observed on the surface of the specimen. Spalling of the salt in the form of fine powder was observed after 3<sup>rd</sup> cycle and continued upto 10 cycles. After completion of 100 cycles, dark grey colour was



observed on the surface. In case of NiCrAl coated Superni 750 alloy (Fig 5.38b), brown color was observed on the specimen after 2<sup>nd</sup> cycle, which subsequently turned into dark grey with brown patches with further exposure. The superficial microspalling of was noticed after 5<sup>th</sup> cycle and continued upto 13 cycles. In case of NiCrAl coated Superfer 800 alloy (Fig.5.38c), after completion of 2<sup>nd</sup> cycle, grey colour was seen on the surface of the specimen. The scale started spalling in the form of fine powder after 6<sup>th</sup> cycle and continued upto 16<sup>th</sup> cycle. The scale turned into dark grey colour with dark green patches after 20 cycles.

### 5.5.3.2 Corrosion Kinetics in molten salt environment

The mass gain per unit area versus number of cycles plots for the bare as well as coated superalloys exposed to molten salt ( $\text{Na}_2\text{SO}_4$ -60% $\text{V}_2\text{O}_5$ ) environment at 900°C under cyclic conditions is shown in Fig. 5.39. It is noticed that the mass gain of the NiCrAl coated Superni 76 and Superni 750 are much lower as compared to Superfer 800. In case of NiCrAl coated Superfer 800, the weight gain is high during the initial period of exposure and leveled off with further exposure in the molten salt environment. The higher weight gain was observed in case of bare superalloys. The higher mass gain in case of bare superalloys indicates that they are more prone to hot corrosion attack. The parabolic rate constant  $k_p$  is calculated from the slope of the linear regression fitted line from  $(\text{mass gain/area})^2$  versus number of cycles as shown in Fig. 5.40. The  $k_p$  values for NiCrAl coated Superni 76, Superni 750 and Superfer 800 are  $0.35 \times 10^{-10} \text{ g}^2 \text{ cm}^{-4} \text{ s}^{-1}$ ,  $1.64 \times 10^{-10} \text{ g}^2 \text{ cm}^{-4} \text{ s}^{-1}$  and  $12.40 \times 10^{-10} \text{ g}^2 \text{ cm}^{-4} \text{ s}^{-1}$ , respectively. The bare superalloys deviated from the parabolic rate law, whereas the NiCrAl sputtered specimens (Superni 76 and 750) followed the parabolic behaviour up to 100 cycles. NiCrAl coated Superfer 800 deviated from the parabolic rate law. The cumulative weight gain/unit area in all three cases of bare/coated superalloys is shown in Fig. 5.41.

### 5.5.3.3 X-ray diffraction analysis

The XRD diffractograms of the coated hot corroded samples after 100 cycles are shown in Fig.5.42. XRD patterns of the NiCrAl coated Superni 76 after exposure to molten salt environment at 900°C revealed the presence of  $\text{Cr}_2\text{O}_3$ ,  $\text{NiCr}_2\text{O}_4$ , and  $\text{FeVO}_4$  as the main phases along with some minor phase of  $\text{Al}_2\text{O}_3$  and  $\text{NiVO}_4$ . In case of NiCrAl coated Superni 750 alloy, the surface scale after 100 hours exposure indicated the presence of  $\text{Cr}_2\text{O}_3$ , and  $\text{NiCr}_2\text{O}_4$  as the main phases and some minor phases such as  $\text{FeVO}_4$ ,  $\text{NiO}$  and  $\text{Al}_2\text{O}_3$ . The phases formed on the surface of the NiCrAl coated Superfer 800 alloy indicated the presence of major phases such as  $\text{Fe}_2\text{O}_3$ ,  $\text{NiCr}_2\text{O}_4$ ,  $\text{NiO}$  and a minor phase of  $\text{Al}_2\text{O}_3$ .

### 5.5.3.4 FESEM/EDAX analysis

#### 5.5.3.4.1. Surface analysis

FESEM micrographs showing the surface morphology and EDAX analysis at some selected points of interest of hot corroded NiCrAl coated specimens are shown in Fig. 5.43. The scale formed on NiCrAl coated Superni 76 alloy after 100 cycles shows (Fig. 5.43a) that the formation of small granules through out the surface indicating the formation of oxides of nickel, iron, chromium on the top scale. The subscale region is rich in oxides of iron and chromium. Small amount of manganese, copper and tungsten are detected on the surface of the scale. The SEM/EDAX analysis of the top surface of the scale for NiCrAl coated Superni 750 alloy (Fig. 5.43b) indicates the formation massive scale with tiny crystals consisting of mainly oxides of nickel, iron and chromium. In case of NiCrAl coated Superfer 800 (Fig. 5.43c) alloy, the scale formed on the surface consists of irregular shaped crystals consisting of mainly oxides of nickel, chromium and iron on both top scale and subscale regions.

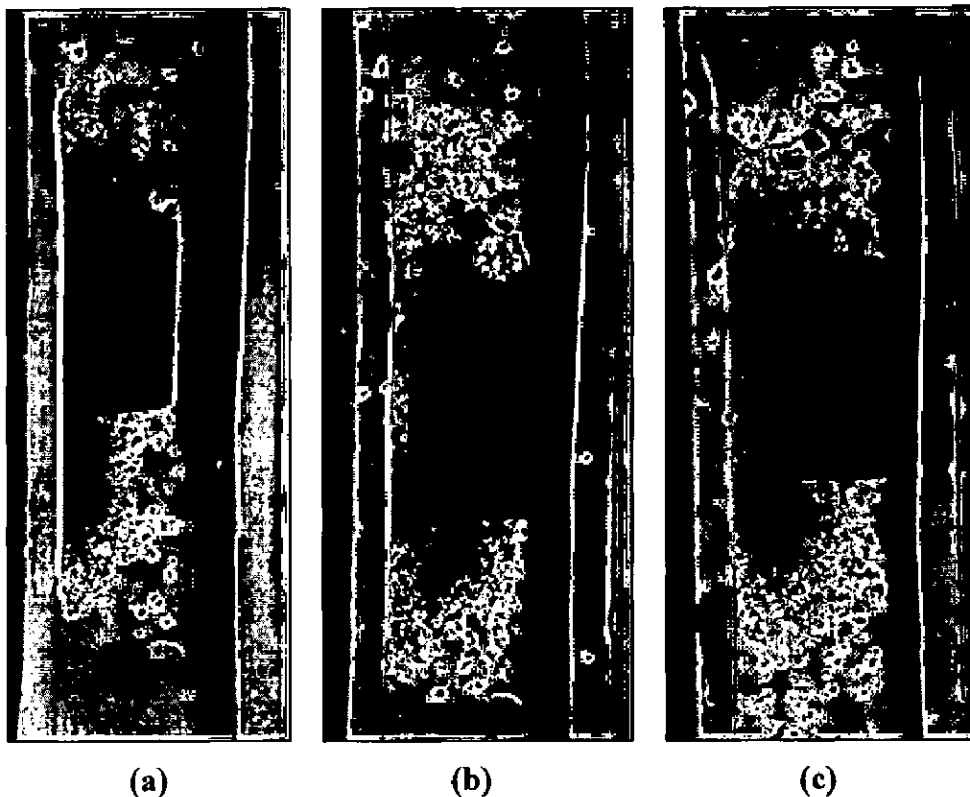


**Fig. 5.38:** Surface macrographs of RF sputtered NiCrAl films on (a) Superni 76, (b) Superni 750, and (c) Superfer 800 after 100 hr exposure to molten salt environment at 900°C.

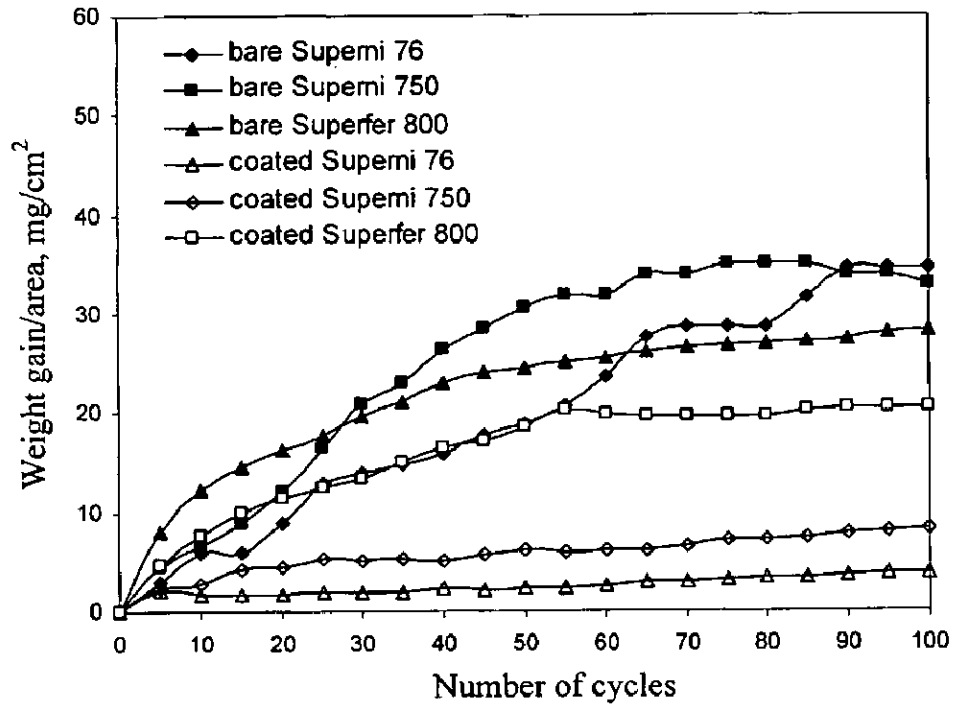


**Fig. 5.39:** Mass gain/area versus number of cycles plot for NiCrAl coated specimens oxidized in molten salt environment at 900°C for 100 cycles.

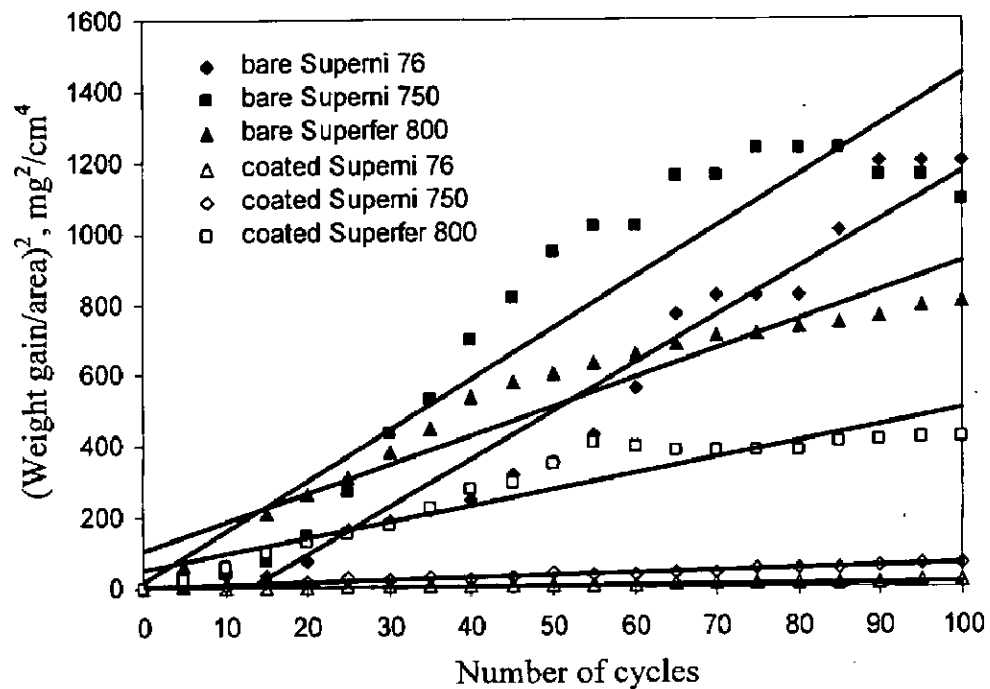


**Fig. 5.40:** (Mass gain/area)<sup>2</sup> versus number of cycles plot for NiCrAl after exposure to molten salt environment at 900°C for 100 cycles.

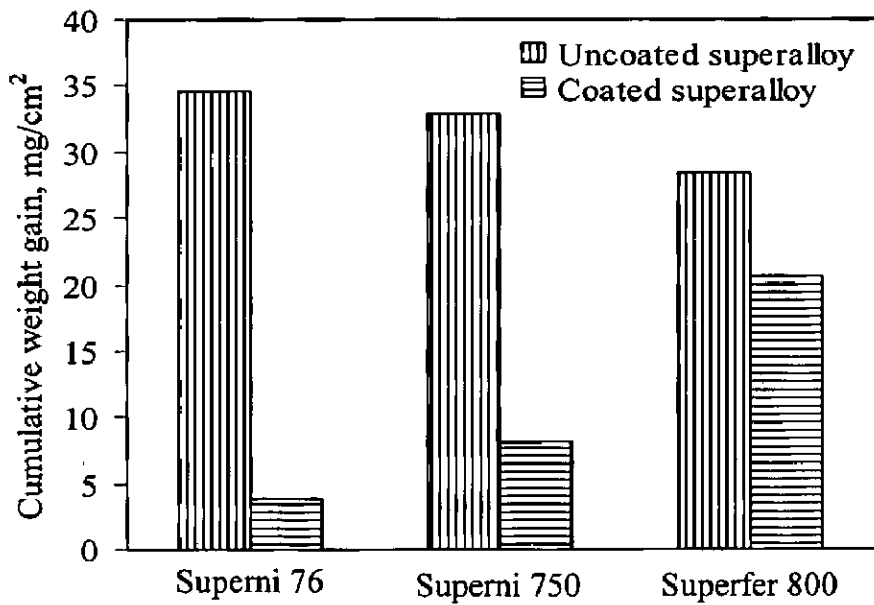


**Fig. 5.41:** Bar chart showing cumulative weight gain per unit area for uncoated and RF sputtered NiCrAl film on superalloys subjected to molten salt environment at 900°C for 100 cycles.

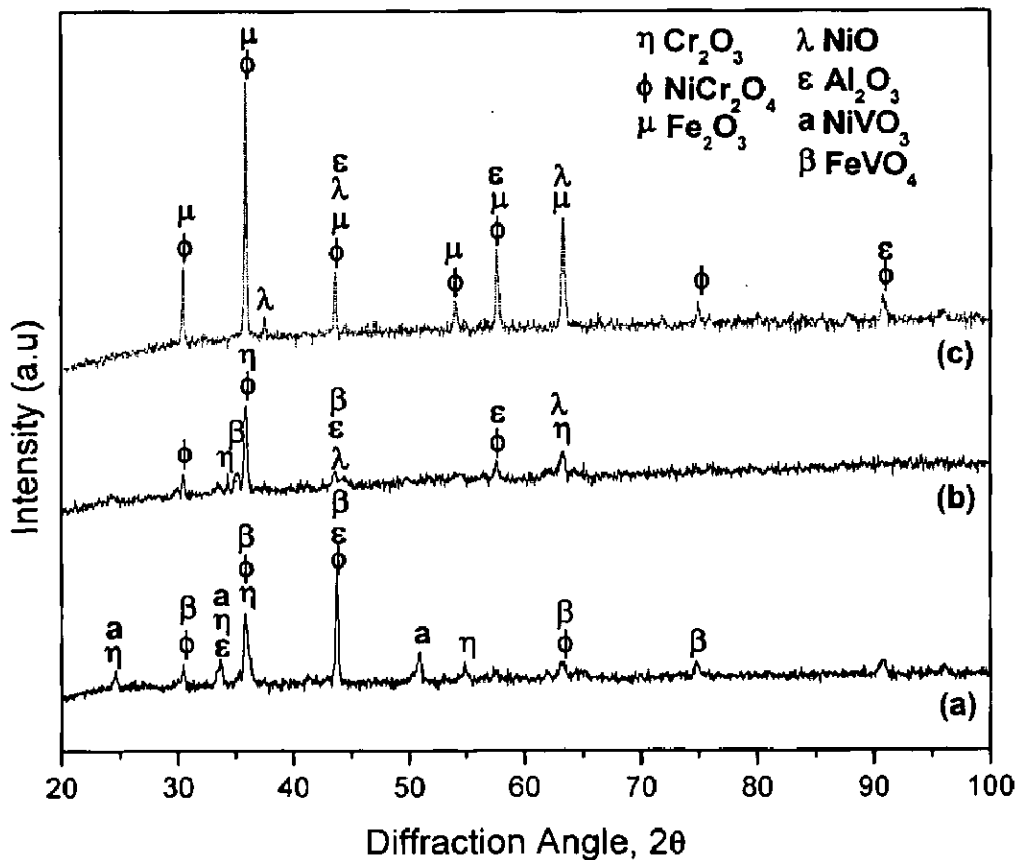


**Fig. 5.42:** X-ray diffractograms of NiCrAl coated thin films on (a) Superni 76, (b) Superni 750 and (c) Superfer 800 after 100 hrs exposure to molten salt environment at 900°C.

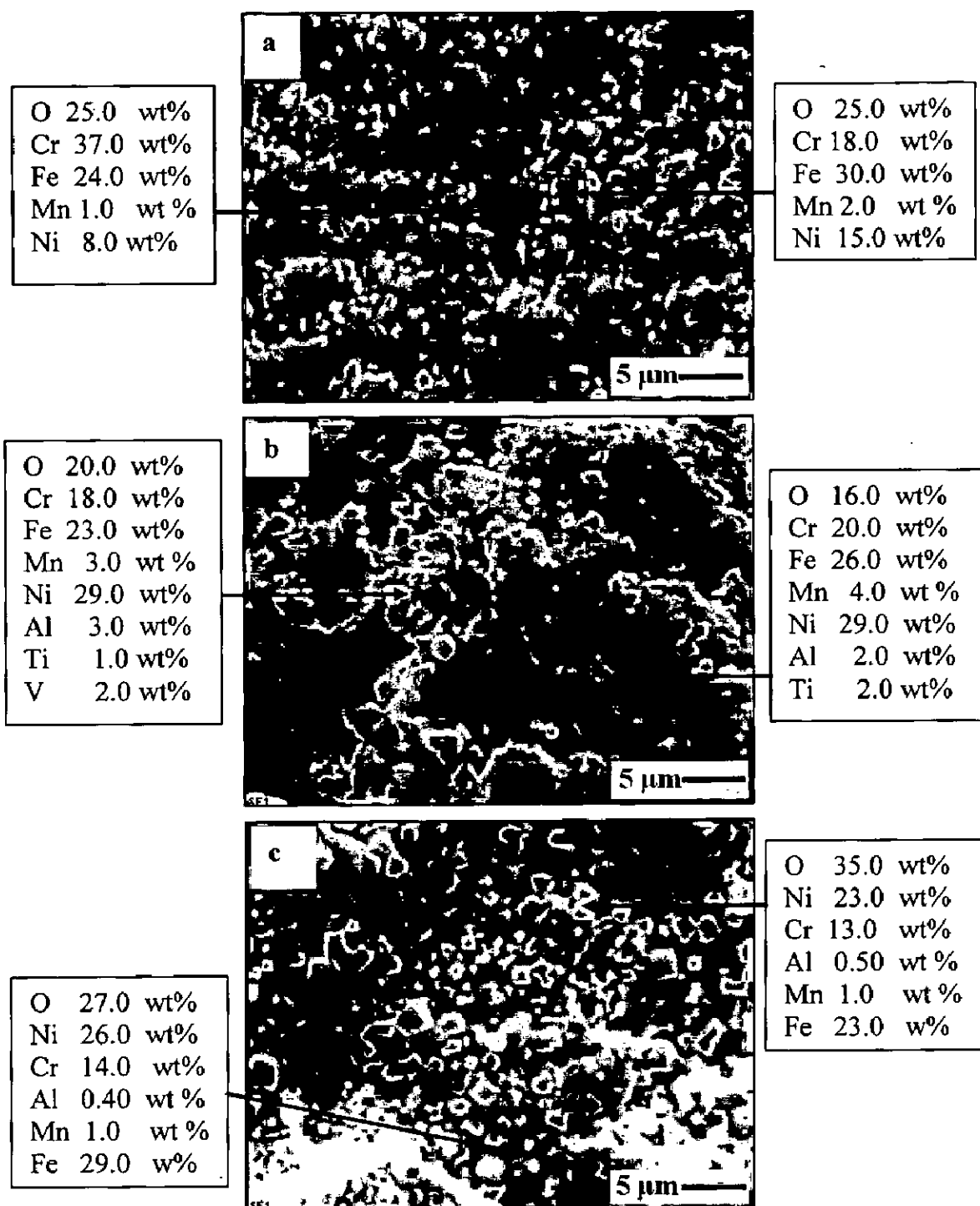


**Fig. 5.43:** Surface scale morphology and EDAX composition of NiCrAl coated thin film for (a) Superni 76, (b) Superni 750 and (c) Superfer 800 after exposure to molten salt environment at 900°C.

### 5.5.3.5 X ray mapping analysis

X-ray mapping for the NiCrAl coated film on Ni- and Fe-based superalloy after hot corrosion studies is shown in Fig. 5.44. In case of coated Superni 76, the topmost scale consists of nickel. It is noticed from the X-ray mapping analysis that chromium is present in the subscale region and iron is distributed along the scale. Oxygen is existing with chromium in the subscale region as it is evident from (Fig 5.44a). Small amount of aluminum is present in the scale, and elements like manganese and tungsten have diffused into the scale from the substrate alloy.

X-ray mapping analysis of Superni 750, (Fig 5.44b), shows that the top layer is rich in nickel and chromium. Chromium and oxygen are coexisting in the coating-substrate interface forming a thick band of chromium oxide. Iron is distributed in the scale and also along the scale substrate interface. Presence of oxygen is observed along the scale-substrate interface. Elements such as manganese and titanium have moved from the substrate into the scale.

In case of coated Superfer 800 (Fig.5.44c), the topmost layer consists of chromium and iron. Nickel is present in the subscale region. Aluminum is present in negligible amount in the scale. Oxygen is present in the scale wherever nickel is absent and is coexisting with chromium and iron. Perceptible amount of silicon has moved from the substrate into the top scale and manganese also has migrated from the substrate into the scale.

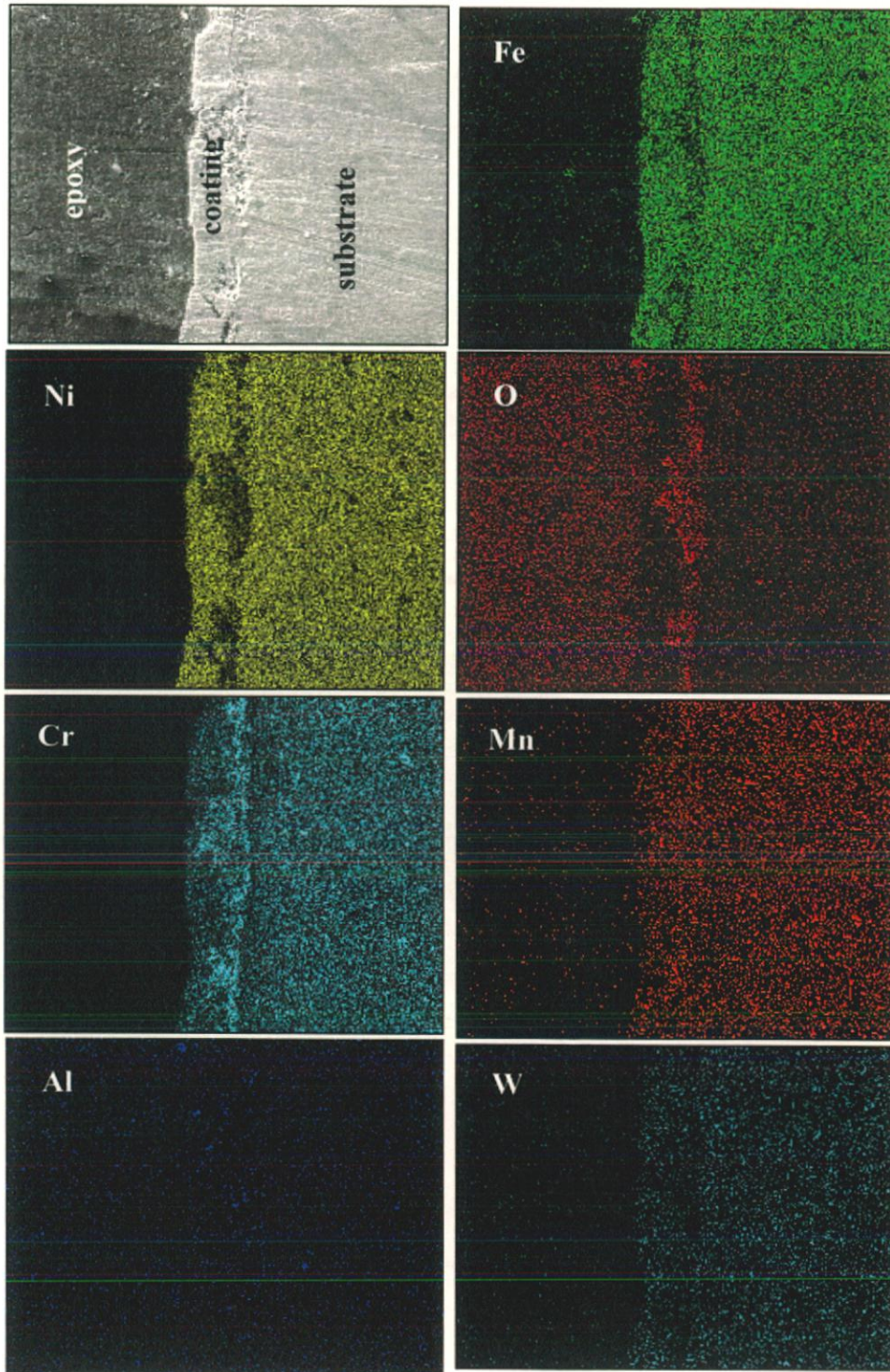


**Fig. 5.44(a):** Compositional image (SEI) and X-ray mapping of the cross-section of NiCrAl coated Superni 76 subjected to molten salt environment at 900°C.

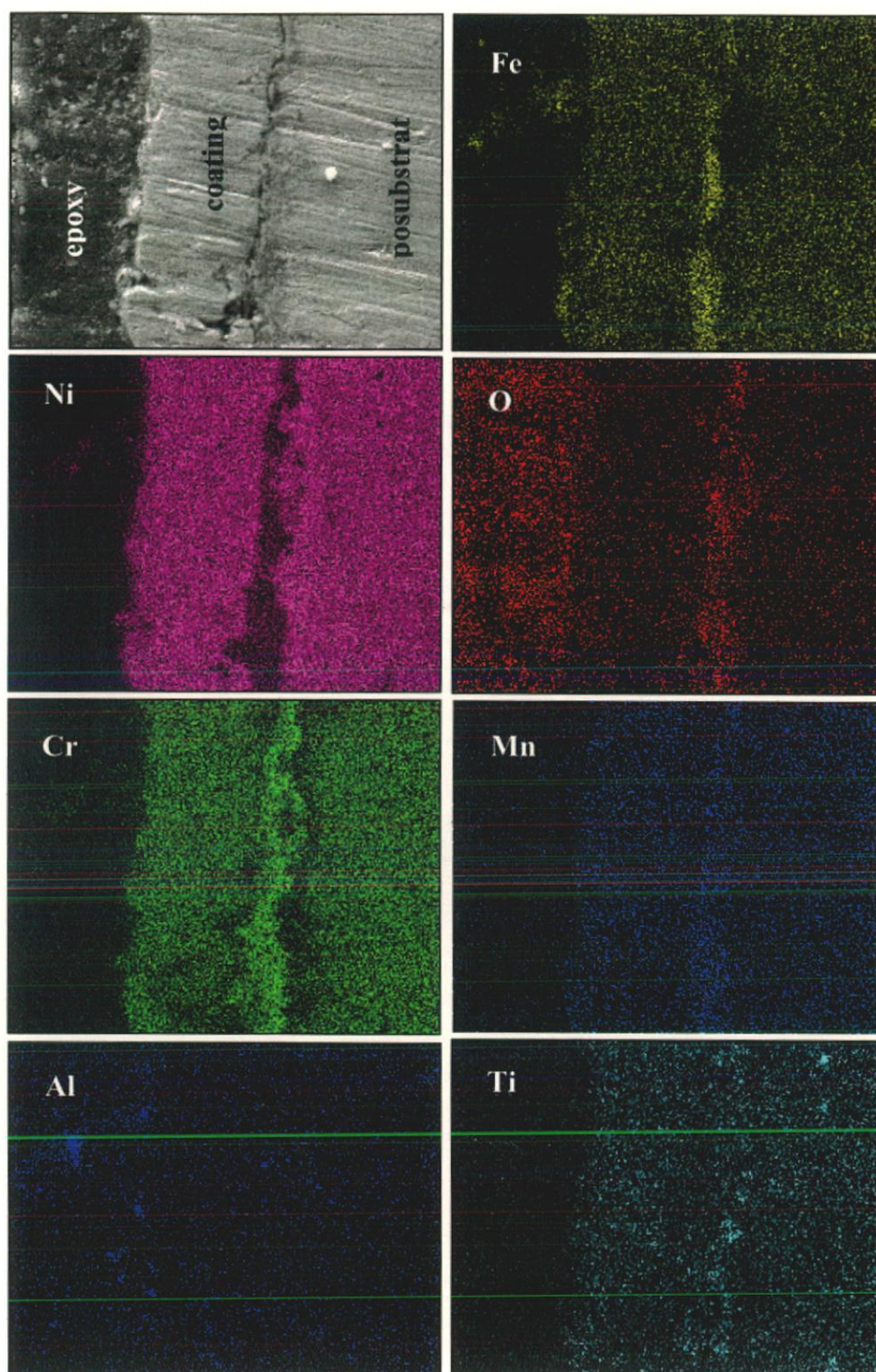


**Fig. 5.44(b):** Compositional image (SEI) and X-ray mapping of the cross-section of NiCrAl coated Superni 750 subjected to molten salt environment at 900°C.



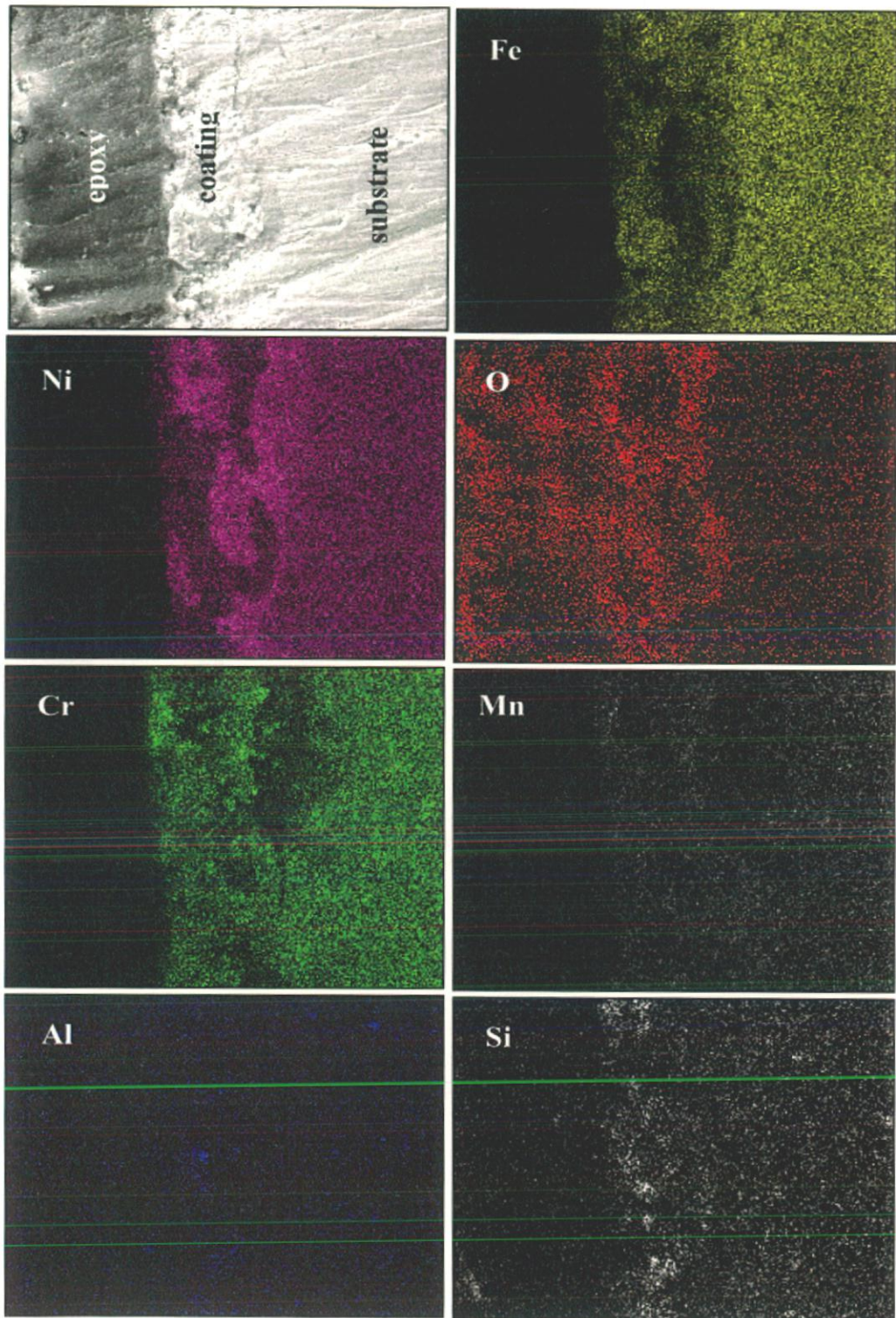


**Fig. 5.44(c):** Compositional image (SEI) and X-ray mapping of the cross-section of NiCrAl coated Superfer 800 subjected to molten salt environment at 900°C.

#### 5.5.4 Discussion

The macrographs of NiCrAl coated superalloys after exposure to molten salt environment shows that the scale has spalled in the form of fine powder in the initial stages of the exposure to the given environment (Fig.5.38). The spalling tendency of the scale stopped with the course of the experiment. The scale formed on the corroded surface was dark grey with some green patches. The uncoated specimen showed higher weight gain in the given environment due to intense spalling of the scale (Fig 5.39). The mass gain of the bare alloys during the initial period is high and due to the penetration of corroding species and spallation of the scale from the surface causes exposure of the fresh surface to the given molten salt environment thus increasing the weight. In case of coated superalloys, the weight gain increases during the initial period of exposure. Once the oxide layer is formed on the surface, the weight gain becomes gradual as observed in the weight gain graph. In case of coated Superfer 800, the weight gain is high compared to other coated superalloys. The higher weight gain in case of coated Superfer 800 is attributed to the spalling of the scale from the surface during the exposure in the given environment. All the uncoated superalloys have deviated from the parabolic rate law. The NiCrAl coated Superfer 800, also deviated from the parabolic rate law, whereas the NiCrAl coated Superni 76 and Superni 750 have followed the parabolic rate law. RF sputtered NiCrAl coating has led to the reduction in the weight of about 89% in Superni 76, whereas, 75% and 30% for Superni 750 and Superfer 800 alloys, respectively (Fig.5.41). It can be inferred that the RF sputtered NiCrAl coating on Superni 76 and Superni 750 have provided the better protection to the superalloys.

The XRD analysis (Fig. 5.42) of the coated superalloys after hot corrosion studies at 900°C in molten salt environment indicates the formation of oxides of nickel, chromium, aluminum and spinel of nickel and chromium. The fine grains of nanoscale range helps in faster diffusion of elements such as aluminum, chromium and nickel through the grain boundaries thus providing the selective oxidation of these elements. Once the oxide layer is formed uniformly over the surface then it prevents the diffusion of corroding species into the substrate alloy. The better protection to the superalloys from hot corrosion may also be due to the formation of spinel on the top scale, which further enhances the corrosion resistance in the aggressive environment. EDAX analysis on the surface indicated the presence of oxides of nickel, chromium and iron which is supported by XRD analysis. These oxides offer better protection to the superalloy substrates due to their low growth rate, strongly bounded compositions and ability to act as effective barriers against ionic migration (Stott, 1989).

The X-ray mapping analysis of coated Superni 76 (Fig.5.44a) indicates that the topmost scale formed on the surface consists of nickel and iron. Chromium is present in the subscale region and co-existing with oxygen forming chromium oxide which is protective at elevated temperature. Chromium from the substrate has move into the coating as observed in the chromium mapping image. In case of coated Superni 750 (Fig 5.44b), the coating consists of nickel and chromium along with some iron. A thick band of chromium is observed near the coating-substrate interface with oxygen indicating the formation of chromium oxide. Chromium has depleted from the substrate and moved into the coating. In case of coated Superfer 800 (Fig. 5.44c), the X-ray mapping analysis shows that the topmost scale consists of oxides of chromium and iron, whereas, the subscale contains nickel oxide. Silicon has migrated to the topmost part of scale. Small amount of manganese has also moved from the substrate into scale.

### 5.5.5 Conclusions

1. The RF magnetron sputtered NiCrAl film on superalloys indicated lower weight gain as compared to the uncoated superalloys in the molten salt environment under study. The coated superalloys showed the superficial microspalling in the form of fine powder, whereas, the in case of uncoated superalloys, intense spalling was observed during the course of the experiment.
2. The parabolic rate constant of NiCrAl coated film on superalloys after 100 hours cyclic exposure to the molten salt environment showed much lower values compared to the uncoated superalloys indicating a better protection to the substrate superalloys in the given environment.
3. The RF sputtered NiCrAl film has led to the reduction in weights of about 89%, 75% and 30% for Superni 76, Superni 750 and Superfer 800 alloys, respectively.
4. The hot corrosion resistance of RF sputtered NiCrAl film on Superni 750 has showed better protection compared to other two coated superalloys in the given molten salt environment. This may be due to the presence of thick band of chromium near the coating-substrate interface. The better hot corrosion resistance may also be attributed to the formation of  $\text{Cr}_2\text{O}_3$  and  $\text{NiCr}_2\text{O}_4$  spinel as revealed by XRD analysis. The nanograins in the films facilitate the formation of protective oxide scales.
5. X-ray mapping analysis indicated the diffusion of some alloying elements such as Mn, Ti, S and W from the substrate into the oxide scale at high temperature.

# NiCrAlY-0.4wt% Ceria COATING

---

---

*This chapter presents the detailed analysis of HVOF sprayed NiCrAlY-0.4wt%CeO<sub>2</sub> coating on Ni-and Fe-based superalloys. Microstructural Characterisation, oxidation in air and hot corrosion studies of NiCrAlY-0.4wt%CeO<sub>2</sub> coatings are discussed in this chapter.*

## 6.1 CHARACTERISATION OF THE COATING

### 6.1.1 Introduction

High velocity oxygen-fuel (HVOF) thermal spray technique in open air has been established for producing the coatings with extremely low oxide content, low porosity, and high bonding strength (Parker and Kunter, 1994). It is widely used to deposit the coatings on the surface of hot section components of advanced turbine engines to improve the reliability, durability and performance of the engines. Plasma sprayed coatings pose various problems such as high volume porosity, high surface roughness, poor adhesion and thermal stresses (Krishnan et al, 2006), which are not manifested in HVOF sprayed coatings. The superior performance of the coating is primarily due to an impact of the higher particle velocities, in HVOF technique, in comparison with the other thermal spraying systems (Russo and Dorfman, 1995) and therefore it has been successfully used to protect the gas turbine engine components (Nestler et al, 1995; Clark et al, 1995). Rajan and Zhou (2004) have reported that addition of rare earths as alloying elements have improved the corrosion resistance.

In recent years, rare earths (RE) have been utilized in surface engineering such as chemical treatment, flame spraying, and electric plating (Wang Y., et al, 1993) and thermal spray coatings (Zhang Z., et al, 2006). It is well known that presence of small percentage of reactive elements, especially rare earths render a beneficial effect on the properties of the protective scale (Bonnet et al, 1993; Bonnet et al, 1996). Wang K. L., et al, (2001B) have investigated the microstructure and corrosion resistance of laser clad coatings with rare earth elements and reported that additions of rare earth oxide CeO<sub>2</sub> or La<sub>2</sub>O<sub>3</sub> to the coatings result in the microstructural refinement of the coatings reduces the secondary dendrite spacing and the inclusion percentage of the coatings. It is evident from the published literature (Wang Y., et al, 1998; Wang M, and Wu W, 1995; Cheng and Xie, 2003) that the RE oxides are effective in grain refinement of alloys for realizing the improved mechanical and oxidation resistance properties.

There is no published literature on the characterization of HVOF sprayed NiCrAlY coatings with rare earth CeO<sub>2</sub> addition. It is very important to realise that characterizations of morphologies such as splats structure, shape, porosity, and compositional features of the coatings are critical for understanding the behavior of thermal spray coatings as well as to formulate guidelines for improving coating performance in aggressive environments. In the present investigation, an attempt has been made to characterise the HVOF sprayed NiCrAlY-0.4wt%CeO<sub>2</sub> coating on different grades of superalloys for specific applications. The microstructures, porosity, microhardness, bond strength and phase formation of HVOF sprayed NiCrAlY-0.4wt%CeO<sub>2</sub> coating were characterized using the combined techniques of optical microscopy, XRD, field emission scanning electron microscopy/energy-dispersive X-ray analysis (FESEM/EDAX) with elemental X-ray mapping. The influence of ceria addition on the hardness and bond strength of the coatings has been analyzed using its microstructural features.

### **6.1.2 Experimental Procedure**

The details of the substrate material, coating formulation and characterisation of the coating are explained in Chapter 3.

### **6.1.3 Results**

#### **6.1.3.1 Microstructure and porosity of the coatings**

The FESEM image showing morphology of the powder used and microstructure of the polished surface of the as sprayed coatings is shown in Fig. 6.1. It was noticed that the distribution of ceria was along the splat boundaries. EDAX results indicated that the black chunks and half-penny shaped areas in Fig. 6.2 were found to be oxides. Ceria was observed mostly in the splat boundaries in varying percentage. The mechanism leading to the formation of these oxide chunks and evolution of overall microstructure is of interest in this present work. Porosity measurements were done for NiCrAlY-0.4wt%CeO<sub>2</sub> coated superalloys, which were found to be around 1.40%. The standard deviation of 0.128 for NiCrAlY-0.4wt%CeO<sub>2</sub> coated SuperNi 76 and 0.118, 0.056 for coated Superni 750 and Superfer 800, respectively, were observed.

#### **6.1.3.2 Coating thickness and surface roughness measurement**

The thickness of the NiCrAlY-0.4wt%CeO<sub>2</sub> coated samples were measured by Back Scattered Electron Image (BSEI) across the cross section of the mounted samples shown in Fig. 6.3. The coating thickness was measured at different locations along the cross section for all the three superalloys. The average coating thickness of 203 μm, 275 μm and 215 μm was found in the case of coated Superni 76, Superni 750 and Superfer 800 respectively. The

surface roughness (Ra) values of the as sprayed coatings were found to be in the range of 4.93 –6.58 $\mu\text{m}$ . The centre line average (CLA) method was used to obtain the Ra values.

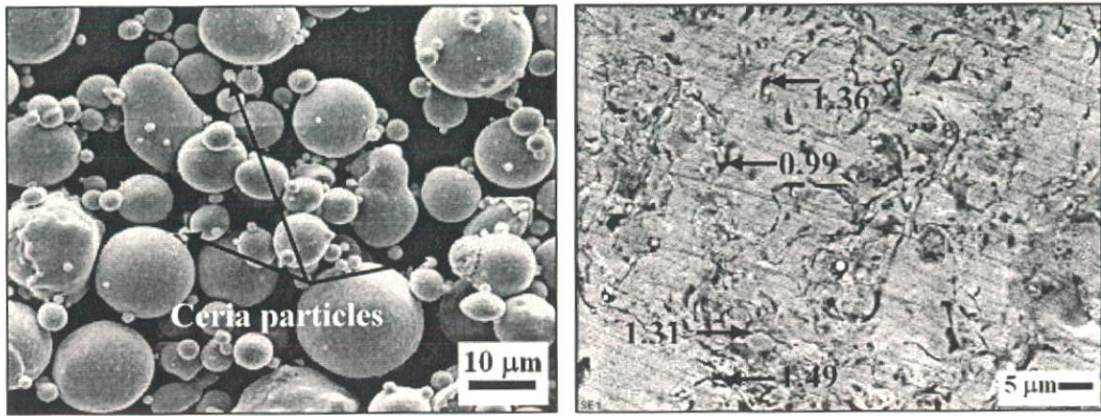


**Fig. 6.1:** FESEM image showing the (a) morphology of NiCrAlY-0.4wt%  $\text{CeO}_2$  powder, (b) ceria distribution along the splat boundaries in the polished as sprayed sample.

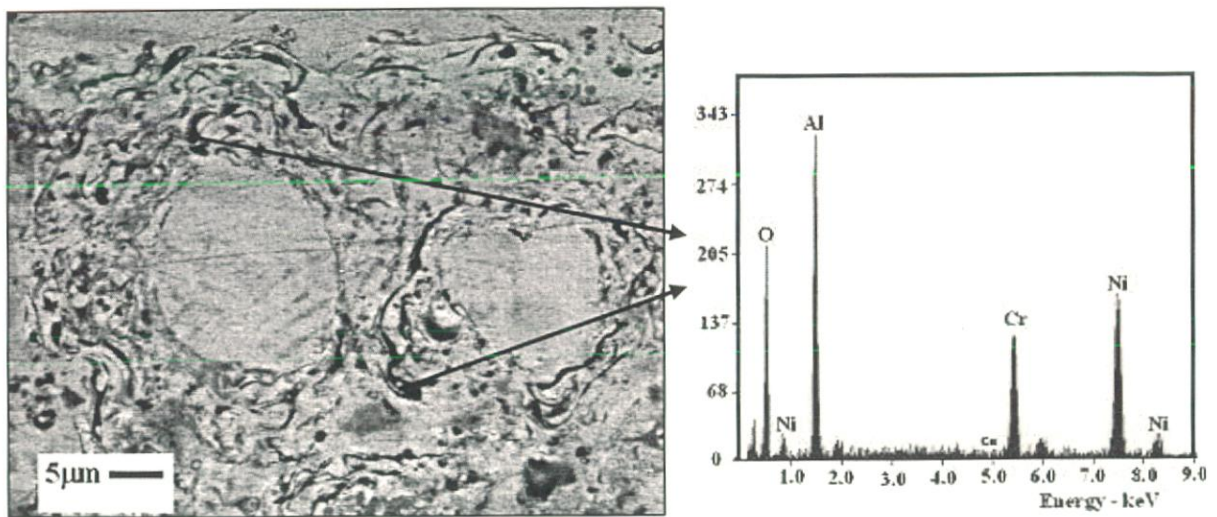


**Fig. 6.2:** EDAX analysis of dark areas in HVOF sprayed coating shows O, Al, Ni, Cr peaks.

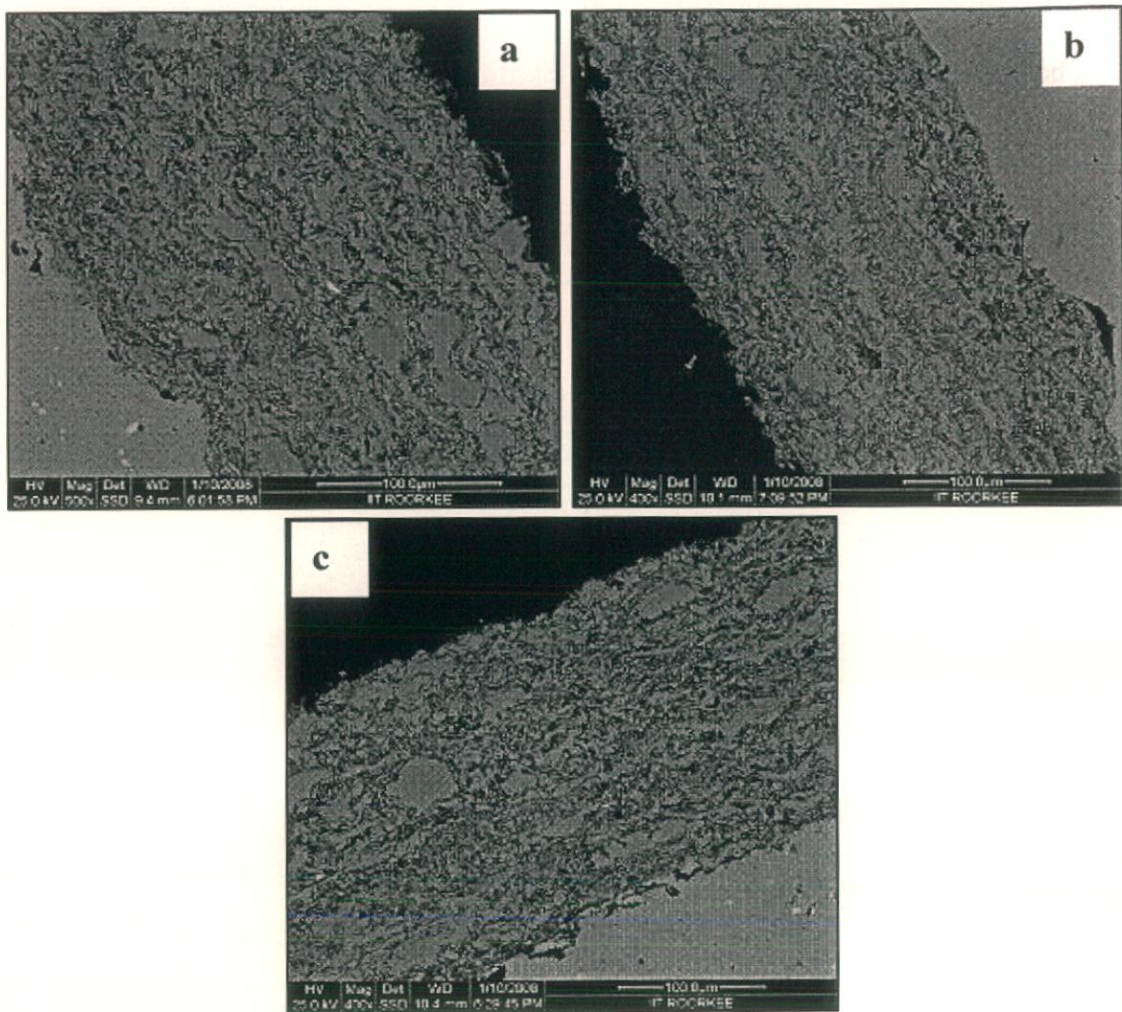


**Fig. 6.3:** Back scattered electron image (BSEI) of coated superalloys showing the cross sectional details for (a) Superni 76, (b) Superni 750 and (c) Superfer 800.

### 6.1.3.3. Microhardness and bond strength of the coating

The microhardness data of the coatings is shown in the Fig. 6.4, which shows the hardness profiles along the cross section of the coatings as a function of distance from the coating–substrate interface. The hardness of the substrates was found to be in the range of 345–360Hv, whereas the hardness of the coatings varied with the distance from the coating–substrate interface. A maximum of 753 Hv and a minimum of 649 Hv were observed in case of coated Superni 76. In case of coated Superni 750, a maximum of 752 Hv and a minimum of 665 Hv were found, whereas coated Superfer 800 alloy indicated a maximum value of 726 Hv and a minimum value of 650 Hv. The fractured surfaces of the coated specimen after ASTM C633 tensile test are shown in Fig. 6.5. The coating failed at the substrate-coating interface which indicates the adhesion failure. Average bond strength of the coating was found to be 45 MPa.

#### 6.1.3.4 X-Ray Diffraction (XRD) analysis

The XRD patterns of the NiCrAlY-0.4wt%CeO<sub>2</sub> coated superalloys are shown in Fig. 6.6. It mainly comprised of  $\gamma$ - nickel and  $\alpha$ -chromium peaks as dominant phases.

#### 6.1.3.5 FESEM/EDAX analysis

##### 6.1.3.5.1 Surface morphology of the as sprayed coating

FESEM micrographs of NiCrAlY-0.4wt%CeO<sub>2</sub> coatings on all three superalloys in the as sprayed condition are shown in Fig.6.7. The coating contains porosity, partially, semi melted particles, and oxide inclusions. The globular/spherical shaped particles are presumably the unmelted and/or partially melted powder particles. It is noticed that the dark grey colored regions are formed from the powder, which might be fully molten at the time of impact. EDAX analysis has detected oxygen in the microstructure of the coating and it showed that the partially melted regions have a composition similar to feedstock powder whereas partially melted regions have higher oxygen content. Some alloying elements such as Fe, Mn, Si and Ti might have diffused from the substrate into the coating.

##### 6.1.3.5.2 EDAX cross sectional analysis

The cross-sectional images and the corresponding elemental analysis of NiCrAlY-0.4wt%CeO<sub>2</sub> coated superalloys viz. Superni 76 and Superni 750 are shown in Fig. 6.8. It is seen that nickel is predominately present in the coating with chromium and aluminum in small amounts. Nickel rich area is depleted of aluminum. The black areas at the coating-substrate interface are identified as the oxides of aluminum.

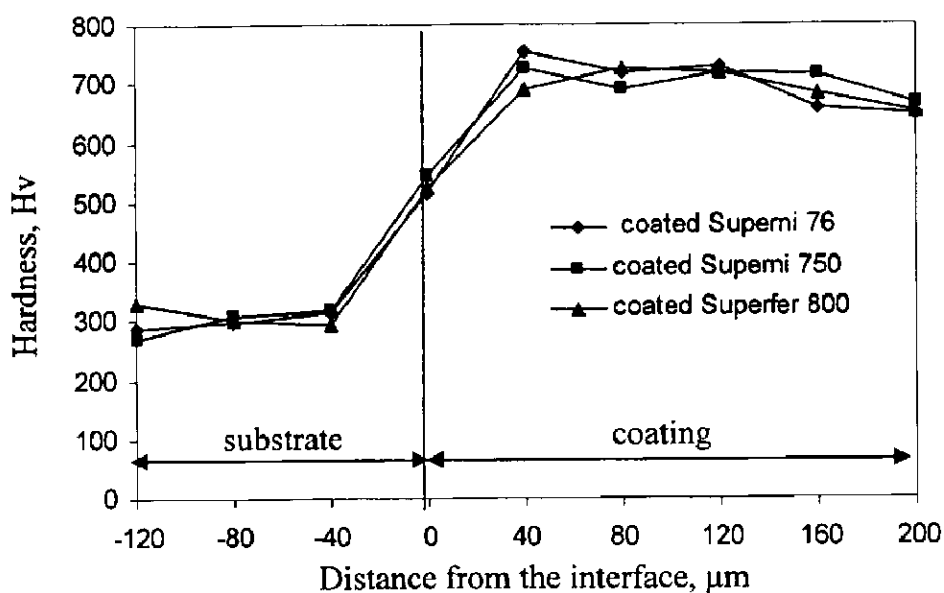


**Fig. 6.4:** Microhardness profiles for HVOF sprayed NiCrAlY-0.4wt% CeO<sub>2</sub> coatings on the superalloys.



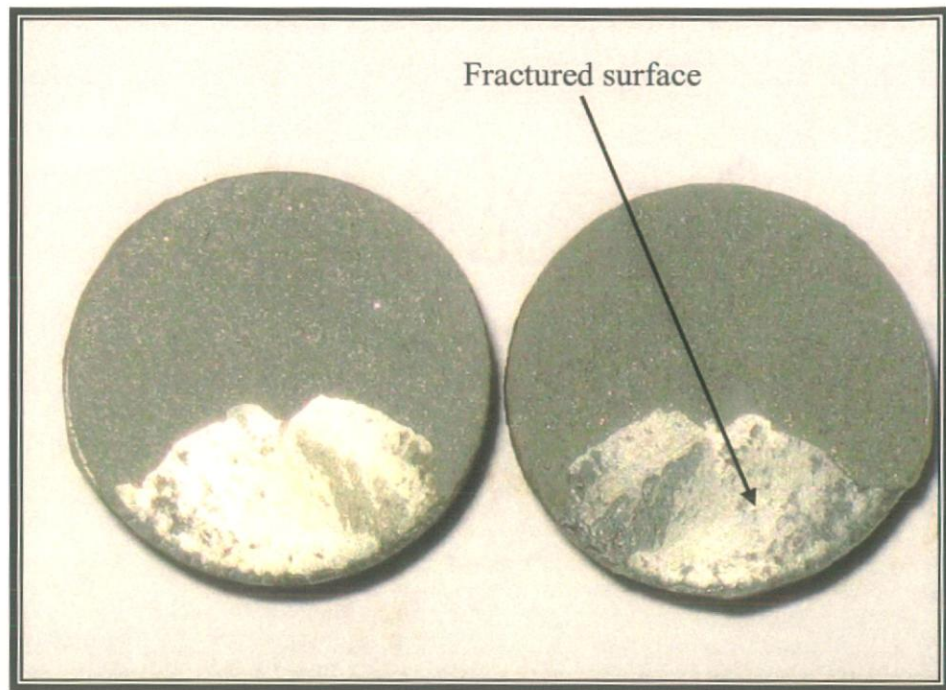


**Fig. 6.5:** Fracture surfaces of a HVOF sprayed NiCrAlY-0.4wt% CeO<sub>2</sub> coated specimen after ASTM C633 tensile test.

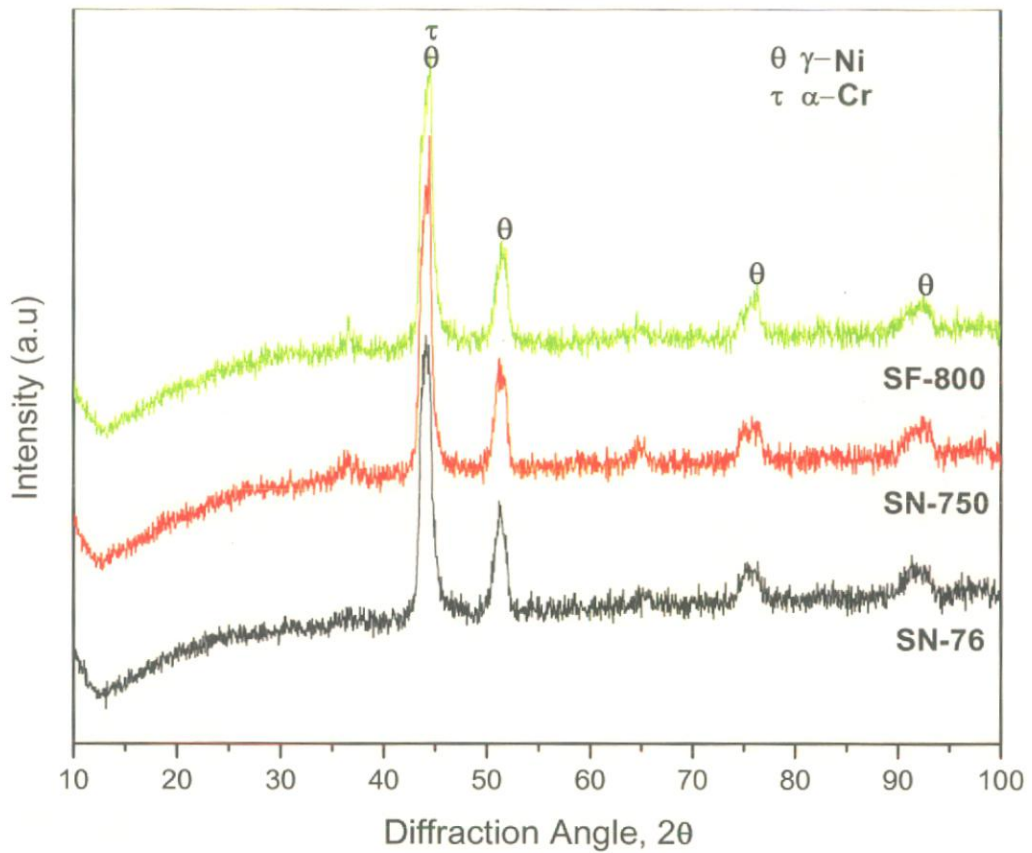


**Fig. 6.6:** XRD diffractograms of HVOF sprayed NiCrAlY-0.4 wt%CeO<sub>2</sub> coating on different superalloy substrates.

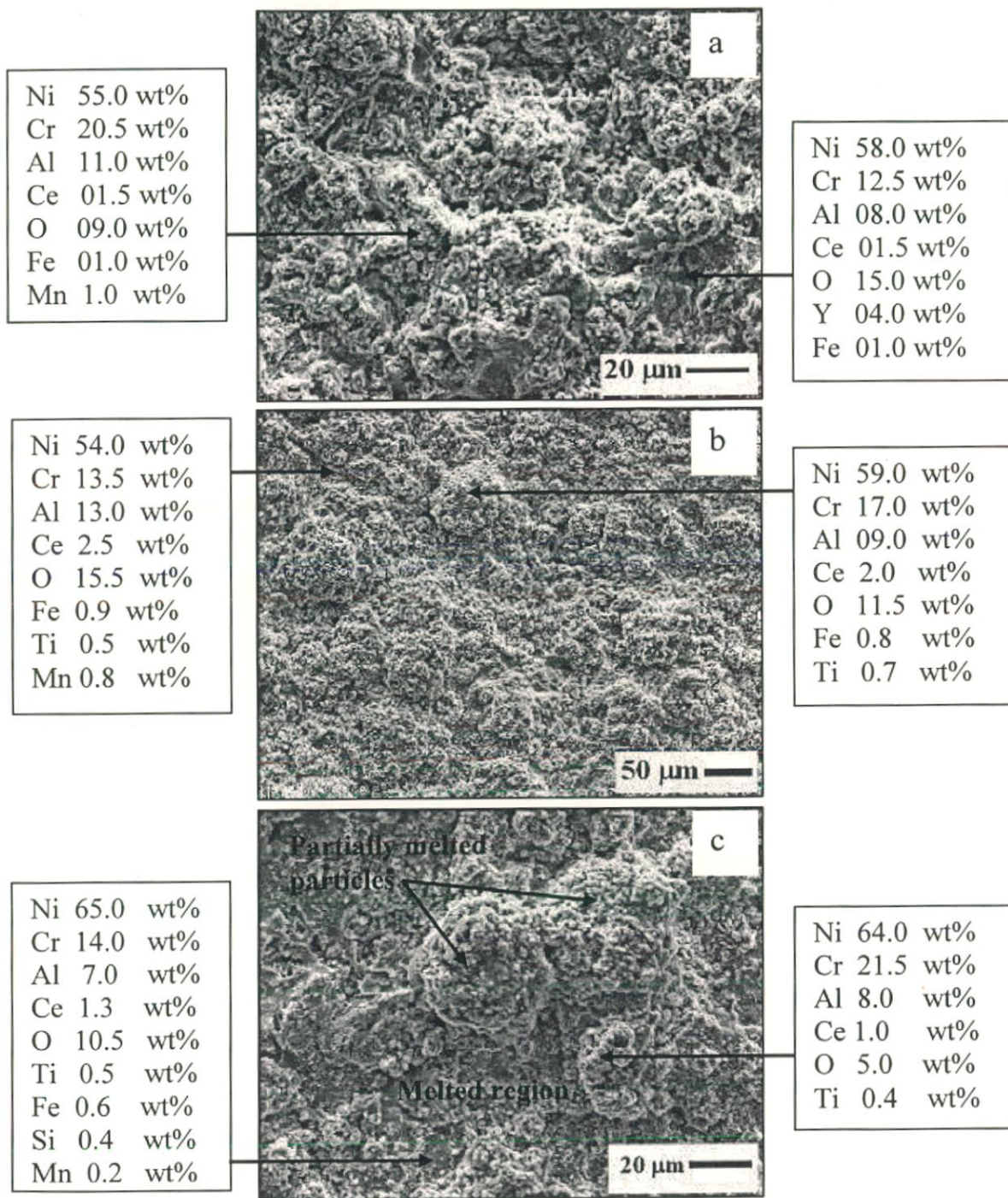


**Fig. 6.7:** FESEM/EDAX analysis of as sprayed NiCrAlY-0.4wt%CeO<sub>2</sub> coating showing surface morphology and elemental composition at different spots on (a) Superni 76, (b) Superni 750 and (c) Superfer 800.

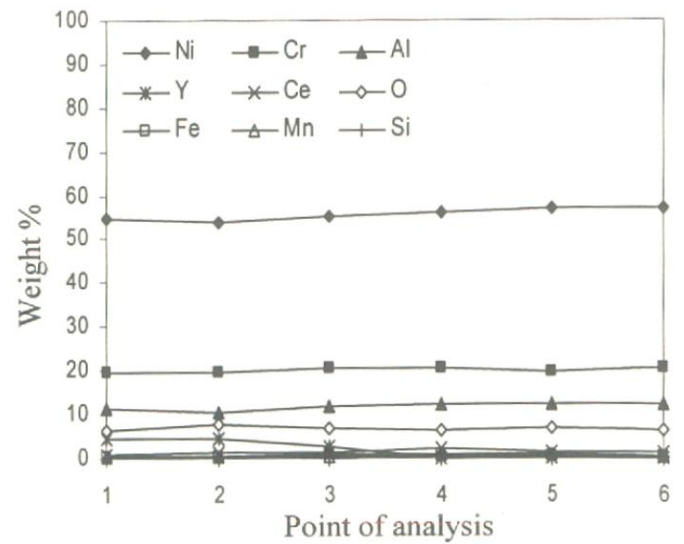
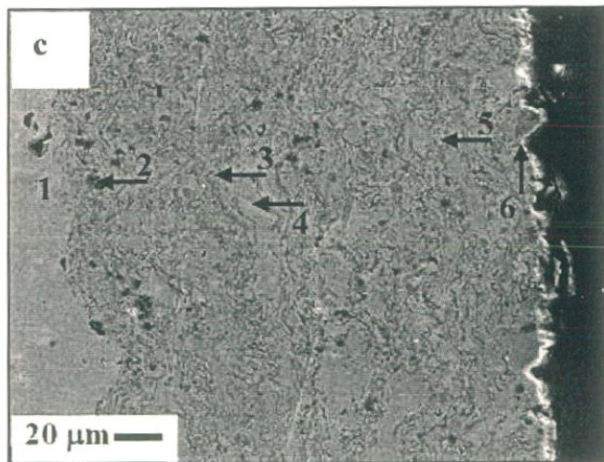
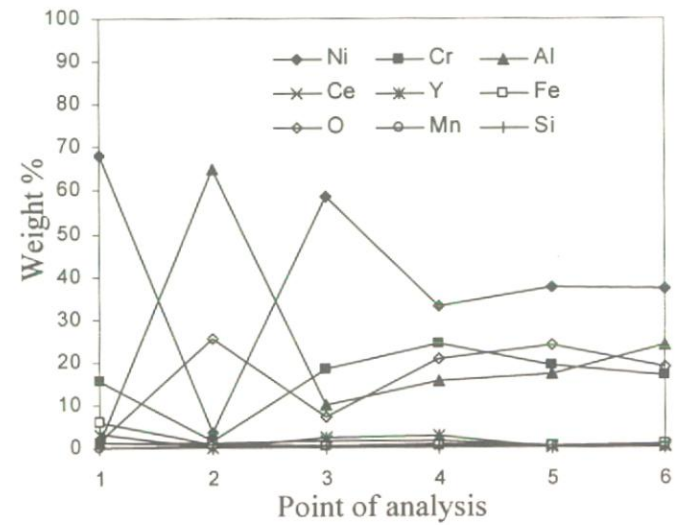
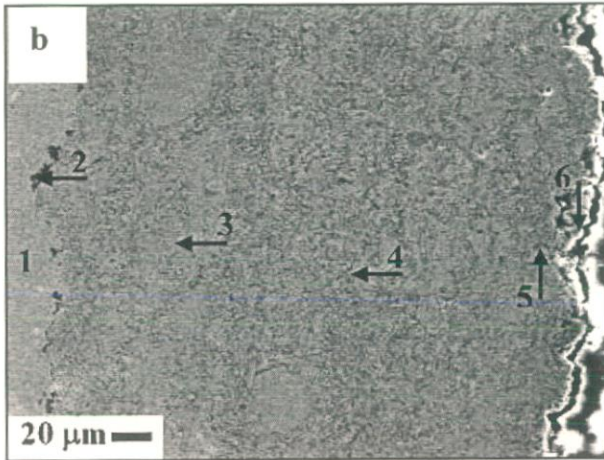
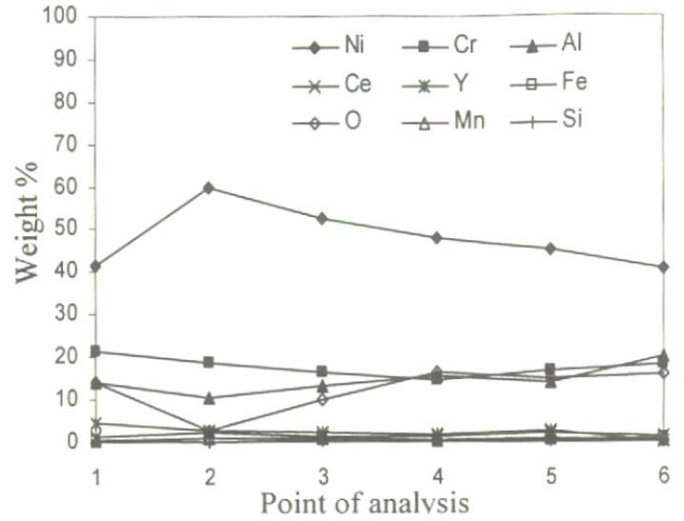
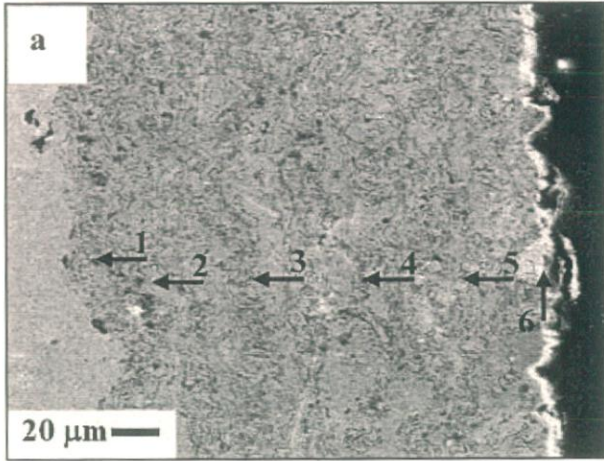


**Fig. 6.8:** Elemental composition across the cross-section of the HVOF sprayed NiCrAlY-0.4wt% CeO<sub>2</sub> coating on (a) Superni 76, (b) Superni 750 and (c) Superfer 800.

### 6.1.3.6 X-ray mapping

X-ray mapping of different elements in the NiCrAlY-0.4wt%CeO<sub>2</sub> coated superalloy samples are shown in Fig.6.9, which illustrate that Ni and Cr are distributed uniformly throughout the coating; whereas, aluminum is existing along the splat boundaries. Oxygen has penetrated upto the coating substrate interface along the intersplat boundaries and existing with Mn, Fe, Y and Ce. Oxygen is absent wherever nickel is present in the coating. Nickel and chromium are found at the location where aluminum is absent. Minor amount of yttrium and cerium are present along the splat boundaries. Iron and manganese have diffused from the substrate into the coating through the intersplat regions during the spraying process.

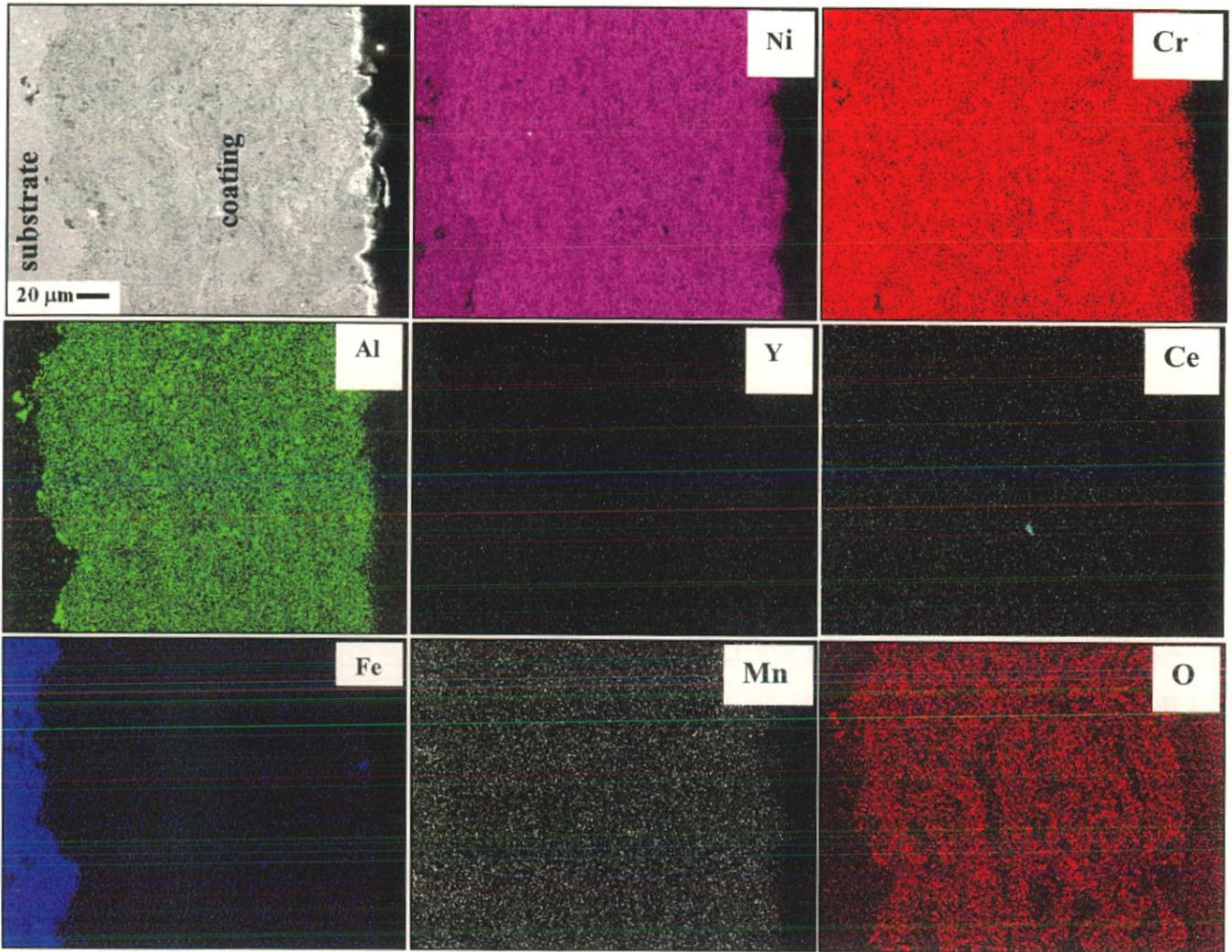


**Fig. 6.9(a):** Compositional image (SEI) and X-ray mapping of the cross-section of the as sprayed NiCrAlY-0.4wt%CeO<sub>2</sub> coating on Superni 76.

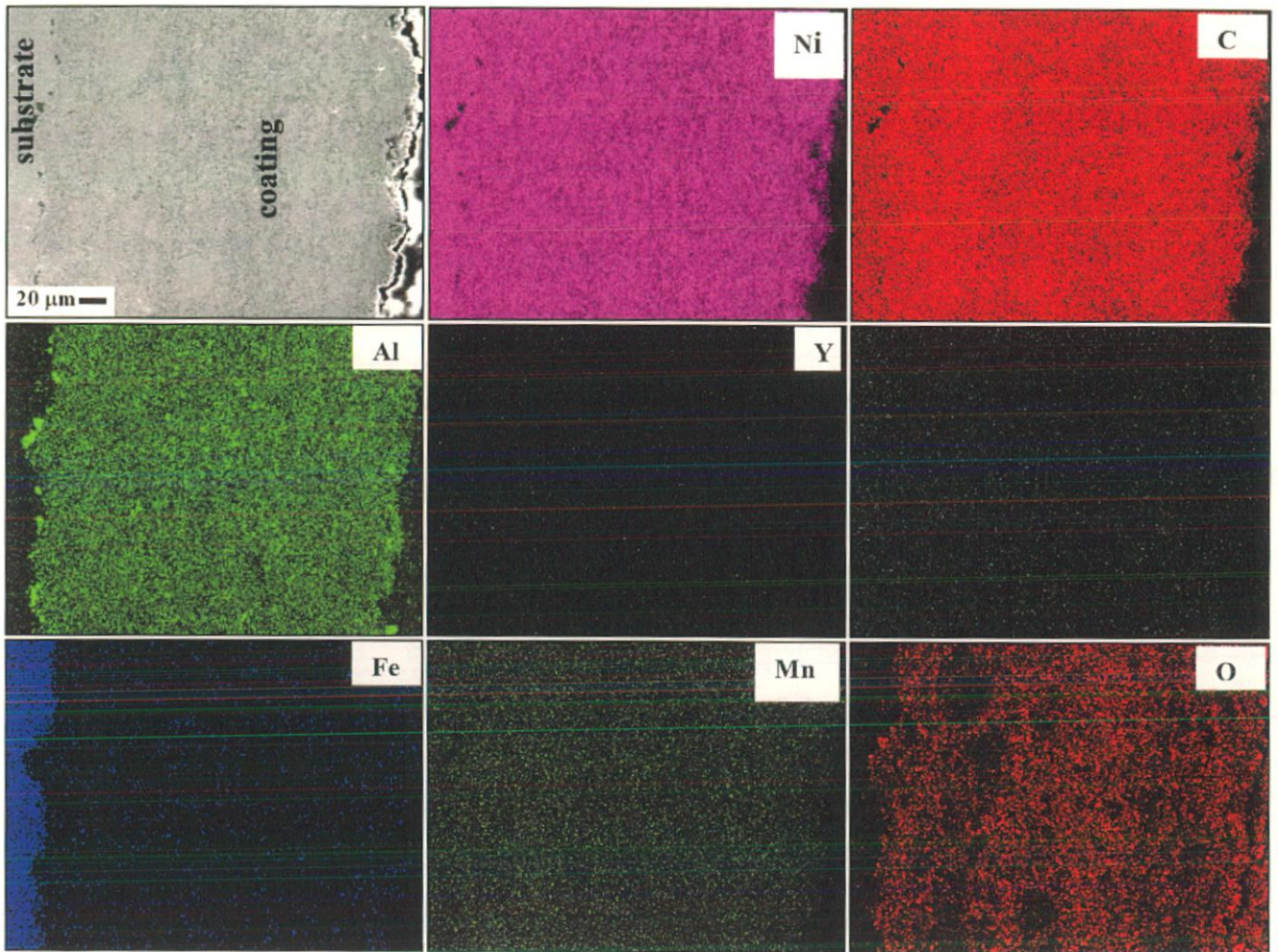


**Fig. 6.9(b):** Compositional image (SEI) and X-ray mapping of the cross-section of the as sprayed NiCrAlY-0.4wt%CeO<sub>2</sub> coating on Superni 750.

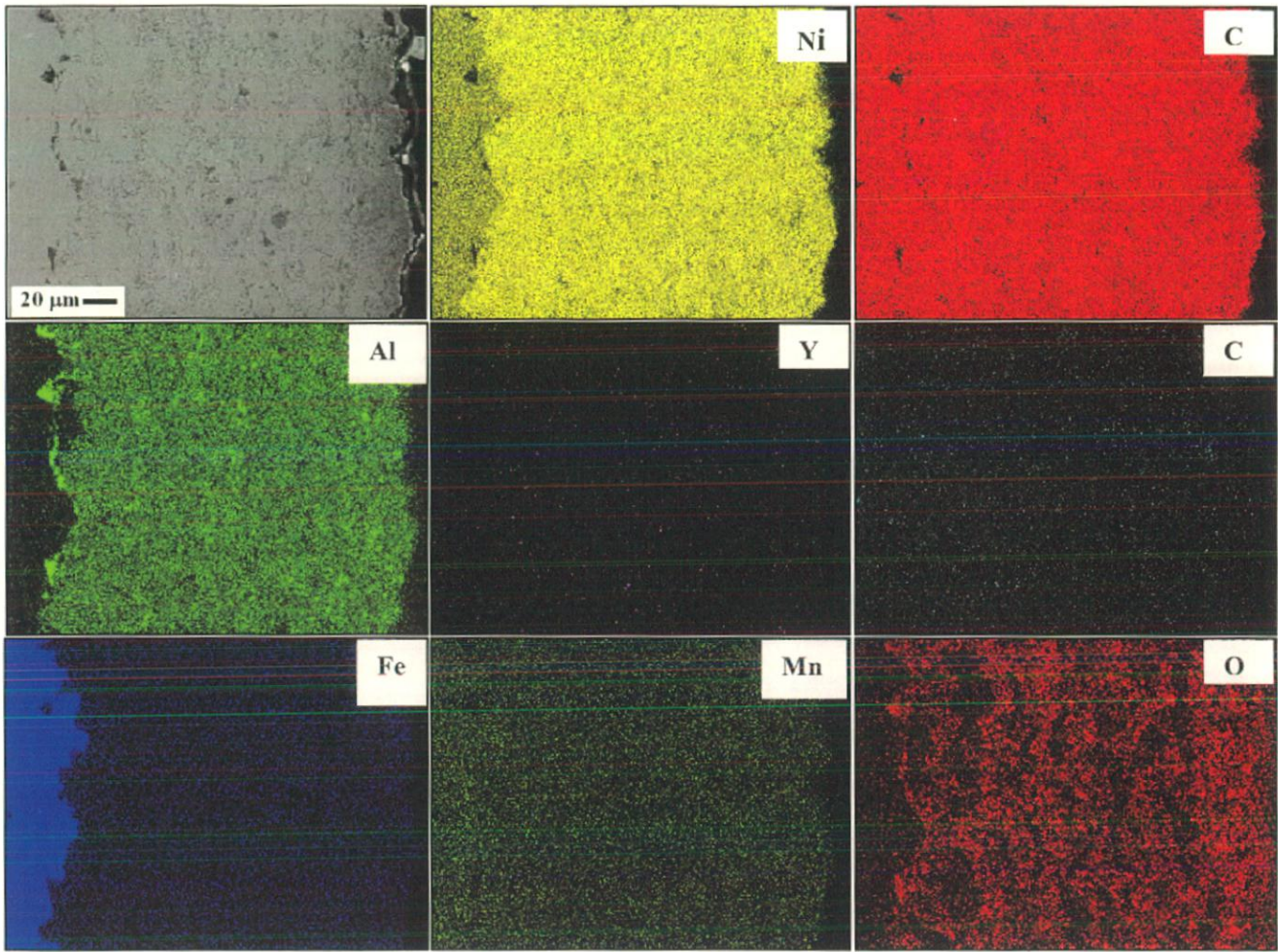


**Fig. 6.9(c):** Compositional image (SEI) and X-ray mapping of the cross-section of the as sprayed NiCrAlY-0.4wt%CeO<sub>2</sub> coating on Superfer 800.

#### 6.1.4 Discussion

NiCrAlY-0.4wt%CeO<sub>2</sub> coating has been successfully obtained by HVOF process on superalloys in the present work. The high velocity and high impact of the sprayed powder particles in the HVOF process produces coatings with very dense structure with very low porosity. The splats obtained were flat in structure (Fig.6.1) with black chunks and half penny shaped areas (Fig.6.2) indicating the oxide phases. Similar findings of formations of oxides in the HVOF coatings have also been reported by Dent et al, (2001) and Sturgeon (2001). The long axis of the impacted splats are oriented parallel to the substrate surface. Lopez et.al, (1998) have reported that in case of powder fed HVOF, the dominant mechanism of oxidation is splat surface oxidation after impact, but in case of wire fed HVOF, it is in-flight oxidation. There have been contradictory reports as to which oxidation mechanism is dominant among the various thermal spray processes.

The porosity of the coating was found to be around 1.4% and it is in tandem with the findings of Aalamialegha et al, (2003), Helali and Hashmi (1992). Sidhu et al, (2006G) and Ak et al, (2003). The coating thickness was measured for all the coated superalloys along the cross section at different locations and the average thickness for Superni 76, Superni 750 and Superfer 800 was 203  $\mu\text{m}$ , 275  $\mu\text{m}$  and 215  $\mu\text{m}$ , respectively. Surface roughness is one of the important parameters of the HVOF sprayed coatings which needs to be evaluated for assessing its performance in the high temperature applications in thermal power plants. The coatings employed on the boiler components are subjected to solid particle erosion and therefore it is essential to ensure the erosion resistance of the coatings with respect to its surface features such as surface roughness, morphology of the grains, etc. The surface roughness values were found to be on the lower side i.e. 4.93-6.58  $\mu\text{m}$ . It may be mentioned that higher surface roughness of the coated component would result in the higher erosion rate. The microhardness values were measured from the interface of the coating as shown in Fig. 6.4. The hardness of the NiCrAlY-0.4wt%CeO<sub>2</sub> coating was around 753 Hv. Harpreet Singh et al, (2005B), have reported lower microhardness values (maximum 373 Hv) for plasma sprayed NiCrAlY coating on Superfer 800 alloy. Mishra et al (2008) have reported a maximum of 552 Hv, 435 Hv for NiCrAlY plasma spray coated Superni 75 and Superni 600 alloys, respectively. Lima and Guilemany (2007) have observed a hardness of 618 Hv for the HVOF sprayed NiCrAlY bond coats on low carbon steel substrates. Belzunce et al, (2001) have reported a lower hardness value of  $433\pm 40$  (HV<sub>300</sub>) for high frequency pulse detonation sprayed NiCrAlY coating on AISI 310 austenitic stainless steel. The higher hardness of ceria



incorporated coatings is perhaps due to refinement of the microstructure and the reduction of inclusion percentage of the coatings as reported in the literature (Wang K L., 2001A; Wang K L., et al, 2001B; Zhang Z., et al, 2006; Tian et al, 2006; Wang K L., et al, 2003).

Tian et al (2006) have reported that during the process of solidification, Ce concentrate at the grain boundaries could recombine with oxygen and other elements to form compounds because of their strong affinity towards oxygen. They further opined that high strain energy in the vicinity of the compounds will be induced due to their large size, which form more effective barriers to grain growth. It is clear that the hardness values are changing across the cross section of the coating with the coating substrate interface. It is believed that the variation in the hardness values of the coating is due to the presence of porosity, oxides, inclusions, unmelted and partially melted powder particles as observed in the microstructure of the coating. Sidhu et al, (2006G) and Ak et al, (2003) have also reported the variation in the hardness of the HVOF sprayed NiCr coating on superalloys and stainless steel. Identical finding was reported by Buta Singh et al, (2004) on the plasma sprayed NiCrAlY bond coat and Ni<sub>3</sub>Al coating on boiler tube steels. The increase in the hardness values of the superalloys substrate near the substrate coating interface perhaps due to work hardening effect of sandblasting of the substrate prior to the coating process as suggested by Sundararajan et al, (2004B). The higher hardness of the substrate near the interface may also be attributed to the high speed impact of coating particles as suggested by Hidalgo et al, (1997; 1998; 1999).

The bond strength is one of most important properties of a thermally sprayed coating. It is generally believed that high velocity of spray particle and an improved melting benefit the adhesion of a coating to substrate (Wang Y.Y., et al, 2006). Recent studies on the adhesion of HVOF sprayed coatings revealed that the bond strength of HVOF coating depends strongly on particle molten state other than particle velocity or temperature (Li and Li, 1998; Li C J., et al, 2000; Li C J., et al, 2001; Li H., et al, 2000). It is reported that the coating strength can be enhanced if droplets penetrate deep into surface cavities of the substrate before they freeze. The coating properties are therefore highly dependent on fluid flow and heat transfer during droplet impact and are affected by both surface roughness and temperature (Pershin et al, 2003). It is noticed that voids created at the coating substrate interface due to splashing and break-up of splats may reduce adhesion (Sobolev et al, 1997). According to Khan et al, (2003), the adhesion of the coating increases with increase of substrate roughness upto certain limits and then decreases due to the increase in the interfacial toughness owing to high compressive stresses associated with the rough surfaces. Lima and Trevisan (1997) found that increasing coating thickness tends to decrease coating

adhesion but also increasing the number of coating layers for the same thickness tends to diminish the coating adhesion due to greater interruption time for the spraying of subsequent layers. The HVOF sprayed NiCrAlY-0.4wt%CeO<sub>2</sub> coatings (Fig. 6.5) on the superalloys failed at the coating-substrate interface and the average bond strength was found to be 45 MPa in the present work. Normally, the HVOF-sprayed coatings tend to exhibit higher bond strength levels than those of atmospheric plasma sprayed (APS) coatings and it is because of higher particle velocities attained by the HVOF-sprayed particles when compared to APS process (Pawłowski, 1995).

The XRD analysis of the HVOF sprayed coating (Fig.6.6) on different superalloys depicts the formation of  $\gamma$ -nickel as a prominent phase with  $\alpha$ -chromium as other phase. The surface morphology (Fig.6.7) of the as sprayed coating indicates that the splats are rich in nickel with chromium and aluminum as other elements. This is further supported by cross sectional EDAX analysis. The dark areas in coating substrate interface as noticed by cross sectional EDAX analysis of the coated samples indicate the oxides of aluminum. It is believed that the some alumina particles might have been retained in the asperities during the grit blasting of the substrate prior to the deposition of the coatings and appeared in the interface as an oxide. The splats are rich in nickel which is presumed to be unoxidised as oxygen is found to be absent or minimum. The presence of oxide stringers in the intersplat boundaries indicates the possible in-flight oxidation of the coating during deposition over the substrate superalloys. This is supplemented by X-ray mapping analysis of different elements across the cross section. It is observed that minor amount of yttrium and cerium is present in the intersplat boundaries with oxygen indicating the possible formation of oxides. Minor diffusion of alloying elements such as iron and manganese has been noticed along the intersplat regions, which eventually got oxidised.

### 6.1.5 Conclusions

1. HVOF spray process has been used to deposit NiCrAlY-0.4wt%CeO<sub>2</sub> coatings (200-275  $\mu\text{m}$  thick) on Ni- and Fe-based superalloys. The coatings exhibited dense and splat like layered morphology with porosity less than 1.5%.
2. The hardness of the coatings was around 753Hv. This higher hardness of the coatings is due to the presence of small percentage of ceria in the coatings. The average bond strength and surface roughness of the coatings were 45 MPa and 4.93 – 6.58  $\mu\text{m}$ , respectively,

3. X-ray diffraction patterns revealed the presence of  $\gamma$ -nickel structure as the dominant phase along with  $\alpha$ -chromium. EDAX analysis of the splat indicated the presence of higher amount of nickel along with small amount of chromium, aluminum and oxygen. EDAX analysis of the as sprayed coating confirmed the formation of required composition of the coating.
4. X-ray mapping indicates that nickel and chromium are coexisting in the splats and aluminum along the splat boundaries. Oxygen has penetrated along the intersplat boundaries and minor amount of alloying elements have diffused into the coating and got oxidised.

## 6.2 OXIDATION STUDIES IN AIR

### 6.2.1 Introduction

The oxidation of metals depends on the rates at which anion and cation transport can occur through the crystal lattice or along the grain boundaries in the oxide (Pomeroy, 2005). The oxidation behavior is characterized by the inward diffusion of species from gaseous environments; the most important one is oxygen. This in turn, causes loss of ductility, which thereby significantly affects the mechanical properties (Mahesh et al, 2007). The oxides formed on iron, nickel or cobalt based alloys are not sufficiently protective above 500°C and are alloyed with chromium, aluminum or silicon to form more protective oxides (scales) of chromia, alumina or silica respectively. The protective oxide scales should be non-volatile, stoichiometric to maintain low ionic transport, stress free at operating high temperatures to reduce scale failure, adherent, free of defects like pores and cracks to prevent short circuit transport of reactants (Ramanathan et al, 2008), homogeneous and stable as possible to constitute a good diffusion barrier (Bonnet et al, 1996). As the interactions of materials with the environment begin at the surfaces, surfaces play a crucial role in many physical phenomena (Krishnan et al, 2006).

Ramanathan et al, (2008) investigated the role of rare earth oxides coatings on oxidation resistance of the chromia forming alloys and shown that the growth rate of chromia has been reduced due to the slow diffusion rate of large sized rare earth ions, which block the outward transport of alloy cations along the scale grain boundaries. In addition to impeding the movements of chromium along the grain boundaries, rare earth ions have minimized the oxide scale grain growth due to its solute drag effect.

The decrease in the oxidation rate and improvement in the adherence of scales are due to prevention of void formation at the alloy-oxide interface and to structure of the scales. The addition of reactive elements also reduces the segregation of impurities at the oxide-alloy interface which otherwise degrades the adherence of oxide scales (Mobin et al, 2002). The adherence of scale is very important in service conditions, where alloys are subjected to thermal cycles of heating and cooling. To improve the adherence of protective oxide scales to the substrates, attempts have largely centered on rare earth effects. It is well known that the presence of small percentage of active elements has a beneficial effect on the properties of these protective scales (Bonnet et al, 1993; Bonnet et al, 1996). It is reported in the literature (Oishi et al, 2000; Rhys-Jones et al, 1987) that the addition of small amounts of reactive

elements to high temperature alloys produces a marked improvement in their oxidation and corrosion resistance under isothermal and cyclic conditions.

DeMasi-Marcin and Gupta (1994) reported that the metallic coating systems used for oxidation resistance are basically designed to form a thin tenacious uniform aluminum oxide layer and acts as a barrier to further oxidation and resultant deterioration of the substrate alloy. The oxidation resistance of high-temperature alloys and metallic coating is dependent on the formation of protective surface oxide. Transport processes in growing scales are of importance primarily because they determine the rate of oxidation, but they also affect the other properties of the scale such as resistance to penetration by aggressive species, stress development, grain growth and creep behavior (Prescott and Graham, 1992).

Little information is available in the open literature on high temperature oxidation behavior of HVOF sprayed NiCrAlY coatings with ceria addition on Ni- and Fe- based superalloys. Degradation by oxidation is one of the main failure modes of hot-section components in gas turbines, so an understanding of the oxidation resistance is very necessary for superalloys (Li M H., et al, 2003). In this present investigation, the high temperature oxidation behaviour of HVOF sprayed NiCrAlY-0.4wt% CeO<sub>2</sub> coatings on Ni- and Fe- based superalloys at 900°C has been studied to assess its performance. It is reported (Sadique et al, 2000) that oxidation under cyclic condition constitutes more realistic approach towards solving metal corrosion problems. The experiment was carried out under cyclic conditions for 100 hours. The oxidised specimens were analysed by various analytical techniques such as XRD, SEM/EDAX and X-ray mapping to characterise the oxide scales. The analysis of transport of various elements occurring from the superalloy substrates into the coating during oxidation is presented to determine their resistance to high temperature oxidation in critical applications.

## **6.2.2 Experimental procedure**

The details of the substrate material, coating formulation and oxidation studies of the coating are explained in section 3.4 and 3.5 of Chapter 3.

## **6.2.3 Results**

### **6.2.3.1 Visual Observation**

Visual examination was carried out after each cycle and changes in colour, luster, adherence-spalling tendency, and cracks in the coatings/oxide scales were recorded. After the completion of 100 cycles (each cycle of 1 hr heating and 20 minutes cooling), the specimens

were examined in detail and their macrographs were taken as shown in Fig 6.10. In all the cases, a green color was observed on the top scale. The scale formed on the surface of the coated specimens were adherent with negligible spalling. Few small cracks were observed along the edges of the specimens.

### 6.2.3.2 Oxidation studies in air

The weight gain per unit area versus number of cycles plots for the bare and coated alloys is depicted in Fig. 6.11. In case of bare alloys, the weight gain is high compared to coated superalloys and the weight gain gradually levels off with the course of the experiment. The square of weight gain per unit area versus number of cycles indicates that the bare alloys slightly deviate from the parabolic rate law, whereas the coated superalloys follow the parabolic rate law as shown in Fig. 6.12. The maximum weight gain ( $\text{mg}/\text{cm}^2$ ) was observed in case of bare Superni 750; whereas, bare Superfer 800 showed a minimum weight gain in the given environment. In case of NiCrAlY-0.4wt%  $\text{CeO}_2$  coated superalloys, Superfer 800 alloy indicated the least weight gain and coated Superni 750 has shown the higher weight gain. The parabolic rate constant  $k_p$  values for the bare and coated superalloy substrates subjected to air oxidation at  $900^\circ\text{C}$  after 100 cycles are shown in Table 6.1. The  $k_p$  values are lower for all coated superalloys as compared to that of bare superalloys thereby indicating better resistance to oxidation in the given environment at  $900^\circ\text{C}$ . Cumulative weight gain/unit area for both bare and coated superalloys is shown in Fig. 6.13.

### 6.2.3.3. X ray diffraction analysis

X-ray diffractograms of oxidised surface of the coated superalloys is shown in Fig. 6.14. X-ray diffraction patterns of the samples were obtained by a Bruker AXS D-8 Advance Diffractometer (Germany) with  $\text{Cu K}_\alpha$  radiation and nickel filter at 30mA under a voltage of 40kV. The specimens were scanned with a scanning speed of  $2^\circ/\text{min}$  in  $2\theta$  range of  $10^\circ$  to  $100^\circ$  and the intensities were recorded. The diffractometer interfaced with Bruker DIFFRAC<sup>plus</sup> X-ray diffraction software provides values directly on the diffraction pattern. These 'd' values were then used for identification of various phases with the help of JCPDS data cards. The oxide phases found on the surface were  $\text{Al}_2\text{O}_3$ ,  $\text{Cr}_2\text{O}_3$ , NiO,  $\text{NiCr}_2\text{O}_4$  and Ni. The presence of Ni indicates the unoxidised state of nickel present in the coatings.

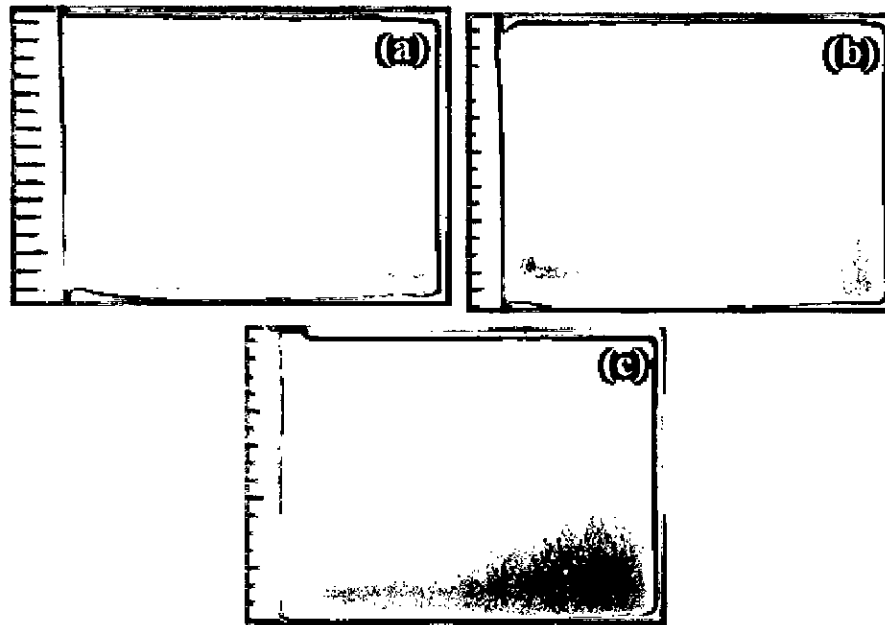


**Fig. 6.10:** Surface photograph of the NiCrAlY-0.4wt% CeO<sub>2</sub> coating oxidised in air at 900°C for 100 cycles for (a) Superni 76, (b) Superni 750 and (c) Superfer 800.

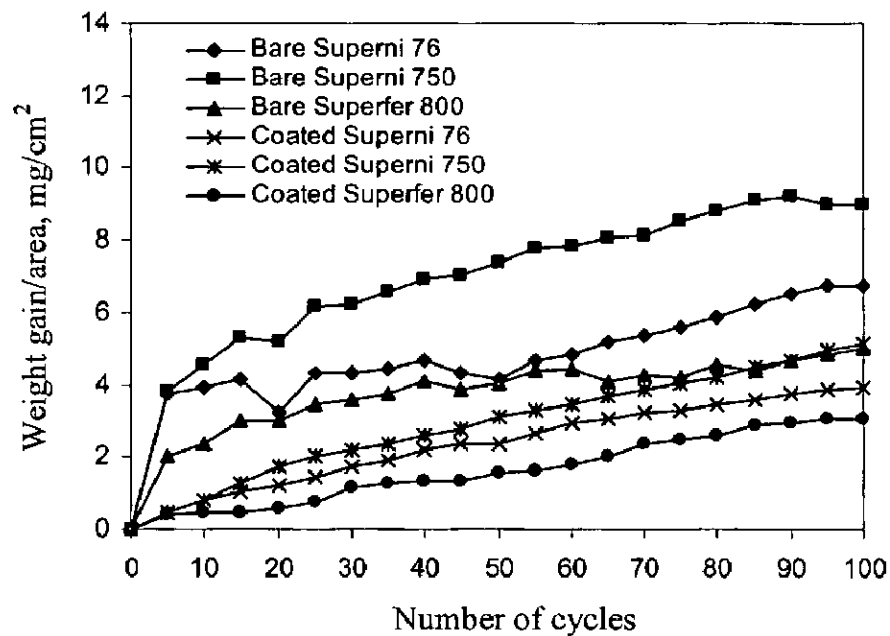


**Fig. 6.11:** Mass gain/area versus. Number of cycles for bare and NiCrAlY-0.4wt%CeO<sub>2</sub> coated superalloys oxidised in air at 900°C for 100 cycles.

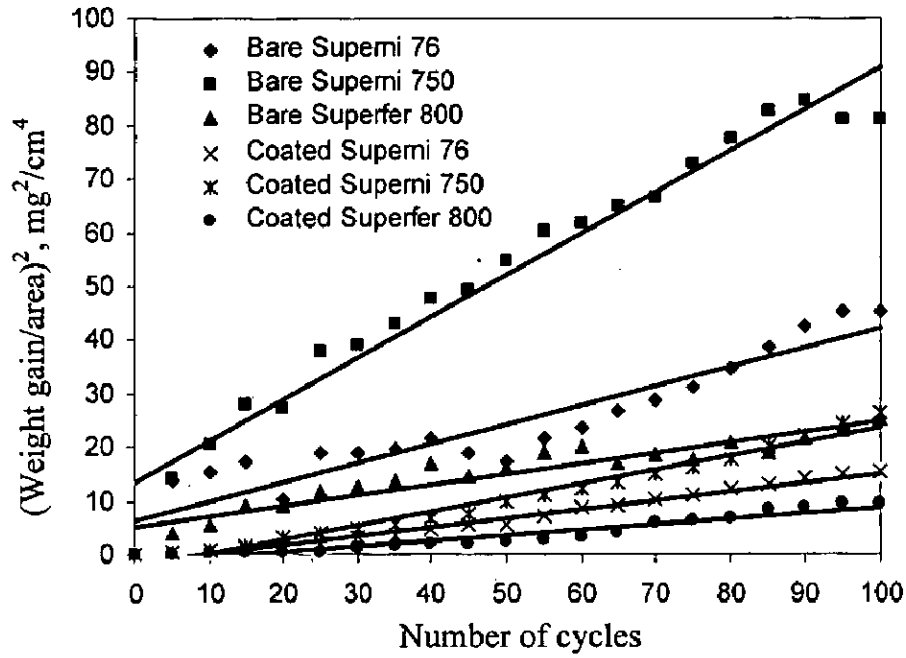


**Fig.6.12:**  $(\text{Mass gain/area})^2$  vs. number of cycles for bare and NiCrAlY-0.4wt%CeO<sub>2</sub> coated superalloys oxidised in air at 900°C for 100 cycles.

**Table 6.1:** Parabolic rate constants of bare and coated superalloys under the similar conditions.

Substrate used	Parabolic rate constant $k_p (10^{-10} \text{g}^2 \text{cm}^{-4} \text{s}^{-1})$
Bare Superni 76	1.0
Bare Superni 750	2.16
Bare Superfer 800	0.55
Coated Superni 76	0.46
Coated Superni 750	0.73
Coated Superfer 800	0.28



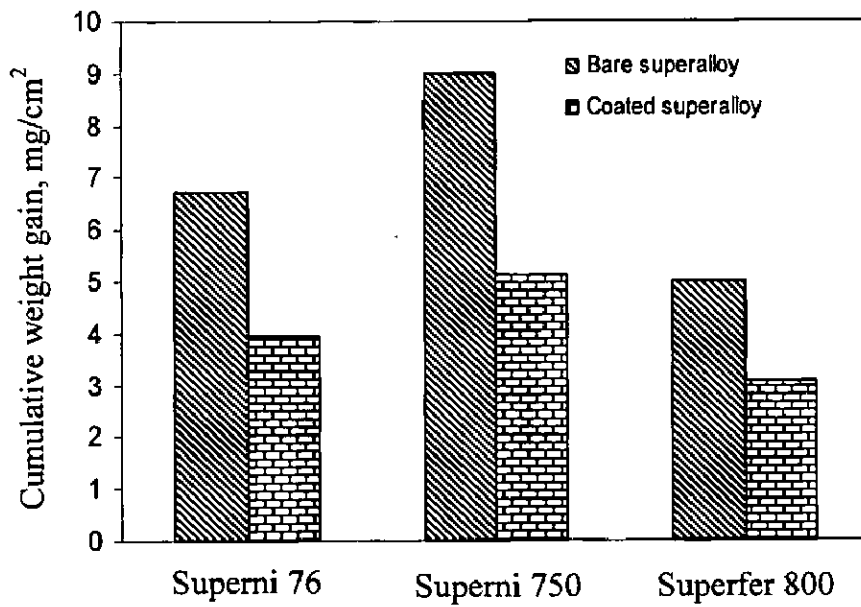


**Fig. 6.13:** Cumulative weight gain per unit area for bare and NiCrAlY-0.4wt%CeO<sub>2</sub> coated superalloys subjected to cyclic oxidation in air at 900°C for 100 cycles.

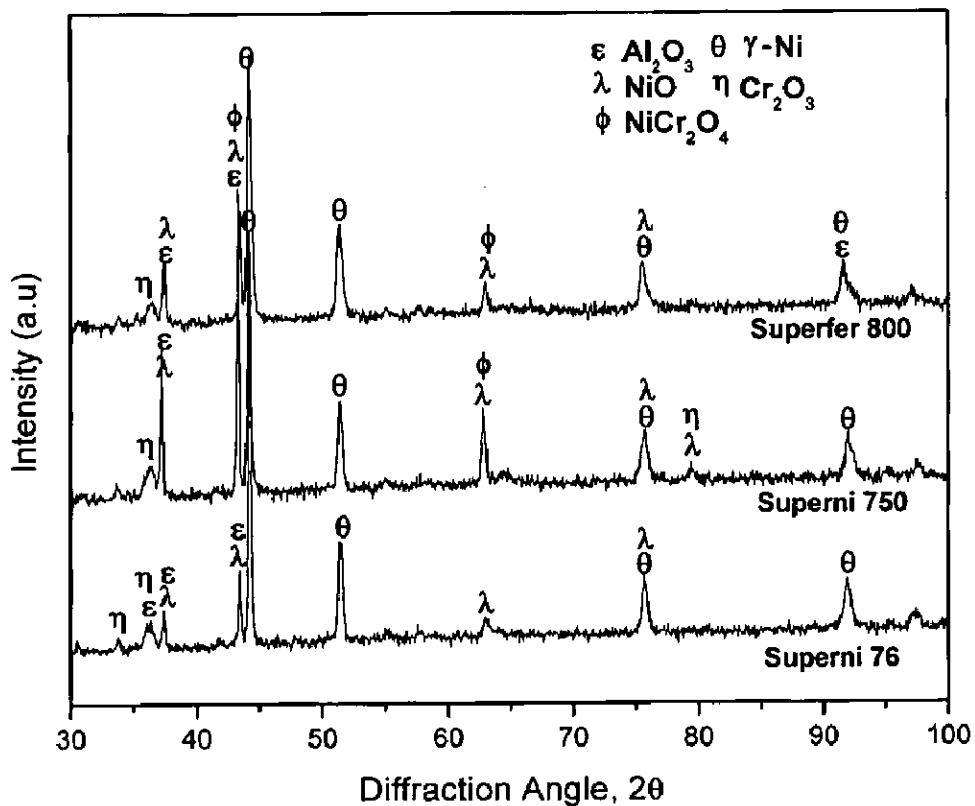


**Fig. 6.14:** X-ray diffraction pattern of NiCrAlY-0.4wt%CeO<sub>2</sub> coated superalloys after oxidation in air for 100 h at 900°C.

## 6.2.3.4 Diffusion of species and reaction products

### 6.2.3.4.1 Surface scale analysis

The FESEM/EDAX micrographs of the surface morphology of the NiCrAlY-0.4wt%CeO<sub>2</sub> coatings oxidised at 900°C under cyclic conditions are shown in Fig.6.15. The scale formed on the coated Superni 76 after oxidation studies indicated the presence of NiO, Cr<sub>2</sub>O<sub>3</sub> and Al<sub>2</sub>O<sub>3</sub>. Small amount of cerium oxide (Ce<sub>2</sub>O<sub>3</sub>) is also formed on the surface of the oxidised scale. Minor amount of manganese oxide and iron oxide have also been detected in the scale thereby indicating the diffusion of these substrate elements into the coating. The oxide scale formed on the surface was adherent and free of cracks. In case of oxidation of coated Superni 750, the surface scale is rich in NiO along with Cr<sub>2</sub>O<sub>3</sub> and Al<sub>2</sub>O<sub>3</sub>. Oxides such as TiO<sub>2</sub>, MnO, and Fe<sub>2</sub>O<sub>3</sub> are also present on the surface of the oxidised samples indicating the transport of elements from the substrate into the coating and their subsequent oxidation. In case of coated Superfer 800, the surface scale consists of NiO, Cr<sub>2</sub>O<sub>3</sub> and Al<sub>2</sub>O<sub>3</sub>. Small amount of alloying elements such as Fe, Mn and Ti have diffused along the splat boundaries and got oxidised.

### 6.2.3.4.2 Cross sectional scale analysis

The oxidised samples were cut across the cross section with slow speed cutting machine (Isomet 1000 precision saw). The samples were then mounted in a transoptic mounting resin, mirror polished and gold coated to study the cross sectional details of the coating using EDAX and X-ray mapping analysis. The EDAX analysis of the coated specimens after oxidation at 900°C is shown in Fig. 6.16. The scale is formed on the surface is adherent with the substrate and without any sign of cracks.

In case of coated Superni 76 (Fig. 6.16a), the top scale (point 1) is rich in nickel, chromium, aluminum along with oxygen. The dark phase around the splat boundaries (point 2 & 3) consists of oxide stringers of chromium and aluminum. It is noticed that the splats formed are elongated and are mainly consisting of nickel (point 4). At point 5, the oxides of nickel, chromium and aluminum have formed. The dark phase (point 6) along the substrate coating interface mainly consists of aluminum along with oxygen. Point 7 indicates that the substrate is rich in nickel along with chromium and iron. Oxygen is almost absent which indicates that the substrate superalloy remained unaffected during the oxidation studies.

In case of coated Superni 750 (Fig. 6.16b), the EDAX analysis indicates the presence of higher weight percent of Ni (point 1) with small amount of oxygen indicating the

partial/unoxidised nickel along with chromium. The dark phase (point 2, 3, 4, & 5) near the splats consists of aluminum, chromium and nickel which are coexisting with oxygen. The dark phase (point 6) near the coating substrate interface indicates the presence of higher amount of aluminum and at point 7, oxygen is not seen in the substrate region.

The EDAX analysis of Superfer 800 (Fig. 6.16c) shows that the top scale (point 1) consists of Ni, Al, Cr along with oxygen reveals the formation of oxides. At point 2, Ni, Cr, and Al coexist along with oxygen. The presence of Al, Ni, and Cr along with oxygen indicates the formation of oxide stringers at point 3. The white phase at point 4 & 5 shows the Ni-rich splats which coexist with chromium and negligible amount of oxygen indicates that the Ni rich splats are unoxidised. The presence of higher amount of aluminum and oxygen at point 6 confirms the formation of aluminum oxide. Absence of oxygen (point 7) shows that the substrate is unaffected and is safe in the given environment.

#### **6.2.3.5 X ray mapping**

The X-ray mapping analysis of the oxidised samples (coated Superni 76 coated Superni 750 and coated Superfer 800) is shown in Fig. 6.17. The splats consist of nickel and chromium. Aluminum is present at the splat boundaries only. The top scale is a combination of oxides of nickel, chromium, aluminum and also spinel of nickel and chromium which is supported by XRD analysis. It is noticed that wherever Ni is present Al is absent. The dark phase at the coating substrate interface indicates the presence of aluminum and oxygen forming aluminum oxide which is supplemented by cross sectional EDAX analysis. The nickel splats are unoxidised indicating the as sprayed nature of the coating, in the intersplat regions; oxygen, chromium, aluminum, manganese and cerium are coexisting indicating the formation of oxides. In case of all coated superalloys, alloying elements like Fe and Mn have diffused from the substrate into the coating along the splat boundaries and got oxidised. Cerium was found in the intersplat regions.

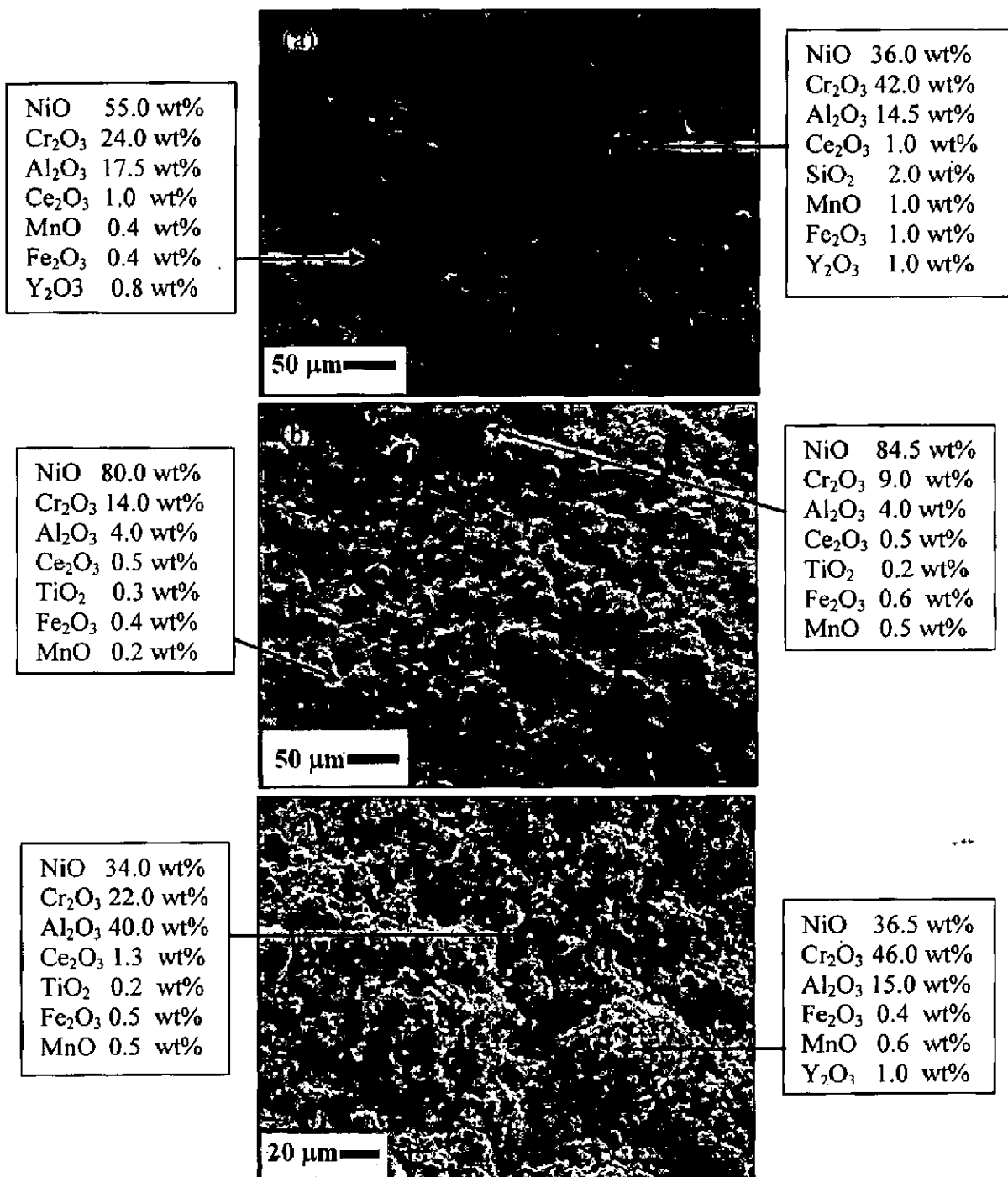


**Fig. 6.15:** Surface-scale morphology and EDAX analysis of NiCrAlYCeO<sub>2</sub> coated (a) Superni 76, (b) Superni 750 and (c) Superfer 800 alloys after oxidation for 100 cycles at 900°C.

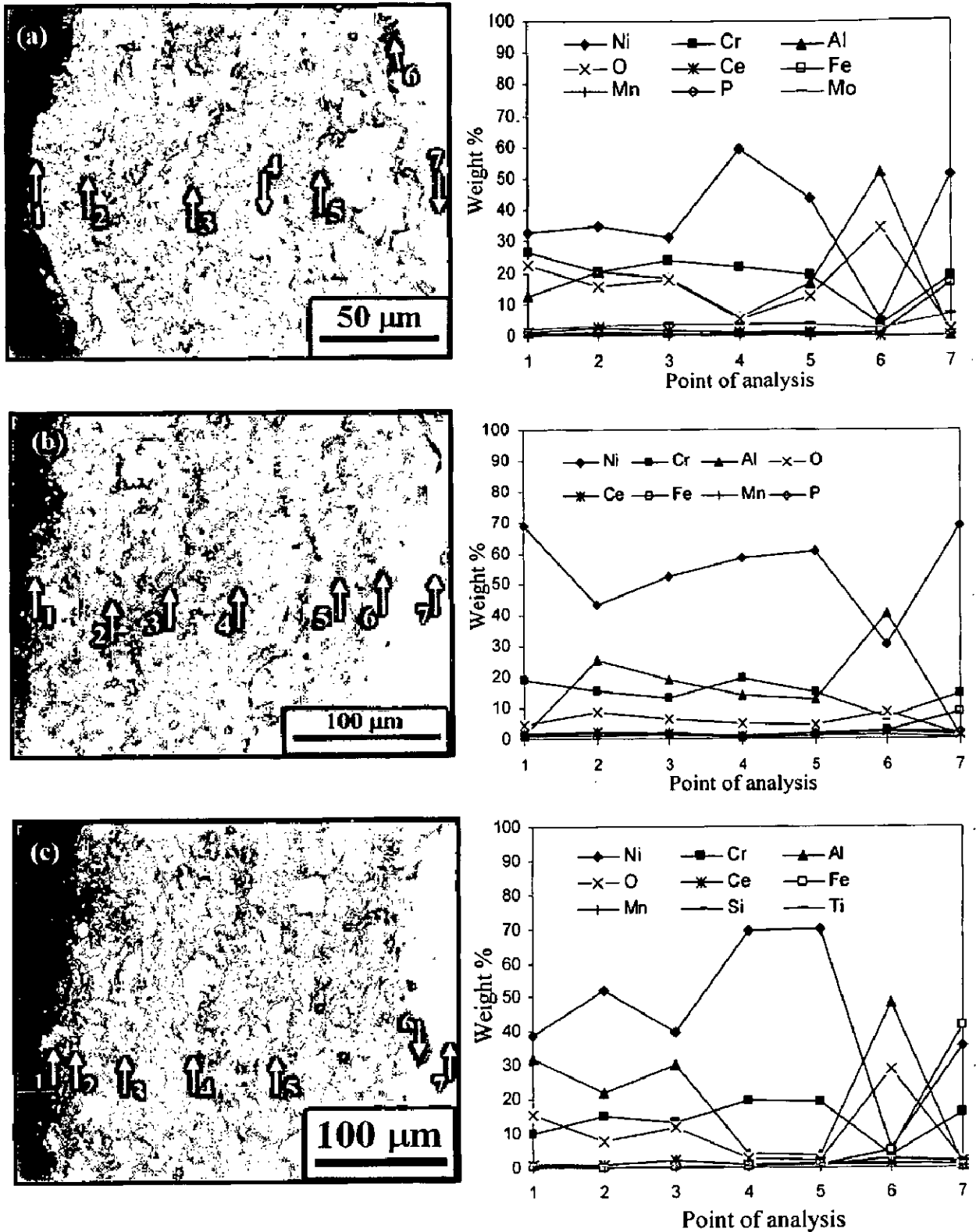


**Fig. 6.16:** Cross sectional morphology and variation of elemental composition across the cross-section of the NiCrAlY-0.4wt% CeO<sub>2</sub> coated (a) Superni 76, (b) Superni 750 and (c) Superfer 800 subjected to the cyclic oxidation at 900°C after 100 cycles.

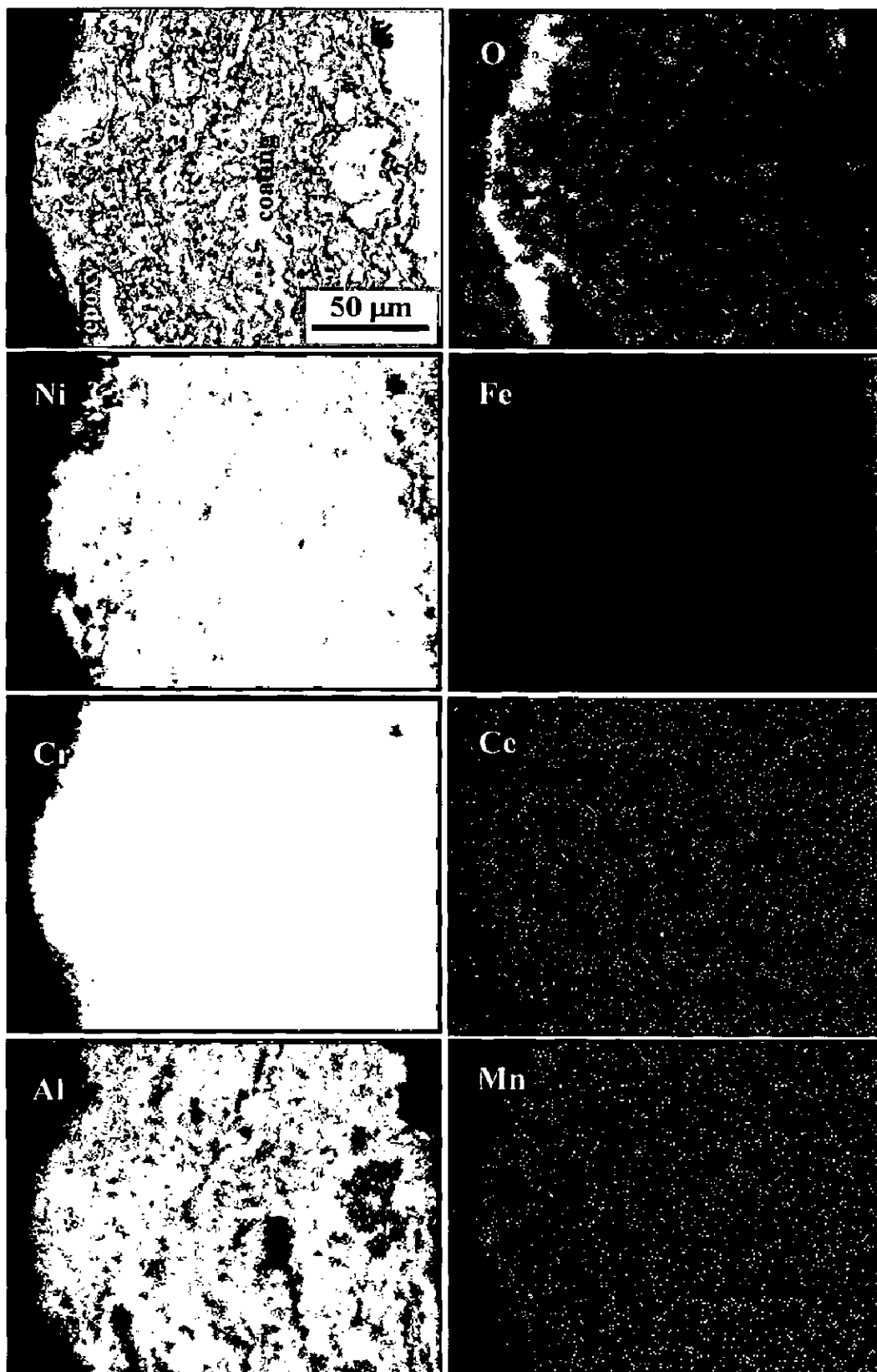


**Fig 6.17(a):** Composition image (SEI) and X-ray mapping of the NiCrAlY-0.4wt%CeO<sub>2</sub> coated Superni 76 subjected to cyclic oxidation in air at 900°C.

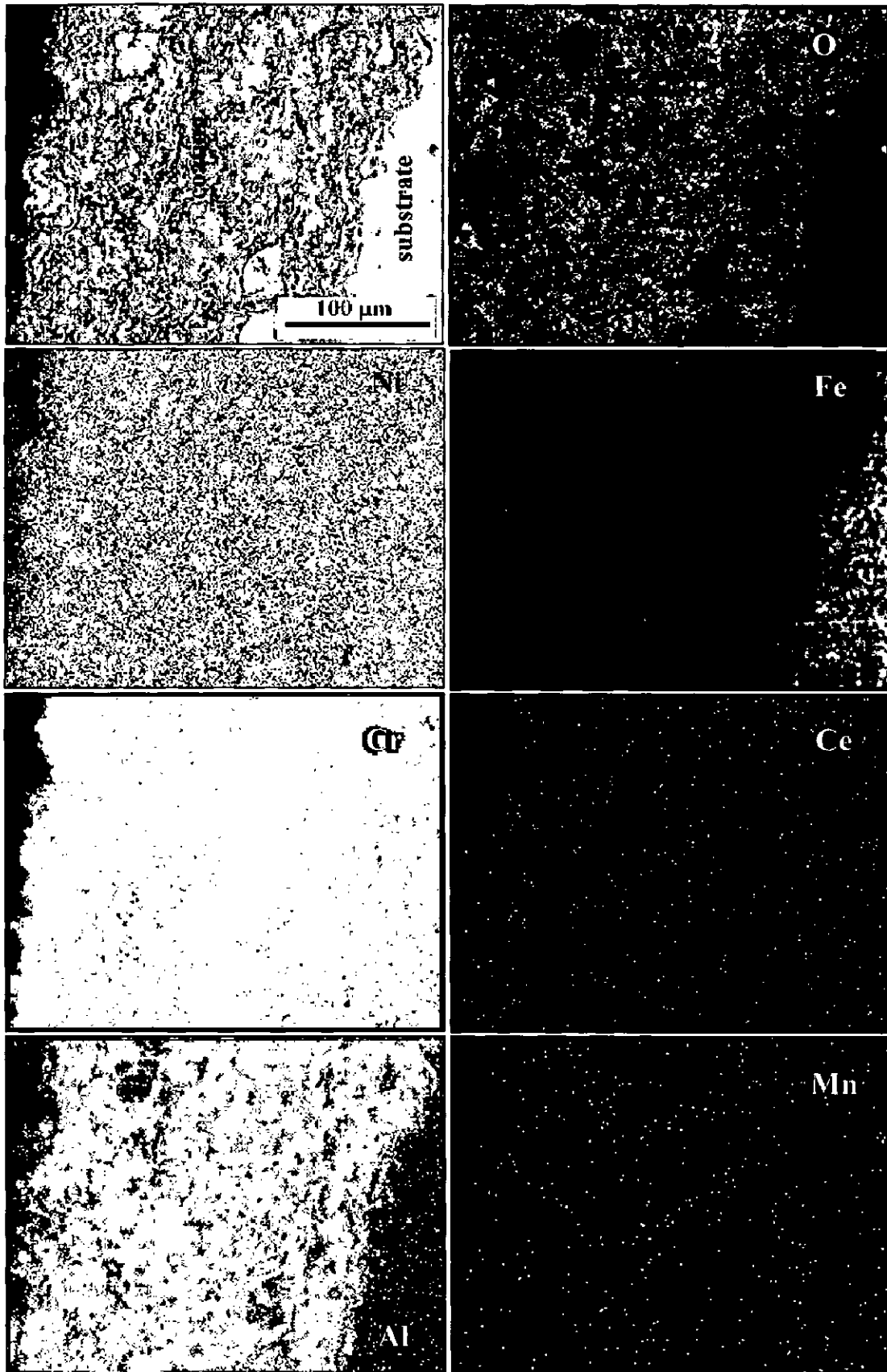


**Fig 6.17(b):** Composition image (SEI) and X-ray mapping of the NiCrAlY-0.4wt%CeO<sub>2</sub> coated Superni 750 subjected to cyclic oxidation in air at 900°C.

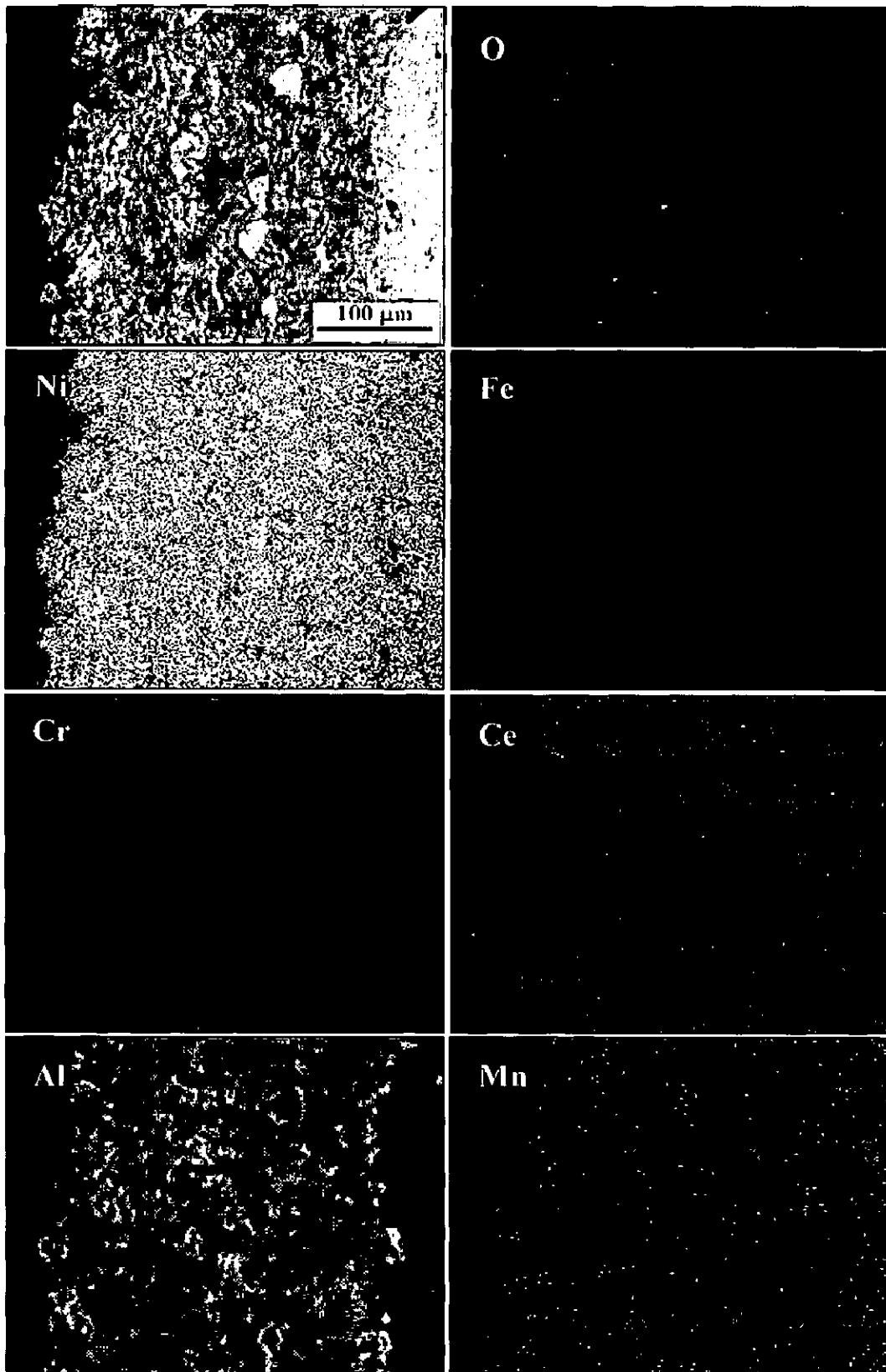


**Fig 6.17(c):** Composition image (SEI) and X-ray mapping of the NiCrAlY-0.4wt%CeO<sub>2</sub> coated Superfer 800 subjected to cyclic oxidation in air at 900°C.



## 6.2.4 Discussion

The NiCrAlY-0.4wt%CeO<sub>2</sub> powder (Fig. 6.1) shows a spherical morphology and ceria is present in the void area. The high temperature oxidation process has followed a diffusion controlled mechanism at 900°C. It is noticed from the visual observation (Fig. 6.10) that the scale formed on the surface of the coating was uniform and free from cracks. The green color of the oxide scale indicates the presence of NiO, which is similar to the findings of Bornstein et al, (1975), Buta Singh (2003), and Mahesh et al, (2008B & 2008C). The weight gain per unit area versus number of cycle is shown in Fig 6.11. In case of bare superalloys, the initial rate of oxidation was high which gradually levels off with the formation of oxide layers. It was clearly seen that the bare superalloys deviated from the parabolic law. Bare Superni 750 showed the maximum weight gain but the minimum was shown by bare Superfer 800. In case of NiCrAlY-0.4wt% CeO<sub>2</sub> coated superalloys, the rapid weight gain of the coated alloys was observed only during initial cycles of oxidation study and it may be attributed to the rapid formation of oxides at the coating-splat boundaries as well as due to the penetration of the oxidizing species along the splat boundaries/open pores. However, the coating subsequently becomes dense and diffusion of oxidizing species into the inner portion of the coating gets slowed down once the oxides are formed at pores and splat boundaries. This would relatively minimize the weight gain and result in the steady state oxidation behavior even with the prolonged exposure time. Zhang Y J., et al, (2002, 2003) have also observed the rapid weight gain during the early stages of oxidation. This supports the fact that partially oxidised coatings acts as a diffusion barrier to the oxidising species. The weight gain per unit area in case of NiCrAlY-0.4wt%CeO<sub>2</sub> coated Superni 76 has reduced to 41% of the bare Superni 76. Further, in case of coated Superni 750 and Superfer 800 alloys, there is a reduction of 43% and 39% weight gain per unit area, respectively.

XRD analysis (Fig. 6.14) of NiCrAlY-0.4wt%CeO<sub>2</sub> coated superalloys oxidised in air at 900°C under cyclic conditions indicates the presence of Ni, NiO and Al<sub>2</sub>O<sub>3</sub> as major phases along with weak phases of Cr<sub>2</sub>O<sub>3</sub>, which is identical to the findings of Zhang Y J., et al, (2002). The formations of these phases are further supplemented by EDAX and X-ray mapping analysis. These oxides are very protective at elevated temperature as reported by Ul-Hamid (2003), Sundararajan et.al, (2004A) and Mahesh et al, (2008D). The presence of Ni indicates the unoxidised state of the nickel rich splats which is further supported by cross sectional EDAX and X-ray mapping analysis. The NiCr<sub>2</sub>O<sub>4</sub> spinel is formed in case of coated Superni 750 and Superfer 800 respectively. According to Zhao S., et al, (2004), NiCr<sub>2</sub>O<sub>4</sub> spinel forms as a results of solid state reaction between NiO and Cr<sub>2</sub>O<sub>3</sub> particles in the scale gradually and forms the external oxide layer.



The formation of spinels on the top scale may further enhance the oxidation resistance due to their much smaller diffusion coefficients of the cations and anions than those in their parent oxides (Chatterjee et al, 2001).

The surface EDAX analysis revealed the presence of cerium oxide in scale in a minor amount. This cerium oxide helps in better adhesion of the oxide scale with the coating when exposed at 900°C. Top scale consists of mainly NiO and with Al<sub>2</sub>O<sub>3</sub> and Cr<sub>2</sub>O<sub>3</sub>. The top surface of the scale consists of oxides of aluminum, chromium and nickel. It is noticed from the X-ray mapping analysis that the coating is partially oxidised and oxygen has not penetrated into the substrate superalloys. This indicates the protective nature of the coating in the given environment at elevated temperature. The formation of cerium oxide along the intersplat regions in the top surface of the scale and in the cross section might have attributed to the better adhesion of the oxide scale to the coating and thus enhanced the performance of the coating at elevated temperature. The oxides of aluminum and chromium have formed along the splat boundaries in all the cases and might have clogged the diffusion of the oxidising species into the substrate superalloy. Transport of some alloying elements has been observed from the substrate into the coating which is also supplemented by the X-ray mapping analysis. Presence of oxides of Fe, Mn and Ti on the top surface of the scale and along the intersplat boundaries indicates diffusion of these elements from the substrate into the coating. The compositional gradient may be the driving force for the transport of alloying elements from the substrate into coatings. The probable oxidation mechanism for the NiCrAlY-0.4wt%CeO<sub>2</sub> coated Superni 750 exposed to air at 900°C for 100 cycles is shown in Fig. 6.18.

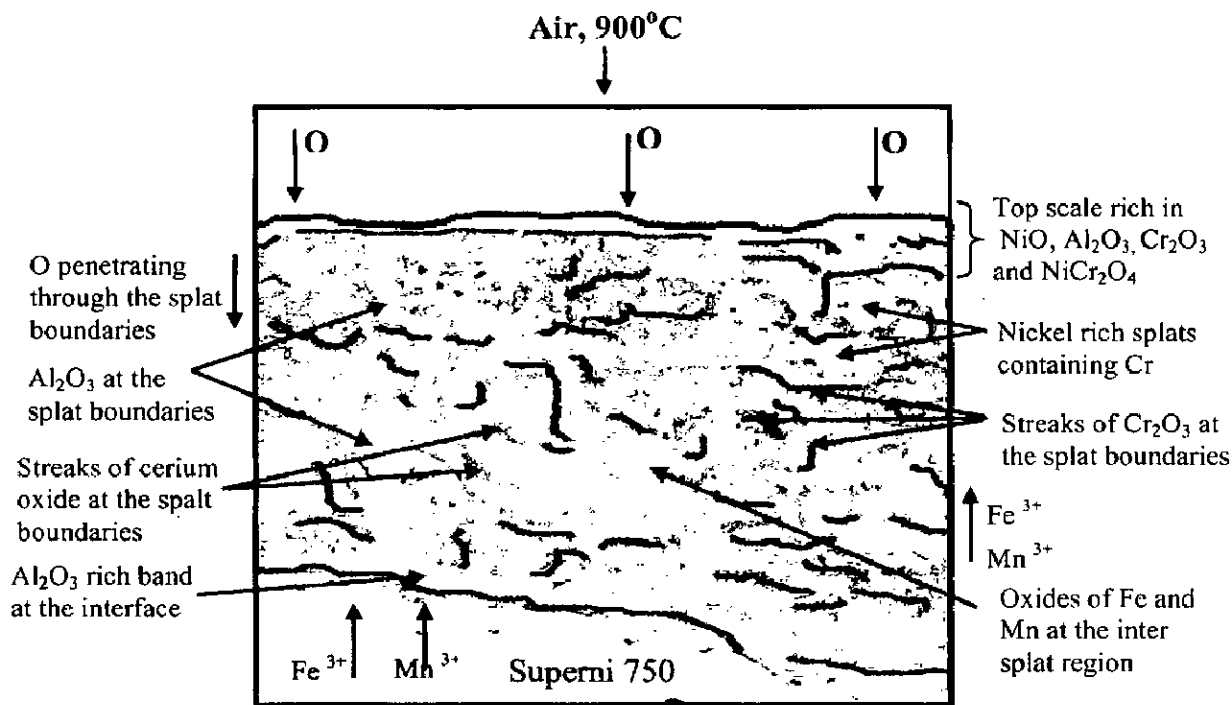


**Fig. 6.18:** Schematic diagram showing probable oxidation mechanism for the NiCrAlY-0.4wt%CeO<sub>2</sub> coated Superni 750 exposed to air at 900°C for 100 cycles.

## 6.2.5 Conclusions

The high temperature oxidation behavior of HVOF sprayed NiCrAlY-0.4wt%CeO<sub>2</sub> coating on Ni- and Fe-based superalloys have been studied and the following conclusions are made.

1. The HVOF spraying process is used successfully used to deposit the NiCrAlY-0.4wt%CeO<sub>2</sub> using LPG as a fuel gas on Ni- and Fe- based superalloys. The scale formed on the surface of the coating is intact without any sign of cracks. There is only superficial microspalling of the scale during the course of the study.
2. The weight gain of the coated superalloys is less compared to that of the bare superalloys. NiCrAlY-0.4wt%CeO<sub>2</sub> coatings lead to a reduction in weight of about 41% in case of Superni 76, whereas 43% and 39% for Superni 750 and Superfer 800 respectively.
3. The NiCrAlY-0.4wt%CeO<sub>2</sub> coated superalloys followed the parabolic rate law after exposing at 900°C for 100 cycles. In case of bare superalloys, deviations from parabolic rate law are observed.
4. The scales formed on the surface of the coating after 100 cycles of exposure to consist of mainly oxides of chromium, aluminum, nickel and spinel of nickel and chromium. Oxides of iron, manganese and titanium are also present in the surface scale in smaller amounts. It must have formed by the diffusion of these elements from the substrate to the top scale through the intersplat regions in the initial stages.
5. The formation of aluminum oxide, chromium oxide, nickel oxide and spinel of nickel and chromium has provided better protection to the substrate superalloys. The formations of these oxides are confirmed by XRD, SEM/EDS and X-ray mapping analysis. The presence of cerium oxide in the oxide scale might have helped the scale to be intact with the coatings as revealed by EDAX and X-ray mapping analysis.

## 6.3 HOT CORROSION STUDIES IN MOLTEN SALT ENVIRONMENT

### 6.3.1 Introduction

It is well known in the literature (Wood, 1970) that the addition of small amounts of reactive metals to high temperature alloys produces a marked improvement in their oxidation and corrosion resistance under isothermal and cyclic conditions. Cerium and lanthanum, as rare earth (RE) elements, have been applied successfully both in steel and for the chemical heat treatment of steel (Wang K L., et al, 2001B). The usage of Ce and La are increasing in several fields of surface engineering such as flame spraying, diffusion heat treatment, electric plating. A minor addition of rare earth elements (REEs) has decreased the oxidation rate of chromia forming alloys and improved the adhesion strength of oxide scales as reported in the literature (Mitra et al, 1993; Landkof et al, 1985; Roure et al, 1994). Seybolt (1971) studied the role of rare earth additions on the hot corrosion behavior of various Ni based alloys in liquid  $\text{Na}_2\text{SO}_4$  in still air at  $1000^\circ\text{C}$ . He has concluded that the rate of hot corrosion attack is reduced by the addition of rare earth and apparently reduced the various sulphides formed. Further, it was observed that rare earth addition in the form of oxides are very effective in minimizing the hot corrosion as it forms oxysulfides by combining with sulphur. The rare earth additions to Ni-base alloys, in particular cerium, lanthanum and gadolinium, in fractional wt. % amounts, has considerably reduced the extent of hot corrosion attack. Wang K L., et al, (2001B) have investigated the effects of rare earth oxides  $\text{CeO}_2$  and  $\text{La}_2\text{O}_3$  on the microstructure and hot corrosion resistance of laser clad nickel based alloy coatings on steel substrate in different corrosive solutions. It was reported that RE addition in the alloys resulted in the microstructural refinement, decreased inclusion percentage, and improved corrosion resistance of the coatings in the given medium. The oxidation behavior of arc ion plated NiCrAlY coating on Ni-based superalloy was studied at the temperature 900 and  $1000^\circ\text{C}$  and reported that the coating gained more weight under cyclic condition than isothermal oxidation (Wang B., et al, 2002; Wang B., et al, 2003). According to them, the oxidation resistance of the coated alloys has improved significantly compared to that of the bare alloys and the oxide scales such as  $\alpha\text{-Al}_2\text{O}_3$  and  $\text{Cr}_2\text{O}_3$  were formed at  $900^\circ\text{C}$ . Huang et al, (2006) studied the effect of rhenium addition on the oxidation resistance of NiCrAlY coatings on the superalloy and observed that the long-term oxidation resistance of the coatings has improved due to its influence on the increased stability of  $\alpha\text{-Cr}$  in the coating during oxidation. Due to the similar CTE values of  $\alpha\text{-Cr}$  and  $\text{Al}_2\text{O}_3$ -rich scale, the induced thermal stress is very less and therefore scale adhesion was observed on the coatings. The hot

corrosion behavior HVOF, atmospheric plasma (APS), and high frequency pulse detonation (HFPD) sprayed NiCrAlY coatings deposited on metallic substrates was investigated and found that the depletion of Al is heavily consumed during interparticle oxidation especially for the APS sprayed coatings (Mayoral et al, 2008). The depletion of Al has involved intrinsic chemical failure and the surface layer is comprised mainly of porous spinel of mixed oxides. The fused salt has also hindered the formation of protective thermally grown surface alumina layer. However, HVOF and HFPD techniques have produced dense coatings and suffered a lesser extent of internal oxidation with less Al consumption in the coatings. Gitanjaly (2003) has reported that, superficial application of ceria on Fe- and Ni- based superalloys lead to the marked reduction in oxidation rate under aggressive environment of molten salt at 900°C. She reported that presence of CeO<sub>2</sub> on the surface led to the possible formation of CeVO<sub>4</sub>, which may be contributing to the reduction in the corrosion attack, as CeVO<sub>4</sub> is solid at the reaction temperature of 900°C.

There is no reported study so far on the high temperature oxidation behaviour of NiCrAlY coatings with rare earth (cerium oxide) addition on superalloys in aggressive environment of molten salt under cyclic conditions. Therefore, the present work has been focused at evaluating the hot corrosion performance of cerium oxide added NiCrAlY HVOF sprayed coatings in a simulated environment of boilers. The hot corrosion experiments were conducted under cyclic conditions as it constitute a very realistic approach towards solving the problem of metal corrosion in actual applications, where cyclic rather than isothermal conditions prevail (Sadique et al, 2000).

### **6.3.2. Experimental Procedure**

The substrate materials, coating formulation and the hot corrosion studies are explained in detail in section 3.4.3 and 3.5 of Chapter 3.

### **6.3.3. Results**

#### **6.3.3.1 Visual observation**

Bare Superni 76 alloy, as shown in Fig. 6.19(a), has started spalling after the completion of 2nd cycle during the hot corrosion experiments. The scale formed on the surface of the alloy was brownish grey in color, which subsequently turned dark in color with the course of the experiment. Little sputtering was observed after 21 cycles and some cracks were seen on the oxide scale. The spalled scale was included in the boat during the mass

change measurements. In case of bare Superni 750 alloy, Fig. 6.19(b), the scale formed on the surface was brown in color as observed during the thermogravimetric analysis after 2nd cycle, which turned into dark brown after subsequent cycles. The scale started spalling after the completion of 7th cycle and the surface scale started cracking. The spalled scale was included in the boat during the weight change measurements. In case of bare Superfer 800 alloy, Fig. 6.19(c), brown color was observed after the 2nd cycle, which turned dark during the study. The spallation of the scale has started after 10th cycle and it was accounted during the mass change measurements.

The HVOF sprayed NiCrAlY with cerium oxide coated Superni 76 alloy indicated a grey scale with some light green patches and few cracks at the edges or near the corners when subjected to oxidation for 100 cycles in molten salt environment (40%Na<sub>2</sub>SO<sub>4</sub>-60%V<sub>2</sub>O<sub>5</sub>) at 900°C. In case of coated Superni 750 alloy, green patches were seen with grey colored scale in the background on the surface. The green colored scale was observed on the surface in case of coated Superfer 800 alloy. Overall, the scale was smooth with minor cracks along or near the edges of the samples. The scale showed a little tendency of microspalling in the form of fine powder. However, the scale showed a good adherence with the superalloys during the course of the hot corrosion studies.

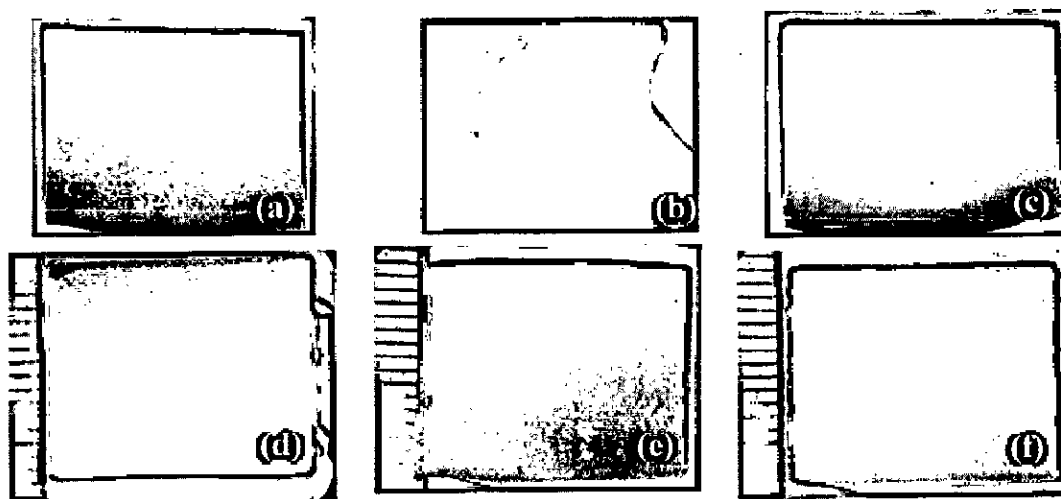


**Fig 6.19:** Surface macrographs of bare Superni 76 (a), Superni 750 (b), Superfer 800 (c) and NiCrAlY-0.4wt%CeO<sub>2</sub> coated Superni 76 (d), Superni 750 (e) and Superni 800 (f) after 100 cycles in 40%Na<sub>2</sub>SO<sub>4</sub>-60%V<sub>2</sub>O<sub>5</sub> environment at 900°C.

### 6.3.3.2 Thermogravimetric studies

The weight change ( $\text{mg}/\text{cm}^2$ ) variation as a function of time expressed in number of cycles for the bare and ceria added NiCrAlY coating on superalloys are shown in Fig 6.20. It shows that the bare superalloys underwent higher weight gain during the exposure periods in the molten salt environment. The bare Superni 76 alloy has showed a maximum weight gain. The cumulative weight gain at the end of 100 cycles for the bare superalloys i.e. Superni 76, Superni 750 and Superfer 800 has been found to be 34.61, 32.93 and 28.35  $\text{mg}/\text{cm}^2$ , respectively. However, in case of ceria added NiCrAlY coated superalloys, the cumulative weight gain at the end of 100 cycles for Superni 76, Superni 750 and Superfer 800 was found to be 7.6, 5.35 and 3.2  $\text{mg}/\text{cm}^2$  respectively. It can be inferred from the weight gain plots that the coated superalloys show the tendency to approach a gradual weight gain after the initial accelerated weight gain under cyclic conditions. The oxidation kinetics of bare superalloys showed a deviation from the parabolic rate law. In case of bare Superni 76 alloy, the weight gain was high during initial period and an oxide layer has formed on the surface during the course of exposure to the molten salt environment. Furthermore, the scale got cracked and spalled after 21<sup>st</sup> cycle and again a fresh surface was exposed to the given environment, thus increasing the weight gain. This was clearly observed from Fig 6.19(a) and Fig 6.20. The same was observed for other two superalloys. Fig. 6.21 shows the  $(\text{weight gain}/\text{area})^2$  versus number of cycles for uncoated and coated superalloys. It is clearly noticed that the coated superalloys followed the parabolic rate law through out the total period of exposure, whereas the uncoated deviated from the parabolic rate law. The values of parabolic rate constants for both bare and coated superalloys are given the Table 6.2. The bar chart showing the cumulative weight gain of the bare and coated samples is shown in Fig. 6.22.

### 6.3.3.3 XRD analysis of the powder and the scale

The XRD pattern of corroded coated superalloy samples after 100 cycles is shown in Fig. 6.23. It is observed that  $\text{NiCr}_2\text{O}_4$ ,  $\text{NiO}$ ,  $\text{Al}_2\text{O}_3$ , and  $\text{CrS}$  phases are formed in the scale of coated Superni 76 after corrosion studies along with relatively weak peaks of  $\text{FeS}$ ,  $\text{Ce}_2\text{O}_3$  and  $\text{FeVO}_4$  phase. Coated Superni 750 alloy on exposure to given environment has developed a scale containing  $\text{NiCr}_2\text{O}_4$ ,  $\text{NiO}$ ,  $\text{Al}_2\text{O}_3$  as the strong phases with  $\text{Cr}_2\text{O}_3$ ,  $\text{FeS}$  and  $\text{Fe}_2\text{O}_3$  as weak phases. The coated Superfer 800 showed that the scale was composed of  $\text{NiO}$ ,  $\text{Cr}_2\text{O}_3$ ,  $\text{Al}_2\text{O}_3$ ,  $\text{NiCrFeO}_4$  phases along with weak peaks of  $\text{NiFeO}_4$ ,  $\text{FeVO}_4$  phases.



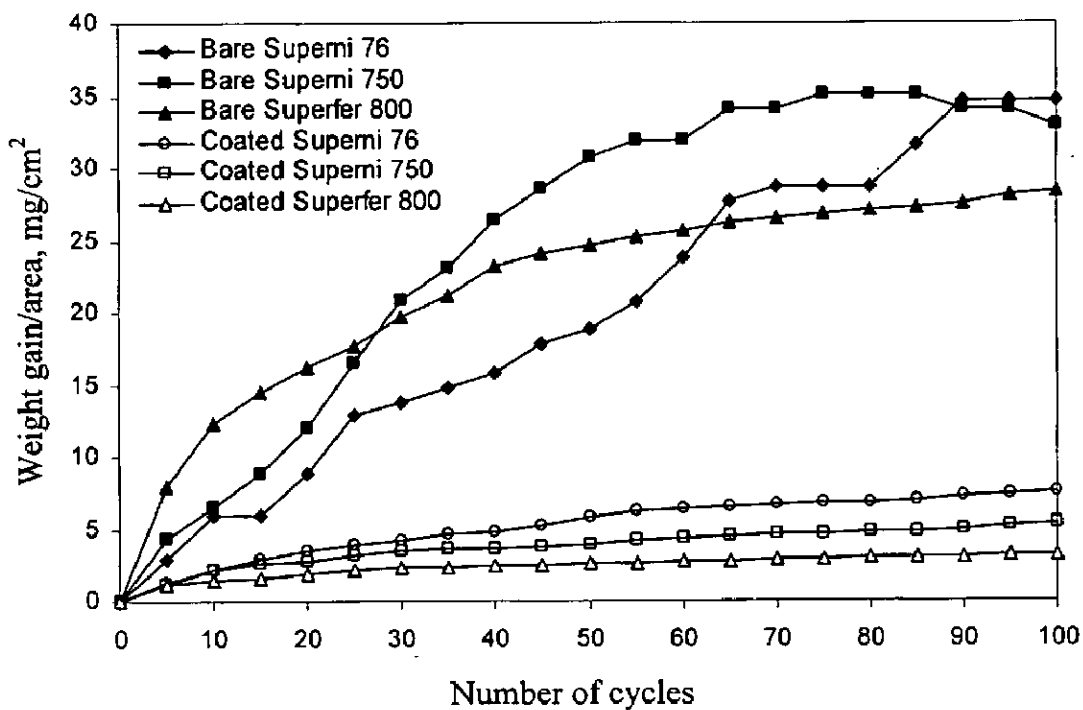


**Fig 6.20:** Mass gain/area versus. number of cycles for bare and NiCrAlY-0.4wt%CeO<sub>2</sub> coated superalloys subjected to 40% Na<sub>2</sub>SO<sub>4</sub>- 60% V<sub>2</sub>O<sub>5</sub> environment at 900°C for 100 cycles.

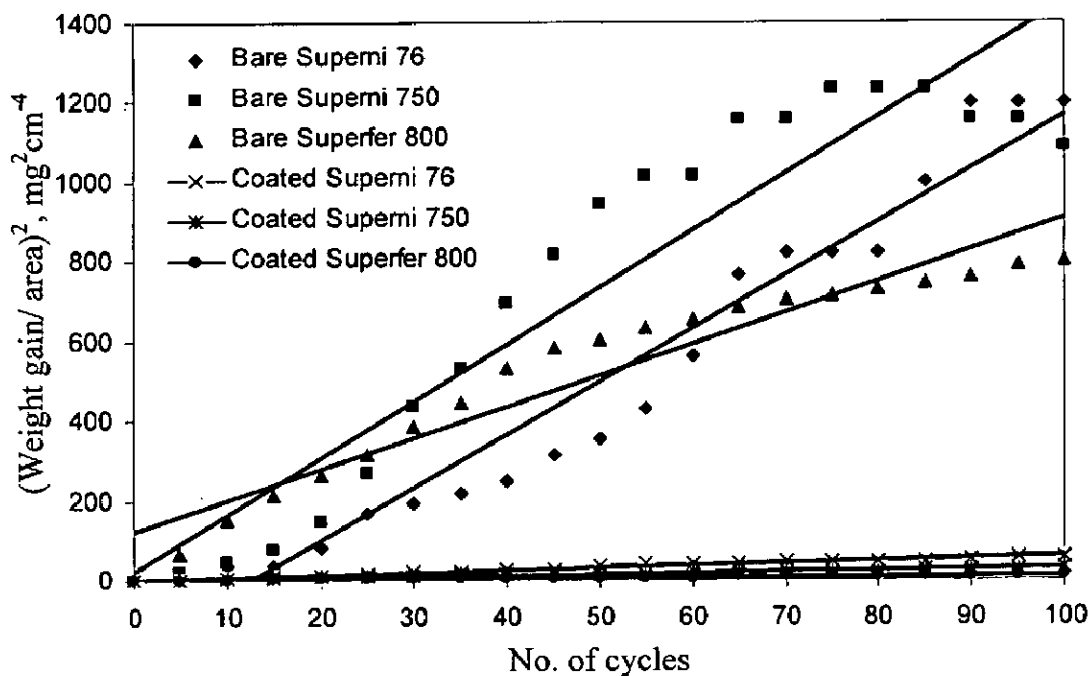


**Fig 6.21:** (Mass gain/area)<sup>2</sup> vs. number of cycles for bare and NiCrAlY-0.4wt%CeO<sub>2</sub> coated superalloys subjected to 40% Na<sub>2</sub>SO<sub>4</sub>-60% V<sub>2</sub>O<sub>5</sub> environment at 900°C for 100 cycles.

**Table 6.2:** Parabolic rate constants of bare and coated superalloys in molten salt environment.

Substrate used	Parabolic rate constant $K_p (10^{-10} \text{ g}^2 \text{ cm}^{-4} \text{ s}^{-1})$
Bare Superni 76	37.08
Bare Superni 750	39.71
Bare Superfer 800	22.36
Coated Superni 76	1.66
Coated Superni 750	0.734
Coated Superfer 800	0.26

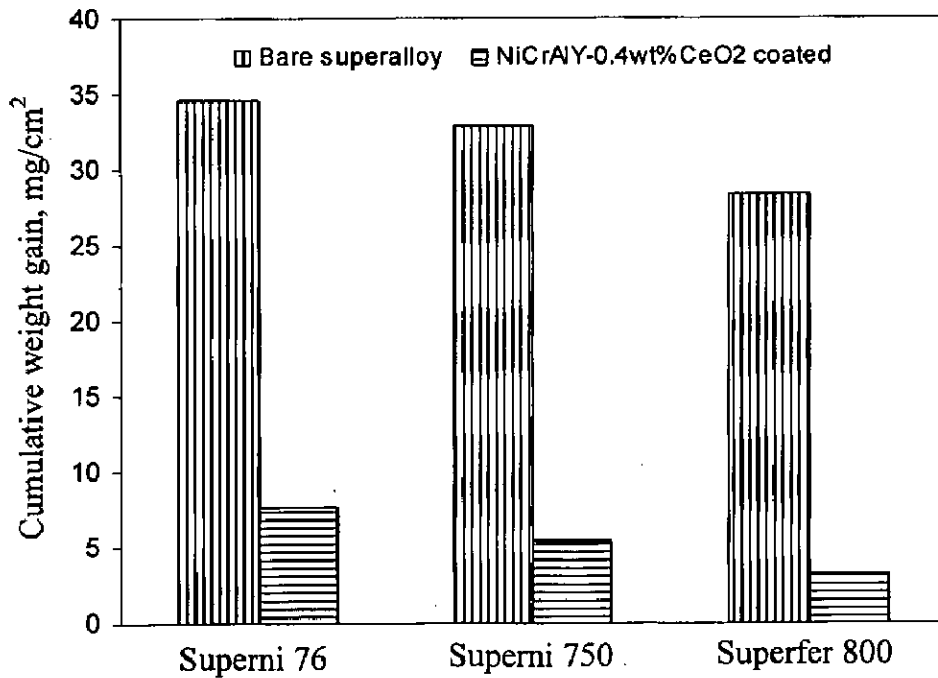


**Fig. 6.22:** Cumulative weight gain per unit area for bare and NiCrAlY-0.4wt%CeO<sub>2</sub> coated superalloys subjected to cyclic oxidation in air at 900°C for 100 cycles.

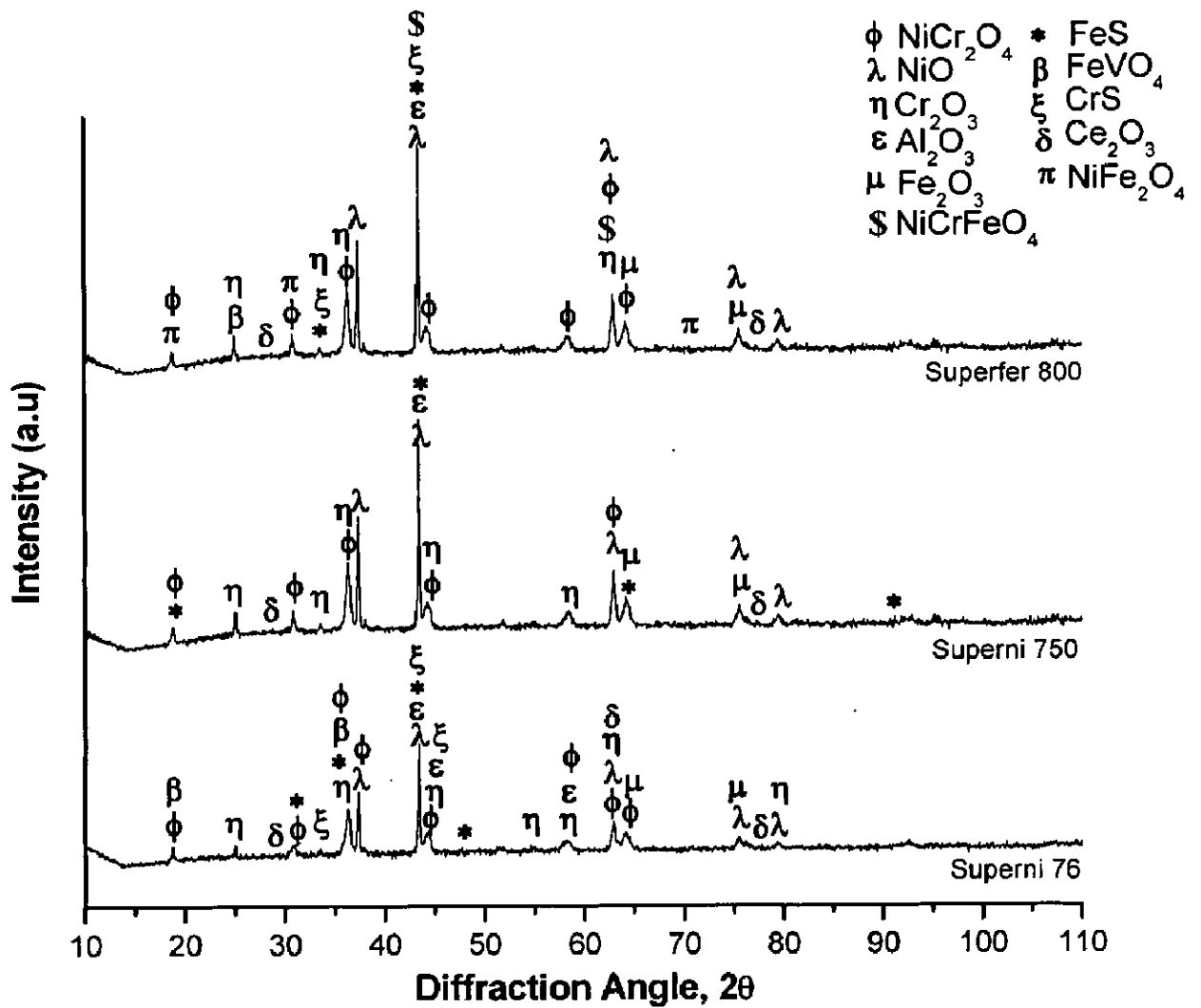


**Fig 6.23:** X-Ray Diffraction pattern of NiCrAlY-0.4wt%CeO<sub>2</sub> coated superalloys after 100h exposure to 40% Na<sub>2</sub>SO<sub>4</sub>- 60%V<sub>2</sub>O<sub>5</sub> environment at 900°C.

### 6.3.3.4 FESEM/EDAX analysis of the scale

#### 6.3.3.4.1 Surface analysis

The FESEM micrographs and EDAX analysis of the corroded NiCrAlY-0.4wt%CeO<sub>2</sub> coated Superni 76, Superni 750 and Superfer 800 are given in Fig.6.24. The surface morphology of the coated Superni 76 (Fig.6.24a), after 100 cycles of hot corrosion shows the formation of continuous homogeneous scale with indications of microspalling. The EDAX analysis shows that the scale formed on the NiCrAlYCeO<sub>2</sub> coated Superni 76 is rich in nickel oxide (77 to 87 wt pct), along with yttrium oxide, aluminum oxide and chromium oxide. Small amounts of vanadium oxide and cerium oxides have been found on the surface of the scale. In case of Superni 750 (Fig.6.24b), the top surface scale is rich in nickel oxide (94 wt pct) with small amount of chromium oxide (3 wt pct); whereas, the subscale consists of nickel oxide (69 wt pct), chromium oxide (20 wt pct), and aluminum oxide (3 wt pct). The scale formed on the surface is uniform and dense with a slight superficial microspalling of the oxide scale. In case of the coated Superfer 800 (Fig.6.24c), the scale formed on the surface is uniform, dense, and adherent. The scale consists of nickel oxide (47 wt pct), chromium oxide (30 wt pct), and aluminum oxide (13 wt pct) with small amount of vanadium oxide and cerium oxide.

#### 6.3.3.5 X-Ray mapping

The corroded samples were cut using Buehler ISOMET 1000 precision saw and then they were mounted in transoptic powder. The samples were mirror polished prior to studying its cross sectional features. The polished samples were then gold coated to facilitate the X-ray mapping of different elements present across the corroded samples by using FESEM (FEI, Quanta 200F). X-ray mapping for the NiCrAlY-0.4wt%CeO<sub>2</sub> corroded coating on all three superalloys at 900°C after 100 cycles in molten salt (40%Na<sub>2</sub>SO<sub>4</sub>-60%V<sub>2</sub>O<sub>5</sub>) environment indicated that oxygen has penetrated along the splat boundaries to oxidise aluminum and chromium. The splats consisting of mainly nickel appeared to be mostly in an unoxidised state. However, the top scale consisted of oxides of nickel, chromium, and aluminum. Furthermore, wherever nickel is present, oxygen is absent. In case of coated Superni 76 alloy (Fig. 6.25a), after corrosion studies, the diffusion of Si, Mn, S and W from the substrate into the coating has been observed. In case of coated Superni 750 alloy (Fig. 6.25b), a thick band of chromium is present on the top scale. Fe and Si as well as traceable amount of Ti have diffused from the substrate into the coating, whereas in case of Superfer 800 alloy (Fig. 6.25c), elements such as Fe, Si and Mn have diffused from the substrate into the scale. A thin layer of Fe has formed on the surface along with oxygen in case of coated Superni 750 and Superfer 800 alloy after exposure to the given environment. Traceable amount of cerium has distributed across the coating in all the three cases.

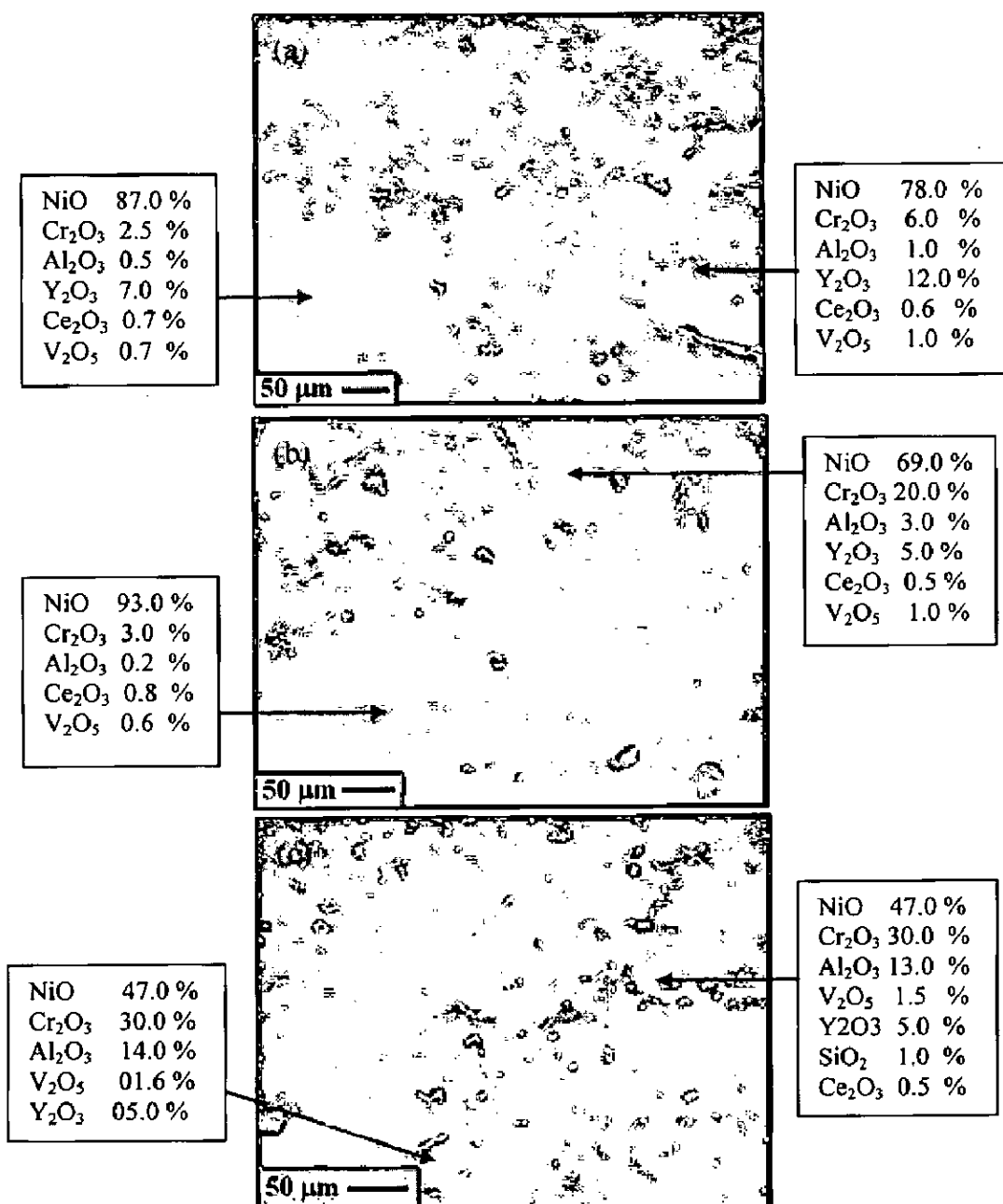


**Fig 6.24:** Surface-scale morphology and EDAX patterns from different spots on NiCrAlY-0.4wt%CeO<sub>2</sub> coated (a) Superni 76, (b) Superni 750 and (c) Superfer 800 in 40% Na<sub>2</sub>SO<sub>4</sub> -60% V<sub>2</sub>O<sub>5</sub> environment at 900°C after 100 cycles.

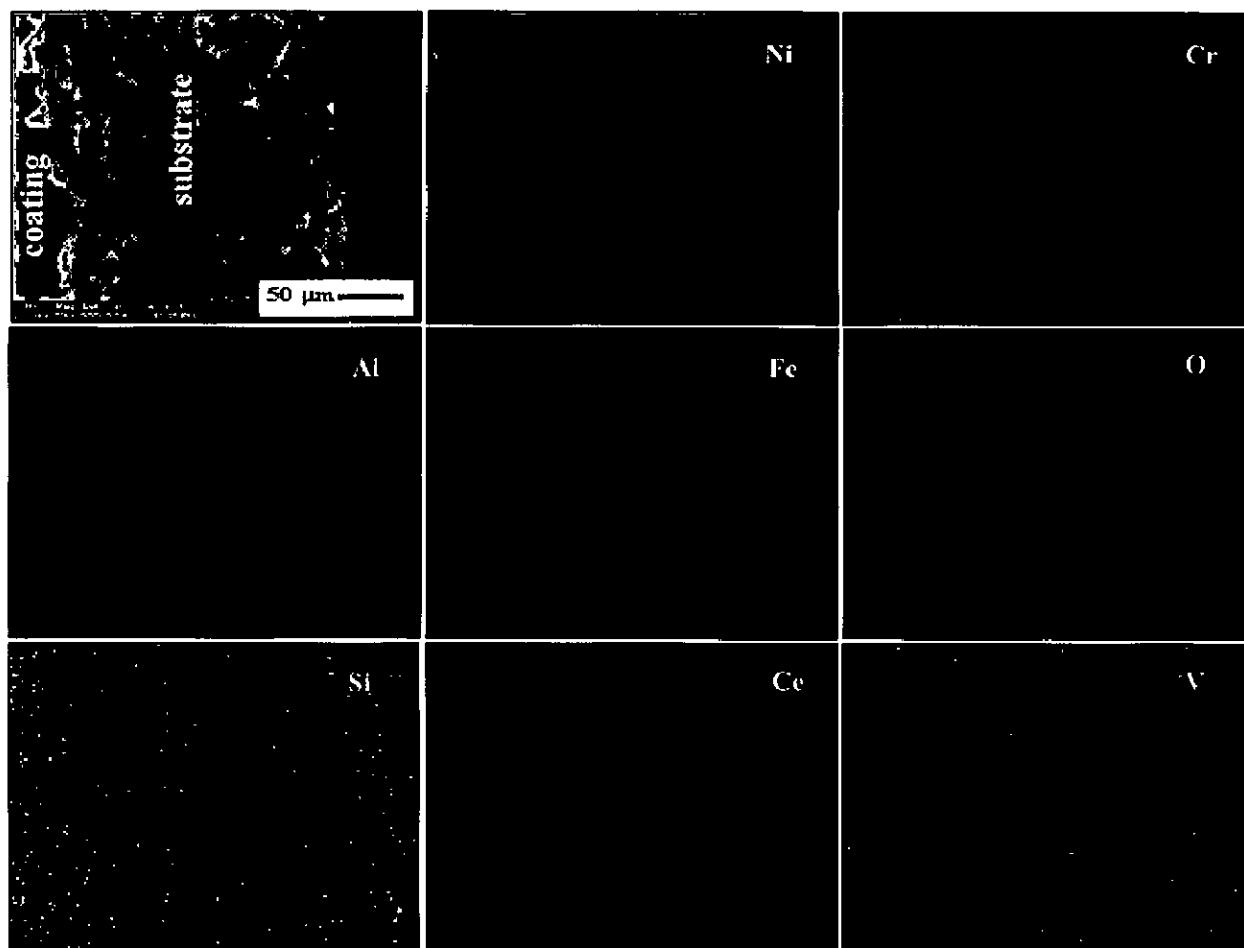


**Fig 6.25(a):** Composition image (SEI) and X-ray mapping of the cross-section of Superalloy 76 coated with NiCrAlY-0.4wt%CeO<sub>2</sub> subjected to cyclic oxidation in 40% Na<sub>2</sub>SO<sub>4</sub>-60%V<sub>2</sub>O<sub>5</sub> environment at 900°C.

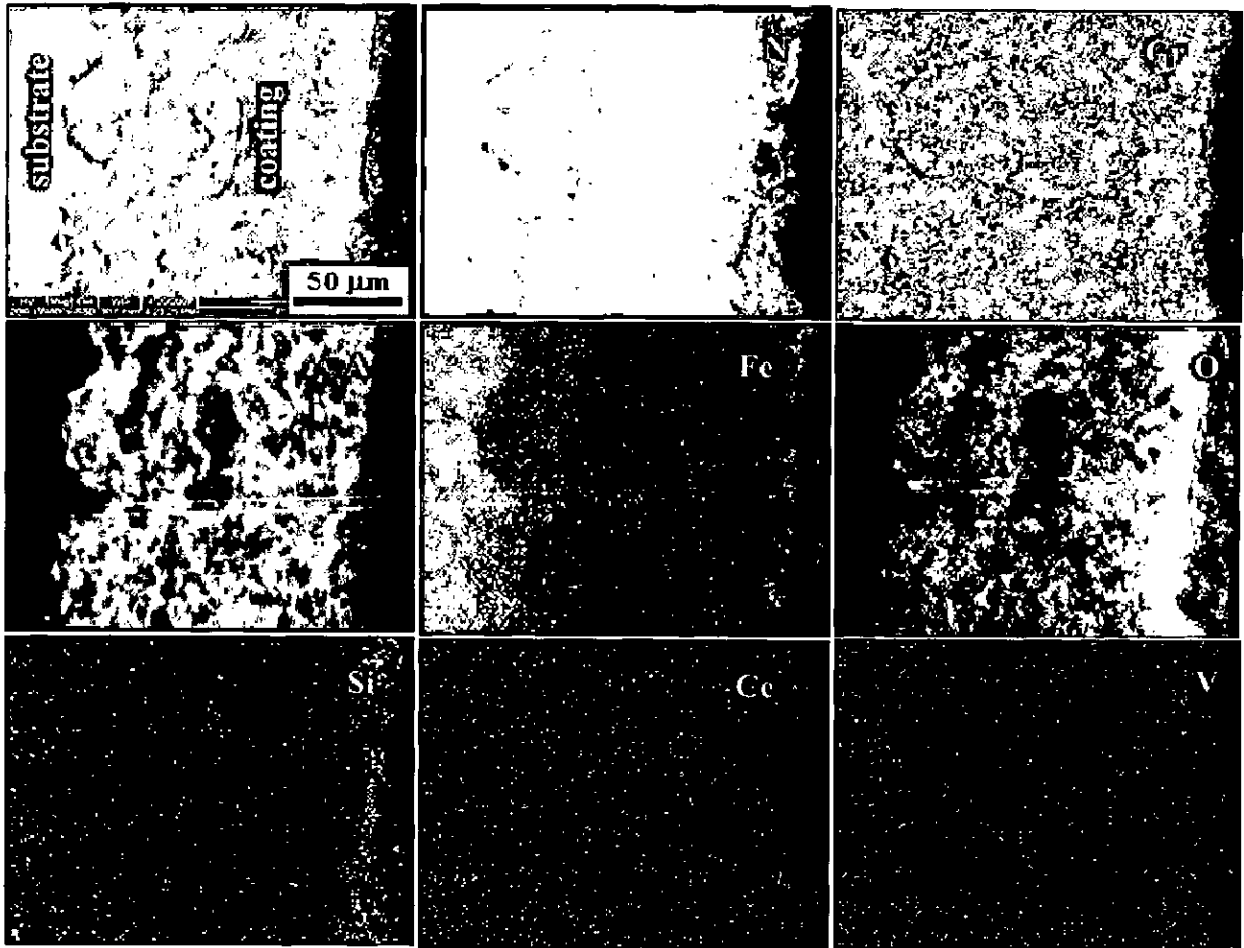


**Fig 6.25(b):** Composition image (SEI) and X-ray mapping of the cross-section of Superni 750 coated with NiCrAlY-0.4wt%CeO<sub>2</sub> subjected to cyclic oxidation in 40% Na<sub>2</sub>SO<sub>4</sub>-60%V<sub>2</sub>O<sub>5</sub> environment at 900°C.

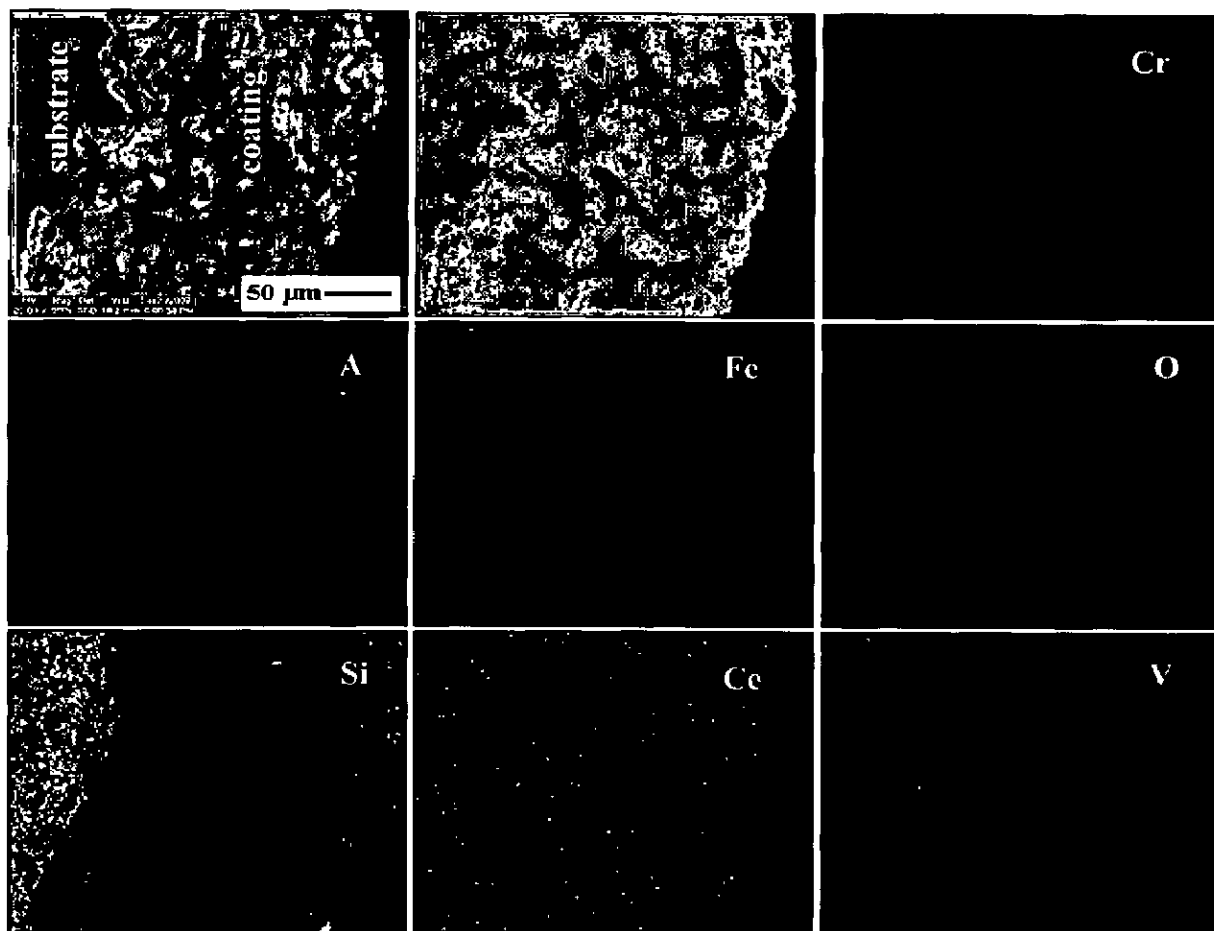
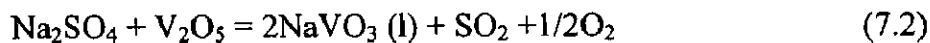


**Fig 6.25(c):** Composition image (SEI) and X-ray mapping of the cross-section of Superfer 800 coated with NiCrAlY-0.4wt%CeO<sub>2</sub> subjected to cyclic oxidation in 40% Na<sub>2</sub>SO<sub>4</sub>-60%V<sub>2</sub>O<sub>5</sub> environment at 900°C.



### 6.3.4 Discussion

The morphology of ceria added NiCrAlY powder is shown in Figure 6.1. The NiCrAl powder particles are spherical in shape and ceria is present in void area. The EDAX analysis of the as sprayed coating surface indicates the presence of cerium along the splat boundaries in the form of streaks. The surface macrographs of bare and coated superalloys after hot corrosion studies are shown in Fig. 6.19. It is observed from the macrographs that the oxide scale was intact with the coating and marginal microspalling was noted from the surface. The scale formed on the corroded surface was light green in color, which may be attributed to the presence of NiO in the scale, which is in tandem with the findings of Mahesh et al, (2008B). The mass gain of the bare alloys during the initial period was high and then becomes gradual during the course of the exposure at 900°C. The uncoated specimen showed a significant spalling during cyclic oxidation in the given environment with a substantial weight gain. It is evident from the Fig. 6.20 that the rate of weight gain is relatively high during the initial period of exposure, which may be attributed to the formation of NaVO<sub>3</sub> (mp ~610°C) as a result of following reaction at 900°C (Kolta et al, 1972).



This NaVO<sub>3</sub> acts as a catalyst and also serves as oxygen carrier to the base alloy, leading to rapid oxidation of the basic elements of the superalloy thereby forming the protective oxide scales. After the initial period of high corrosion rate, it has been observed that the rate of corrosion tends to be nearly uniform with the increase in the period of exposure. In case of coated superalloys subjected to cyclic oxidation in the given environment, significant weight gains were noticed in the early cycles of the exposure, but it became almost uniform with the exposure time obeying the parabolic rate law. This supports the fact that the partially oxidised coatings act as a diffusion barrier to the corroding species over the longer periods of exposure. The initial high oxidation rates may be due to the rapid formation of oxides at the coating surface and ingress of oxidising species along the splat boundaries resulting in the formation of oxides. Once the oxides are formed, the coating becomes dense and the diffusion of oxidising species to the internal portions of the coatings gets slowed down and the growth of the oxides becomes limited mainly to the surface of the specimens. This has caused the weight gain and the oxidation rate reaching a steady condition with the further progress of exposure time, indicating the protective nature of coatings in the given environment. Microspalling of the scale in the form of fine powder was observed in all the three cases from the coated surface after exposure to 900°C for 100 cycles which is identical to the findings of

Chan et al, (2000) for oxidised atmospheric plasma sprayed (APS) NiCrAlY coatings. Coefficient of thermal expansion (CTE) mismatch between the oxide scale and the coating plays an important role in oxide scale spallation. The formation of oxides leads to the development of thermal stresses in the resultant scale. In cyclic conditions, expansion and contraction of substrate and scale may lead to cracking and spallation. These cracks provide direct access to corroding species to the substrate. The parabolic rate constant for the bare superalloy is found to be greater than that of coated superalloys. The NiCrAlY-0.4wt%CeO<sub>2</sub> coating on superalloys has improved the oxidation resistance of the coatings through its segregation at the splat-splat interfaces and grain boundaries as evident from the SEM/EDAX analysis. The oxidation of other alloying elements at these active sites are minimised due to the preferential accumulation of ceria over there. It can be inferred that the HVOF sprayed NiCrAlY with CeO<sub>2</sub> coating has provided the necessary protection to the superalloys. Particularly, coating on Superfer 800 has shown the best protection. From the surface EDAX analysis it is observed that chromium oxide formed on the surface is in higher amount, which might have imparted the best resistance to hot corrosion in the given environment. The oxide scale formed on the three superalloys was dense and adherent. The  $k_p$  values for the ceria added NiCrAlY coatings on Superfer 800 ( $0.26 \times 10^{-10} \text{ g}^2 \text{ cm}^{-4} \text{ s}^{-1}$ ) are less compared to NiCrAlY coating ( $1.378 \times 10^{-10} \text{ g}^2 \text{ cm}^{-4} \text{ s}^{-1}$ ) without ceria addition by plasma spray process (Harpreet Singh et al, 2005C).

The XRD analysis (Fig. 6.23) of the coated superalloys after hot corrosion study at 900°C in molten salt environment indicates that the coating has provided the better protection to the superalloys. The protection to the superalloys from hot corrosion might be partially due to the formation of oxides of nickel, aluminum and chromium, which is supported by EDAX analysis. The phases formed are identical to the findings of Gitanjaly (2003). These oxides especially Al<sub>2</sub>O<sub>3</sub> and Cr<sub>2</sub>O<sub>3</sub> offer a better protection against oxidation/hot corrosion due to their low growth rate, strongly bounded compositions and ability to act as effective barriers against ionic migration (Stott, 1989). The presence of these phases is further confirmed by X-ray mapping analysis. The formation of spinels on the top scale may further enhance the oxidation resistance due to their much smaller diffusion coefficients of the cations and anions than those in their parent oxides (Chatterjee et al, 2001).

EDAX analysis on the surface and cross section indicated the presence of ceria in the scale. The better protection provided by the coating in the given environment may be due to the presence of ceria in the scale and possible formation of CeVO<sub>4</sub> might have contributed to the reduction in the corrosion rate. Furthermore, Ce, V and O coexisted as indicated by X-ray

mapping analysis. XRD and EDAX analysis failed to detect the presence of  $\text{CeVO}_4$  on the surface perhaps due to its lower concentration (0.4 wt% ceria). Aluminum and chromium are present wherever nickel is absent. X-ray mapping analysis (Fig. 6.25) indicates that the coatings are found to be dense and successful in maintaining their continuous surface contact with the substrate superalloy when exposed to the given aggressive environment. Moreover, it is clear from the oxygen map that the base superalloy has not undergone internal oxidation, which indicates the protective nature of the coating. The surface scale for the NiCrAlY-0.4wt%CeO<sub>2</sub> coating has shown very good spallation resistance against the cyclic oxidation, which indicates the effectiveness of the coatings under study. The schematic representation of the possible hot corrosion mode for the NiCrAlY-0.4wt%CeO<sub>2</sub> coated Superfer 800 subjected to the molten salt environment for 100 cycles at 900°C is shown in Fig. 6.26.

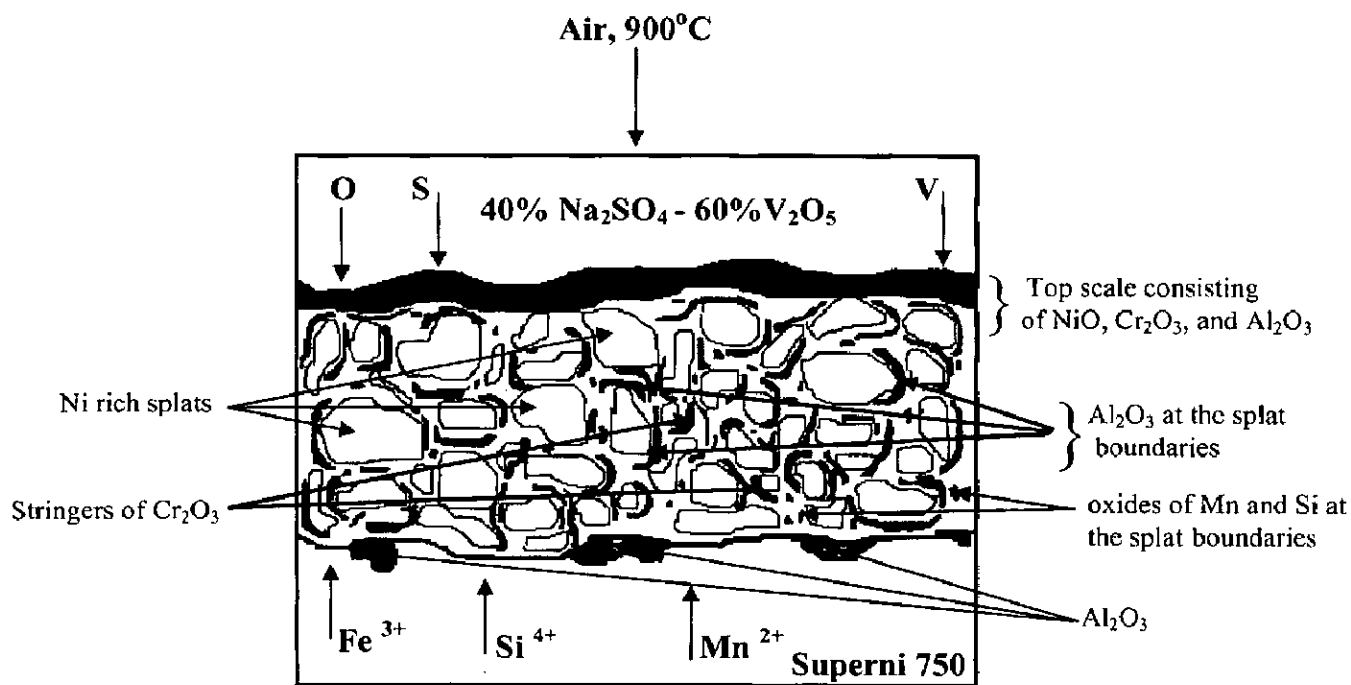


**Fig 6.26:** Schematic diagram showing the possible hot corrosion mode for the NiCrAlY-0.4wt%CeO<sub>2</sub> coated Superfer 800 exposed to the 40%Na<sub>2</sub>SO<sub>4</sub>-60%V<sub>2</sub>O<sub>5</sub> environment at 900°C for 100 cycles

### 6.3.5 Conclusions

1. The HVOF process using LPG as fuel gas has been used to deposit NiCrAlY-0.4wt%CeO<sub>2</sub> coatings on the superalloys in the present work. The coatings were found to be dense and adherent to the base superalloys with negligible spalling of the oxide scale.
2. The bare superalloys showed significant increase in the weight gain in the given environment which was accompanied by cracking and spalling of the oxide scale during the exposure at 900°C. The coated superalloys after exposure to molten salt environment at 900°C for 100 cycles showed comparatively very little weight gain and the scale formed on the surface were dense and adherent to superalloy substrates.
3. The parabolic rate constant for the coated superalloys was found to be very less as compared to the bare superalloys in the given environment at 900°C; thus indicating a better resistance of the coating to the hot corrosion.
4. The NiCrAlY-0.4wt%CeO<sub>2</sub> coating has led to the reduction in weight per unit area of about 1/20 in Superni 76, whereas 1/50 and 1/100 for Superni 750 and Superfer 800, respectively.
5. The formations of oxides of nickel, chromium, aluminum, and spinel of nickel and chromium as indicated by XRD analysis provide a better protection to the superalloys in the given environment at 900°C. It is further supplemented by SEM/EDAX line scan analysis and X-ray mapping analysis. Furthermore, formations of ceria in the scale and the possible formation of cerium vanadates (CeVO<sub>4</sub>) might have contributed for better corrosion resistance of the superalloys in the given environment.
6. The hot corrosion resistance provided by the NiCrAlY-0.4wt%CeO<sub>2</sub> coating to the superalloys in the given environment at 900°C followed the sequence,

Superfer 800 > Superni 750 > Superni 76.

# **HOT CORROSION STUDIES IN INDUSTRIAL ENVIRONMENT**

---

---

This chapter focuses on the study of hot corrosion behaviour of the uncoated, HVOF coated and RF magnetron sputter coated Superfer 800 exposed to low temperature superheater zone of the coal fired boiler of Guru Gobind Singh Super Thermal Power Plant, Ropar, Punjab, India. The specimens were hanged in the low temperature superheater zone where the gas temperature was around  $700^{\circ}\text{C} \pm 10^{\circ}\text{C}$ . Hot corrosion studies were performed for 100 cycles, each cycle consists of 100 hours exposure followed by 1 hour cooling at ambient temperature. The specimens were visually examined at the end of each cycle for any change in colour, luster, spalling tendency and other physical changes of the scale, if any. Weight change measurements were made at the end of each cycle but it could not be of much use for predicting hot corrosion behaviour of suspected spalling and ash deposition on the samples. The extent of corrosion has been evaluated by measuring thickness of the unreacted portion of the samples after the total exposure of 1000 hours. The different phases and their distribution in the hot corroded specimens were analysed with the help of XRD, FESEM/EDAX and X-ray mapping.

## **7.1 EXPERIMENTAL DETAILS**

The details of the studies in the industrial environment of uncoated, HVOF coated and RF sputtered specimens are explained in Chapter 3

## **7.2 RESULTS AND DISCUSSION**

### **7.2.1 Visual Examination**

#### **7.2.1.1 Uncoated and HVOF coated Superfer 800**

The macrographs for the uncoated Superfer 800 and HVOF sprayed Ni-5Al, NiCrAl and NiCrAlY-0.4wt%CeO<sub>2</sub> coatings on Superfer 800 after 1000 hours of exposure to low temperature superheater zone of the coal fired boiler are shown in Fig. 7.1. After exposure of 300 hours, light grey coloured scale formed on the surface of the uncoated Superfer 800 (Fig. 7.1a), which subsequently turned into light brownish grey colour after 1000 hours of exposure to the boiler environment. No spallation from the surface was observed upto 1000 hours of exposure.

The macrographs of HVOF sprayed coatings on Superfer 800 after exposing to the boiler environment are shown in Fig. 7.1(b) to 7.1(d). The Ni-5Al coated specimen shows spallation from the surface after 200 hours of exposure. The spallation has continued upto 400 hours and then stopped with further exposure to the boiler environment. Light grey coloured scale formed on the surface of the specimen after 300 hours and turned into yellowish grey with green shade after 1000 hours (Fig. 7.1b). The NiCrAl coated Superfer 800 (Fig. 7.1c) shows grey colour after 200 hours and it turned into light yellowish grey after 1000 hours of exposure. The spallation of scale has not occurred during the course of the study in the given environment. In case of NiCrAlY-0.4wt%CeO<sub>2</sub> coated Superfer 800 (Fig. 7.1d), light yellowish grey colour with green tinge has formed on the surface after 1000 hrs of exposure, but with no spallation during the course of the study.

#### **7.2.1.2 RF magnetron sputtered films on Superfer 800**

The macrographs for the RF magnetron sputtered Ni-Al and NiCrAl films on Superfer 800 after 1000 hour exposure to low temperature superheater zone of the coal fired boiler are shown in Fig. 7.2. The RF sputtered Ni-Al film (Fig. 7.2a) indicates a grey coloured scale after 200 hours of exposure in the given environment, which subsequently turned into grey colour with brown and reddish patches on the surface of the specimen. In case of RF sputtered NiCrAl film on Superfer 800 (Fig. 7.2b), grey with green shades on the surface has formed after 1000 hrs of exposure to boiler environment. In both the cases, spallation of the scale is not observed during the study.

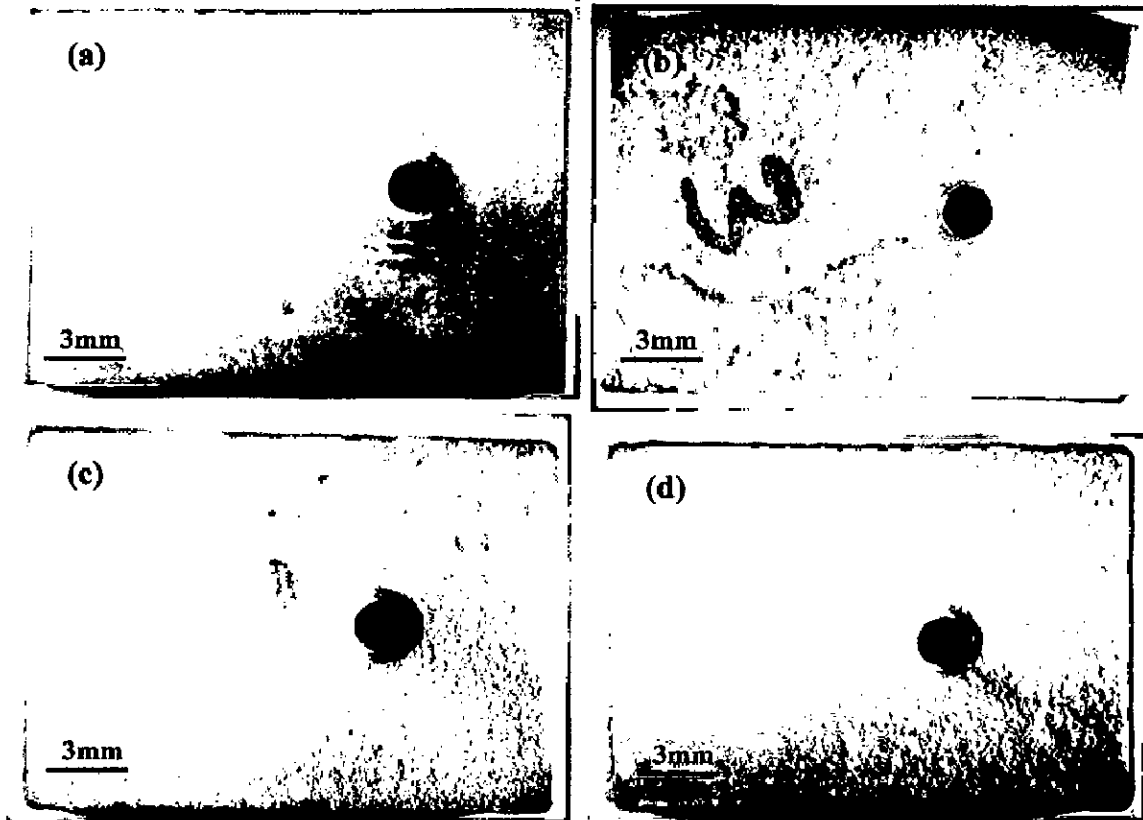


**Fig. 7.1:** Macrographs of the (a) uncoated, and HVOF sprayed (b) Ni-5Al, (c) NiCrAl and (d) NiCrAlY-0.4wt%CeO<sub>2</sub> coated on Superfer 800 after 1000 hrs exposure to low temperature superheater zone of the boiler at 700 °C.

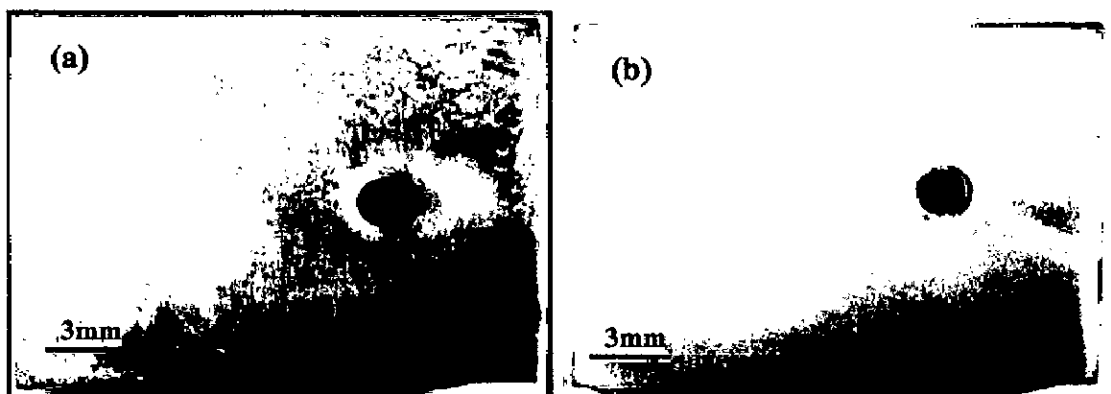


**Fig. 7.2:** Macrographs of RF magnetron sputtered (a) Ni-Al and (b) NiCrAl coated films on Superfer 800 after 1000 hrs exposure to low temperature superheater zone of the boiler at 700 °C.

## 7.2.2 Hot Corrosion of uncoated and coated Superfer 800

The hot corrosion behaviour of uncoated, HVOF coated and RF magnetron sputtered films on Superfer 800 in the given environment has been assessed by evaluating the weight change data, the metal thickness loss corresponding to the combined effects of average thickness of scale, loss of scale thickness due to spallation or evaporation, and the depth of internal corrosion attack after 1000 hours of exposure. The uncoated Superfer 800 showed no scale thickness loss, whereas in case of HVOF sprayed Ni-5Al coated Superfer 800, an average of 65  $\mu\text{m}$  scale thickness loss was found. In case of HVOF sprayed NiCrAl and NiCrAlY-0.4wt%CeO<sub>2</sub> coated Superfer 800 and RF sputtered Ni-Al and NiCrAl films on Superfer 800, in general, the scale thickness loss was not found.

### 7.2.2.1 Corrosion Kinetics

The weight change per unit area ( $\text{mg}/\text{cm}^2$ ) versus time plot for 1000 hours exposure of bare, HVOF coated Ni-5Al, NiCrAl, NiCrAlY-0.4wt%CeO<sub>2</sub> on Superfer 800 and RF magnetron sputtered Ni-Al and NiCrAl films on Superfer 800 to the boiler environment is shown in Fig. 7.3 and Fig. 7.4. The weight change consists of weight gain owing to the formation of the oxides scale, deposition of ash and weight loss due to the suspected spalling and fluxing of the oxide scale. The net weight change of the specimens in the given environment represents the combined effects of these two processes.

The HVOF sprayed NiCrAl and NiCrAlY-0.4CeO<sub>2</sub> coated Superfer 800 shows the lowest weight gain and the uncoated Superfer 800 shows the highest weight gain, which is around 58% more than that gained by the former. In case of RF magnetron sputtered films on Superfer 800, NiCrAl film shows marginal increase in the weight gain as compared to the Ni-Al coated Superfer 800 after exposure to the boiler environment.



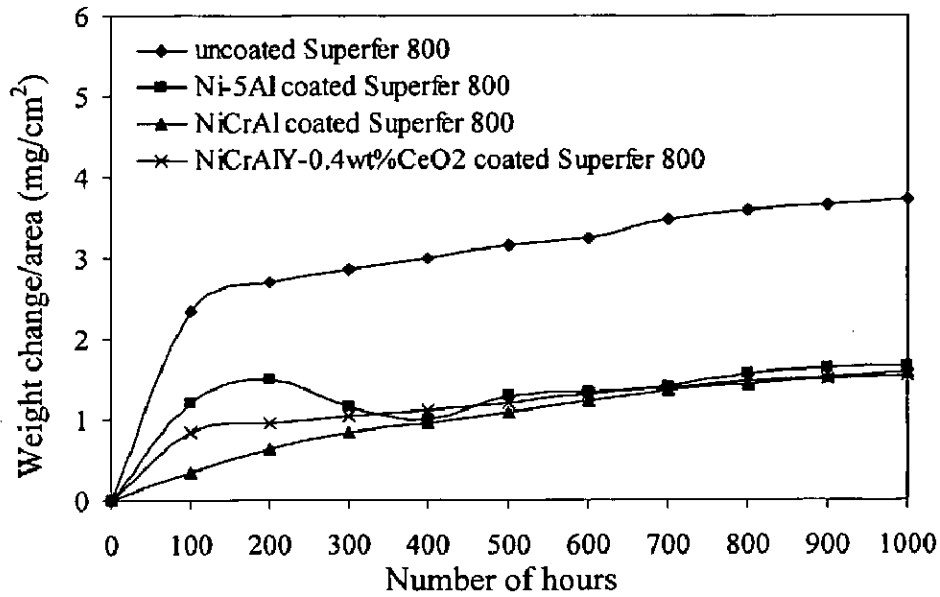


**Fig. 7.3:** Weight change vs. time plots for the uncoated and HVOF coated Superfer 800 subjected to 1000 hrs cyclic exposure to low temperature superheater zone of the coal fired boiler at 700 °C.

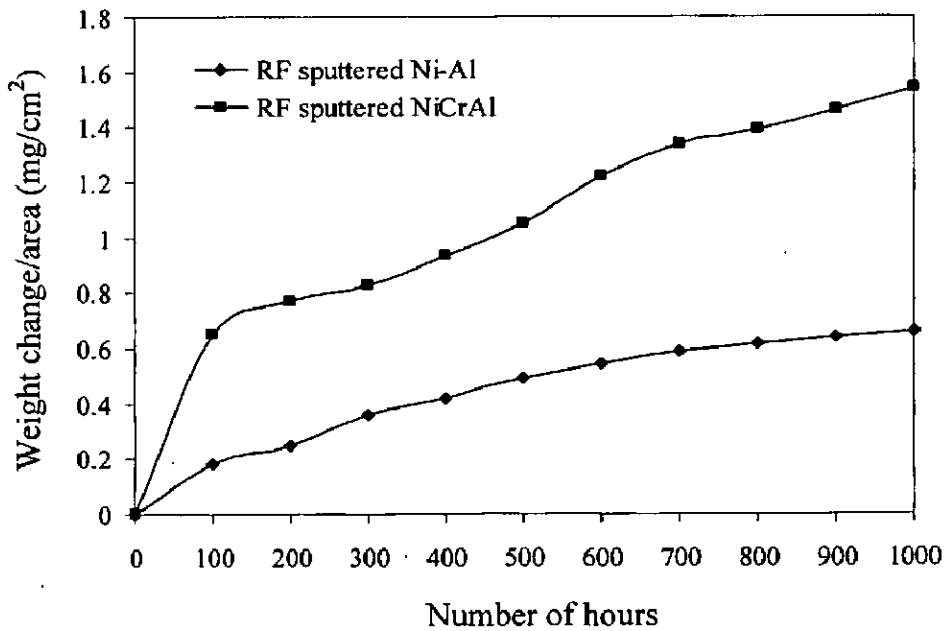


**Fig. 7.4:** Weight change vs. time plots for the RF sputtered Ni-Al and NiCrAl coated films on Superfer 800 subjected to 1000 hrs cyclic exposure to low temperature superheater zone of the coal fired boiler at 700 °C

The  $(\text{weight change/area})^2$  versus time plot for uncoated and HVOF coated Superfer 800 is shown in Fig. 7.5. It can be noted from the graph that the uncoated and Ni-5Al coated Superfer 800 show some deviations from the parabolic rate law. The NiCrAl and NiCrAlY-0.4wt%CeO<sub>2</sub> coated Superfer 800 follow a parabolic rate law. The parabolic rate constants ( $k_p$  in  $10^{-12} \text{ g}^2 \text{ cm}^{-4} \text{ s}^{-1}$ ) for the NiCrAl, NiCrAlY-0.4wt%CeO<sub>2</sub> coated Superfer 800 was found to be 0.75 and 0.60 respectively. The parabolic rate constants for Ni-5Al coated Superfer 800 could not be calculated as it did not follow the parabolic rate law. Fig. 7.6 shows  $(\text{weight change/area})^2$  versus time plots for RF magnetron sputtered Ni-Al and NiCrAl coated Superfer 800. It can be seen from the graph that the Ni-Al coated Superfer 800 followed the parabolic rate law, whereas NiCrAl coated Superfer 800 slightly deviated from the parabolic rate law. The parabolic rate constants ( $k_p$  in  $10^{-12} \text{ g}^2 \text{ cm}^{-4} \text{ s}^{-1}$ ) for Ni-Al and NiCrAl coated Superfer 800 are 0.13 and 0.38 respectively.

#### 7.2.2.2 Average scale Thickness and Depth of Internal Attack

The BSE images across the cross-section of the scales formed on bare and HVOF coated Superfer 800 are shown in Fig.7.7. The average scale thickness for uncoated Superfer 800 is found to be 75  $\mu\text{m}$ , and that for HVOF sprayed Ni-5Al, NiCrAl and NiCrAlY-0.4wt%CeO<sub>2</sub> coated Superfer 800 are 165, 245, and 230  $\mu\text{m}$ , respectively. The uncoated and the coated superalloy showed no internal corrosion attack. The average scale thickness, scale thickness lost (reported under section 7.2.2) and depth of internal corrosion attack for uncoated and HVOF coated Superfer 800 are given in Fig. 7.8.

The BSE images across the cross section of the scale formed on the RF magnetron sputtered Ni-Al and NiCrAl coated Superfer 800 are shown in Fig. 7.9. The average scale thickness of Ni-Al and NiCrAl coated Superfer 800 are 35 and 18  $\mu\text{m}$ , respectively. No internal attack was observed after exposure to 1000 hrs in the boiler environment. The average scale thickness of the RF sputtered Superfer 800 is shown in Fig. 7.10.

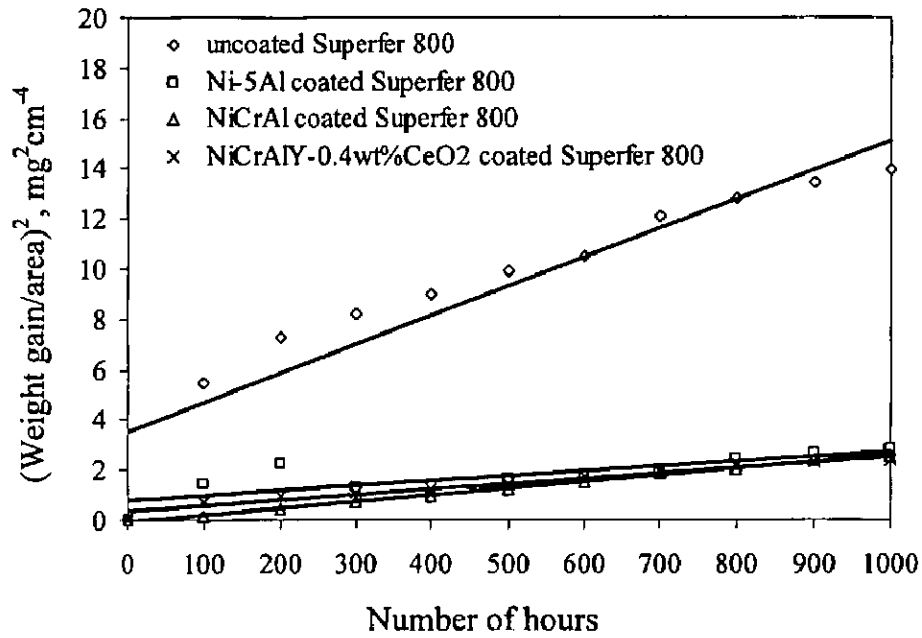


**Fig.7.5:** (Weight gain/area)<sup>2</sup> vs. number of hours plots for the uncoated and HVOF coated Superfer 800 subjected to 1000 hrs cyclic exposure to low temperature superheater zone of the coal fired boiler at 700°C.

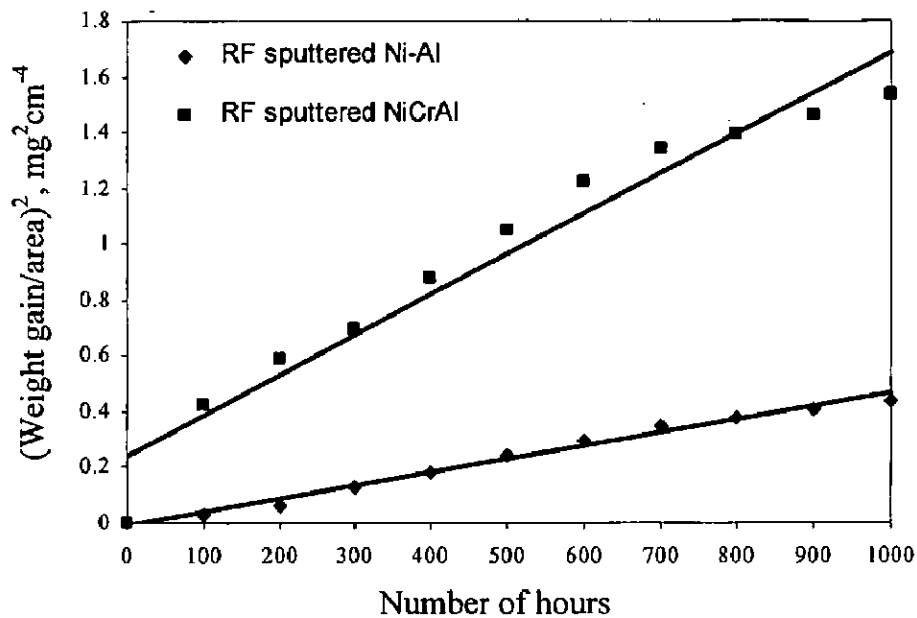


**Fig.7.6:** (Weight gain/area)<sup>2</sup> vs. number of hours plots for the RF magnetron sputtered Ni-Al and NiCrAl coated Superfer 800 subjected to 1000 hrs cyclic exposure to low temperature superheater zone of the coal fired boiler at 700°C.

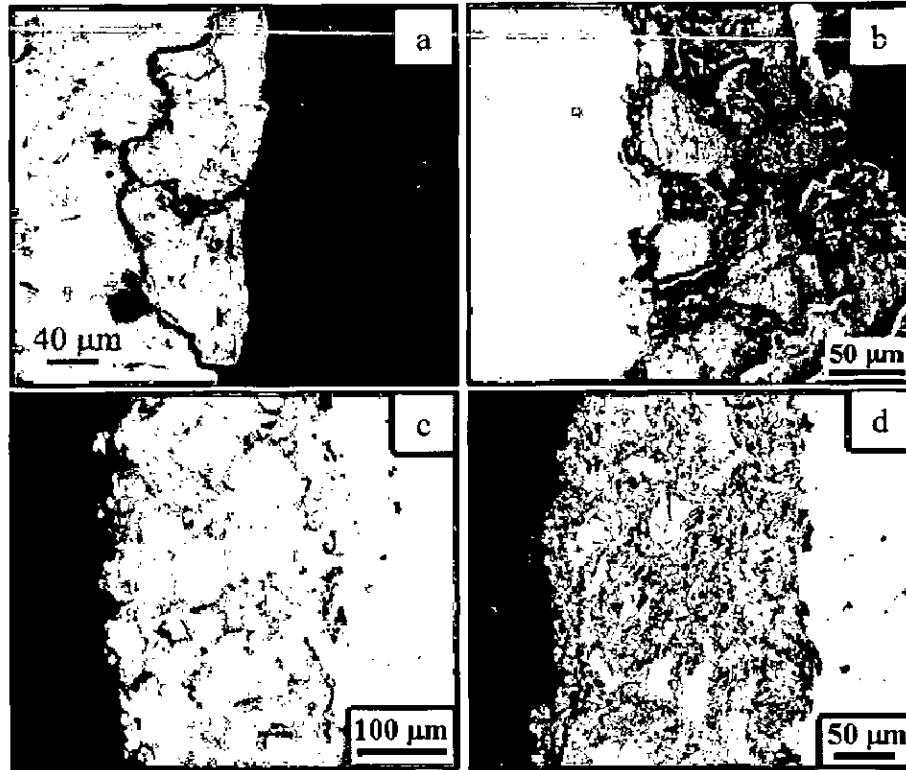


**Fig. 7.7:** BSE images for the uncoated and HVOF coated Superfer 800 after 1000 hrs exposure to low temperature superheater zone of the coal fired boiler at 700 °C: (a) Uncoated superalloy (b) Ni-5Al coated (c) NiCrAl coated (d) NiCrAlY-0.4wt%CeO<sub>2</sub> coated

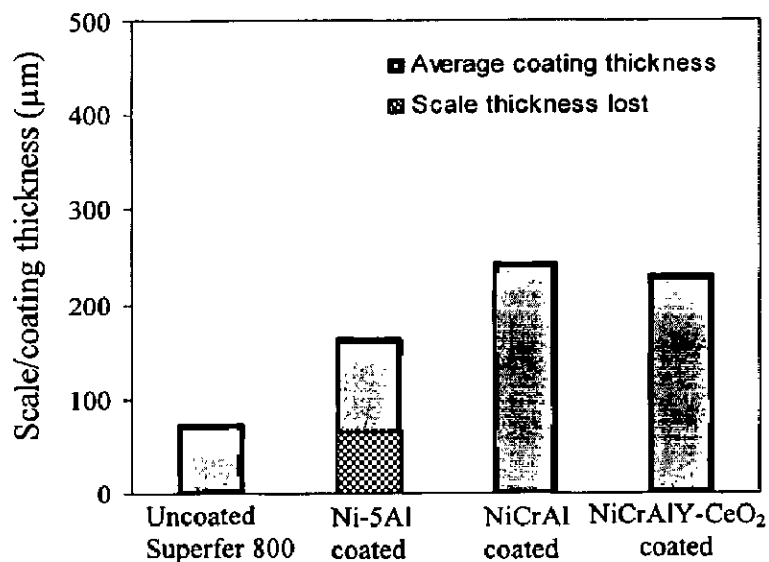


**Fig. 7.8:** Bar charts indicating the scale thickness for the bare and HVOF coated Superfer 800 after 1000 hrs exposure to the coal fired boiler at 700 °C.

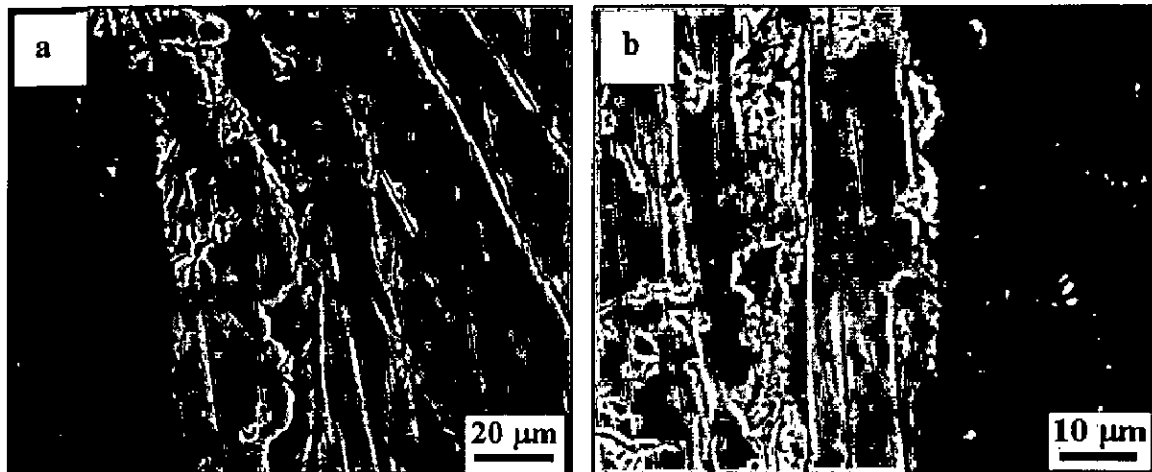


**Fig. 7.9:** BSE images for the RF sputtered (a) Ni-Al and (b) NiCrAl films on Superfer 800 after 1000 hrs exposure to low temperature superheater zone of the coal fired boiler at 700 °C.

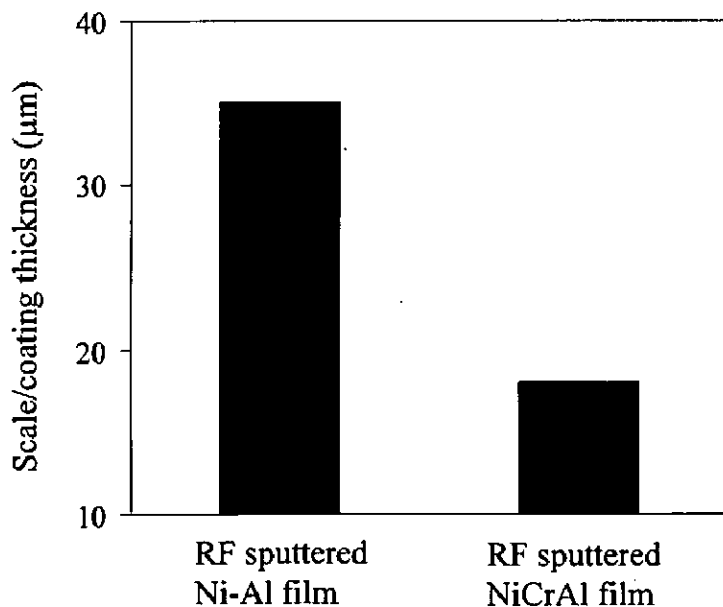


**Fig. 7.10:** Bar charts indicating the scale thickness for the RF sputtered Ni-Al and NiCrAl film on Superfer 800 after 1000 hrs exposure to the coal fired boiler at 700 °C.

### 7.2.2.3 X-ray Diffraction Analysis

The X-ray diffraction patterns for the corroded bare and HVOF coated Superfer 800 are shown in Fig. 7.11. The uncoated Superfer 800 after exposure to the boiler environment (700°C) for 1000 hrs indicates the presence of AlNi<sub>3</sub> on the surface of the specimen. In case of Ni-5Al coated Superfer 800, the scale surface shows the presence of NiO, Fe<sub>3</sub>O<sub>4</sub>, Al<sub>2</sub>O<sub>3</sub>, and  $\gamma$ -Ni. The phases formed on the NiCrAl coated Superfer 800 indicates the presence of AlNi and  $\gamma$ -Ni as the main phases along with a minor phase of  $\alpha$ -Cr. In case of NiCrAlY-0.4wt%CeO<sub>2</sub> coated Superfer 800, the phases formed on the surface consist of  $\gamma$ -Ni,  $\alpha$ -Cr and AlNi.

The X-ray diffraction patterns for the RF sputtered Superfer 800 specimens after exposing to the boiler environment are shown in Fig. 7.12. The Ni-Al coated Superfer 800 after exposure for 1000 hrs indicated the presence of AlNi and  $\gamma$ -Ni on the surface of the specimen. In case of NiCrAl coated Superfer 800, the surface scale indicated only the presence of AlNi<sub>3</sub>.

### 7.2.2.4 FESEM/EDAX Analysis

#### 7.2.2.4 (a) Surface Analysis

The FESEM micrographs showing surface morphology of the scale formed on uncoated and HVOF coated Superfer 800 are given in Fig. 7.13. The black areas present on the surface of uncoated Superfer 800 indicate that the scale formed on the surface may consists of oxides of nickel, chromium, aluminum, silicon and iron (Fig. 7.13a). The EDAX analysis shows that the white phase of the scale consists mainly of SiO<sub>2</sub>, Al<sub>2</sub>O<sub>3</sub>, and some amounts of Fe<sub>2</sub>O<sub>3</sub>, TiO<sub>2</sub>, CaO and K<sub>2</sub>O. It is inferred that the composition of the white phase is almost similar to ash composition along with some other oxides of the scale.

In case of Ni-5Al and NiCrAl coated Superfer 800 (Fig. 7.13b and 7.13c), uniform and adherent surface scale which is rich in silica and alumina are formed on the surface without indication of any crack. The scale formed on the surface of NiCrAlY-0.4wt%CeO<sub>2</sub> coated Superfer 800 (Fig. 7.13d) contain higher amount of alumina and silica. The EDAX analysis of dark areas on the surface indicates the presence of ash deposition along with

oxides of nickel, chromium, and iron. The presence of Ti in the surface scale indicates its outward diffusion from the substrate, whereas presence of Fe in the surface scale is due to diffusion from the substrate and partly due to interaction with ash.

The FESEM micrographs showing surface morphology of the scale formed on RF sputtered Ni-Al and NiCrAl films on Superfer 800 after exposure to boiler environment for 1000 hrs are given in Fig. 7.14. The dark area on the surface of the Ni-Al coated Superfer 800 (Fig. 7.14a) show the presence of oxides of nickel, aluminum, silicon. The presence of oxides of chromium, iron, titanium and manganese on the surface might be attributed either to the diffusion from the substrate or to the deposition of these elements from the stainless steel target into the coating. In case of RF sputtered NiCrAl on Superfer 800 (Fig. 7.14b), granular scales rich in silica and alumina are formed on the surface of the specimen. Higher amount of manganese present in the scale may be due to its deposition from the stainless steel target. It is inferred that the composition of the white phase is almost similar to ash composition along with some other oxides of the scale.

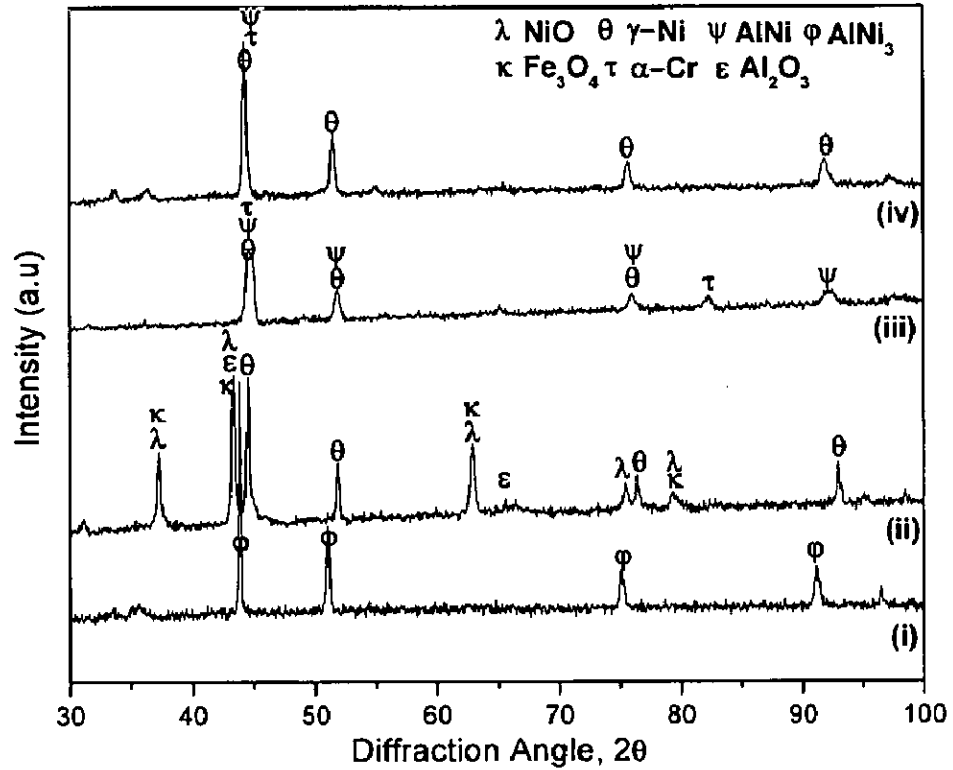


**Fig. 7.11:** X-ray diffraction patterns for the (i) uncoated and HVOF sprayed (ii) Ni-5Al, (iii) NiCrAl, (iv) NiCrAlY-0.4wt%CeO<sub>2</sub> coatings on Superfer 800 after 1000 hrs exposure to low temperature superheater zone of the coal fired boiler at 700 °C.

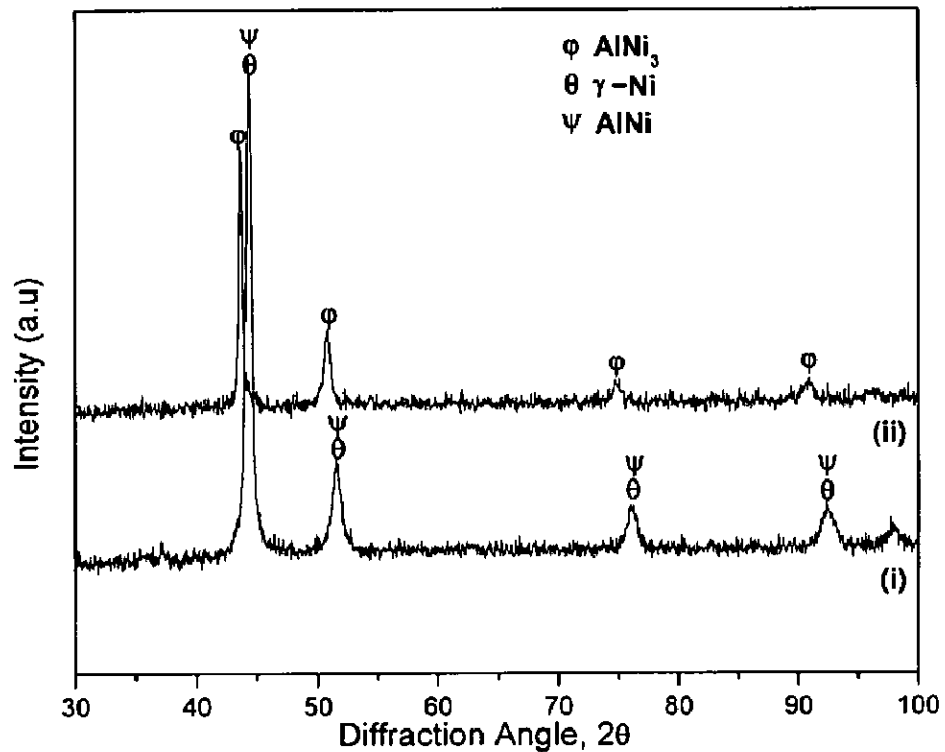


**Fig. 7.12:** X-ray diffraction patterns of RF sputtered (i) Ni-Al and (ii) NiCrAl coatings on Superfer 800 after 1000 hrs exposure to low temperature superheater zone of the coal fired boiler at 700 °C.



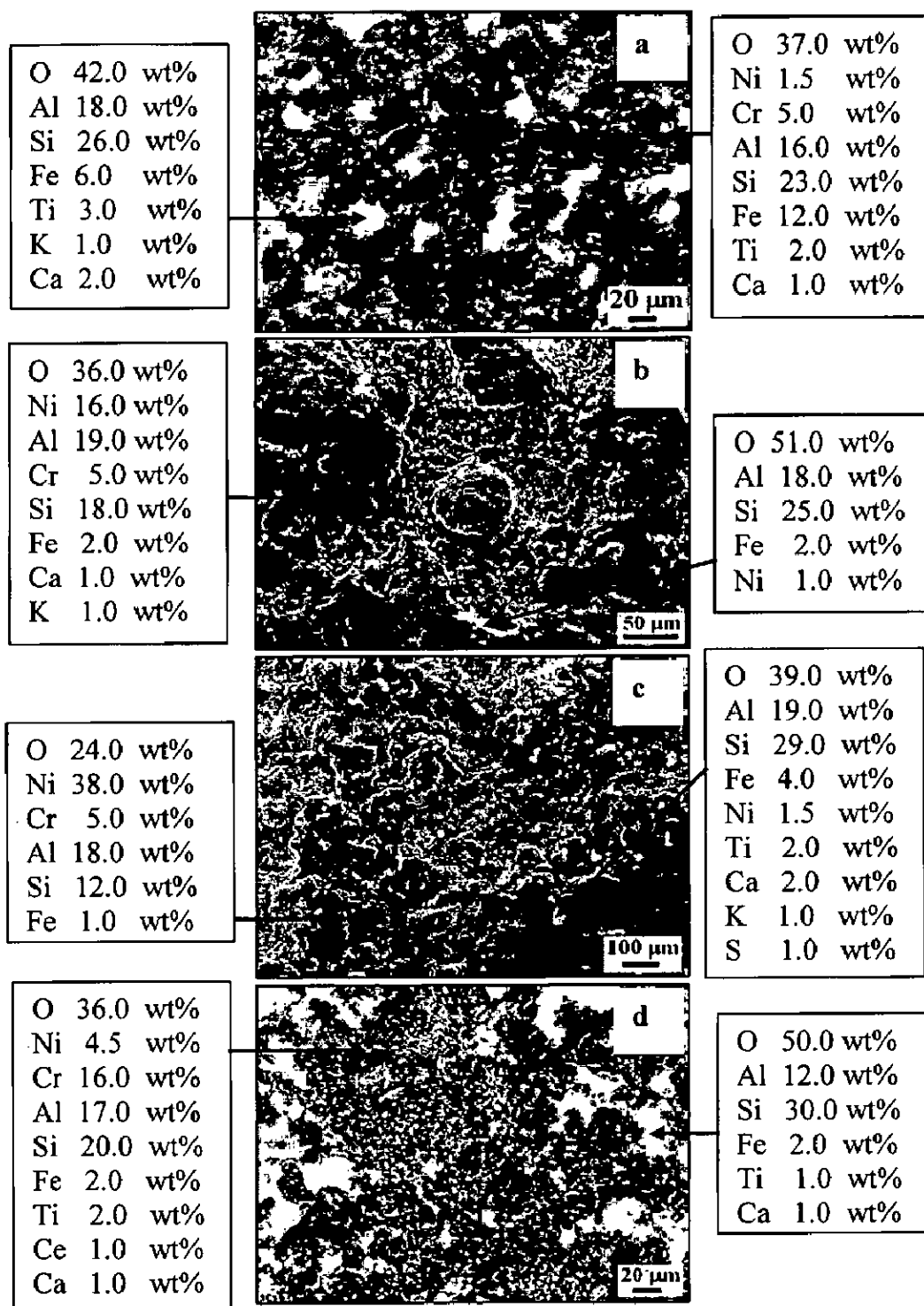


**Fig. 7.13:** FESEM/EDAX analysis showing elemental composition (wt.%) for the bare and HVOF coated Superfer 800 after 1000 hrs exposure to low temperature superheater zone of the coal fired boiler at 700 °C: (a) Bare Superfer 800 (b) Ni-5Al coated (c) NiCrAl coated (d) NiCrAlY-0.4wt%CeO<sub>2</sub> coated.

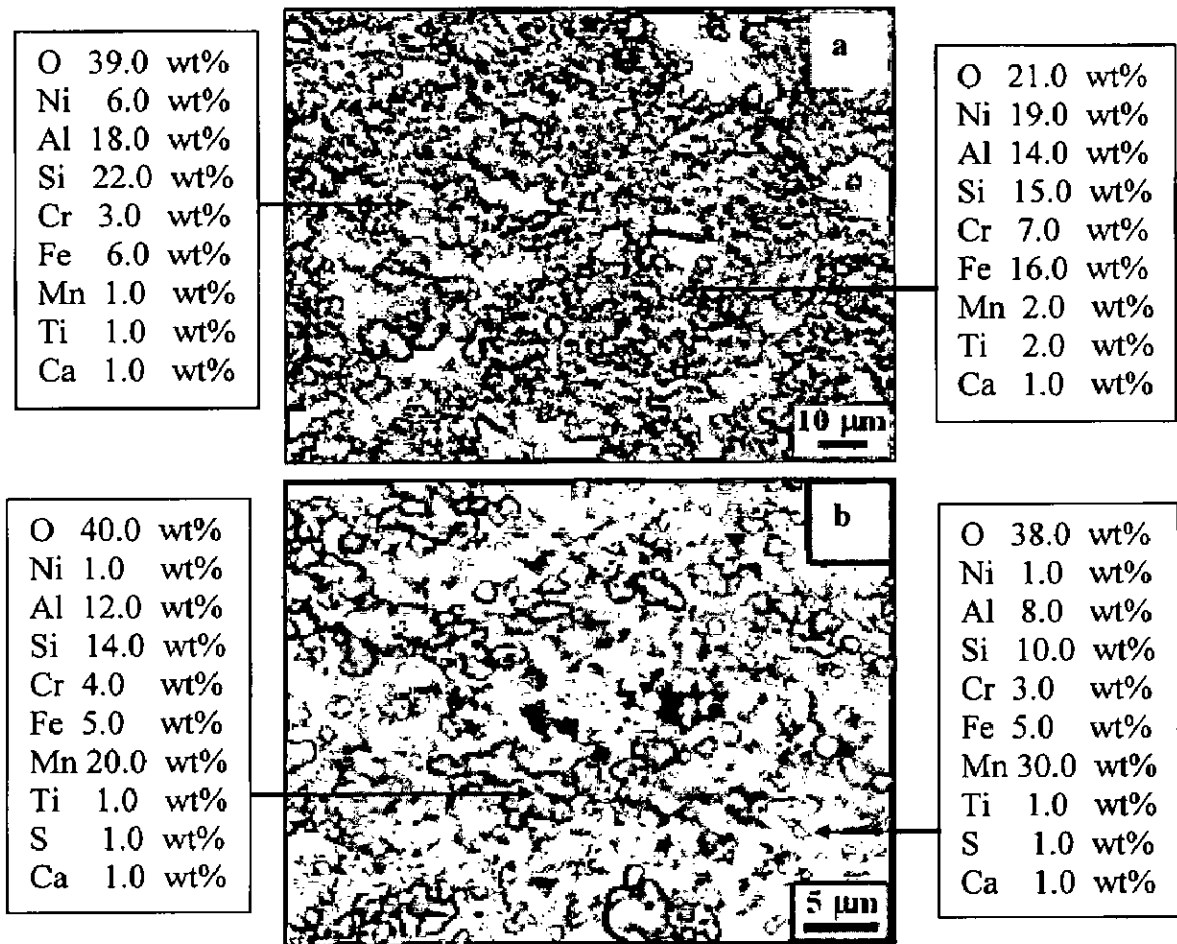


**Fig. 7.14:** FESEM/EDAX analysis showing elemental composition (wt.%) for the RF sputtered (a) Ni-Al and (ii) NiCrAl films on Superfer 800 after 1000 hrs exposure to low temperature superheater zone of the coal fired boiler at 700 °C.

#### 7.2.2.4 (b) Cross-Section Analysis

The BSE images and EDAX analysis at some selected points of interest across the cross-section of corroded uncoated and HVOF coated Superfer 800 are shown in Fig. 7.15-7.16. Very thin scale has formed on the top surface of the corroded uncoated Superfer 800 (Fig. 7.15a). EDAX analysis shows that mainly iron, nickel and chromium are found at the substrate (point 1). At the intermediate region (point 3), the EDAX analysis has shown the presence of oxygen. The top surface is unoxidised and consists mainly iron, nickel and chromium.

BSE image of the corroded Ni-5Al coated Superfer 800 (Fig. 7.15b) gives no indication of adhesion loss of the scale. The EDAX analysis shows the absence of oxygen near the coating-substrate interface (Point 1). Therefore, it can be inferred that Ni-5Al coating has developed a barrier to the penetration of oxygen. At the coating-substrate interface (Point 2), amount of Ni has reduced but aluminum content has increased with oxygen. The white areas (Point 3) in the scales are found to be Ni-rich splats and presence of small amount of oxygen at this point suggests that the Ni-rich splats are partially oxidised. The top surface of the scale (Point 4) is rich in aluminum and oxygen, which increased marginally with a substantial decrease in nickel suggesting that the top scale is rich in  $Al_2O_3$ .

The cross sectional BSE images of corroded NiCrAl coated Superfer 800 (Fig. 7.16a) shows the white areas (Point 1 and 4) in the scale are nickel rich splats with small amount of aluminum and chromium. Oxygen is absent at these points suggests that these nickel rich splats are in unoxidised state. The grey coloured area (Point 2 and 3) along the splat boundaries shows chromium and aluminum. There is a substantial decrease in nickel content and marginal increase in oxygen amount suggesting the formation of oxide stringers of chromium and aluminum. The dark areas (Point 5) near the coating-substrate interface are rich in aluminum and the amount of oxygen at this point also increased suggesting the formation of  $Al_2O_3$ . Further, there is a substantial decrease in the nickel and chromium content. At point 6, absence of oxygen indicates that the coating has prevented the penetration of oxygen into the substrate, thus protecting it from the corrosive species.

The BSE image of corroded NiCrAlY-0.4wt%CeO<sub>2</sub> coated Superfer 800 (Fig. 7.16a) shows the white areas (Point 1 and 4) are Ni-rich splats in the scale with small amount of chromium and aluminum. Point 2 and 3 shows the region where there is a substantial decrease in nickel content and increase in the oxygen and aluminum amount suggesting the formation of oxide stringers of Al<sub>2</sub>O<sub>3</sub> and Cr<sub>2</sub>O<sub>3</sub>. The dark areas (Point 5) near the coating-substrate interface indicate the presence of higher amount of aluminum and oxygen indicating the formation of Al<sub>2</sub>O<sub>3</sub>. Absence of oxygen (Point 6) shows that the coating has prevented the penetration of oxygen into the substrate superalloy.

The cross sectional BSE images of corroded RF sputtered Ni-Al coated film on Superfer 800 (Fig. 7.17a) shows that the film has not oxidised after 1000 hours of exposure to coal fired boiler environment. The film formed on the surface mainly consists of iron, nickel and chromium. Negligible amount of oxygen is present in the film. It is noted that the film formed on the surface is continuous and adherent as seen in the macrograph (Fig. 7.2a). Absence of oxygen in the substrate indicates the protective behaviour of the Ni-Al film in the given environment.

The BSE images of corroded RF sputtered NiCrAl coated film on Superfer 800 (Fig. 7.17b) shows that the film formed (Point 4 and 5) on the surface mainly consists of iron, nickel, chromium and aluminum. The Point 2 in the substrate indicates presence of some inclusion. The NiCrAl film has not oxidised during the exposure and only a very thin scale might have formed on the top surface of the film. The presence of silica on the top surface may be attributed to ash deposition during exposure to the boiler environment.

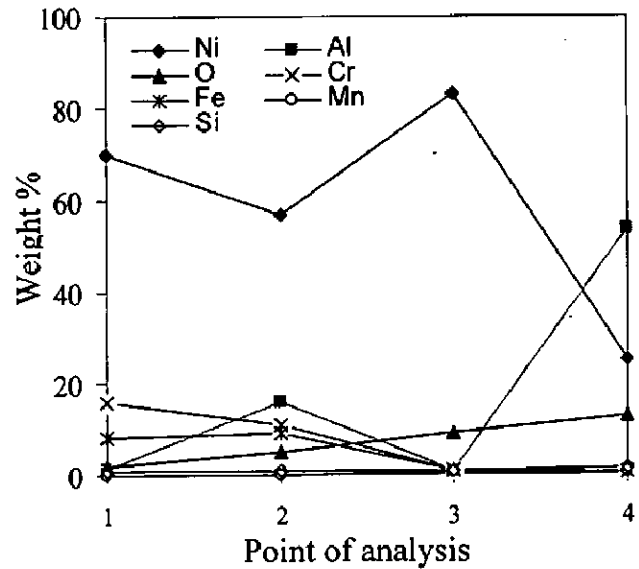
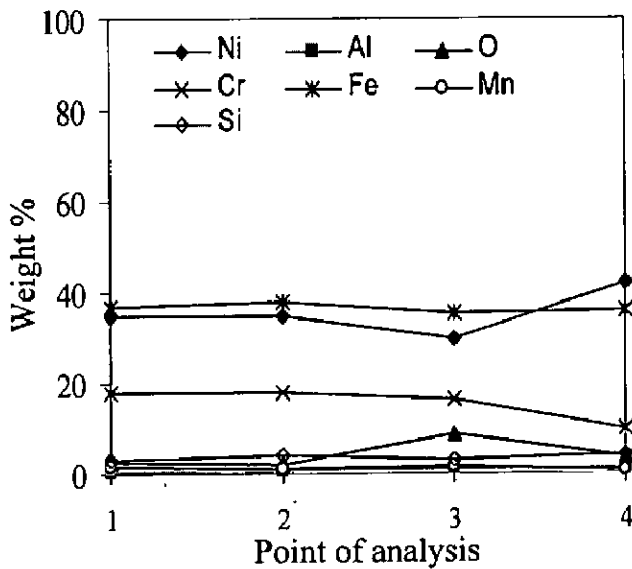
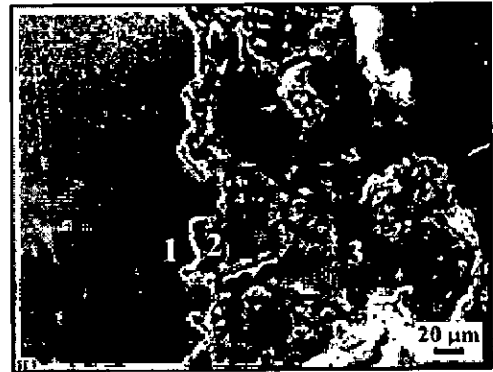


**Fig 7.15:** Oxide scale morphologies and variations of elemental composition (wt%) across the cross section of (a) bare and (b) HVOF sprayed Ni-5Al coating on Superfer 800 after 1000 hrs exposure to low temperature superheater zone of the coal fired boiler at 700 °C.

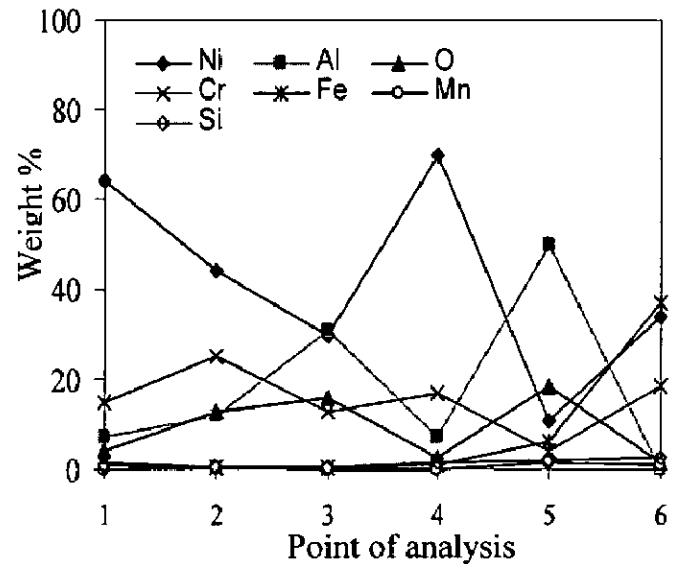
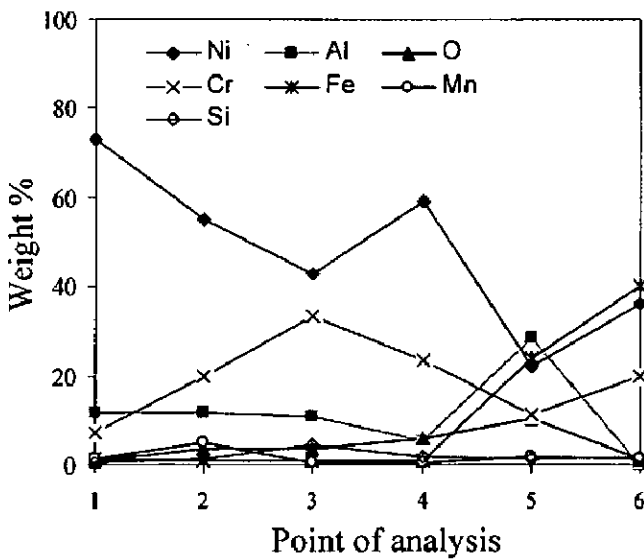
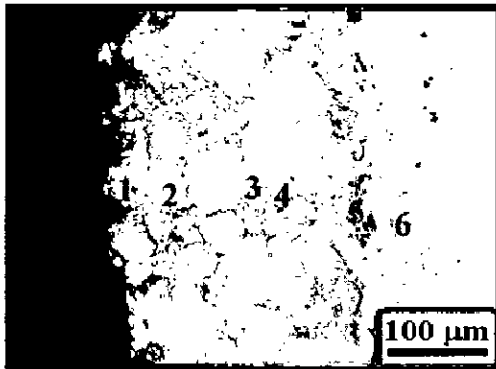


**Fig 7.16:** Oxide scale morphologies and variations of elemental composition (wt%) across the cross section of HVOF sprayed (a) NiCrAl and (b) NiCrAlY-0.4wt%CeO<sub>2</sub> coating on Superfer 800 after 1000 hrs exposure to low temperature superheater zone of the coal fired boiler at 700 °C.

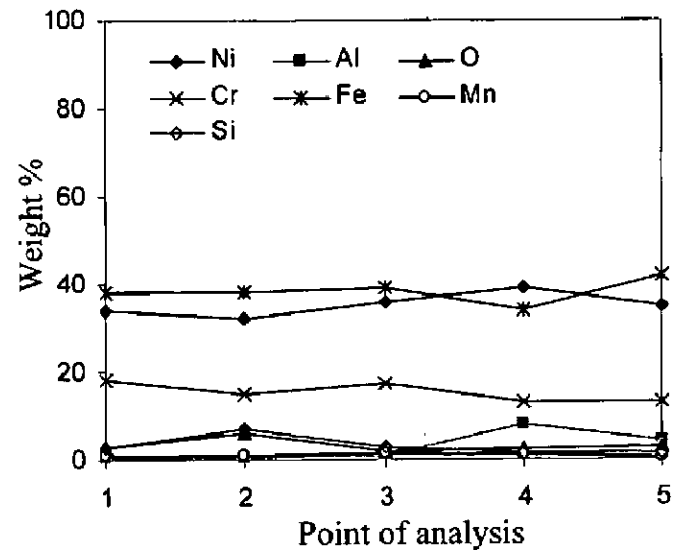
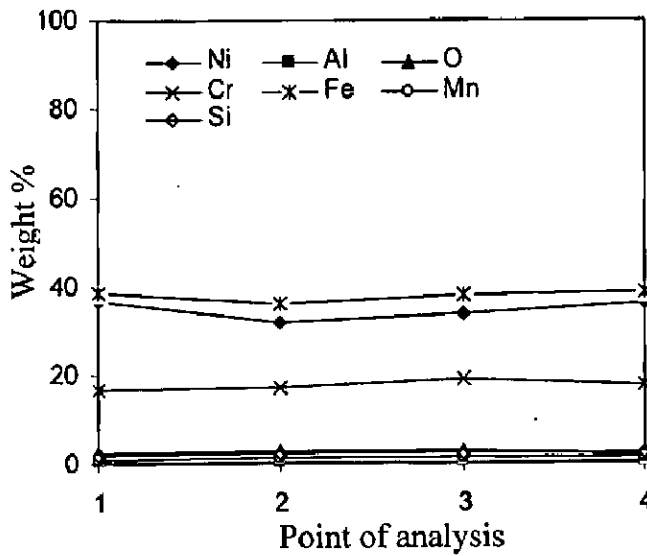
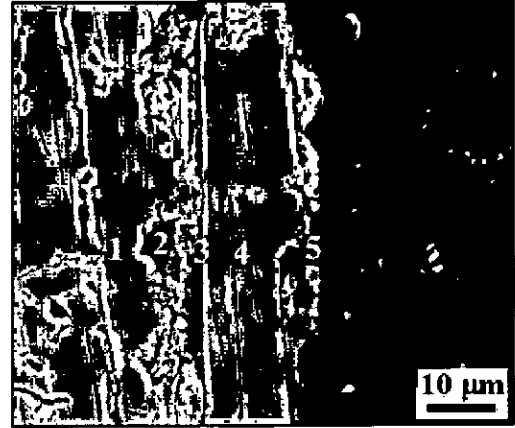
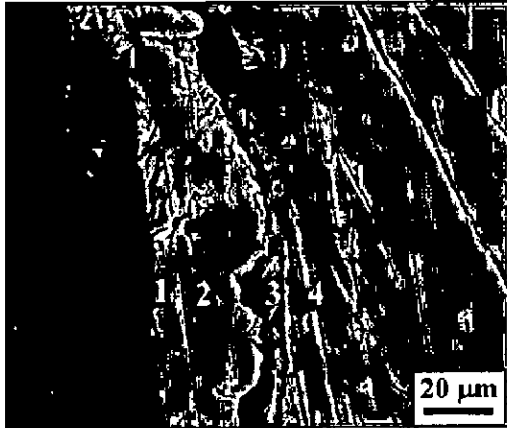


**Fig 7.17:** Oxide scale morphologies and variations of elemental composition (wt%) across the cross section of RF sputtered (a) Ni-Al and (b) NiCrAl films on Superfer 800 after 1000 hrs exposure to low temperature superheater zone of the coal fired boiler at 700 °C.

### 7.2.2.5 X-ray mapping analysis

BSE images and elemental X-ray maps for the uncoated and HVOF coated Superfer 800 after cyclic exposure to the given environment is shown in Fig. 7.18 to 7.21. The BSE images of the uncoated Superfer 800 shows no internal attack as the oxygen has not penetrated into the substrate (Fig. 7.18). Elemental maps show that the surface has not oxidised in the given environment under study.

The elemental map of different elements for Ni-5Al coated Superfer 800 (Fig. 7.19) indicate that the scale formed on the surface is adherent and continuous. The topmost layer of the scale is found to be enriched with aluminum oxide. The Ni-rich splats are present

throughout the scale which remain unoxidised whereas aluminum forms oxides at their boundaries. Small amount of Fe, Mn and Ti have diffused from the substrate into the coating. The penetration of oxygen is restricted upto scale-substrate interface thereby indicating the protective nature of the coating in the given environment.

The NiCrAl coated Superfer 800 forms a continuous and adherent oxide scale after exposure to boiler environment for 1000 hours at 900°C (Fig. 7.20). The scale consists of lamellar splat structure and it mainly consists of nickel with some amount of chromium existing together. Aluminum is present along the splat boundaries and existing with oxygen forming  $\text{Al}_2\text{O}_3$ . Iron has diffused from the substrate to reach the topmost scale. Small amounts of Mn and Si have diffused from the substrate into the coating.

The scale formed on the NiCrAlY-0.4wt%CeO<sub>2</sub> coated Superfer 800 after 1000 hrs exposure to the boiler environment has a lamellar structure with elongated splats (Fig. 7.21). The elemental mapping indicates that the splats consist of Ni and Cr, Al, and Cr are present along the splat boundaries with oxygen suggesting the formation of  $\text{Al}_2\text{O}_3$  and  $\text{Cr}_2\text{O}_3$ . Some islands of aluminum are present at the scale- substrate interface, where all other elements are found to be absent. The presence of oxygen at these places indicates that these islands are inclusions of aluminum oxide.

The X-ray mapping of different elements for RF sputtered Ni-Al film is shown in Fig.7.22. The top layer of the film consists of Ni, Cr and Fe. Chromium is absent in the interface and aluminum is also not found in the top surface of the film. Silicon is present along the interface with oxygen. The oxygen map indicates that the Ni-Al film has not oxidised after exposure to boiler environment for 1000 hours. The Ni-Al film on Superfer 800 has prevented the penetration of oxygen into the substrate.

The oxide scale formed on the RF sputtered NiCrAl coated film on Superfer 800 is very thin (Fig.7.23) in the given environment. The top scale consists of  $\text{Al}_2\text{O}_3$  and  $\text{SiO}_2$  indicating the deposition of ash. NiCrAl film is intact on the substrate and there is no oxygen penetration along the film-substrate interface. A nickel rich band is present on the top surface of the film followed by a chromium rich band in the subsurface region. It is observed that wherever nickel is present in the film, aluminum is absent. The dark area in the substrate may be some inclusion consisting of silicon. Manganese is present throughout the film and the film has not oxidised after 1000 hours of exposure in the boiler environment.



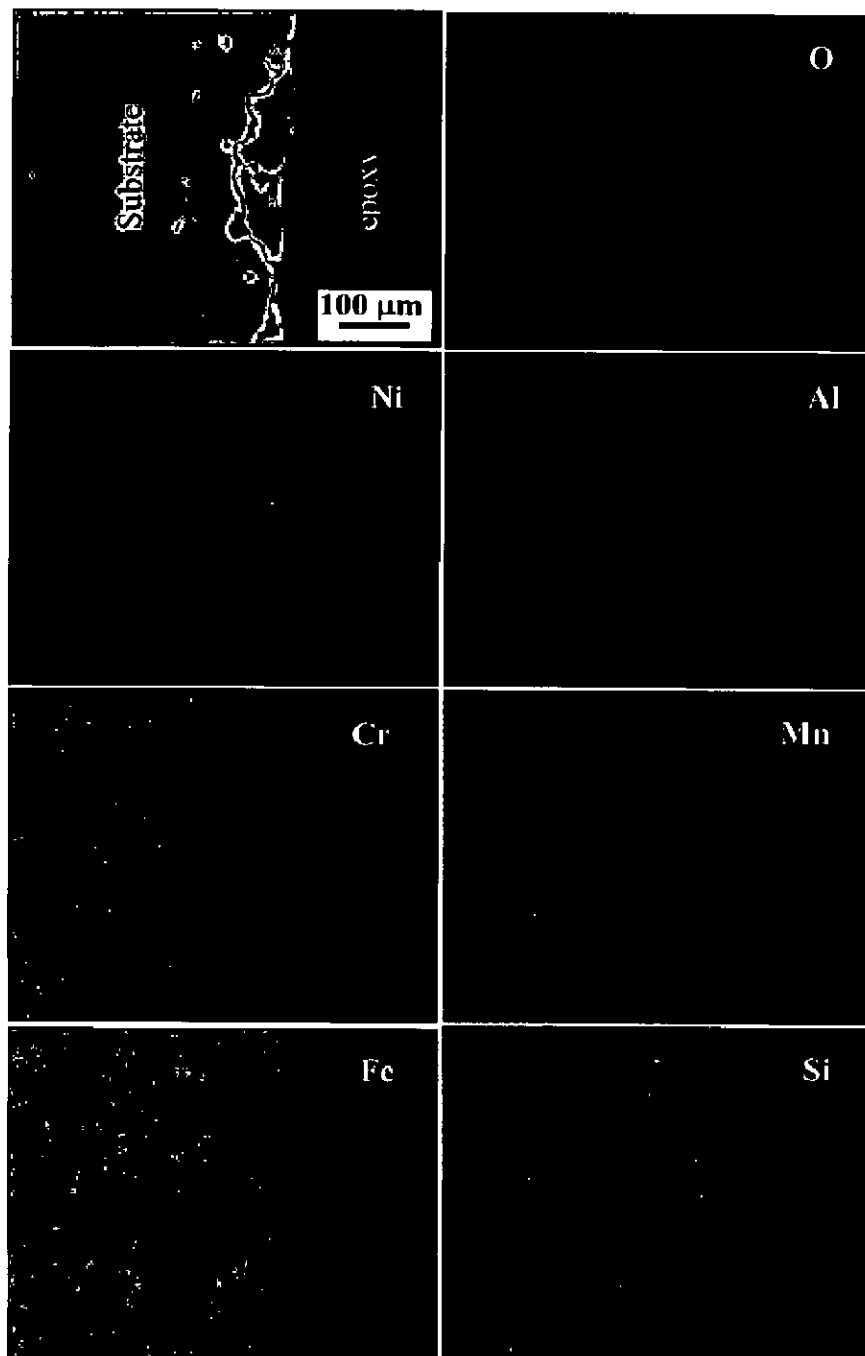


**Fig. 7.18:** Composition image (BSEI) and X-ray mappings across the cross-section of uncoated Superfer 800 after 1000 hrs exposure to low temperature superheater zone of the coal fired boiler at 700 °C.

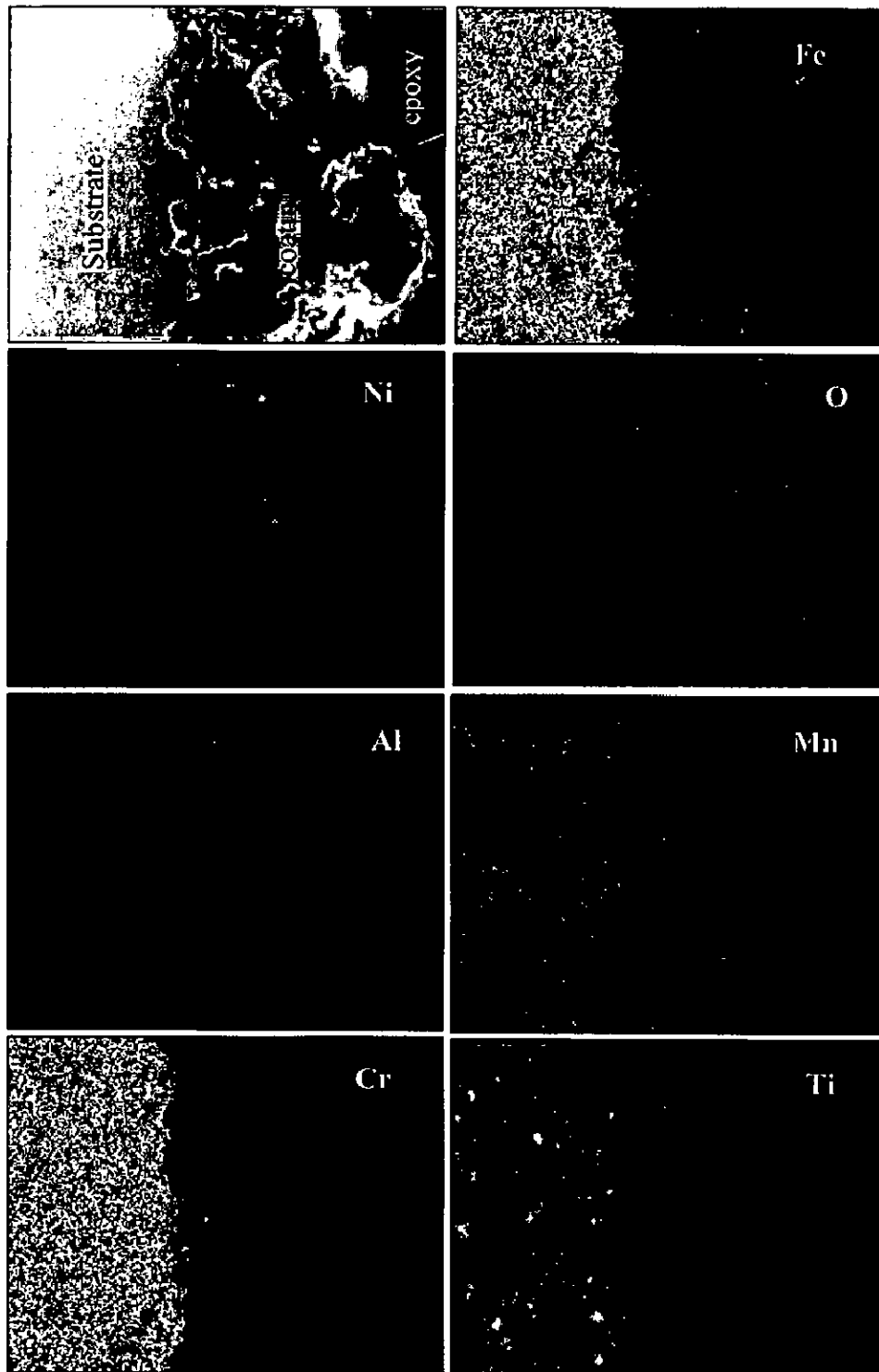


**Fig. 7.19:** Composition image (BSEI) and X-ray mappings across the cross-section of HVOF sprayed Ni-5Al coated Superfer 800 after 1000 hrs exposure to low temperature superheater zone of the coal fired boiler at 700 °C.

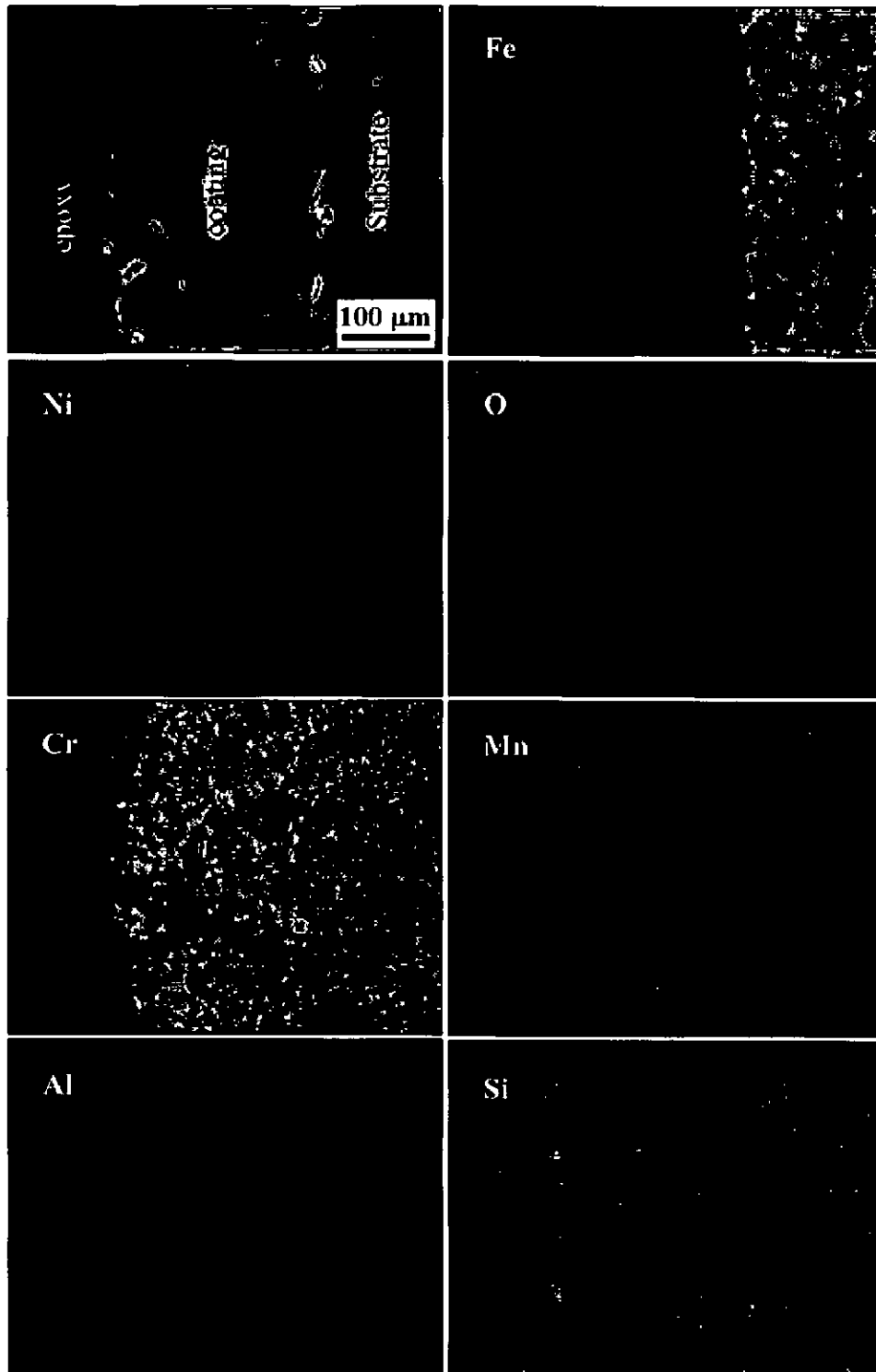


**Fig. 7.20:** Composition image (BSEI) and X-ray mappings across the cross-section of HVOF sprayed NiCrAl coated Superfer 800 after 1000 hrs exposure to low temperature superheater zone of the coal fired boiler at 700 °C.

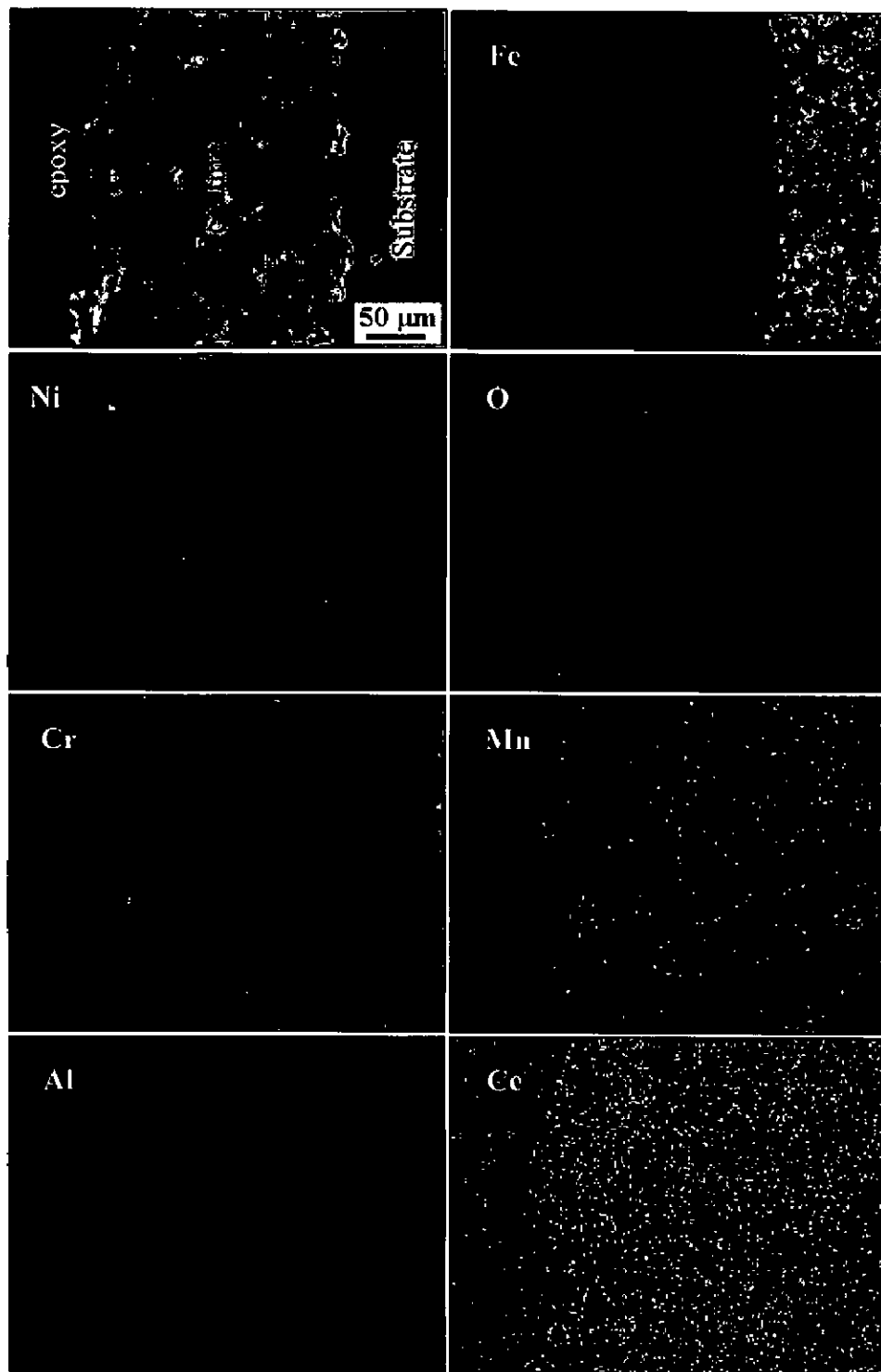


**Fig. 7.21:** Composition image (BSEI) and X-ray mappings across the cross-section of HVOF sprayed NiCrAlY-0.4wt%CeO<sub>2</sub> coated Superfer 800 after 1000 hrs exposure to low temperature superheater zone of the coal fired boiler at 700 °C.

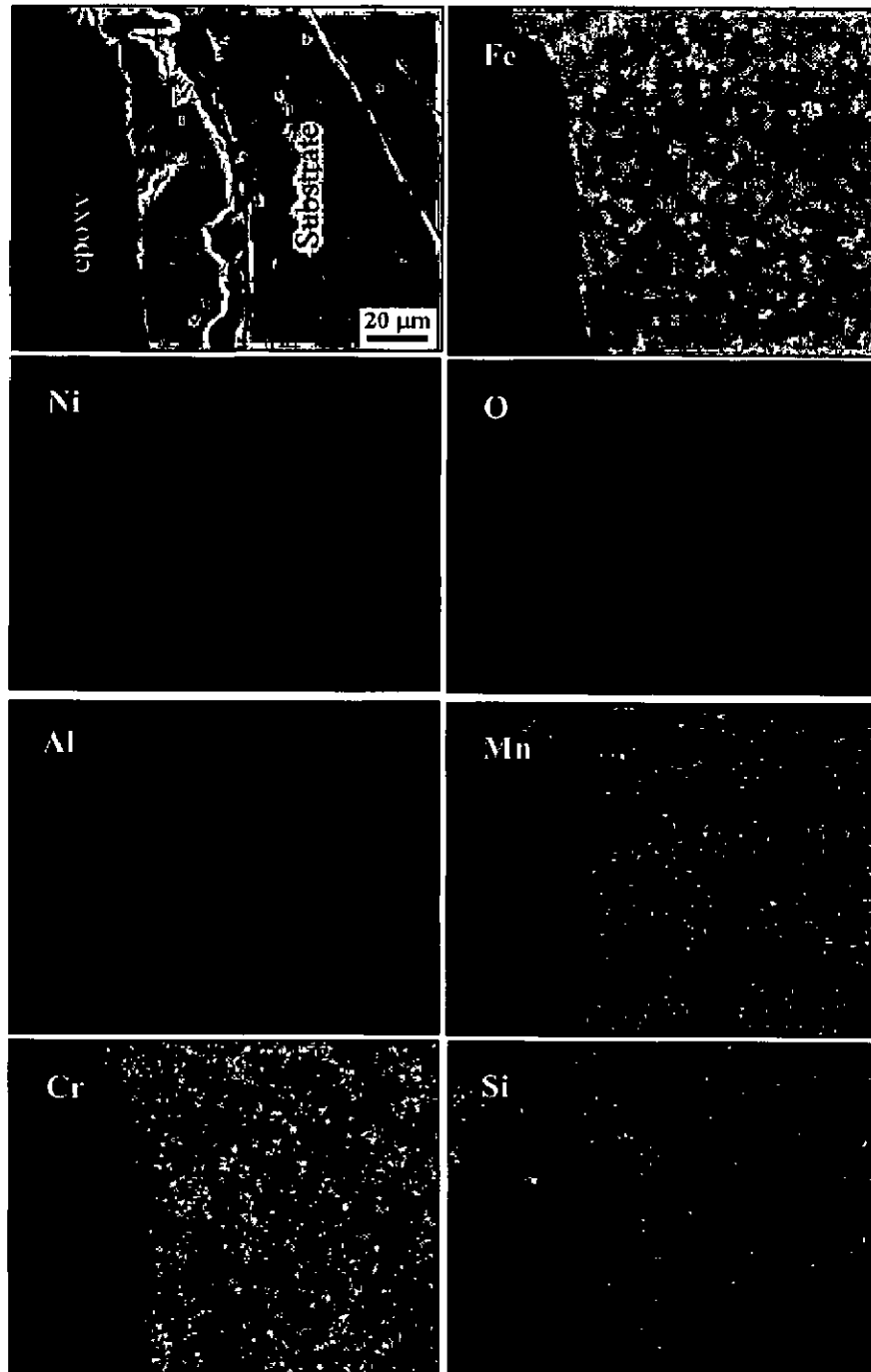


**Fig. 7.22:** Composition image (BSEI) and X-ray mappings across the cross-section of RF sputtered Ni-Al film on Superfer 800 after 1000 hrs exposure to low temperature superheater zone of the coal fired boiler at 700 °C.

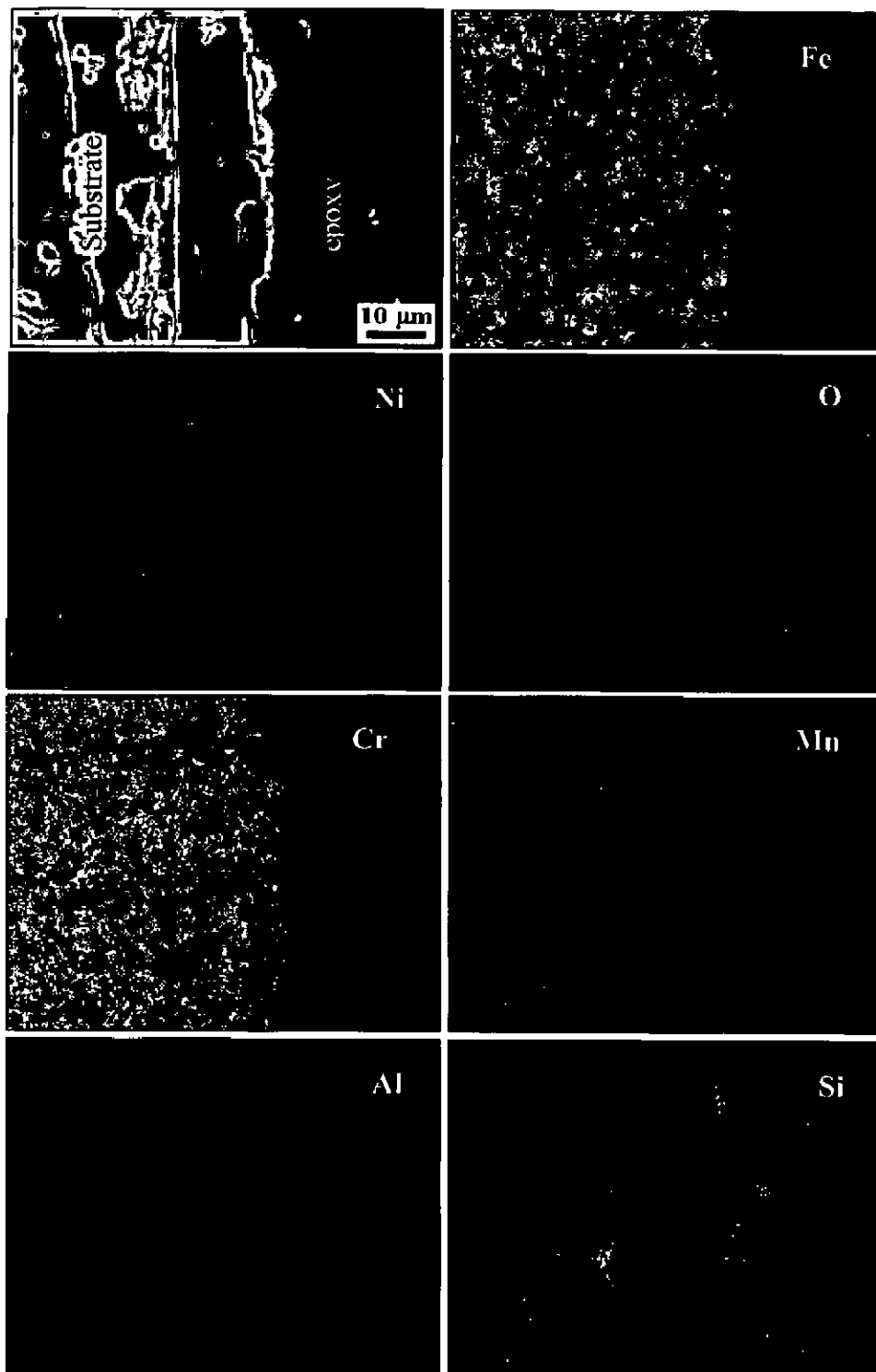


**Fig. 7.23:** Composition image (BSEI) and X-ray mappings across the cross-section of RF sputtered NiCrAl film on Superfer 800 after 1000 hrs exposure to low temperature superheater zone of the coal fired boiler at 700 °C.

### 7.3 SUMMARY OF RESULTS

Results obtained after 1000 hours exposure of uncoated and coated (HVOF and RF sputtered) Superfer 800 to the low temperature superheater zone of the coal fired boiler at  $700 \pm 10^\circ\text{C}$  are summarised in Table 7.1.

**Table 7.1:** Summary of the results for uncoated and coated Superfer 800 exposed to low temperature superheater zone of the coal fired boiler at around  $700^\circ\text{C}$  for 1000 hours.

Bare Super alloy	Coating	Weight gain $\text{mg}/\text{cm}^2$	$k_p \times 10^{-12} \text{ g}^2 \text{ cm}^{-4} \text{ s}^{-1}$	coating thickness $\mu\text{m}$	Major XRD phases	Minor XRD Phases	Remarks
Superfer 800	Uncoated	3.73	----	75	$\text{AlNi}_3$	----	Light brownish grey colored scale is formed. No spallation from the surface is observed.
	HVOF coated Ni-5Al	1.67	----	100	$\gamma\text{-Ni}$	$\text{Fe}_2\text{O}_3$ and NiO	Coating spalled from the surface after 200 hrs of exposure. Light grey coloured scale formed on the surface turned into yellowish grey with green shade after 1000 hrs.
	HVOF coated NiCrAl	1.58	0.75	245	$\gamma\text{-Ni}$ and $\text{AlNi}_3$	$\alpha\text{-Cr}$	Grey coloured scale formed after 200 hrs and turned into light yellowish grey after 1000 hrs of exposure. No spallation is observed during the course of the study.

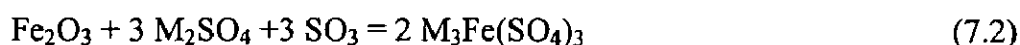
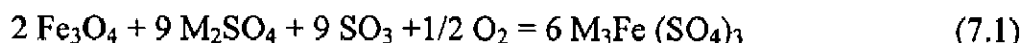
	HVOF coated NiCrAlY-0.4wt%CeO <sub>2</sub>	1.55	0.6	230	γ-Ni, AlNi and α-Cr	----	Light yellowish grey colour with green patch is formed on the surface after 1000 hrs. No spallation is observed during the course of the study.
Superfer 800	RF sputtered Ni-Al	0.66	0.13	75	γ-Ni and AlNi	----	Grey colored scale after 200 hours turned into grey color with brown and reddish patches. No spallation from the surface is observed.
	RF sputtered NiCrAl	1.54	0.38	100	AlNi <sub>3</sub>	----	The scale formed on the surface show grey with green shades after 1000 hrs.



## 7.4 COMPREHENSIVE DISCUSSION

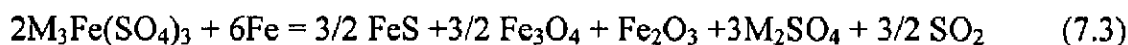
### 7.4.1 Uncoated Superalloys

The EDAX analysis (Fig.7.13a) shows the presence of ash deposition on the surface of the specimens. The interaction of ash ( $\text{Na}_2\text{O}$ ,  $\text{K}_2\text{O}$  etc.) with the boiler gas ( $\text{SO}_2$ ,  $\text{SO}_3$ ,  $\text{O}_2$  etc.) results in the formation of alkali sulphates ( $\text{K}_2\text{SO}_4$ ,  $\text{Na}_2\text{SO}_4$ ). These alkali sulphates react with iron oxides (present in the scale or in the ash itself), in presence of  $\text{SO}_3$  in the gas, to form alkali-ion trisulphates  $(\text{Na,K})_3\text{Fe}(\text{SO}_4)_3$  according to the following reactions.



Where  $\text{M} = \text{Na}$  or  $\text{K}$

These alkali-iron trisulphates are molten at the operating temperature of the boiler due to their low melting temperatures:  $624^\circ\text{C}$  for  $\text{Na}_3\text{Fe}(\text{SO}_4)_3$ ,  $618^\circ\text{C}$  for  $\text{K}_3\text{Fe}(\text{SO}_4)_3$  and  $552^\circ\text{C}$  for the mixed compound  $(\text{Na,K})_3\text{Fe}(\text{SO}_4)_3$  (Srivastava et al. 1997; Weulersse-Mouturat et al., 2004). These molten compounds can flux the scale or react with the metal to form internal sulphides as per reaction given below:



Therefore, these alkali-iron trisulphides are responsible for the degradation of superheater in the coal-fired plants.

The XRD analysis of the corroded uncoated Superfer 800 did not indicate the presence of the sulphides in the oxide scale. This may be due to the formation of very thin oxide scale on the surface. Weulersse-Mouturat et al. (2004) reported that due to their low content, alkali-iron-trisulphates were not identified in the scale. The (weight change/area)<sup>2</sup> versus time plots also show deviations from the parabolic rate law (Fig.7.5) indicating inhomogeneous formation of oxide scale on the surface during the experiments.

The X-ray mapping analysis indicates that the scale formed on the surface is continuous with the substrate in the given environment. Overall analysis of the substrate specimen indicates that a thin layer of the scale has formed on the surface when exposed to coal fired boiler environment. The presence of ash deposits on the surface of the specimen is an indication of negligible erosion mode of degradation in this particular zone of the boiler.

## 7.4.2 HVOF Coated Superfer 800

### 7.4.2.1 Ni-5Al Coating

The weight change data and the corrosion rate show that the Ni-5Al coating provides relatively less protection to the base alloy in the give boiler environment as compared to other coatings under study. The coating indicated the spallation during the initial period of cyclic study (Fig 7.1b). The BES images of the coated Superfer 800 show no indication of internal attack (Fig. 7.7b). Oxygen elemental map for coated Superfer 800 alloy confirms that the permeation of oxygen is restricted to scale-substrate interface and substrate superalloys indicate no sign of oxidation (Fig. 7.19). The partially oxidised coating is in intimate contact with the substrate as it is evident from the BSEI micrograph shown in Fig. 7.7b.

The partial oxidation of the coating at the splat boundaries is observed. The presence of oxygen in the coating might be attributed to the penetration of some oxidising species through the open pores and along the splat boundaries of the coating during the initial period of exposure. Once the protective layer is formed on the surface and oxides are formed in the intersplat region, the penetration of the corroding species is clogged. Identical findings have been reported by Belzunce et al (2001) where they observed internal oxidation during earlier stages of the study and suggested the penetration of oxidising species into the coatings through the open pores until all the accessible internal surfaces got oxidised. Niranatlumpong et al. (2000) also opined that internal oxidation takes place due to porosity in the thermal spray coatings.

The weight change curve for Ni-5Al coated Superfer 800 showed the deviation from the parabolic rate law. It is due to the spalling of the scale during the exposure. The weight gain is high during the initial period of exposure due to the formation of oxides at the surface and splat boundaries and within the open pores due to the penetration of oxygen.

The XRD analysis indicates the formation of  $\gamma$ -Ni. It is believed that the scale formed on the surface of the Ni-5Al coated specimen is very thin and the X-rays have penetrated deep into the coating and indicated the presence of nickel as the main phase. XRD also indicates the minor phases such as NiO and Fe<sub>2</sub>O<sub>3</sub>. The EDAX analysis of the corroded surface after 1000 hrs of exposure shows the presence of higher amount of aluminum, silicon and oxygen indicating the composition of the ash. The cross sectional EDAX analysis shows that the aluminum oxide formed along the splat boundaries is responsible for blocking the transport of degrading species through Ni-5Al coating. X-ray mapping analysis further supported the results of EDAX analysis.

#### 7.4.2.2 NiCrAl Coating

This coating is effective in imparting necessary protection to Superfer 800 and has shown no spalling during the course of the study. The BSE images of the coated Superfer 800 show no indications of any internal corrosion attack (Fig.7.7c). Oxygen elemental map for the coated superalloy confirm that the permeation of oxygen is restricted to scale-substrate interface and substrate alloy indicate no sign of oxidation (Fig. 7.20). The partially oxidised coating is in intimate contact with the substrate as it is evident from the BSEI micrograph (Fig.7.7c). Therefore, it is concluded that the NiCrAl coating has provided necessary protection to Superfer 800 alloy in the coal fired boiler environment.

The superior corrosion resistance of NiCrAl coated Superfer 800 is due to the formation of thin layer of oxides of chromium and nickel in the topmost part of the scale as revealed by cross sectional X-ray mapping analysis (Fig. 7.20). The greenish colored scale formed on the surface is an indication for the formation of NiO. The NiCrAl coated Superfer 800 followed the parabolic rate law during cyclic exposure to boiler environment. Hence, it can be inferred from that the coating shows a tendency to act like a barrier to the corroding species in the given environment of the coal fired boiler.

The main phases identified by the XRD analysis on NiCrAl coated Superfer 800 after exposure to boiler environment are  $\gamma$ -Ni and AlNi with some minor phases of  $\alpha$ -Cr. The phases are similar to the as sprayed condition of the coating. It is believed that the scale formed on the surface is very thin and X-rays penetrated deep into the coating indicating the phases of as sprayed coating. Whereas, the surface EDAX analysis indicated the white phase of the scale consists mainly alumina and silica along with some amounts of  $\text{Fe}_2\text{O}_3$ ,  $\text{TiO}_2$ , CaO and  $\text{K}_2\text{O}$ . The cross sectional EDAX analysis show that oxides of aluminum and chromium have formed along the nickel rich splat boundaries, which were responsible for blocking the transport of degrading species through the NiCrAl coatings. The X-ray mapping analysis further supported the EDAX results.

#### 7.4.2.5 NiCrAlY-0.4wt%CeO<sub>2</sub> Coating

This coating is shown to be excellent in imparting necessary protection to Superfer 800 after 1000 hrs exposure to the coal fired boiler environment. The BSE images of the coated Superfer 800 show that the partially oxidised coating is in intimate contact with the substrate and shows no indications of any internal corrosion attack (Fig.7.7d). The presence of oxygen in the coating indicates the penetration of oxygen during the initial exposure to the environment. The selective oxidation of chromium and aluminum along the splat boundaries (as seen by combining the x-ray maps of O, Al and Cr) helps in blocking the corrosive species through it.

The coating consists of dense and elongated splats in the coating, the distance for the corrosive species to traverse from the coating surface to the substrate along the splat boundaries are long. These combined advantages restrict the corrosive species reaching the substrate. Oxygen elemental maps for the coated superalloy confirm that the permeation of oxygen is restricted to scale-substrate interface and substrate alloy indicate no sign of oxidation (Fig. 7.21). Therefore, it is concluded that the NiCrAlY-0.4wt%CeO<sub>2</sub> coating has provided necessary protection to Superfer 800 alloy in the coal fired boiler environment.

The weight gain per unit area is increasing during the initial period of exposure and then become gradual with further exposure. The weight change curve for NiCrAlY-0.4wt%CeO<sub>2</sub> coated Superfer 800 follows the parabolic rate law. It is observed from the macrograph that light yellowish grey colour with green patch has formed on the surface after 1000 hrs of exposure. No spallation is observed during the course of the cyclic study.

The XRD analysis indicates the formation of  $\gamma$ -Ni, AlNi and  $\alpha$ -Cr. This suggests the formation of as sprayed coating phases. The scale formed on the surface of the NiCrAlY-0.4wt%CeO<sub>2</sub> coated specimen may be very thin and the X-rays might have penetrated deep into the coating and indicated the presence of nickel as the main phase. The surface EDAX analysis shows that the white phase of the scale consists mainly of SiO<sub>2</sub>, Al<sub>2</sub>O<sub>3</sub>, and some amounts of Fe<sub>2</sub>O<sub>3</sub>, TiO<sub>2</sub>, CaO and K<sub>2</sub>O. It is inferred that the composition of the white phase is almost similar to ash composition along with some other oxides of the scale. The cross sectional EDAX analysis shows that the elongated splats with oxide stringers of chromium and aluminum at the splat boundaries which is further supported by X-ray mapping analysis.

### **7.4.3 RF Magnetron Sputtered Superfer 800**

#### **7.4.3.1 Ni-Al Coating**

The RF sputtered Ni-Al film on Superfer 800 exhibit good resistance to corrosion in coal fired boiler environment. The fluctuation in the weight gain data may be due to fly ash deposition, rapid thermal cycling on the exposed sample. The coating indicated the spalling tendency after 200 hours of exposure and it continued upto 400 hours of exposure. The BSE images of the Ni-Al coated Superfer 800 show no indication of internal attack (Fig. 7.9a). The scale formed on the exposed surface is very thin and it has cracked during cutting across the cross section. Oxygen elemental map for coated Superfer 800 alloy shows that the permeation of oxygen is restricted to scale-substrate interface and substrate superalloy indicate no sign of oxidation (Fig. 7.22). Thus, it provides a better protection to the substrate Superfer 800. The cross sectional EDAX analysis indicates that the film contains iron, nickel and chromium.

The XRD analysis indicates the formation of  $\gamma$ -Ni and AlNi after 1000 hrs exposure. This suggests the Ni-Al coated surface of the specimen has not oxidised and shows the as sprayed phases of the coating. From the macrographs (Fig. 7.2a), it could be noted that a very thin layer has formed on the surface after exposing to the boiler environment. The surface EDAX analysis shows that the scale consists mainly of  $\text{SiO}_2$ ,  $\text{Al}_2\text{O}_3$ , and some amounts of  $\text{Fe}_2\text{O}_3$ ,  $\text{TiO}_2$ , CaO and  $\text{TiO}_2$ . The X-ray mapping analysis indicates that the film formed on the surface is rich in iron, nickel and chromium which is also supported by cross sectional EDAX analysis. Presence of manganese in the top layer may be attributed to the deposition of manganese from the steel target.

#### 7.4.3.2 NiCrAl Coating

The NiCrAl film has been successful in providing protection to Superfer 800 in the actual coal fired boiler. The weight change data show that the RF sputtered NiCrAl coating has shown slightly higher weight gain as compared to that of Ni-Al coating on Superfer 800. No spallation is observed during cyclic study and the weight gain is rapid during the initial period of exposure. The fluctuations in the weight gain may be due to the deposition of ash in the coal fired boiler environment. This is a result of fly ash deposit formation and fouling of the samples. The falling off and the regeneration of the ash deposits and oxide layer on the coating are repeated during the exposure of the sample. Palit and Mandal, (1994), Mukhopadhyay and Mandal (1999), and Stringer (1995) have reported the incidence of fly ash erosion, fouling and fireside deposit formation in pulverised coal fired boiler. It is observed from the  $(\text{weight gain/area})^2$  versus time graph that NiCrAl coated film on Superfer 800 show some deviation from the parabolic rate law. The cross sectional BES images of the NiCrAl coated Superfer 800 show that no indication of internal attack (Fig. 7.9b). Oxygen elemental map for NiCrAl coated film on Superfer 800 alloy show that oxygen has penetrated upto coating-substrate interface and formed oxide band thus indicating better protection to the Superfer 800 in the boiler environment.

The FESEM/EDAX analysis indicates the presence of granular scale on the surface after exposure to the given environment. The surface EDAX analysis shows that the white phase of the scale consists of mainly alumina and silica along with some amounts of  $\text{Fe}_2\text{O}_3$ ,  $\text{TiO}_2$ . Presence of higher amount of manganese in the surface scale indicates the manganese deposition during sputtering process. X-ray mapping analysis indicate that the top scale consist of  $\text{SiO}_2$  (as seen by combining the X-ray maps of oxygen and silicon), which may be attributed to the deposition of ash during the period of exposure.

# COMPARATIVE DISCUSSION

---

---

This chapter describes the comparative performance of the uncoated, HVOF coated and RF magnetron sputtered superalloys in air, molten salt ( $\text{Na}_2\text{SO}_4\text{-60\%V}_2\text{O}_5$ ) environment as well as in the actual working environment of the coal fired boiler at  $700^\circ\text{C}$  under cyclic conditions.

### 8.1 OXIADATION IN AIR

The bar charts showing the overall weight gains for the uncoated and coated superalloys after 100 cycles in air is presented in Figs. 8.1. From the bar charts, it can be inferred that the superalloys under study have shown higher oxidation resistance as compared to that in the given molten salt environment under cyclic conditions. Superfer 800 has indicated higher resistance to air oxidation, whereas Superni 750 shows minimum resistance to air oxidation among all the superalloys on the basis of weight gain data. From the bar charts, it is evident that the coatings, used in the present investigation, have successfully reduced the overall weight gain in all the cases. Among HVOF coated superalloys, NiCrAlY-0.4wt%  $\text{CeO}_2$  coated Superfer 800 has provided the best protection compared to other two HVOF coated superalloys. The BSE images show that the partially oxidised coatings are in good contact with the substrate superalloy (Fig 7.17). The better protection of ceria added NiCrAlY coating may be attributed to the formation of elongated splats in the coating structure and also the presence of streaks of chromium oxide and aluminum oxide along the nickel rich splat boundaries (Fig 7.18) acts as a barrier to the oxidising species diffusing into the coating and ultimately into the substrate superalloy. The presence of small concentrations of Y within the scale in solid solution could have reduced the scale growth rate. The segregation of yttrium to the grain boundaries of the  $\alpha\text{-Al}_2\text{O}_3$  scale could also reduce its growth rate (Stott, 1989) as well as improve its elevated temperature mechanical strength. According to Nicholls and Hancock (1989), Y could segregate to fill voids or pores along the grain boundaries of the scale, improving its cohesion. All the coatings follow the parabolic rate law of oxidation, whereas the uncoated superalloys deviated from the parabolic rate law. Therefore it is concluded that coated superalloys have performed better than the bare superalloys in the given environment under cyclic conditions at elevated temperature of

900°C. In case of RF sputtered coatings, Ni-Al coated film on Superni 76 and Superfer 800 have provided best protection to the superalloys in air at 900°C under cyclic conditions. Ni-Al coated film on Superni 750 show slightly higher weight gain. The better protection by RF sputtered films may be attributed to the formation of an adherent and continuous film on the specimens at elevated temperature. Figure 8.1 leads to the conclusion that the RF-sputtered Ni-Al coating provide maximum resistance, whereas HVOF coated NiCrAl indicate lower resistance to oxidation in air. Coated film is about 10 µm and after oxidation and hot corrosion experiment, most of the film remains unaffected but only reaction is confined to the surface and the weight change during the experiments is negligible.

## 8.2 MOLTEN SALT ENVIRONMENT

The bar charts showing the overall weight gains for the uncoated and coated superalloys after 100 cycles in molten salt environment is presented in Fig. 8.2. From the bar charts, it can be inferred that the uncoated superalloys have shown higher weight gain as compared to coated superalloys in the given molten salt environment under cyclic conditions. The uncoated Superni 76 has shown lower resistance to the molten salt environment, whereas Superfer 800 has shown higher resistance in the given environment. The accelerated corrosion of the Superni 76 might be attributed to presence of 9.0% molybdenum content in the basic composition of this alloy and it was suggested that the additional presence of molybdenum compounds  $\text{Na}_2\text{MoO}_4\text{-MoO}_3$  cause enhanced degradation (Swaminathan and Raghavan, 1994). The X-ray maps obtained after 100 cycles of exposure to the molten salt environment indicate that all the HVOF coatings protect the base superalloy against the penetration of oxygen and other corrosive species, and the BSE images show that the partially oxidised coatings are in good contact with the substrate in all the cases (Fig.5.24b, Fig. 8c (1047-hot cor-750 X-ray), Fig. 7.25c). The coatings get oxidised only at the splat boundaries which act as diffusion barriers against the penetration of corroding species. In case of RF sputtered Ni-Al coating, the film formed on the surface is uniform, continuous and adherent with the substrate and the film formed on the substrate is very thin (Fig.1.13a, Fig.1.16a). The grain size of the Ni-Al film is found around 18 nm from the XRD analysis. The RF sputtered NiCrAl coated film on Superfer 800 suffered accelerated attack in the molten salt environment. On the other hand, the oxide scale formed on the bare superalloy is fragile and spalled continuously during the course of the experiment, thereby reducing the thickness of the sound metal. All the coatings followed the parabolic rate law, whereas the

uncoated superalloys deviated from the parabolic rate law. Therefore, it is concluded that the coated superalloys have performed better than the bare superalloys in the given molten salt environment of  $\text{Na}_2\text{SO}_4$ -60% $\text{V}_2\text{O}_5$  salt mixture at  $900^\circ\text{C}$  under cyclic conditions.

### 8.3 INDUSTRIAL ENVIRONMENT

As observed in oxidation and molten salt environment, all the coatings, in general have shown good resistance to hot corrosion in the industrial environment consisting of actual working condition of the coal fired boiler. The uncoated Superfer 800 has suffered minor internal attack in the coal fired boiler environment at  $700^\circ\text{C}$ . The BSE images show that the partially oxidised coatings are in good contact with the substrates (Fig 7.7). In case of HVOF coated Ni-5Al on Superfer 800, some spalling has been observed during the initial period of exposure (Fig. 7.1b). The fluctuation in weight gain data during the experiment can be attributed to the fly ash deposition and rapid thermal cycling which leads to falling off and the regeneration of the ash deposit and the oxide scale. The  $(\text{weight gain/area})^2$  plot for the uncoated and HVOF coated Ni-5Al coated Superfer 800 show slight deviations from the parabolic rate law due to the rapid weight change and spalling of the scale during the experiment.

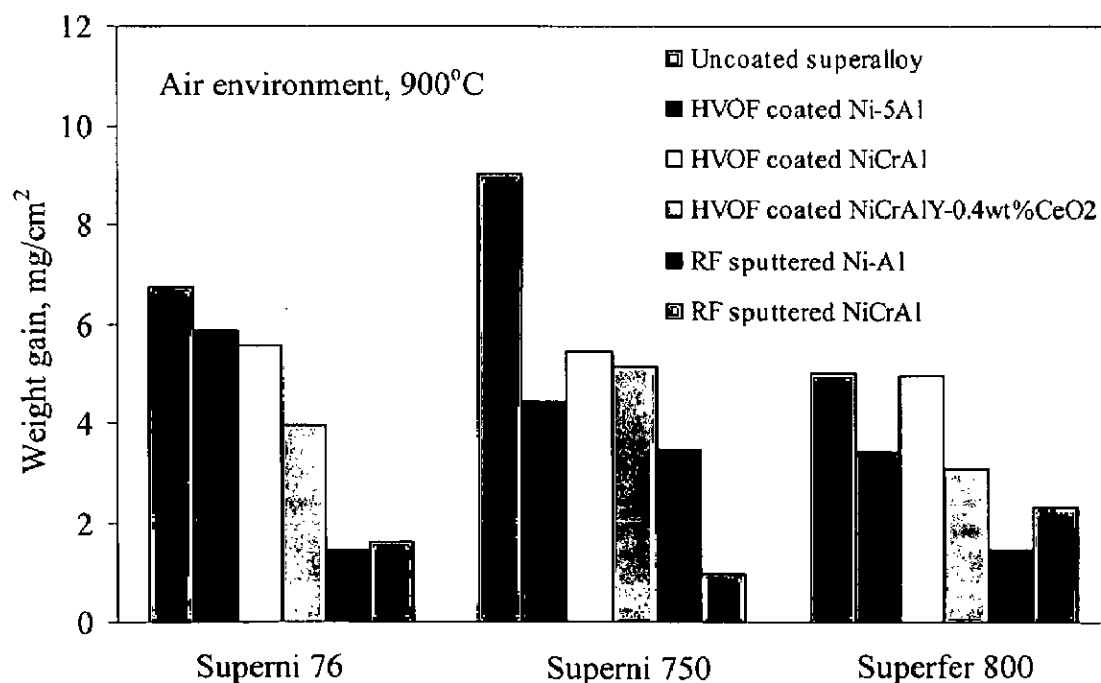


**Fig.8.1:** Bar charts showing cumulative weight gain ( $\text{mg/cm}^2$ ) for the uncoated and coated superalloys subjected to cyclic oxidation in air at  $900^\circ\text{C}$  for 100 cycles



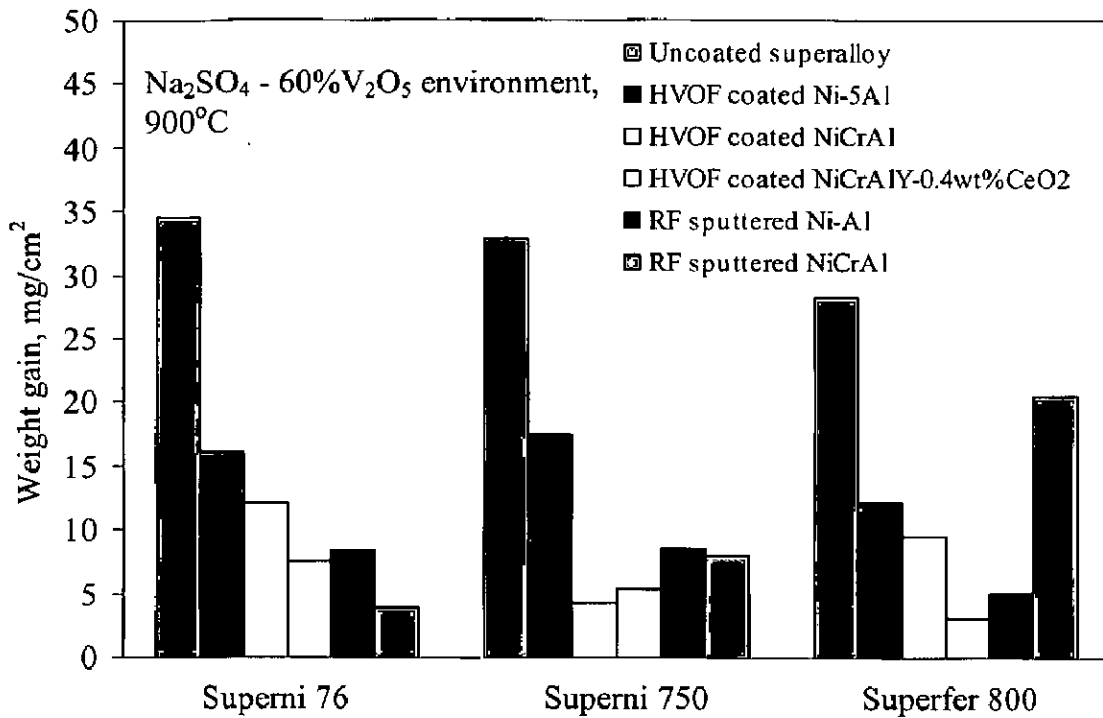


**Fig.8.2:** Bar charts showing cumulative weight gain ( $\text{mg}/\text{cm}^2$ ) for the uncoated and coated superalloys subjected to cyclic oxidation in  $\text{Na}_2\text{SO}_4 - 60\%\text{V}_2\text{O}_5$  environment at  $900^\circ\text{C}$  for 100 cycles.

Fig. 8.3 and 8.4 shows a bar chart indicating the partially oxidised coating thickness and weight gain for uncoated, HVOF coated and RF sputtered films on Superfer 800 after 1000 hours of exposure to low temperature superheater zone of coal fired boiler. In general, all the coatings which are partially oxidised under study show no measurable thickness loss except HVOF coated Ni-5Al on Superfer 800 and uncoated Superfer 800 also shows no thickness loss in the given environment. The uncoated Superfer 800 and all the coatings on Superfer 800 have provided protection from the internal attack in the coal fired boiler environment. The uncoated Superfer 800 indicates higher weight gain and among coated Superfer 800, RF sputtered Ni-Al film on Superfer 800 has indicated a minimum weight gain in the coal fired boiler, thus providing better protection to the superalloy.

The hot corrosion resistance of HVOF coatings in the coal fired boiler environment may be attributed to the selective oxidation of chromium and aluminum along the nickel rich splat boundaries and helps in clogging the diffusion of corroding species through the splat boundaries. The formation of oxides on the surface of the coated specimen helps in blocking the inward diffusion of oxidising or corrosive species through the open pores and voids. The oxidation kinetics of all the coatings followed the nearly parabolic rate law. The HVOF coated Ni-5Al on Superfer 800 showed lower resistance to hot corrosion. This might be associated with relatively higher porosity content in the coating.

In case of RF magnetron sputtered films, Ni-Al film on Superfer 800 show excellent protection in the boiler environment as compared to NiCrAl film on Superfer 800. The better protection may be attributed to the formation of nanostructured grains which helps in forming an adherent, thin and continuous scale on the surface after exposure to the boiler environment.

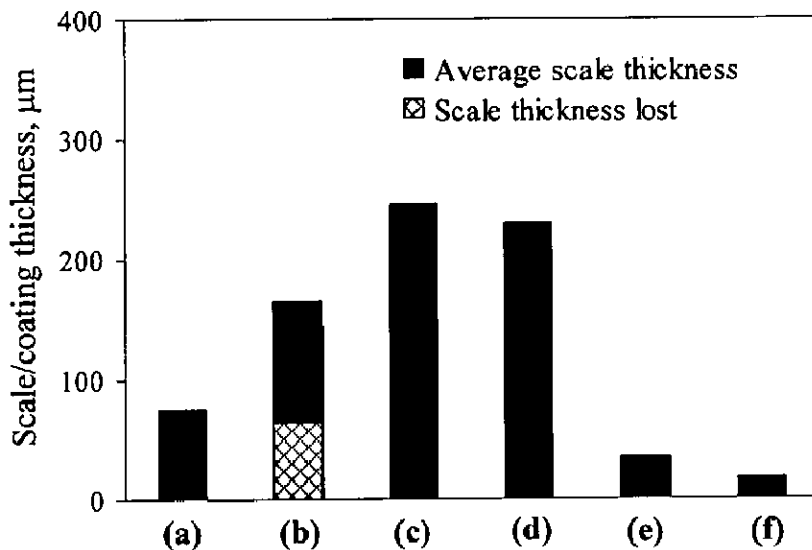


**Fig. 8.3:** Bar charts indicating the scale thickness for the (a) uncoated Superfer 800; (b) HVOF coated Ni-5Al; (c) HVOF coated NiCrAl; (d) HVOF coated NiCrAlY-0.4wt%CeO<sub>2</sub>; (e) RF sputtered Ni-Al and (f) RF sputtered NiCrAl coated Superfer 800 after 1000 hrs exposure to the coal fired boiler at 700 °C.

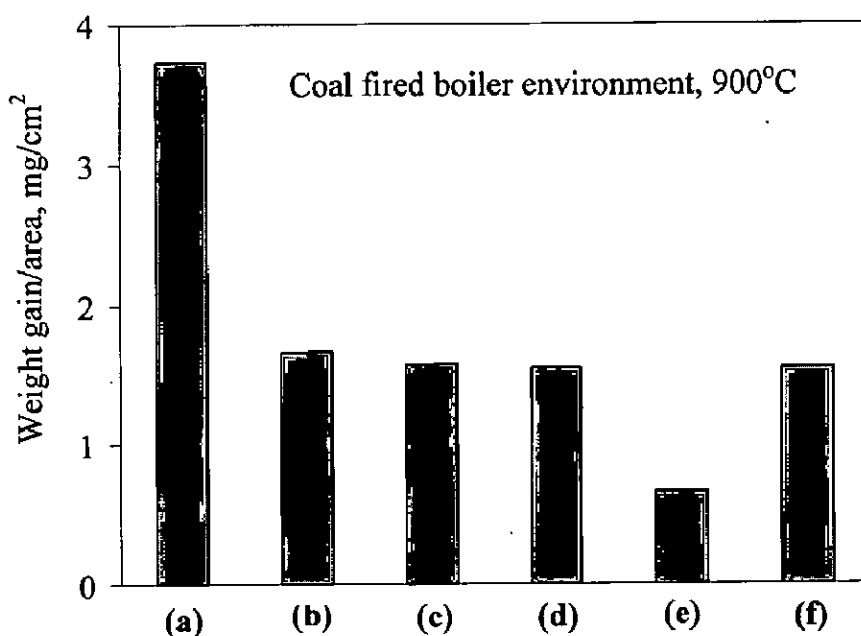


**Fig. 8.4:** Bar charts showing weight gain for the (a) uncoated Superfer 800; (b) HVOF coated Ni-5Al; (c) HVOF coated NiCrAl; (d) HVOF coated NiCrAlY-0.4wt%CeO<sub>2</sub>; (e) RF sputtered Ni-Al and (f) RF sputtered NiCrAl coated Superfer 800 after 1000 hrs exposure to the coal fired boiler at 700°C.

# CONCLUSIONS

---

---

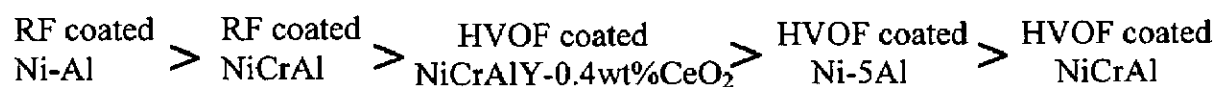
The conclusions from the present investigation pertaining to oxidation behaviour of Ni-5Al, NiCrAl and NiCrAlY-0.4wt%CeO<sub>2</sub> coatings formulated by HVOF process and Ni-Al and NiCrAl coated thin films by RF magnetron sputtering process on three types of superalloys namely Superni 76, Superni 750 and Superfer 800 are presented in this chapter. The oxidation studies were conducted in air as well as in molten salt (Na<sub>2</sub>SO<sub>4</sub>-60%V<sub>2</sub>O<sub>5</sub>) environments under cyclic conditions, in a laboratory furnace, at an elevated temperature of 900°C for an oxidation run of 100 cycles in all the cases. In addition to the laboratory tests, an attempt has been made to evaluate the performance of these coatings in the actual environment of coal fired boiler of Guru Gobind Singh Super Thermal Power Plant, Ropar, Punjab, India. All the coating powders were commercially available except NiCrAlY-0.4wt%CeO<sub>2</sub>, which was prepared by mixing NiCrAlY with 0.4wt%CeO<sub>2</sub>. Salient conclusions from the present study are summarized below:

- (1) The HVOF thermal spray process with liquid petroleum gas as fuel could be used successfully to deposit all the coating powders on the given superalloys. All the coatings exhibit low porosity, which was in the range of 1.4 - 2.0% and thickness in the range of 100-250 μm.
- (2) The cross-sectional microhardness of the coatings was found to be variable with the distance from the coating-substrate interface. As far as the upper values of the hardness range are concerned, NiCrAlY-0.4wt%CeO<sub>2</sub> coating showed a maximum limit of 753 Hv (highest among all the coatings), while Ni-5Al coatings exhibited a minimum limit of 210 Hv (lowest among all the coatings). The higher hardness in case of NiCrAlY-0.4wt%CeO<sub>2</sub> coating is perhaps due to refinement of the microstructure and the reduction of inclusion percentage of the coatings as reported in the literature (Wang 2001A; Wang et al, 2001B; Zhang et al, 2006; Tian et al, 2006; Wang et al, 2003).
- (3) The bond strength of the HVOF sprayed coating was determined as per ASTM standard C633-01. It was noticed that 43MPa, 59MPa and 45 MPa in case of Ni-5Al, NiCrAl and NiCrAlY-0.4wt%CeO<sub>2</sub> coatings.

- (4) The interdiffusion of alloying elements from the substrate to the HVOF sprayed coatings was observed to be marginal as indicated by cross sectional X-ray mapping analysis. It shows that the adhesion between the coating and the substrate is due to mechanical interlocking and metallurgical bonding effect.
- (5) The RF magnetron sputtered coatings indicated uniform deposition on all the superalloy substrates with a grain size ranging from 8 nm to 16 nm.

## OXIDATION STUDIES IN AIR

- (6) RF magnetron sputtered Ni-Al and NiCrAl coated superalloys subjected to cyclic oxidation in air for 100 cycles at 900°C showed considerably lower weight gain than that of HVOF coated and uncoated superalloys. The uncoated Superni 76 and Superni 750 have shown higher weight gain, whereas uncoated Superfer 800 has shown comparatively lower weight gain.
- (7) Based on the thermogravimetric (weight change with respect to time) data, the relative oxidation resistance attained by various coatings under study can be arranged in the following sequence:



- (8) The better protection provided by RF sputtered thin films to the superalloys may be attributed to very fine grains in the nanoscale range. The fine grains helps in rapid diffusion of the elements from the deposited film such as nickel, chromium and aluminum, thus providing selective oxidation of the elements. This helps in forming a uniform oxide layer on the exposed surface and prevents the further diffusion of oxidising species into the base alloy.
- (9) In case of RF magnetron coated specimens, formation of very thin and uniform film consisting of oxides of chromium, iron and nickel on the surface was observed and most of the film below the thin oxide layer remained unoxidised.
- (10) In case of HVOF sprayed coatings, NiCrAlY-0.4wt%CeO<sub>2</sub> coating has provided better protection in the given environment at 900°C under cyclic conditions. The better protection provided by NiCrAlY-0.4wt%CeO<sub>2</sub> coating might be due to the formation of streaks of cerium oxide along the splat boundaries and also the coating consists of dense and elongated splats, the distance for the oxidising species to traverse from the coating surface

to the substrate along the splat boundaries are long. These combined advantages restrict the corrosive species reaching the substrate, hence better protection to the substrate alloy.

- (11) In case of HVOF sprayed Ni-5Al coated specimens, the formation of aluminum oxide along the splat boundaries helps in clogging the diffusion of oxidising species into the coating and finally into the substrate superalloys. Whereas in case of HVOF sprayed NiCrAl and NiCrAlY-0.4wt%CeO<sub>2</sub> coated specimens, formation of oxides of aluminum, chromium and streaks of cerium oxide along the splat boundaries might be preventing the permeation of the oxidising species into the substrate superalloys.

## HOT CORROSION STUDIES IN MOLTEN SALT ENVIRONMENT

- (12) The oxidation rates for the investigated superalloys based on the overall weight gains after 100 cycles of oxidation in the Na<sub>2</sub>SO<sub>4</sub>-60%V<sub>2</sub>O<sub>5</sub> environment could be arranged in the following order:



- (13) Rate of hot corrosion was observed to be high in the early cycles of the study in the given environment for all types of coatings, which may be attributed to the fact that during transient period of oxidation, the corroding species might have penetrated into the coating along the splat boundaries and the open pores to cause rapid oxidation. However, once all these possible diffusion paths are blocked by the formation of the oxides, the oxidation then becomes limited mainly to the surface of the coatings resulting in a steady state.
- (14) The cumulative weight gain in case of RF magnetron sputtered films (Ni-Al & NiCrAl) were relatively high as compared to the HVOF sprayed NiCrAlY-0.4wt%CeO<sub>2</sub> coating. The higher weight gain in case of RF magnetron sputtered coating may be due to the observed microspalling of thin scale during the initial period of exposure to the molten salt environment thereby exposing a fresh surface to the corrosive species.
- (15) The HVOF sprayed NiCrAlY-0.4wt%CeO<sub>2</sub> coating has provided best protection in the given aggressive environment under study. The enhanced protection of the ceria added NiCrAlY coating by HVOF process may be due to the possible formation of CeVO<sub>4</sub> and the presence of streaks of cerium oxide along the splat boundaries. This helps in enhancing the performance of the coating in the molten salt environment. It is reported in the literature (Wood, 1970; Seybolt 1971; Wang et al., 2001) that the presence of small amount of ceria helps in improving the hot corrosion resistance by reducing the amount of various sulfides formed.

## ACTUAL INDUSTRIAL ENVIRONMENT

- (16) In case of RF magnetron sputtered Ni-Al and NiCrAl coated specimens, the colour became grey with brownish and reddish patches after 1000 hours of exposure and no spallation was observed during the study.
- (17) The samples were hanged in the low temperature Superheater zone ( $700 \pm 10^{\circ}\text{C}$ ) for 1000 hrs and negligible effect was observed on all the coatings.
- (18) The weight gain in case of uncoated Superfer 800 is slightly more as compared to the HVOF coated and RF magnetron sputtered film on Superfer 800 alloy for 1000 hours of cyclic exposure.
- (19) In case of HVOF sprayed Ni-5Al coating, the spalling of the coating was observed during the cyclic exposure to the boiler environment. The fluctuation in the weight gain is due to the fly ash deposition, removal and the redeposition of the ash on the surface of the specimen. The presence of  $\text{SiO}_2$  and  $\text{Al}_2\text{O}_3$  was confirmed by FESEM/EDAX analysis.
- (20) In case of bare superalloy, no spallation was observed whereas, in case of HVOF sprayed Ni-5Al coated Superfer 800 showed spallation after 200 hours of exposure which continued upto 400 hours. The final corroded specimen indicated yellowish grey with green shade after 1000 hours. In case of HVOF sprayed NiCrAl and NiCrAlY-0.4wt% $\text{CeO}_2$  coated Superfer 800, light yellowish color was observed on the surface and no spallation was observed during the study.

## SUGGESTIONS FOR FUTURE WORK

---

---

In light of the significant results obtained in the present study, some of the recommendations for future work are as follows:

1. All the investigated coatings showed promising results in laboratory and in the actual coal fired boiler environment. High temperature erosion studies of the coated superalloys may also be evaluated in the laboratory as well as in actual boiler environment at elevated temperature.
2. A mathematical model could be developed using the laboratory and industrial environment data, to predict the life of the coatings.
3. Hot stage microscopy may also be used to understand the development of the scale as well as mechanism of transport of species during the oxidation and hot corrosion runs.
4. The influence of different HVOF process parameters such as spraying distance, fuel/oxygen ratio, powder feed rate etc., of the powders used in the present investigation as well as other powders could be studied to evaluate the hot corrosion behaviour of the coatings.
5. The effect of different process parameters used in RF magnetron sputtering process such as power, bias voltage, sputtering pressure, temperature and deposition time etc., with high purity targets could be studied for evaluating their influence on the microstructural characteristics and hot corrosion behaviour of the superalloy coatings.
6. The tailoring of coating powder compositions especially by alloying the coating powders with rare earth elements could be made prior to the HVOF spray process.

## REFERENCES

---

---

1. **Aalamialeagha**, M.E., Harris, S.J. and Emamighomi, M., (2003), "Influence of the HVOF Spraying Process on the Microstructure and Corrosion Behaviour of Ni-20%Cr Coatings," *J. Mater. Sci.*, Vol. 38, pp. 4587-4596.
2. **Ak**, N.F., Tekmen, C., Ozdemir, I., Soykan, H.S. and Celik, E., (2003), "NiCr Coatings on Stainless Steel by HVOF Technique," *Surf. Coat. Technol.*, Vol. 173-174, pp.1070-1073.
3. **Almeida**, P. de, Schaublin, R., Almazouzi, A., Victoria, M., and Levy F., (2000), "Microstructure and growth modes of stoichiometric NiAl and Ni<sub>3</sub>Al thin films deposited by r.f.-magnetron sputtering," *Thin Solid Films*, Vol. 368, pp. 26-34.
4. **ASM Handbook**, (1995), "Metallography and Microstructures," Vol. 9, Sixth Printing, ASM Publication, Metals Park Ohio.
5. **Barrett** C. A, Khan A. S., and Lowell C. E., (1981), "The Effect of Zirconium on the Cyclic Oxidation of NiCrAl Alloys," *J. Electrochem. Soc.*, Vol. 128, No. 1, pp. 25-32.
6. **Basu**, S. N. and Yurek, G. J., (1991), "Effect of Alloy Grain Size and Silicon Content on the Oxidation of Austenitic Fe-Cr-Ni-Mn-Si Alloys in Pure O<sub>2</sub>," *Oxid. Met.*, Vol. 36, pp. 281-315.
7. **Barbooti**, M.M., Al-Madfai, S.H. and Nassouri, H.J., (1988), "Thermochemical Studies on Hot Ash Corrosion of Stainless Steel 304 and Inhibition by Magnesium Sulphate," *Thermochim. Acta*, Vol. 126, pp. 43-49.
8. **Beele** W., Czech N., Quadackers W.J. and Stamm W., (1997), "Long-term oxidation tests on a re-containing MCrAlY coating," *Surf. Coat. Technol.* Vol. 94-95, pp.41-45.
9. **Beltran**, A.M., and Shores, D.A., (1972), "Ch. 11: Hot Corrosion," in 'The Superalloys,' Eds. Sims, C.T. and Hagel, W.C., Wiley Publ., John Wiley and Sons, N. Y.
10. **Belzunce**, F.J., Higuera, V. and Poveda, S., (2001), "High Temperature Oxidation of HFPD Thermal-Sprayed MCrAlY Coatings," *Mater. Sci. & Engg. A*, Vol. 297, No. 1-2, pp. 162-167.
11. **Bettridge** D. F., and Ubank R. G., (1986), "Quality Control of High-Temperature Protective Coatings," *Mater. Sci. Technol.*, Vol. 2, pp. 232-242.
12. **Bhushan**, B. and Gupta, B. K. (1991), 'Handbook of Tribology: Materials, Coatings and Surface Treatments,' McGraw-Hill, New York.



13. **Bonnet G., Aguilar G., Colson J.C. and Larpin J. P., (1993), "The effect of rare earths deposited on steel surfaces by different processes (sol/gel, electrophoresis, OMCVD) on high temperature corrosion behaviour," Corros. Sci., Vol. 35(5-8), pp. 893-899.**
14. **Bonnet G., Silva M., Chevalier S., Larpin J. P., and Colson J. C., (1996), "Effect of chromia and alumina coatings on the high-temperature behaviour of F17Ti stainless steel in air: effect of a rare earth element oxide," Surf. Coat. Technol., Vol. 80, No. 1-2, pp. 76-79.**
15. **Bornstein, N. S. and DeCrescente, M.A., (1970), "The Role of Sodium and Sulfur in the Accelerated Oxidation Phenomena-Sulphidation," Corros., Vol. 26, No. 7, pp. 209-214.**
16. **Bornstein, N.S., DeCrescente, M.A. and Roth, H.A., (1973), "The Relationship Between Relative Oxide Ion Content of Na<sub>2</sub>SO<sub>4</sub>, the Presence of Liquid Metal Oxides and Sulfidation Attack," Metall. Trans., Vol. 4, pp. 1799-1810.**
17. **Bornstein N. S., Decrescente M. A. and Roth H. A., (1975), Proc. in conf. on Gas turbine Mater. In the Marine environment, MMIC-75-27, Columbus, Ohio, USA, p. 115.**
18. **Byrnes L. and Kramer M., (1994), "Method and Apparatus for the Application of Thermal Spray Coatings onto Aluminium Engine Cylinder Bores," Proceedings of the 7<sup>th</sup> National Thermal Spray Conference, Boston, pp. 39-48.**
19. **Buta Singh, (2003), 'Studies on the Role of Coatings in Improving Resistance to Hot Corrosion and Degradation,' Ph.D. Thesis, Met. & Mat. Eng. Dept., Indian Institute of Technology Roorkee, Roorkee.**
20. **Buta Singh Sidhu., Puri D., and Prakash S., (2004), "Characterisations of plasma sprayed and laser remelted NiCrAlY bond coats and Ni<sub>3</sub>Al coatings on boiler tube steels," Mater. Sci. Eng. A., Vol. 368, pp. 149-158.**
21. **Buta Singh Sidhu., Puri D., and Prakash S., (2005A), "Mechanical and Metallurgical Properties of Plasma Sprayed and Laser Remelted Ni-20Cr and Stellite-6 Coatings," Jour. Mater. Process. Technol., Vol. 159, pp. 347-355.**
22. **Buta Singh Sidhu, and Prakash S., (2005B), "High-Temperature Oxidation Behavior of NiCrAlY Bond Coats and Stellite-6 Plasma-Sprayed Coatings," Oxid. Met., Vol. 63, No. 3-4, pp. 241-259.**
23. **Buta Singh Sidhu., and Prakash, S., (2006), "Erosion-corrosion of plasma as sprayed and laser remelted Stellite-6 coatings in a coal fired boiler," Wear, Vol. 260, pp. 1035-1044.**
24. **Budinski, K. G., (1998), 'Engineering Materials, Properties and Selection,' Pub. Prentice-Hall of India, New Delhi, India.**

25. **Burakowski, T. and Wierzchon, T., (1999), 'Surface Engineering of Metals, Principles, Equipment, Technology,' CRC Press, N. W., Boca Raton, Florida.**
26. **Burman, C. and Ericsson, T., (1983), "Study of Plasma Sprayed FeCrAlY Coatings after Various Post-Treatments," Proc. Sympos. High-Temperature Protective Coatings, March 7-8, Atlanta, GA, USA, Ed. Singhal, S.C., Pub. Metall. Soc of AIME, Warrendale, PA, USA, pp. 51-59.**
27. **Chan W. Y., Evans H. E., Ponton C. B., Nicholls J. R., and Simms N. J., (2000), "The influence of NiAl<sub>3</sub> on the high temperature oxidation of a plasma-sprayed overlay coating," Mater. High Temp., Vol. 17, No. 2, pp. 173-178.**
28. **Chang, J.T., Davison, A. He, J.L. Matthews, A., (2006), "Deposition of Ni-Al-Y alloy films using a hybrid arc ion plating and magnetron sputtering system," Surf. Coat. Technol., Vol. 200, pp. 5877-5883.**
29. **Chatterjee, U. K, Bose S. K., and Roy S. K., (2001), "Environmental Degradation of Metals," Pub., Marcel Dekkar, Inc. 270 Madison Avenue, New York.**
30. **Chattopadhyay, B., and Wood G. C., (1970), "The Transient Oxidation of Alloys," Oxid.Met. Vol. 2, No. 4, pp. 373-399.**
31. **Chen, G., Lou, H., (1999), "Oxidation behavior of sputtered Ni-3Cr-20Al nanocrystalline coating," Mater. Sci. Eng. A, Vol. 271, pp. 360-365.**
32. **Chen, G., and Lou, H., (2000), "Oxidation behavior of sputtered Ni-Cr-Al-Ti nanocrystalline coating," Surf. Coat. Technol., Vol. 123, (2000) 92-96.**
33. **Chen, G., and Lou, H., (2003), "Effect of  $\gamma'$  precipitation on oxide formation on the Ni-3Cr-20Al and Ni-10Cr-11Al-8Ti nanocrystalline coatings," Corros. Sci., Vol. 42, pp.1185-1195.**
34. **Cheng X. H., and Xie C. Y., (2003), "Effects of rare earth elements on the erosion resistance of nitrided 40Cr steel," Wear, Vol. 254, pp. 415-420.**
35. **Cheruvu N.S., Chan K. S., and Viswanathan R., (2006), "Evaluation, degradation and life assessment of coatings for land based combustion turbines," Energy Mater., Vol. 1, No. 1, pp. 33-47.**
36. **Choi H., Yoon B., Kim H., and Lee C., (2002), "Isothermal oxidation of air plasma spray NiCrAlY bond coatings," Surf. Coat. Technol. Vol. 150, No. 2-3, pp. 297-308.**
37. **Clark, R., Barbezat, G., Keller, S., and Nicoll, A. R., (1995), "A Review of HVOF System Process Considerations for Optimizing Coatings in Turbo-Machinery", Proceedings, 14th Inter. Thermal Spray Conf., JPN, pp. 1173-1178.**

38. **Culha O., Celik E., Ak Azem N.F., Birlik I., Toparli M., and Turk A., (2008),** "Microstructural, thermal and mechanical properties of HVOF sprayed Ni-Al based bond coatings on stainless steel substrate," *Jour. Mater. Process. Technol.*, Vol. 204, pp. 221-230.
39. **Cullity, B.D.,** *Elements of X-ray Diffraction*, Addison-Wesley, 1970.
40. **Czech N., Schmitz F. and Stamm W., (1995),** "Microstructural analysis of the role of rhenium in advanced MCrAlY coatings," *Surf. Coat. Technol.* Vol. 76, No.1-3, pp. 28-33.
41. **Danyluk S. and Park J.Y., (1979),** "Technical Note: Corrosion and Grain boundary Penetration in Type 316 Stainless Steel Exposed to a Coal Gasification Environment," *Corrosion*, Vol. 35, No.12, pp. 575-576.
42. **Deb, D., Ramakrishna Iyer, and S., Radhakrishnan, V. M., (1996),** "A comparative study of oxidation and hot corrosion of a cast nickel base superalloy in different corrosive environments," *Mater. Lett.*, Vol. 29, pp. 19-23.
43. **Dent A. H, Horlock A. J, McCartney D.G, and Harris S. J., (1999),** "The Corrosion Behavior and Microstructure of High-Velocity Oxy-Fuel Sprayed Nickel-Base Amorphous/Nanocrystalline Coatings," *J. Thermal Spray Technol.*, Vol. 8, pp. 399-404.
44. **Dent A. H, Horlock A. J., McCartney D. G., Harris S. J., (2001),** "Microstructural characterisation of a Ni-Cr-B-C based alloy coating produced by high velocity oxy-fuel thermal spraying," *Surf. Coat. Technol.* Vol. 139, pp. 244-250.
45. **DeMasi-Marcin, J. T. and Gupta, D. K., (1994),** "Protective Coatings in the Gas Turbine Engine," *Surf. Coat. Technol.*, Vol. 68-69, pp. 1-9.
46. **Deshpande S, Sampath S, and Zhang H., (2006),** "Mechanisms of oxidation and its role in microstructural evolution of metallic thermal spray coatings - Case study for Ni-Al," *Surf. Coat. Technol*, Vol. 200, pp. 5395-5406.
47. **Dieter, L., (2007),** "Corrosion and surface Chemistry of Metals", EPFL Press, Lausanne, Switzerland.
48. **Driver, D., Hall, D.W. and Meetham, G.W.;** (1981), "The Gas Turbine Engine," In: G.W. Meetham, Editor, *The Development of Gas Turbine Materials*, Applied Science Publishers, London, pp. 1-30.
49. **Edris H., McCartney D. G, and Sturgeon A. J, (1997),** "Microstructural Characterization of High Velocity Oxy-Fuel Sprayed Coatings of Inconel 625," *J. Mater Sci.*, Vol. 32, pp. 863-872.
50. **Eliasz, N., Shemesh G., and Latanision R. M., (2002),** "Hot corrosion in gas turbine components," *Engineering Failure Analysis*, Vol. 9, pp. 31-43.

51. **Fitzer F., J. Schlichting,** (1981), "Coatings containing chromium, aluminum, and silicon for high temperature alloys," in R. A. Rapp (Ed.), High Temperature Corrosion, NACE, San Diego, CA, Houston, TX, March 2–6, pp. 604–614.
52. **Fukutome H., Shimizu H., Yasmashita N., and Shimizu Y.,** (1995), "The Application of Cermet Coating on Piston Ring by HVOF," Proceedings of the 14<sup>th</sup> International Thermal Spray Conference, Kobe, Japan, pp. 21-26.
53. **Geibel A., Froyen L., Delaey L., and Leuven K. U.,** (1996), "Plasma Spray Forming: An alternative Route for Manufacturing Free-Standing Components," Jour. Thermal Spary Technol., Vol. 5. No. 4, pp. 419-429.
54. **Geng S., Wang F., Zhu S., and Wu W.,** (2002), "Hot-Corrosion Resistance of a Sputtered K38G Nanocrystalline Coating in Molten Sulfate at 900°C," Oxid. Met., Vol. 57, No. 5-6, pp. 549-557.
55. **Geng, S., Wang, F., and Zhang S.,** (2003), "High temperature oxidation behavior of a sputtered pure Ni nanocrystalline coating at 700–900°C," Surf. Coat.Technol., Vol. 167 pp. 212–216.
56. **Gitanjaly, Prakash, S. and Singh, S.,** (2002), "Effects of MgO and CaO on Hot Corrosion of Fe Base Superalloy Superfer 800H in Na<sub>2</sub>SO<sub>4</sub>-60%V<sub>2</sub>O<sub>5</sub> Environment," Brit. Corros. J., Vol. 37, No. 1, pp. 56-62.
57. **Gitanjaly,** (2003), 'Role of Inhibitors on Hot Corrosion of Superalloys in Na<sub>2</sub>SO<sub>4</sub>-V<sub>2</sub>O<sub>5</sub> Environment,' Ph.D. Thesis, Met. Mat. Engg. Deptt., Indian Institute of Technology Roorkee, Roorkee, India.
58. **Goebel, J. A. and Pettit, F. S.,** (1970A), "Na<sub>2</sub>SO<sub>4</sub> - Induced Accelerated Oxidation (Hot Corrosion) of Nickel," Metall. Trans., Vol. 1, pp. 1943-1954.
59. **Goebel, J. A. and Pettit, F. S.,** (1970B), "The Influence of Sulphides on the Oxidation Behaviour of Nickel-base Alloys," Metall Trans, Vol.1, pp.3421-3429.
60. **Goebel, J. A., Pettit, F. S. and Goward, G. W.,** (1973), "Mechanisms for the Hot Corrosion of Nickel-Base Alloys," Metall. Trans., Vol. 4, pp. 261-275.
61. **Gonzalez-Rodriguez, J. G., Haro, S., Martinez-Villafane, A., Salinas-Bravo, V. M., and Porcado-Calderon, J.,** (2006), "Corrosion performance of heat resistant alloys in Na<sub>2</sub>SO<sub>4</sub>-V<sub>2</sub>O<sub>5</sub> molten salts," Mater. Sci. Eng A, Vol. 435-436, pp. 258-265.
62. **Goward, G. W.,** (1998), "Progress in coatings for gas turbine airfoils," Surf. Coat. Technol., Vol. 108-109, pp. 73-79.
63. **Goward, G.W.,** (1970), "Surface protection of superalloys for gas turbine engines," J. Metals, Vol. 10, p. 31-39.

64. **Goward G. W., and Boone D. H., (1971),** "Mechanisms of formation of diffusion aluminide coatings on nickel-base superalloys," *Oxid. Met.*, Vol. 3, No. 5, pp. 475-495.
65. **Graham M. J., and Hussey R. J., (1995),** "Analytical techniques in High Temperature Corrosion," *Oxid. Met.*, Vol. 44, pp. 339-374.
66. **Grabke H. J., (1999),** "Oxidation of NiAl and FeAl", *Intermetallics*, Vol. 7, pp. 1153-1158.
67. **Gupta, N., (2003),** "Technical Talk on Cathodic Protection," *IIM Metal News*, Vol. 16, No. 1, pp. 38.
68. **Guilemany, J. M., Fernandez, J., Delgado, J., Benedetti, A. V. and Climent, F., (2002),** "Effects of Thickness Coating on the Electrochemical Behaviour of Thermal Spray Cr<sub>3</sub>C<sub>2</sub>-NiCr Coatings," *Surf. Coat. Technol.*, Vol. 153, No. 2-3, pp. 107-113.
69. **Gurrappa I., (2001),** "Identification of Hot Corrosion Resistant MCrAlY Based Bond Coatings for Gas Turbine Engine Applications," *Surf. Coat. Technol.* Vol. 139, No. 2-3, pp. 272-283.
70. **Gurrappa I., (2003),** "Influence of alloying elements on hot corrosion of superalloys and coatings: necessity of smart coatings for gas turbine engines", *Mater. Sci. Technol.*, Vol. 19, No. 2, pp. 178-183.
71. **Gurumoorthy, K., Kamaraj, M., Prasad Rao, K., Sambasiva Rao, A., Venugopal, S., (2007),** "Microstructural aspects of plasma transferred arc surfaced Ni-based hard facing alloy," *Mater. Sci. Eng A* Vol. 456, pp. 11-19.
72. **Guo, M. H., Wang, Q. M., Gong, J., Sun, C., and Wen L. S., (2006),** "Preparation and oxidation of a gradient NiCoCrAlYSiB coating deposited by a combined system of arc ion plating and magnetron sputtering," *Surf. Coat. Technol.*, Vol. 201, pp.1302-1308.
73. **Hancock, P. and Hurst R.C., (1974),** "The Mechanical Properties and Breakdown of Surface Oxide Films at Elevated Temperatures," in 'Advances in Corrosion Science and Technology,' Vol.4, Eds. Fontana, M.G. and Staehle, R.W., Pub. Plenum Press, New York.
74. **Handbook of Thermal Spray Technology, (2004),** Ed, Davis, J. R., Davis & Associates, ASM International, Materials Park, OH, USA.
75. **Harpreet Singh, (2005A),** "Hot corrosion Studies of Plasma Sprayed Coatings over Some Ni- and Fe- Based Superalloys," Ph.D. Thesis, Met. & Mat. Eng. Dept., Indian Institute of Technology Roorkee, Roorkee.

76. **Harpreet, S., Puri D., and Prakash S., (2005B),** "Studies of plasma spray coatings on a Fe-base superalloy, their structure and high temperature oxidation behaviour," *Anti-Corrosion Methods and Materials*, Vol. 52, No. 2, pp. 84–95.
77. **Harpreet Singh., Puri D. and Prakash S., (2005C),** "Some studies on the hot corrosion performance of plasma sprayed coatings on a Fe based superalloy," *Surf. Coat. Technol.*, Vol. 192, pp. 27-38.
78. **Harpreet Singh, Puri, D. and Prakash, S., (2005D),** "Corrosion Behaviour of Plasma Sprayed Coatings on a Ni-base Superalloy in Na<sub>2</sub>SO<sub>4</sub>-60%V<sub>2</sub>O<sub>5</sub> Environment at 900°C," *Metall. Mater. Trans. A*, Vol. 36, No 4, pp. 1007-1015.
79. **Hazoor Singh Sidhu, Buta Singh Sidhu, and S. Prakash., (2006),** "Mechanical and microstructural properties of HVOF sprayed WC–Co and Cr<sub>3</sub>C<sub>2</sub>–NiCr coatings on the boiler tube steels using LPG as the fuel gas," *Jour. Mater. Process. Technol.* Vol. 171, pp. 77-82.
80. **Haugrud, R., (2003),** "On the high temperature oxidation of nickel", *Corros. Sci.*, Vol. 45, pp. 211-235.
81. **He, J. L., Chen K.C., Chen C.C., Leyland A., and Matthews A., (2001),** "Cyclic oxidation resistance of Ni-Al alloy coatings deposited on steel by a cathodic arc plasma process," *Surf. Coat. Technol.*, Vol. 135, pp. 158-165.
82. **Heath, G. R., Heimgartner, P., Irons, G., Miller, R. and Gustafsson, S., (1997),** "An Assessment of Thermal Spray Coating Technologies for High Temperature Corrosion Protection," *Mater. Sci. Forum*, Vol. 251-54, pp. 809-816.
83. **Helali M. M., and Hashmi M. S. J., (1992),** "A comparative study of plasma spraying and high velocity oxy-fuel (HVOF) thermal spraying," *Proc. of the 10th Conf. of the Irish Manufacturing Committee (IMC 10), Galway, Ireland*, pp. 377–387.
84. **Herman, H., Sampath, S. and Mccune, R., (2000),** "Thermal Spray: Current Status and Future Trends," *MRS Bull*, Vol. 25, No. 7, pp.17-25.
85. **Hearley J.A, Little J.A., and Sturgeon A.J., (2000),** "The effect of spray parameters on the properties of high velocity oxy-fuel NiAl intermetallic coatings," *Surf. Coat. Technol.* Vol. 123, pp. 210-218.
86. **Hidalgo, V.H., Varela, F.J.B. and Rico, E.F., (1997),** "Erosion Wear and Mechanical Properties of Plasma-Sprayed Nickel- and Iron-Based Coatings Subjected to Service Conditions in boilers," *Tribol. Int.*, Vol. 30, No. 9, pp. 641-649.

87. **Hidalgo** V.H., Varela F.J.B., and Menendez A.C., (1998), "Characterization and high temperature behaviour of thermal sprayed coatings used in boilers," Proceedings of the 15th International Thermal Spray Conference, Nice, France, May 25–29, pp. 617–621.
88. **Hidalgo**, V.H., Varela, F.J.B., Martinez, S.P. and Espana, S.G., (1999), "Characterization and High Temperature Behaviour of Cr<sub>3</sub>C<sub>2</sub>-NiCr Plasma Sprayed Coatings," Proc. of the United Thermal Spray Conf., Germany, pp. 683-686.
89. **Huang**, L., Sun X. F., Guan H. R., and Hu Z. Q., (2005), "Oxidation Behaviour of Directionally Solidified Ni-base Superalloy DS951 in Air," Oxid. Met., Vol. 64, No. 5/6, pp. 303-318.
90. **Huang** L., Sun X. F., Guan H. R. and Hu Z. Q., (2006), "Improvement of the oxidation resistance of NiCrAlY coatings by the addition of rhenium," Surf. Coat. Technol., Vol. 201, pp. 1421-1425.
91. **Hussain**, H., Shahid K. A., Khan I. H., and Rahman S., (1994), "Oxidation of High-Temperature Alloys (Superalloys) at elevated Temperatures in Air: I", Oxid. Met., Vol. 41, Nos. 3/4, pp. 251-269.
92. **Hwang**, Y. S., and Rapp, R. A., (1989), "Thermochemistry and Solubilities of Oxides in Sodium Sulphate-Vanadate Solutions," Corrosion, Vol. 45, No. 11, pp. 933-937.
93. **Ilavsky**, J., Pisacka, J., Chraska, P., Margandant, N., Siegmann, S., Wagner, W., Fiala, P. and Barbezat, G., (2000), "Microstructure-Wear and Corrosion Relationships for Thermally Sprayed Metallic Deposits," Proc. 1<sup>st</sup> Inter. Thermal Spray Conf., Montreal, Quebec, Canada, May 8-11, pp. 449-454.
94. **Kawahara** Y., (2002), "High temperature corrosion mechanisms and effect of alloying elements for materials used in waste incineration environment," Corros. Sci., Vol. 44, pp. 223-245.
95. **Kawase**, R. and Nakano, A., (1996), "Production of Heat and Corrosion-Resistant Plastic Coatings," Proc. of the 9<sup>th</sup> National Thermal Spray Conference, Cincinnati, Ohio, pp. 257-262.
96. **Khalid**, F.A., Hussain, N. and Shahid, K.A., (1999), "Microstructure and Morphology of High Temperature Oxidation in Superalloys," Mater. Sci. Eng. A, Vol. 265, pp. 87-94.
97. **Khan** A.N., Lu J., and Liao H., (2003), "Effect of residual stresses on air plasma sprayed thermal barrier coatings," Surf. Coat. Technol., Vol. 168, pp. 291-299.
98. **Khanna** A. S., Quadackers W. J., Yang X., and Schuster H., (1993), "On the Mechanism of the Oxidation of NiCrAl-Base Alloys in Air and Air Containing Sulphur Dioxide," Oxid. Met., Vol. 40, Nos. (3/4), pp. 275-294.

99. **Khanna, A. S., and Jha, S. K., (1998), "Degradation of Materials under hot corrosion conditions,"** *Trans. Indian Inst. Met.*, Vol. 51, No. 5, pp. 279-290.
100. **Khanna, A. S., (2005), Ch. 6: "Handbook of environmental degradation of Materials,"** Pub., William Andrew, 13 Eaton Avenue, New York.
101. **Khor, K. A., and Loh N. L., (1994), "Hot Isostatic Pressing of Plasma Sprayed Ni-based Alloys,"** *Jour. of Thermal Spray Techno.*, Vol. 3. No. 1, pp. 57-62.
102. **Knight R and Smith R.W., (1992). "HVOF Sprayed 80/20 NiCr Coatings - Process Influence Trends,"** *Proc. 13th Int'l. Thermal Spraying Conference, Thermal Spray: International Advances in Coatings Technology*, ed. Berndt, C.C., ASM Int'l Orlando, FL, USA, 28 May-5 June, pp. 159-164.
103. **Knotek, O., (2001), "Chapter 3: Thermal Spraying and Detonation Spray Gun Processes,"** in 'Handbook of Hard Coatings: Deposition Technologies, Properties and Applications,' Ed. Bunshah, R. F., Noyes Pub. Park Ridge, New Jersey, U. S.
104. **Knoll, A., Smigiel E., Broll N., and Cornet A., (1999), "Study of high temperature oxidation kinetics of steel using grazing X-ray reflectometry",** *JCPDS-International Centre for Diffraction Data*, pp.170-178.
105. **Kofstad, P., (1988), "Chapter 14" in 'High Temperature Corrosion,'** Elsevier Applied Science, London & New York, pp. 465.
106. **Kolta G.A, Hewaidy I.F. and Felix N.S., (1972), "Reactions between Sodium Sulphate and Vanadium Pentoxide,"** *Thermochim. Acta*, Vol. 4, pp. 151-164.
107. **Krishnan R., Dash S., Kesavamoorthy R., Babu Rao C., Tyagi A.K., and Baldev Raj, (2006), "Laser surface modification and characterization of air plasma sprayed alumina coatings,"** *Surf. Coat. Technol.*, Vol. 200, pp. 2791-2799.
108. **Krisch, H., (1963), "Corrosion in Combustion Chambers Caused by Slag Attack and Flue gases of Varying Composition,"** in *Proceedings of Conference Mechanism of Corrosion by Fuel Impurities*, Marchwood, UK (Butterworth, London), p. 508.
109. **La, P., Bai M., Xue Q. and Liu W., (1999), "A study of Ni<sub>3</sub>Al coating on carbon steel surface via the SHS casting route,"** *Surf. Coat. Technol.* Vol. 113, pp. 44-51.
110. **Landkof M., Levy A. V., Boone D. H., Gray R., and Yaniv E., (1985), "The effect of surface additives on the oxidation of chromia-forming alloys,"** *Corrosion*, Vol. 41, pp. 344-357.
111. **Lai, G. Y., (2007), "High-Temperature Corrosion and Materials Applications,"** Pub., ASM International, Materials Park, OH.



112. **Leyens, C., Pint, B.A., and Wright, I.G., (2000), "Effect of composition on the oxidation and hot corrosion resistance of NiAl doped with precious metals", Surf. Coat. Technol., Vol. 133-134, pp. 15-22.**
113. **Lee W.H and Lin R. Y., (2003), "Hot corrosion mechanism of intermetallic compound Ni<sub>3</sub>Al," Mater. Chem. Phy., Vol. 77, pp. 86-96.**
114. **Lee, L. L., Laughlin, D.E. and Lambeth, D. N., (1995), "Effects of Cr intermediate layers on CoCrPt thin film media on NiAl underlayers," IEEE Trans., Vol. 31, No. 6, pp. 2728-2730.**
115. **Lih W., Chang E., Wu, B.C. and Chao, C.H., (1992), "The effect of pack-aluminisation on the microstructure of MCrAlY and the performance of thermal barrier coatings," Surf. Coat. Technol. Vol. 50, No.3, pp. 277-288.**
116. **Lih W., Chang E., Wu B.C., Chao C.H. and Peng A., (1993), "Effect of Bond-Coat Pre-Aluminization and Pre-Oxidation Duplex Pretreatment on the Performance of ZrO<sub>2</sub>-8 wt.% Y<sub>2</sub>O<sub>3</sub>/Co - 29Cr- 6Al- 1Y Thermal-Barrier Coatings," Oxid. Met. Vol. 40, No. 3-4, pp. 229-243.**
117. **Liu, P. S., Liang K. M., and Gu S. R., (2001), "High-temperature oxidation behavior of aluminide coatings on a new cobalt-base superalloy in air," Corros. Sci., Vol. 43, pp.1217-1226.**
118. **Liu, Z., Gao, W., Dahm, K. L., and Wang, F., (1998), "Oxidation Behaviour of Sputter- Deposited Ni-Cr-Al Micro-crystalline Coatings," Acta. Mater., Vol. 46, pp. 1691-1700.**
119. **Li C. J., and Li H., (1998), "Effect of WC-Co addition on the adhesion of HVOF Ni-based coatings," in C. Coddet (Ed.), Thermal Spray: Meeting the Challenges of the 21<sup>st</sup> Century, ASM International, Materials Park, OH, pp. 723-728.**
120. **Li, C.-J., Wang, Y. Y., and Ohmori, A., (2000), "Effect of Melting State of Spray Particles on the Adhesion Strength of HVOF Nickel-Based Alloy Coatings," Thermal Spray Surface Engineering via Applied Research: Proc. Int. Therm. Spray Conf., Montreal, QUE, United States, ASM International, May 8-11, pp. 791-796.**
121. **Li H., Khor K.A., and Cheang P., (2000), "Effect of the powders' melting state on the properties of HVOF sprayed hydroxyapatite coatings," Mater. Sci. Eng. A, Vol. 293, pp. 71-80.**
122. **Li C.J., Wang Y.Y., Wu T., Ji G. C., and Ohmori A., (2001), "Effect of types of ceramic materials in aggregated powder on the adhesive strength of high velocity oxy-fuel sprayed cermet coatings," Surf. Coat. Technol., Vol. 145, pp. 113-120.**

123. **Li, M. H., Sun, X. F., Li, J. G., Zhang, Z. Y., Jin, T., Guan, H.R. and Hu, Z. Q.,** (2003), "Oxidation Behaviour of a Single-Crystal Ni-Base Superalloy in Air-I: At 800 and 900°C," *Oxid. Met.*, Vol. 59, No. 5-6, pp.591-605.
124. **Lima C.R.C., and Trevisan R.E.,** (1997), "Graded plasma spraying of premixed metalceramic powders on metallic substrates," *Jour. Thermal Spray Technol.*, Vol. 6, No.2, pp. 199-204.
125. **Lima C.R.C. and Guilemany J. M.,** (2007), "Adhesion improvements of Thermal Barrier Coatings with HVOF thermally sprayed bond coats," *Surf. Coat. Technol.*, Vol. 201, pp. 4694–4701.
126. **Liu Zhenyu and Gao Wei,** (1998), "Oxidation Behaviour of Microcrystalline Ni-Cr-Al Alloy Coatings at 900°C," *Scripta Materialia*, 38 (6), pp.877-885.
127. **Lou, H., Tang, Y., Sun, X., and Guan, H.,** (1996), "Oxidation behavior of sputtered microcrystalline coating of superalloy K17F at high temperature," *Mater. Sci. Eng.A*, Vol. 207, pp. 121- 128.
128. **Lowell C. E., Deadmore D. L., and Daniel Whittenberger J.,** (1982), "Long-term high-velocity oxidation and hot corrosion testing of several NiCrAl and FeCrAl base oxide dispersion strengthened alloys," *Oxid. Met.*, Vol. 17, No.3-4, pp. 205-221.
129. **Lopez A. R., Hassan B., Oberkampf W. L., Neiser R. A. and Roemer T. J.,** (1998), "Computational fluid dynamics analysis of a wire-feed, high-velocity oxygen fuel (HVOF) thermal spray torch," *Jour. of Thermal Spray Technol.* Vol. 7, No. 3, pp. 374-382.
130. **Lugscheider, E., Herbst, C., and Zhao, L.,** (1998), "Parameter studies on high-velocity oxy-fuel spraying of MCrAlY coatings," *Surf. Coat. Technol.*, Vol. 108-109, pp. 16-23.
131. **Luthra, K. L.,** (1983), "Mechanisms of Low Temperature Hot Corrosion," in 'High Temperature Corrosion,' Houston, NACE, Ed. Rapp, R.A., pp. 507-518.
132. **Luthra, K.L. and Spacil, H.S.,** (1982), "Impurity Deposits in Gas Turbines from Fuels Containing Sodium and Vanadium," *J. Electrochem. Soc.*, Vol:129, No. 3, pp. 649-656.
133. **Mahesh A., Jayaganthan R., Tewari, V. K., Arivazhagan, N.,** (2007), "A study on the hot corrosion behavior of Ti–6Al–4V alloy," *Mater. Lett.*, Vol. 61, pp. 1483-1488.
134. **Mahesh R.A., Jayaganthan R., Prakash S.,** (2008A), "Microstructural characteristics and mechanical properties of HVOF sprayed NiCrAl coating on superalloys", *Jour. Alloys Compd.*, in press.

135. **Mahesh R.A.**, Jayaganthan R. and Prakash S., (2008B), "Oxidation behavior of HVOF sprayed Ni-5Al coatings deposited on Ni- and Fe-based superalloys under cyclic condition," *Mater. Sci. Eng. A*, Vol. 475, pp. 327-335.
136. **Mahesh R.A.**, Jayaganthan R., and Prakash S., (2008C), "A study on hot corrosion behaviour of Ni-5Al coatings on Ni- and Fe-based superalloys in an aggressive environment at 900°C," *Jour. Alloys Comp.*, Vol. 460, pp. 220-231.
137. **Mahesh R.A.**, Jayaganthan R., and Prakash S., (2008D), "Hot corrosion behaviour of HVOF sprayed NiCrAlY-0.4wt%CeO<sub>2</sub> coatings on superalloys in aggressive environment at 900°C," *Corros. Eng. Sci. Technol.*, in press (DOI 10.1179/174327808X303473).
138. **Malik A.U.**, Ahmad R., Ahmad S., Ahmad S., (1992), *Pract. Metallogr.* Vol. 29, pp. 255-268.
139. **Matthews, A.**, Artley, R.J. and Holiday, P., (1998), "Future's Bright for Surface Engineering," *Mater. World*, Vol. 6, pp. 346-347.
140. **Matsubara Y.** and Tomiguchi A., (1992), "Surface Texture and Adhesive Strength of High Velocity Oxy-Fuel Sprayed Coatings for Rolls of Steel Mills," *Proceedings of 13<sup>th</sup> International Thermal Spray Conference*, Florida, USA, pp. 637-645.
141. **Mayoral M. C.**, Andres J. M., Bona M. T., Higuera V., and Belzunce F. J., (2008), "Aluminium depletion in NiCrAlY bond coatings by hot corrosion as a function of projection system," *Surf. Coat. Technol.*, Vol. 202, pp. 1816-1824.
142. **Metals Handbook**, (1972), "Atlas of Microstructures of Industrial Alloys," Vol. 7, ASM Publication, Metals Park OH, USA.
143. **Metals Handbook**, (1975), "Failure analysis and Prevention," Vol.10, ASM Publication, Metals Park OH, USA.
144. **Merz, M. D.**, (1979), "The oxidation resistance of fine-grained sputter-deposited 304 stainless steel," *Metall. Trans. A*, Vol. 10, 71-77.
145. **Mevrel, R.**, (1989), "State of the Art on High-Temperature Corrosion-Resistant Coatings," *Mater. Sci. Engg. A*, Vol. 120, pp.13-24.
146. **Mitra S. K.**, Roy S. K., and Bose S., (1993), "Influence of Superficial Coating of CeO<sub>2</sub> on the Oxidation Behavior of AISI 304 Stainless Steel", *Oxid. Met.*, Vol. 39, No. 3/4, pp. 221-229.
147. **Mishra S. B.**, Chandra K., and Prakash S., (2008), "Characterisation and erosion behaviour of NiCrAlY coating produced by plasma spray method on two different Ni-based superalloys," *Mater. Lett.*, Vol. 62, pp. 1999-2002.

148. **Mobin M., Sharma H.K., and Hasan S.K,** (2002), "High temperature oxidation behaviour of CeO<sub>2</sub> and La<sub>2</sub>O<sub>3</sub> modified aluminide coatings on carbon steel," *Anti Corros. Methods and Mater*, Vol. 49, No. (4), pp. 283-294.
149. **Modi, S.C. and Calla, Eklavya,** (2001), "Structure and Properties of HVOF Sprayed NiCrBSi Coatings," *Thermal Spray 2001: New Surfaces for New Millennium*, ASM International, Materials Park, Ohio, USA, pp. 281-284.
150. **Mondal, K., Chatterjee, U. K., Murty, B. S.,** (2007), "Oxidation behavior of multicomponent Zr-based amorphous alloys," *Jour. Alloy. Compd.*, Vol. 433, pp. 162–170.
151. **Moskowitz L.N.,** (1992), "Application of HVOF Thermal Spraying to Solve Corrosion Problems in the Petroleum Industry," *Proceedings of 13<sup>th</sup> International Thermal Spray Conference*, Florida, USA, pp. 611-618.
152. **Murthy, K. S. N., Ambat, R., and Dwarakadasa, E. S.,** (1994), "The Role of Metal Cations on the Corrosion Behaviour of 8090-T851 Alloy in a pH 2.0 solution," *Corros. Sci.*, Vol. 36, No. 10, pp. 1765-1775.
153. **Mukhopadhyay, R., and Mandal, P. K.,** (1999), "Clinkering problem in 500MW unit of a pulverised coal based power station," *R & D Journal (NTPC)*, Vol.5, pp. 9-12.
154. **Nakagawa, P.M., Kawakami, F. and Kudoh, T.,** (1994) "Trends in Automotive Applications of Thermal Spray Technology in Japan," *Proc. of the 7<sup>th</sup> National Therm. Spray Conf.*, Boston, pp. 1-6.
155. **National Materials Advisory Board,** (1996), "Coatings for High-Temperature Structural Materials: Trends and Opportunities," *National Academy Press Washington D.C.*, <http://www.nap.edu/openbook/0309053811/html>, pp 1-85.
156. **Nesbitt J. A., and Heckel R. W.,** (1984), "Modeling Degradation and Failure of Ni-Cr-Al Overlay Coatings," *Thin Solid Films*, Vol. 119, pp. 281-290.
157. **Nestler, M. C., Hohle, R. M., Balbach, W. M., and Koromzay, T.,** (1995), "Economical Advantages of HVOF-Sprayed Coatings for the Land Based Gas Turbine Industry," *Proceedings, 14<sup>th</sup> International Thermal Spray Conference*, JPN, pp. 101–106.
158. **Nicoll, A. R.,** (1984), "Chapter 13: The Production and Performance Evaluation of High Temperature Coatings," in 'Coatings and Surface Treatment for Corrosion and Wear Resistance,' Eds. Strafford, K. N., Datta, P. K. and Googan, C. G., (1984), *Institution of Corros. Sci. and Techol.*, Birmingham, Pub. Ellis Horwood Ltd., Chichester.

159. **Nicholls, J. R., and Hancock, P.,** (1989), in 'The Role of Active Elements in the Oxidation of High Temperature Metals and Alloys,' Ed. Lang, E., Elsevier Applied Science, London, pp. 195.
160. **Nicholls, J. R., and Stephenson, D.J.,** (1991), "High Temperature Coatings for Gas Turbines," Surf. Engg., Vol. 22, pp. 156-163.
161. **Nicoll, A.R.,** (1994), "Production Plasma Spraying in the Automotive Industry: A European Viewpoint," Proc. of the 7<sup>th</sup> National Therm. Spray Conf., Boston, pp. 7-17.
162. **Nicholls, J. R. and Stephenson, D.J.,** (1995), "Ch. 22: High-Temperature Coatings for Gas Turbines," in 'Intermetallic Compounds, Principles and Practice, Vol. 2-Practice,' Eds. Westbrook, J.H. and Fleischer, F.L., Pub. John Wiley & Sons Ltd., England.
163. **Nicholls, J.R.,** (2000), "Design of Oxidation-Resistant Coatings," JOM, Vol. 52, No. 1, pp. 28-35.
164. **Niranatlumpong, P., Ponton, C.B. and Evans, H.E.,** (2000), "The Failure of Protective Oxides on Plasma-Sprayed NiCrAlY Overlay Coatings," Oxid. Met., Vol. 53, No. 3-4, pp. 241-58.
165. **Nguyentat, T., Dommer, K.T. and Bowen, K.T.,** (1992), "Metallurgical Evaluation of Plasma Sprayed Structural Materials for Rocket Engines," Proc. of 13<sup>th</sup> Int. Therm. Spray Conf., Florida, USA, pp. 321-326.
166. **Ohring, M.,** (2002), "Materials Science of thin Films," Academic Press, London, NW1 7BY, UK.
167. **Oishi, N, Tatsuru Namikawa, and Yohtaro Yamazaki,** (2000), "Oxidation behaviour of a La-coated chromia-forming alloy and the electrical property of oxide scales," Surf. Coat. Technol., Vol. 132, pp. 58-64.
168. **Otero, E., Merino, M. C., Pardo, A., Biezma, M. V. and Buitrago, G.,** (1987), "Study on Corrosion Products of IN657 Alloy in Molten Salts," Proc. of 10th ICMC, Madras, India, Vol. IV, pp. 3583-91.
169. **Otsuka, N. and Rapp, R.A.,** (1990), "Effects of Chromate and Vanadate Anions on the Hot Corrosion of Preoxidized Ni by a Thin Fused Na<sub>2</sub>SO<sub>4</sub> Film at 900°C," J. Electrochem. Soc., Vol. 137, No. 1, pp. 53-60.
170. **Otsuka, N,** (2002), "Effects of Fuel Impurities on the Fireside Corrosion of Boiler Tubes in Advanced Power Generating Systems-A Thermodynamic Calculation of Deposit Chemistry," Corros. Sci., Vol. 44, No. 2, pp. 265-283.
171. **Palit, A., and Mandal, P. K.,** (1994), "Slagging and clinkering problem at vindhyachal super thermal power station," R & D Journal (NTPC), Vol. 1, pp. 1-11.

172. **Parker D. W., and Kunter G. L., (1994), "HVOF Moves into Industrial Mainstream,"** Adv. Mat. Proc., Vol. 146, No. 1, pp. 31–35.
173. **Pawlowski, L., (1995), "The Science and Engineering of Thermal Spray Coatings,"** John Wiley & Sons, Chichester, England, 1995.
174. **Perkin Elsmer, (1989), "Diamond Jet System and Gun Manual,"** Metco, 1989.
175. **Pershin V., Lufitha M., Chandra S., and Mostaghimi J., (2003), "Effect of Substrate Temperature on Adhesion Strength of Plasma-Sprayed Nickel Coatings,"** Jour. Thermal Spray Technol., Vol. 12, No. 3, pp. 370-376.
176. **Pettit, F. S. and Meier, G. H., (1985), "Oxidation and Hot corrosion of Superalloys,"** Superalloys 85, Eds. Gell, M., Kartovich, C. S., Bricknel, R. H., Kent W. B. and Radovich, J. F., Met. Soc. of AIME, Warrendale, Pennsylvania, pp. 651-687.
177. **Pettit, F. S. and Giggins, C. S., (1987), "Hot Corrosion, Ch. 12,"** Superalloys II, Sims, C. T., Stoloff, N. S. and Hagel, W. C. (Eds.), Wiley Pub., N. Y.
178. **Picas J.A., Forn A., Igartua A. and Mendoza G., (2003), "Mechanical and tribological properties of high velocity oxy-fuel thermal sprayed nanocrystalline CrC–NiCr coatings,"** Surf. Coat. Technol. Vol. 174–175, pp. 1095-1100.
179. **Pichoir, R., (1978), "Influence of the mode of formation on the oxidation and corrosion behaviour of NiAl-type protective coatings, in Materials and Coatings to Resistant High Temperature Corrosion,"** (D.R. Holmes and A. Rahmel, eds.), Applied Science Publishers, London, p. 271.
180. **Pomeroy M. J., (2005), "Coatings for gas turbine materials and long term stability issues,"** Mater. Design, Vol. 26, pp. 223-231.
181. **Prakash, S., Singh S., Sidhu B.S., and Madeshia A., (2001), "Tube failures in coal fired Boilers, Proc. National Seminar on Advances in Material and Processing, IIT, Roorkee, India, pp. 245-253.**
182. **Prakash, S., Puri, D. and Singh, H., (2005), "Hot Corrosion Behaviour of Plasma Sprayed Coatings on a Ni-Based Superalloy in Na<sub>2</sub>SO<sub>4</sub>-60%V<sub>2</sub>O<sub>5</sub> Environment,"** ISIJ Int., Vol.45, No.6, pp. 886-895.
183. **Prescott R., and Graham M. J., (1992), "The formation of aluminum oxide scales on High-temperature alloys",** Oxid. Met., Vol. 38, No. (3/4), pp. 233-254.
184. **Priyantha, N., Jayaweera, P., Sanjurjo, A., Lau, K., Lu, F. and Krist, K., (2003), "Corrosion-Resistant Metallic Coatings for Applications in Highly Aggressive Environments,"** Surf. Coat. Technol., Vol. 163-64, pp. 31-36.

185. **Raffaitin A.**, Monceau D., Andrieu E. and Crabos F., (2006), "Cyclic oxidation of coated and uncoated single-crystal nickel-based superalloy MC2 analysed by continuous thermogravimetry analysis," *Acta Mater.*, Vol. 54, pp. 4473-4487.
186. **Rajan Ambat**, Zhou, W., (2004), "Electroless nickel-plating on AZ91D magnesium alloy: effect of substrate microstructure and plating parameters", *Surf. Coat. Technol.*, Vol. 179, pp. 124–134.
187. **Ramanathan L. V.**, Pillis M.F. and Fernandes S. M. C., (2008), "Role of rare earth oxide coatings on oxidation resistance of chromia-forming alloys," *J. Mater. Sci.*, Vol. 43, pp. 530-535.
188. **Rapp, R. A.** and Goto, K. S., (1981), "The Hot Corrosion of Metals by Molten Salts," *Sympos. on Fused Salts*, Eds. Braunstein, J. and Selman, J. R., The Electrochem. Soc., Pennington, N. J., p.159.
189. **Rapp, R. A.**, (1986), "Chemistry and Electrochemistry of the Hot Corrosion of Metals," *Corros.*, Vol. 42, No. 10, pp. 568-577.
190. **Rapp, R. A.** and Zhang, Y. S., (1994), "Hot Corrosion of Materials: Fundamental Studies," *JOM*, Vol. 46, No. 12, pp. 47-55.
191. **Rapp, R. A.**, (2002), "Hot Corrosion of Materials: A Fluxing Mechanism," *Corros. Sci*, Vol. 44, No. 2, pp. 209-221.
192. **Rastogi, R. S.**, and Pourrezaei, K., (1994), "Deposition, characterization, thermochemical compatibility and failure analysis of multi-layer coated silicon-carbide fiber-reinforced metal-matrix composites," *J. Mater. Process. Technol.* Vol. 43, pp. 89-107.
193. **Ren, X.**, and Wang, F, (2006), "High-temperature oxidation and hot-corrosion behavior of a sputtered NiCrAlY coating with and without aluminizing," *Surf. Coat. Technol.*, Vol. 201, pp. 30–37.
194. **Rhys-Jones, T. N.**, and Swindells, (1985), "The high temperature corrosion of a commercial aluminide coating on IN738-LC and MARMOO2 at 700°C and 830°C," *Corros. Sci.*, Vol. 25, No. 7, pp. 559-576.
195. **Rhys-Jones T. N.**, Grabke H. J., and Kudielka H., (1987), "The effects of various amounts of alloyed cerium and cerium oxide on the high temperature oxidation of Fe-10Cr and Fe-20Cr alloys," *Corros. Sci.*, Vol. 27, No. 1, pp. 49-73.
196. **Roure S.**, Czerwiski F., and Petric A., (1994), "Influence of CeO<sub>2</sub>-coating on the high-temperature oxidation of chromium," *Oxid. Met.*, Vol. 42, No. 1-2, pp. 75-102.

197. **Rybicki, G. C., and Smialek J. L., (1989),** "Effect of the  $\theta$ - $\alpha$ - $\text{Al}_2\text{O}_3$  Transformation on the Oxidation Behavior of  $\beta$ -NiAl + Zr," Vol. 31, Nos 3/4, pp. 275-304.
198. **Russo L., and Dorfman M., (1995),** "High Temperature Oxidation of MCrAlY Coatings Produced by HVOF," Proceedings, 14th International Thermal Spray Conference, JPN, pp. 1179-1184.
199. **Sadique, S. E., Mollah, A. H., Islam, M. S., Ali, M. M., Megat, M. H. H. and Basri, S., (2000),** "High-Temperature Oxidation Behavior of Iron-Chromium-Aluminum Alloys," *Oxid. Met.*, Vol. 54, Nos. 5-6, pp. 385-400.
200. **Sampath S., Herman H., and Rangaswamy S., (1987),** "Ni-Al Re-evaluated, Thermal Spray-Advances in Coating Technology, National Thermal Spray Conference, Orlando, D.L. Houck (Ed), ASM International. pp 47-53.
201. **Sampath S., Jiang X.Y, Matejicek J, Prchlik L, Kulkarni A., and Vaidya A., (2004),** "Role of thermal spray processing method on the microstructure, residual stress and properties of coatings: an integrated study for Ni-5wt.%Al bond coats," *Mater. Sci. Eng., A.*, Vol. 364, pp. 216-231.
202. **Santoro G. J., and Barrett C. A., (1978),** "Hot Corrosion Resistance of Nickel-Chromium-Aluminum Alloys," *J. Electrochem, Soc*, Vol. 125, No. 2, pp. 271-278.
203. **Santoro G. J., (1979),** "Hot Corrosion of Four Superalloys: HA-188, S-57, IN-617, and TD-NiCrAl," *Oxid. Met.*, Vol. 13, No. 5, pp. 405-435.
204. **Santorelli, R., Sivieri, E. and Reggiani, R.C., (1989),** "High-Temperature Corrosion of Several Commercial Fe-Cr-Ni Alloys Under a Molten Sodium Sulphate Deposit in Oxidizing Gaseous Environments," *Mater. Sci. Eng. A* Vol. 120, pp. 283-291.
205. **Saunders, S.R.J. and Nicholls, J.R., (1984),** "Hot Salt Corrosion Test Procedures and Coating Evaluation," *Thin Solid Films*, Vol. 119, pp. 247-269.
206. **Schutze, M., (1993),** "Mechanical Aspects of High-Temperature Oxidation," *Corros. Sci.*, Vol. 35, Nos 5-8, pp. 955-963.
207. **Schneibel J. H., and Becher P.F., (1999),** "Iron and nickel aluminide composites," *J. Chin. Inst. Eng.*, Vol. 22, No.1, pp. 1-12.
208. **Scrivani, A., Ianelli, S., Rossi, A., Groppetti. R., Casadei, F., and Rizzi, G., (2001),** "A contribution to the surface analysis and characterisation of HVOF coatings for petrochemical application," *Wear*, Vol. 250, pp. 107-113.
209. **Seiersten M., and Kofstad P., (1987),** "Effect of  $\text{SO}_3$  on Vanadate Induced Hot Corrosion," *High Temp. Technol.* Vol. 5, No. 3, pp. 115-122.



210. **Seybolt A. U.**, (1971), "Role of rare earth additions in the phenomenon of hot corrosion," *Corros. Sci.*, Vol. 11, pp. 751-761.
211. **Shifler, David A.**, (2004), "Substrate-Coating Interactions and Their Effects on Hot Corrosion Resistance," *Proc. Electrochemical Society*, v PV 2004-16, High Temperature Corrosion and Materials Chemistry V-International Symposium, Electrochemical Society Inc., Pennington, NJ 08534-2896, United States, Oct 3-8, 2004, pp. 294-305.
212. **Sierra C.**, and **Vazquez A. J.**, (2005), "NiAl coatings on carbon steel by self-propagating high-temperature synthesis assisted with concentrated solar energy: mass influence on adherence and porosity," *Solar Energy Materials & Solar Cells.*, Vol. 86, pp. 33-42.
213. **Smeggil, J. G.** and **Bornstein, N. S.**, (1983), "Study of Interdiffusion Effects on Oxidation/Corrosion Resistant Coatings for Advanced Single Crystal Superalloys," *Proc. Sympos. High-Temperature Protective Coatings*, March 7-8, Atlanta, GA, USA, Ed. Singhal, S.C., *Pub. Metall. Soc of AIME*, Warrendale, PA, USA, pp. 61-74.
214. **Smith, R.W.** and **Knight, R.**, (1995), "Thermal spraying I: Powder Consolidation - From Coating to Forming," *J. Mater.*, Vol. 47, No. 8, pp.32-39.
215. **Smith, D. L.**, (1995), *Thin Film Deposition*, McGraw-Hill, New York.
216. **Smialek, J. L.**, (2001), "Advances in the oxidation resistance of high-temperature turbine materials," *Surf. Interface Anal.*, Vol. 31, pp. 582-592.
217. **Sidhu T. S.**, (2006), "Studies on The Hot corrosion behaviour of HVOF Coatings on Some Ni- and Fe-based Superalloys", Ph.D. Thesis, *Met. & Mat. Eng. Dept.*, Indian Institute of Technology Roorkee, Roorkee.
218. **Sidhu, T. S.**, **Prakash S.**, and **Agarwal R.D.**, (2006C), "Performance of High-velocity Oxyfuel Sprayed coatings on a Fe-based Superalloy in Na<sub>2</sub>SO<sub>4</sub>-60%V<sub>2</sub>O<sub>5</sub> environment at 900°C Part I: Characterization of the coating," *Mat Engg & Perfor.*, Vol. 15, pp. 122-129.
219. **Sidhu, T.S.**, **Prakash S.**, and **Agrawal R.D.**, (2006D), "Characterizations of HVOF sprayed NiCrBSi coatings on Ni- and Fe-based superalloys and evaluation of cyclic oxidation behaviour of some Ni-based superalloys in molten salt environment," *Thin Solid Films*, Vol. 515, pp. 95-105.
220. **Sidhu T.S.**, **Prakash S.** and **Agarwal R.D.**, (2006C), "Hot corrosion studies of HVOF sprayed Cr<sub>3</sub>C<sub>2</sub>-NiCr and Ni-20Cr coatings on nickel based superalloy at 900°C," *Surf. Coat. Technol.*, Vol. 201, pp. 792-800.

221. **Sidhu T. S., Prakash S., Agrawal R. D., (2006D),** "Studies of the metallurgical and mechanical properties of high velocity oxy-fuel sprayed stellite-6 coatings on Ni- and Fe-based superalloys," *Surf.Coat. Technol.* Vol. 201, pp. 273-281.
222. **Sidhu T. S., Prakash S., Agrawal R. D., (2006E),** "Characterisation of NiCr wire coatings on Ni- and Fe based superalloys by the HVOF process," *Surf. Coat. Technol.* Vol. 200, pp. 5542-5549.
223. **Sidhu, T. S., Prakash, S., Agrawal, R. D., (2006F)** "Hot corrosion behaviour of HVOF-sprayed NiCrBSi coatings on Ni and Fe-based superalloys in Na<sub>2</sub>SO<sub>4</sub>-60% V<sub>2</sub>O<sub>5</sub> environment at 900°C," *Acta Mater.*, Vol. 54, pp. 773-784.
224. **Siddu T. S., Prakash S., and Agrawal R. D., (2007),** "Study of Molten Salt Corrosion of High Velocity Oxy-Fuel Sprayed Cermet and Nickel-Based Coatings at 900°C," *Metall. Mater. Trans A.* Vol. 38A, pp. 77-85.
225. **Sidhu, T.S., Prakash, S., and Agrawal, R.D., (2006A),** "Hot corrosion studies of HVOF NiCrBSi and Stellite-6 coatings on a Ni-based superalloy in an actual industrial environment of a coal fired boiler," *Surf. Coat. Technol.*, Vol. 201, pp. 1602-1612.
226. **Sidhu, T.S., Prakash, S., and Agrawal, R.D., (2006B),** "Hot corrosion performance of a NiCr coated Ni-based alloy", *Scripta Materialia*, Vol. 55, pp.179-182.
227. **Sidky, P. S., and Hocking M. G., (1999),** "Review of Inorganic Coatings and Coating Processes For Reducing Wear and Corrosion," *Brit. Corros. J.*, Vol. 34, No. 3, pp. 171-183.
228. **Sims, C.T., Stoloff, N.S., and Hagel, W.C., (1987)** "The superalloys," John Wiley and Sons, Inc, New York.
229. **Sivakumar, R., and Mordike, B. L., (1989),** "High Temperature Coatings for Gas Turbine Blades: A review," *Surf. Coat. Technol.*, Vol. 37, pp. 139-160.
230. **Srinivas, V., Barua, P., Ghosh, T.B. and Murty, B.S., (2004),** "Oxidation Behaviour of Al-Cu-Fe Nanoquasicrystal Powders," *Journal of Non-Crystalline Solids*, Vol. 334-335, pp. 540-543.
231. **Srivastava, S. C., Godiwalla, K. M., and Banerjee, M. K., (1997),** "Fuel ash corrosion of boiler and superheater tubes," *Jour. Mater. Sci.*, Vol. 32, pp. 835-849.
232. **Sobolev V.V., Guilemany J.M., Nutting J., and Miquel J.R., (1997),** "Development of substrate-coating adhesion in thermal spraying," *Int. Mater. Rev.*, Vol. 42, No. 3, pp. 117-136.
233. **Sobolev, V.V., Guilemany, J.M. and Nutting, J., (2004),** "High Velocity Oxy-Fuel Spraying," B0655, IOM3, Maney Publishing, London.

234. **Stokes, J. and Looney, L.,** (2001), "HVOF System Definition to Maximise the Thickness of Formed Components," *Surf. Coat. Technol.*, Vol. 48, No. 1, pp. 18-24.
235. **Stokes J. and Looney L.,** (2004), "Residual stress in HVOF thermally sprayed thick deposits," *Surf. Coat. Technol.* Vol. 177-178, pp.18-23.
236. **Stewart D.A., Shipway P.H. and McCartney D.G.,** (1999), "Abrasive wear behaviour of conventional and nanocomposite HVOF-sprayed WC-Co coatings," *Wear*, Vol. 225- 229, pp. 789-798.
237. **Sturgeon A. J.,** (2001), "Microstructure characteristics and corrosion behaviour of HVOF sprayed metallic coatings," *Proc. of International Thermal Spray Conference*, pp. 1149-1155.
238. **Streief Roland,** (1993), "Databases and expert systems for high temperature - corrosion and coatings," *Corros. Sci.*, Vol. 35, No. 5-8, pp. 1177-1187.
239. **Stringer, J.,** (1987), "High Temperature Corrosion of Superalloys," *Mater. Sci. Technol.*, Vol. 3, No. 7, pp. 482-493.
240. **Stringer, John.,** (1995), "Practical experience with wastage at elevated temperatures in coal combustion systems," *Wear*, Vol. 186-187, Part1, pp. 11-27.
241. **Stott, F. H.,** (1998), "The role of oxidation in the wear of alloys", *Trib. Int.*, Vol. 31, No. 1-3, pp. 61-71.
242. **Stott, F.H.,** (1989B), "Influence of Alloy Additions on Oxidation," *Mater. Sci. Technol.*, Vol. 5, pp. 734-740.
243. **Stroosnijder, M. F., Mevrel, R. and Bennet, M. J.,** (1994), "The Interaction of Surface Engineering and High Temperature Corrosion Protection," *Mater. High Temp.*, Vol. 12, No. 1, pp. 53-66.
244. **Sundararajan, T., Kuroda, S., Itagaki, T. and Abe F.,** (2003A), "Steam Oxidation Resistance of Ni-Cr Thermal Spray Coatings on 9Cr-1Mo Steel. Part 1: 80Ni-20Cr," *ISIJ Int.*, Vol. 43, No.1, pp. 95-103.
245. **Sundararajan S., Kuroda S, Nishida K, Itagaki T., and Abe F.,** (2004A), "Behaviour of Mn and Si in the spray powders during steam oxidation of Ni-Cr thermal spray coatings", *ISIJ Int.*, Vol. 44, pp. 139-144.
246. **Sundararajan, T., Kuroda, S. and Abe, F.,** (2004B), "Steam Oxidation Studies on 50Ni-50Cr HVOF Coatings on 9Cr-1Mo Steel: Change in Structure and Morphology across the Coating/Substrate Interface," *Mater. Trans.*, Vol. 45, No. 4, pp.1299-1305.
247. **Sundararajan, T., Kuroda, S. and Abe, F.,** (2005), "Steam Oxidation of 80Ni-20Cr High Velocity Oxy-fuel Coatings on 9Cr-1 Mo Steel: Diffusion-Induced Phase

Transformations in the Substrate Adjacent to the Coating,” *Metallurgical and Materials Transactions A: Physical Metallurgy and Materials Science*, Vol. 36, No. 8, pp. 2165-2174.

248. **Swaminathan, J.**, Raghavan, S. and Iyer, S. R., (1993), “Studies on the Hot Corrosion of Some Nickel-Base Superalloys by Vanadium Pentoxide,” *T. Indian I. Metals*, Vol. 46, No. 3, pp. 175-181.
249. **Swaminathan, J.** and Raghavan, S., (1994), “Vanadic Hot Corrosion-Creep Interaction of Superni-C 276 in the Temperature Range 650-750<sup>0</sup>C,” *High Temp. Mater. Processes*, Vol. 13, No. 4, pp. 277-297.
250. **Tan, K.S.**, Wharton, J.A. and Wood, R.J.K., (2005), “Solid Particle Erosion-Corrosion Behaviour of a Novel HVOF Nickel Aluminium Bronze Coating for Marine Applications-Correlation Between Mass Loss and Electrochemical Measurements,” *Wear*, Vol. 258, No. 1-4, pp. 629-640.
251. **Tian Y. S.**, Chen C. Z., Chen L. X., and Huo Q.H., (2006), “Effect of RE oxides on the microstructure of the coatings fabricated on titanium alloys by laser alloying technique,” *Scripta Mater.*, Vol. 54, pp. 847-852.
252. **Tiwari, S. N.**, (1997), “Investigations on Hot Corrosion of Some Fe-, Ni- and Co-Base Superalloy in Na<sub>2</sub>SO<sub>4</sub>-V<sub>2</sub>O<sub>5</sub> Environment under Cyclic Conditions,” Ph. D. Thesis, Met. Mat. Engg. Deptt., University of Roorkee, Roorkee, India.
253. **Tiwari S.N** and Prakash S., (1997), “Studies on the hot corrosion behaviour of some superalloys in Na<sub>2</sub>SO<sub>4</sub>-60%V<sub>2</sub>O<sub>5</sub>, Paper presented at symposium on localised corrosion and environmental cracking (SOLCEC), Kalpakkam (India), C-33.
254. **Tiwari, S. N.** and Prakash, S., (1998), “Literature Review-Magnesium Oxide as Inhibitor of Hot Oil Ash Corrosion,” *Mater. Sci. Technol.*, Vol. 14, pp. 467-172.
255. **Tobe S.**, (1998-1047-char), “A Review on Protection from Corrosion, Oxidation and Hot Corrosion by Thermal Spray Coatings,” *Proceedings of the 15<sup>th</sup> International Thermal Spray Conference*, Nice, France, May 25-29; pp. 3-11.
256. **Toma D.**, Brandl W., and Koster U., (2000), “The Characteristics of Alumina Scales Formed on HVOF-Sprayed MCrAlY Coatings,” *Oxid. Met.*, Vol. 53, No. 1-2, pp. 125-137.
257. **Tucker Jr R.C.**, (1994) Chapter 11, *Advanced Thermal Spray Deposition Techniques*, Norwich, NY, *Handbook of Deposition Technologies for Films & Coatings*, R.F. Bunshah, Ed., William Andrew Publ./Noyes, p 591

258. **Ul-Hamid A.**, (2003), "Diverse scaling behaviour of the Ni-20Cr alloy," *Mater. Chem. Phys.*, Vol. 80, pp. 135-142.
259. **Uusitalo, M.A., Vuoristo, P.M.J., and Mantyla, T.A.**, (2003), "High temperature corrosion of coatings and boiler steels in oxidizing chlorine-containing atmosphere," *Mater. Sci. Eng. A* Vol. 346, pp. 168-177.
260. **Varacalle, D. J. Jr., Couch, K.W. and Budinger, V.S.**, (1996), "Studies of the Flame Spraying of Polymers," *Proc. of the 9<sup>th</sup> National Thermal Spray Conference, Cincinnati, Ohio*, pp. 251-255.
261. **Wang D.**, (1988-1037-HC), "Corrosion Behaviour of Chromized and/or Aluminized 21/4Cr-1Mo Steel in Medium-BTU Coal Gasified Environments," *Surf. Coat. Technol.* Vol. 36, pp. 49-60.
262. **Wang, Y., Liu, J. J., and Yu, Z. H.**, (1993), "Effect of rare earth elements, on microstructure and wear resistance of laser remelted iron alloy coatings containing metalloids," *Surf. Engg.*, Vol, 9, no. 2, pp. 151-155.
263. **Wang M., and Wu W.**, (1995), "Microstructure of laser-surface-alloyed cast iron with Cr-Al-Y alloy," *Surf. Coat. Technol.*, Vol. 72, pp. 181-188.
264. **Wang Y., Kovacevic R. and Liu J.**, (1998), "Mechanism of surface modification of CeO<sub>2</sub> in laser remelted alloy spray coatings," *Wear*, Vol. 221, pp. 47-53.
265. **Wang K. L., Zhang Q.B., Sun M.L., Wei X.G., and Zhu Y. M.**, (2001A), "Rare earth elements modification of laser-clad nickel-based alloy coatings," *Applied Surf. Science*, Vol. 174, pp. 191-200.
266. **Wang K.L., Zhang Q.B., Sun M.L., Wei X.G. and Zhu Y.M.**, (2001B), "Microstructure and corrosion resistance of laser clad coatings with rare earth elements", *Corros. Sci.*, Vol. 43, pp. 255-267.
267. **Wang, B.Q. and Shui, Z.R.**, (2002), "The Hot Erosion Behavior of HVOF Chromium Carbide-Metal Cermets Coatings Sprayed with Different Powders," *Wear*, Vol. 253, pp.550-557.
268. **Wang B., Gong J., Wang A. Y., Sun C., Huang R. F., and Wen L. S.**, (2002), "Oxidation behaviour of NiCrAlY coatings on Ni-based superalloy," *Surf. Coat. Technol.*, Vol. 149, pp. 70-75.
269. **Wang, X. Y., and Li, D. Y.**, (2002), "Mechanical and electrochemical behavior of nanocrystalline surface of 304 stainless steel," *Electrochimica Acta*, Vol. 47, pp.3939-3947.

270. Wang B., Gong J., Sun C., Huang R. F., and Wen L. S., (2003), "The behavior of MCrAlY coatings on Ni<sub>3</sub>Al-base superalloy", *Mater. Sci. Eng. A*, Vol. 357, pp. 39-44.
271. Wang K. L., Zhang Q. B., Sun M. L., and Wei X. G., (2003), "Microstructural characteristics of laser clad coatings with rare earth metal elements," *Jour. Mater. Process. Technol.*, Vol. 139, pp. 448-452.
272. Wang, Y., and Chen, W., (2003), "Effect of ceria on the erosion resistance of HVOF thermal sprayed NiAl intermetallic coatings," *Jour. Mat. Sci. Lett.*, Vol. 22, pp. 845– 848.
273. Wang Y.Y., Li C.J., Ohmori A., (2006), "Examination of factors influencing the bond strength of high velocity oxy-fuel sprayed coatings," *Surf. Coat. Technol.*, Vol. 200, pp. 2923-2928.
274. Weulersse-Mouturat, K., Moulin, G., Billard, P., and Pierotti, G., (2004), "High Temperature Corrosion of Superheater Tubes in Waste Incinerators and Coal-Fired Plants," *Mater. Sci. Forum*, Vol. 461-464, pp. 973-980.
275. Whittle, D. P., (1983), "Oxidation Mechanisms for alloys in single oxidant gases," *High temperature corrosion*. Ed. Rapp R. A., Houston: NACE, pp 171-183.
276. Wirojanupatump S., Shipway P.H., and McCartney D.G., (2001-1037-Hc), "The influence of HVOF powder feedstock characteristics on the abrasive wear behaviour of Cr<sub>x</sub>C<sub>y</sub>-NiCr coatings," *Wear*, Vol. 249, pp. 829-837.
277. Wigren, J. and Tang, K., (2001), "Some Considerations for the Routine Testing of Thermal Sprayed Coatings," *Proc. Inter. Thermal Spray Conference*, May 28-30, Singapore, pp. 1221-1227.
278. Wolfe D. and Singh J., (1998), "Functionally gradient ceramic/metallic coatings for gas turbine components by high-energy beams for high-temperature applications," Vol. 33, No. 14, pp. 3677-3692.
279. Wood G. C., (1970), "High temperature oxidation of alloys," *Oxid Met.*, Vol. 2, No.1, 11-57.
280. Wright, I.G., (1987), "High-Temperature Corrosion," in 'Metals Handbook,' Vol. 13, 9<sup>th</sup> Ed., Metals Park, ASM, pp. 97-103.
281. Xiao, C.B., Han, Y.F., Song, J.X. and Li, J.P., (2006), "Effect of NiCoCrAlYHf Overlay Coating on Performance of Ni<sub>3</sub>Al-Based Alloy IC6A," *Surf. Coat. Technol.*, Vol. 200, No. 9, pp. 3095-3101.

282. **Yang, S., Wang, F., and Wu, W., (2001), "Effect of microcrystallization on the cyclic oxidation behavior of b-NiAl intermetallics at 1000°C in air," Intermetallics, Vol. 9, pp. 741-744.**
283. **Yoshida, M., (1993), "Effect of Hot Corrosion on the Mechanical Performances of Superalloys and Coating Systems," Corros. Sci., Vol. 35, No. 5-8, pp. 1115-1124.**
284. **Zhang, J.S., Hu, Z.Q., Murata, Y., Morinaga, M. and Yukawa, N., (1993), "Design and Development of Hot Corrosion-Resistant Nickel-Base Single Crystal Superalloys by the d-Electron Alloy Design Theory; II: Effects of Refractory Metals Ti, Ta, and Nb on Microstructures and Properties," Metall. Trans. A, Vol. 24, No. 11, pp. 2451-2464.**
285. **Zhang Y. J., Sun X. F., Guan H. R., and Zhuang-Qi Hu, (2002), "1050°C isothermal oxidation behavior of detonation gun sprayed NiCrAlY coating," Surf. Coat. Technol., Vol. 161, pp. 302-305.**
286. **Zhang Y.J., Sun X.F., Zhang Y.C., Jin T., Deng C.G., Guan H.R., and Hu Z.Q., (2003), "A comparative study of DS NiCrAlY coating and LPPS NiCrAlY Coating," Mater. Sci. Eng. A Vol. 360, pp. 65-69.**
287. **Zhang Z., Wang Z., Liang B., and La P., (2006), "Effects of CeO<sub>2</sub> on Friction and Wear Characteristics of Fe-Ni-Cr alloy coatings," Tribol. Int. Vol. 39, pp. 971-978.**
288. **Zhao W. M., Wang Y., Han T., Wu K. Y., Xue J., (2004), "Electrochemical evaluation of corrosion resistance of NiCrBSi coatings deposited by HVOF," Surf. Coat. Technol. Vol. 183, pp. 118-125.**
289. **Zhao, S., Xie X., and Smith G. D., (2004), "The oxidation behavior of the new nickel-based superalloy Inconel 740 with and without Na<sub>2</sub>SO<sub>4</sub> deposit," Surf. Coat. Technol., Vol. 185, pp. 178-183.**
290. **Zhao W. M., Wang Y., Dong L. X., Wu K. Y., Xue J., (2005), "Corrosion mechanism of NiCrBSi coatings deposited by HVOF," Surf. Coat. Technol. Vol. 190, pp. 293-298.**
291. **Zhao, S., Xie, X., Smith, G.D., and Patel, S.J., (2005A), "The Corrosion of Inconel Alloy 740 in Simulated Environments for Pulverized Coal-Fired Boiler," Mater. Chem. Phys., Vol. 90, No. 2-3, pp. 275-281.**
292. **Zhong, D., Moore, J.J., Ohno, T.R., Disam, J., Thiel, S., Dahan, I., (2000), "Deposition and characterization of NiAl and Ni-Al-N thin films from a NiAl compound target," Surf. Coat. Technol., Vol. 130, pp. 33-38.**
293. **Zhu, S., Wang, F., Lou, H., and Wu, W., (1995), "Reactive sputter deposition of alumina films on superalloys and their high-temperature corrosion resistance", Surf. Coat. Technol., Vol. 71, pp. 9-15.**